



**University of Kerbala
College of Science
Department of Chemistry**

Synthesis of Dendrimers, Imidazoles and Study Their Biochemical and Biological Applications

A Thesis

Submitted to the Council of the College of Science, University of
Kerbala, in Partial Fulfillment of the Requirements for the Degree of
Doctor of Philosophy of Science / Chemistry

By

Sawsan Khudair Abbas

B.Sc. Chemistry 2002 –University of Babylon

M.Sc. Chemistry 2014 –University of Kerbala

Supervised by

Prof. Dr. Haitham Dalol Alshebly
Organic Chemistry

Prof. Dr. Narjis Hadi Al-Saadi
Biochemistry

2023 A.D

1445 A.H

بِسْمِ اللَّهِ الرَّحْمَنِ الرَّحِيمِ

وَأَنْزَلَ اللَّهُ عَلَيْكَ الْكِتَابَ وَالْحِكْمَةَ وَعَلَّمَكَ مَا لَمْ تَكُنْ تَعْلَمُ ۖ وَكَانَ فَضْلُ اللَّهِ عَلَيْكَ عَظِيمًا

صدق الله العظيم
(سورة النساء: الآية 113)

Dedication

*To my God and creator
and my support*

*To the Prophet of Mercy,
Muhammad*

*To my warm family,
I present my modest Gift*

Acknowledgments

Initially, I am most grateful to Allah, who gave me strength and guidance throughout my life, especially during this work., I would like to express my deepest thanks and sincere gratitude to my supervisors, Prof. Dr. Haitham Dalloul Hanoun and Prof. Dr. Narjis Hadi Mansoor, for their suggestion of the work plan, and their tremendous guidance, and their kind support, advice, guidance, and continuous encouragement throughout the presented research work.

Also thank the College of Science, represented by the Head of the Chemistry Department, Prof. Dr Luma Majeed Ahmed, and the Dean of the College of Science, Asst. Prof. Dr. Jassim Hanoun Al-Awadi, for their assistance in providing work requirements and support for students.

My sincere thanks and appreciation to Dr. Haider Ali Muhammed, Professor at the College of Veterinary Medicine, for helping me in facilitating my task of working in the college laboratories and preparing all the means to complete the works, my sincere appreciation to my beloved family: dear parents, brothers, and sisters for their endless love their patience, support, sacrifice, and fortitude to stay by my side through these years.

I would also like to thank my colleagues and close friends who have continued to support me through all the difficult times in my work and for their assistance and kindness. Finally, I would like to express my thanks to all the individuals who have helped me in one way or another in the fulfillment of this work.

Supervisor Certification

I certify that this thesis " **Synthesis of Dendrimers, Imidazoles and Study Their Biochemical and Biological Applications**" is conducted under my supervision at the department of chemistry, College of science, University of Kerbala, as a partial fulfillment of the requirements for the degree of philosophy in chemistry.

Supervisor

Name: Prof. Dr. Haithem Dalol Alshebly

**Address: University of Kerbala / College
of Science**

Signature:



Supervisor

Name: Prof. Dr. Narjis Hadi Al-Saadi

**Address: University of Kerbala /
College of Science**


Signature:



Report of the Head of Chemistry Department

According to the recommendation presented by the Chairman of the Postgraduate Studies Committee, I forward this thesis "**Synthesis of Dendrimers, Imidazoles and Study Their Biochemical and Biological Applications**" for discussion.

Signature:

A handwritten signature in blue ink that reads "Luma". The signature is stylized with a large loop at the top and a horizontal line extending to the left.

Prof. Dr. Luma Majeed Ahmed

Head of Chemistry Department

Address: University of Kerbala / College of Science ,Department of Chemistry

Date: 9 / 11 / 2023

Examination Committee Certification

We, the examining committee, certify that we have read this thesis "Synthesis of Dendrimers, Imidazoles and Study Their Biochemical and Biological Applications" and examined the student (Sawsan Khudair Abbas) in its contents and that in our opinion, it is adequate as a thesis for the degree of philosophy of science in chemistry.

(Chairman)

Signature: 


Name: Dr. Zeid Hassan Abood

Title: Professor

Address: University of Kerbala / College of Science

Date: 9/11/2023

(Member)

Signature: 


Name: Dr. Sadiq Abdul Hussein Karim

Title: Professor

Address: University of Babylon / College of Science for Women

Date: 8/11/2023

(Member)

Signature: 


Name: Dr. Suhad Rasheed Majeed

Title: Professor

Address: University of Kufa / college of pharmacy

Date: 8/11/2023

(Member)

Signature: 


Name: Dr. Salam Ahmed Abed

Title: Assistant Professor

Address: University of Kerbala / college of pharmacy

Date: 7/11/2023

(Member)

Signature: 


Name: Dr. Rehab Jasim Mohammad

Title: Assistant Professor

Address: University of Kerbala / College of Education for Pure Sciences

Date: 7/11/2023

(Member & Supervisor)

Signature: 

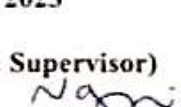
Name: Dr. Haitham Dalol Alshebly

Title: Professor

Address: University of Kerbala / College of Kerbala

Date: 9/11/2023

(Member & Supervisor)

Signature: 

Name: Dr. Narjis Hadi Al-Saadi

Title: Professor

Address: University of Kerbala / College of Kerbala

Date: 9/11/2023

Approved by the council of the College of Science in its session No. in / / 2023

Signature:

Name: Dr. Jasem Hanoon Hashim Al-Awadi

Title: Professor

Address: University of Kerbala - Dean of College of Science

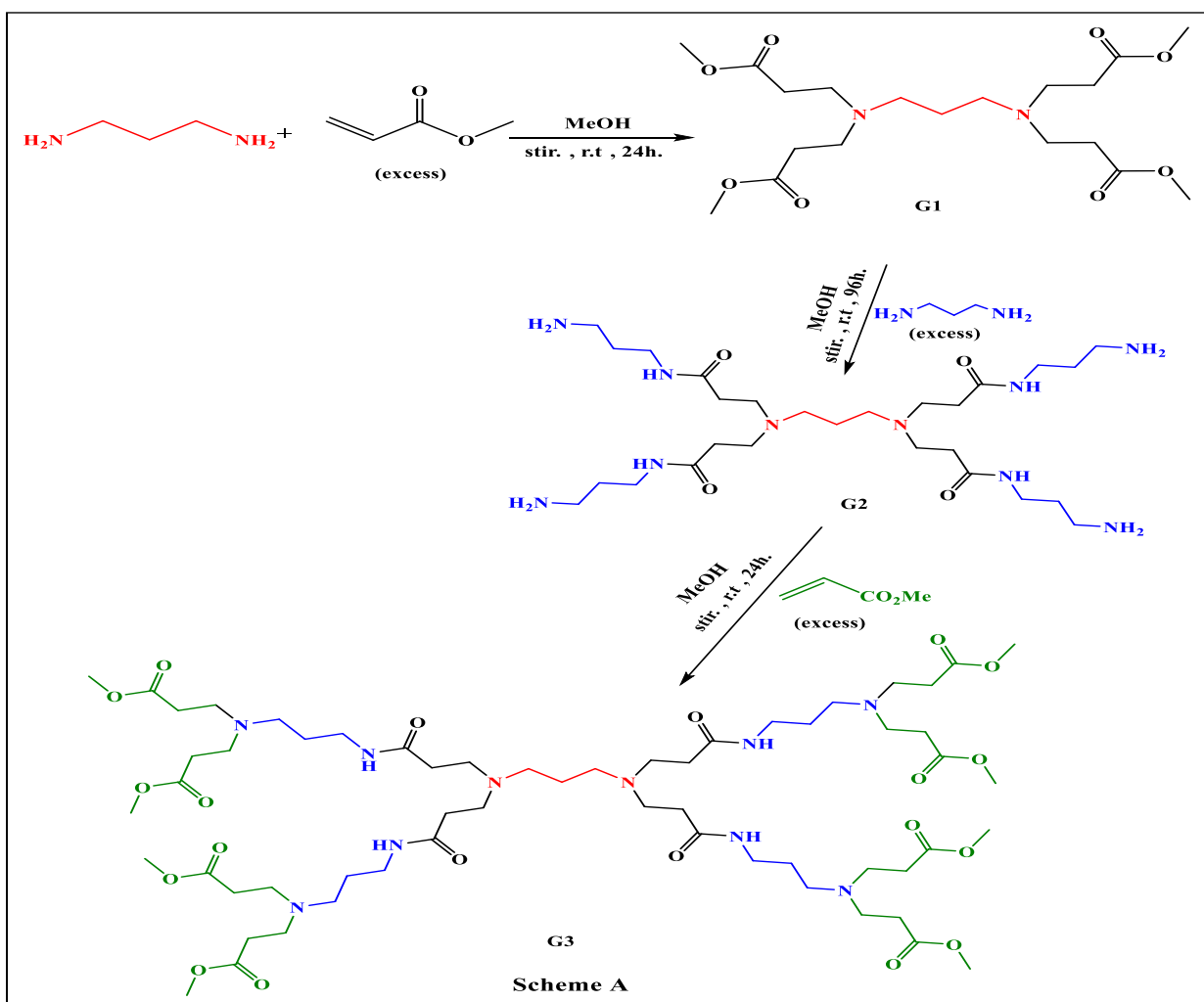
Date: 11/2023

12

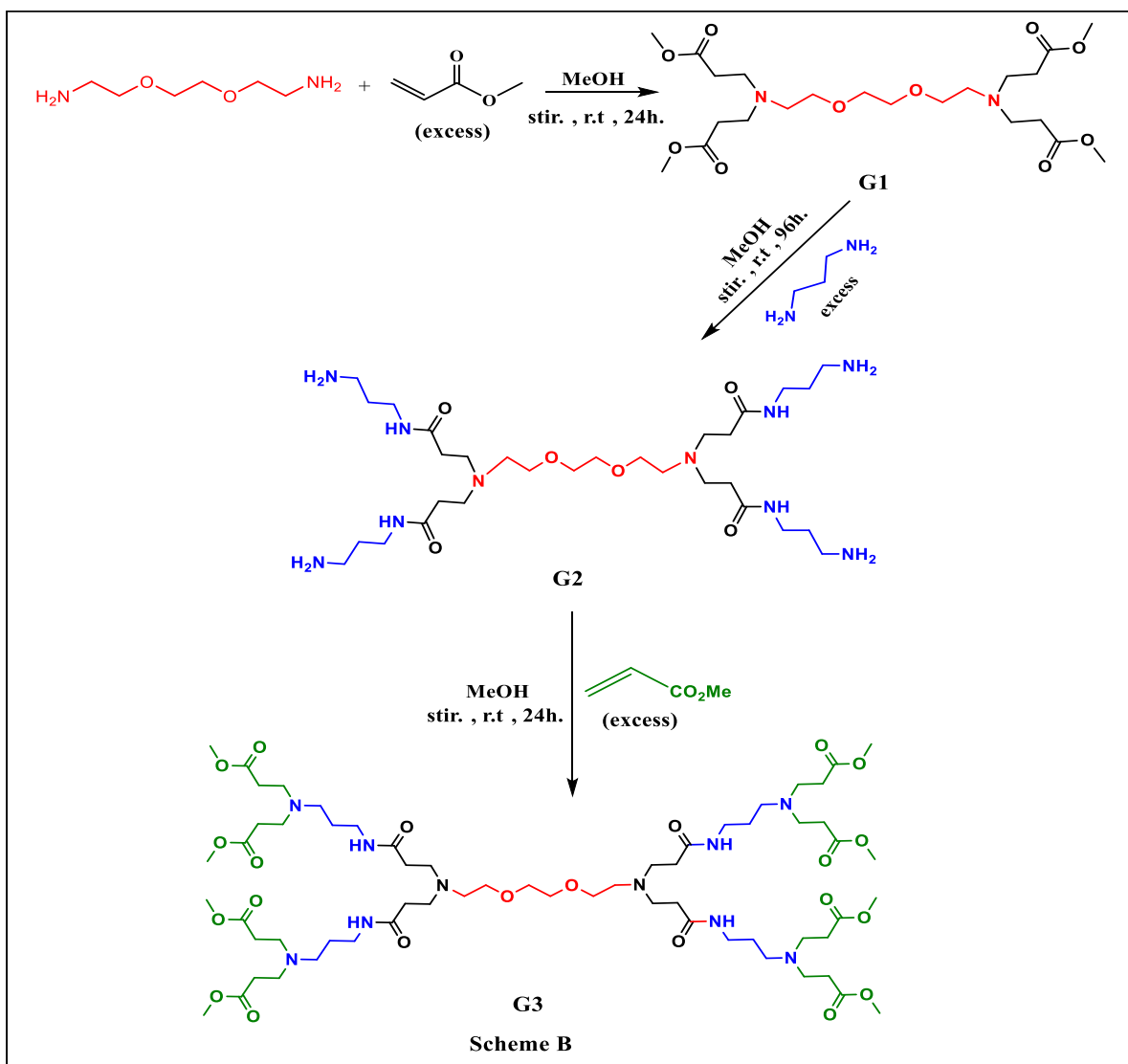
Abstract

Polyamidoamine (PAMAM) dendrimer and imidazole derivatives are essential classes of organic compounds that play a significant role in medicinal chemistry. As a result, this study focuses on the synthesis and characterization of hyperbranched (PAMAM dendrimers) and new substituted imidazoles (Triimidazole and Tetraimidazole derivatives) as well as studies their properties in the biochemical and biological applications. The current research included three parts.

The first part of the thesis outlines the synthesis of PAMAM dendrimers from **G1** to **G3** through a divergent approach that includes two steps; a 1,4-Michael addition which yields ester-terminated dendrimers and an amidation step to generate amine-terminated dendrimers

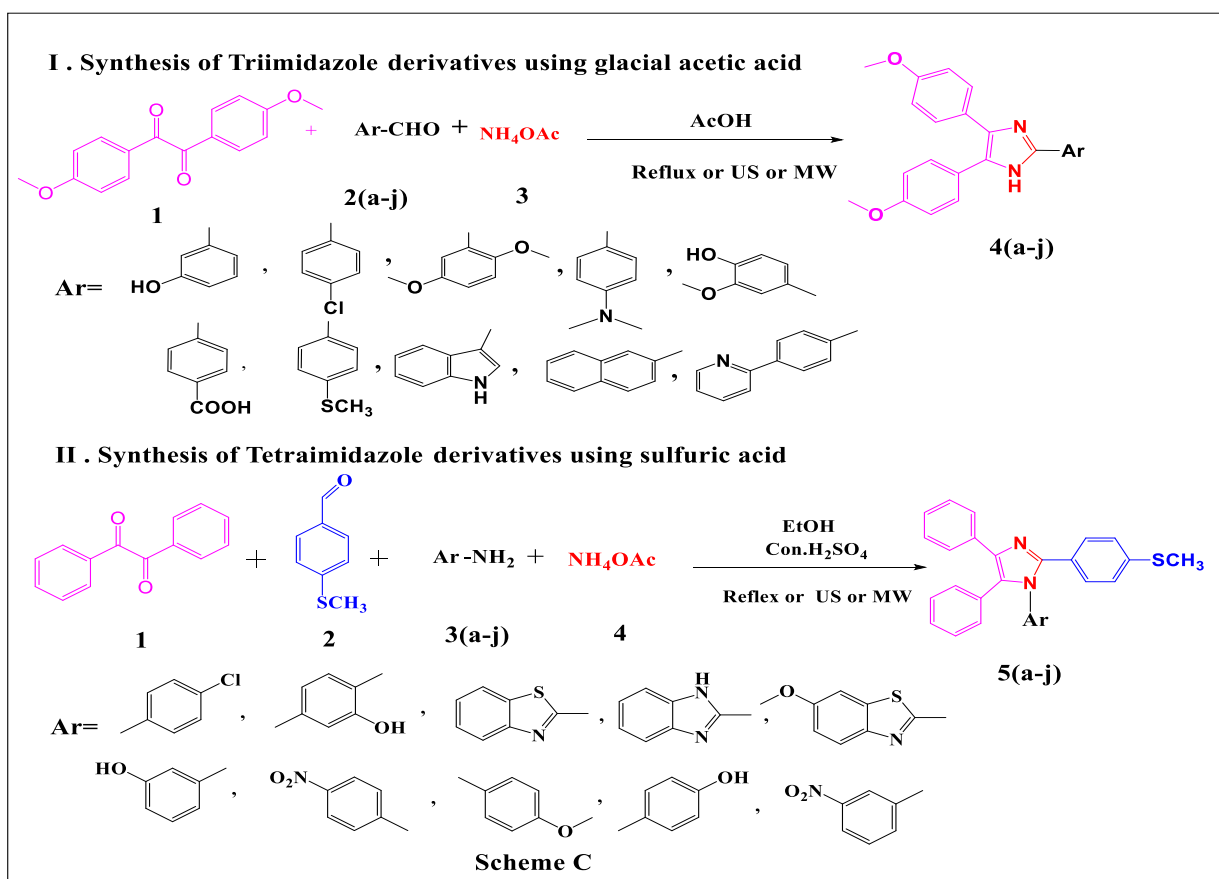


Propane-1,3-diamine and 1,2-bis(2-aminoethoxy) ethane were chosen as various cores for the synthesis of dendrimers to produce primary and secondary amines inside the dendrimer structure (Scheme A and B).



To investigate that dendrimers were successfully prepared different spectroscopic techniques were utilized such as FTIR, (^1H , ^{13}C) NMR and ESI-MS analysis. In addition to, Field Emission Scanning Electron Microscope (FE-SEM) and Energy-dispersive X-ray spectroscopy (EDX).

The second part of the thesis describes the multicomponent coupling reactions via the Debus-Radziszewski reaction to synthesized 2,4,5-triaryl imidazole derivatives ranging from **4a** to **4j** using 4,4'-Dimethoxybenzil, different aldehydes and ammonium acetate in the presence of glacial acetic acid as a catalyst. It also describes the synthesis of 1,2,4,5-tetraarylimidazole derivatives ranging from **5a** to **5j** using benzil, aromatic aldehyde, a variety of aromatic amine and ammonium acetate in the presence of sulfuric acid as a catalyst under reflux (heating conditions). The reactions in traditional heating conditions were compared with Ultrasonic irradiation and Microwave irradiation reactions as effective techniques for green synthesis, ultrasound and Microwave synthesis are being employed increasingly to accelerate organic reactions. In comparison to traditional methods, ultrasonication and microwaves have better yields, faster reaction times, higher selectivity, and fewer side effects (Scheme C).



The characterizations of synthesized imidazole derivatives compounds were mostly carried out by using melting point, FT-IR, ¹HNMR, ¹³CNMR spectroscopy and mass spectroscopy.

The third part of the work examines the biochemical and biological applications of some newly synthesized compounds. The selected compounds were tested for their *in vitro* anti-urolithiasis activity, antidiabetic activity and antibacterial activity. Additionally, the *in vitro* hemolysis assays of selected compounds were performed for a better understanding of toxicity study.

To investigate the anti-urolithiasis potentials of the tested compounds, *in vitro* anti-urolithiasis inhibitory activities have been screened at various concentrations of 50, 100, 150, 200 and 250 µg/mL and various times (0, 30, 60, 180 and 360 minutes) utilizing cystone as the reference drug. The finding showed that compound **G2_(b)** had the highest inhibiting percentage in the nucleation test, which was 91% at a concentration of 250 µg/mL after 360 minutes of the incubation period compared to the positive drug cystone, which had a percentage of 65%. Compound **G2_(a)**, on the other hand, showed the highest inhibition % in the aggregation test when incubated at 360 minutes and the concentration of 250 µg/mL, which was 69%; which was 24% higher than cystone (46%).

The antidiabetic assay at various concentrations (50, 100, 150, 200 and 250) µg/mL demonstrated moderate to good inhibitory potentials, with percentage values ranging from 48% to 90% against α-amylase and 38% to 61% against α-glucosidase. These results were encouraging. The obtained results were compared to the standard acarbose drug, which had values of 32%-65% for α-amylase and 43%-66% for α-glucosidase. Particularly, compounds **4f**, **4e**, **5b**, and **4b** were reported to be the most active, with percentage inhibition values of 90% 78%, 77% and 75%, respectively against α-amylase and compounds **4f** and **4b**, with percentage inhibition values of 61% and 58% against α-glucosidase at concentration 250 µg/mL.

The tested compounds were also screened for their *in vitro* antibacterial activity against four isolated bacteria two Gram-positive (*Staphylococcus aureus*, *Streptococcus agalactiae*) and two Gram-negative (*Proteus mirabilis* and *Escherichia coli*). The findings of the minimum inhibitory concentrations (MICs) of tested compounds at the concentrations of 100, 200, 300, 400 and 500 µg/mL showed comparable values with the standard antibiotics Azithromycin and Amoxicillin-clavulanic acid most notably **4a**, **4e**, **5b**, and **5c** with a MIC of 200 µg/mL against *Staphylococcus aureus* and **4e** and **5b** with a MIC of 300 µg/mL against *Streptococcus agalactiae*. The results of the antibacterial test by Agar well diffusion method demonstrated that among the screened compounds, **G2_(a)** and **G2_(b)** displayed excellent activity (inhibition zones) against all the bacterial strains at concentrations of their MICs as compared to reference drugs Azithromycin and Amoxicillin-Clavulanic acid.

The results of the hemolysis assay at concentrations of 100, 200, 250, 300, 400, and 500 µg/mL displayed that most screened compounds have a low effect on human red blood cells (less than 5%). Specifically, compounds **G2_(a)**, **G3_(a)**, **G2_(b)**, **G3_(b)** and **5g** were demonstrated to be significantly active with percent hemolysis ranging from (0.718% to 2.654%) compared to the standard Triton X-100, which exhibited a positive control of 97.3%. These findings reveal that some of the screened compounds were found to show potent activity, which could make them a promising drug for treatment.

Table of content

No.	Subject	Page
	Dedication	
	Acknowledgments	
	Summary	I
	Contents	VI
	List of tables	XI
	List of figures	XII
	List of Schemes	XVI
	List of symbols and abbreviations	XVII
Chapter1	Introduction	
1.1	Dendrimers	1
1.1.1	Introduction	1
1.1.2	Properties of dendrimers	2
1.1.2.1	Structure and Shape	2
1.1.2.2	Reactivity	5
1.1.2.3	Solubility	6
1.1.2.4	Viscosity	7
1.1.3	Synthesis of dendrimers	7
1.1.3.1	Divergent approach	7
1.1.3.2	Convergent approach	8
1.1.3.3	Double-stage convergent method	9
1.1.3.4	Hyper monomer method	10
1.1.3.5	Click chemistry method	10
1.1.4	Applications of Dendrimers	11
1.1.4.1	Drug delivery	12
1.1.4.2	Sensors	13
1.1.4.3	Catalyst	14
1.1.4.4	Light Harvesting Material	15
1.1.4.5	Cosmetics	16

1.1.4.6	Process of Water Purification	16
1.2	Imidazoles	17
1.2.1	Introduction	17
1.2.2	Structure and properties	18
1.2.3	Synthesis of Imidazole and its derivatives	20
1.2.3.1	Classical methods for the synthesis of imidazole derivatives	20
1.2.3.1.1	Van Leusen synthesis	20
1.2.3.1.2	Wallach synthesis	21
1.2.3.1.3	Marckwald synthesis	21
1.2.3.1.4	Debus-Radziszewski synthesis	22
1.2.3.2	Modern synthetic route towards poly-functionalized imidazoles	22
1.2.4	Applications of Imidazole	28
1.2.4.1	Natural Products	28
1.2.4.2	Pharmacological activates	28
1.2.4.3	Industrial application	33
1.3	Microwave-Assisted Technique	33
1.3.1	Applications of Microwave irradiation	34
1.4	Ultrasound	35
1.4.1	Ultrasound Irradiation in Organic Chemistry	36
1.4.2	Important of ultrasound	37
	Aims & objectives	38
Chapter2	Experimental part	
2.1	General Description of Chemicals and Equipment	39
2.1.1	chemicals and Solvents	39
2.1.2	Instruments and Equipment	39
2.2	Synthesis of the first line of PAMAM dendrimer	40
2.2.1	General procedure for Synthesis of PAMAM dendrimer with 4 OMe terminal groups $G1_{(a)}$	40
2.2.2	General procedure for Synthesis of PAMAM dendrimer with 4 amine terminal groups $G2_{(a)}$	41

2.2.3	Synthesis of PAMAM dendrimer with 8 OMe terminal groups G3_(a)	42
2.3	Synthesis of the second line of PAMAM dendrimer	43
2.3.1	General procedure for Synthesis of PAMAM dendrimer with four OMe terminal groups G1_(b)	43
2.3.2	General procedure for Synthesis of PAMAM dendrimer with four amine terminal groups G2_(b)	44
2.3.3	Synthesis of PAMAM dendrimer with eight OMe terminal groups G3_(b)	45
2.4	Synthesis of Tri-imidazole derivatives(4a-4j)	46
2.4.1	By using traditional methods	46
2.4.2	By using ultrasound methods	46
2.4.2	By using microwave-assisted methods	47
2.5	Spectral and Physical data of Tri-imidazole derivatives (4a-4j)	47
2.6	Synthesis of Tetra-imidazole derivatives(5a-5j)	53
2.6.1	By using traditional methods	53
2.6.2	By using ultrasound methods	54
2.6.3	By using microwave-assisted methods	54
2.7	Spectral and Physical data of Tetra-imidazole derivatives (5a-5j)	55
Chapter 3	Results and Discussion	
3.1	Synthesis of PAMAM dendrimers	62
3.1.1	Synthesis of 1 st generation PAMAM dendrimers G1_(a) .	64
3.1.2	Synthesis of 2 ^{ed} generation PAMAM dendrimers G2_(a)	65
3.1.3	Synthesis of 3 rd generation PAMAM dendrimers G3_(a)	65
3.1.4	Synthesis of G1_(b) , G2_(b) and G3_(b) PAMAM dendrimer	66
3.2	Purification of the PAMAM dendrimer	68
3.3	Characterization of PAMAM dendrimers G1_(a) , G2_(a) and G3_(a)	70
3.4	Characterization of PAMAM dendrimers G1_(b) , G2_(b) and G3_(b)	81
3.5	SEM and EDX analysis	93
3.6	Multi-component reactions	95
3.7	Synthesis of 2,4,5-triimidazole derivatives by using glacial acetic acid	95

3.8	The proposed mechanism for the synthesis of 2,4,5-triimidazole derivatives	98
3.9	Characterization of 2,4,5-Triarylimidazole derivatives	99
3.10	Synthesis of 1,2,4,5-Tetraimidazole derivatives by using sulfuric acid as catalyst	103
3.11	The proposed mechanism for the synthesis of 1,2,4,5-Tetraimidazole derivatives	106
3.12	Characterization of 1,2,4,5-Tetraimidazole derivatives	107
Chapter 4	Applications	
4.1	Introduction	111
4.2	Literature Review	113
4.2.1	Anti-Urolithiasis Activity	113
4.2.1.1	Mechanisms of Stone Formation	114
4.4.1.1.1	Nucleation of Crystals	115
4.4.1.1.2	Growth of Crystal	116
4.4.1.1.3	Aggregation of Crystals	116
4.2.2	Diabetes Mellitus and Management	116
4.2.2.1	Anti-diabetic Drugs	117
4.2.3	Anti-bacterial Activity of Drugs	118
4.2.4	Hemolysis	119
4.3	Apparatuses and Chemicals	121
4.3.1	Apparatuses	121
4.3.2	Chemicals	122
4.4	Methods	122
4.4.1	Urolithiasis Assay	122
4.4.1.1	Nucleation Assay	122
4.4.1.2	Aggregation Assay	123
4.4.2	Antidiabetic Assay	124
4.4.2.1	Inhibition Activity of α -Amylase	124
4.4.2.2	Inhibition Activity of α -Glucosidase	125
4.4.3	Anti-bacterial Assay	125

4.4.3.1	Minimum Inhibitory Concentrations (MICs) Method	125
4.4.3.2	Agar Well Diffusion Method	126
4.4.4	Hemolytic Assay	127
4.5	Results	128
4.5.1	Urolethiasis Assay for Dendrimer (G2_(a) , G3_(a) , G2_(b) , and G3_(b))	128
4.5.2	Urolethiasis assay for Tri-imidazole derivatives (4a,4b,4e , and 4f)	132
4.5.3	Urolethiasis Assay for Tetra-imidazoles (5a, 5b, 5f , and 5g)	135
4.5.4	Microscopy study on the changes of CaOx crystals in nucleation and aggregation assays	138
4.5.5	Antidiabetic Effect of Dendrimers (G2_(a) , G3_(b) , G2_(a) and G3_(b))	140
4.5.6	Antidiabetic Effect of Tri-imidazole (4a,4b,4e,4f and 4g)	141
4.5.7	Antidaibetic Effect of Tetra-imidazole (5a, 5b, 5f and 5g).	143
4.5.8	Anti-bacterial Activity of Dendrimer (Minimum Inhibitory Concentrations (MICs))	145
4.5.9	Anti-bacterial Activity of Tri-imidazoles (Minimum Inhibitory Concentrations (MICs))	146
4.5.10	Anti-bacterial Activity of Tetra-imidazoles (Minimum Inhibitory Concentrations (MICs))	147
4.5.11	Agar Well Method for Dendrimer	149
4.5.12	Agar Well Method for Tri-imidazoles	149
4.5.13	Agar Well Method of Tetra imidazoles	150
4.5.14	Hemolytic Activity of Dendrimer (G2_(a) , G3_(a) , G2_(b) and G3_(b))	154
4.5.15	Hemolytic Activity of Tri-imidazoles(4a, 4b, 4e and 4f)	155
4.5.16	Hemolytic Activity of Tetra-imidazoles(5a, 5b, 5f , and 5g)	156
4.6	Discussion	157
	Conclusions and future works	
	Conclusions	162
	future works	164
	References	165
	Appendix A	182
	Appendix B	236

List of Tables

No.	Subject	Page
1-1	Commercially available drugs having Imidazole nucleus	31
3-1	The molecular weight of PAMAM dendrimer generations from [G1_(a) to G3_(b)]	92
3-2	Comparison of product yield and reaction time utilizing different conditions in the presence of AcOH as catalysts for the synthesis triimidazoles (4a-4j)	97
3-3	Characteristic absorption bands of FT-IR and ¹ HNMR spectra for (4a-4j)	100
3-4	The calculated molecular mass (g/mol) and observed molecular ion mass (m/z) of the synthesized imidazole 4a-4j .	102
3-5	Comparison of product yield using different conditions in the presence of H ₂ SO ₄ as catalysts for the synthesis tetramidazoles (5a-5j)	105
3-6	Characteristic absorption bands of FT-IR and ¹ HNMR spectra for tetramidazoles.	108
3-7	The calculated molecular mass (g/mol) and observed molecular ion mass (m/z) of the synthesized imidazole 5a-5j .	110
4-1	The apparatuses and equipment used in this study	121
4-2	The chemicals used in this study	122
4-3	The percentage inhibition of the enzymes α -amylase and α -glucosidase by compounds G2_(a) , G3_(a) , G2_(b) , and G3_(b) at different concentrations	142
4-4	The percentage inhibition of the enzymes α -amylase and α -glucosidase by compounds 4a , 4b , 4e , 4f , and 4g at different concentrations	143
4-5	The percentage inhibition of the enzymes α -amylase and α -glucosidase by compounds 5a , 5b , 5f , and 5g at different concentrations	145
4-6	MICs test results of Dendrimer (G2_(a) , G3_(a) , G2_(b) , and G3_(b)) against selected Gram-positive and Gram-negative bacteria using resazurin dilution in broth assays at concentrations (100-500 μ g/ mL).	148
4-7	MICs test results of triimidazoles (4a,4b,4e,4f and 4g)	149
4-8	MICs test results of teramidazoles (5a,5b,5c,5e and 5f)	150
4-9	Antibacterial activities of all tested compounds	154
4-10	Hemolytic activity of all tested compounds	161

List of Figures

No.	Subject	Page
1-1	Three main classes of conventional synthetic polymers	3
1-2	Four sub-classes of dendritic polymers	4
1-3	Basic of dendrimer structure	4
1-4	Different types of dendrimers	5
1-5	Synthesis of dendrimer-templated Pt-Cu nanoparticles	6
1-6	The schematic illustration of dendrimer divergent synthesis	8
1-7	The schematic representation of the convergent synthesis of dendrimers	9
1-8	The schematic demonstrates the synthesis of dendrimers by both divergent and convergent methods.	9
1-9	The schematic representation of the hyper monomer method	10
1-10	Dendrimer Diels-Alder reaction	11
1-11	Schematic representation of Various applications of dendrimers	12
1-12	Preparation of biosensor made Au/AuNP/ (FeSH+Cyst) / PAMAM/	14
1-13	Dendrimer used as light-harvesting material	15
1-14	Structural formula of azole ring (including nitrogen only)	17
1-15	Structure of imidazole	18
1-16	Hydrogen bonding in imidazole ring	18
1-17	Tautomeric forms of imidazole structure	19
1-18	Resonating Structures of the imidazole moiety	19
1-19	Imidazole as pseudo acidic Properties and generates acids with Crystalline Salts	19
1-20	Traditional Method for Imidazole derivatives synthesis	20
1-21	chemical structure of histamine	28
1-22	<i>in vitro</i> anti-tubercular activity	29
1-23	<i>in vitro</i> antifungal activity	29
1-24	<i>in vitro</i> anti-inflammatory effects	30
1-25	<i>in vitro</i> antibacterial activities	30
1-26	<i>in vitro</i> α -glucosidase activity	30
1-27	<i>in vitro</i> analgesic activity	31
1-28	A variety of microwave-assisted synthesis types	34
1-29	Frequency variations of sound	35

3-1	FT-IR of G1 _(a)	71
3-2	FT-IR of G2 _(a)	71
3-3	FT-IR of G3 _(a)	72
3-4	¹ HNMR of G1 _(a) (DMSO-d ₆ , 500MHz)	73
3-5	¹ HNMR Zoomed of G1 _(a) (DMSO-d ₆ , 500MHz)	73
3-6	¹ HNMR of G2 _(a) (D ₂ O, 400MHz)	74
3-7	¹ HNMR Zoomed of G2 _(a) (D ₂ O, 400MHz)	74
3-8	¹ HNMR of G3 _(a) (DMSO-d ₆ , 400MHz)	75
3-9	¹³ CNMR of G1 _(a) (DMSO-d ₆ , 125MHz)	76
3-10	¹³ CNMR of G2 _(a) (D ₂ O, 100MHz)	76
3-11	¹³ CNMR of G3 _(a) (DMSO-d ₆ , 100MHz)	77
3-12	Mass spectrum of G1 _(a)	78
3-13	Mass spectrum of G2 _(a)	79
3-14	Mass spectrum of G3 _(a)	80
3-15	FT-IR of G1 _(b)	81
3-16	FT-IR of G2 _(b)	82
3-17	FT-IR of G3 _(b)	82
3-18	¹ HNMR of G1 _(b) (DMSO-d ₆ , 400MHz)	83
3-19	¹ HNMR Zoomed of G1 _(b) (DMSO-d ₆ , 400MHz)	84
3-20	¹ HNMR of G2 _(b) (DMSO-d ₆ , 400MHz)	85
3-21	¹ HNMR Zoomed of G2 _(b) (DMSO-d ₆ , 400MHz)	85
3-22	¹ HNMR of G3 _(b) dendrimer (DMSO-d ₆ , 400MHz)	86
3-23	¹³ CNMR of G1 _(b) dendrimer (DMSO-d ₆ , 100MHz)	87
3-24	¹³ C NMR of G2 _(b) dendrimer (DMSO-d ₆ , 100MHz)	87
3-25	¹³ C NMR of G3 _(b) dendrimer (DMSO-d ₆ , 100MHz)	88
3-26	Mass spectrum of G1 _(b)	89
3-27	Mass spectrum of G2 _(b)	90
3-28	Mass spectrum of G3 _(b)	91
3-29	SEM images of synthesized (a) G1 _(a) , (b) G2 _(a) and (c) G3 _(a)	93
3-30	EDX spectrum of synthesized G1 _(a)	94

3-31	EDX spectrum of synthesized G2 _(a)	94
3-31	EDX spectrum of synthesized G3 _(a)	94
4-1	Schematic diagram that indicates the application of dendrimers in various biomedical fields	111
4-2	Different pharmacological activities of imidazole derivatives	113
4-3	Schematic of the calcium oxalate kidney stone formation	115
4-4	Effect of the G2 _(a) , G3 _(a) , G2 _(b) , and G3 _(b) compounds and cystone (a) at 50 µg/mL (b) at 100 µg/mL (c) at 150 µg/mL (d) at 200 µg/mL (e) at 250 µg/mL on nucleation of calcium oxalate crystallization * <i>p</i> -value ≤ 0.05 vs. cystone, ** <i>p</i> -value ≤ 0.001 vs. cystone	130
4-5	Effect of the G2 _(a) , G3 _(a) , G2 _(b) , and G3 _(b) compounds and cystone (a) at 50 µg/mL (b) at 100 µg/mL (c) at 150 µg/mL (d) at 200 µg/mL (e) at 250 µg/mL on aggregation of calcium oxalate crystallization * <i>p</i> -value ≤ 0.05 vs. cystone, ** <i>p</i> -value ≤ 0.001 vs. cystone	131
4-6	Effect of the 4a, 4b, 4e, and 4f compounds and cystone (a) at 50 µg/ml (b) at 100 µg/mL (c) at 150 µg/mL (d) at 200 µg/mL (e) at 250 µg/mL on nucleation of calcium oxalate crystallization * <i>p</i> -value ≤ 0.05 vs. cystone, ** <i>p</i> -value ≤ 0.001 vs. cystone	133
4-7	Effect of the 4a, 4b, 4e, and 4f compounds and cystone (a) at 50 µg/mL (b) at 100 µg/mL (c) at 150 µg/mL (d) at 200 µg/mL (e) at 250 µg/mL on aggregation of calcium oxalate crystallization * <i>p</i> -value ≤ 0.05 vs. cystone, ** <i>p</i> -value ≤ 0.001 vs. cystone	134
4-8	Effect of the 5a, 5b, 5f, and 5g compounds and cystone (a) at 50 µg/mL (b) at 100 µg/mL (c) at 150 µg/mL (d) at 200 µg/ml, (e) at 250 µg/mL on nucleation of calcium oxalate crystallization * <i>P</i> -value ≤ 0.05 vs. cystone, ** <i>P</i> -value ≤ 0.001 vs. cystone	136
4-9	Effect of the 5a, 5b, 5f, and 5g compounds and cystone (a) at 50 µg/mL (b) at 100 µg/mL (c) at 150 µg/mL (d) at 200 µg/mL (e) at 250 µg/mL on the aggregation of calcium oxalate crystallization * <i>p</i> -value ≤ 0.05 vs. cystone, ** <i>p</i> -value ≤ 0.001 vs. cystone	137
4-10	Light microscopic image of nucleation inhibition activity (40X) magnification (a) negative control (no treatment) (b) positive control (cystone) (250 mg/mL) (c) compound G2 _(b) (250 µg/mL)	139
4-11	Light microscopic image of aggregation inhibition activity (40X) magnification (a) negative control (no treatment) (b) positive control (cystone) (250 mg/mL) (c) compound G2 _(a) (250 µg/mL)	139
4-12	<i>In vitro</i> antidiabetic activity (a) α-amylase inhibition (b) α-glucosidase inhibition by dendrimers G2 _(a) , G3 _(a) , G2 _(b) and G3 _(b)	142

4-13	<i>In vitro</i> antidiabetic activity (a) α -amylase inhibition (b) α -glucosidase inhibition by triimidazole 4a,4b,4e,4f, and 4g	144
4-14	<i>In vitro</i> antidiabetic activity (a) α -amylase inhibition (b) α -glucosidase inhibition by tetraimidazole 5a, 5b, 5f, and 5g	146
4-15	A schematic representation the (MICs) of the 96-well resazurin broth microdilution model (A) for G2 _(a) and G3 _(a) (B) for G2 _(b) and G3 _(b) (C) for 4a and 4b (D) for 4e and 4f (E) for 5a and 5b (F) for 5c and 5e (G) for 5f and 4g and (H) for AZI and AMC against <i>Staphylococcus aureus</i> , <i>Streptococcus agalactiae</i> , <i>Proteus mirabilis</i> , and <i>E. coli</i> , observation: The pink color shows that organisms are active, whereas the blue color shows that growth has been inhibited	151
4-16	The antibacterial activity of G2 _(a) , G3 _(a) , G2 _(b) and G3 _(b) (A) and (B) against Gram-positive bacteria (<i>Staphylococcus aureus</i> and <i>Streptococcus agalactiae</i>) (C) and (D) against Gram-negative bacteria (<i>Proteus mirabilis</i> and <i>E. coli</i>), Negative control represents solvent, (Azithromycin and Amoxicillin-Clavulanic acid) represents positive control	155
4-17	The antibacterial activity of 4a,4b,4e,4f,4g 5a,5b,5c,5e and 5f (E) and (F) against Gram-positive bacteria (<i>Staphylococcus aureus</i> and <i>Streptococcus agalactiae</i>) (G) and (H) against Gram-bacteria (<i>Proteus mirabilis</i> and <i>E. coli</i>), Negative control represents solvent, (Azithromycin and Amoxicillin-Clavulanic acid) represents positive control	156
4-18	Hemolytic activities of G2 _(a) , G3 _(a) , G2 _(b) and G3 _(b) at the concentrations of 100, 200, 250, 300, 400, and 500 μ g/mL	158
4-19	Hemolytic activities of 4a,4b,4e, and 4f at the concentrations of 100, 200, 250, 300, 400 and 500 μ g/mL	159
4-20	Hemolytic activities of 5a, 5b, 5f, and 5g at the concentrations of 100, 200, 250, 300, 400 and 500 μ g/mL	160

List of Schemes

No.	Subject	Page
1-1	Synthesis of “cascade molecules by Vögtle et al	2
1-2	Van Leusen synthesis	21
1-3	Wallach synthesis	21
1-4	Marckwald synthesis	21
1-5	Debus-Radziszewski synthesis	22
1-6	Synthesis of bis(1-methyl-4,5-diphenylimidaz-2-oyl) carbinol derivatives	22
1-7	The Boland method for synthesizing enantiopure imidazole derivatives	23
1-8	Puratchikody and Doble method	24
1-9	Synthesis of imidazole derivatives using an ionic liquid catalyst under ultrasound conditions	24
1-10	Imidazole synthesis with [Hmim]NO ₃ assistance	25
1-11	Glycerol-based imidazole derivative synthesis	25
1-12	The synthesis of poly-functionalized imidazoles has been catalyzed by glacial acetic acid	26
1-13	Synthesis of imidazole derivatives from diphenyl acetylene under Pd-catalyzed	26
1-14	synthesis Imidazole derivatives driven under visible LED light	27
1-15	Synthesis of imidazoles via cyclo-addition reactions	27
3-1	Michael addition mechanism	63
3-2	The mechanism of the amidation reaction step	63
3-3	Synthesis of G1 _(a)	64
3-4	Synthesis of G2 _(a)	65
3-5	Synthesis of G3 _(a)	66
3-6	The synthesis of PAMAM dendrimers G1 _(b) to G3 _(b) with each Michael addition and amidation step	68
3-7	Side -reactions in PAMAM dendrimer synthesis, (A) Incomplete Michael reaction (B) Intermolecular cyclization (C) Dimer formation (D) retro-Michael reaction	70
3-8	Synthesis of 2,4,5-Tri-imidazoles under reflux condition	95
3-9	Synthesis of 2,4,5-Tri-imidazoles under ultrasonic and microwave conditions	96

3-10	Proposed mechanism for the formation of 2,4,5-trisubstituted imidazoles from 1,2-diketone, aldehyde and NH ₄ OAc in the presence of glacial acetic acid	99
3-11	Synthesis of 1,2,4,5-Tetra-imidazoles under reflux condition	103
3-12	Synthesis of 1,2,4,5-Tetra-imidazoles under ultrasonic and microwave conditions	104
3-13	Proposed mechanism for the formation of 1,2,4,5-Tetrasubstituted imidazoles from benzil, aldehyde, amines, and NH ₄ OAc in the presence of H ₂ SO ₄	107

List of symbols and abbreviations

Symbol	Definition
¹³ C-NMR	Carbon Nuclear Magnetic Resonance Spectroscopy
¹ H-NMR	Proton Nuclear Magnetic Resonance Spectroscopy
Abs	Absolute
AcOH	Acetic acid
br	broad
d	doublet
D ₂ O	Deuterated Deuterium Oxide
dd	doublet of doublets
DMSO-d ₆	Deuterated Dimethyl Sulphoxide.
EC ₅₀	Half maximal effective concentration
<i>ELISA</i>	Enzyme-linked immuno-sorbent assay
ESI-MS	Electrospray Mass Spectrometry
EtOH	Ethanol
FT-IR	Fourier Transform Infrared Spectrophotometry.
G	Generation
IC ₅₀	Half maximal inhibitory concentration
<i>J</i>	Coupling constant
m	multiplet
m.p	Melting points
m/z	Mass/charge

M^+	Molecular ion
MeOH	Methanol
MHz	Mega Hertz
MICs	Minimum Inhibitory Concentrations
[Himm]NO ₃	(1-Methyl-3H-imidazolium nitrate)
mmol	millimole
MRCs	Multi-component reactions
MW	Microwave
NH ₄ OAc	Ammonium acetate
O. D	Optical density
PAMAM	Polyamido amine
PDA	Propane 1,3- diamine
ppm	part per million
q	quartet
R_f	Retention factor
rt	Room Temperature
s	singlet
t	triplet
TLC	Thin Layer Chromatography
US	ultrasound
δ	chemical shift in NMR
TsOH	p-Toluenesulfonic acid

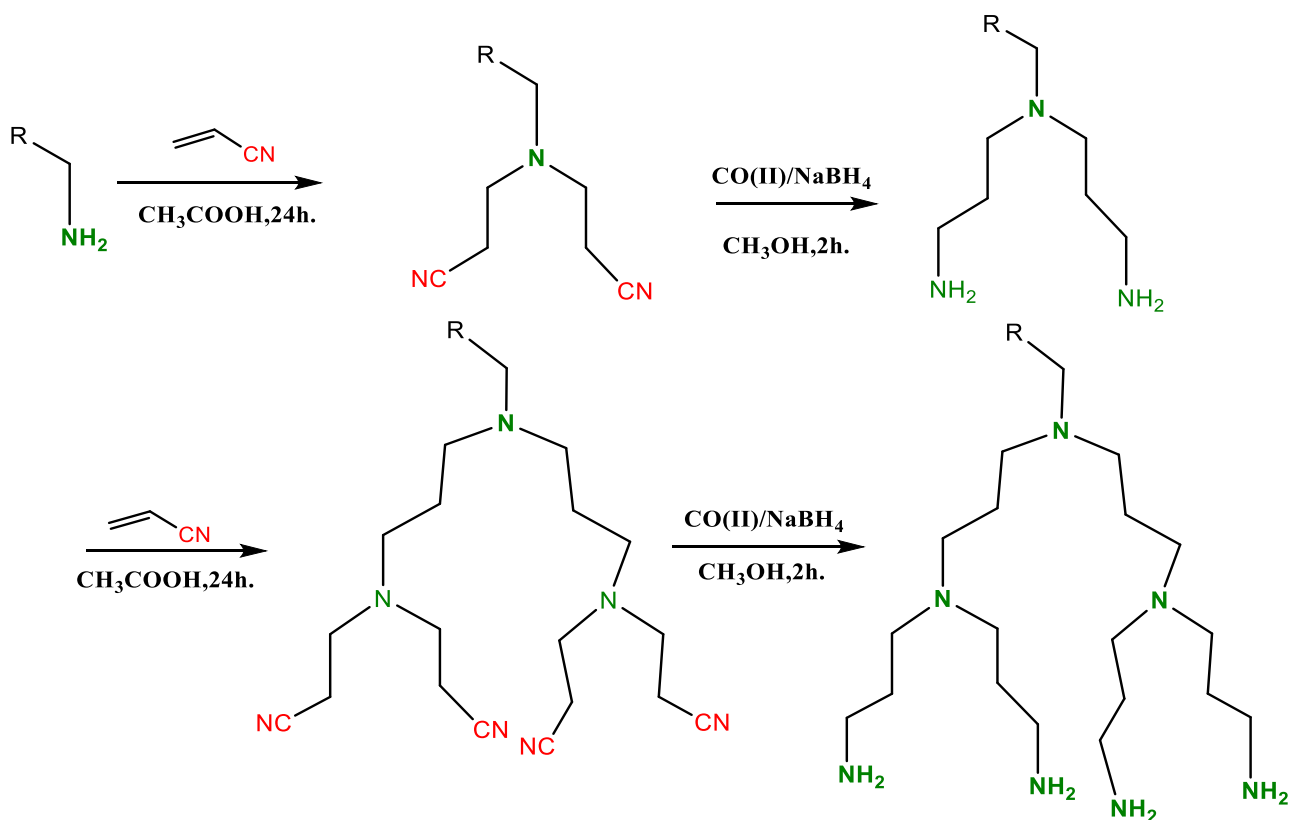
CHAPTER ONE

INTRODUCTION

1.1 Dendrimers

1.1.1 Introduction

Dendrimers are a new class of synthetic macromolecules with well-defined, homogeneous structures that are globular, monodispersed, radially symmetric, and highly branched [1-4]. The term "dendrimer" arises from the Greek words "dendron," that means "tree," and "meros," that means "part." The majority of developments in polymer synthesis and macromolecule design of biodegradable polymers happened in the twentieth century [5]. These advances in this field led to the production of dendrimers, prepared by numerous research groups. At the beginning of the 1940s., Flory offered his first theoretical suggestion for a highly branched macromolecule with a three-dimensional structure [6]. A highly branching macromolecule having a three-dimensional structure was first proposed theoretically by Flory in the 1940s. After Flory, Vogtle described the first dendrimer to be synthesized as a branching polypropylene-amine (PPI) and referred to the molecule as a "cascade polymer as shown in Scheme (1-1). Tomalia and co-workers synthesized polyamidoamine (PAMAM) between 1983 and 1985; Tomalia who generated the term "dendrimers" at the same time, Newkome created the term "arborols" means, in Latin 'trees'. Additionally, in 1984, Tomalia presented the development of dendrimers at the first International Polymer Conference[7]. This study described dendrimer preparation and the preparation of starburst molecules using the divergent method that arrived immediately after. Tomalia has suggested the application of a dendritic polymer as the dendritic box to encapsulate hydrophobic compounds. In 1990, Frechet and Hawker documented how to synthesize dendrimers using the convergent method.



Scheme 1-1 Synthesis of "cascade molecules"

1.1.2 Properties of Dendrimers

1.1.2.1 Structure and Shape

The word "macromolecule" was first used by Hermann Staudinger to describe polymeric materials with long chains or repeating units connected by covalent bonds through a process called polymerization. Staudinger published a paper on the macromolecular hypothesis in 1922, and for this work, he was awarded the Nobel Prize in 1953[8]. The development of drug delivery systems has been significantly assisted by polymers, which can control the release of therapeutic compounds to give a constant dose over long periods. There are four different macromolecular architectures for polymeric molecules, and three of them fall under the traditional synthetic polymer class, including cross-linked, branched, and linear polymers as represented in Figure (1-1).

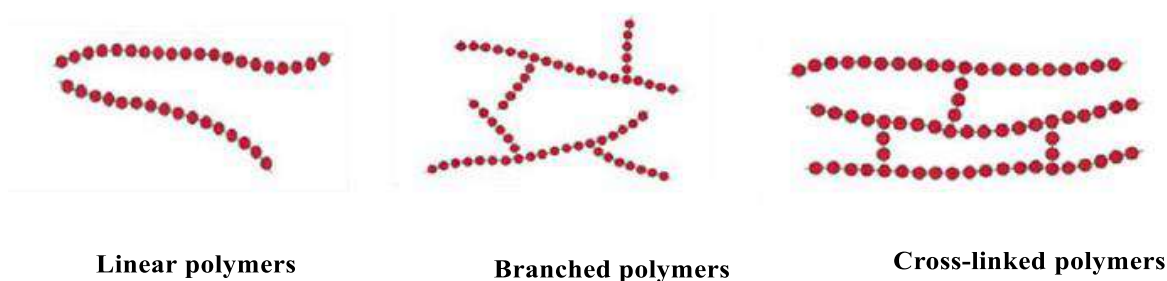


Figure 1-1 Three main classes of conventional synthetic polymers: a) linear polymers, b) branched polymers, and c) cross-linked polymers

Dendritic are the fourth class [9]. Different dendritic have been employed in formulations with controlled release and drugs targeting systems. These molecules are classified into four types: random hyper-branched polymers, dendrigrafts, dendrons, and dendrimers, (Fig. 1-2).

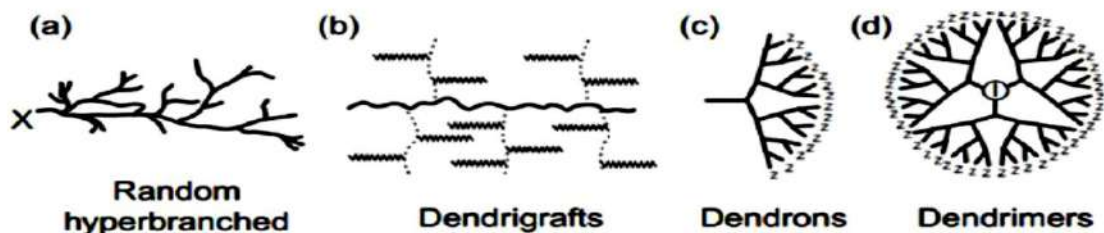


Figure 1-2 Four sub-classes of dendritic polymers: (a) random hyper-branched polymers, (b) dendrigrafts, (c) dendrons, and (d) dendrimers

Typically, dendrimer moiety consists of three different architectural regions: as seen in Figure (1-3): (i) central atom or core; (ii) branches (a layer inside the core composed of repeated units) and (iii) terminal groups linked to the branches (also called surface groups or free functional groups) [10].

Fragments of the dendrimer that are similar are referred to as "dendrons." Each layer of the dendrimer is called a generation. The first generation is produced by combining repeat units and a core (as a single layer). The second generation consists of two layers, and the third generation is composed of three layers of repeated units [11]. In contrast to linear polymers, dendrimers have a known regular shape and size. They are nondispersive macromolecules that were polymerized during synthesis using a specific method and good control.

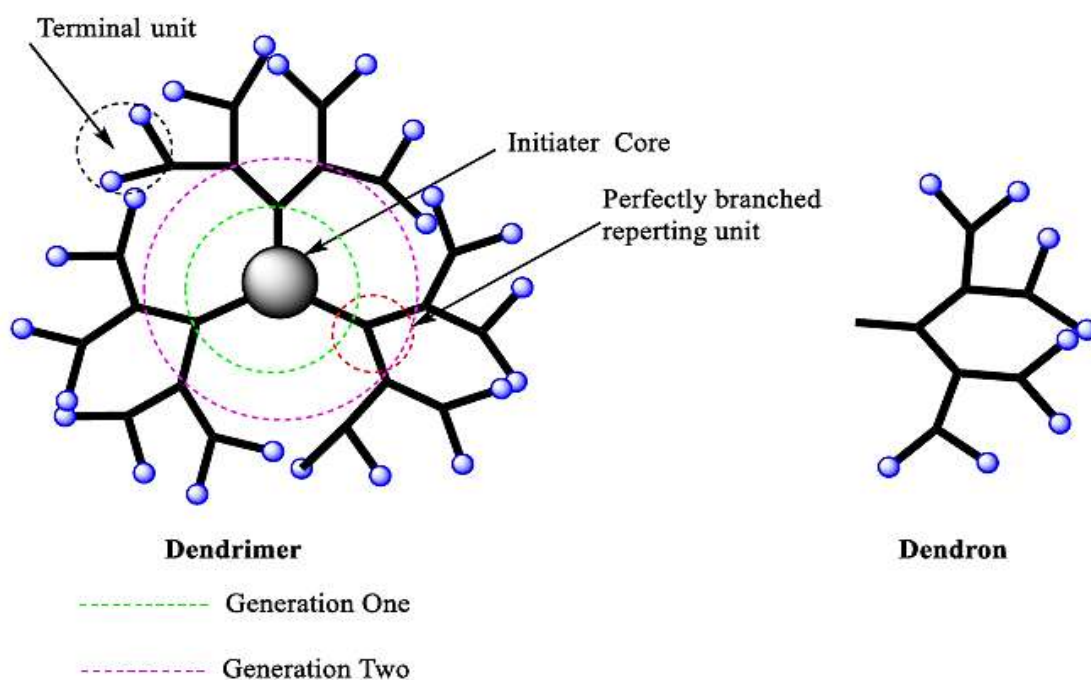


Figure 1-3 Basic of dendrimer structure

Dendrimers can be divided based on their branching units, shape, generation number, and preparation methods [12], (Fig. 1-4) illustrates how dendrimers are classified.

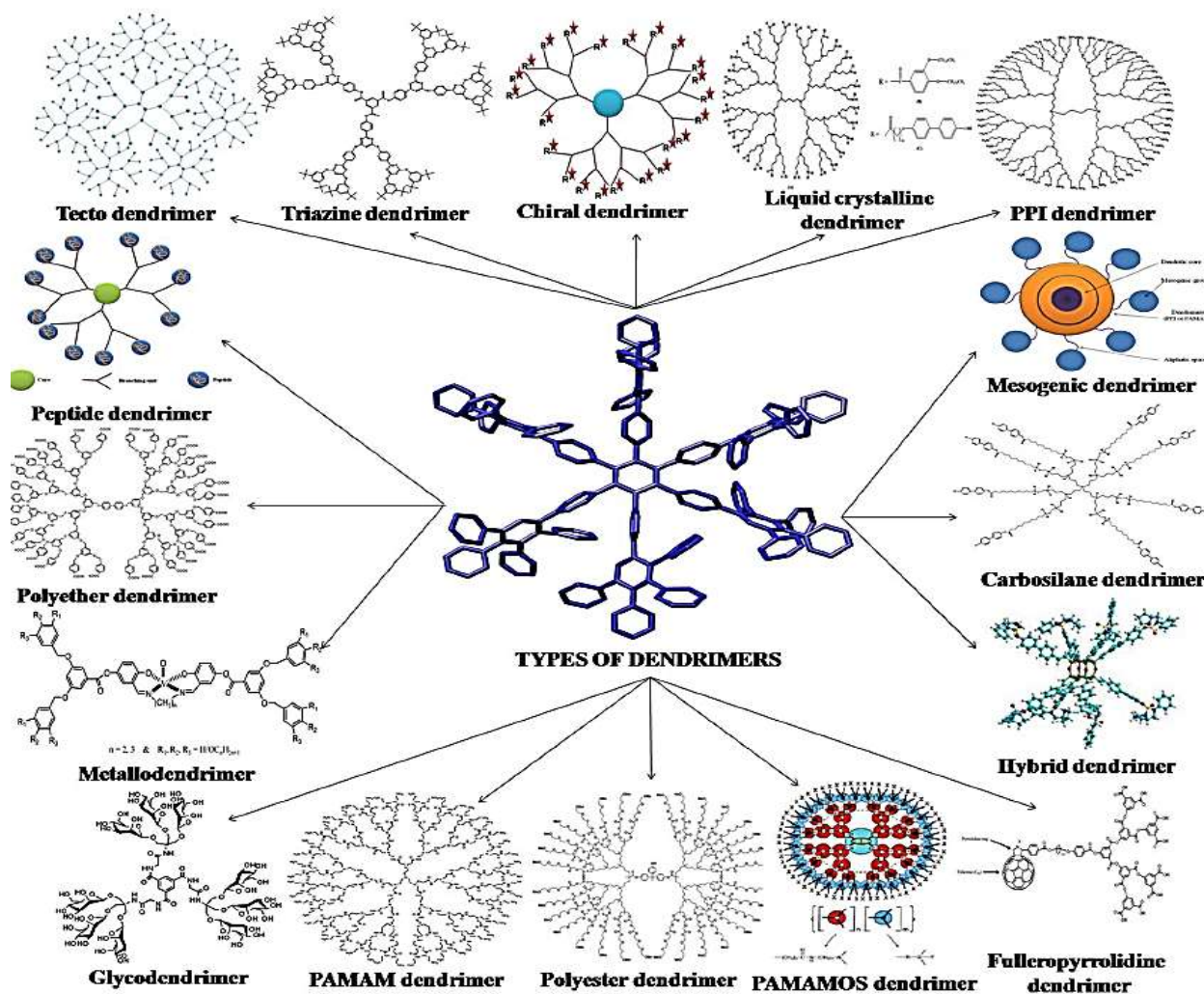


Figure 1-4 Different types of dendrimers

1.1.2.2 Reactivity

The functional groups play an important role in how dendrimers interact with their environment. The management of polymer architecture and the development of molecular interactions, such as hydrogen bonding, have helped improve the interfaces between different types of polymers as well as the interfaces with polymers and other surfaces. Synthetic dendrimers with a three-dimensional structure have been produced to enclose reactive sites and provide highly regulated surfaces and interfaces. Hoover and colleagues show how PAMAM dendrimers may be employed as a template to

generate bimetallic Pt-Cu nanoparticles in a solution that has controlled metal stoichiometries, (Fig. 1-5).

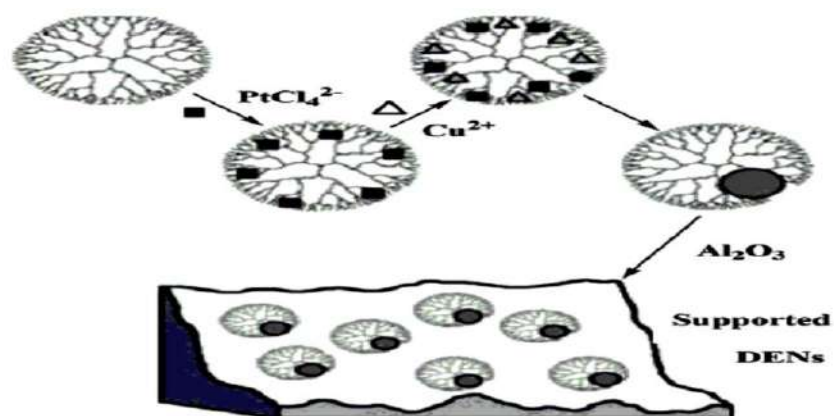


Figure1-5 Synthesis of dendrimer-templated Pt-Cu nanoparticles

By depositing nanoparticles over a high surface-area oxide support and removing dendrimers thermally, active supported bimetallic nanoparticle catalysts may be created. Infrared spectroscopy of adsorbed CO indicates the surface dilution of Pt in Cu and only weakly suggests electronic transfer from Cu to Pt. It is significant to note that the activity of the resultant catalysts is directly influenced by stoichiometry which is used in the original solution syntheses of the nanoparticles. This opens up new possibilities for researching the impact of particle composition on various catalytic processes and catalytic reactions [13].

1.1.2.3 Solubility

Solubility plays a vital role in achieving the objective in a variety of dendrimer applications. The type of functional groups that are present on the dendrimer surfaces determine this property. By replacing the end groups of the dendrimer with suitable functional groups, solubility can be improved. It is possible to achieve the desired solubility in some solvents in the presence of a large number of modified functional groups on the surfaces. These depend on the replacement groups that are used for this.

The presence of several functional groups can enhance the reactivity and binding. Dendrimers have been developed as a suitable molecule to encapsulate hydrophobic pharmaceuticals due to their globular structure and internal cavities, particularly higher generations[14].

1.1.2.4 Viscosity

Solutions of dendrimers are significantly less viscous than those of linear polymers. The degree of branching and molecular weight has a significant effect on the viscosity of dendrimers. The intrinsic viscosity of dendrimers in solution, however, exhibits several anomalous behaviors that, up until this point, have not been properly explained by the available theoretical frameworks. The intrinsic viscosity of conventional polymers rises steadily with molecular mass. It has been discovered that the intrinsic viscosity of polyether dendrimers rises to the fourth generation before decreasing linear polymers don't show this behavior[15].

1.1.3 Synthesis of Dendrimers

The main methods for synthesizing dendritic macromolecules are as follows:

1.1.3.1 Divergent Method

In 1983, Tomalin pioneered the divergent approach as the first method for synthesizing dendrimers. This method involves building the dendrimer generation layer by layer, starting with a central core molecule and progressing outward to the periphery as shown in Figure 1-6. To produce the first generation of the dendrimer, a multifunctional core molecule reacts with monomers containing one reactive and two inactive groups. Then, a reactive group on the periphery reacts with another monomer unit to produce second generation dendrimers. These two steps can be repeated multiple times to form different generations of dendrimers, with the molecular weight doubling after each generation.

This method allows for a higher yield of dendrimers and has become the commercial scale for their synthesis. However, there are some disadvantages to this approach, such as side reactions, ester hydrolysis, and incomplete reactions, which can lead to defects in the dendrimer structure. To avoid these defects, an excess amount of reagent is used to complete both reaction steps [16-18].

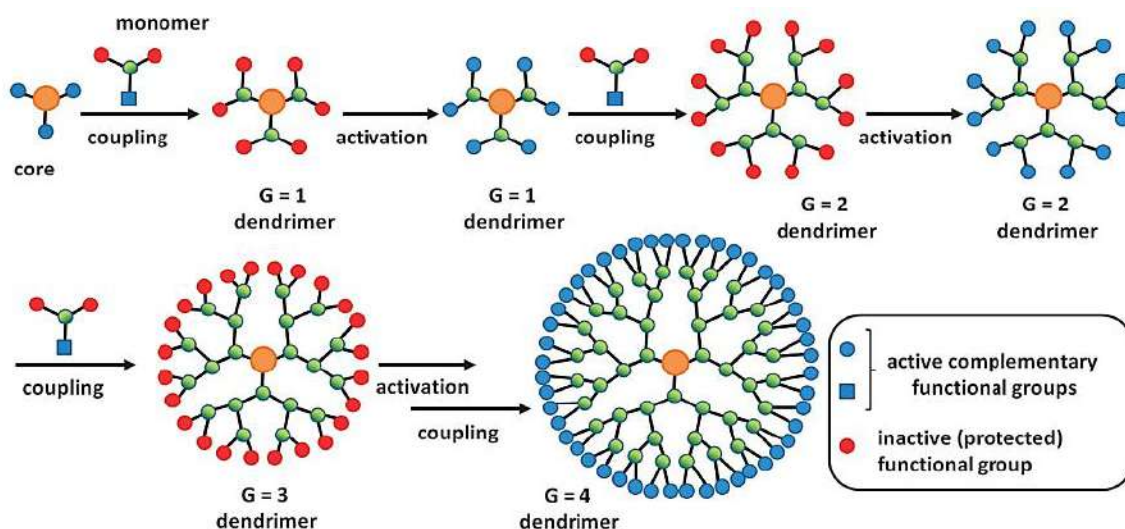


Figure 1- 6 The schematic illustration of dendrimer divergent synthesis

1.1.3.2 Convergent Method

Fréchet et al. developed the convergent method as an alternative method for synthesizing dendrimers in 1990. The synthesis of the dendrimer by using this method starts from the outside part (periphery) and progresses to the inside (core unit). The synthesis involves combining multiple surface molecules to produce large surface molecules (dendrons), which then connect to multifunctional core molecules as shown in Figure 1-7. Unlike the divergent method, the convergent method requires an equal amount of molar concentration to complete the synthesis without an excessive number of branching units. This approach offers better control over the synthesis process, resulting in fewer flaws and an easier purification process. However, this technique

also has a disadvantage, such as steric hindrance on the external surfaces that can hinder the production of high-generation dendrimers[19-21].

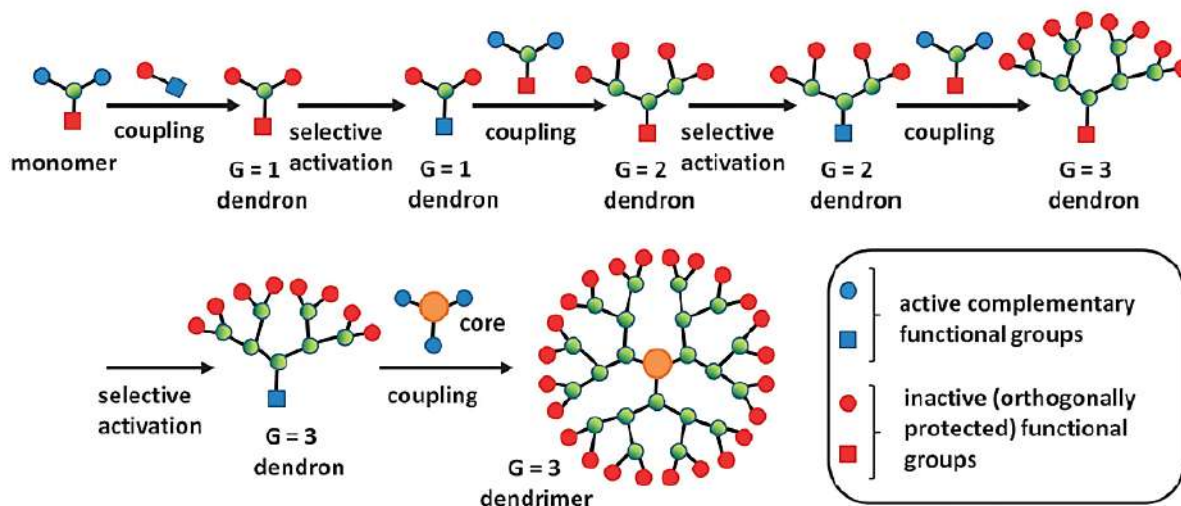


Figure 1-7 The schematic representation of the convergent synthesis of dendrimers

1.1.3.3 Double-stage Convergent Method

A double-stage convergent method, in which the synthesis of building blocks is performed using the divergent approach followed by the convergent dendrimer assembly, may be used in circumstances needing a more complex structure. Figure (1-8) displays a schematic illustration of the divergent route.

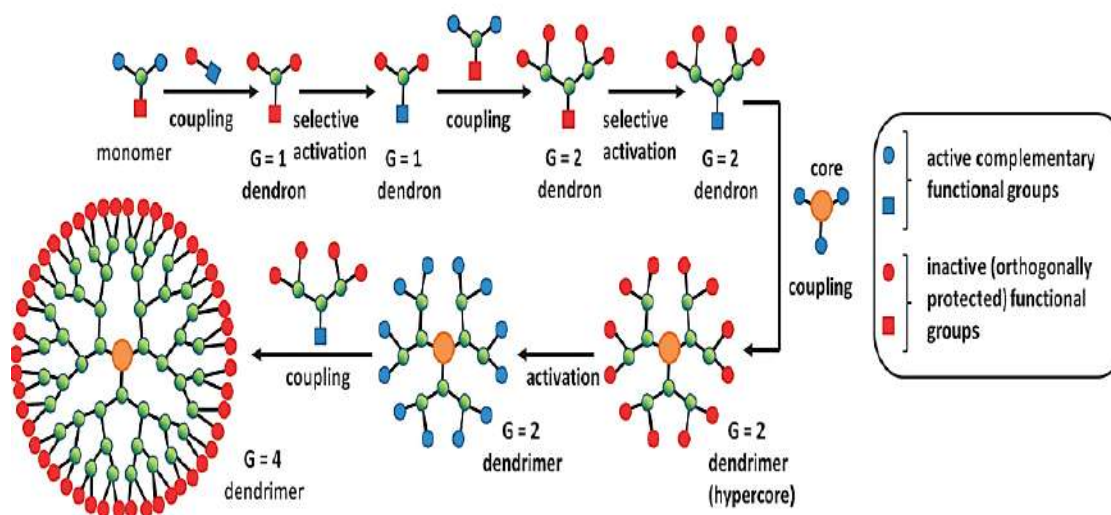


Figure 1-8 The schematic demonstrates the synthesis of dendrimers by both divergent and convergent methods

The figure demonstrates that the initial step involves synthesizing a low-generation multifunctional dendrimer that has external coupling sites. The second step involves synthesizing a small dendron that has an active functional group at the focal point. These two molecules are coupled together in the reaction that results from the convergent route[22,23].

1.1.3.4 Hypermonomer Method

This method utilizes hypermonomeric synthetic building blocks to form 14 branching, which enables the number of terminal groups to increase rapidly. The figure illustrates the reaction between the active coupling groups of the core molecule and the four AB_4 branching units that have an active functional group at their focal point [24], (Fig. 1-9).

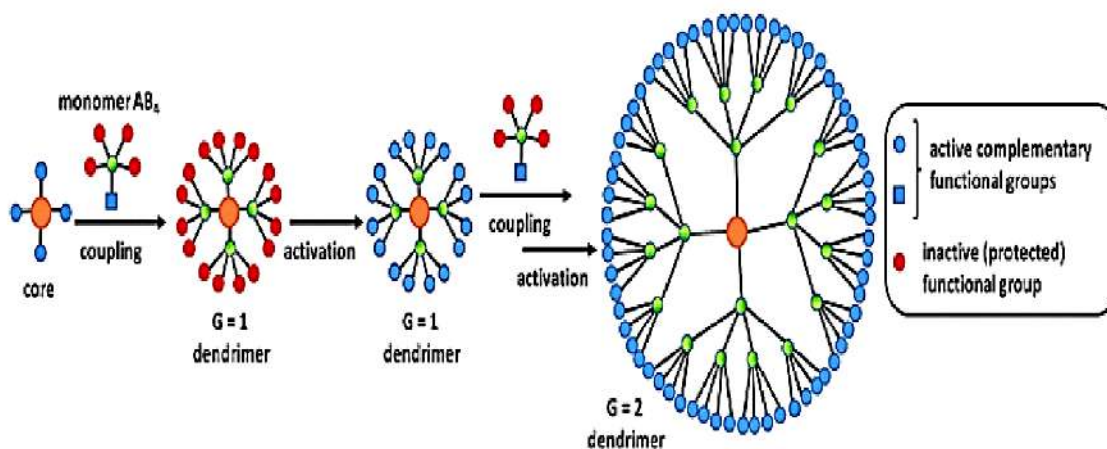


Figure 1-9 The schematic representation of the hyper monomer method

1.1.3.5 Click Chemistry Method

K. Barry Sharpless first fully outlined the principles of click chemistry in 2001. In this approach, smaller units are joined by heteroatom bonds C-X-C, where X is heteroatom [25]. High chemical yields, commercially available starting compounds, readily removed or inoffensive byproducts, simple product isolation and purification, and stereospecificity are the characteristics of the "click reaction".

Diels-Alder reactions, thiol-yne reactions, and azide-alkyne reactions are the three types of reactions used in click chemistry to synthesize dendrimers [26], (Fig. 1-10).

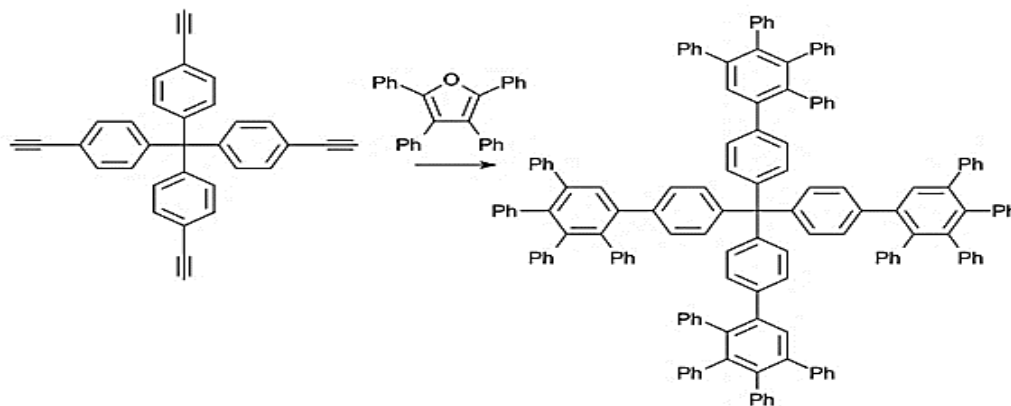


Figure 1-10 Dendrimer Diels-Alder reaction

1.1.4 Applications of Dendrimers

Dendrimers are a good candidate for a wide range of prospective applications because of their unique structural characteristics such as high branching spheroidal surface, nanoscopic scale, cavernous core, and unique features including higher solubility, higher reactivity and low viscosity. Dendritic macromolecules are playing an important role in anticancer medicines, diagnostic imaging, and nanoscale delivery systems. Chemical sensors and gene therapy and drug delivery systems are examples of combined medicinal and diagnostic applications. Furthermore, these particular groups of materials have uses in coatings and adhesives, light harvesting materials, catalysts, separating agents, electrical applications, and a variety of other fields. The illustration of numerous dendrimer applications is presented in Figure (1-11).

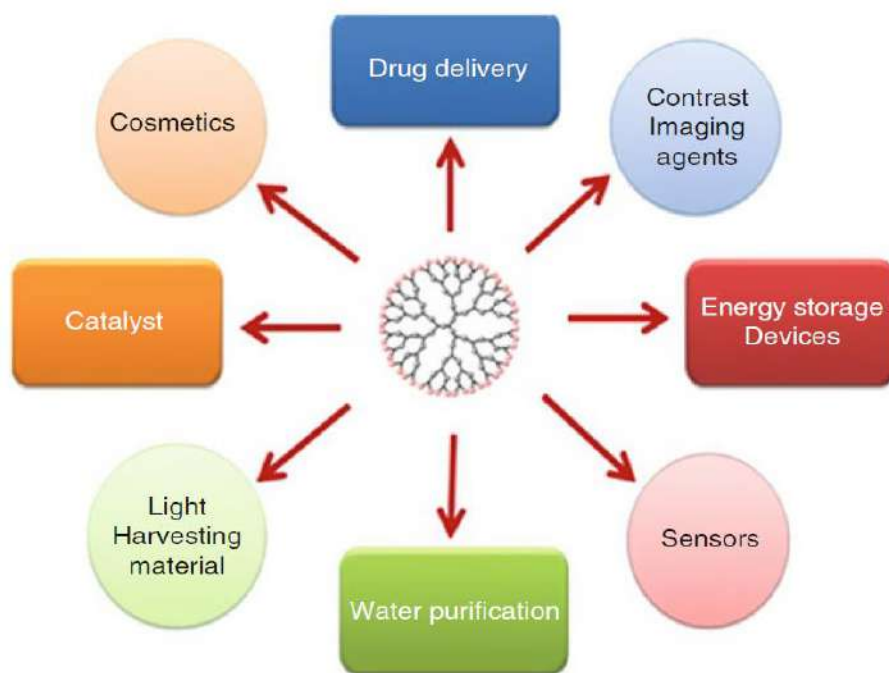


Figure 1-11 Schematic representation of various applications of dendrimers

- Some of the applications of Dendrimers are discussed below:

1.1.4 .1 Drug delivery

Szoka and Haesler [27] showed the gene transfection use of PAMAM dendrimers. Attaching DNA and organic molecules to dendrimers and directing them to the cell nucleus is possible. Dendrimers are useful as agents for the targeted delivery of drugs to a specific location of an organism, organ, or cell due to their multi-functionality. Their applications in medicinal and pharmaceutical chemistry are especially appealing due to the existence of interior holes for the storage of drugs and outside functional groups for drug molecule binding. Drug molecules can be linked to a dendrimer through its end groups or stored in its interior cavities. Existing agents for the transport of medicine molecules are unsatisfactory, thus scientists are searching for alternatives. There is still a need for innovative transport systems with a high affinity for the human body, affinity for many types of pharmacological molecules, and cell membrane

penetration. In addition to facilitating drug transfer, dendrimers assist in overcoming obstacles such as limited bioavailability, insolubility, toxicity, and drug breakdown under biological circumstances. PAMAM dendrimers have thus far been studied for oral, ophthalmic, and pulmonary drug delivery. In addition to these qualities, dendrimers can be utilized to improve the solubility of dosage forms. Because of the hydrophilic perimeter and exterior, poorly soluble drugs can be dissolved by encapsulating them in dendritic polymers [28].

1.1.4 .2 Sensors

Special attention has been paid to the development of dendrimer-based sensors because they have many important properties that can improve the performance of optical sensors. Dendrimers possess potential utility in sensor applications when they exhibit reactivity towards the analyte, leading to consequential interactions including absorption, reflectance, lifetime, luminescence, scattering, refractive index, diffraction, and polarization, changes in a quantifiable way. Several studies [29] have shown that dendrimers can be used to make electrochemical biosensors for analytical purposes. These biosensors can be used to detect analytes like, ascorbic acid, uric acid, phenols, dopamine, glucose, and hydrogen peroxide. Despite undergoing several iterations of regeneration for deoxyribonucleic acid hybridization and antigen-antibody tests, dendrimer-modified sensor surfaces have shown to be very stable. These matrices are stable in stripping using urea [30] glycine-HCl stripping [31] heating stripping [32] and alkaline stripping [33]. The high degree of stability of the dendrimer film is due to the fact that each bioreceptor molecule is affixed to the sensor substrates by forming multiple interactions with multiple functional groups and the affinity regions can hold more. Polyvalent interactions, like surface coatings, adhesives, or polymer crosslinking can be used to keep dendrimers from moving around the surfaces of electrodes and in the bulk of materials [34].

Karadag et al. [35] recently wrote about how to make the glucose biosensor via an [Au/AuNP/(FeSH+Cysteamine)/ PAMAM/GOD], as shown in Figure 1-12. This group's idea for a biosensor worked well when it was used to test the amount of glucose in drinks.

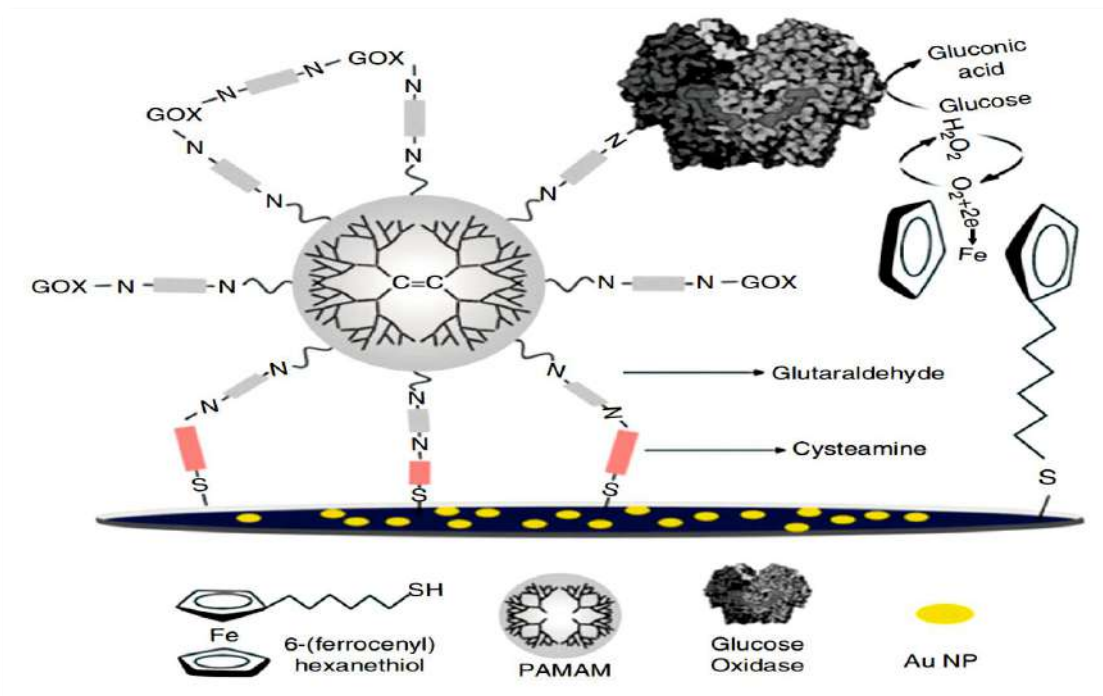


Figure 1-12 Preparation of biosensor made Au/AuNP/(FeSH+Cyst)/PAMAM/GOx system

1.1.4 .3 Catalyst

Dendrimers can be used in the field of catalytic chemistry because they retain the advantages of homogeneous catalysts, including a high degree of activity, excellent repeatability, higher selectivity, easy access to the site of metals, and so on. In contrast to most other polymeric substances, they exhibit a high degree of recoverability after a reaction. Basically, dendrimers are the most likely to meet all of the requirements for an ideal catalyst: nanoscale dimensions that stay the same and can be controlled, a surface that reacts chemically, a good shape in which all of the active sites are always facing the reaction mixture so that they are easy for migrate the reactants to reach, and solubility that makes them easy to recover by filtration[36,37] . Dendrimers are very attractive as scaffolds for polymer catalysts because the size and shape of their

molecules can be controlled and their functional groups can be put where they are needed. Zhao and his coworker prepared dendrimers encapsulated with platinum (Pt) and palladium (Pd) nanoparticles and discovered good catalytic activity for the hydrogenation of simple alkenes and electron-deficient alkenes. The incorporation of metal ions into hydroxy-terminated PAMAM dendrimers was followed by reduction with BH_2 to produce these catalysts. High-resolution transmission electron microscopy (TEM) reveals that the interdendrimer metal nanoparticles are remarkably monodispersed and stable before, during, and after hydrogenation processes[38].

1.1.4.4 Light Harvesting Material

Dendrimers are completely branching synthetic macromolecules that have many ends all extending from the center that serves as amazing scaffolds for light harvesting uses, (Fig. 1-13). Light harvesting is the process of converting light energy into chemical energy or photon energy by capturing it with peripheral chromophores [39]. Nantalaksakul et al. produced π -conjugated dendrimers using thienyl ethynylene, which demonstrated an inherent energy gradient from the periphery to the core, as well as extensive (UV-vis) absorption and adept transfer of energy to the lower energy center. They have a strong potential for use as light-harvesting substances.

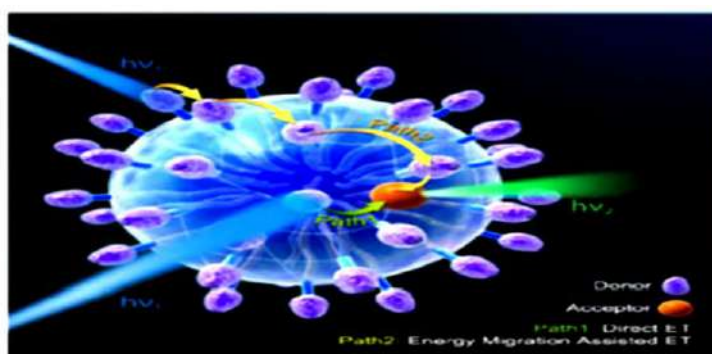


Figure 1-13 Dendrimer used as light-harvesting material

Xu et al. demonstrated an effective, one-way energy transfer to a chromophore with a single core. The robust, high-yielding synthesis made it possible to prepare high-generation (G-n) compounds up to (G-6). These cross-conjugated structures exhibit significant ultraviolet radiation (UV) absorption in the region of (250-350) nm, which is twice as strong as the rising generation. Furthermore, these dendrimers emit light in the (350-450) nm region [40].

1.1.4.5 Cosmetics

Dendrimers have a broad variety of cosmetic applications, including UV sunscreens, hair care products, and oxidants. Due to its ability to absorb UV radiation, dendrimers are used in sunscreen compositions. These dendrimer compounds will be used in a range of hair grooming formulations, including hair care compositions, permanent shaping compositions, hair bleaching compositions, hair fixing compositions and oxidative after-treatment compositions [41].

1.1.4.6 Process of Water Purification

Dendrimers possess many important physicochemical properties that make them ideal for use as reaction media and separation in water purification. Various types of solutes can be found in water, including anions such as nitrate, perchlorate, and phosphate, cations such as uranium, silver, gold, and copper, and organic molecules like pesticides and pharmaceuticals. One method for containing these solutes is through the use of dendritic nano polymers, which have been utilized as catalysts and reactors on a nanoscale level [42]. Diallo and colleagues have developed methods to recover dissolved anions and cations from aqueous solutions through Enhancing Microfiltration (EMF). These methods can also bind and deactivate bacteria and viruses [43].

1.2 Imidazoles

1.2.1 Introduction

Nitrogen-based heterocyclic organic chemistry is a significant and unique class. Among the branches of application in organic chemistry, many N-heterocyclic compounds, which are widely distributed in nature, exhibit pharmacological and physiological properties and are components of numerous biologically active molecules, such as nucleic acids, vitamins, antibiotics, dyes, pharmaceuticals, natural or synthetic alkaloids, and agricultural chemicals, amongst many others [44]. A broad and promising class of heterocyclic compounds is azole, a five-membered heterocyclic aromatic compound whose structure includes from one and up to five nitrogen atoms. The parent azole compounds, as represented by, ('pyrrole', 'pyrazole', 'imidazole', '1,2,3-triazole', '1,2,4-triazole', 'tetrazole', and pentazole) with aromatic structures and two double bonds as indicated in Figure (1-14). These azoles are also found as core structures in many natural and artificially synthesized compounds. Imidazole motifs have been discovered to be the most commonly detailed keyword [45].

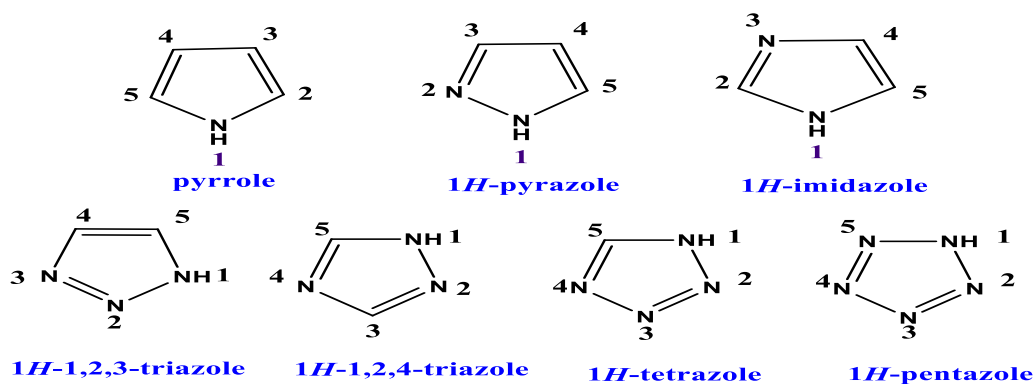


Figure 1-14 Structural formula of azole ring (including nitrogen only)

1.2.2 Structure and Properties

Imidazole is a 5-membered planar nitrogenous heterocyclic organic molecule that contains two nitrogens, three carbon, four hydrogen atoms, and two double bonds with formula $C_3H_4N_2$. It is additionally named (*1,3-diaza-2,4-cyclopentadiene*) with pyrrole type (-NH) and pyridine type nitrogen (=N) annular nitrogen, (Fig. 1-15), it was reported in 1858 as glyoxaline (the first synthesis with glyoxal and ammonia) [46].

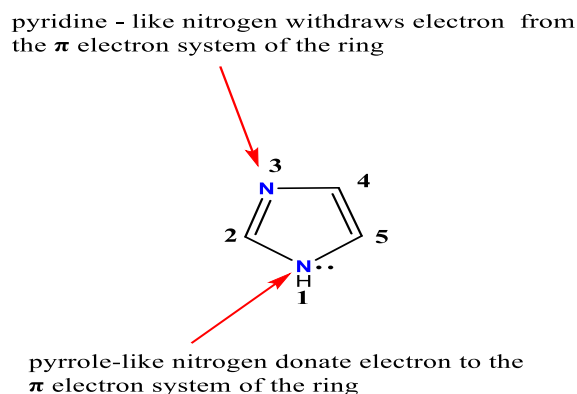


Figure 1-15 Structure of imidazole

Imidazole is a colorless liquid due to intermolecular H-bonding. It has a higher boiling point of about 256°C than all other five-membered heterocyclics (Fig. 1-16) and it is highly soluble in both water and other polar solvents, as demonstrated by a determined electric dipole moment of 3.67D so it is a highly polar compound [47].

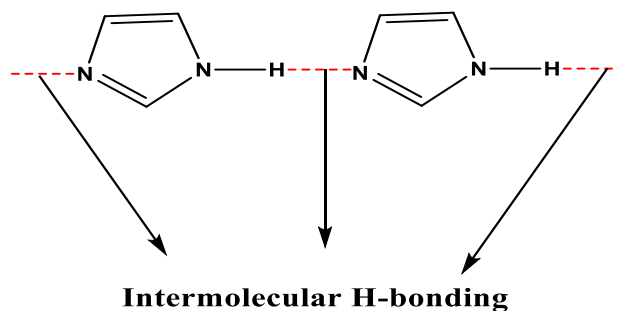


Figure 1-16 Hydrogen bonding in imidazole ring

It is found in two equivalent tautomeric forms, *1H*-imidazole and *3H*-imidazole [48], (Fig. 1-17).

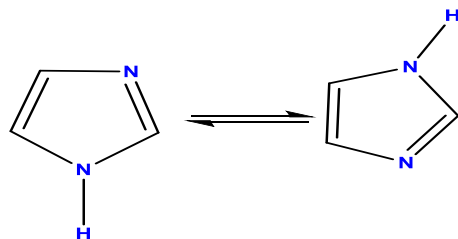


Figure 1-17 Tautomeric forms of imidazole structure

Imidazole compound is considered as aromatic heterocyclic because of the presence of delocalized 6π -electrons with a resonance value of 14.2 Kcal/mol, and found in resonating forms at room temperature (I-IV)[49], (Fig. 1-18).

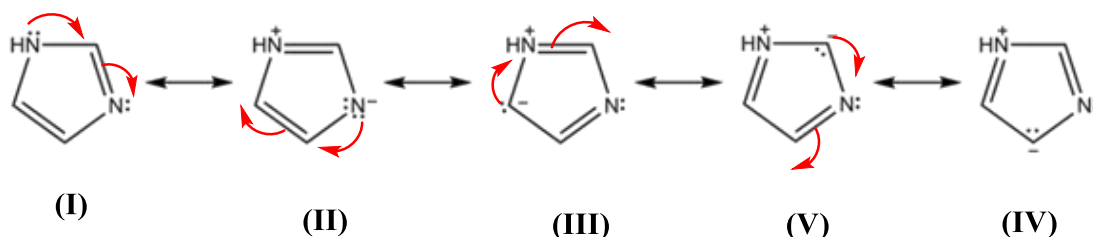


Figure 1-18 Resonating Structures of the imidazole moiety

Imidazole is considered an amphoteric molecule (it can act as a weak acid or a weak base) a strong base when compared with other compounds like; pyrrole, pyrazole, or pyridine. The electrophilic reagent would attack the N atom in position three of the imidazole ring instead of the 'pyrrole' nitrogen because the second nitrogen is a part of the aromatic system, but nucleophilic substitution happens if a strong electron-withdrawing group is present in its nucleus. imidazole also shows weakly acidic properties by forming salt with metals such as soluble silver salt [50], (Fig. 1-19).

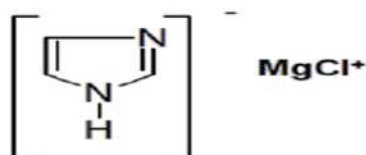


Figure 1-19 Imidazole as pseudo-acidic properties and generates acids with Crystalline Salts

1.2.3 Synthesis of Imidazole and its derivatives

There are various synthetic methodologies described in the literature of the many physicochemical and biological properties of imidazole. Different classical and modern methods for the preparation of imidazole derivatives have been summarized.

1.2.3.1 Classical methods for the synthesis of imidazole derivatives

Figure (1-20) shows four types of traditional methods for the synthesis of (poly-functionalized imidazole derivatives) such as Van Leusen synthesis, Wallach synthesis, Marckwald synthesis, and Debus-Radziszewski synthesis. Each synthetic approach is described in detail below.

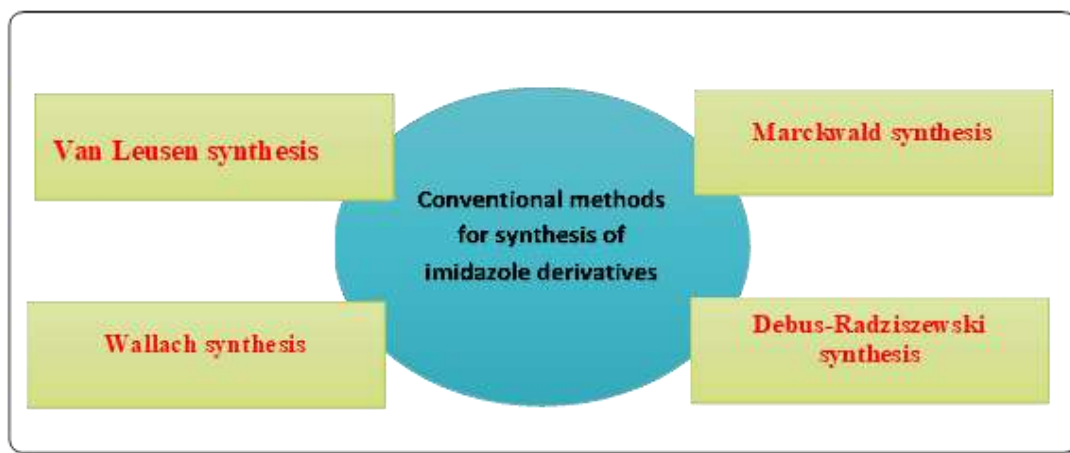
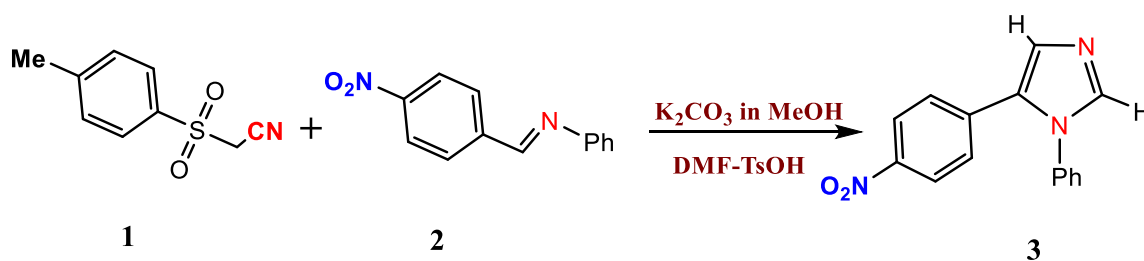


Figure 1-20 Traditional method for Imidazole derivatives synthesis

1.2.3.1.1 Van Leusen synthesis

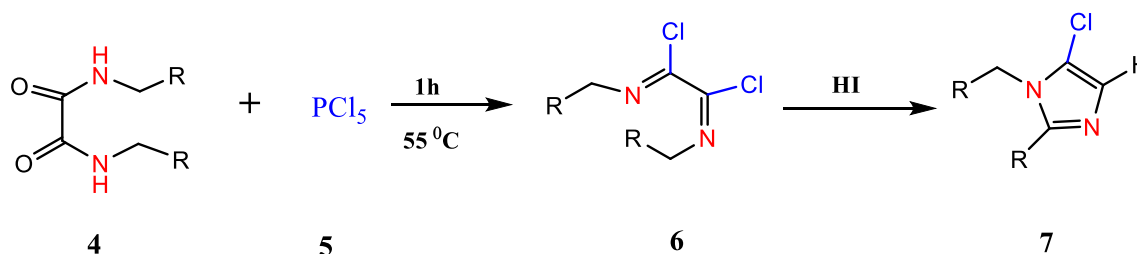
1,5-disubstituted imidazole derivatives have been synthesized by Van Leusen et al. [51] in 1977 with the reactions between (tosyl methyl isocyanide) and (aldimines) under basic medium, with the presence of K_2CO_3 in [(MeOH/DMF)-TsOH] at $20^\circ C$. This method gives an 82% yield of the product (3), (Scheme 1-2).



Scheme 1-2 Van Leusen synthesis

1.2.3.1.2 Wallach synthesis

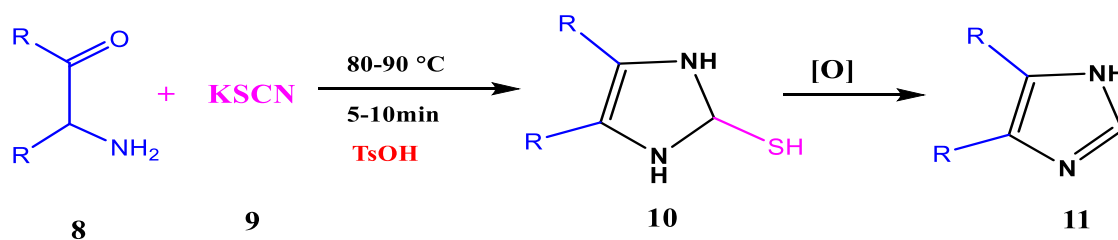
Wallach has studied [52] the preparation of imidazole derivatives via the reaction of *N,N*-dimethylformamide (4) with PCl_5 (5) to obtain dichloride derivatives (6) which then reduced with hydroiodic acid (HI) to give imidazole derivative (7), (Scheme 1-3).



Scheme 1-3 Wallach synthesis

1.2.3.1.3 Marckwald synthesis

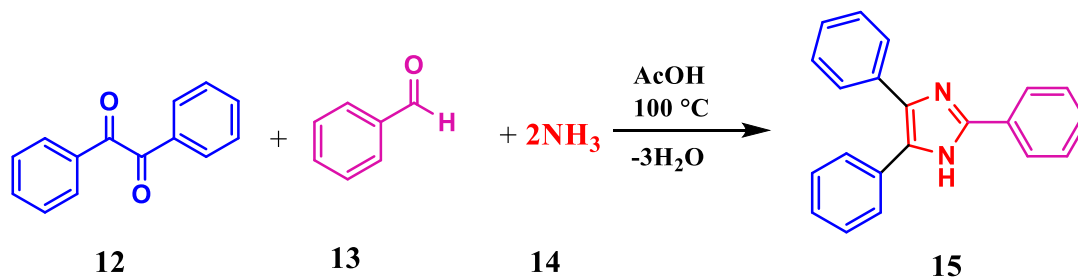
This synthetic method [53] was used for the preparation of 2-mercapto imidazoles (11) from an aldehyde or α -amino ketone (8) in the presence of potassium thiocyanate (9) to obtain 2-thiol substituted imidazole (10) and by using various types of oxidative methods the sulfur can easily be removed to give the desired product in yield 86.97%, (Scheme 1-4).



Scheme 1-4 Marckwald synthesis

1.2.3.1.4 Debus-Radziszewski synthesis

The Debus-Radziszewski [54] synthesis involved the condensation of the α -dicarbonyl compound, benzil (12) with aldehydes (13) and ammonia (14) to give 2,4,5-trisubstituted imidazole core (15), (Scheme 1-5).

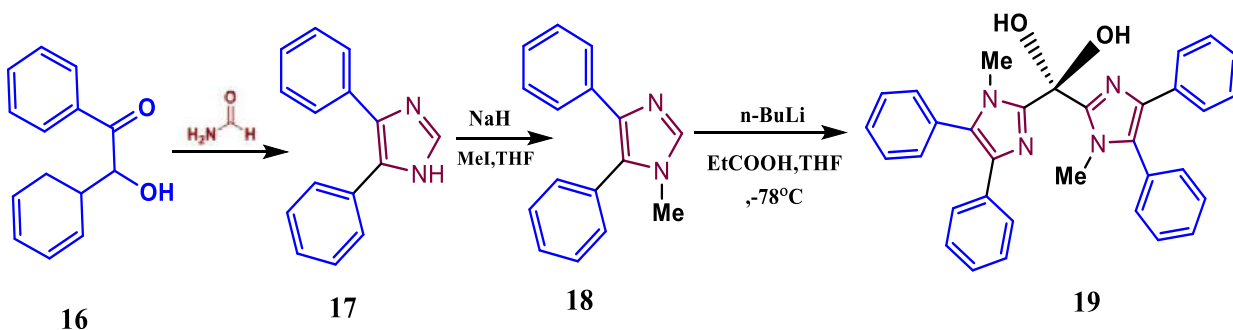


Scheme 1-5 Debus-Radziszewski synthesis

1.2.3.2 Modern synthetic route towards poly-functionalized imidazoles

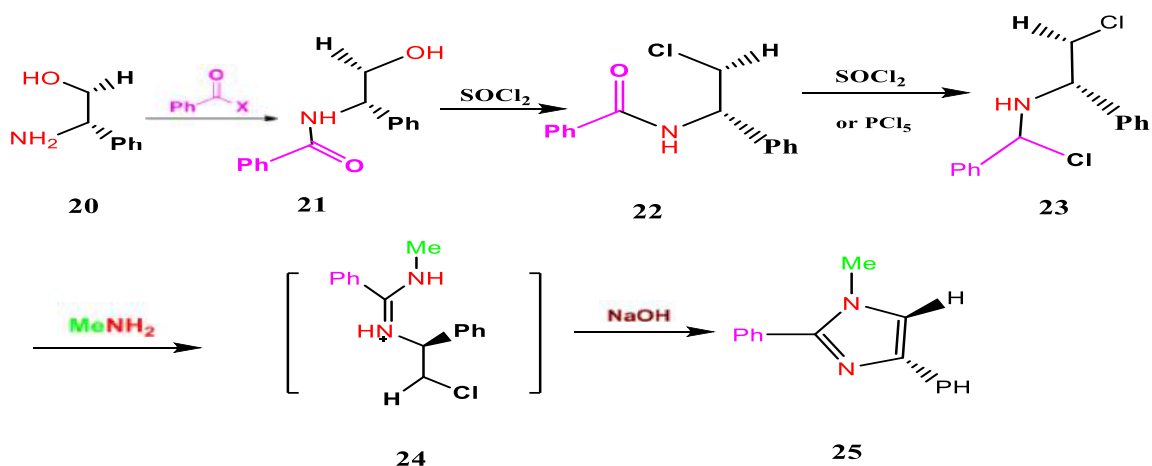
There are various route of synthesis part of imidazole's and functionalization at its different positions involve various name reaction, multi-step strategy, multicomponent reaction, harsh condition, and use of Lewis acid and Lewis's base, metal-free condition, expensive transition metal catalyst or in solvent and solvent-free condition.

In 1996 [55] Bhalla and coworkers synthesis of bis [(1-methyl-4,5-diphenylimidaz-2- oyl)]carbinol derivatives via the reaction of benzoin (16) and amino aldehyde to obtain imidazole derivative (17) and that then react with (NaH/MeI) in tetrahydrofuran (THF) followed by the addition of (n-BuLi/EtCOOH) in tetrahydrofuran to give bis -imidazole derivatives (19), (Scheme 1-6).



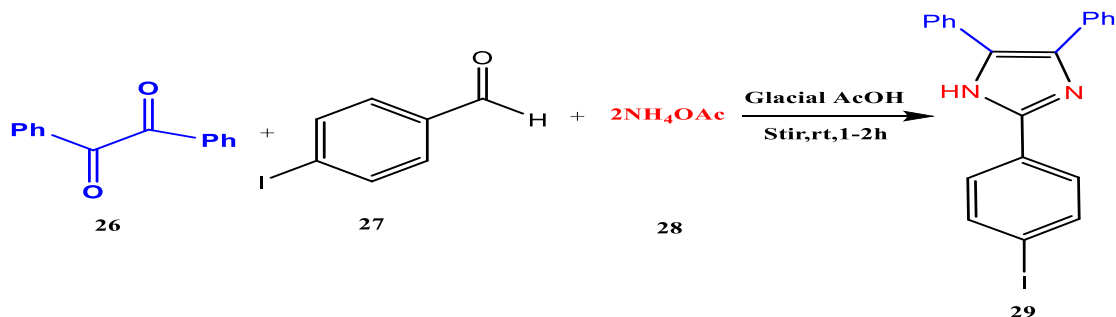
Scheme 1-6 Synthesis of bis[(1-methyl-4,5-diphenylimidaz-2-oyl)] carbinol derivatives

In 2002, a new preparation method for the synthesis of enantiopure imidazole derivatives was developed by Boland and coworkers [56], initially, β -amino alcohols are converted into *N*-hydroxyethylamides (21) followed by the reaction with thionyl chloride to the formation of chloroethyl amide (22), and this further reacted with excess(PCl_5) or (SOCl_2) to yield chloroethyl imidoyl chloride (23) then this intermediate was undergo reactions with aqueous sodium hydroxide (NaOH) to form imidazolidines (24). This procedure is effective for the synthesis of enantiopure imidazolines but the longer reaction is the important limitation of this method, (Scheme 1-7).



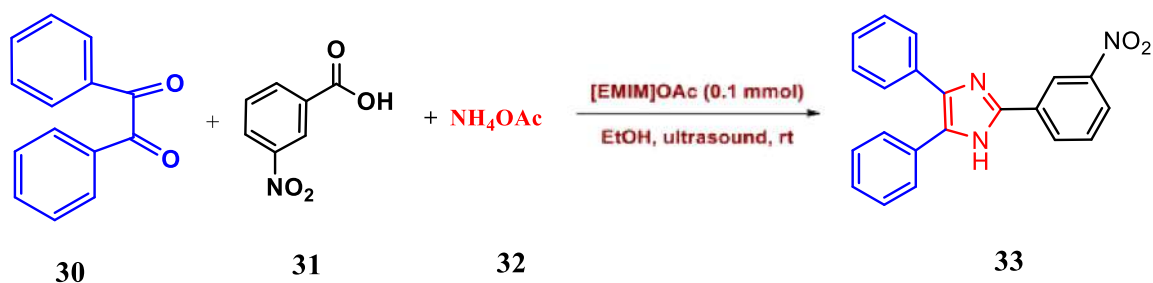
Scheme 1-7 The Boland method for synthesizing enantiopure imidazole derivatives

In 2007 Puratchikody and Doble [57] performed this reaction in a one pot at room temperature, which made it particularly appealing for the preparation of imidazole derivatives in comparison to previously reported approaches. Additionally, it satisfies all requirements for green and sustainable chemistry via benzil (26) condensation reactions with aryl aldehydes (27), ammonium acetate (28), and glacial acetic acid. The mixture was stirred for (1-2) hours at room temperature, resulting in the formation of pharmacologically active substances 2-substituted-4,5-diphenyl-1*H*-imidazoles (29), (Scheme 1-8).



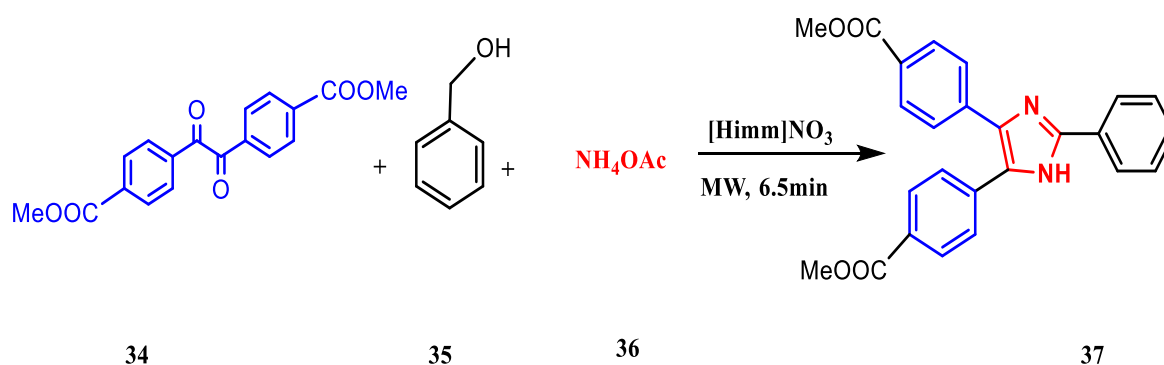
Scheme 1-8 Puratchikody and Doble method

Zang and coworkers in 2010[58] performed a simple one-pot method to synthesize tri-substituted imidazole derivatives (33) at 25°C under ultrasonic conditions by using an ionic liquid as the catalyst. When benzil (30) is treated with the suitable aldehyde (31) and NH_4OAc (32), the ionic liquid (1-ethyl-3-methylimidazole acetate) serves as a mild and efficient catalyst during the formation of 2-aryl-4,5-diphenyl-1H-imidazoles (33). This approach has numerous benefits, such as mild reaction conditions producing high yields, avoiding the use of hazardous catalysts /solvents, and simplicity of the method, (Scheme 1-9).



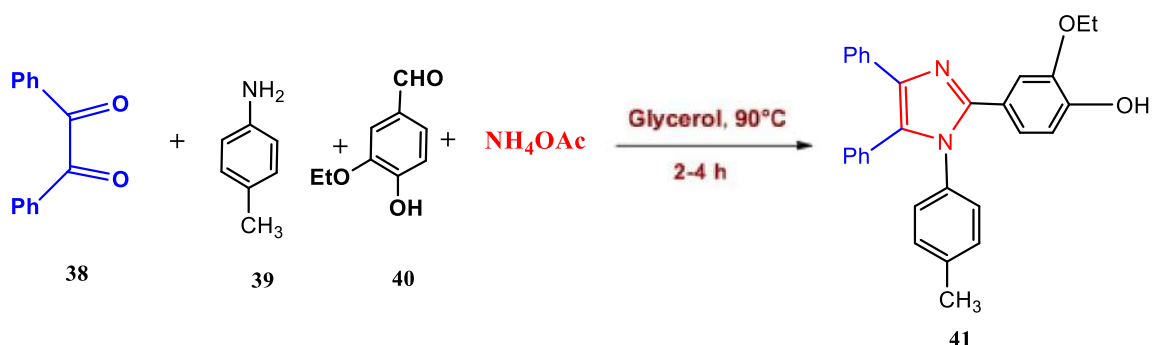
Scheme 1-9 Synthesis of imidazole derivatives using an ionic liquid catalyst under ultrasound conditions

Mirjafriin 2014 [59] has developed an effective and single-pot synthetic approach under microwave irradiation. The tri-substituted imidazole (37) was synthesized using a multi-component condensation reaction that included 1,2-diketone (34), primary alcohol (35), and ammonium acetate (36) in the presence of ionic liquid, Brønsted acidic, (1-Methyl-3*H*-imidazolium nitrate), (Scheme 1-10).



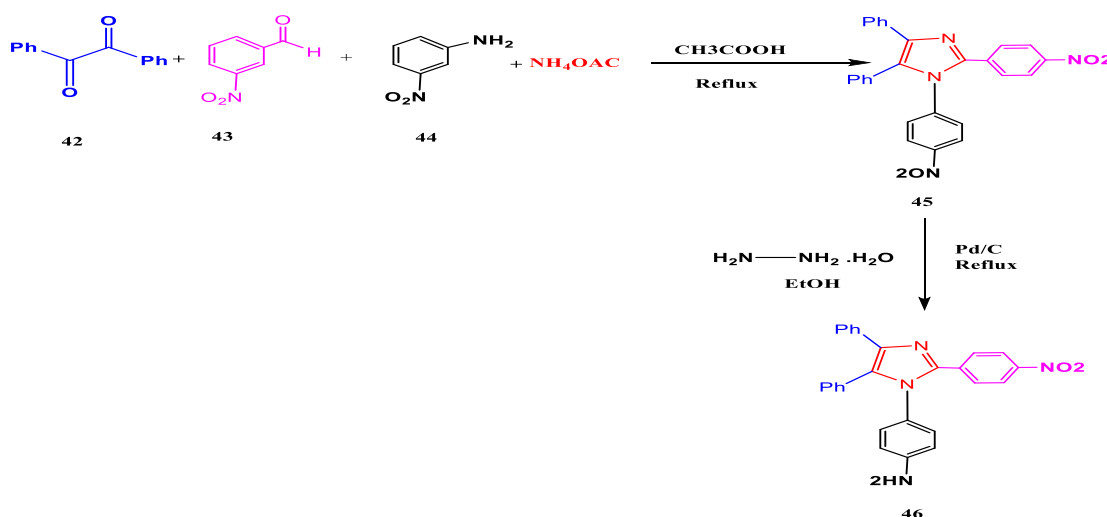
Scheme 1-10 Imidazole synthesis with [Hmim]NO₃ assistance

In 2016, Nemati et al. [60] demonstrated an efficient, simple and catalyst-free technique for the preparation of imidazole derivatives (41) in the presence of glycerol which serves as a green solvent through the reactions of 1,2-diketone (38), amine (39), aldehyde (40) and NH₄OAc (Scheme 1-11).



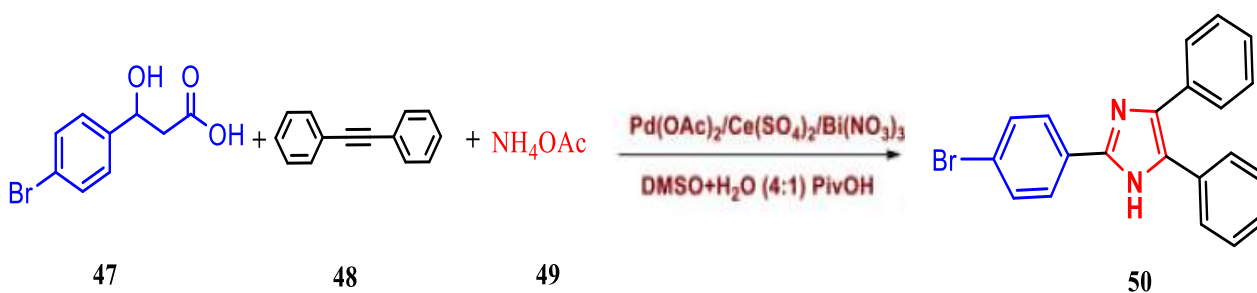
Scheme 1- 11 Glycerol-based imidazole derivative synthesis

In 2018, Hariharan et al. [61] described the reaction of benzil (41), 4-nitrobenzaldehyde (42) and 4-nitroaniline (43) with ammonium acetate at 120 °C with (10-15) mL of acetic acid to produce 1,2-bis (4-nitrophenyl)-4,5-diphenyl-1*H*-imidazole (44). When 1,2-bis(4-nitrophenyl)-4,5-diphenyl-1*H*-imidazole is treated with (hydrazine monohydrate) in the presence of (Pd/C) as a catalyst in ethanol as a solvent under conditions of reflux, 4,4'-(4,5-diphenyl-1*H*-imidazole-1,2-diyl)dianiline (45) is obtained, (Scheme 1- 12).



Scheme 1-12 The synthesis of poly-functionalized imidazole derivatives has been catalyzed by glacial acetic acid

In 2109, Sun et al. [62] described the one-pot synthesis of (poly-substituted imidazole derivatives) via the reactions of hydroxyaryl acetic acid (47) with diphenylacetylene (48) and NH_4OAc (49), by employing a trimetallic catalytic system in a mixture of (DMSO/ H_2O) as a solvent to generate tri phenyl imidazole derivatives (50) in high yield, (Scheme 1-13).



Scheme 1-13 Synthesis of imidazole derivatives from diphenyl acetylene under Pd-catalyzed

1.2.4 Applications of Imidazole

1.2.4.1 Natural Products

Many complex natural products, including histamine, vitamin B12, deoxyribonucleic acid (DNA), hemoglobin, etc., contain the structural subunit imidazole heterocycle, which is necessary for performing several physiological actions for vital biological processes. Histidine (56), which is essential for the structure and binding properties of hemoglobin, is found in a wide variety of proteins and enzymes. The biological substance histidine may be converted into histamine (57) by a process called decarboxylation. Imidazole, a substance present in tea and coffee beans and part of theophylline, is a chemical that activates the central nervous system [65], (Fig. 1-21).

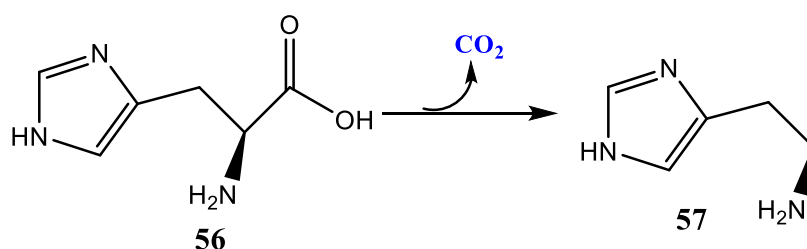


Figure 1-21 chemical structure of histamine

1.2.4.2 Pharmacological activities

According to the literature reviews, imidazole derivatives exhibit a wide spectrum of pharmacological activities, such as anti-tubercular, anti-cancer, anti-fungal, anti-bacterial, anti-inflammatory, antidiabetic, antimalarial, and analgesic activity.

Ramya V. and coworkers developed several new 5-(nitro/bromo)-styryl-2-benzimidazoles derivatives, which were then screened for *in vitro* anti-tubercular activity against Mycobacterium TB. These compounds demonstrated excellent antitubercular activities. streptomycin was used as a standard drug [66], (Fig. 1-22).

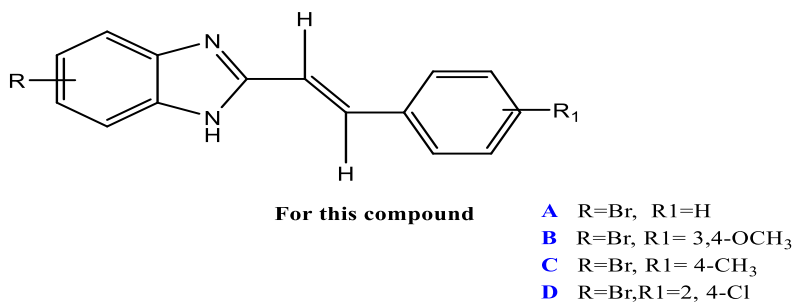


Figure 1-22 *In vitro* anti-tubercular activity

Zhao Shizhen and a coworker synthesized and investigated a series of biphenyl imidazole derivatives for *in vitro* antifungal activity. Several of the prepared compounds exhibited good activity against *C. tropicalis*, *C. albicans*, and *C. neoformans*. Furthermore, some compounds displayed a low inhibition in human cytochrome P450 isoforms [67], (Fig. 1-23).

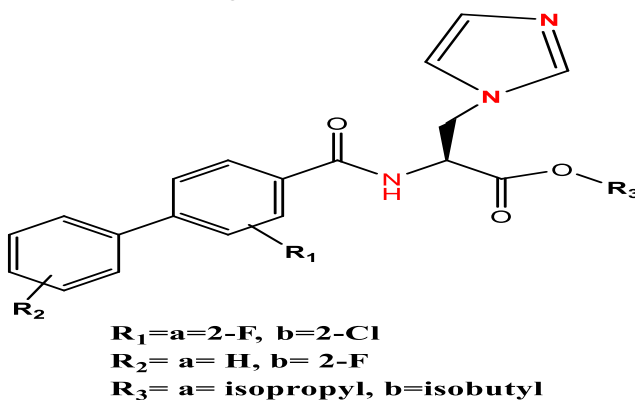


Figure 1-23 *In vitro* antifungal activity

Two new series of (4,5- diarylthiazole and diarylimidazole derivatives) were synthesized by Abdelazeem and colleagues. *In vitro*, COXs inhibition assay results showed that products with an acetic acid constituent attached to a thiazole or imidazole core have the strongest anti-inflammatory effects. Among them, compound 15b was the most potent. Celecoxib and Indomethacin were used as reference drugs [68], (Fig. 1-24).

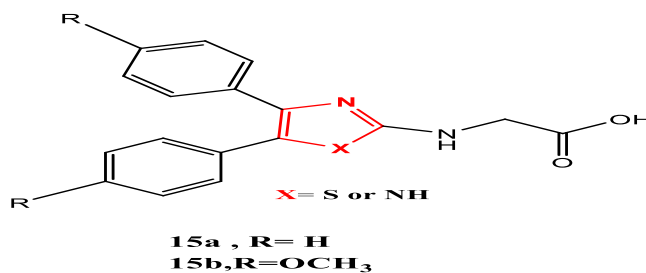


Figure 1-24 *In vitro* anti-inflammatory effects

Jain et al. developed a novel molecule of triphenyl-substituted imidazole derivatives and synthesized by for investigation of antibacterial activities which demonstrated activity against *S. aureus*, *B. subtilus* and *E. coli* [69] , (Fig. 1-25).

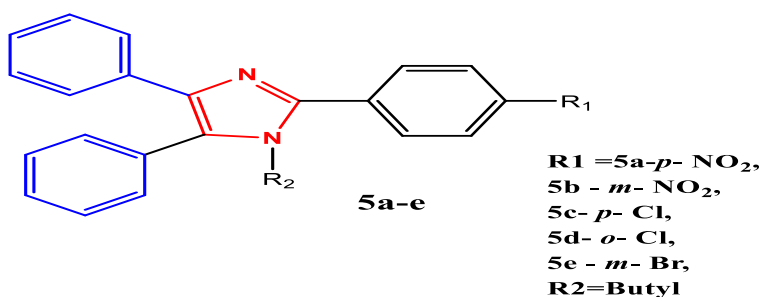


Figure 1-25 *In vitro* antibacterial activities

Chaudhry et al. showed the design and synthesis of tetra-substituted imidazole-pyrazole hybrids as potential anti-diabetic agents. Based on the results of an *in vitro* α -glucosidase inhibitory assay, hybrids 49a (IC₅₀ = 25.19 M μ M) and 49b (IC₅₀ = 33.62 μ M) demonstrated the most potent inhibition of the α -glucosidase enzyme[70] , (Fig. 1-26).

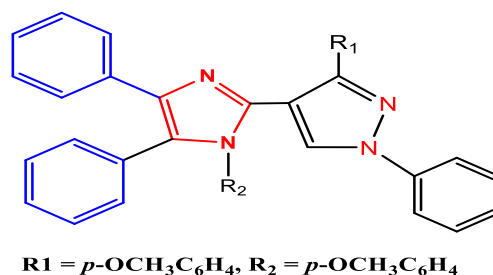


Figure 1-26 *In vitro* α -glucosidase activity

The *in vitro* series of novel 5-substituted-1-(phenylsulfonyl)-2-methylbenzimidazole derivatives have been synthesized by Gaba et.al and evaluated for analgesic activity. Derivatives 143a–c exhibited moderate to good analgesic activity [71], (Fig. 1-27).

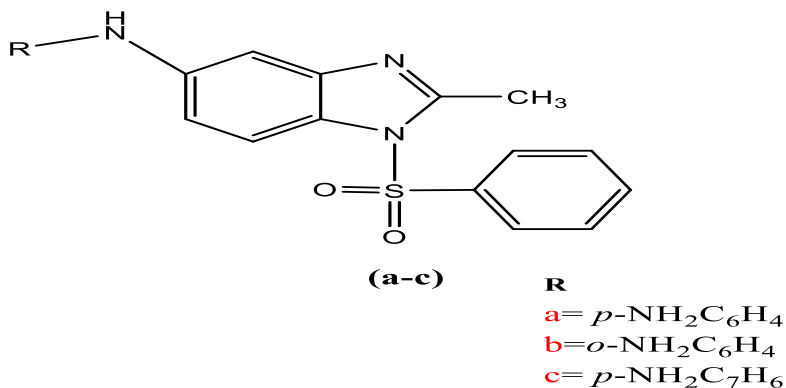
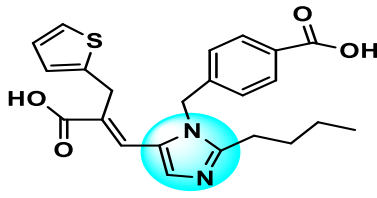
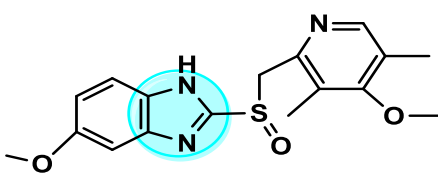
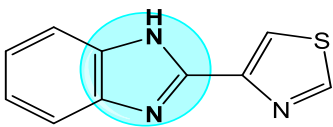
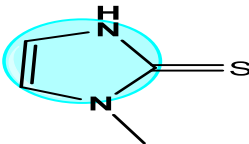
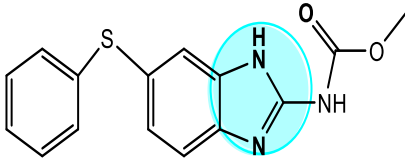
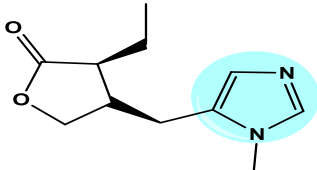
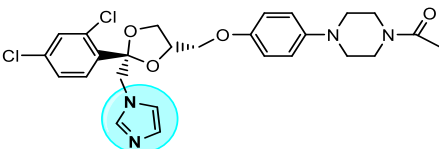


Figure 1-27 *In vitro* analgesic activity

There are various examples of pharmaceutical imidazole-based drug rings that are used clinically for the treatment of different infections, Table (1-1).

Table 1-1 Commercially available drugs having Imidazole nucleus

NO.	Drug	Structure	Activity	Ref.
1	Clemizole		Anti-histaminic Agent	[72]
2	Azathioprine		Anti-rheumatoid Arthritis	[73]
3	clotrimazole		antitubercular	[74]

NO.	Drug	Structure	Activity	Ref.
4	Eprosartan		antihypertensive	[75]
5	Omeprazole		antiulcer	[76]
6	Thiabendazole		Anti-helminthic	[77]
7	Methimazole		Antithyroid	[78]
8	Fenbendazole		Anti-helminthic	[79]
9	Pilocarpine		Cholinergic agent	[80]
10	Ketoconazole		Antifungal	[81]

1.2.4.3. Industrial Application

The N-heterocyclic imidazole family has a wide spectrum of applications in several fields, including materials chemistry, optical electronics, and dye-sensitized solar cells [82]. In addition to being utilized in the industry as a corrosion inhibitor for definite transition metals, imidazole derivatives are also employed in photography as photosensitive chemicals[83].

1.3 Microwave-Assisted Technique

Microwaves are a form of electromagnetic radiation with wavelengths varying from (0.1 to 100 cm) in other words, their frequencies can vary from (0.3 to 300) GHz. One interesting application of microwave technology is in dielectric heating, which can drive chemical reactions through the conversion of electromagnetic radiation into heat in certain liquids and solids[84]. Chemists have effectively carried out a wide variety of organic reactions using microwave irradiation over the years. There are several benefits to microwave-assisted organic synthesis over traditional methods [85]. The use of microwaves (reduces the time reaction from many days and hours to minutes and seconds). It offers efficient and uniform heating, proving to be a faster way than traditional methods. When microwave heating is used, the reactants are directly heated, whereas traditional methods heat the reaction vessel first and then transfer the heat to the contributing reactants via convection [86].

The microwave provides short reaction time, enhanced conversions, clear formation of products, high efficacy and selectivity, fewer by-products and simple separation, environmental acceptability, a wide range of new reaction conditions, and rapid analog synthesis. Furthermore, it reduces energy and chemical consumption[87].

1.3.1 Applications of Microwave Irradiation

Microwave heating has advantages for chemical processes and has become a commonly accepted nonconventional source of energy for organic synthesis. This statement is supported by the increasing volume of associated publications in recent years, especially since 2003, that have accompanied the widespread availability of novel and accurate microwave instrumentation. A large number of examples of reactions have been described in organic synthesis[88], (Fig. 1-28).

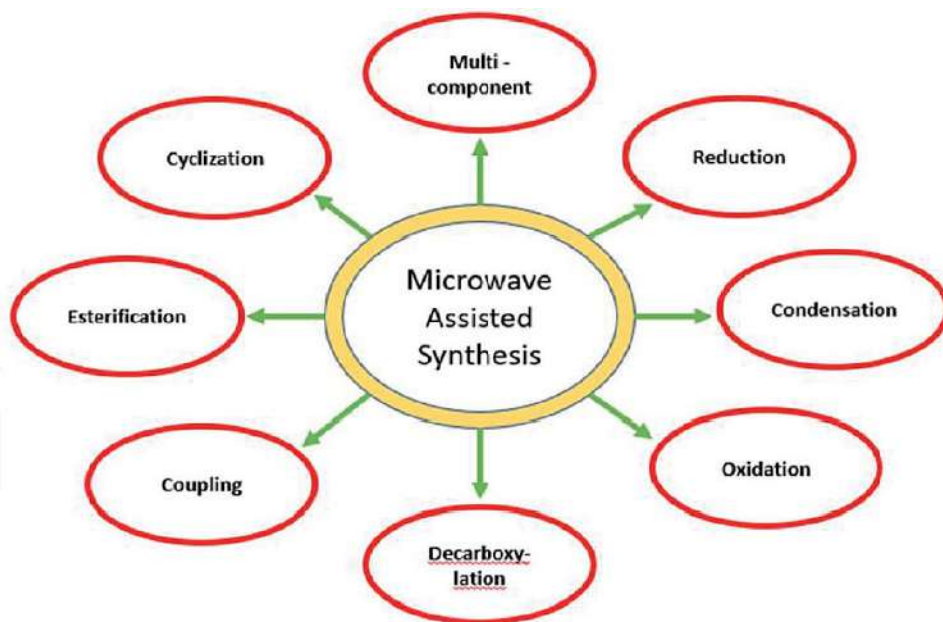


Figure 1-28 A variety of microwave-assisted synthesis types

There have been several published reviews on the use of microwaves in various chemical reactions. These include solvent-free conditions [89], radioisotope synthesis[90], cycloaddition reactions[91], polymer compounds, fullerene chemistry, heterocyclic chemistry, heterogeneous as well as homogeneous catalysis, carbohydrates, green chemistry, medicinal and combinatorial chemistry and

nanomaterial synthesis[92]. Additionally, microwaves have been utilized in decomposition processes such as the hydrolysis of proteins and peptides. Microwave irradiation has been applied to a variety of organic reactions including substitution, alkylation, condensation reaction, esterification, Coupling reactions, and introduction or removal of the protecting groups. Microwaves have been used successfully in the preparation of aromatic five-membered heterocyclic systems with excellent results in terms of yields and purities of the products prepared[93].

1.4 Ultrasound

Ultrasonic is a widely known thermal cracking technique and a reliable instrument for preparing samples in the laboratory. It is commonly utilized in chemistry because it has been associated with several important benefits including safety, reduced energy consumption, prevention of waste, use of ambient conditions, as well as mass transfer improvement [94,95].

Sonochemistry is the branch of chemical study that focuses on the reactions and applications of ultrasonic waves, which are high-frequency sound waves that are difficult for the human ear to detect but can be heard by adults at a threshold of around (18-20) kHz. Ultrasound covers a range of frequencies from (20 kHz to 100) MHz, with no clear upper limit. Therapeutic and diagnostic uses of ultrasound typically fall between (1 MHz and 10) MHz, while sonochemistry usually operates in the (20-40) kHz range, which is common in laboratory equipment as seen in Figure (1-29).

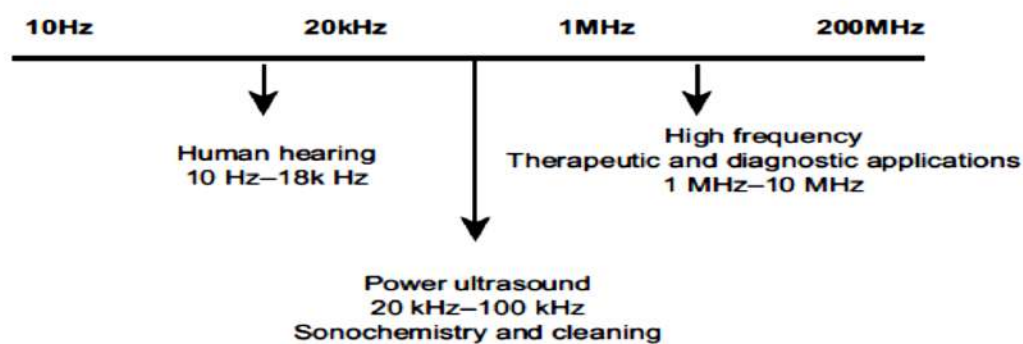


Figure 1-29 Frequency variations of sound

Using ultrasound to speed up traditional chemical reactions has been crucial in achieving environmentally conscious goals, such as minimizing waste and reducing time and energy [96].

1.4.1 Ultrasound Irradiation in Organic Chemistry

The process of ultrasound irradiation, also known as sonochemistry, is a valuable tool in synthetic organic chemistry. This method has become increasingly popular since the 1990s [97-99], and this approach has become extremely common in promoting different chemical reactions. In a variety of reaction systems, ultrasound has been helpful in accelerating dissolution, increasing the rate of reaction, and/or renewing the surface of the solid reactant or catalyst[100]. Sonochemistry is now widely used in both homogeneous and heterogeneous processes for synthesizing organic compounds [101-103].

By utilizing this method, researchers can achieve higher reaction rates and substance yields, in comparison to traditional methods. One of the most important types of organic compounds is heterocycles, which are used extensively in various fields, including industry, agriculture, pharmaceuticals, material science, and medicinal chemistry. Therefore, the synthesis of heterocycles is an ongoing area of research.

Sonochemistry is an excellent alternative method for synthesizing both heterocycles and fused heterocycles under mild conditions, high yields, and short reaction times[104,105]. Recent studies have focused on the use of ultrasound waves as a form of alternative energy in green as well as pharmaceutical chemistry, particularly in heterocyclic chemistry. Sonication enhances reactions such as condensation, replacement, addition, reduction, oxidation, protection/deprotection, coupling reactions, polymerization, and photochemical[106,107].

1.4.2 Important of Ultrasound

Ultrasound has a wide range of applications. Ultrasonic instruments are used to detect objects and measure distances. Researchers have studied the chemical effects caused by high-power ultrasound since 1927, when Loomis and Richards [108] introduced a hydrolysis product of dimethyl sulfate and iodine as a catalyst. Then, in 1963, Demaggio and colleagues [109] utilized ultrasonic radiation for the isolation of alkaloids. Since the late 1970s and the beginning of the 1980s, a number of the chemical uses for ultrasound have included material science and organic chemistry. In addition, these waves have been employed extensively in fields like medicine and biology [110]. Using sonar devices to detect objects or echography in medicine is the most well-known application of ultrasound. During nondestructive testing, ultrasound is employed to discover faults in products and structures.

In industry, ultrasound has been utilized for cleaning, mixing, and accelerating chemical reactions. Animals such as bats and porpoises use ultrasound to discover food and prevent obstacles[111].

Aims & objectives

This study aims to synthesize new compounds which have biochemical applications and can be used in pharmaceutical fields. So, the major objectives of the present thesis project are outlined below:

1. Selection of a suitable core molecule for the production of PAMAM dendrimer generations.
2. Produce dendrimers of the first, second, and third generations employing a simple, effective two-step synthesis that does not require any complicated protecting group approach.
3. Synthesis of two new series of imidazole derivatives (2,4,5-trisubstituted imidazole and 1,2,4,5-tetrasubstituted imidazole derivatives).
4. Confirm the resulting structures via FT-IR, ^1H NMR, ^{13}C NMR, and Mass spectrometry.
5. Evaluation of *in vitro* antiuorlthesis , antidiabetic, antibacterial, and hemolysis assay for the selected compounds.

CHAPTER TWO

EXPERIMENTAL

PART

2.1 General Description of Chemicals and Equipment

2.1.1 Chemicals and Solvents

All of the chemicals and solvents employed for the project were purchased commercially from (Sigma Aldrich, Macklin, HI Media, Fluka and BDH Chemicals) and they were utilized without any extra purification.

2.1.2. Instruments and Equipment

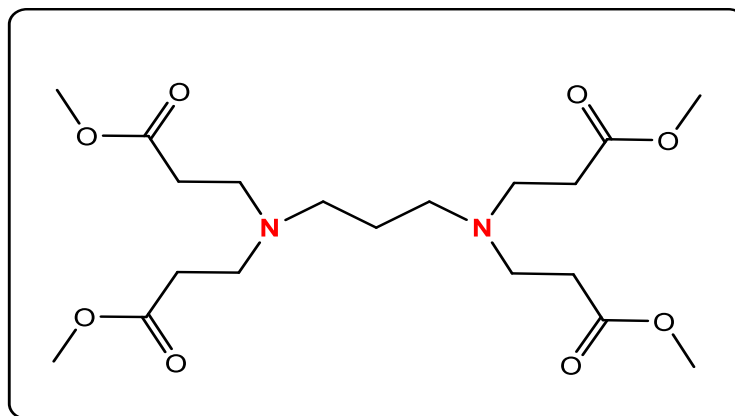
- ❖ Thin-layer chromatography (TLC) silica plate (60 F₂₅₄) was used to monitor the reactions visualization of spots was done by heating plates coated with KMnO₄ stain.
- ❖ The melting point of the compounds was determined by the capillary melting point apparatus, a UK device at Kerbala University, College of Science.
- ❖ The functional groups and composition of the compounds were determined using Fourier transform infrared spectroscopy SHIMADZU FTIR-8400S (FTIR and ATR) in Kerbala University, College of Science and College of Education for Pure Sciences.
- ❖ The ¹H and ¹³CNMR spectra were measured on a Varian INOVA and Bruker (500 MHz and 400 MHz for ¹HNMR) and (125 MHz and 100 MHz for ¹³CNMR) using DMSO-d₆ as the solvent and Tetramethylsilane (TMS) as a reference standard. Center Tehran Laboratory College, University of Tehran, Iran.
- ❖ Electrospray ionization mass spectrometry (ESI-MS 70 eV): was performed using Shimadzu LCMS 2010. Center Tehran Laboratory College, University of Tehran, Iran.
- ❖ Field-emission images scanning electron microscopy (FE-SEM) were taken using, Fei, Inspect 50 Dutch. Alkhora company for general trading -Nano lab.
- ❖ A SAMx analyzer was used to monitor energy-dispersive X-ray spectroscopy (EDX). Alkhora company for general trading -Nanolab.

- ❖ Ultrasonic wise clean frequency 60kHz ultrasonic bath was used for ultrasonic irradiation, Kerbala University, College of Science.
- ❖ A domestic microwave oven in a crucible was used to carry out reactions at Kerbala University, College of Science.
- ❖ Rotary evaporators were used for the removal of solvents from samples Kerbala University, College of Science

2.2 Synthesis of the first line of PAMAM dendrimer

2.2.1 General procedure for Synthesis of PAMAM dendrimer with 4 OMe terminal groups (G1_(a))

In a 100 mL round bottom flask, the propane-1,3-diamine (5.6 mL, 0.067 mol.) was dissolved in methanol (20 mL) using a magnetic stirrer, and an excess amount of methyl acrylate (30.5 mL, 0.33mol.) was added drop-wise at 0°C for 45 minutes. The reaction was stirred at room temperature for 24 hours. The progress of the reaction was monitored on TLC with CH₂Cl₂: MeOH, 9:1 as eluent. The unreacted methyl acrylate and methanol were removed using a rotary evaporator, and a vacuum was utilized to ensure the product's purity was confirmed from the remains of the reactants and the solvent. The result was a colorless liquid oil (Yield: 21.2g; 87.62%).



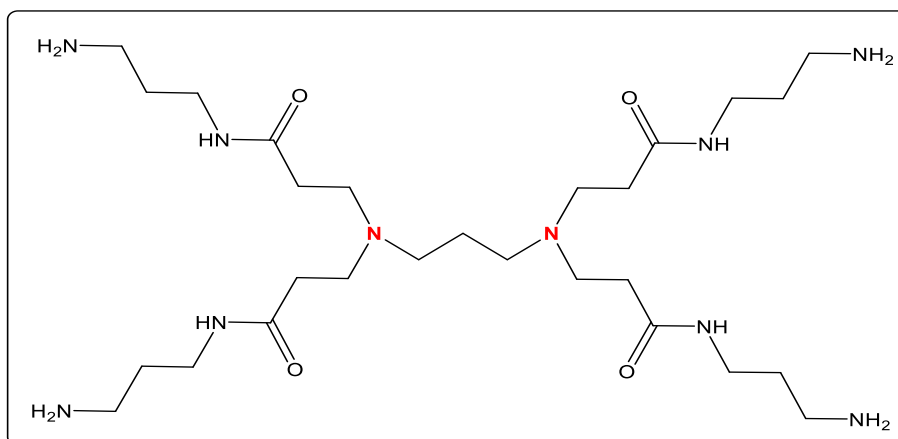
[G1_(a)]

Molecular Formula: $C_{19}H_{34}N_2O_8$, $R_f = 0.56$

FT-IR-ATR (cm^{-1}): 2951, 2820 (C–H aliphatic), 1737 (ester, C=O). **1H NMR** (500 MHz, DMSO- d_6) δ_H (ppm): 3.59 (s, 12H, 4OCH \underline{H}_3), 2.65 (t, $J = 5.0$ Hz, 8H), 2.40 (t, $J = 7.5$ Hz, 4H), 2.33 (t, $J = 7.5$ Hz, 8H), 1.43 (p, $J = 5.0$ Hz, 2H). **^{13}C NMR** (DMSO- d_6 , 125 MHz) δ_c (ppm): 172.9, 51.58, 51.31, 49.20, 32.34, 24.96. **ESI-MS**: $m/z = 418.2$ (M^+).

2.2.2 General procedure for Synthesis of PAMAM dendrimer with 4 amine terminal groups($G2_{(a)}$)

A solution of ($G1_{(a)}$); precursor (10 g, 0.023 mol.) in methanol (25 mL) had been carefully added drop-wise to a vigorously stirred solution of propane-1,3-diamine (89 mL, 1.045 mol.) in methanol (100 mL) at $0^\circ C$ over 40 minutes. The rate of addition was selected so that the temperature did not exceed $40^\circ C$. The final mixture was then stirred at room temperature for 96 hours, The progress of the reaction was monitored on TLC with CH_2Cl_2 : MeOH, 9:1 as eluent, after which time no ester groups were apparent by FT-IR spectroscopy. The solvent was removed under the rotary evaporator and maintained at a temperature below $40^\circ C$. An azeotropic mixture of toluene and methanol (9:1) was used to remove the excess propane-1,3-diamine. This purification process was carried out several times until all PDA was removed. Finally, the product was vacuumed for 48 hours, yielding the tetra-amine terminated $G2_{(a)}$ precursor as a pale-yellow vacuous oil (Yield:11.5 g; 90.01%).



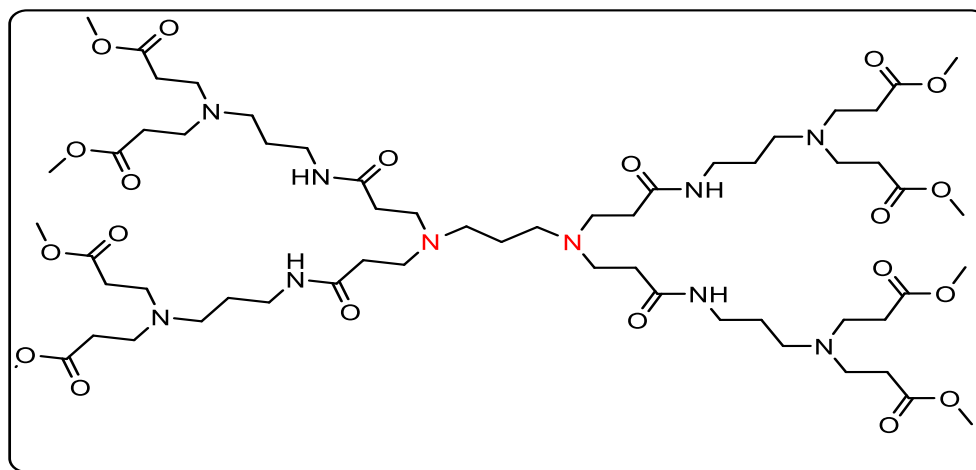
[$G2_{(a)}$]

Molecular Formula: $C_{27}H_{58}N_{10}O_4$, $R_f = 0.60$

FT-IR-ATR (cm^{-1}): 3356 (amide, N-H), 3294, 3240 (NH_2 , amine) 2935, 2866 (C–H aliphatic), 1641 (amide, C=O). **1H NMR** (400 MHz, D_2O) δ_H (ppm): 7.27 (s, 4H, 4NH), amide), 3.05 (td, $J = 8.0, 4.0$ Hz, 8H), 2.89 (t, $J = 6.0$ Hz, 8H), 2.63 - 2.55 (m, 8H), 2.53 – 2.46 (m, 12H), 2.24 (t, $J = 6.0$ Hz, 8H, 4NH₂), 1.46 (p, $J = 8.0$ Hz, 10H). **^{13}C NMR** (100MHz, D_2O) δ_C (ppm):174.59, 50.58, 48.84, 38.01, 37.78, 33.21,31.54,29.21. **ESI-MS**: $m/z = 586.46$ (M^+).

2.2.3 Synthesis of PAMAM dendrimer with 8 OMe terminal groups **G3_(a)**

A stirred solution of methyl acrylate (13.1 mL, 0.14 mol.) in methanol (20 mL) was added to a solution of (**G2_(a)**) precursor (8.0 g, 0.013 mol.) in methanol (20 mL) at 0°C for one hour. The resulting mixture was then stirred for 24 hours. The progress of the reaction was monitored on TLC with CH_2Cl_2 : MeOH, 9:1 as eluent. The final product (14.5 g, 83.84%) was produced after the solvent was removed under a rotary evaporator at 40°C and the final product as a sticky yellow oil was vacuum dried for 12 hours at 50°C (10 mm Hg).



[G3_(a)]

Molecular Formula: $C_{59}H_{106}N_{10}O_{20}$, $R_f = 0.71$

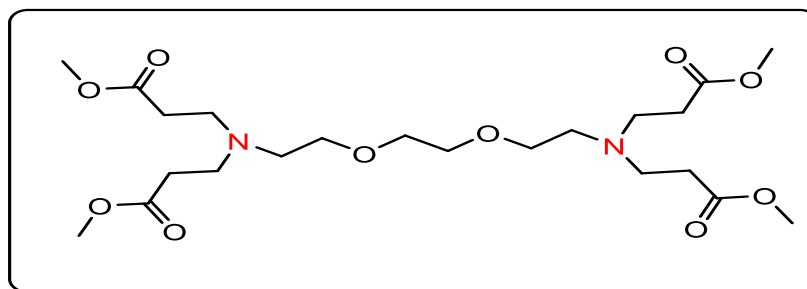
FT-IR-ATR (cm^{-1}): 3273 (amide, N-H), 2951, 2821 (C–H aliphatic), 1735 (ester, C=O), 1649 (amide, C=O). **1H NMR** (400 MHz, DMSO- d_6) δ_H (ppm): 8.14 (s, 4H, NH, amide), 3.57 (s, 24H, 8OCH₃), 2.90 (t, $J = 8.0$ Hz, 8H), 2.75 (t, $J = 8.0$ Hz,

16H), 2.51 (t, $J = 6.0$ Hz, 8H), 2.51 – 2.25 (m, 32H), 1.66 (t, $J = 8.0$ Hz, 4H), 1.50 – 1.39 (m, 10H). ^{13}C NMR (100 MHz, DMSO- d_6) δ_{C} (ppm): 174.79, 174.54, 53.16, 52.6, 51.7, 50.44, 48.84, 38.05, 37.73, 33.31, 25.02, 24.29. **ESI-MS**: $m/z = 1274.75$ (M^+).

2.3 Synthesis of the second line of PAMAM dendrimer

2.3.1 General procedure for preparation of PAMAM dendrimer with four OMe terminal groups G1_(b)

A solution of 1,2-bis(2-aminoethoxy) ethane (4.9 mL, 0.033 mol.) in methanol (25 mL) was added dropwise at 0°C for one hour to a solution of methyl acrylate (18 mL, 0.20 mol.) in Methanol (15 mL). The final mixture was stirred at 0°C for 45 minutes before being warmed to room temperature and stirred for 24 hours. The progress of the reaction was monitored on TLC with CH_2Cl_2 : MeOH 9:1 as eluent. The solvent and excess methyl acrylate were removed under reduced pressure at 40°C using a rotary evaporator, and the resulting colorless oily liquid was dried overnight to yield the final product (15 g, 90%).



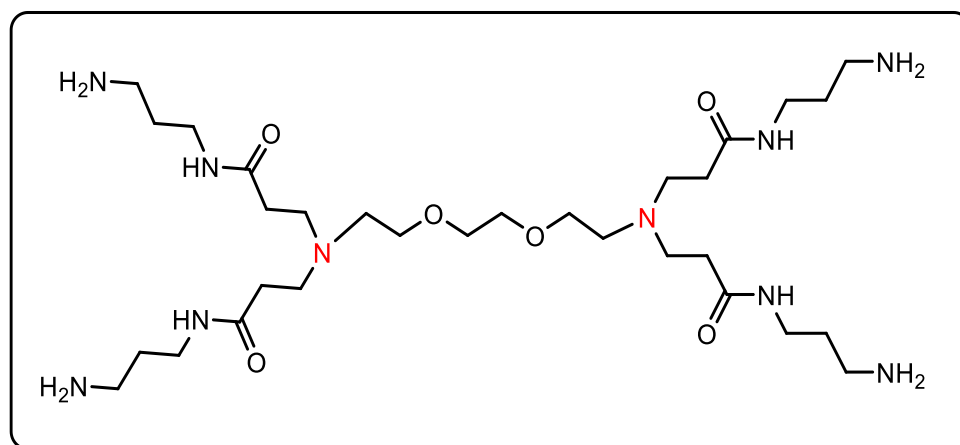
[G1_(b)]

Molecular Formula $\text{C}_{22}\text{H}_{40}\text{N}_2\text{O}_{10}$, $R_f = 0.69$,

FT-IR-ATR (cm^{-1}): 2951, 2862(C–H aliphatic), 1732 (ester, C=O); **^1H NMR** (400 MHz, DMSO- d_6) δ_{H} (ppm): 3.58 (s, 12H, 4OCH₃), 3.52 (s, 4H), 3.41 (t, $J = 6.0$ Hz, 4H), 2.71 (t, $J = 6.0$ Hz, 8H), 2.56 (t, $J = 6.0$ Hz, 4H), 2.40 (t, $J = 8.0$ Hz, 8H). **^{13}C NMR** (100MHz, DMSO- d_6) δ_{C} (ppm) 172.88, 70.19, 69.39, 52.97, 51.57, 49.77, 32.48; **ESI-MS**: $m/z = 492.26$ (M^+).

2.3.2 General procedure for preparation of four amine-terminated PAMAM dendrimer G2_(b)

A solution of (G1_(b)); PAMAM (5g,0.010mol.) in Methanol (15 mL) was slowly added to a vigorously stirred solution of Propane-1,3-diamine (40 mL, 0.01 mol.) in Methanol (50 mL) at 0°C over 40 minutes. The mixture was stirred after complete addition for 4 days at room temperature. The progress of the reaction was monitored on TLC with (CH₂Cl₂: MeOH 9:1 as eluent). At reduced pressure, the solvent was removed while maintaining the temperature below 50°C. The excess of Propane-1,3-diamine was then removed by washing the mixture with an azeotropic solution of a (9:1) toluene: methanol. Methanol azeotropic distillation was used to remove any remaining toluene. Finally, the remaining methanol is removed under a vacuum for 4 hours. The product was pale yellow sticky oil (Yield:6 g, 88.12 %).



[G2_(b)]

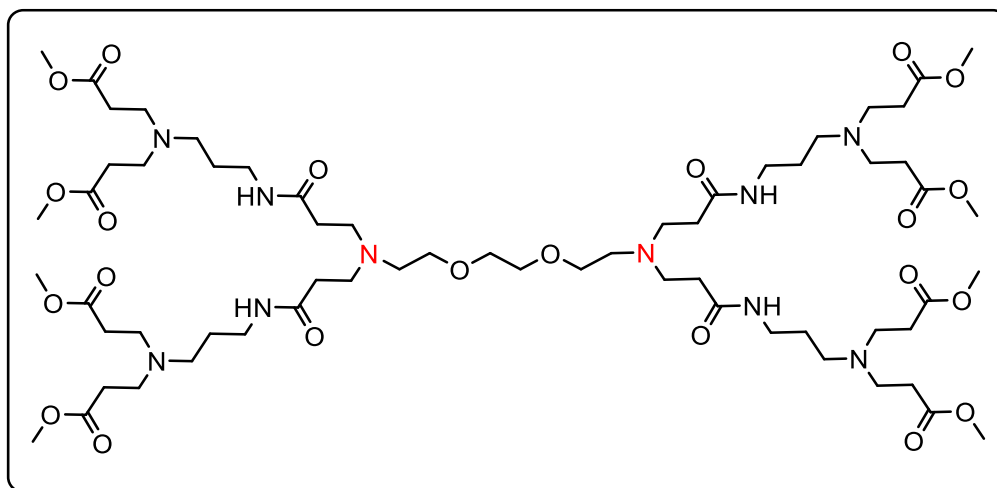
Molecular Formula C₃₀H₆₄N₁₀O₆ R_f = 0.56

FT-IR-ATR (cm⁻¹): 3342 (amide, N-H), 3275, 3245 (NH₂, amine) 2933, 2868 (C-H aliphatic), 1643 (amide, C=O). **¹HNMR** (400 MHz, DMSO-d₆) δ (ppm): 8.05 (bt, J = 5.8 Hz, 4H, 4NH), 3.48 – 3.40 (m, 8H), 3.06 (t, J = 6.0 Hz, 8H), 2.93 (t, J = 6.0 Hz, 4H), 2.66-2.49 (m, 24H), 2.17 (t, J = 8.0 Hz, 8H, 4NH₂), 1.41 (p, J = 8.0 Hz,

8H). ^{13}C NMR (100MHz, DMSO- d_6) δ (ppm) 171.77, 70.14, 69.16, 52.74, 48.85, 39.73, 37.20, 36.48, 33.40. **ESI-MS**: m/z = 660.50 (M^+).

2.3.3 General procedure for preparation of PAMAM dendrimer with eight OMe terminal groups $G3_{(b)}$

A solution of ($G2_{(b)}$); PAMAM (4g, 0.006 mol.) in methanol (15 mL) was added to a stirred solution of methyl acrylate (3 mL, 0.260 mol) in methanol (15 mL). The final mixture was stirred at 0°C for one hour before being allowed to warm to room temperature and stirred for another 24 hours. The progress of the reaction was monitored on TLC with CH_2Cl_2 : MeOH, 9:1 as eluent. The solvent was removed at 40°C under reduced pressure, and the resulting was dried under vacuum for 4 hours to obtain the final product as a sticky colorless oil (Yield:17.5 g, 83.34%).



[$G3_{(b)}$]

Molecular Formula $\text{C}_{62}\text{H}_{112}\text{N}_{10}\text{O}_{22}$, $R_f = 0.73$

FT-IR-ATR (cm^{-1}): 3284 (amide, N-H), 2937, 2823(C-H aliphatic), 1734 (ester, C=O), 1643 (amide, C=O). ^1H NMR (400 MHz, DMSO- d_6) δ_{H} (ppm): 8.12 (bt, $J = 4.0$ Hz, 4H, 4NH), 3.65 (s, 24H, 8OCH₃), 3.37-2.73 (m, 61H), 2.64 (t, $J = 8.0$ Hz, 4H), 2.53 - 1.65 (m, 19H). ^{13}C NMR (100 MHz, DMSO- d_6) δ_{C} (ppm): 174.97, 173.01, 70.14, 69.16, 54.70, 52.65, 51, 79,50.43, 49.42, 38.11, 36.35, 33.14, 25.02. **ESI-MS**: m/z =1348.80 (M^+).

2.4 Synthesis of Tri-imidazole derivatives (4a-4j)

2.4.1 By using traditional methods

General method

A mixture of 4,4'-dimethoxybenzil (0.270 g, 0.001mol.), various aromatic aldehyde (0.001 mol.), and NH₄OAc, (0.385 g ,0.005 mol.) with glacial acetic acid (15 mL) as solvent and catalyst in 50 mL round-bottom flask, the mixture was reflux at 120°C for (6-8) hours until the reaction was completed. The progress of the reaction was monitored by TLC with *n*-hexane: ethyl acetate 3:2 as eluent. A sufficient amount of cold water was added to the reaction vessel, followed by the addition of ammonium hydroxide solution drop by drop with stirring to obtain the solid, then the product was filtered and washed well with deionized water to remove any remnants of base and salts, the product was dried, and recrystallized from hot ethanol to offer the corresponding 2,4,5-triaryl-1*H*-imidazoles (**4a-4j**).

2.4.2 By using ultrasound methods

General method

4,4'-dimethoxybenzil (0.270g, 0.001mol), various aromatic aldehydes (0.001mol.) and ammonium acetate (0.385g, 0.005mol.) dissolved in glacial acetic acid (10 mL) were taken in a single neck round bottom flask. The flask with the reaction mixture was immersed in the water bath of an ultrasonic cleaner at room temperature for the prescribed time. The progress of the reaction was monitored on TLC with *n*-hexane: ethyl acetate 3:2 as eluent. The reaction mixture was poured on ice water (50 mL), and a precipitated solid was filtered, washed with water, dried and recrystallized from hot ethanol to get the corresponding 2,4,5-triaryl-1*H*-imidazoles (**4a-4j**).

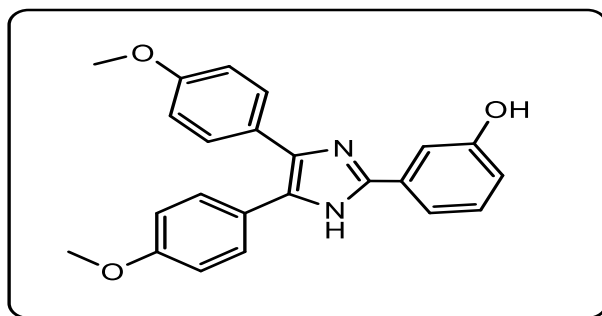
2.4.3 By using microwave-assisted methods

General method

4,4'-dimethoxybenzil (0.270 g, 0.001 mol), various aromatic aldehyde (0.001 mol.) and ammonium acetate (0.385g, 0.005 mol.) were taken in a flask with (1mL) of glacial acetic acid and subjected to microwave irradiation (380W) for an appropriate time until the reaction completion by TLC with *n*-hexane/ethyl acetate 3:2 as eluent. The mixture was cooled to room temperature and the resulting product was diluted with water and poured on crushed ice. The crude solid product was filtered, dried, and recrystallized from hot ethanol to obtain the corresponding 2,4,5-triaryl-1*H*-imidazoles (**4a-4j**).

2.5 Spectral and physical data of Tri-imidazole derivatives (4a-4j)

1) 3-(4,5-bis(4-methoxyphenyl)-1*H*-imidazole-2-yl) phenol (**4a**)

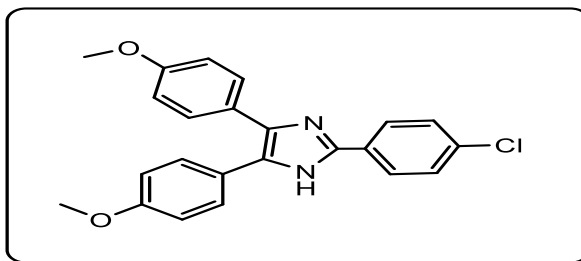


[4a]

Molecular formula: **C₂₃H₂₀N₂O₃**

Color: off-white powder. m.p.: 110-111°C, *R_f* = 0.65. **FT-IR** (KBr (cm⁻¹)): 3302 (N-H), 3151 (OH), 3055 (C-H, aromatic), 1654 (C=N). **¹H NMR** (500 MHz, DMSO-*d*₆) δ (ppm): 12.43 (s, 1H, **NH**), 9.54 (s, 1H, **OH**), 7.55 – 7.50 (m, 3H, ph-H), 7.45 (d, *J* = 5.0 Hz, 4H, ph-H), 7.26 (t, *J* = 10.0 Hz, 1H, ph-H), 6.96 (s, 1H, ph-H), 6.79 (dd, *J* = 10.0, 5.0 Hz, 3H, ph-H), 3.79 (s, 6H, (**OCH₃**)₂). **¹³C NMR** (125 MHz, DMSO-*d*₆) δ (ppm): 162.49, 158.79, 158.03, 145.42, 138.25, 135.22, 132.21, 130.09, 129.08, 128.89, 123.11, 119.99, 118.09, 116.42, 115.66, 114.30, 112.51, 55.54. **MS**: *m/z* = 372.1 (**M⁺**).

2)2-(4-chlorophenyl)-4,5-bis(4-methoxyphenyl)-1H-imidazole (4b)

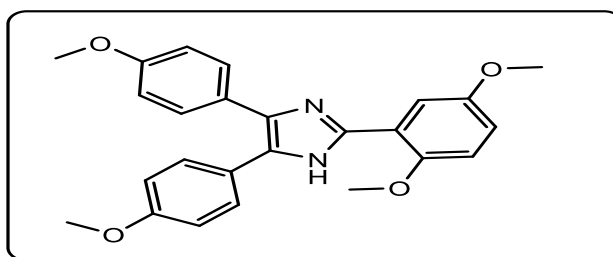


[4b]

Molecular formula: $C_{23}H_{19}ClN_2O_2$

Color: white powder, m.p.; 116-118 °C, $R_f = 0.72$. **FT-IR** (KBr (cm^{-1})): 3398 (N-H), 3097 (C-H, aromatic), 1654 (C=N). **1H NMR** (500 MHz, DMSO- d_6) δ_H (ppm): 12.61 (s, 1H, **NH**), 8.09 (d, $J = 5.0$ Hz, 2H, ph-H), 7.96 (d, $J = 10.0$ Hz, 1H, ph-H), 7.88 (d, $J = 10.0$ Hz, 1H, ph-H), 7.55 (dd, $J = 10.0, 5.0$ Hz, 3H, ph-H), 7.46 (d, $J = 5.0$ Hz, 4H, ph-H), 7.14 (d, $J = 10.0$ Hz, 1H, ph-H), 3.79 (s, 6H, (**OCH₃**)₂). **^{13}C NMR** (125 MHz, DMSO- d_6) δ_C (ppm): 166.94, 165.25, 150.48, 144.20, 138.27, 132.94, 132.49, 131.60, 129.83, 129.48, 129.17, 127.14, 125.91, 115.28, 114.34, 55.55. **MS**: $m/z = 390.1$ (M^+).

3) 2-(2,5-dimethoxyphenyl)-4,5-bis(4-methoxyphenyl)-1H-imidazole(4c)



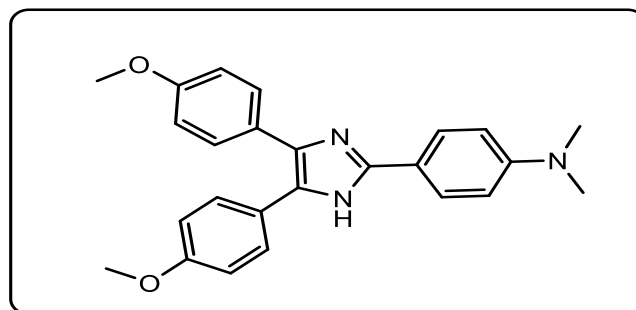
[4c]

Molecular formula: $C_{24}H_{24}N_2O_4$

Color: dark yellow powder, m.p.; 176-177°C, $R_f = 0.66$. **FT-IR** (KBr (cm^{-1})): 3352 (N-H), 3059 (C-H, aromatic), 1658 (C=N). **1H NMR** (500 MHz, DMSO- d_6) δ_H (ppm): 11.68 (s, 1H, **NH**), δ 7.63 (d, $J = 5.0$ Hz, 1H ph-H), 7.48 (d, $J = 10.0$ Hz, 2H ph-H),

7.40 (d, $J = 10.0$ Hz, 2H, ph-H), 7.09 (d, $J = 10.0$ Hz, 1H, ph-H), 7.01 (d, $J = 5.0$ Hz, 2H, ph-H), 6.95 (dd, $J = 10.0, 5.0$ Hz, 1H, ph-H), 6.89 (d, $J = 5.0$ Hz, 2H, ph-H), 3.88 (s, 3H, OCH₃), 3.81 (s, 3H, OCH₃), 3.76 (s, 6H, (OCH₃)₂). ¹³CNMR (125 MHz, DMSO-d₆) δ_C (ppm) 159.20, 158.37, 153.58, 150.64, 142.73, 136.29, 130.36, 128.67, 128.36, 127.00, 124.11, 120.03, 115.22, 114.49, 114.07, 113.74, 113.24, 56.40, 55.95, 55.63, MS: m/z = 416.2 (M⁺).

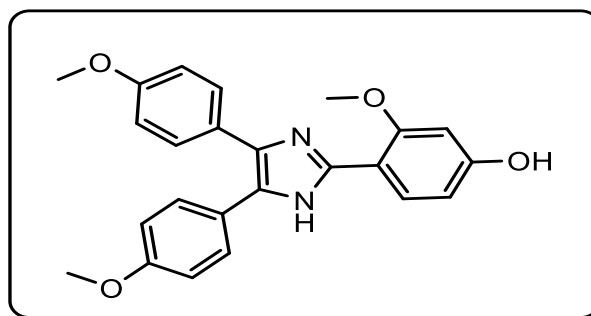
4) 4-(4,5-bis(4-methoxyphenyl)-1H-imidazol-2-yl)-N,N-dimethylaniline(4d)



[4d]

Molecular formula: C₂₅H₂₅N₃O₂

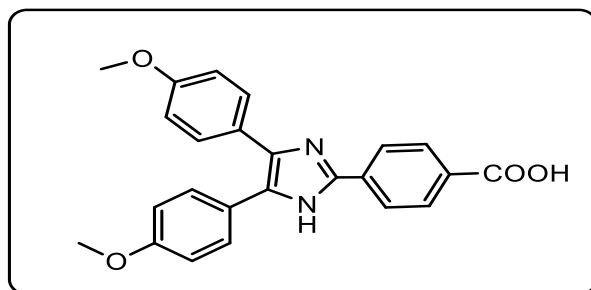
Color: grey powder, m.p.; 88-90°C, R_f = 0.71. FT-IR (KBr (cm⁻¹)) : 3414(N-H), 3047(C-H, aromatic) 1657 (C=N). ¹HNMR (500 MHz, DMSO-d₆) δ_H (ppm): 12.66 (s, 1H, NH), 7.92 (d, $J = 10.0$ Hz, 2H ph-H), 7.84 (d, $J = 10.0$ Hz, 1H ph-H), 7.46 (d, $J = 5.0$ Hz, 3H ph-H), 6.94 (d, $J = 10.0$ Hz, 3H ph-H), 6.80 (d, $J = 10.0$ Hz, 2H ph-H), 6.62 (d, $J = 5.0$ Hz, 1H ph-H), 3.78 (s, 6H, (OCH₃)₂), 2.96 (s, 6H, (NCH₃)₂). ¹³CNMR (125 MHz, DMSO-d₆) δ_C (ppm): 160.35, 158.62, 150.60, 146.26, 139.35, 136.83, 129.33, 126.66, 123.38, 122.65, 121.51, 119.02, 114.25, 112.38, 110.35, 55.51, 40.39. MS: m/z = 399.2 (M⁺).

5) 4-[(4,5-bis(4-methoxyphenyl)-1*H*-imidazol-2-yl)]-3-methoxyphenol(4e)

[4e]

Molecular formula: $C_{24}H_{22}N_2O_4$

Color: yellow-colored powder, m.p.; 123-125°C, $R_f = 0.68$. **FT-IR** (KBr (cm^{-1})): 3448 (N-H), 3236(O-H), 3088 (C-H aromatic), 1651(C=N). **1H NMR** (500 MHz, DMSO- d_6) δ_H (ppm): 12.28 (s, 1H, **NH**), 9.25 (s, 1H, **OH**), 7.87 (d, $J = 10.0$ Hz, 1H, ph-H), 7.61 (d, $J = 5.0$ Hz, 1H, ph-H), 7.50 (dd, $J = 10.0, 5.0$ Hz, 1H, ph-H), 7.43 (d, $J = 10.0$ Hz, 3H, ph-H), 7.14 (d, $J = 10.0$ Hz, 1H, ph-H), 6.94 (d, $J = 10.0$ Hz, 3H, ph-H), 6.85 (d, $J = 10.0$ Hz, 1H, ph-H), 3.86 (s, 3H, **OCH₃**), 3.77 (s, 6H, (**OCH₃**)₂). **^{13}C NMR** (125 MHz, DMSO- d_6) δ_C (ppm): 165.23, 163.25, 158.72, 148.14, 147.35, 145.86, 137.57, 132.50, 128.27, 125.91, 122.65, 118.70, 116.07, 115.28, 114.29, 109.74, 103.24, 56.14, 55.52. **MS**: $m/z = 400.2$ (M^+).

6) 4-[(4,5-bis(4-methoxyphenyl)-1*H*-imidazol-2-yl)] benzoic acid (4f)

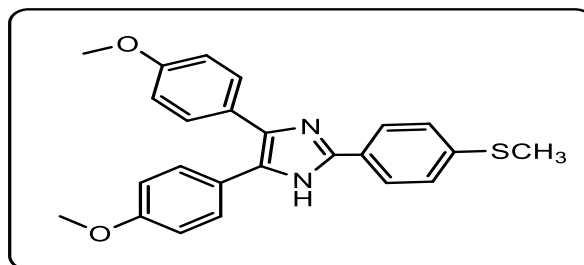
[4f]

Molecular formula: $C_{24}H_{20}N_2O_4$

Color: pale yellow colored powder, m.p.; 220-222°C, $R_f = 0.81$. **FT-IR** (KBr (cm^{-1})): 3483 (N-H), 3066 (C-H aromatic), 1647 (C=N). **1H NMR** (500 MHz, DMSO- d_6)

δ_{H} (ppm): δ 12.77 (s, 1H, COOHH), 12.48 (s, 1H, NHH), 8.21 (d, $J = 5.0$ Hz, 3H, ph-H), 8.05 (d, $J = 5.0$ Hz, 3H, ph-H), 7.48 (d, $J = 10.0$ Hz, 4H, ph-H), 6.96 (d, $J = 10.0$ Hz, 2H, ph-H), 3.79 (s, 6H, (OCHH₃)₂). ¹³CNMR (125 MHz, DMSO-*d*₆) δ_{C} (ppm): 167.97, 160.65, 160.25, 150.51, 138.36, 135.20, 133.43, 131.23, 129.89, 128.83, 127.91, 126.65, 123.60, 122.97, 114.26, 113.96, 55.56. MS: $m/z = 400.1(\text{M}^+)$.

7) 4,5-bis(4-methoxyphenyl)-2-(4-(methylthio) phenyl)-1*H*-imidazole(4g)

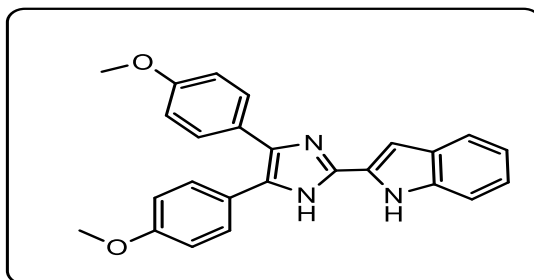


[4g]

Molecular formula: **C₂₄H₂₂N₂O₂S**

Color: white powder, m.p.; 112-114°C, $R_f = 0.73$. FT-IR (KBr (cm⁻¹)): 3402 (N-H), 3093 (C-H, aromatic), 1647 (C=N), 1570 (C=C). ¹HNMR (400 MHz, DMSO-*d*₆) δ_{H} (ppm): δ 12.49 (s, 1H, NHH), 8.01 (d, $J = 8.0$ Hz, 2H, ph-H), 7.44 (d, $J = 8.0$ Hz, 4H, ph-H), 7.35 (d, $J = 8.0$ Hz, 2H, ph-H), 7.01 (d, $J = 8.0$ Hz, 4H, ph-H), 3.77 (s, 6H, (OCHH₃)₂), 2.52 (s, 3H). ¹³CNMR (100 MHz, DMSO-*d*₆) δ_{C} (ppm): 162.52, 160.38, 152.80, 148.82, 144.97, 138.53, 127.55, 126.28, 125.94, 122.56, 121.34, 117.43, 115.90, 115.16, 111.96, 55.54, 14.94. MS: $m/z = 402.1(\text{M}^+)$.

8) 2-(4,5-bis(4-methoxyphenyl)-1*H*-imidazol-2-yl)-1*H*-indole(4h)

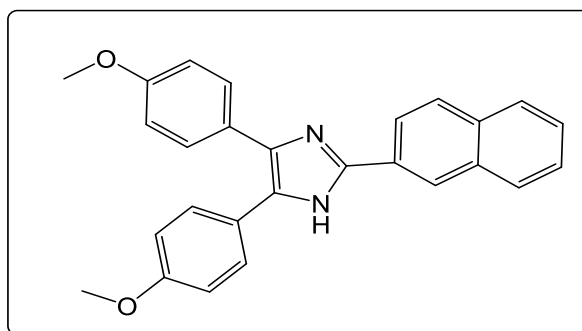


[4h]

Molecular formula: $C_{27}H_{22}N_2O_2$

Color: off-white, m.p.; 118-120°C, $R_f = 0.56$. **FT-IR** (KBr (cm^{-1})): 3367 (N–H), 3063(C–H, aromatic)1654 (C=N), 1573 (C=C). **1H NMR** (400 MHz, DMSO- d_6) δ_H (ppm): 12.12 (s, 1H, **NH**), 11.35 (s, 1H, **NH**), 8.47 (d, $J = 8.0$ Hz, 1H, ph-H), 7.97 (d, $J = 4.0$ Hz, 1H, ph-H), 7.87 (d, $J = 8.0$ Hz, 2H, ph-H), 7.45 (d, $J = 8.0$ Hz, 2H, ph-H), 7.14 (d, $J = 8.0$ Hz, 4H, ph-H), 6.97 (d, $J = 8.0$ Hz, 3H, ph-H), 3.87 (s, 6H, (O**H**₃)₂). **^{13}C NMR** (100 MHz, DMSO- d_6) δ_C (ppm) 165.24, 164.44, 147.50, 143.46, 136.69, 132.51, 125.86, 125.52, 123.94, 122.25, 121.99, 121.28, 120.06, 115.31, 112.88, 112.01, 107.48, 105.87, 103.76, 56.32. **MS**: $m/z = 395.2(M^+)$.

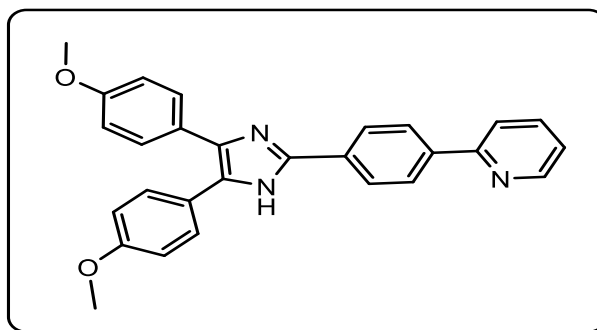
9) 4,5-bis(4-methoxyphenyl)-2-(naphthalen-2-yl)-1H-imidazole(4i)



[4i]

Molecular formula: $C_{27}H_{22}N_2O_2$

Color: pale green, m.p.; 109-111°C, $R_f = 0.62$. **FT-IR** (KBr (cm^{-1})) :3360 (N–H), 3066(C–H, aromatic)1654 (C=N), 1570 (C=C). **1H NMR** (400 MHz, DMSO- d_6) δ_H (ppm): 12.01 (s, 1H, **NH**), 8.60 (s, 1H, ph-H), 8.26 (d, $J = 7.6$, 1H, ph-H), 8.01 – 7.93 (m, 3H, ph-H), 7.87 (d, $J = 8.9$ Hz, 1H, ph-H), 7.56 – 7.49 (m, 6H, ph-H), 6.97 (d, $J = 8.3$ Hz, 3H, ph-H), 3.79 (s, 6H, (O**H**₃)₂). **^{13}C NMR** (100 MHz, DMSO- d_6) δ_C (ppm) 165.24, 158.86, 150.63, 145.24, 133.48, 133.07, 132.51, 128.66, 128.52, 128.37, 128.18, 127.13, 126.68, 125.86, 123.91, 123.86, 115.30, 114.34, 112.96, 55.5. **MS**: $m/z = 406.2(M^+)$.

10) 2-(4-(4,5-bis(4-methoxyphenyl)-1*H*-imidazol-2-yl)phenyl)pyridine(4j)

[4j]

Molecular formula: $C_{28}H_{23}N_3O_2$

Color: dark yellow, m.p.; 103-105°C, $R_f = 0.60$, **FT-IR** (KBr (cm^{-1})): 3441 (N-H), 3073 (C-H, aromatic) 1651 (C=N), 1570 (C=C). **1H NMR** (400 MHz, DMSO- d_6) δ_H (ppm): 12.66 (s, 1H, **NH**), 8.69 (d, $J = 8.0, 1.7$ Hz, 1H, ph-H), 8.20 (d, $J = 8.0$ Hz, 2H, ph-H), 8.04 (d, $J = 8.0$ Hz, 1H, ph-H), 7.90 – 7.86 (m, 4H, ph-H), 7.49 – 7.35 (m, 5H, ph-H), 7.13 (d, $J = 8.0$ Hz, 2H, ph-H), 6.96 (d, $J = 8.0$ Hz, 1H, ph-H), 3.78 (s, 6H, (OCH $_3$) $_2$). **^{13}C NMR** (100 MHz, DMSO- d_6) δ_C (ppm): 165.24, 155.89, 150.30, 150.03, 144.86, 138.33, 137.95, 137.69, 136.69, 132.50, 131.71, 131.42, 130.42, 127.60, 127.22, 125.86, 125.76, 123.09, 120.62, 115.29, 55.55. **MS**: $m/z = 433.2$ (M^+).

2.5 Synthesis of Tetra-imidazole derivatives (5a-5j)

2.5.1 By using traditional methods

General method

4-(methylthio) benzaldehyde (0.132 mL, 0.001 mol.), benzil (0.210 g, 0.001 mol.), aromatic substituted amines (0.001 mol.), and NH_4OAc (0.385 g, 0.005 mol.) were placed in a round bottom flask and reflux with (15 mL) of absolute ethanol and (3 drops) of conc. H_2SO_4 as a catalyst for (8-10) hours. The reaction progress was monitored using thin-layer chromatography TLC *n*-hexane: ethyl acetate 3:2 as eluent.

After the completion of the reaction, the reaction was cooled to room temperature, after that the precipitated product was filtered, washed with an excess amount of water, and recrystallized with absolute ethanol to obtain the desired imidazoles (**5a-4j**).

2.5.2 By using ultrasounds methods

General method

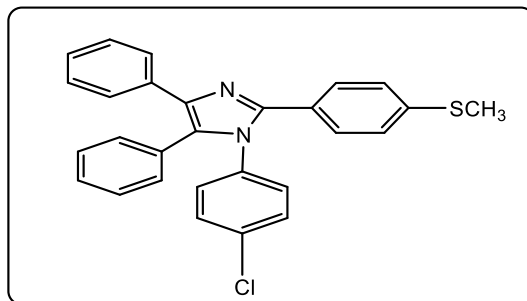
A mixture of benzil (0.210 g, 0.001 mol.), 4-(methylthio) benzaldehyde (0.132 mL, 0.001 mol.), and ammonium acetate (0.385 g, 0.005 mol.) in ethanol (10 mL) was taken, and conc. H₂SO₄ as a catalyst (3 drops) was added. Then, the reaction mixture was exposed to ultrasonic irradiation at 40°C for a prescribed time. Thin layer chromatography (TLC) was used to monitor the progress of the reaction *n*-hexane: ethyl acetate 3:2 as eluent. After that, the reaction mixture was filtered, and the resulting solid was washed successively with distilled water, dried, and recrystallized with hot ethanol to get the corresponding imidazole derivatives (**5a-5j**).

2.5.3 By using microwave-assisted methods

General method

Benzil (0.210g,0.001mol), 4-(methylthio) benzaldehyde (0.132 mL, 0.001mol.), aromatic substituted amines (0.001mol.) and ammonium acetate (0.385 g0.005 mol.) were taken in a flask with ethanol (1 mL) and (3 drops) of conc. H₂SO₄ as a catalyst and subjected to microwave irradiation (380W) for an appropriate time until the completion of reaction by TLC with *n*-hexane: ethyl acetate, 3:2 as eluent. The mixture was cooled to room temperature and the resulting product was diluted with water and poured on crushed ice. The crude solid product was filtered, dried, and recrystallized with hot ethanol to obtain the corresponding imidazoles (**5a-5j**).

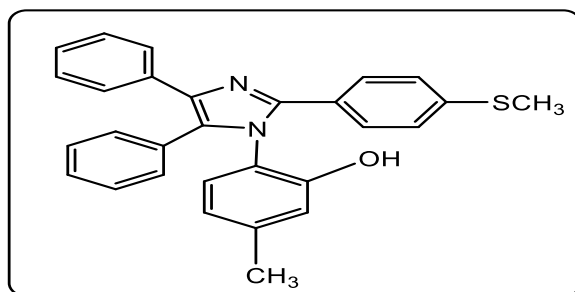
2.6 Spectral and physical data of Tetra-imidazole derivatives

1)1-(4-Chlorophenyl)-2-(4-(methylthio) phenyl)-4,5-diphenyl-1*H*-imidazole (5a)

[4a]

Molecular formula: $C_{28}H_{21}ClN_2S$

Color: White solid, m.p.:196-198°C, $R_f = 0.75$. **FT-IR** (KBr, cm^{-1}): 3061 (C–H aromatic), 2983(C–H aliphatic), 1602 (C=N), 1558 (C=C), 653 (C-S), 756 (C-Cl); **1H NMR** (500 MHz, DMSO- d_6) δ_H (ppm): δ 7.53 (d, $J = 10.0$ Hz, 2H, ph-H), 7.41 (d, $J = 10.0$ Hz, 3H, ph-H), 7.34 (t, $J = 7.5$ Hz, 6H,ph-H), 7.28 – 7.24 (m, 4H,ph-H), 7.19 (dd, $J = 15.0, 10.0$ Hz, 3H, ph-H), 2.46 (s, 3H, SCH₃). **^{13}C NMR** (125 MHz, DMSO) δ_C (ppm) :148.11, 141.21, 139.58, 137.40, 136.09, 135.05, 134.73, 133.78, 131.62, 131.04, 130.68, 129.71, 129.13, 129.03, 128.64, 126.98, 126.88, 126.81, 125.65, 14.64. **MS**: $m/z = 452.1$ (M^+).

2)5-methyl-2-{2-[4-(methylthio) phenyl]-4,5-diphenyl-1*H*-imidazol-1-yl}phenol(5b)

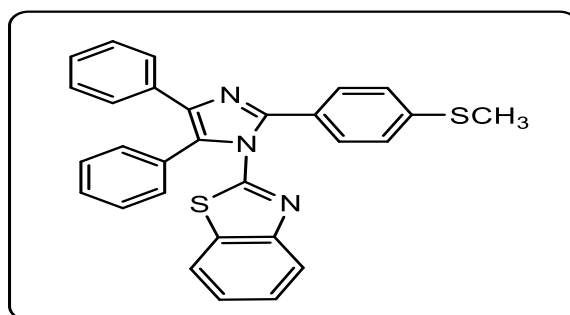
[5b]

Molecular formula: $C_{29}H_{24}N_2OS$

Color: Pale yellow powder, m.p.:256-258°C, $R_f = 0.40$ **FT-IR** (KBr, cm^{-1}): :3224(OH), 3064 (C–H aromatic), 2964 (C–H aliphatic), 1604 (C=N), 1517(C=C), 617(C-S). **1H NMR** (500 MHz, DMSO- d_6) δ_H (ppm): 9.67 (s, 1H, OH), 7.49(dd, J

= 10.0, 5.0 Hz, 4H, ph-H), 7.30 – 7.24 (m, 7H, ph-H), 7.18 (d, $J = 10.0$ Hz, 3H, ph-H), 6.99 (d, $J = 10.0$ Hz, 1H, ph-H), 6.93 (s, 1H), 6.78 (d, $J = 5.0$ Hz, 1H, ph-H), 2.46 (s, 3H, SCH₃), 2.08 (s, 3H, CH₃). ¹³CNMR (125 MHz, DMSO-*d*₆) δ_c (ppm): 151.91, 146.28, 139.07, 137.04, 135.16, 132.00, 131.74, 131.17, 130.97, 130.60, 128.76, 128.70, 128.56, 128.36, 128.24, 127.73, 126.78, 126.71, 125.61, 124.26, 116.62, 20.20, 14.69. MS : $m/z = 448.2$ (M⁺).

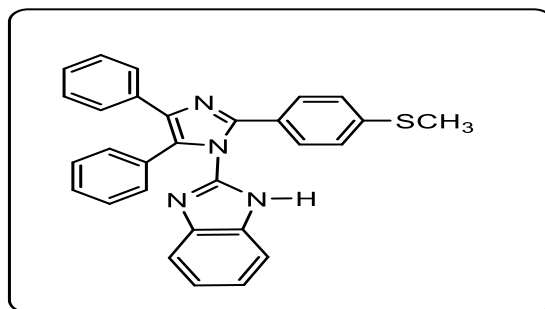
3)2-{2-[4-(Methylthio)phenyl]-4,5-diphenyl-1H-imidazolyl}benzo[d]thiazole(5c)



[5c]

Molecular formula: C₂₉H₂₁N₃S₂

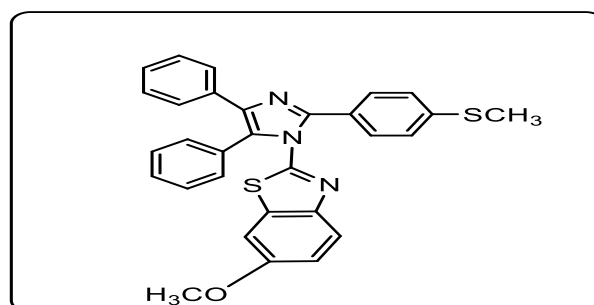
Color: Cream powder, m.p.: 240-241°C, $R_f = 0.53$. FT-IR (KBr, (cm⁻¹)): 3076 (C–H aromatic), 2969 (C–H aliphatic), 1602 (C=N), 1502 (C=C), 673 (C–S). ¹HNMR (500 MHz, DMSO-*d*₆) δ_H (ppm): 8.03 (d, $J = 10.0$ Hz, 2H), 7.53 (dd, $J = 20.0, 10.0$ Hz, 2H, ph-H), 7.44 (t, $J = 10.0$ Hz, 3H, ph-H), 7.37 (t, $J = 10.0$ Hz, 3H, Ph-H), 7.30 (t, $J = 10.0$ Hz, 2H, Ph-H), 7.23 (d, $J = 5.0$ Hz, 1H, ph-H), 2.53 (s, 3H, SCH₃). ¹³CNMR (125 MHz, DMSO-*d*₆) δ_c (ppm): 157.61, 156.42, 145.71, 142.39, 138.29, 133.80, 132.00, 131.27, 131.18, 129.92, 129.41, 129.12, 128.51, 128.41, 128.34, 128.19, 127.17, 125.95, 125.84, 123.08, 120.75, 120.42, 14.95. MS: $m/z = 457.1$ (M⁺).

4)2-{2-[4-(Methylthio) phenyl]-4,5-diphenyl-1*H*-imidazol-1-yl}-1*H*-benzo[d]imidazole(5d)

[5d]

Molecular formula: **C₂₉H₂₂N₄S**

Color: white powder, m.p. :248-250°C, R_f=0.65. **FT-IR** (KBr, (cm⁻¹)): 3318 (N-H), 3028 (C-H aromatic), 2978 (C-H aliphatic), 1602 (C=N), 1508 (C=C), 677(C-S). **¹H NMR** (500 MHz, DMSO-d₆) δ_H (ppm): 12.66 (s, 1H, **NH**), 8.08 (d, *J* = 8.4 Hz, 2H, Ph-H), 7.57 (dd, *J* = 30.0, 10.0 Hz, 5H, ph-H), 7.45 (t, *J* = 7.5 Hz, 3H, ph-H), 7.39 (d, *J* = 10.0 Hz, 4H, ph-H), 7.32 (t, *J* = 7.5 Hz, 3H, ph-H), 7.25 (t, *J* = 5.0 Hz, 2H, ph-H), 2.54 (s, 3H, **SCH₃**). **¹³CNMR** (125 MHz, DMSO-d₆) δ_C (ppm): 154.71, 148.73, 145.73, 138.91, 137.57, 135.69, 131.60, 129.10, 128.90, 128.64, 128.58, 128.19, 127.57, 127.44, 126.97, 126.35, 126.14, 125.54, 125.11, 124.74, 121.14, 112.24, 14.99. **MS**: m/z = 458.2 (M⁺).

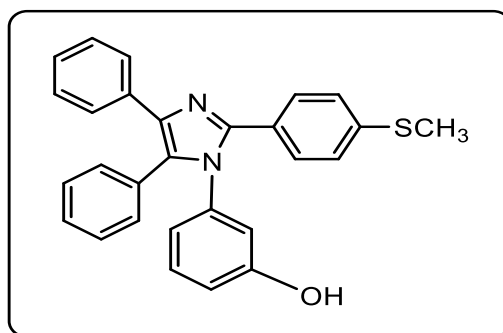
5)6-Methoxy-2-{2-[4-(methylthio) phenyl]-4,5-diphenyl-1*H*-imidazol-yl}benzo[d]thiazole(5e)

[5e]

Molecular formula: $C_{30}H_{23}N_3OS_2$

Color: cream crystal, m.p.:206-207°C, $R_f = 0.83$. **FT-IR** (KBr, cm^{-1}):3022(C-H aromatic), 2914 (C-H aliphatic), 1606 (C=N), 1502 (C=C), 671 (C-S). **1H NMR** (400 MHz, DMSO-d6) δ_H (ppm) : 8.03 (d, $J = 8.0$ Hz, 2H, ph-H), 7.53 (dd, $J = 8.0, 4.0$ Hz, 4H, ph-H), 7.44 (t, $J = 8.0$ Hz, 3H, ph-H), 7.36 (d, $J = 8.0$ Hz, 4H, ph-H), 7.30 (t, $J = 6.0$ Hz, 3H, ph-H), 7.23 (d, $J = 8.0$ Hz, 1H, ph-H), 3.80 (s, 3H, OCH_3), 2.53 (s, 3H, SCH_3). **^{13}C NMR** (100 MHz, DMSO-d6) δ_C (ppm): 157.11, 156.42, 156.00, 143.60, 142.41, 137.27, 134.42, 134.42, 132.53, 131.45, 129.92, 129.35, 129.05, 128.87, 128.55, 128.47, 128.21, 128.13, 125.95, 122.24, 110.82, 106.76, 54.56, 14.92. **MS**: $m/z = 505.1$ (M^+).

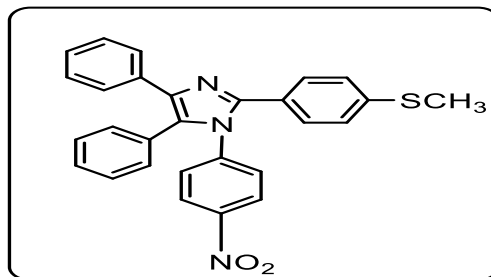
6) 3-{2-[4-(Methylthio) phenyl]-4,5-diphenyl-1H-imidazol-1-yl} phenol(5f)



[5f]

Molecular formula: $C_{28}H_{22}N_2OS$

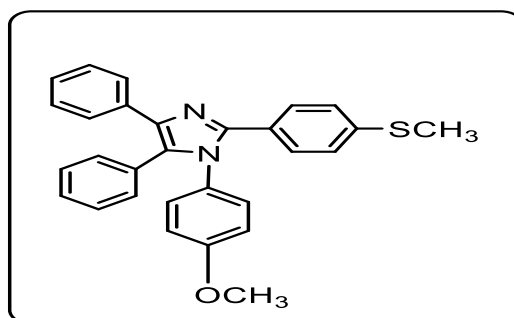
Color: brown powder, m.p.:223-226°C, $R_f = 0.43$ FT-IR (KBr, cm^{-1}): 3433(OH),3053 (C-H aromatic), 2924 (C-H aliphatic), 1620 (C=N), 1600 (C=C), 677(C-S). **1H NMR** (400 MHz, DMSO-d6): δ_H (ppm): 9.78 (s,1H, OH), 8.04 (d, $J = 8.0$ Hz, 2H,Ph-H), 7.55 (dd, $J = 16.0, 8.0$ Hz, 5H, Ph-H), 7.44 (t, $J = 8.0$ Hz, 3H,Ph-H), 7.36 (d, $J = 8.0, Hz, 4H,Ph-H$), 7.31 (t, $J = 8.0$ Hz, 3H Ph-H,), 7.23 (d, $J = 8.0$ Hz, 1H Ph-H) 2.54 (s, 3H, SCH_3). **^{13}C NMR** (125 MHz, DMSO-d6) δ_C (ppm):155.19,145.71, 138.90, 136.01, 135.62, 132.73,131.56,130.07, 129.29, 129.12,128.95, 128.89, 128.84, 128.65, 128.16,127.40, 126.65, 126.12, 125.60, 117.41,113.60,14.68 .**MS**: $m/z = 434.1$ (M^+).

7)2-{4-[(Methylthio)phenyl]-1-(4-nitrophenyl)}-4,5-diphenyl-1*H*-imidazole (5g)

[5g]

Molecular formula: $C_{28}H_{21}N_3O_2S$

Color: pale yellow crystal, m.p.:247-248°C, $R_f=0.58$. **FT-IR** (KBr, cm^{-1}): 3030 (C–H aromatic), 2983 (C–H aliphatic), 1608 (C=N), 1508 (C=C), 1539 and 1379 (NO_2),672(C-S). **1H NMR** (500 MHz, DMSO- d_6) δ_H (ppm): 8.06 (d, $J = 10.0$ Hz, 2H, Ph-H), 7.55 (dd, $J = 10.0, 5.0$ Hz, 5H ,Ph-H), 7.46 (t, $J = 10.0$ Hz, 3H ,Ph-H), 7.38 (d, $J = 10.0$ Hz, 3H ,Ph.-H), 7.32 (t, $J = 10.0$ Hz, 3H ,Ph-H), 7.24 (d, $J = 5.0$ Hz, 1H, Ph-H),2.55(s, 3H,SCH₃). **^{13}C NMR** (125 MHz, DMSO- d_6) δ_C (ppm):148.81 145.71, 138.90, 137.55, 135.67, 131.58, 129.11, 128.89, 128.64, 128.57, 128.30, 128.17, 127.55, 127.42, 126.97, 126.34, 126.12,124.44,124.12,14.97.**MS**: $m/z = 463.1$ (M^+).

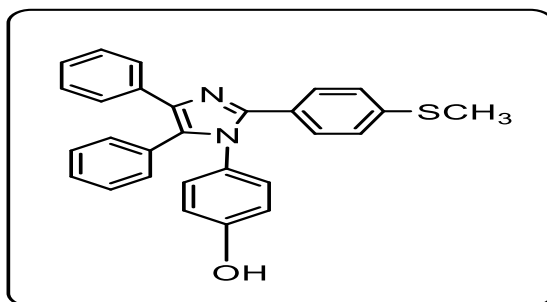
8)1-(4-Methoxyphenyl)-2-(4-(methylthio) phenyl)-4,5-diphenyl-1*H*-imidazole(5h)

[5h]

Molecular formula: **C₂₉H₂₄N₂OS**

Color: pale green powder, m.p.: 118-119°C, $R_f=0.63$. **FT-IR** (KBr, (cm⁻¹)): 3045 (C–H aromatic), 2985 (C–H aliphatic), 1602(C=N), 1512 (C=C), 1251(C-O) 731(C-S). **¹H NMR** (400 MHz, DMSO-*d*₆) δ_H (ppm) : 8.57 (d, $J = 8.0$ Hz, 2H , Ph-H), 8.05 (d, $J = 8.0$ Hz, 1H , Ph-H), 7.94 (d, $J = 8.0$ Hz, 3H , Ph-H), 7.84 (d, $J = 8.0$ Hz, 2H, Ph-H), 7.65 – 7.16 (m, 7H, ph-H), 6.97 (d, $J = 8.0$ Hz, 3H , Ph-H), 6.86 (d, $J = 8.0$ Hz, 2H , Ph-H), 3.77 (s, 3H, OCH₃), 2.53 (s, 3H, SCH₃). **¹³CNMR** (100 MHz, DMSO-*d*₆) δ_C (ppm): 158.06, 146.26, 142.76, 137.12, 132.69, 131.59, 130.32, 130.08, 129.97, 129.24, 128.94, 128.60, 126.80, 126.28, 126.10, 125.80, 125.54, 122.82, 114.84, 55.73, 14.62. **MS**: $m/z = 448.2$ (M⁺)

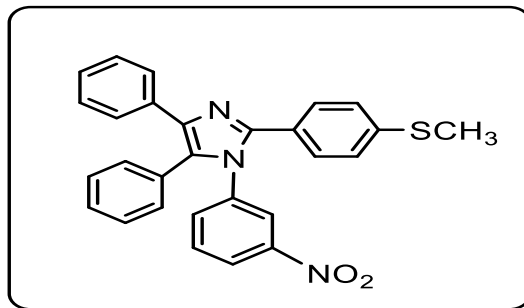
9) 4-(2-(4-(Methylthio) phenyl)-4,5-diphenyl-1H-imidazol-1-yl)phenol(5i)



[5i]

Molecular formula: **C₂₈H₂₂N₂OS**

Color: pale orange powder, m.p.: 288-290°C, $R_f = 0.51$. **FT-IR** (KBr, (cm⁻¹)) : 3273(OH), 3032 (C–H aromatic), 2970 (C–H aliphatic), 1608 (C=N), 1506(C=C), 651(C-S). **¹H NMR** (400 MHz, DMSO-*d*₆) δ_H (ppm) : 10.13 (s, 1H, OH), 8.04 (d, $J = 8.4$ Hz, 1H ,Ph-H), 7.51 – 7.36 (m, 5H, Ph-H), 7.26 (dd, $J = 16.0, 8.0$ Hz, 6H ,Ph-H), 7.15 (t, $J = 8.0$ Hz, 4H, Ph-H), 6.86 (d, $J = 8.0$, Hz, 1H, Ph-H), 6.73 (t, $J = 8.0$ Hz, 1H ,Ph-H), 2.45 (s, 3H, SCH₃). **¹³CNMR** (100 MHz, DMSO-*d*₆) δ_C (ppm): 154.12, 146.30, 145.69, 139.11, 137.01, 135.09, 131.93, 131.13, 130.98, 128.78, 128.26, 127.64, 126.74, 126.28, 126.09, 125.56, 124.56, 119.64, 116.80, 14.67. **MS**: $m/z = 434.1$ (M⁺)

10)2-(4-(Methylthio) phenyl)-1-(3-nitrophenyl)-4,5-diphenyl-1*H*-imidazole(5j)

[5j]

Molecular formula: $C_{28}H_{21}N_3O_2S$

Color: yellow powder, m.p.: 242-244°C, $R_f=0.61$. **FT-IR** (KBr, cm^{-1}): 3057 (C–H aromatic), 2982 (C–H aliphatic), 1600 (C=N), 1508(C=C), 1512,1365 (NO_2), 651(C–S). **1H NMR** (400 MHz, DMSO- d_6) δ_H (ppm) : δ 8.70 (s, 1H, Ph-H), 8.11 – 7.89 (m, 5H, Ph-H), 7.81 (t, $J = 8.0$ Hz, 1H, Ph-H), 7.64 (t, $J = 8.0$ Hz, 4H, Ph-H), 7.53 (dd, $J = 16.0, 8.0$ Hz, 2H, Ph-H), 7.40 (d, $J = 8.0$ Hz, 2H, Ph-H), 7.32 (d, $J = 8.0$ Hz, 3H, Ph-H), 2.53 (s, 3H, SCH₃). **^{13}C NMR** (100 MHz, DMSO- d_6) δ_C (ppm): 149.00, 145.68, 144.38, 138.88, 136.03, 132.68, 131.04, 130.08, 129.98, 129.92, 129.11, 128.87, 128.72, 128.64, 127.52, 127.34, 126.27, 126.08, 125.74, 120.75, 115.74, 14.52. **MS**: $m/z = 468.1$ (M^+).

CHAPTER THREE

RESULTS AND

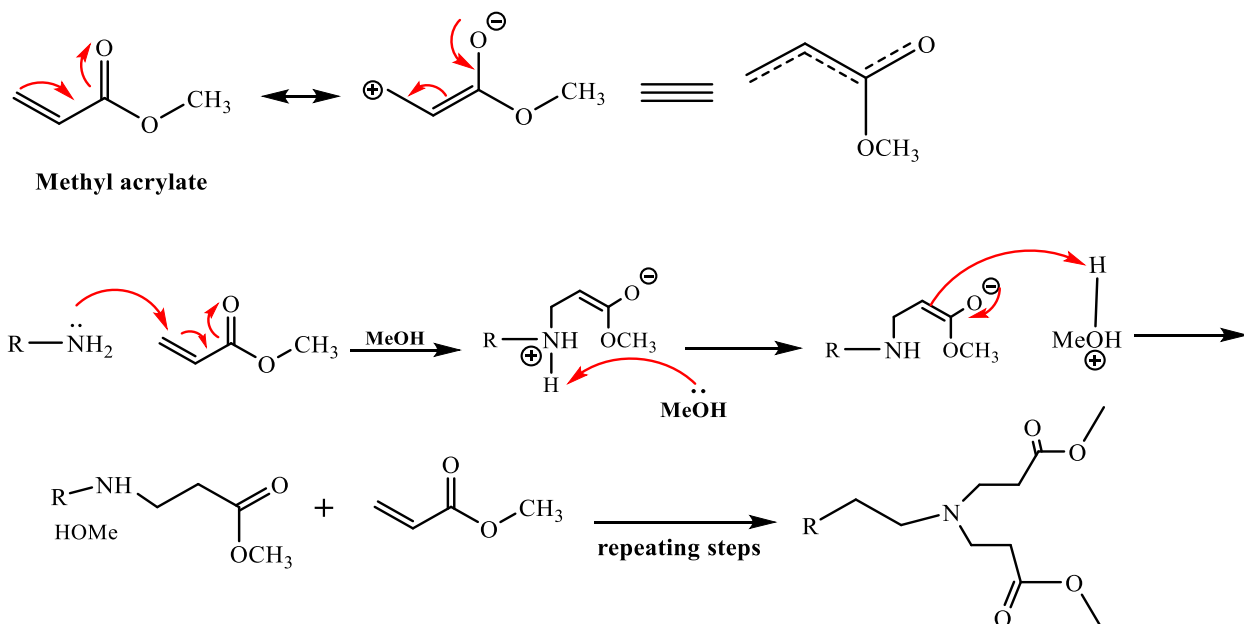
DISCUSSION

3.1. Synthesis of PAMAM dendrimers

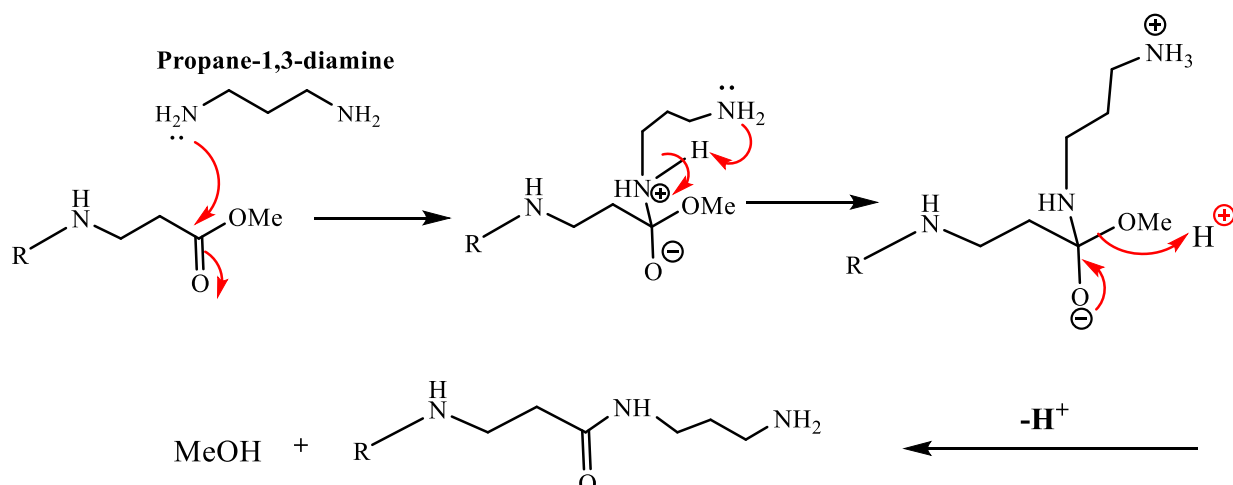
The selection of a core molecule is the most important stage in the divergent synthesis of the dendrimer since the shape and number of generations are largely dependent on the structure of the core. We carried out an initial synthesis using two different primary amines as potential cores for this purpose. PAMAM dendrimers were selected because they are simple to synthesize and modify. The divergent strategy was chosen since it has proven successful in generating PAMAM dendrimers [112,113]. This approach needs the formation of dendrimers of the smallest generation, starting with (**G1**) and continuing to greater generation dendrimers. Repeated reactions produce higher than three generations.

The synthesis of PAMAM dendrimers includes a repeating series of two simple reactions: 1,4-Michael addition to producing ester-terminated PAMAM dendrimers and followed by an amination process to generate amine-terminated PAMAM dendrimers [114].

Methyl acrylate (serving as the α, β -unsaturated carbonyl molecule) is used during the 1,4-Michael addition stage. The carbonyl substituent exerts an electron-withdrawing action on the alkene, resulting in the formation of δ -positive on the terminal carbon, which is finally stabilized by resonance. Thus, the β -carbon will be electropositive, exposing it to Propane-1,3-diamine (PDA) as a nucleophilic attack. When the first step finishes, the second Michael reactions take place. The Scheme (3-1) illustrates the mechanism of the 1,4-Michael addition.

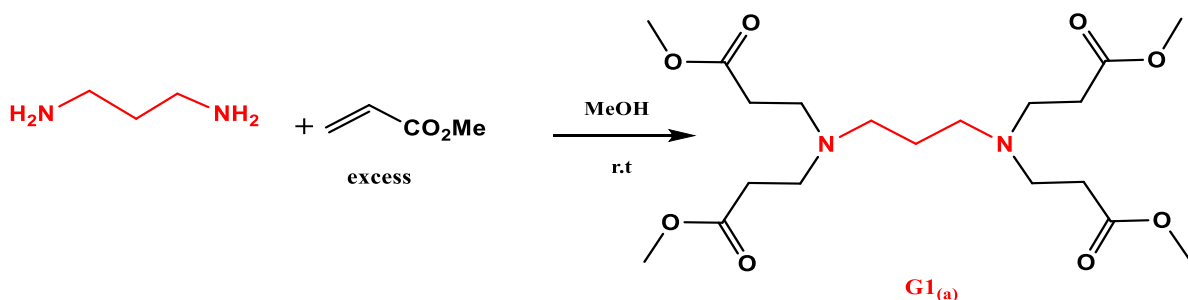


After the 1,4-Michael addition is complete, the second step occurs. At this step, the lone pair of nitrogen from PDA serves as a nucleophile, attacking the carbonyl carbon of the methoxy group. The resulting intermediate is then protonated by the second terminal amine. After this, the methoxy group is converted into a good leaving group, and the positive charge is removed through deprotonation, yielding the end product and alcohol. This step is known as the amidation reaction and is illustrated in Scheme below (3-2). The size of the dendrimer is increased by repeating the two steps. The following sections provide additional detail about the process.



3.1.1 Synthesis of 1st generation PAMAM dendrimers (**G1_(a)**)

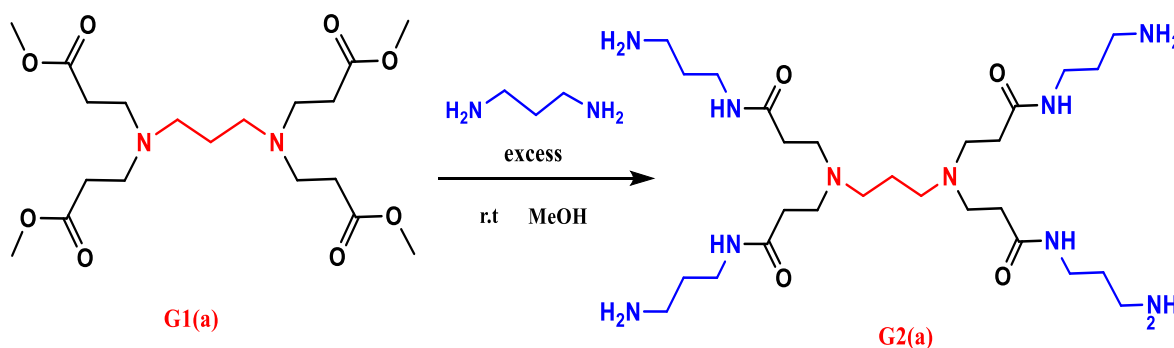
The first-generation dendrimers (**G1_(a)**) were produced by adding an excess of methyl acrylate (MA) and six equivalents of methyl acrylate drop by drop to PDA dissolving in methanol at 0°C (Scheme 3-3). The solution was then stirred at room temperature. The amount of methyl acrylate added increased in proportion to the dendrimer size but remained constant in comparison to the number of amines. The size of the generation determined how long it took for the reaction to complete; after each generation, tiny amounts of reaction solution were taken and Monitor by TLC to see whether the reaction was complete or not. It took 24 hours to synthesize **G1_(a)**, 96 hours to synthesize **G2_(a)**, and 24 hours to synthesize **G3_(a)**. The most crucial step was at the end of the reaction when any starting material had to be removed to avoid unwanted side reactions during the synthesis of the next generation. The excess of methyl acrylate was then removed from the solvent using a rotary evaporator. ¹HNMR was used to establish that all MA had been eliminated. By following this decrease, the alkene peaks at 6.14 ppm and 6.36 ppm become reduced as shown in Figure (3-4). The product was next placed under a vacuum to ensure complete elimination; dendrimers were obtained as viscous oil products. The viscosity of dendrimers increased as the size of PAMAM dendrimers increased, and the color gradually darkened.



Scheme 3-3 Synthesis of **G1_(a)**

3.1.2 Synthesis of 2nd generation PAMAM dendrimers (G_{2(a)})

The second-generation PAMAM dendrimers (G_{2(a)}) were synthesized by adding an excess of PDA to solutions of ester-terminated PAMAM dendrimers at 0°C, drop by drop. After that, the mixture was stirred at room temperature. 12.5-fold of PDA per ester group is required to ensure that the reaction proceeds to completion, producing homogenous dendrimers and preventing undesirable side reactions. In general, the reaction to produce second-generation dendrimers was longer than the reaction to produce one-generation dendrimers, and the amination reaction was much slower than the 1,4-Micheal reaction. After the reaction, the excess PDA was removed using a 9:1 azeotropic mixture of toluene and methanol. At this stage, it was crucial to completely remove PDA since it bonds to the amide or amine groups of the dendrimers, making it much more difficult to remove than methyl acrylate. The washing process was continued until this spectral peak was no longer visible. (Scheme 3-4) shows the synthesis of PAMAM dendrimers of the second generation.

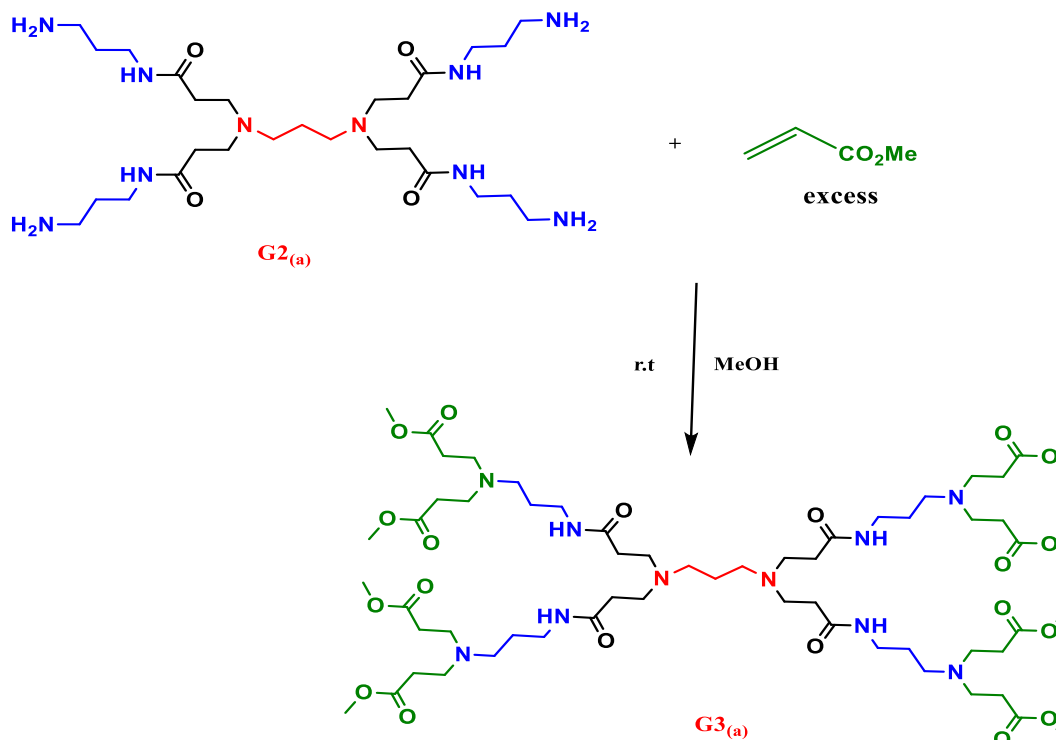


Scheme 3- 4 Synthesis of G_{2(a)}

3.1.3 Synthesis of 3rd generation PAMAM dendrimers (G_{3(a)})

In methanol, the amine-terminated PAMAM (G_{2(a)}) was dissolved. Methyl acrylate was poured into the G_{2(a)} solution drop by drop at 0 °C. At room temperature, the reaction mixture was allowed to stir. The rotary evaporation device then

removed the solvent and the methyl acrylate. The conversion of the $G2_{(a)}$ dendrimer amine-terminated groups into the dendrimer ester-terminated group ($G3_{(a)}$) was depicted in Scheme (3-5).



Scheme 3- 5 Synthesis of $G3_{(a)}$

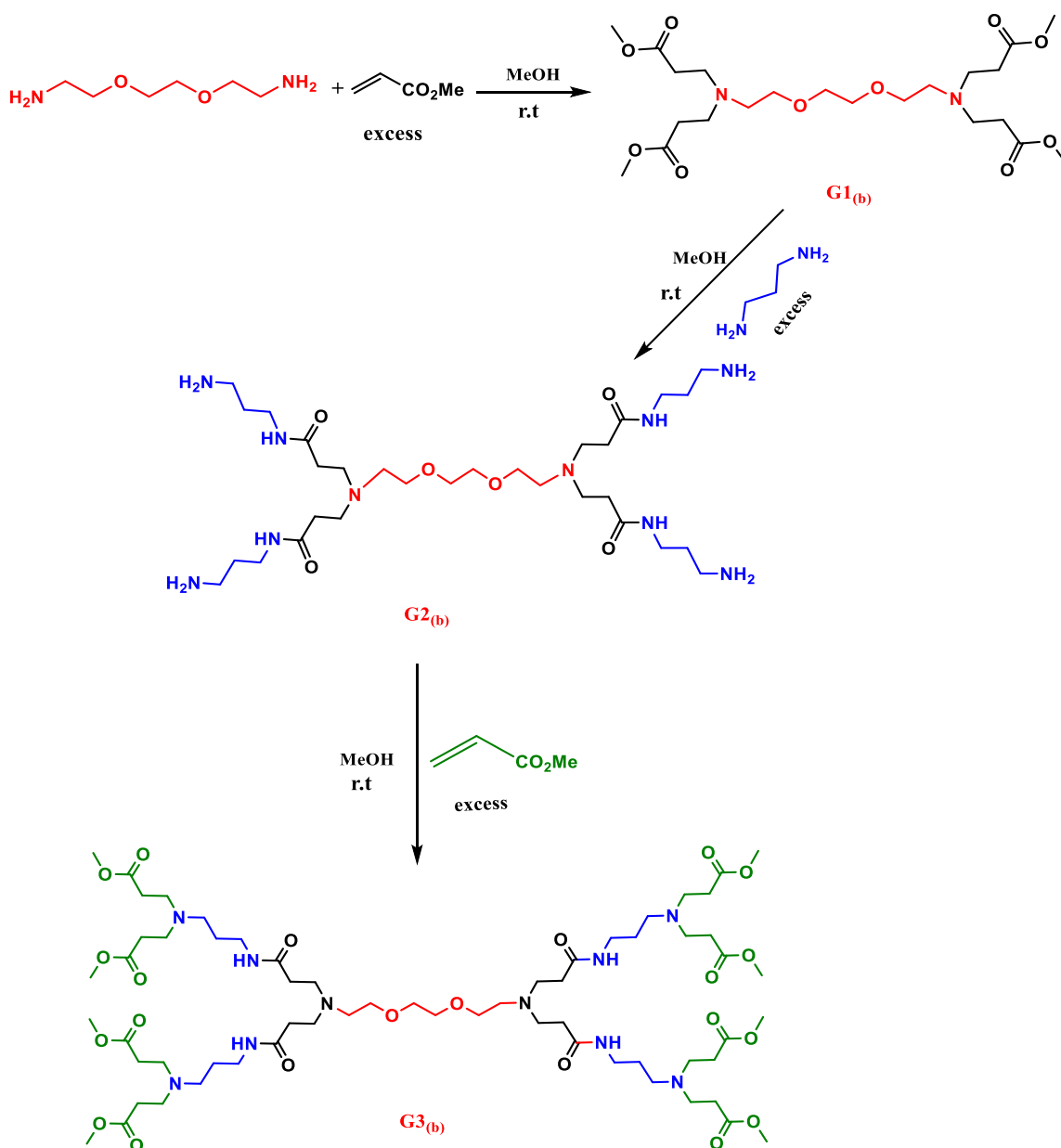
3.1.4 Synthesis of PAMAM dendrimers ($G1_{(b)}$, $G2_{(b)}$ and $G3_{(b)}$)

A $G1_{(b)}$ (PAMAM dendrimer) was synthesized by adding methyl acrylate dropwise to 1,2-bis(2-aminoethoxy) ethane dissolved in methanol at 0°C . This was allowed to return to room temperature before being stirred for 24 hours. Under vacuum, the excess of methanol and methyl acrylate was removed. Using FTIR, the complete removal of these compounds was monitored. The product was a colorless and viscous oil. This is the result of the Michael addition involving the nucleophilic center of 1,2-bis(2-aminoethoxy) ethane.

The nucleophilic core reacted with six equivalents of methyl acrylates to generate a **G1_(b)** containing four ester terminal groups. This ester-terminated compound (**G1_(b)**) was next dissolved in methanol and added dropwise to (PDA) and stirred at 0 °C for one hour. The solution was cooled to room temperature and allowed to stirring for 96 hours. An azeotropic mixture of toluene and methanol ratio (9:1) was used to remove excess PDA. FTIR confirmed the complete elimination of PDA. The oil was mildly viscous and honey-colored.

This was a product of the amidation reaction, which produced a **G2_(b)** along with four amine terminal groups. Both of these steps, namely Michael addition and amidation, were employed iteratively to produce higher generations of dendrimers.

In methanol, the **G2_(b)** was dissolved, methyl acrylate was next added drop by drop to the stirred solution at 0 °C for one hour. The mixture was brought down to room temperature and allowed to stirring for 24 hours. Utilizing a rotary evaporator, excess methyl acrylate was removed. This product was a **G3_(b)** with eight ester terminal groups along with higher viscosity. The growth of **G1_(b)** into **G3_(b)** is depicted schematically in Scheme (3-6). This schematic reaction demonstrates how the Michael addition process and amidation process can be used repeatedly to generate dendrimers of higher generations.



Scheme 3-6 The synthesis of PAMAM dendrimers G1_(b) to G3_(b), with each Michael addition and amidation step

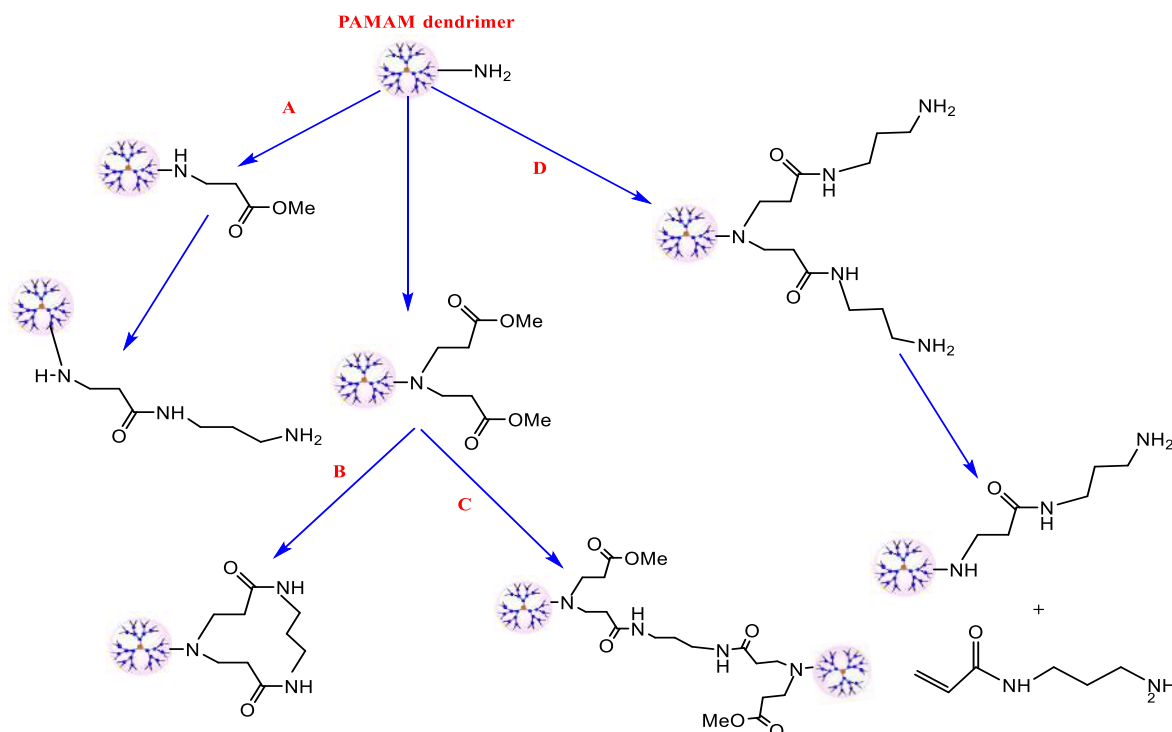
3.2 Purification of the PAMAM dendrimers

Purification for the dendrimer is essential for removing excess reactants from the final products, as their presence causes problems in the next generation.

The Michael addition reaction was carried out on the PAMAM dendrimer of the G1 generation, and due to the highly volatile nature of the methyl acrylate, the excess

compound that had been employed could be rapidly removed using a rotary evaporator made the process of removal quite simple. On the other hand, Propane-1,3-diamine (PDA) is difficult to remove from an amidation step, which means it affects the synthetic procedure that comes after it. Incomplete removal of PDA can act as a new initiator core, which will react with MA to generate unwanted by-products if the process is not carried out correctly. Incomplete purification of PDA may also lead to unwanted side effects including cross-linking products or cyclization substances. The effects of residual diamine are depicted in Scheme (3-7). Because of their physical and structural similarity to the wanted dendrimer, these different side reactions generations were very difficult to remove.

Strong hydrogen bonds that exist between the dendrimer and diamine are responsible for the difficulty that is associated with the purification process. Methanol is an excellent competitor for hydrogen bonding and can displace an excess of diamine. When employing a rotary evaporator, however, because methanol has a lower boiling point than diamine, it is removed from the mixture before any of the diamine is completely evaporated. This provides an obstacle to the process. Washing repeatedly using an azeotropic combination was the most effective method to eradicate diamine. This mixture contains a 9:1 ratio of toluene and methanol. Methanol can be a beneficial competition when using an azeotropic solution because toluene will increase the boiling point of the solution and make it easier to remove the diamine.



Scheme 3-7 Side -reactions in PAMAM dendrimer synthesis, **(A)** Incomplete Michael reaction **(B)** Intermolecular cyclization **(C)** Dimer formation **(D)** retro-Michael reaction

3.3 Characterization of PAMAM dendrimers ($G_{1(a)}$, $G_{2(a)}$ and $G_{3(a)}$)

FTIR (ATR) ^1H NMR, ^{13}C NMR spectroscopy, and Mass spectrometry are the most essential tools for the analysis of dendrimers. Initially, FT-IR spectroscopy is useful for identifying the main functional group in the all-generations structure. The FTIR spectrum was measured to distinguish between the functional groups of the three generations as shown in Figures (3-1, 3-2, and 3-3). For the 1st generation ($G_{1(a)}$) (Fig. 3-1), the presence of a carbon carbonyl ester peak at 1737 cm^{-1} gives good evidence that ester-terminated groups are formed. For the 2nd generation ($G_{2(a)}$), there is one peak for the amide carbonyl at 1641 cm^{-1} as shown in Figure (3-2). The 3rd generation ($G_{3(a)}$) exhibits two peaks, one for the ester carbonyl at around 1735 cm^{-1} and a second for the amide carbonyl at about 1649 cm^{-1} , (Fig. 3-3).

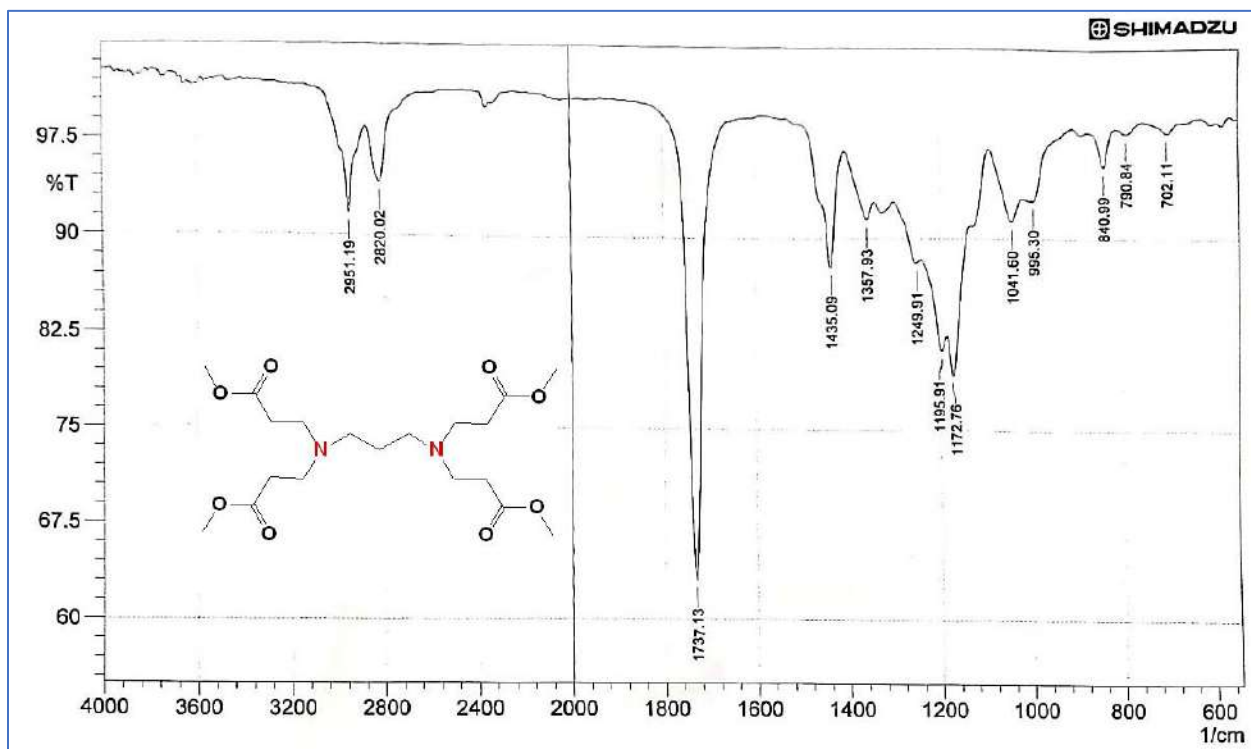


Figure 3-1 FTIR of G1(a)

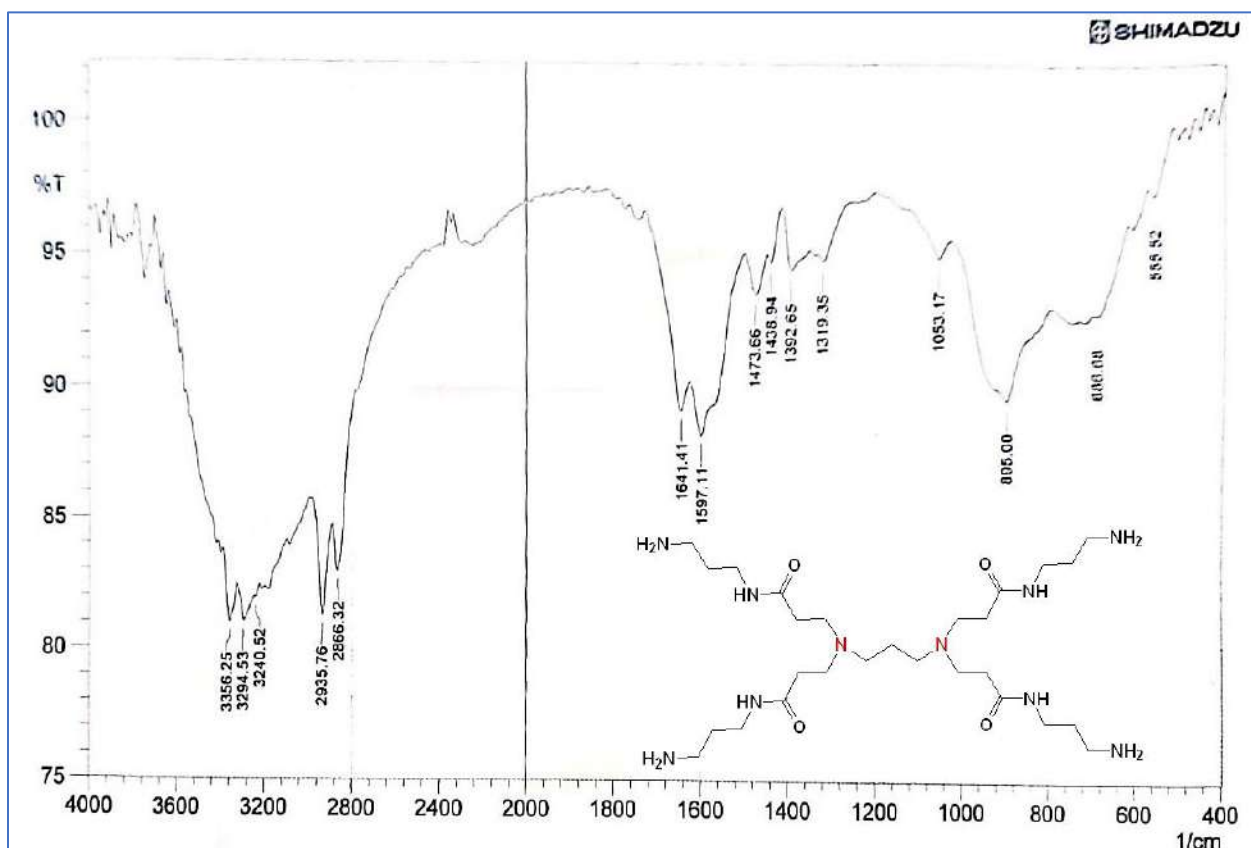


Figure 3-2 FTIR of G2(a)

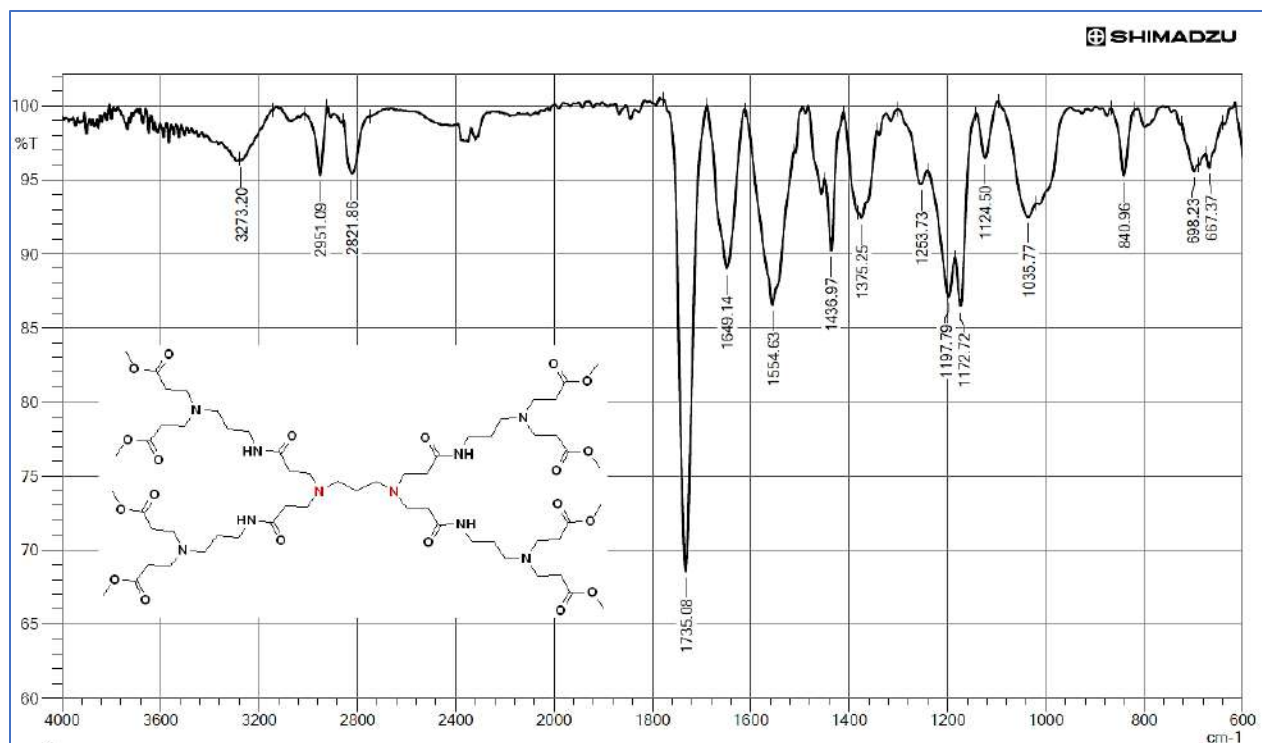
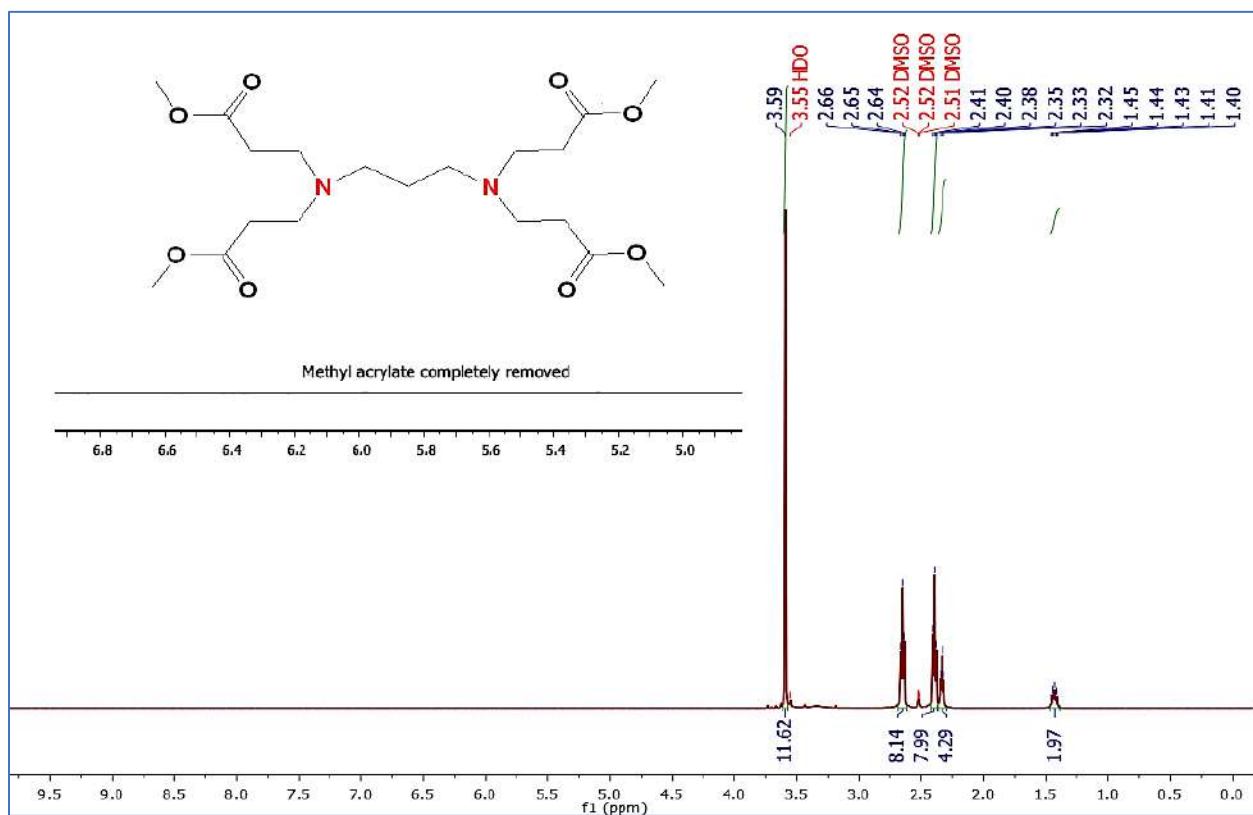
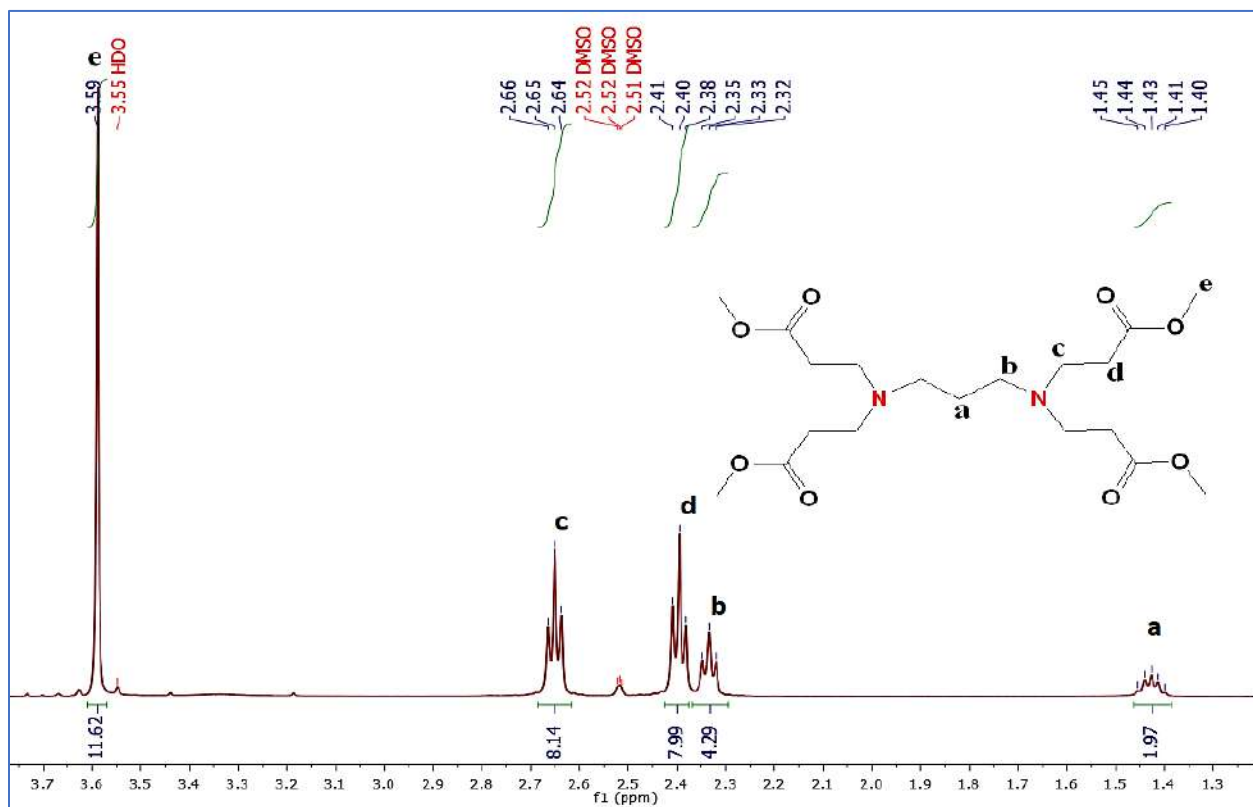
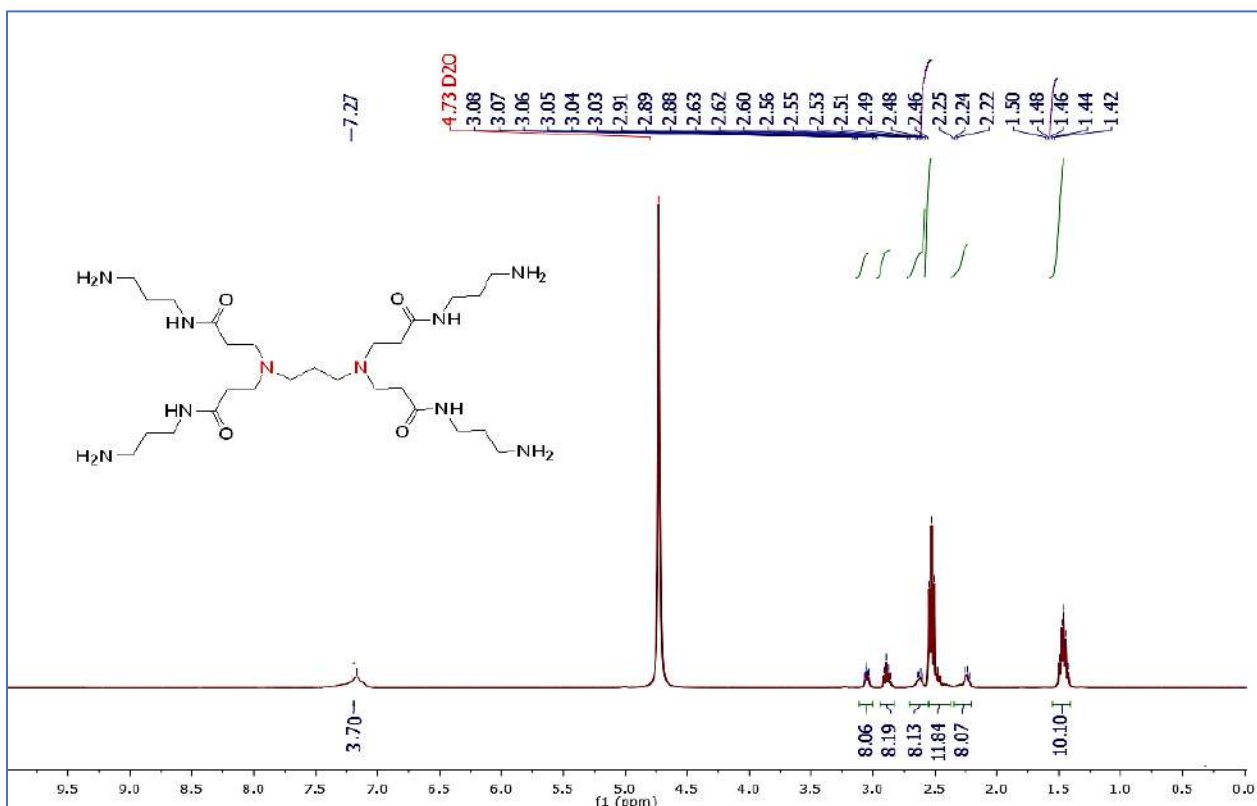
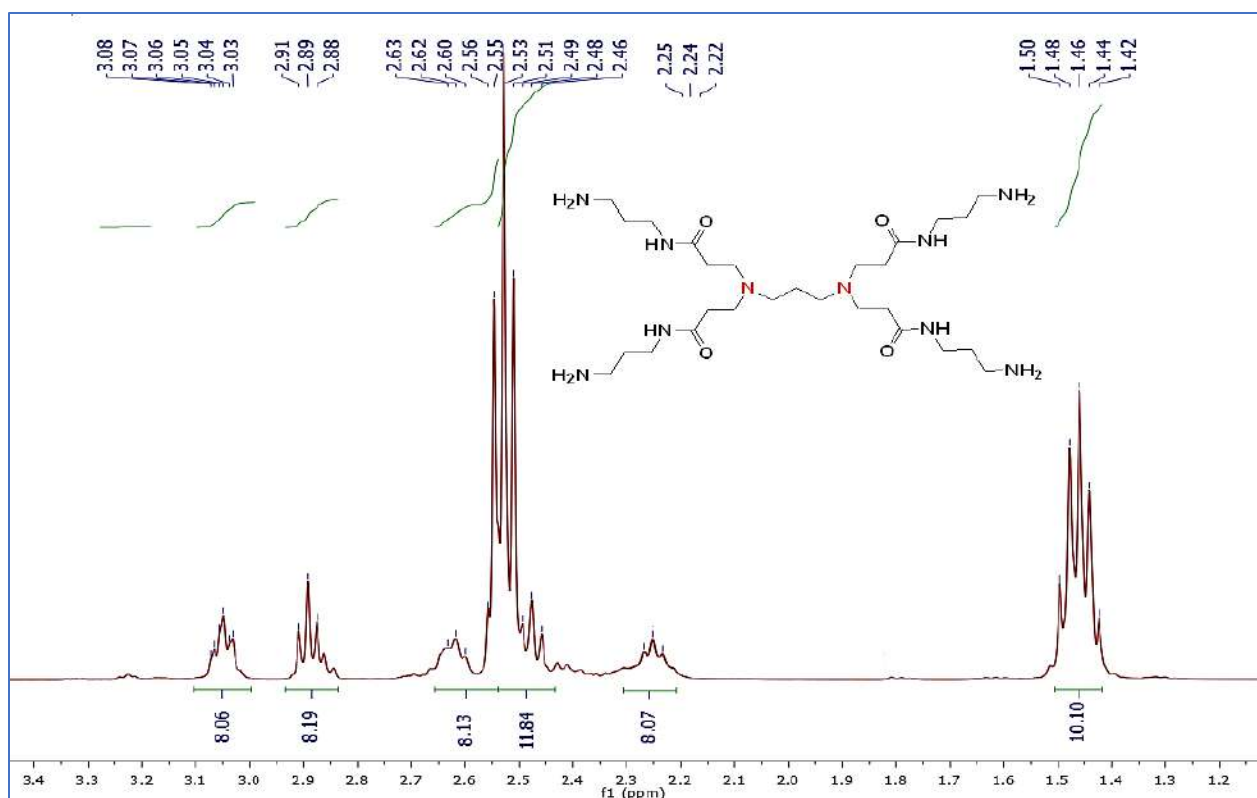


Figure 3-3 FTIR of $G3_{(a)}$

^1H NMR is suitable for all generations of dendrimers. For the spectrum of the $G1_{(a)}$, (Fig. 3-4), the absence of peaks between 5.52 ppm and 6.52 ppm in the spectrum indicates that all methyl-acrylate has been removed, (Fig. 3-5) for zoomed $G1_{(a)}$ exhibited five different peaks; there is a singlet peak at 3.59 ppm that corresponds to 12 methoxy protons (e) in the first-generation dendrimers. The two methylene-proton groups in the dendrimer correspond to two triplet peaks at 2.66 ppm and 2.32 ppm (c, d) the peak of the core protons (PDA) is observed at 2.40 ppm (b) and 1.94 ppm (a). As for the $G2_{(a)}$, it exhibited the same peaks, as well as the amide proton (NH) peak at 7.27 ppm, (Figs. 3-6 and 3-7). However, as the size of the generation increases, some of the peaks appear broader and overlap. The spectrum of PAMAM dendrimer ($G3_{(a)}$) with eight terminal (OCH_3 groups) exhibits a strong peak at 3.65 ppm from the ester terminal, (Fig. 3.8). Integration values are consistent with the structure's theoretical values, which is compelling evidence that all PAMAM dendrimers have formed.

Figure 3-4 ^1H NMR of G1_(a) (DMSO-d₆, 500MHz)Figure 3-5 ^1H NMR Expanded of G1_(a) (DMSO-d₆, 500MHz)

Figure 3-6 $^1\text{H NMR}$ of G2(a) (D₂O, 400MHz)Figure 3-7 $^1\text{H NMR}$ Expanded of G2(a) (D₂O, 400MHz)

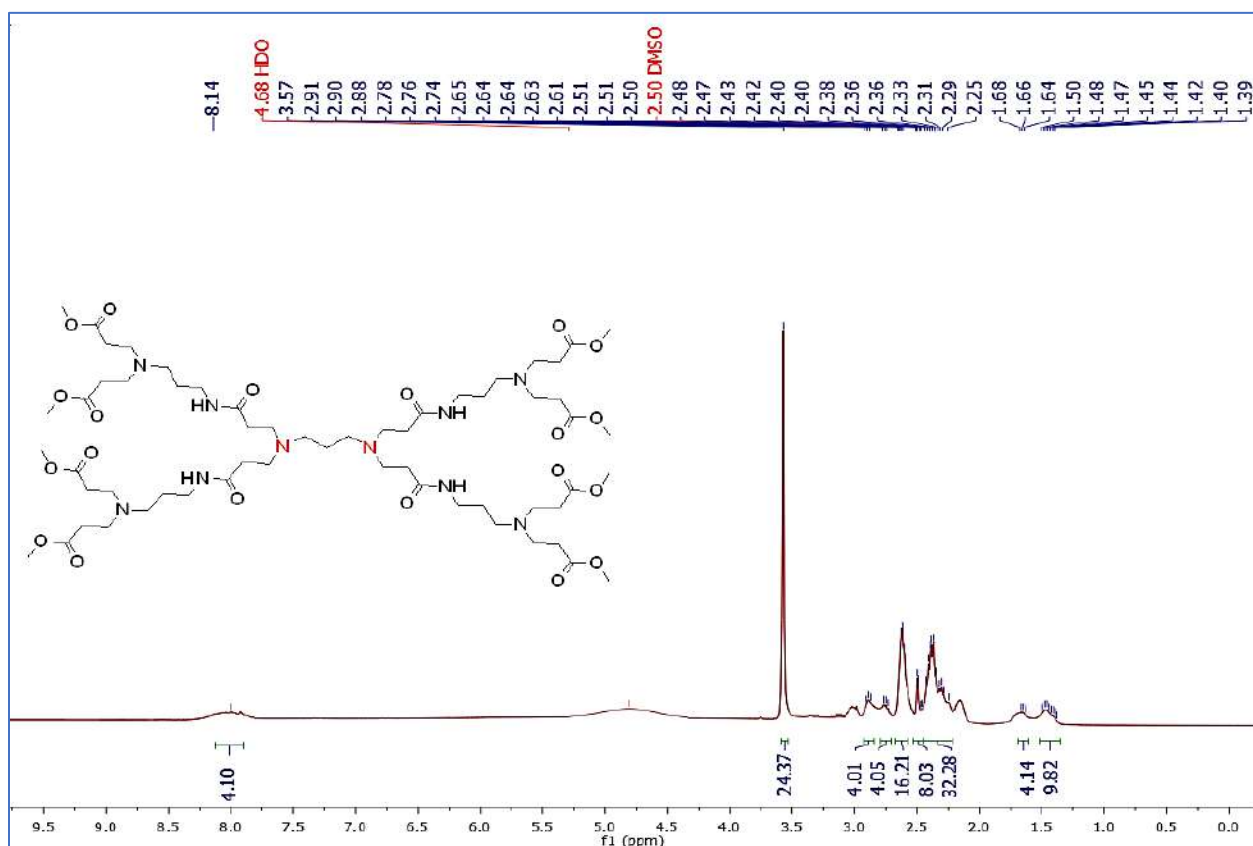
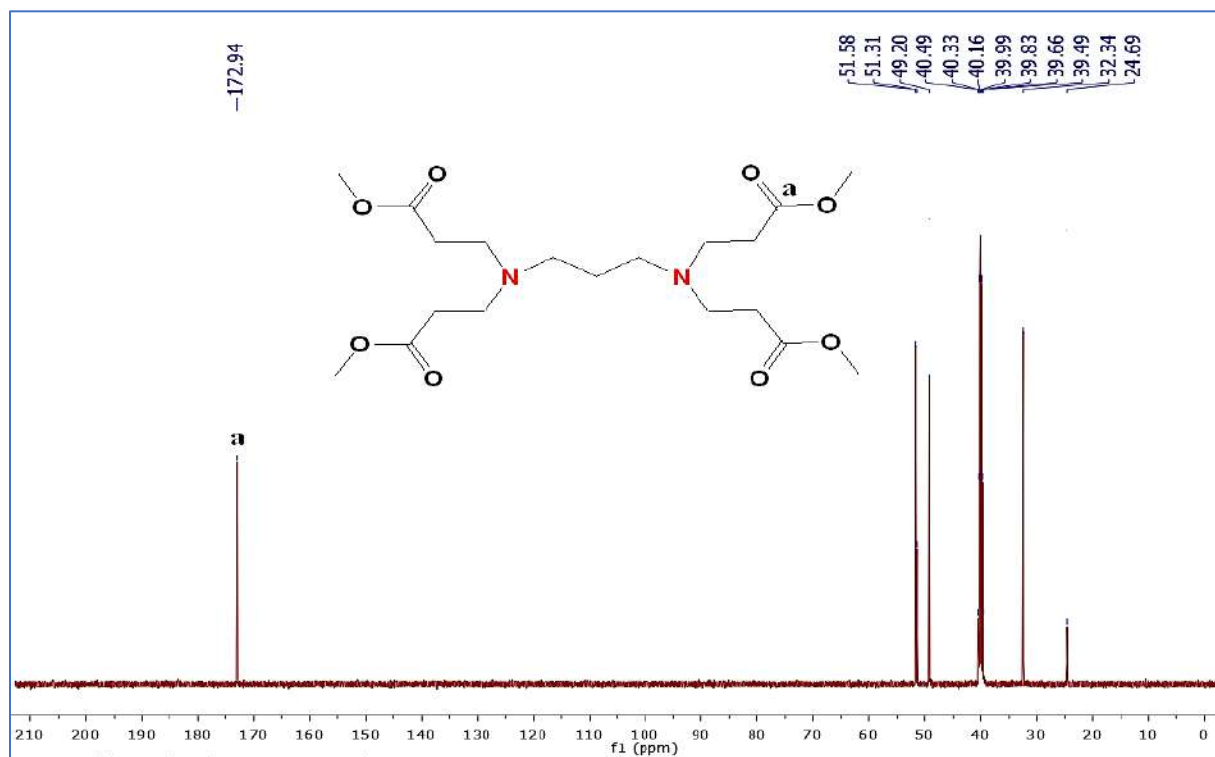
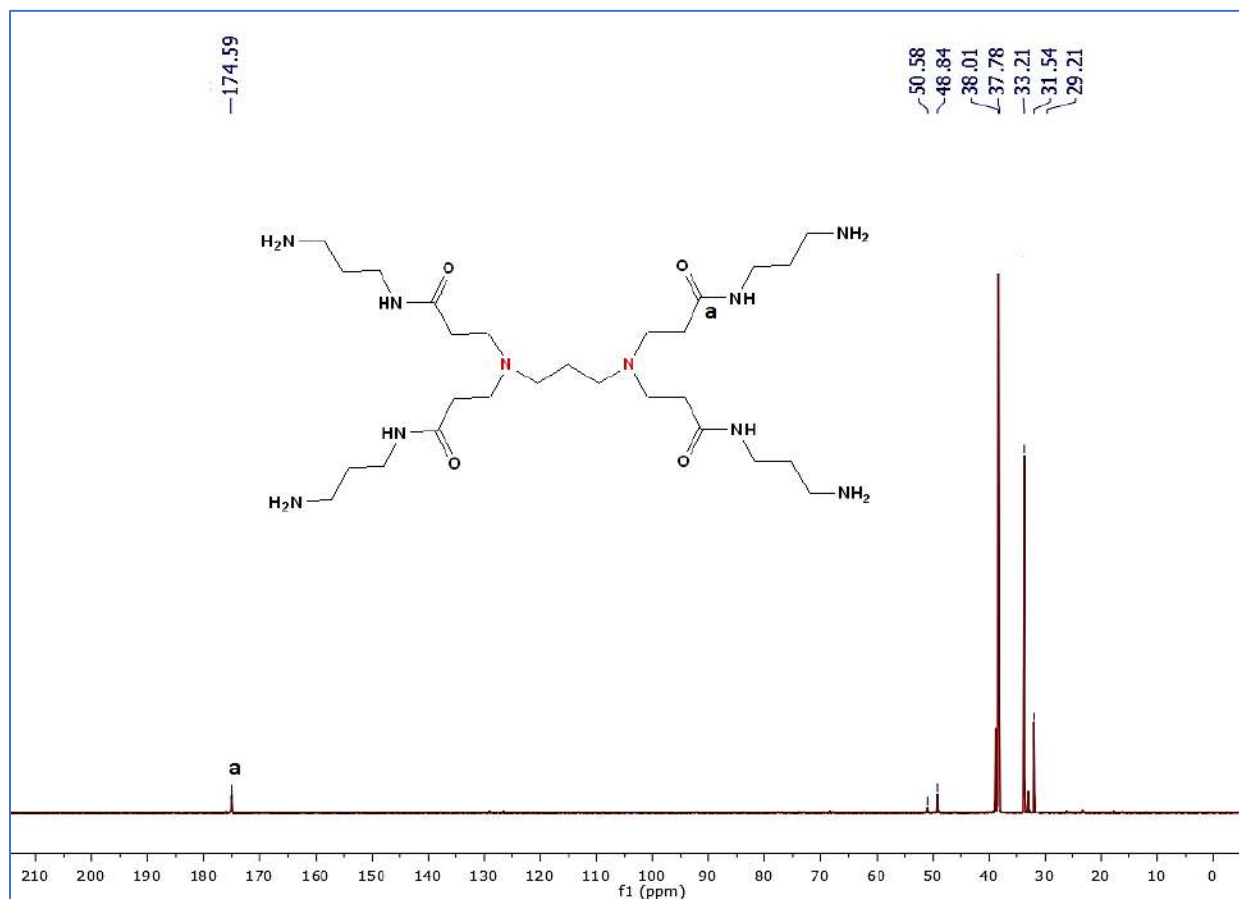


Figure 3-8 ^1H NMR of $\text{G3}_{(a)}$ (DMSO-d_6 , 400MHz)

^{13}C NMR was utilized to confirm the dendrimer structures; the $\text{G1}_{(a)}$ exhibited one signal for ester carbonyl at 172.94 ppm (a) and there are signals between 51.58- 24.69 ppm, confirming the number of CH_2 -proton environments,) (Fig. 3-9) and the $\text{G2}_{(a)}$ dendrimer showed one signal for amide carbonyl at 174.59 ppm (a), (Fig. 3-10). Meanwhile, the higher generation dendrimers $\text{G3}_{(a)}$ have two signals that derive from the ester carbonyl at 174.5 ppm (a) and amide carbonyl at 174.6 ppm (b), (Fig. 3-11). There are signals in the ^{13}C NMR spectra between 53.16 ppm and 24.29 ppm, demonstrating the enormous number of CH_2 -proton environments for $\text{G3}_{(a)}$. Utilizing ^{13}C NMR helps to validate the structure and is the most accurate approach to detect the existence of PDA.

Figure 3-9 ^{13}C NMR of G1(a) (DMSO- d_6 , 125MHz)Figure 3-10 ^{13}C NMR of G2(a) (D $_2$ O, 100MHz)

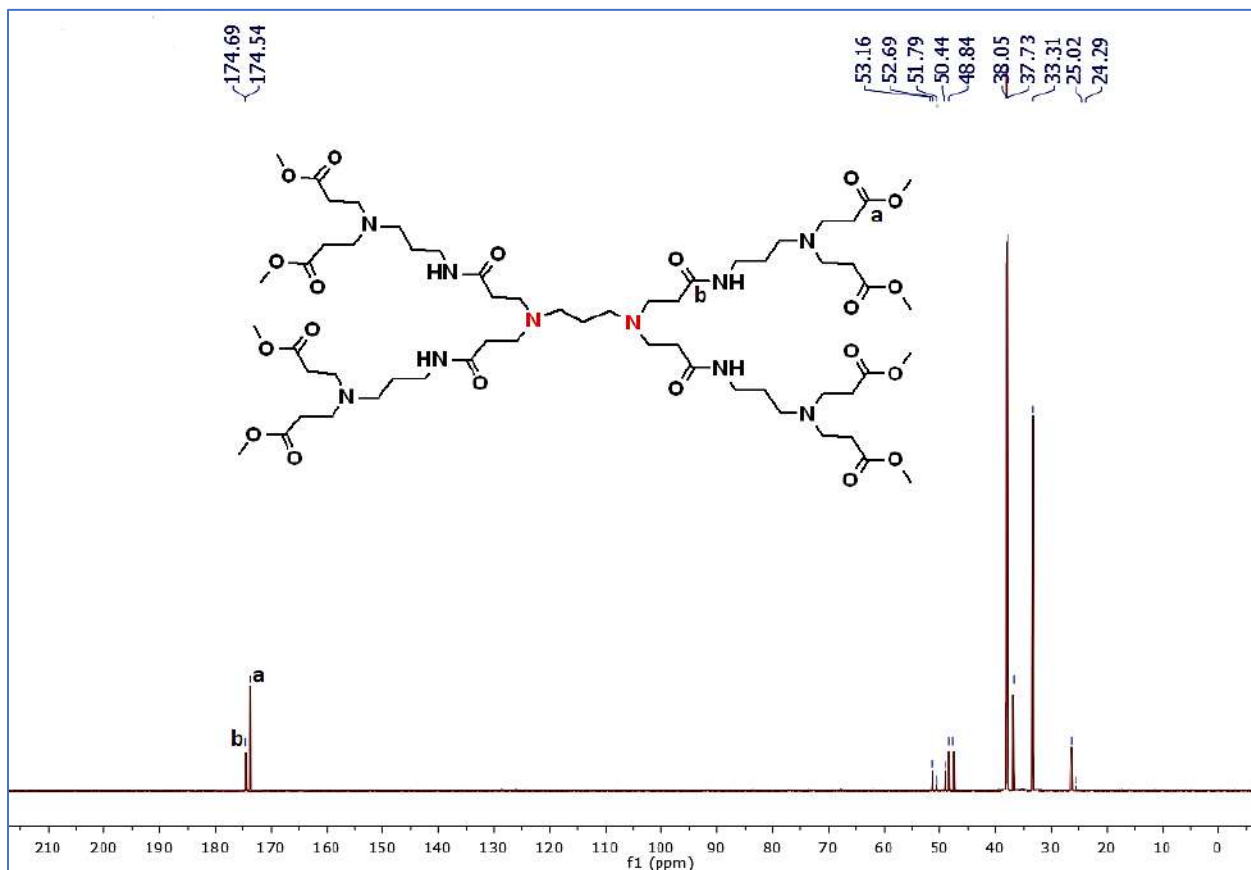


Figure 3-11 ^{13}C NMR of G3 (a) (DMSO- d_6 , 100MHz)

Mass spectrometry (MS) is a very useful technique for examining the presence of structural defects in dendrimers as shown in Figures (3-12, 3-13 and 3-14). Dendrimers have structural homogeneity, which allows them to have accurate molecular weights. The values obtained for molecular ion peaks in all dendrimer generations were similar to the calculated molecular weights from the structure, confirming the product purity, (See Table 3.1).

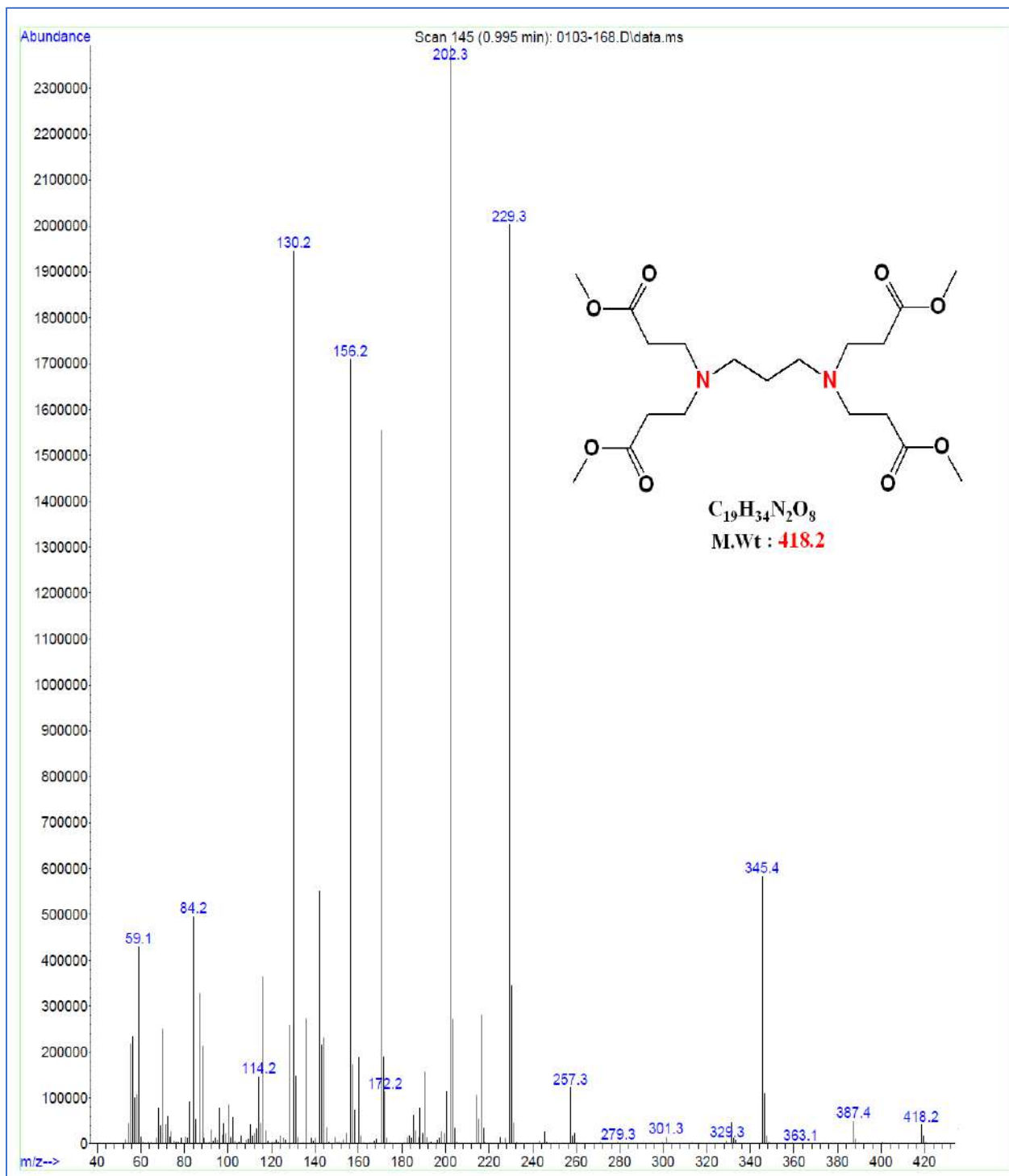


Figure 3-12 Mass spectrum of G1(a)

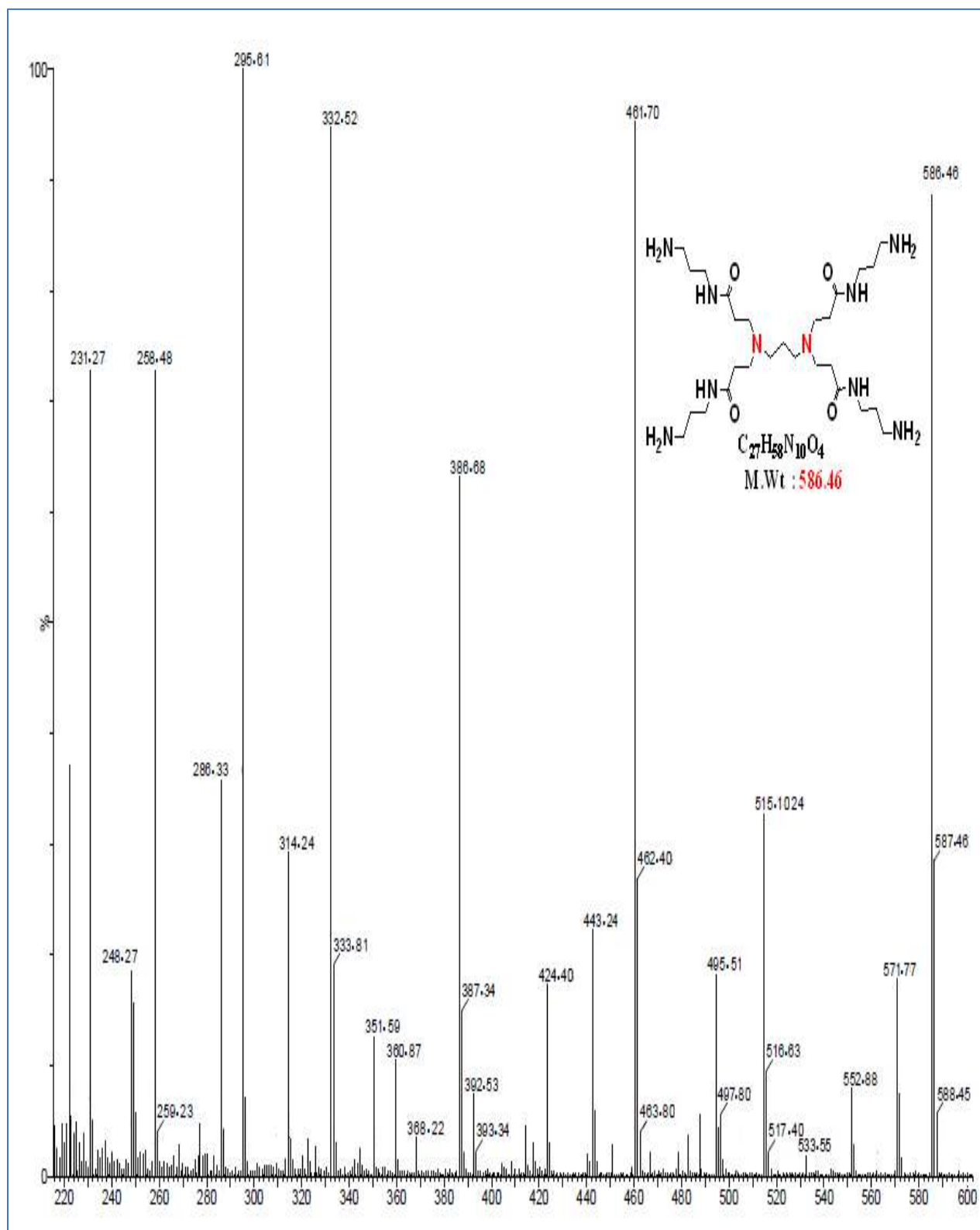


Figure 3-13 Mass spectrum of G2(a)

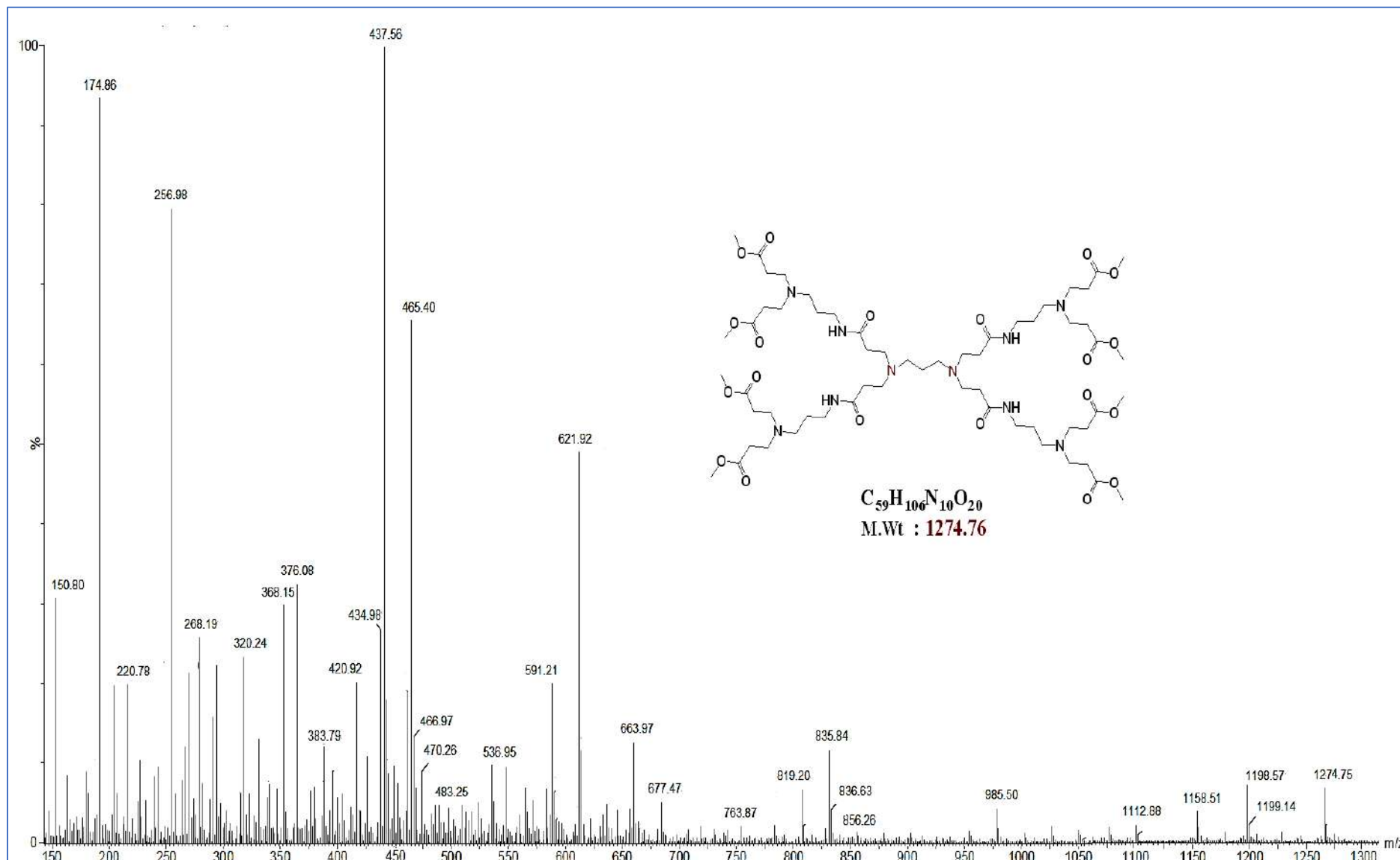


Figure 3-14 Mass spectrum of G3(a)

3.4 Characterization of PAMAM dendrimers **G1_(b)**, **G2_(b)** and **G3_(b)**

Several characterization techniques, such as FTIR spectroscopy, (¹H and ¹³C) NMR spectroscopy, and mass spectrometry, were employed to ensure that all synthesized dendrimers (**G1_(b)**, **G2_(b)** and **G3_(b)**) were in good agreement with the theory discussed previously.

FTIR spectroscopy assists in identifying the functional group within the dendrimers' structure. For PAMAM dendrimer that ends in an ester **G1_(b)**, the spectrum showed a strong ester peak at 1732 cm⁻¹. For PAMAM dendrimer that ended in an amine **G2_(b)**, amine peaks appeared at 3342 cm⁻¹ and 3275 cm⁻¹, and an amide carbonyl peak was observed at 1643 cm⁻¹. For PAMAM dendrimer **G3_(b)**, the spectrum showed two significant peaks: one for the amide carbonyl at 1643 cm⁻¹ and another for carbon carbonyl ester dendrimer at about 1734 cm⁻¹ as shown in Figures (3-15, 3-16, and 3-17).

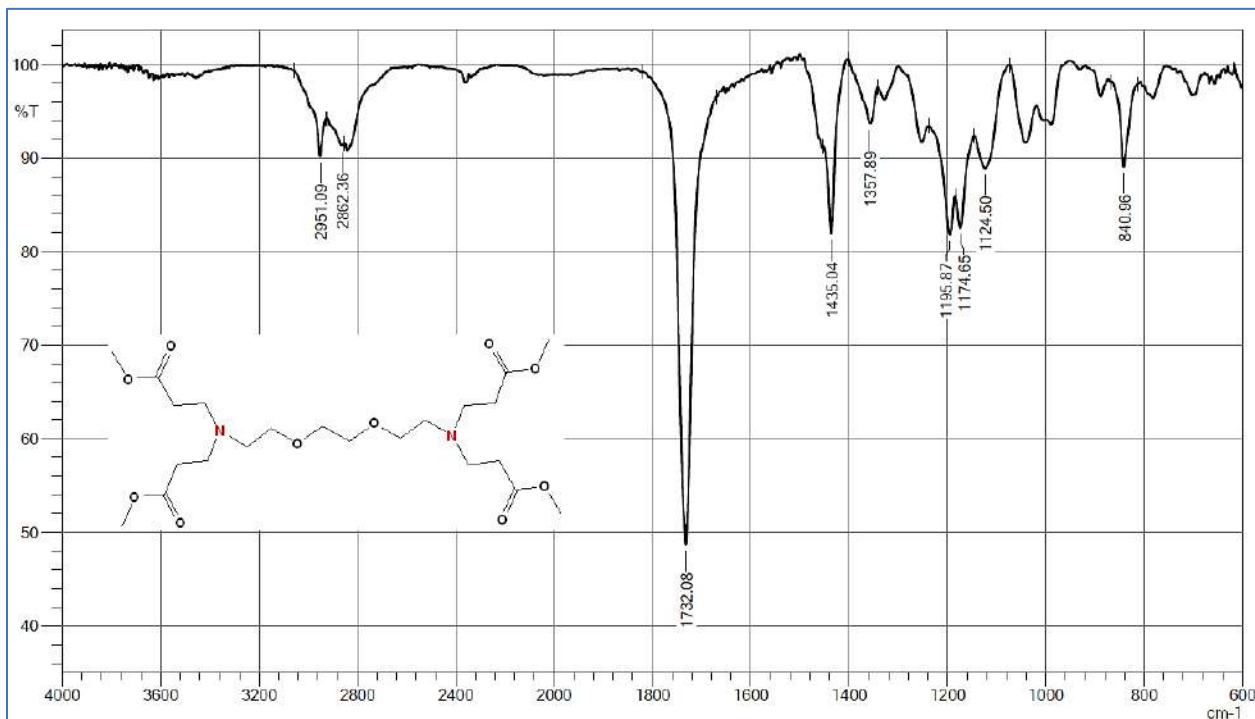


Figure 3-15 FTIR of **G1_(b)**

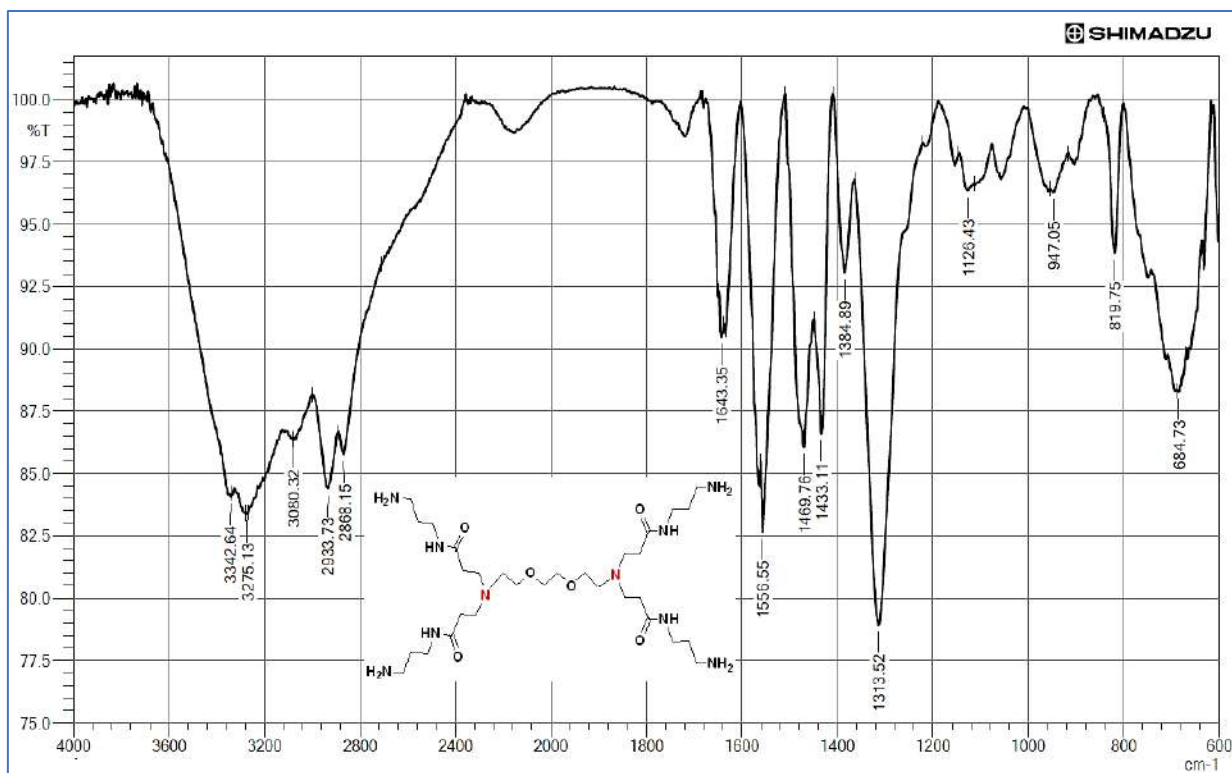


Figure 3-16 FTIR of G2(b)

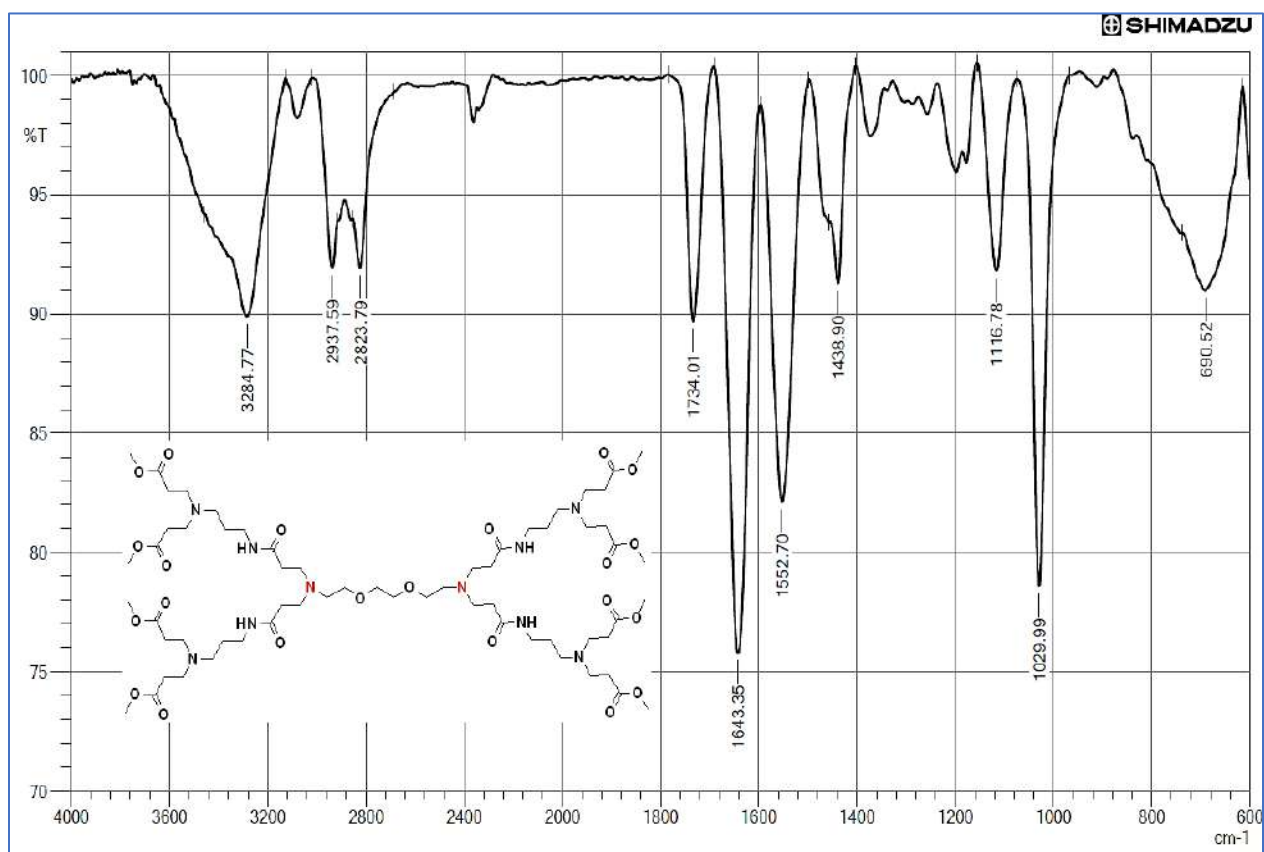
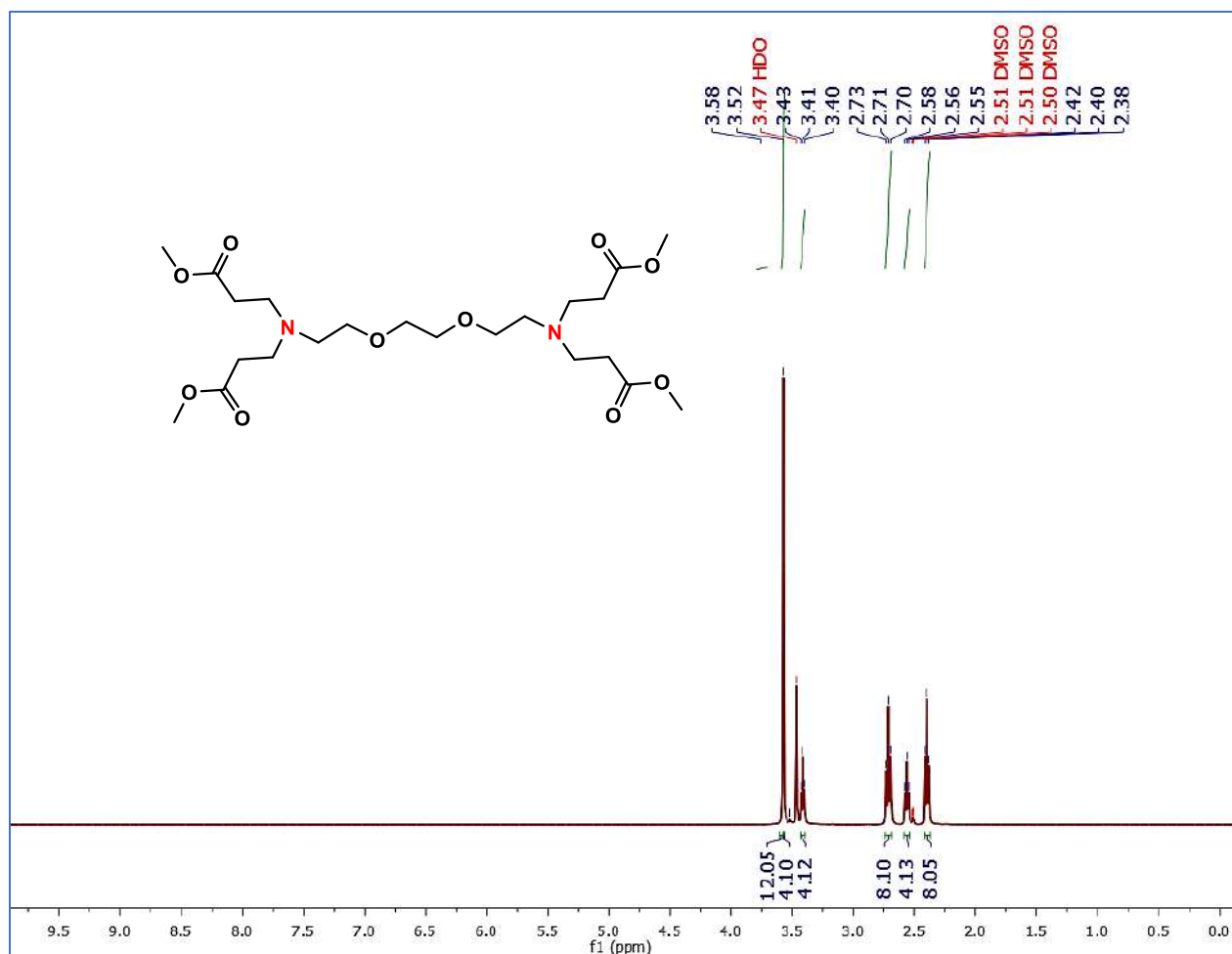


Figure 3-17 FTIR of G3(b)

The ^1H NMR technique is a useful tool for determining hydrogen abundance and relative abundance. Figures 3.18 and 3.19 depict the ^1H NMR spectrum of **G1**_(b) and zoomed **G1**_(b) which reveals a singlet signal at 3.58 ppm which matches twelve methoxy protons (a). Two triplets at 2.40 ppm (b) and 2.71 ppm (c), revealed the presence of newly produced CH_2 groups, whereas another two triplets at 2.56 ppm (d) and 3.41 ppm (e). In addition, a singlet at 3.52 ppm (f) indicated the presence of a proton from the core 1,2-bis(2-aminoethoxy) ethane.



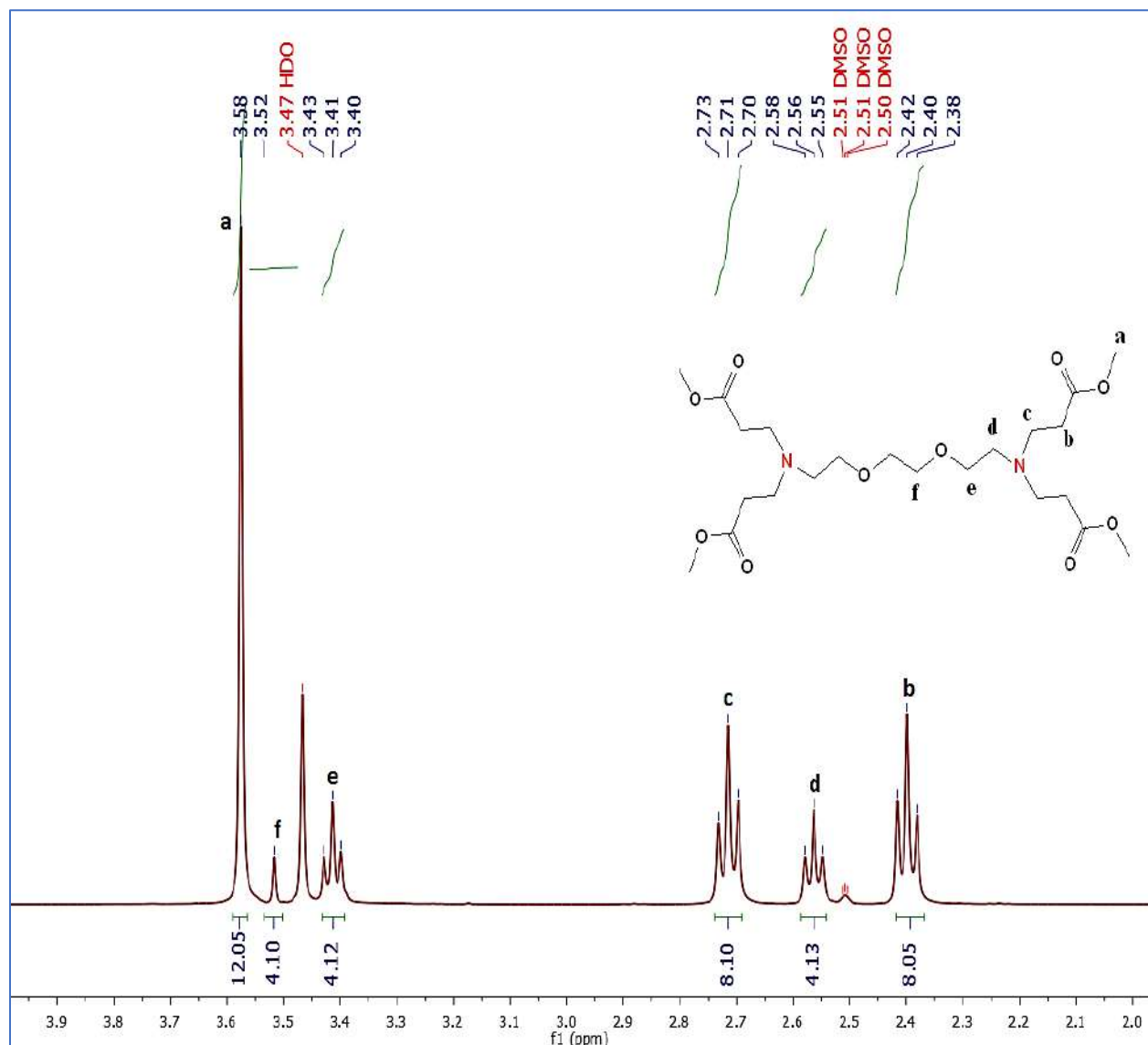
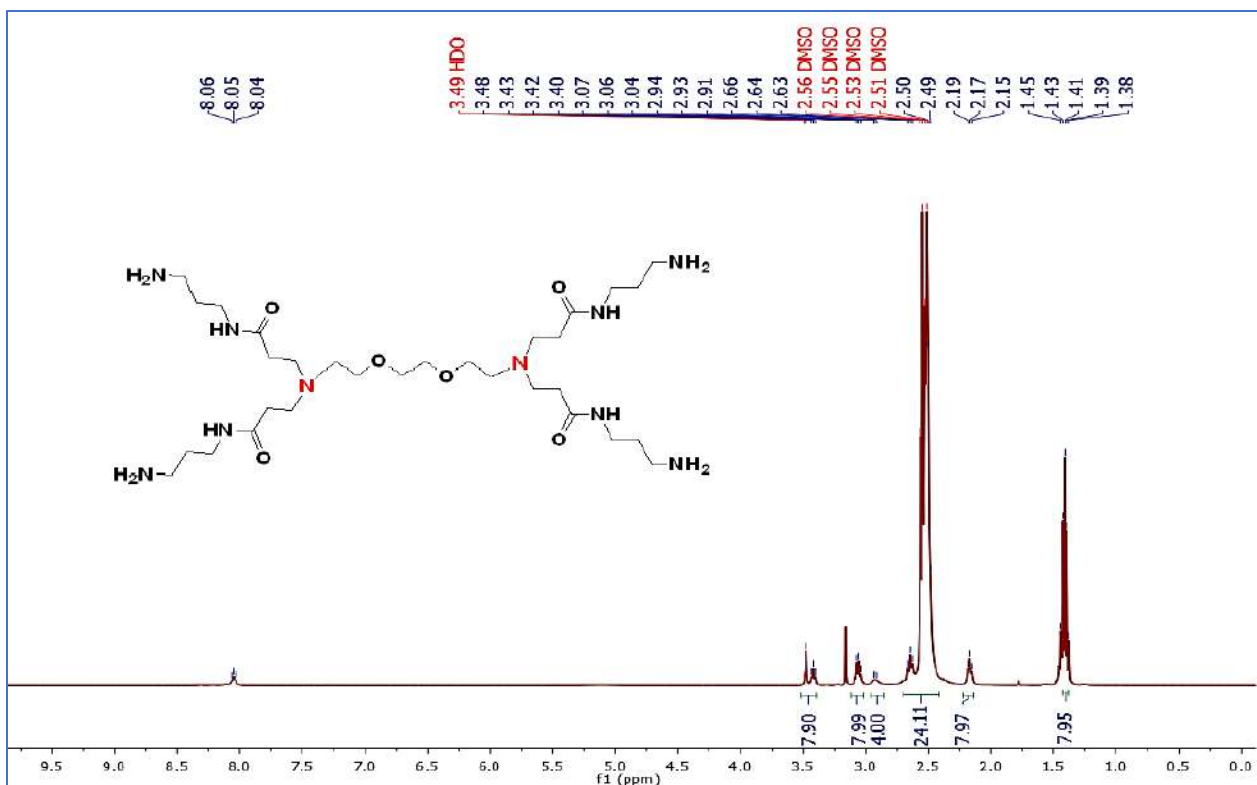
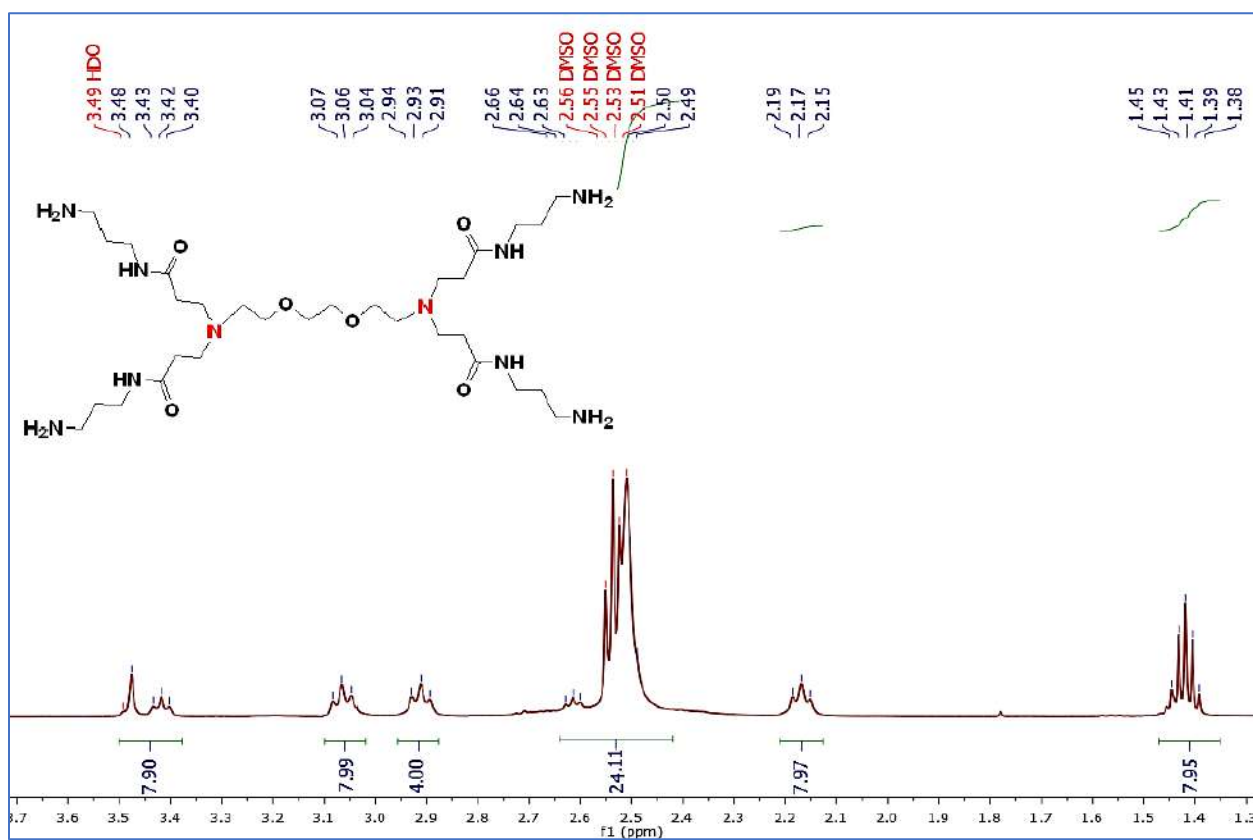


Figure 3-19 $^1\text{H NMR}$ Expanded of $\text{G1}_{(b)}$ dendrimer (DMSO-d_6 , 400MHz)

As well as the $\text{G2}_{(b)}$, displayed the same signals as well as the existence of an amide proton (NH) as a triplet signal at 8.05 ppm [115] as shown in Figures (3-20 and 3-21).

Figure 3-20 ^1H NMR of G2(b) dendrimer (DMSO- d_6 , 400MHz)Figure 3-21 ^1H NMR Expanded of G2(b) dendrimer (DMSO- d_6 , 400MHz)

The spectra of dendrimers of higher generations **G3_(b)** are more complicated to interpret. This is owing to the abundant number of protons. As a result, there were wide overlapping regions and expanded triplets and multiples. This is illustrated in Figure 3.22. At 3.65 ppm, a very significant singlet signal (a) related to methoxy was observed on the **G3_(b)** spectrum. Multiplets at 3.37-2.73 ppm (b) and 2.53-1.65 ppm (c) indicate the presence of CH₂ groups in the dendrimer structure.

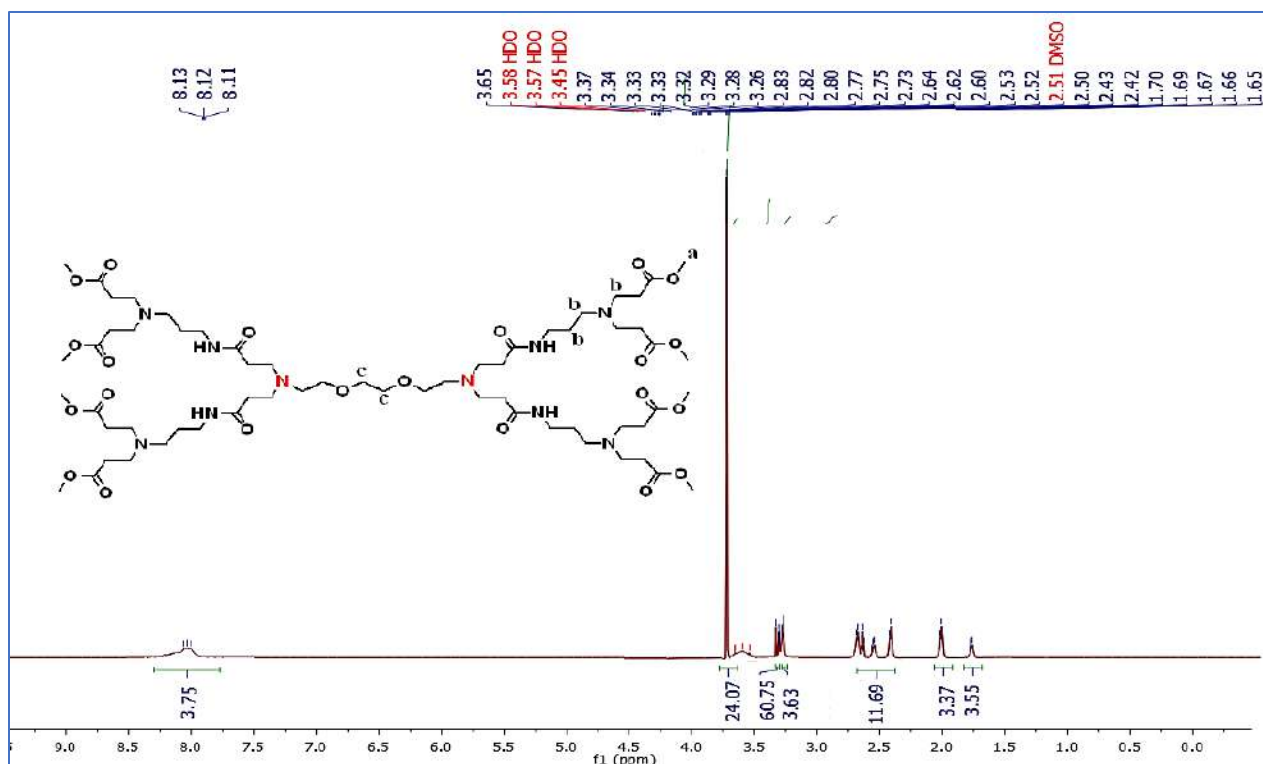
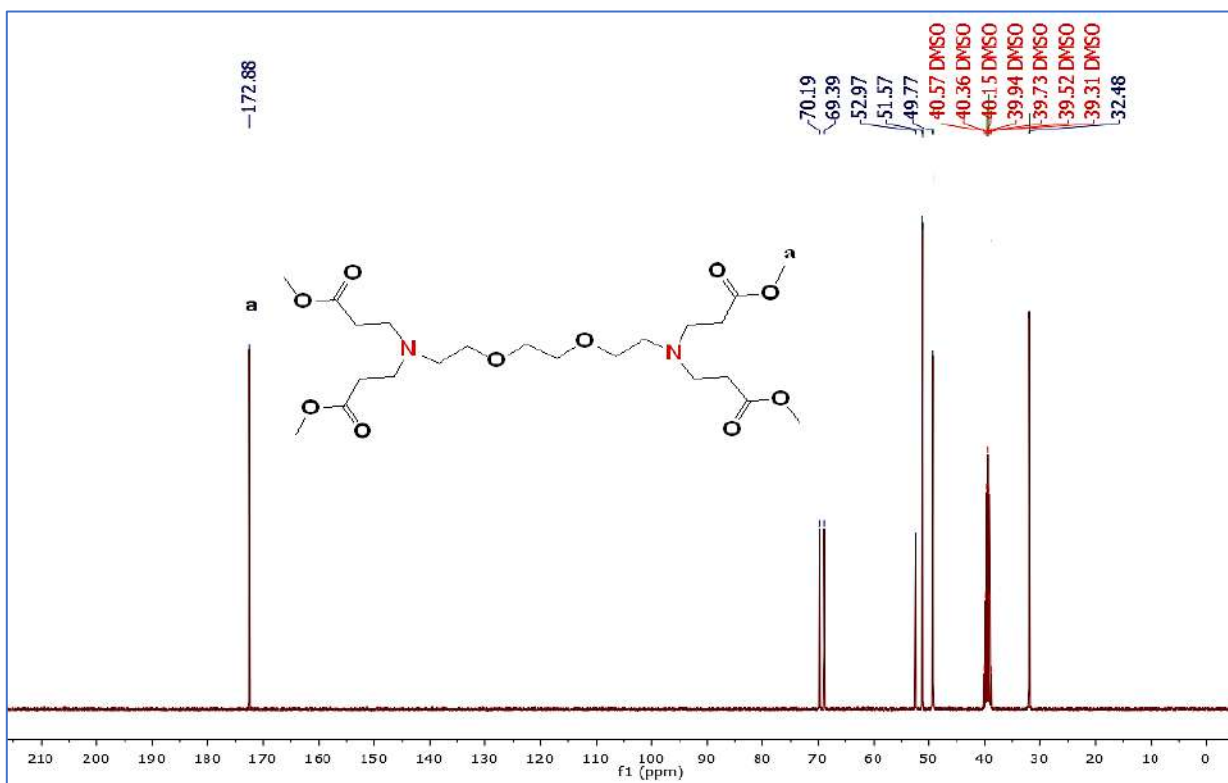
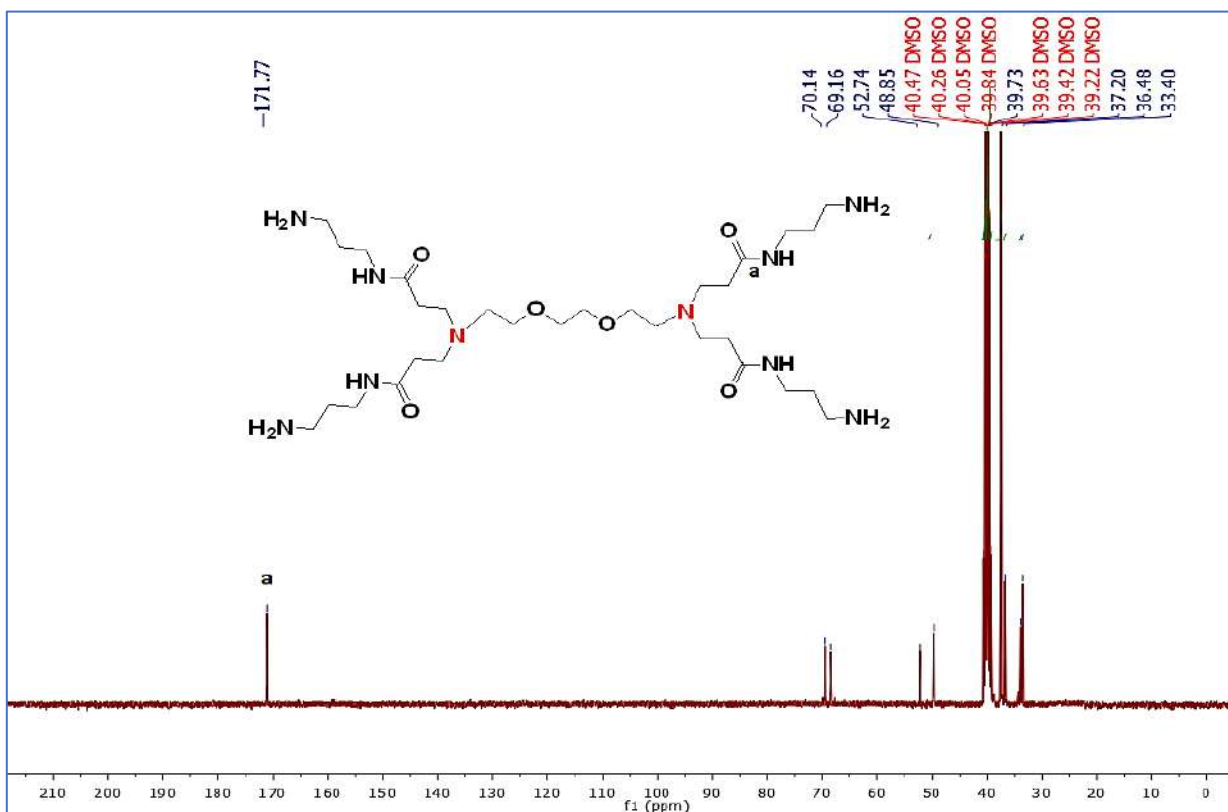


Figure 3-22 ¹H NMR of **G3_(b)** dendrimer (DMSO-d₆, 400MHz)

To confirm the structure of the **G1_(b)**, ¹³C NMR spectroscopy was performed. The methoxycarbonyl (a) was represented by a signal in the ¹³C NMR spectrum at 172.88 ppm as shown in Figure (3-23). **G2_(b)** generation exhibits a signal of 171.77 ppm, which can be attributed to carbonyl amide carbon (a) as illustrated in Figure (3-24). As for the **G3_(b)** the ¹³C NMR spectrum shows two various carbonyl signals, 174.97 ppm (a) and 173.01 ppm (b), corresponding to ester carbon, and amide carbon, respectively as shown in Figure (3-25).

Figure 3-23 ^{13}C NMR of G1 (b) dendrimer (DMSO- d_6 , 100 MHz)Figure 3-24 ^{13}C NMR of G2 (b) dendrimer (DMSO- d_6 , 100 MHz)

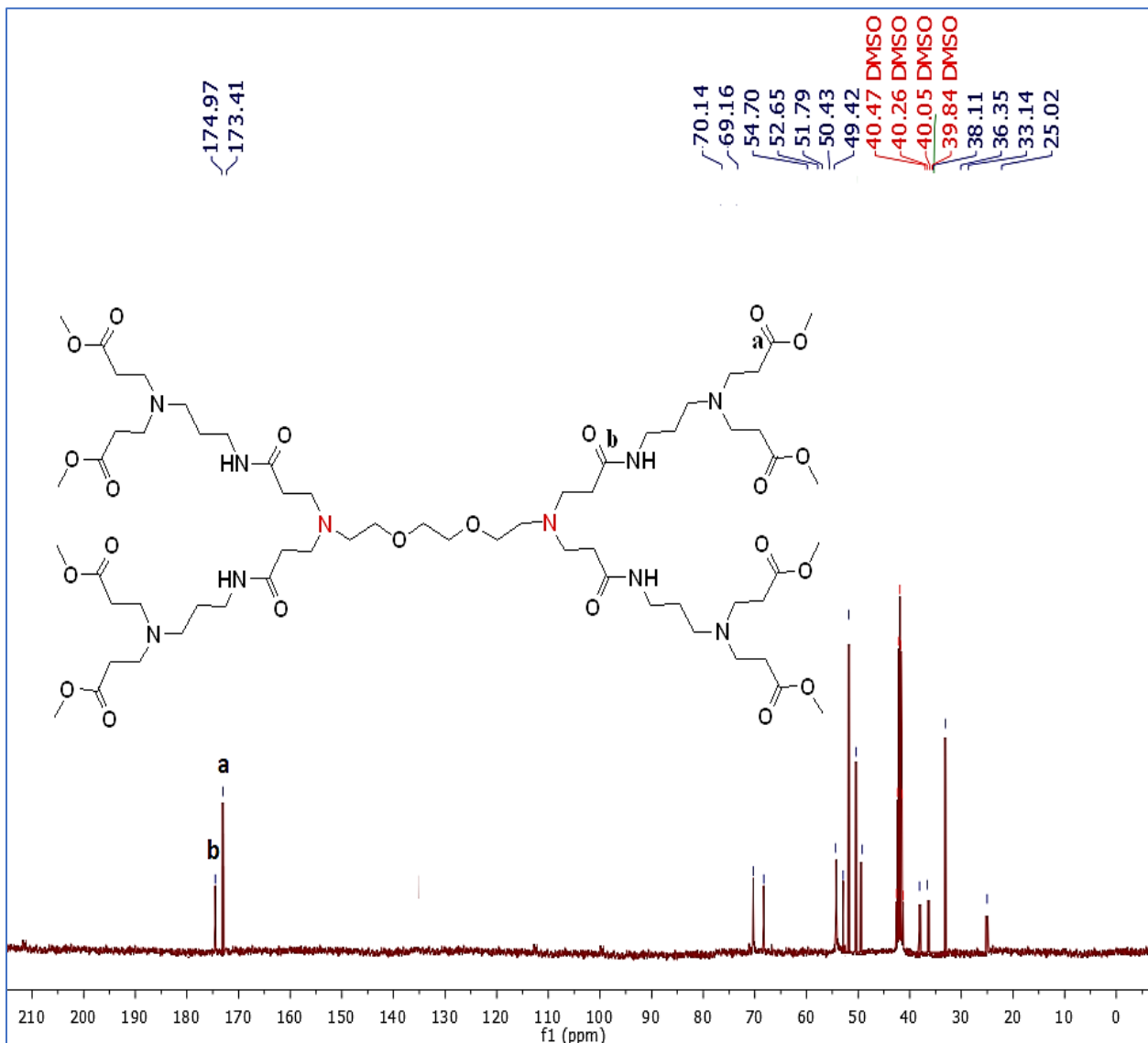


Figure 3-25 ^{13}C NMR of G3 (b)dendrimer (DMSO- d_6 , 100MHz)

Mass spectroscopy was another technique utilized for confirming the dendrimers (**G1**(b), **G2**(b), and **G3**(b)). This demonstrated that the peak of molecular ions was almost identical, as demonstrated in Figures (3-26, 3-27 and 3-28), as well as, Table (3-1) displays the molecular ion peak values for all dendrimer generation. More details about FTIR and (^1H NMR, ^{13}C NMR) spectroscopy data are presented in the experimental part.

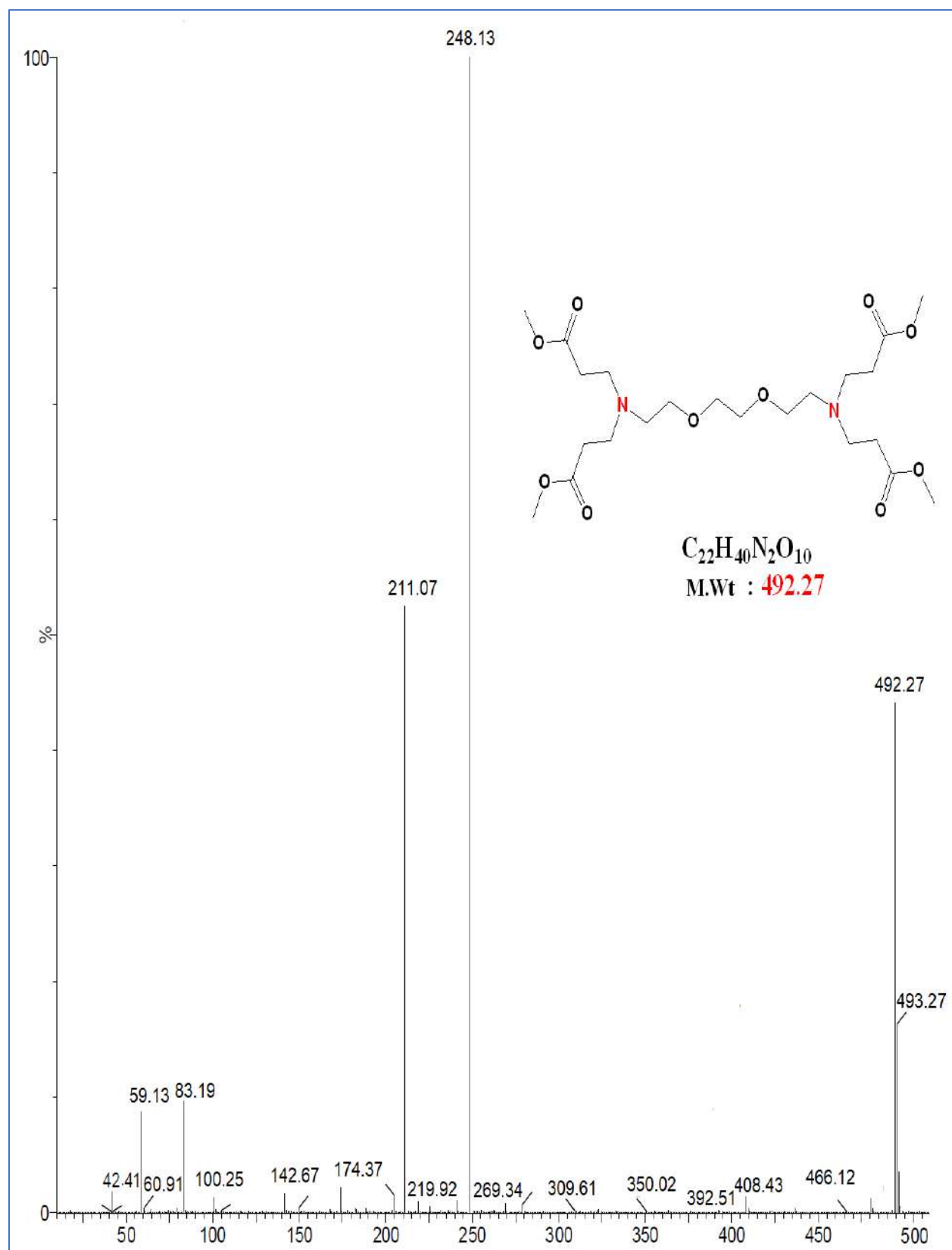


Figure 3-26 Mass spectrum of G1(b)

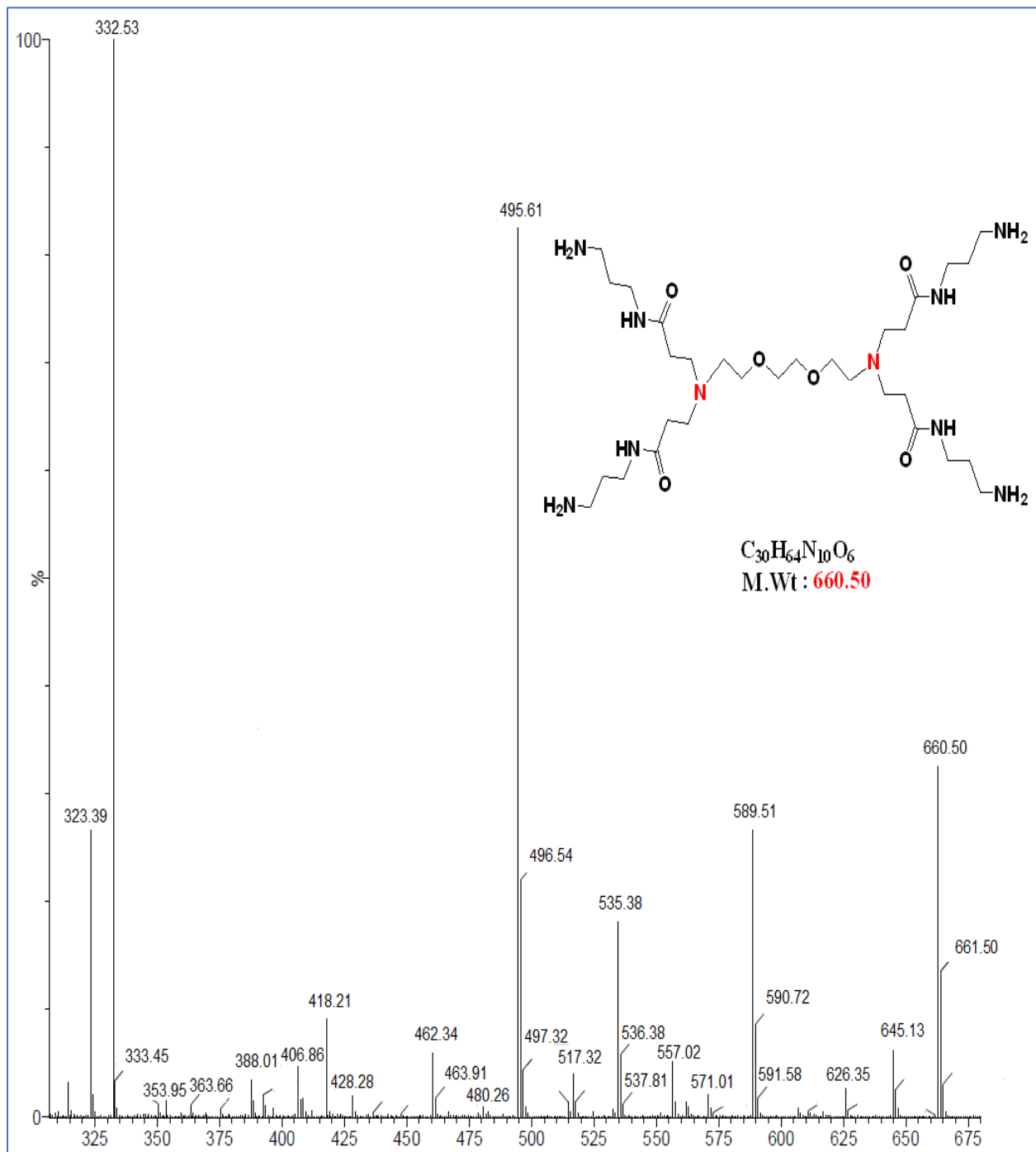


Figure 3-27 Mass spectrum of G2(b)

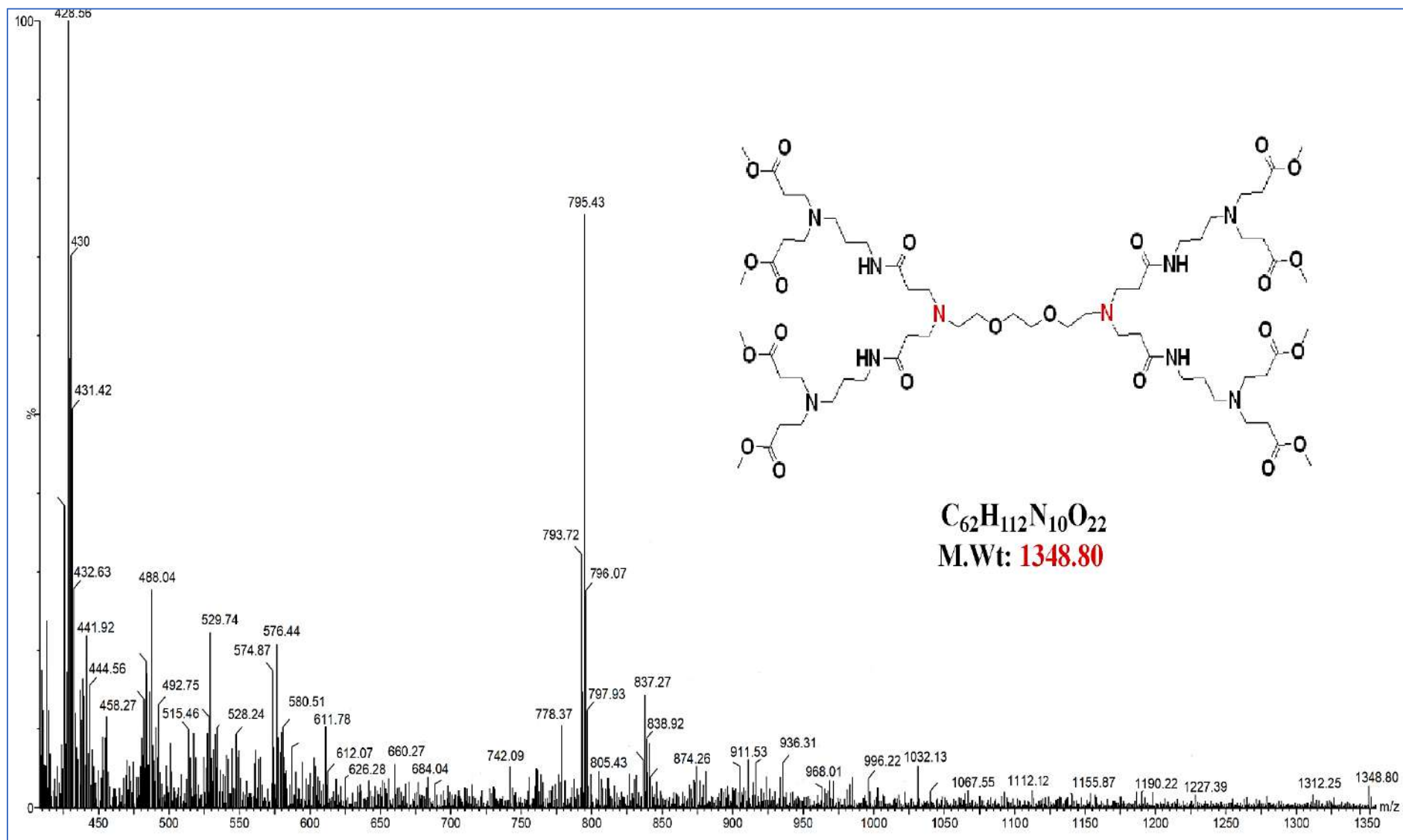


Figure 3-26 Mass spectrum of G3(b)

Table 3-1 The molecular weight of PAMAM dendrimer generations from [G1_(a) to G3_(b)]

PAMAM generation	Molecular Formula	End Groups	M+ peak	Expected M.Wt
G1 _(a)	C ₁₉ H ₃₄ N ₂ O ₈	CO ₂ OMe (4)	418.2	418.2
G2 _(a)	C ₂₇ H ₅₈ N ₁₀ O ₄	NH ₂ (4)	586.46	586.46
G2 _(a)	C ₅₉ H ₁₀₆ N ₁₀ O ₂₀	CO ₂ OMe (8)	1274.75	1274.76
G1 _(b)	C ₂₂ H ₄₀ N ₂ O ₁₀	CO ₂ OMe (4)	492.27	492.27
G2 _(b)	C ₃₀ H ₆₄ N ₁₀ O ₆	NH ₂ (4)	660.50	660.50
G3 _(b)	C ₆₂ H ₁₁₂ N ₁₀ O ₂₂	CO ₂ OMe (8)	1348.80	1348.80

3.5 SEM and EDX analysis of G1_(a), G2_(a) and G3_(a)

Scanning Electron Microscope (SEM) micrographs were employed to study the surface morphology of the dendrimer samples (G1_(a), G2_(a) and G3_(a)) as shown in Figure 3-29 (a, b and c). The synthesized compounds show a model aggregated (cluster type) morphology. To check the composition of (G1_(a), G2_(a) and G3_(a)), EDX analysis was also carried out (Figs. 3-30, 3-31 and 3-32), respectively. The EDX spectrum shows the presence of C, O, and N elements in synthesized compounds[116].

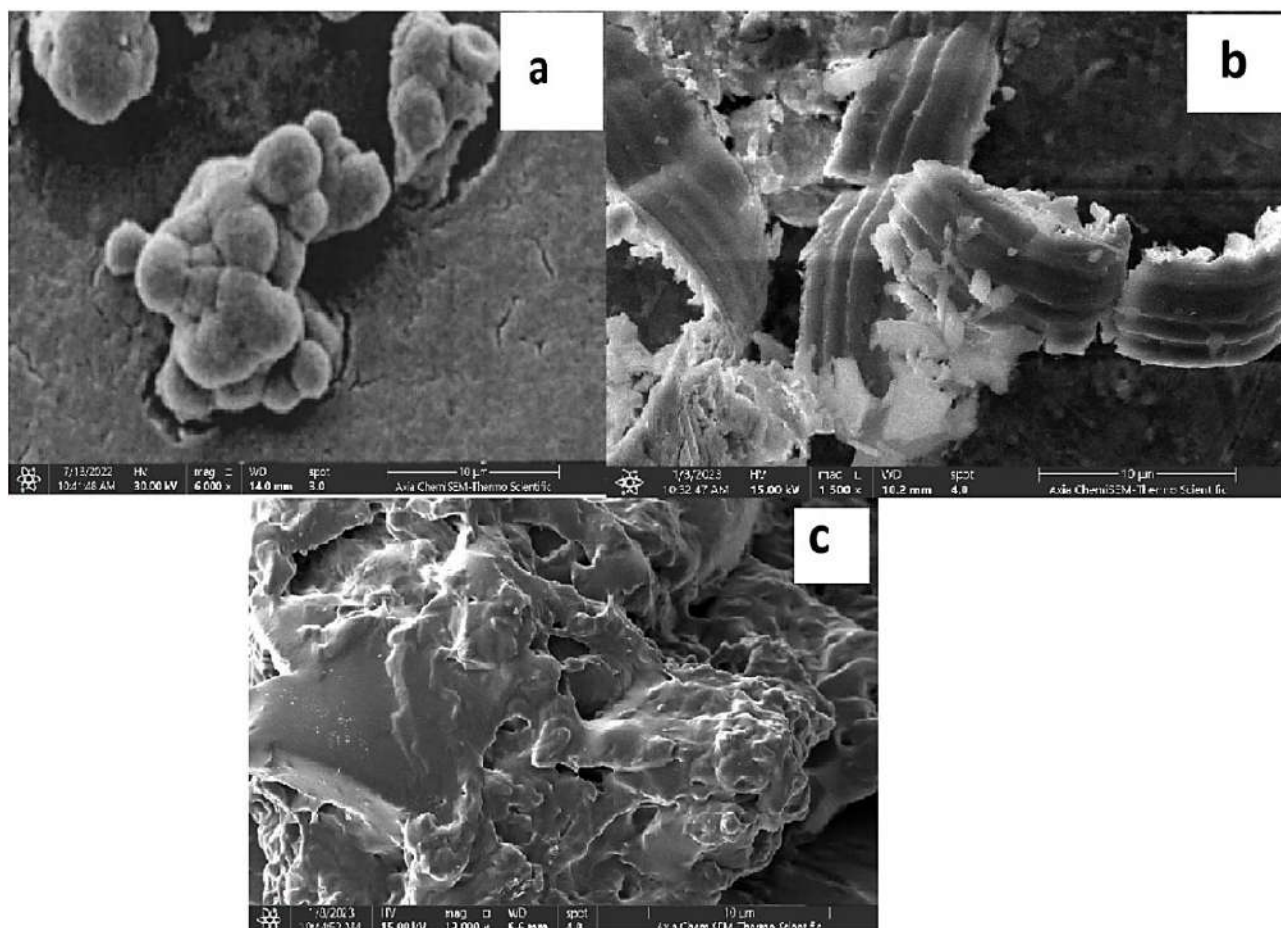


Figure 3.29 SEM images of synthesized (a) G1_(a), (b) G2_(a) and (c) G3_(a)

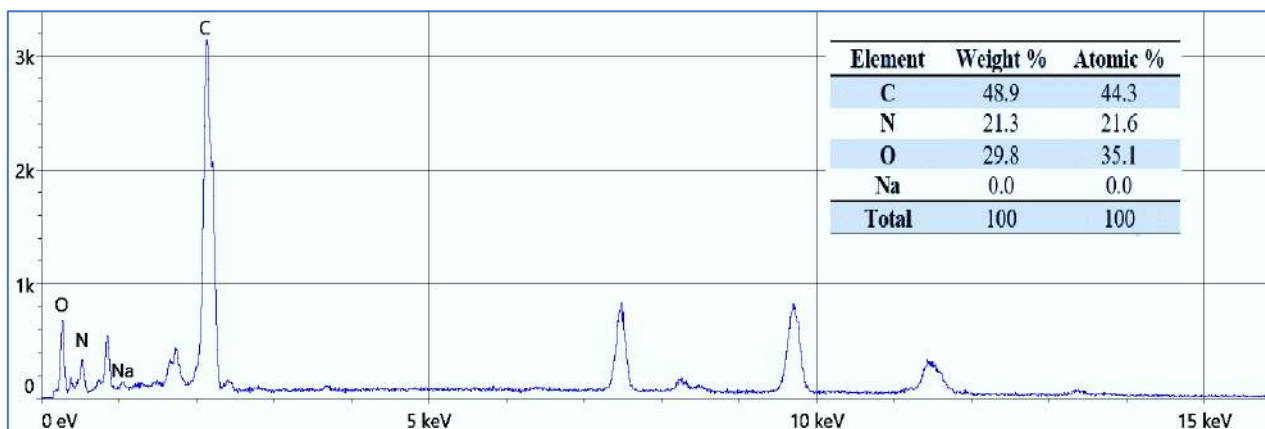


Figure 3-30 EDX spectrum of synthesized G1(a)

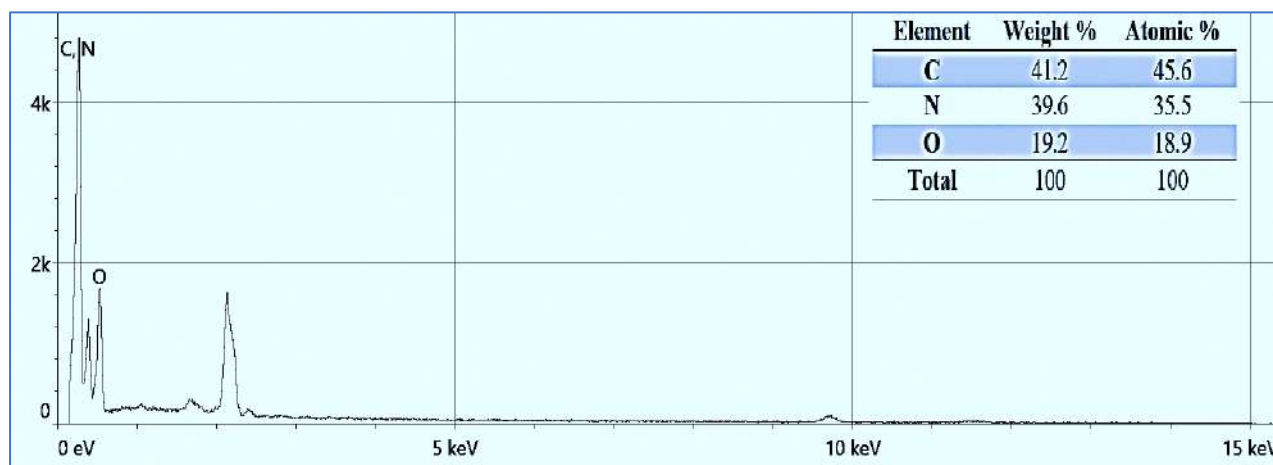


Figure 3-31 EDX spectrum of synthesized G2(a)

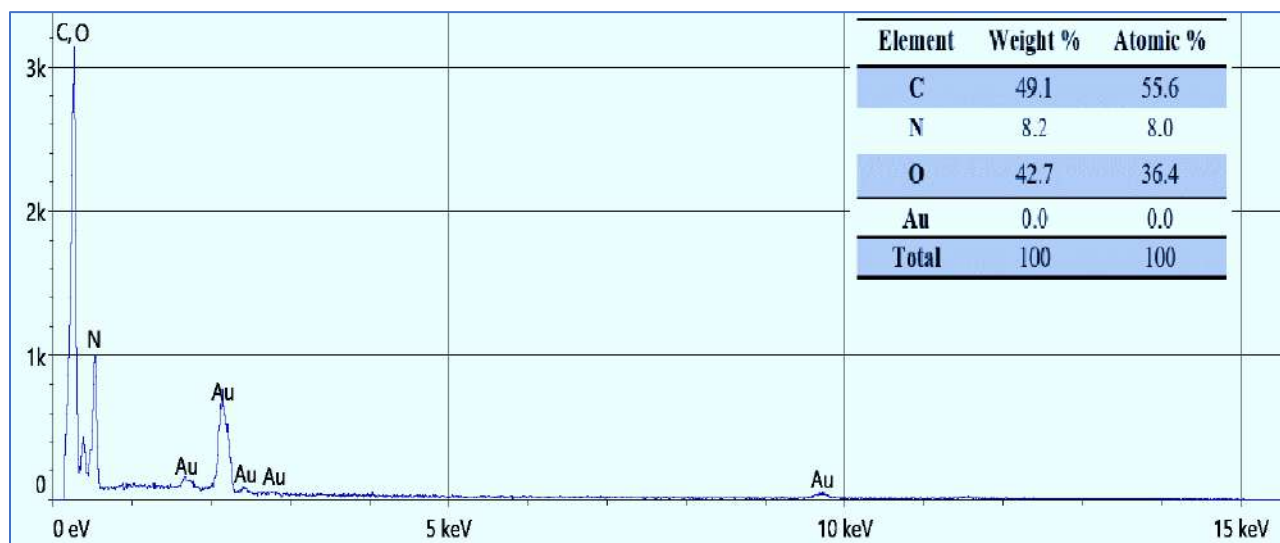


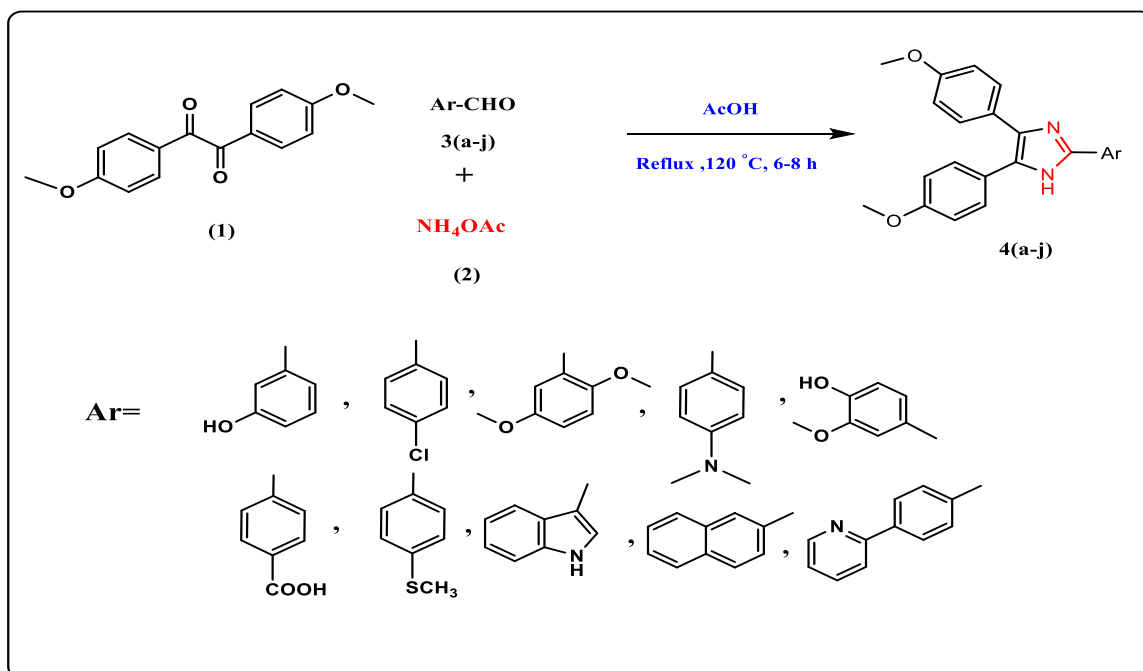
Figure 3-32 EDX spectrum of synthesized G3(a)

3.76 Multi-Component Reactions

Multicomponent reactions (MCRs) are considered an effective and powerful tool for use in the field of organic synthesis because complex organic compounds can be obtained from simple and readily available starting materials without the isolation of any intermediate[117,118]. As a result, new approaches for MCRs are being developed, and attempts are being made to improve current MCRs methods. The formation of imidazoles is one of these reactions[119].

3.7 Synthesis of 2,4,5-Tri-substituted imidazole derivatives (4a-4j) by using glacial acetic acid

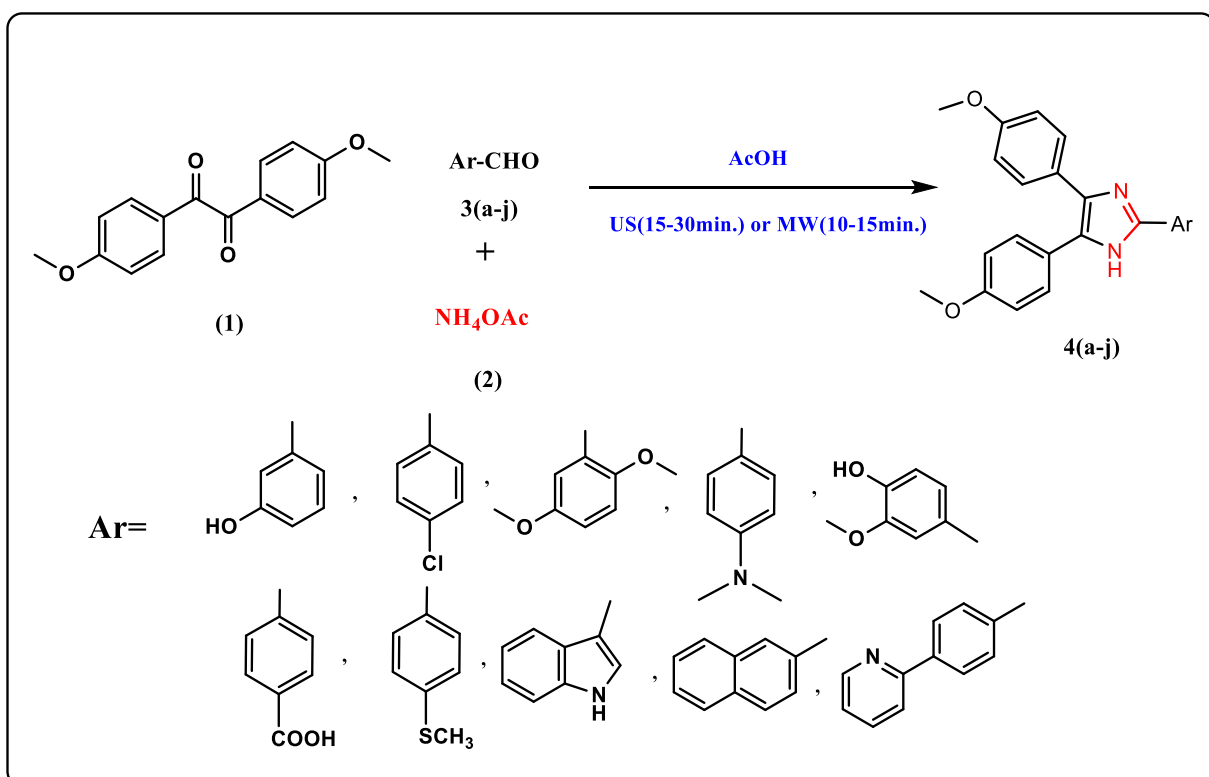
A new series of 2,4,5-trisubstituted imidazole derivatives were synthesized using glacial acetic acid as a catalyst and suitable solvent involving condensation of 1,2-diketone, aromatic substituted aldehydes and ammonium acetate. At first, a mixture consisting of equal amounts of 4,4'-Dimethoxybenzil (0.001mol), aromatic aldehydes (0.001mol.), and ammonium acetate (0.005mol.) in 15mL of glacial acetic acid was refluxed for 6-8 hours yielding a good product, (Scheme 3-8).



Scheme 3-8 Synthesis of 2,4,5-Tri-imidazole derivatives under reflux condition

The presence of glacial acetic acid increases the reactivity of aromatic aldehydes and 1,2-diketone. The use of a suitable catalyst is essential for improving product yield. It is necessary to use an appropriate catalyst to increase product yield.

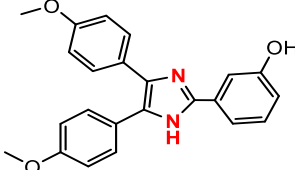
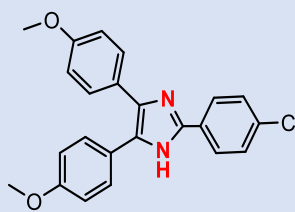
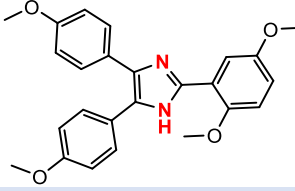
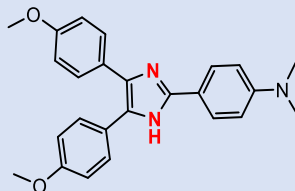
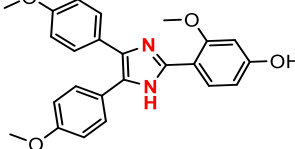
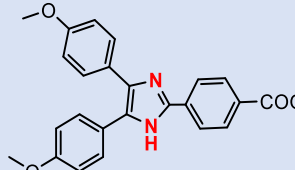
To increase both the reaction speed and the product yield, the reaction was carried out under ultrasonic irradiation and microwave conditions, which offered promising results in a shorter period, (Scheme 3-9).

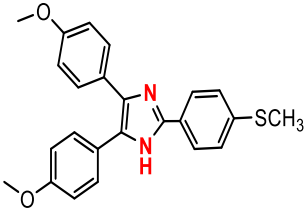
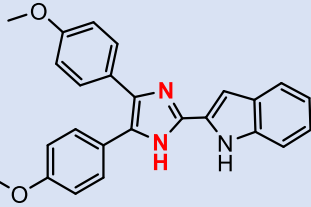
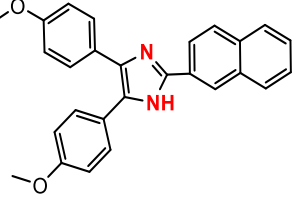
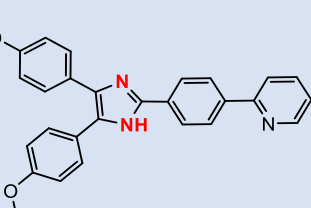


Scheme 3-9 Synthesis of 2,4,5-Tri-imidazole derivatives under ultrasonic and microwaves conditions

A Comparison of product yield and reaction time using different reaction conditions for the synthesis of 2,4,5-trisubstituted imidazole derivatives was summarized in Table (3-2).

Table 3-2 Comparison of product yield and reaction time utilizing different conditions in the presence of AcOH as a catalyst for the synthesis of triimidazole derivatives (4a-4j)

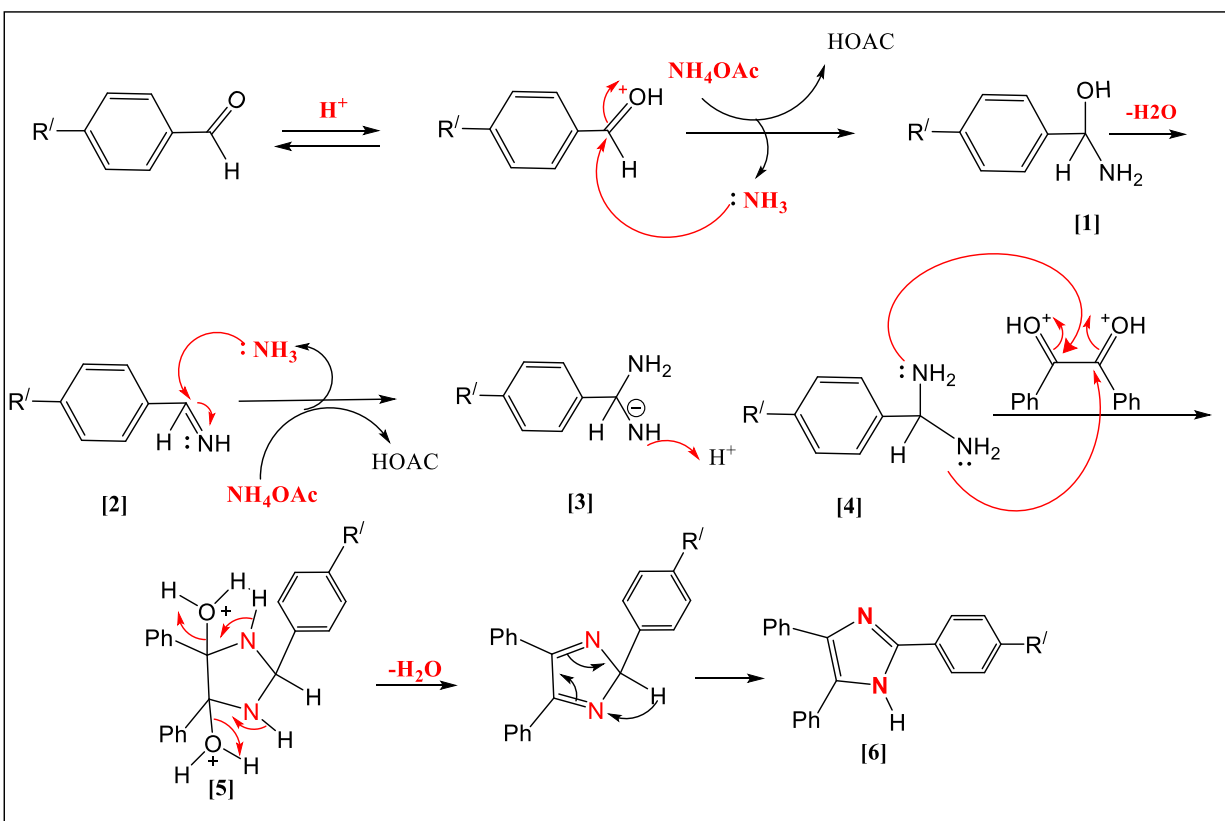
Entry	Product	Conventional heating (reflux)		Ultrasound Condition		Microwave Condition	
		Time(h)	Yield(%)	Time (min.)	Yield(%)	Time (min.)	Yield(%)
4a		7	81	20	88	10	90
4b		7	78	25	88	12	91
4c		6	79	25	85	12	86
4d		7	81	20	87	15	89
4e		7	81	25	90	13	90
4f		8	78	25	86	13	87

Entry	Product	Conventional heating (reflux)		Ultrasound Condition		Microwave Condition	
		Time(h)	Yield(%)	Time (min.)	Yield(%)	Time (min.)	Yield(%)
4g		6	78	15	88	10	89
4h		8	78	30	84	15	88
4i		7	80	25	89	15	93
4j		7	73	20	85	12	89

3.8 The proposed mechanism for the synthesis of 2,4,5-Tri-substituted imidazoles (General mechanism)

The same pattern described in the literature[120] may be followed by the reaction mechanism for the synthesis of tri-imidazole derivatives as shown in Scheme (3-10). The first step includes the formation of an *H*-bond between the catalyst and the aldehyde, Glacial acetic acid donates a proton to the carbonyl group to activate it and produce the hydroxylamine intermediate (1) hydroxylamine dehydration leads to the generation of imine intermediate (2) the nucleophilic attack by another NH₃ on imine leads to the formation of a diamine intermediate (4) this is followed by the nucleophilic

attack of diamine intermediate (4) on the activated carbonyl group of benzil to produce cycle intermediate (5), which then undergoes water molecule release and proton transfer to yield 2,4,5-tri imidazole (6).



Scheme 3-10 Proposed mechanism for the formation of 2,4,5-trisubstituted imidazole from 1,2-diketone, aldehyde and NH_4OAc in the presence of glacial acetic acid

3.9 Characterization of 2,4,5-Tri-arylimidazole derivatives (4a-4j).

The Melting point and spectral analyses (FT-IR, ^1H NMR, ^{13}C NMR, and mass spectra) were utilized to characterize the products formed (See Appendix A). The FTIR spectra of derivatives (4a-4j) exhibited ten peaks for (N-H) and (C=N) groups at 3416-3446 and 1647-1657 cm^{-1} , respectively. The (N-H) proton of the imidazole moiety demonstrated signals at 11.68-12.66 ppm on the ^1H NMR spectrum. Other Characteristic FTIR and ^1H NMR absorption peaks for compounds (4a-4j) are listed in Table (3-3).

Table 3-3 Characteristic absorption bands of FT-IR and ¹H NMR spectra for (4a-4j)

Comp. No.	FT-IR (cm ⁻¹)			¹ H NMR (ppm)
	ν (C=N)	ν (N-H)	others	
4a	1654	3302	ν (O-H) 3151	12.43 (s, 1H, NH), 9.54 (s, 1H, OH), 7.55 – 7.50 (m, 3H, ph-H), 7.45 (d, $J = 5.0$ Hz, 4H, ph-H), 7.26 (t, $J = 10.0$ Hz, 1H, ph-H), 6.96 (s, 1H, ph-H), 6.79 (dd, $J = 10.0, 5.0$ Hz, 3H, ph-H), 3.79 (s, 6H, (OCH ₃) ₂)
4b	1654	3398	ν (C-Cl) 840	12.61 (s, 1H, NH), 8.09 (d, $J = 5.0$ Hz, 2H, ph-H), 7.96 (d, $J = 10.0$ Hz, 1H, ph-H), 7.88 (d, $J = 10.0$ Hz, 1H, ph-H), 7.55 (dd, $J = 10.0, 5.0$ Hz, 3H, ph-H), 7.46 (d, $J = 5.0$ Hz, 4H, ph-H), 7.14 (d, $J = 10.0$ Hz, 1H, ph-H), 3.79 (s, 6H, (OCH ₃) ₂)
4c	1658	3253	ν (C-O-C) 1246, 1172	11.68 (s, 1H, NH), δ 7.63 (d, $J = 5.0$ Hz, 1H ph-H), 7.48 (d, $J = 10.0$ Hz, 2H ph-H), 7.40 (d, $J = 10.0$ Hz, 2H, ph-H), 7.09 (d, $J = 10.0$ Hz, 1H, ph-H), 7.01 (d, $J = 5.0$ Hz, 2H, ph-H), 6.95 (dd, $J = 10.0, 5.0$ Hz, 1H, ph-H), 6.89 (d, $J = 5.0$ Hz, 2H, ph-H), 3.88 (s, 3H, OCH ₃), 3.81 (s, 3H, OCH ₃), 3.76 (s, 6H, (OCH ₃) ₂).
4d	1657	3414	ν (C-N) 1296	12.66 (s, 1H, NH), 7.92 (d, $J = 10.0$ Hz, 2H ph-H), 7.84 (d, $J = 10.0$ Hz, 1H ph-H), 7.46 (d, $J = 5.0$ Hz, 3H ph-H), 6.94 (d, $J = 10.0$ Hz, 3H ph-H), 6.80 (d, $J = 10.0$ Hz, 2H ph-H), 6.62 (d, $J = 5.0$ Hz, 1H ph-H), 3.78 (s, 6H, (OCH ₃) ₂), 2.96 (s, 6H, (NCH ₃) ₂).
4e	1651	3448	ν (O-H) ν (C-O-C) 1249, 1172	12.28 (s, 1H, NH), 9.25 (s, 1H, OH), 7.87 (d, $J = 10.0$ Hz, 1H, ph-H), 7.61 (d, $J = 5.0$ Hz, 1H, ph-H), 7.50 (dd, $J = 10.0, 5.0$ Hz, 1H, ph-H), 7.43 (d, $J = 10.0$ Hz, 3H, ph-H), 7.14 (d, $J = 10.0$ Hz, 1H, ph-H), 6.94 (d, $J = 10.0$ Hz, 3H, ph-H), 6.85 (d, $J = 10.0$ Hz, 1H, ph-H), 3.86 (s, 3H, OCH ₃), 3.77 (s, 6H, (OCH ₃) ₂).
4f	1647	3443	ν (O-H) 3213 ν (C=O) 1705	12.77 (s, 1H, COOH), 12.48 (s, 1H, NH), 8.21 (d, $J = 5.0$ Hz, 3H, ph-H), 8.05 (d, $J = 5.0$ Hz, 3H, ph-H), 7.48 (d, $J = 10.0$ Hz, 4H, ph-H), 6.96 (d, $J = 10.0$ Hz, 2H, ph-H), 3.79 (s, 6H, (OCH ₃) ₂).
4g	1647	3402	ν (C-S) 636	12.49 (s, 1H, NH), 8.01 (d, $J = 8.0$ Hz, 2H, ph-H), 7.44 (d, $J = 8.0$ Hz, 4H, ph-H), 7.35 (d, $J = 8.0$ Hz, 2H, ph-H), 7.01 (d, $J = 8.0$ Hz, 4H, ph-H), 3.77 (s, 6H, (OCH ₃) ₂), 2.52 (s, 3H).
4h	1654	3397	-	12.12 (s, 1H, NH), 11.35 (s, 1H, NH), 8.47 (d, $J = 8.0$ Hz, 1H, ph-H), 7.97 (d, $J = 4.0$ Hz, 1H, ph-H), 7.87 (d, $J = 8.0$ Hz, 2H, ph-H), 7.45 (d, $J = 8.0$ Hz, 2H, ph-H), 7.14 (d, $J = 8.0$ Hz, 4H, ph-H), 6.97 (d, $J = 8.0$ Hz, 3H, ph-H), 3.87 (s, 6H, (OCH ₃) ₂).

Comp. No.	FT-IR (cm ⁻¹)			¹ HNMR (ppm)
	ν (C=N)	ν (N-H)	others	
4i	1654	3360	-	12.01 (s, 1H, <u>NH</u>), 8.60 (s, 1H, ph-H), 8.26 (d, <i>J</i> = 7.6, 1H, ph-H), 8.01 – 7.93 (m, 3H, ph-H), 7.87 (d, <i>J</i> = 8.9 Hz, 1H, ph-H), 7.56 – 7.49 (m, 6H, ph-H), 6.97 (d, <i>J</i> = 8.3 Hz, 3H, ph-H), 3.79 (s, 6H, (OCH ₃) ₂).
4j	1651	3441	ν (C-N) 1296	12.66 (s, 1H, <u>NH</u>), 8.69 (d, <i>J</i> = 8.0, 1.7 Hz, 1H, ph-H), 8.20 (d, <i>J</i> = 8.0 Hz, 2H, ph-H), 8.04 (d, <i>J</i> = 8.0 Hz, 1H, ph-H), 7.90 – 7.86 (m, 4H, ph-H), 7.49 – 7.35 (m, 5H, ph-H), 7.13 (d, <i>J</i> = 8.0 Hz, 2H, ph-H), 6.96 (d, <i>J</i> = 8.0 Hz, 1H, ph-H), 3.78 (s, 6H, (OCH ₃) ₂).

¹³CNMR spectra of compounds (**4a-4j**) exhibited signals of the three carbon atoms of imidazole moiety as (H-N-C=C) signals ranging from 125.94 to 126.68 ppm, (H-N-C=C) signals ranging from 127.00 to 128.66 ppm, and (H-N-C=N) signals ranging from 130.36 to 131.71 ppm. The rest of the spectral results are outlined in detail in the experimental section.

All mass spectral analyses of the prepared imidazoles (**4a-4j**), revealed a peak of molecular ions with a (m/z) value equal to the corresponding calculated value mass as indicated in Table (3-4).

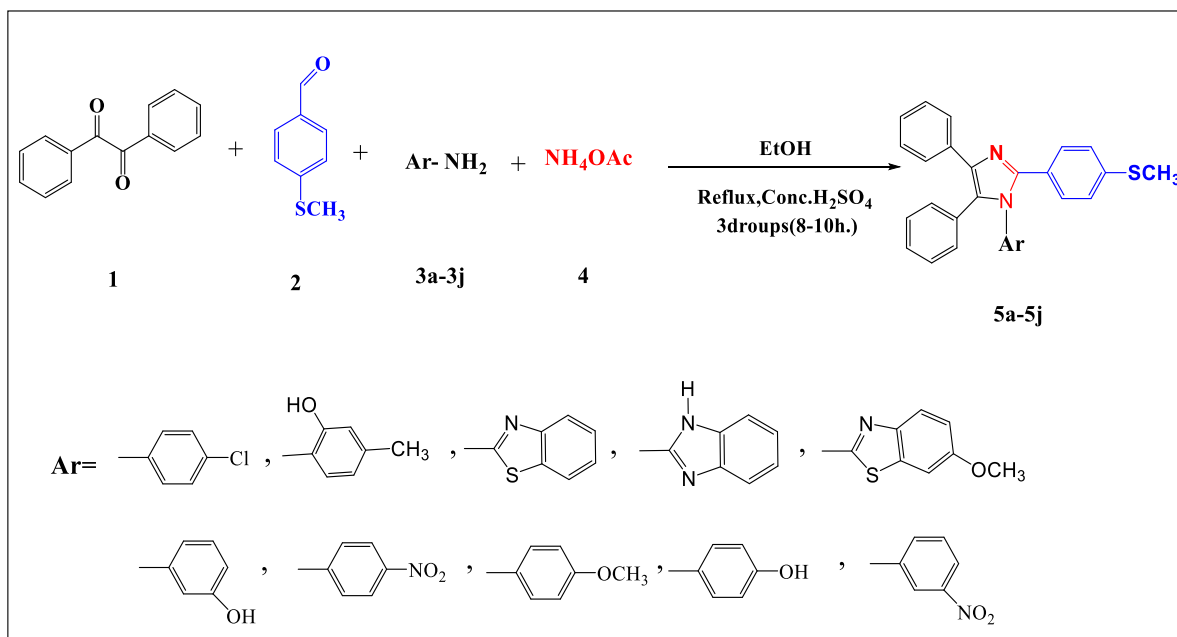
Table 3-4 The calculated molecular mass (g/mol) and observed molecular ion mass (m/z) of the synthesized imidazoles (4a-4j)

Entry	Molecular weight (g/mol)	Molecular ion mass (m/z)
4a	372.1	372.1
4b	390.1	390.1
4c	416.2	416.2
4d	399.2	399.2
4e	402.2	402.2
4f	400.1	400.1
4g	402.1	402.1
4h	395.2	395.2
4i	406.2	406.2
4j	433.2	433.2

3.10 Synthesis of 1,2,4,5-Tetra-substituted imidazole derivatives (5a-5j) by using sulfuric acid as a catalyst

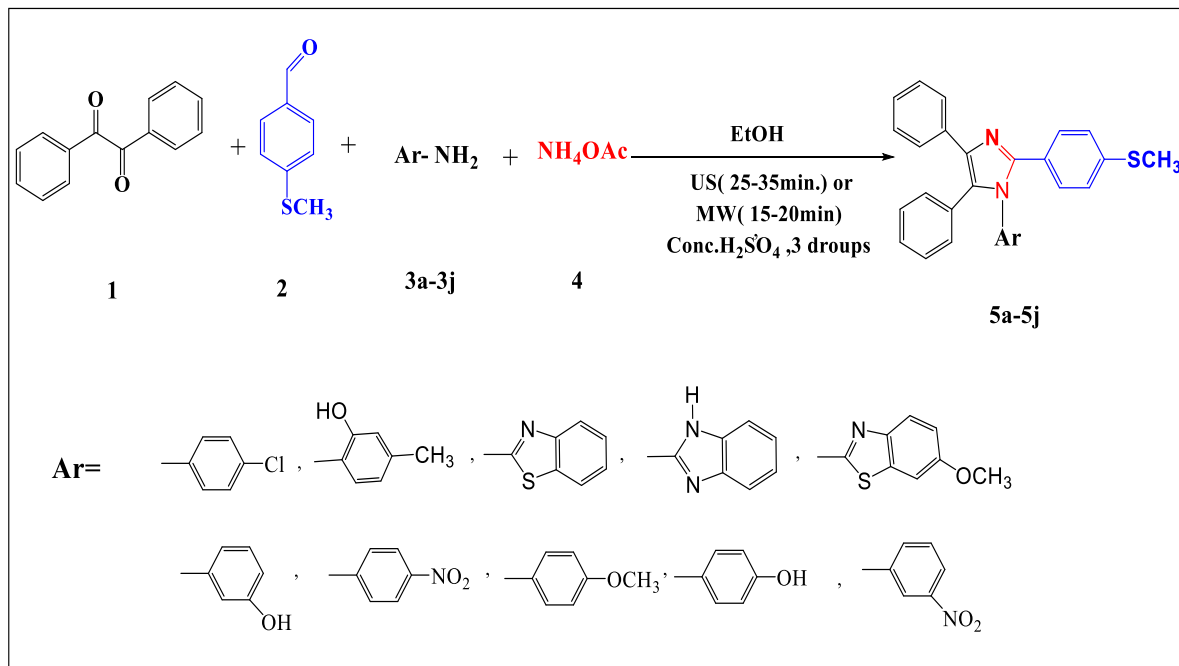
A new series of 1,2,4,5-tetrasubstituted imidazole derivatives (5a-5j) were synthesized using sulfuric acid as a catalyst and suitable solvents like ethyl alcohol which involving the condensation of benzil, aromatic aldehyde, and a variety of amines (aromatic and heteroaromatic).

Initially, equimolar amounts of benzil (0.001mol.), aromatic aldehyde (0.001 mol.), various aromatic amine 3a-3j (0.001mol.), and ammonium acetate (0.005mol.) in 15 mL of ethyl alcohol were refluxed for (8-10 hours) using H₂SO₄ as a catalyst that resulted in good yields. Four components are condensed during the reaction to produce the desired products 5a-5j as shown in Scheme (3-11). The reactivity of aryl aldehyde and benzil increases with the addition of sulfuric acid H₂SO₄.



Scheme 3-11 Synthesis of 1,2,4,5-Tetra-imidazole derivatives under reflux condition

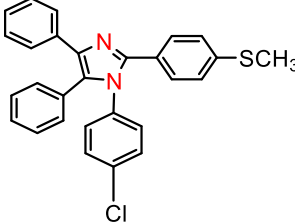
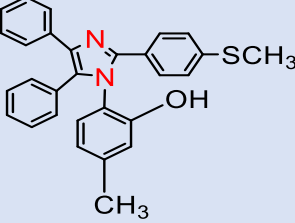
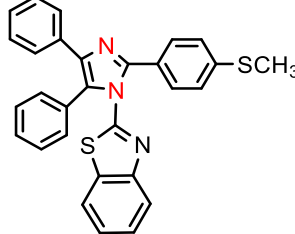
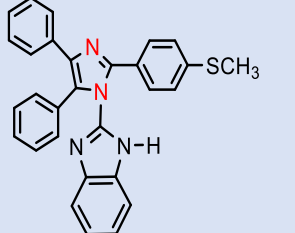
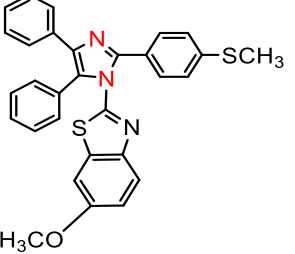
The same protocol was repeated employing both ultrasonic energy and microwave irradiation using a few drops of H₂SO₄ as a catalyst which took a shorter time and better yields, (Scheme 3-12).

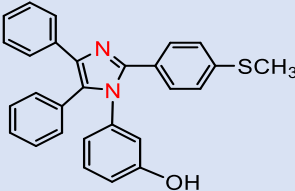
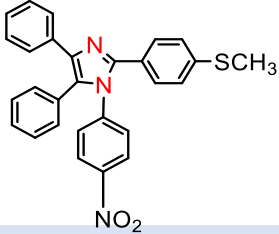
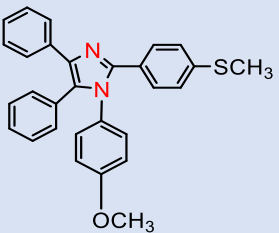
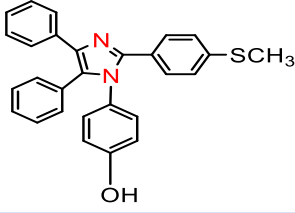
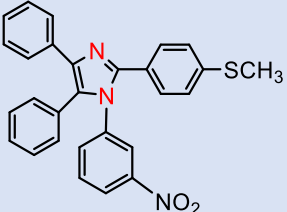


Scheme 3-12 Synthesis of 1,2,4,5-Tetra-imidazole derivatives under ultrasonic and microwaves conditions

A comparison of product yield utilizing various methods for the synthesis of 1,2,4,5-tetraimidazoles (**5a-5j**) is given in Table (3.5).

Table 3-5 Comparison of product yield using different conditions in the presence of H₂SO₄ as a catalyst for the synthesis of tetramidazoles (5a-5j)

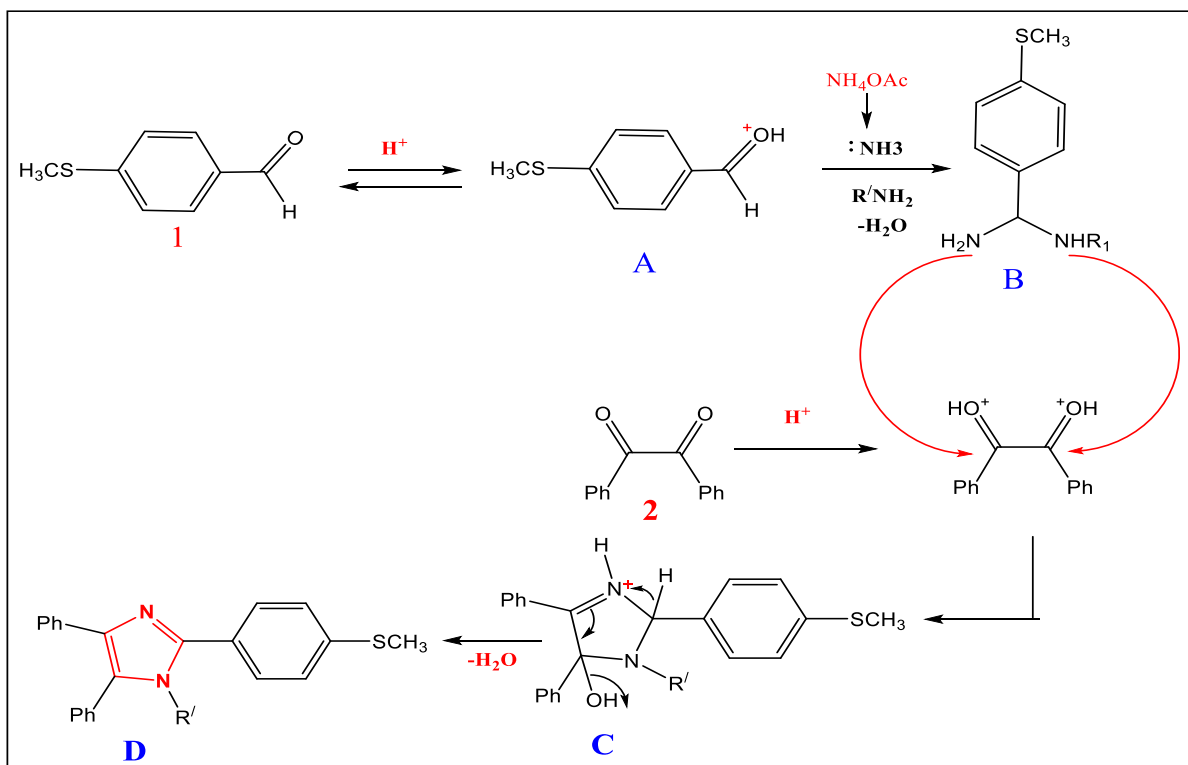
Entry	Product	Conventional heating (reflux)		Ultrasounds Condition		Microwave Condition	
		Time(h)	Yield (%)	Time(min.)	Yield (%)	Time(min.)	Yield (%)
5a		8	70	25	76	15	79
5b		8	72	25	78	20	83
5c		10	67	35	75	20	80
5d		10	68	30	73	15	82
5e		10	70	30	78	15	83

Entry	Product	Conventional heating (reflux)		Ultrasounds Condition		Microwave Condition	
		Time(h)	Yield (%)	Time(min.)	Yield (%)	Time(min.)	Yield (%)
5f		8	78	30	81	20	84
5g		9	65	35	70	20	80
5h		8	82	30	87	15	89
5i		9	80	25	84	15	87
5j		10	73	30	79	20	84

3.11 The proposed mechanism for the synthesis of 1,2,4,5-Tetra-imidazoles (General mechanism)

A suitable mechanism is outlined in Scheme (3-13) based on the literature [121]. In the first step, the carbonyl group in aldehyde (**1**) was protonated by the catalyst and then the intermediate (A) condensed with ammonia (which was generated from

NH_4OAc) and attacked as a nucleophile to the protonated carbonyl. After that reacting with the amine to produce compound (**B**). The nucleophilic reaction of compound (**B**) with protonated benzil (**2**) is followed by ring closure to obtain intermediate (**C**). Finally, the dehydration step is obtained with electronic rearrangements to give compound (**D**).



Scheme 3-13 Proposed mechanism for the formation of 1,2,4,5-tetra-substituted imidazoles from benzil, aldehyde, amines, and NH_4OAc in the presence of H_2SO_4

3.12 Characterization of 1,2,4,5-Tetra-imidazole derivatives (5a-5j)

All synthesized compounds were proven using several spectral studies (FTIR, ^1H NMR, ^{13}C NMR and mass spectra) see Appendix A. Furthermore, the melting points have been determined.

The FT-IR spectra of all synthesized compounds exhibit the absence of the strong peak which is attributed to the stretching vibration of the N-H group of the amine, which indicates that the reaction has taken place, around $3030\text{-}3061\text{ cm}^{-1}$ (C-H) aromatic stretch was observed. Also, around $1517\text{-}1585\text{ cm}^{-1}$ (C=C) stretch and around $1602\text{-}1612\text{ cm}^{-1}$ (C=N) stretch in the side imidazole ring as expected. FT-IR data clearly

show the successful completion of cycloaddition reactions and the formation of the imidazole ring. The FT-IR spectra of all synthesized compounds are provided in the appendix A.

¹HNMR spectra of all imidazoles in DMSO-d₆ show peaks at expected chemical shift values (See appendix A). The number of signals and their integration are in agreement with the proposed structures. The signals of aromatic protons are indicated in the form of a multiplet around 7.10 to 7.37 ppm [122]. Table (3-6) lists other characteristic bands of the FTIR and ¹H NMR and their interpretations.

Table 3-6 Characteristic absorption bands of FT-IR and ¹HNMR spectra for (5a-5j)

Comp. No.	FT-IR (cm ⁻¹)			¹ HNMR (ppm)
	ν (C-H) aromatic	ν (C=N)	others	
5a	3061	1602	ν (C-Cl) 756	7.53 (d, $J = 10.0$ Hz, 2H, ph-H), 7.41 (d, $J = 10.0$ Hz, 3H, ph-H), 7.34 (t, $J = 7.5$ Hz, 6H, ph-H), 7.28 – 7.24 (m, 4H, ph-H), 7.19 (dd, $J = 15.0, 10.0$ Hz, 3H, ph-H), 2.46 (s, 3H, SCH ₃).
5b	3064	1604	ν (O-H) 3224	9.67 (s, 1H, <u>OH</u>), 7.49 (dd, $J = 10.0, 5.0$ Hz, 4H, ph-H), 7.30 – 7.24 (m, 7H, ph-H), 7.18 (d, $J = 10.0$ Hz, 3H, ph-H), 6.99 (d, $J = 10.0$ Hz, 1H, ph-H), 6.93 (s, 1H), 6.78 (d, $J = 5.0$ Hz, 1H, ph-H), 2.46 (s, 3H, SCH ₃), 2.08 (s, 3H, CH ₃).
5c	3076	1602	-	8.03 (d, $J = 10.0$ Hz, 2H), 7.53 (dd, $J = 20.0, 10.0$ Hz, 2H, ph-H), 7.44 (t, $J = 10.0$ Hz, 3H, ph-H), 7.37 (t, $J = 10.0$ Hz, 3H, Ph-H), 7.30 (t, $J = 10.0$ Hz, 2H, Ph-H), 7.23 (d, $J = 5.0$ Hz, 1H, ph-H), 2.53 (s, 3H, SCH ₃).
5d	3028	1602	ν (N-H) 3318	12.66 (s, 1H, <u>NH</u>), 8.08 (d, $J = 8.4$ Hz, 2H, Ph-H), 7.57 (dd, $J = 30.0, 10.0$ Hz, 5H, ph-H), 7.45 (t, $J = 7.5$ Hz, 3H, ph-H), 7.39 (d, $J = 10.0$ Hz, 4H, ph-H), 7.32 (t, $J = 7.5$ Hz, 3H, ph-H), 7.25 (d, $J = 5.0$ Hz, 1H, ph-H), 2.54 (s, 3H, SCH ₃).

Comp. No.	FT-IR (cm ⁻¹)			¹ HNMR (ppm)
	ν (C-H) aromatic	ν (C=N)	others	
5e	3022	1606	ν (C-O-C) 1281,1199	8.03 (d, $J = 8.0$ Hz, 2H, ph-H), 7.53 (dd, $J = 8.0, 4.0$ Hz, 4H, ph-H), 7.44 (t, $J = 8.0$ Hz, 3H, ph-H), 7.36 (d, $J = 8.0$ Hz, 4H, ph-H), 7.30 (t, $J = 6.0$ Hz, 3H, ph-H), 7.23 (d, $J = 8.0$ Hz, 1H, ph-H), 3.80 (s, 3H, OCH ₃), 2.53 (s, 3H, SCH ₃)
5f	3053	1620	ν (O-H) 3433	9.78 (s, 1H, OH), 8.04 (d, $J = 8.0$ Hz, 2H, Ph-H), 7.55 (dd, $J = 16.0, 8.0$ Hz, 5H, Ph-H), 7.44 (t, $J = 8.0$ Hz, 3H, Ph-H), 7.36 (d, $J = 8.0$ Hz, 4H, Ph-H), 7.31 (t, $J = 8.0$ Hz, 3H Ph-H), 7.23 (d, $J = 8.0$ Hz, 1H Ph-H) 2.54 (s, 3H, SCH ₃).
5g	3030	1608	ν (NO ₂) 1539 asym. 1379 sym.	8.06 (d, $J = 10.0$ Hz, 2H, Ph-H), 7.55 (dd, $J = 10.0, 5.0$ Hz, 5H, Ph-H), 7.46 (t, $J = 10.0$ Hz, 3H, Ph-H), 7.38 (d, $J = 10.0$ Hz, 3H, Ph-H), 7.32 (t, $J = 10.0$ Hz, 3H, Ph-H), 7.24 (d, $J = 5.0$ Hz, 1H, Ph-H), 2.55 (s, 3H, SCH ₃)
5h	3045	1602	ν (C-O-C) 1296,1251	8.58 (d, $J = 1.3$ Hz, 1H, Ph-H), 8.05 (d, $J = 8.2$ Hz, 2H, Ph-H), 7.94 – 7.82 (m, 4H, Ph-H), 7.63 (t, $J = 7.7$ Hz, 6H, Ph-H), 6.97 (d, $J = 8.8$ Hz, 3H, Ph-H), 6.86 (d, $J = 7.2$ Hz, 2H, Ph-H), 3.77 (s, 3H, OCH ₃), 2.53 (s, 3H, SCH ₃).
5i	3032	1608	ν (O-H) 3273	10.13 (s, 1H, OH), 8.04 (d, $J = 8.4$ Hz, 1H, Ph-H), 7.52 – 7.35 (m, 5H, Ph-H), 7.26 (dd, $J = 14.4, 6.2$ Hz, 6H, Ph-H), 7.15 (t, $J = 8.0$ Hz, 4H, Ph-H), 6.86 (dd, $J = 8.2, 1.3$ Hz, 1H, Ph-H), 6.73 (t, $J = 7.6$ Hz, 1H, Ph-H), 2.45 (s, 3H, SCH ₃).
5j	3057	1600	ν (NO ₂) 1512 asym. 1365 sym.	8.70 (s, 1H, Ph-H), 8.24 – 7.87 (m, 5H, Ph-H), 7.81 (t, $J = 7.5$ Hz, 1H, Ph-H), 7.64 (t, $J = 7.8$ Hz, 4H, Ph-H), 7.53 (dd, $J = 18.6, 7.4$ Hz, 2H, Ph-H), 7.40 (d, $J = 8.2$ Hz, 2H, Ph-H), 7.34 (dd, $J = 18.3, 8.4$ Hz, 3H, Ph-H), 2.53 (s, 3H, SCH ₃).

¹³CNMR spectra of compounds (**5a-5j**) exhibited signals of the three carbon atoms of imidazole moiety as (Ar-N-C=C) signal ranging from 125.94 to 126.68 ppm, (Ar-N-C=C) signals ranging from 127.00 to 128.66 ppm, and (N-C=N) signals ranging from 130.36 to 131.71 ppm. The rest of the spectral results are outlined in detail in the experimental section.

Furthermore, as presented in Table (3-7), the mass spectroscopy of products with an electron energy of 70 eV revealed molecular ion peaks M^+ at m/z matching their calculated molecular masses.

Table 3-7 The calculated molecular mass (g/mol) and observed molecular ion mass (m/z) of the synthesized imidazoles (5a-5j)

Entry	Molecular weight (g/mol)	Molecular ion mass (m/z)
5a	452.1	452.1
5b	448.2	448.2
5c	475.1	475.1
5d	458.2	458.2
5e	505.1	505.1
5f	434.1	434.1
5g	463.1	463.1
5h	484.2	484.2
5i	434.1	434.1
5j	463.1	463.1

CHAPTER FOUR

APPLICATIONS

4.1. Introduction

The use of chemical research methodologies to synthesize pharmaceutical substances is known as medicinal chemistry. Scientists were mainly concerned with the isolation of therapeutic compounds found in plants throughout the beginning stages of therapeutic chemical development. Researchers in this field are now equally concerned with developing novel synthetic drug molecules. Medicinal chemistry is usually used virtually to discover and develop new drugs.

Dendrimers possess a structure that can be modified according to various applications. The multi-functionality of its surface and the internal cavity along with the core make it widely applicable in various fields such as biomedical, diagnostics, cancer therapy, and tissue engineering [123], (Fig. 4-1).

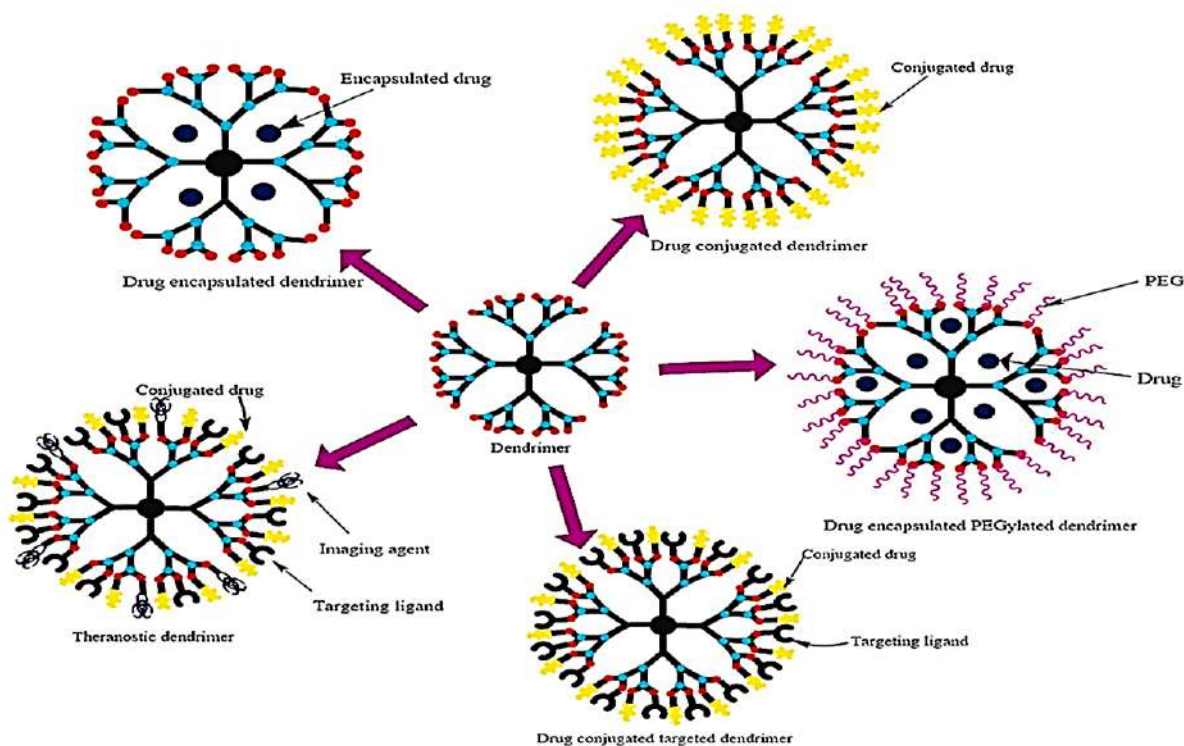


Figure 4-1 Schematic diagram that indicates the application of dendrimers in various biomedical fields [124]

They also impart utility in drug delivery, gene delivery, oligonucleotide labeling, photodynamic therapy, vaccine delivery, boron neutron capture therapy (BNCT), and targeted drug delivery. Further, they mimic the nature of proteins; hence they can be modified into drug molecules[124] .

Thus, the unique structure and features of dendrimers make them a potential candidate for use in many purposes. Recent research in this area also include the study of the antimicrobial activities of dendrimer derivatives. Poly amido amine (PAMAM) and other dendrimers with peripheral amino groups have been used as carriers or scaffolds for the covalent attachment of antimicrobial agents, such as quaternary ammonium[125,126] , carbohydrates[127] and boron complexes[128]. However, the antimicrobial activity of the PAMAM dendrimers has recently been discovered [129].

In the last decades, an aromatic heterocycle, especially the imidazole compounds ring, has been used as the structural skeleton for obtaining various types of bioactive compounds. According to a variety of literature surveys, imidazole derivatives exhibit a wide spectrum of pharmacological activities including Anticancer, Antibacterial, Antifungal, Anti-tubercular, Anti-HIV, and Analgesic activity. A variety of imidazole compounds have medicinal importance and are employed as powerful drugs, such as etomidate (A), ketoconazole (B), cimetidine (C), and clotrimazole (D) [130], (Fig.4-2). Particularly, heterocyclic compounds containing imidazole exhibit strong biological activity and have low toxicity [131]. These facts prompted us to search for the synthesis of new dendrimers and imidazoles and demonstrate their various activities.

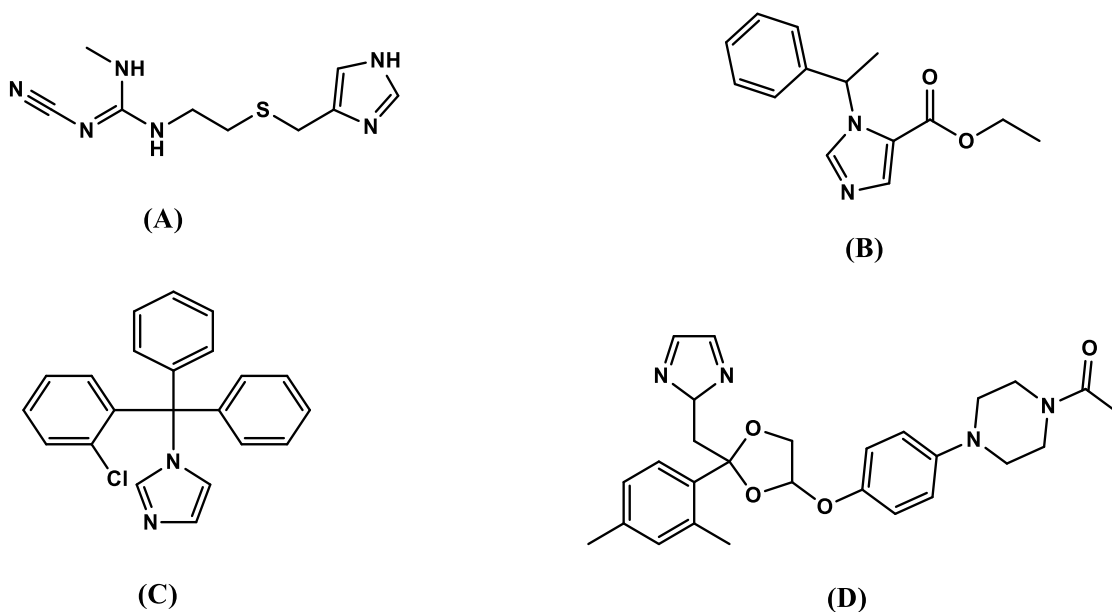


Figure 4-2 Different pharmacological activities of imidazole derivatives [130]

4.2 Literature Review

4.2.1 Anti-Urolithiasis Activity

The term urolithiasis derives from the Greek words ouron, which means urine, and lithos, which means stone. Urolithiasis is a condition in which a stone form in the renal system or urinary tract in numerous individuals of people. Approximately 10-15% of people are presently affected by kidney stones[132]. It is the third most common urological disorder, following urinary tract infections and prostate disorders [133] with a rate of recurrence of 70-81% in males and (47-60%) in females and is more common in both sexes[134]. Renal calculi production is a complex process resulting from several physicochemical activities, such as incredible saturation, nucleation, increased aggregation, and retention within the renal tubules[135]. Although many different types of stones have been identified, such as those made of monosodium urate monohydrate, ammonium urate, uric acid mono and di-hydrate, uric acid anhydrous [136], calcium oxalate monohydrate (CaOx) and cystine[137]. Calcium stones are the most prevalent (approximately 80%)[138]. Although the reason for urolithiasis remains unknown, it is likely caused by a positive family history, being overweight, obese, or having a high body mass index (BMI)[139].

Recent therapies, like Extracorporeal Shock Wave Lithotripsy (ESWL) as well as percutaneous nephrolithotomy, are costly, risk recurrence, and have severe adverse effects. There are very few medicinal products accessible to treat urolithiasis. Thiazides, potassium magnesium citrate, and allopurinol are useful in the treatment of urolithiasis. Cystone is a commercialized herbal formulation that inhibits the production of lithogenic compounds, causes urinary calculi disintegration, as well as has antibacterial properties that aid in the avoidance of stone-related urinary tract infections. On the other hand, drugs that specifically inhibit CaOx crystallization in urine would constitute a novel class of drug for the treatment of urolithiasis[140] .

4.2.1.1 Mechanisms of Stone Formation

There are numerous opinions involving the mechanism of CaOx renal stone formation, Figure (4-3) shows the steps of CaOx urinary stone growth and development. Renal stones form when there is too much salt in the urine, which causes crystalline particles to form. The driving factor for crystallization in fluids such as urine is supersaturating. When salt is given to a solvent, it dissolves until a certain concentration is achieved, after which further dissolving is impossible. The solvent is considered to be saturated with salt at this point. If the temperature and pH remain constant, more salt crystallizes in the solution. The thermodynamic solubility product is the concentration at which saturation occurs and crystallization begins. If crystallization inhibitors are unable to act, the end effect will be urolithiasis[141].

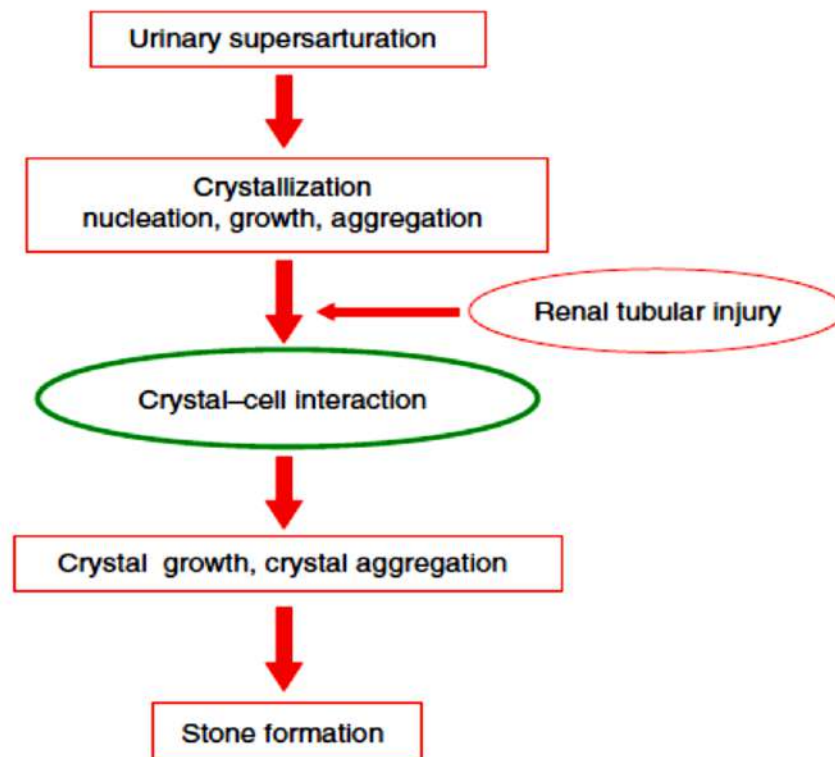


Figure 4-3 Schematic of the calcium oxalate kidney stone formation

4.4.1.1.1 Nucleation of Crystals

Nucleation is the first step in the transformation of a supersaturated solution from a liquid state to a solid state. This process starts with the coalescence of stone ions in the solution through loose clusters that might increase in size as new components or clusters are added. Nucleation can be classified into two types: homogeneous and heterogeneous. Homogeneous nucleation happens when the process proceeds spontaneously in a purified solution. Since impurities always exist in human urine, heterogeneous nucleation will typically occur at a lower supersaturation level compared to that needed for homogeneous nucleation induction. The function of heterogeneous nucleation in the formation of stones is unknown. Nonetheless, several investigations have found that most stones are composed of several crystals with one or two main constituents[142].

4.4.1.1.2 Growth of Crystal

Crystals can grow up through epitaxial (overgrowth of one crystalline material on another or the substrate of the crystalline lattice) mediated during the crystal growth process. Adsorption of molecules or ions separately on the crystal surface with supersaturated urine leads to the direct formation of one crystal on a surface that has various compositions or the surfaces of the crystal or substrate. Crystal growth is determined by the molecular shape, size of components, pH, and physical properties, or defects that can occur in the crystal structure. One of the most important steps in stone production is crystal growth[143].

4.4.1.1.3 Aggregation of Crystals

Aggregation is the process by which crystals in fluids stick to one another to produce larger particles. According to some researchers, crystal aggregation was the most crucial stage in stone formation. Although crystal growth is a necessary step in the shape of CaOx renal stones, the process occurs so slowly that crystals cannot grow sufficiently large to block the tubules of the renal system and can stay there by this process alone, as it takes several minutes for the tubular fluid to pass via the kidney [143,144]. Consequently, crystal aggregation is believed to be the most important phase. The various theories of CaOx urolithiasis believe that crystal aggregation likely plays a role in crystal retention inside the kidneys, given that crystal aggregation significantly influences particle size and aggregating crystals are frequently observed in urine and renal stones [145].

4.2.2 Diabetes Mellitus and Management

Diabetes mellitus is a health disease caused by an increase in blood glucose concentrations mainly because of the disorder of carbohydrate metabolism, which is characterized by a deficiency in the production of insulin and/or insulin action[146]. Diabetes mellitus is a non-communicable disease whose prevalence is increasing globally[147]. Over 300 million persons globally are diagnosed with diabetes [148].

Diabetes causes ketoacidosis, visual problems, nerve damage, decreased consciousness, and even death[149,150]. Diabetes deaths about 80% of people in countries with low or middle incomes. It is anticipated that around 366 million people worldwide will have diabetes by 2030 [151]. one study also revealed that the "diabetes epidemic" will continue even if obesity levels remain steady [152].

Diabetes mellitus is classified into two types: type I (T_1D) and type II (T_2D). Diabetes type I commonly known as insulin-dependent diabetes, occurs by the body's immune system destroying pancreatic beta cells, resulting in the body producing no insulin [153]. It has accounted for around 10% of all diabetes cases during the last two decades [154], but it is the most frequent form of diabetes among children, accounting for around eighty percent of pediatric diabetes cases[155]. Exogenous insulin injections are the only treatment for this metabolic condition. Diabetes type II, on the other hand, is non-insulin dependent and arises as a result of insulin resistance or insensitivity by peripheral tissues or receptors that regulate the utilization of glucose in the body[156]. The series of events that contribute to the progression of T_2D has not been thoroughly investigated. However, several hereditary factors, such as metabolic syndrome (MetS), as well as environmental causes, such as obesity, have been linked to the development of insulin resistance [157]. According to reports, 90% of diabetic cases are non-insulin dependent diabetes [156,158].

4.2.2.1 Anti-diabetic Drugs

The normalization of blood glucose is the goal of diabetes management. Antidiabetic drugs have several mechanisms, including reducing the production of glucose in the liver, stimulating the secretion of insulin (sulfonylureas and glinides drugs), improving insulin receptor sensitivity and circulating glucose absorption (thiazolidinediones and metformin), and insulin. Delaying the absorption and digestion of intestinal carbohydrates to maintain the postprandial glucose level (α -amylase and α -glucosidase drugs inhibitors)[159]. Increased blood glucose levels are

caused by enzymes such as α -amylases and α -glucosidases, which hydrolyze starch molecules (found in food) into their absorbable monomers. For instance, maltose, dextrin, and glucose are oligosaccharides that are produced by the activity of the α -amylase, and α -glucosidase enzyme are responsible for converting complex carbohydrates to glucose. It particularly hydrolyzed the α -1,4 glucopyranoside bond, which resulted in the release of an α -D-glucose from the sugar's non-reducing end. The α -antidiabetic inhibitors work by slowing the breakdown of complex carbohydrates into glucose and reducing the rate of absorption from the stomach, resulting in a lower postprandial blood sugar level [160].

Diabetes can be managed with the assistance of synthetic drugs such as miglitol metformin, alogliptin, and acarbose that act as α -amylase and α -glucosidase inhibitors [161,162]. Studies have demonstrated that, in addition to lowering blood glucose levels in type II diabetics, these inhibitory drugs have been reported to cause side effects, including raised serum transaminases and causes diarrhea, and abdominal pain [161-163]. This makes it useful for searching for alternative α -amylase inhibitors with few adverse effects.

4.2.3 Anti-bacterial Activity of Drugs

Humans have been perpetually exposed to various pathogens on a daily for many years, and such invasive infections caused by bacteria are regarded as significant problems, especially for immunocompromised individuals[164]. Antibiotics are a class of anti-bacterial compounds that can be used to prevent, manage, and treat bacterial infections. Antibiotics are natural, semi-synthetic, or synthetic substances that kill bacteria or inhibit their growth. When the bacteria are exposed to an antibiotic, they can respond in one of two ways, they can be sensitive, which inhibits their growth, division, and death or they can be unaffected or resistant[165].

The antibiotic resistance of microorganisms can be genetic (intrinsic) or acquired. Gene mutations occur spontaneously to produce natural resistance

mutation. After contact with an antibiotic, bacteria develop acquired resistance as a consequence of a species' adaptation to difficult environmental conditions.

In like a population, an antibiotic works as a selective agent on susceptible individuals, while resistant individuals survive and grow dominant. There are three mechanisms by which bacteria can develop antibiotic resistance : (i) modification of the active site of the target, which reduces the binding efficiency of the drug; (ii) direct damage or modification of an antibiotic by enzymes generated by the organism; and (iii) release of the antibiotic from the cell [166]. Imidazoles have many different mechanisms for their activity. One study suggests that nitroimidazoles enter the cell via passive diffusion, where they undergo reduction to produce nitro radical anion. The anion oxidizes DNA, causing DNA strand breakage and cell death [167].

Another study revealed that flavohaemoglobins in bacteria convert nitric oxide (NO) to nitrates (NO₃), preventing NO-mediated damage, inhibition of growth, and death rates. The imidazoles work by coordinating flavohaemoglobin and inhibiting its NO dioxygenase (NOD), hence inhibiting NO metabolism and eventually leading to bacterial cell death [168]. According to another group of studies, inhibiting enoyl acyl carrier protein reductase (fatty acid biosynthesis inhibitor), an enzyme that facilitates the production of bacterial fatty acids, provides a new target for antibacterial activity[169]. Therefore, bacteria that are resistant to antibiotics are a significant public health problem. Overcoming the problem and seeking new sources of antimicrobial agents is a global challenge and the objective of numerous types of research carried out by scientists, academic institutions, and pharmaceutical companies. This application is an attempt to investigate the potential antibacterial effects of dendrimer and imidazole derivatives against a variety of bacterial isolates.

4.2.4 Hemolysis

Red blood cells (RBC), also known as erythrocytes, are among the most numerous cells in the human body. Their main function is to carry oxygen (O₂) from

the lungs to all of the body's cells utilizing hemoglobin, a metalloprotein with heme groups whose iron atoms briefly bind with the O₂ [170]. Human RBCs are extensively used as a model for evaluating the cytotoxicity of natural and synthesized chemical compounds. To evaluate the hem biocompatibility of products for potential biomedical applications, the hemolytic assay is required. Compounds that produce more than 5% hemolysis at different concentrations are considered non-hemocompatible[171]. Several compounds have the potential to be biologically active, however, they can also cause toxic effects such as hemolysis (i.e., the rupture of erythrocytes), which may damage vital organs including the liver, kidney, and heart[172,173]. Therefore, it is necessary to test the hemolytic effect of biologically active compounds. The hemolytic assay is one of the simplest, inexpensive, and most rapid methods for preliminary toxicity examination, as it is evident from numerous studies that the findings obtained with this method complement those obtained with the cytotoxicity assay performed on normal cell lines [174].

Hemolysis is defined as the rupture of red blood cells (erythrocytes) and the discharge of their contents (e.g., hemoglobin) into the external environment[175], which causes anemia, jaundice, and renal failure [176].

4.3. Apparatuses and Chemicals

4.3.1. Apparatuses

The apparatuses and equipment used in the study are summarized in Table (4-1).

Table (4-1): The apparatuses and equipment used in this study

Instruments	Company
Autoclave	Hirayama (Japan)
Electronic balance	ABS 220-4/KERN
Incubator	Gallen Kamp (England)
Light microscopic (40X)	BioLab-103B
Micro-titer plate reader	Bio Tek (U.S.A)
Microplate 96 well	LabTech/Korea
Micropipette	DragoLAB/China
Oven	Memmert
Table Top Centrifuge	PLC-05 Taiwan
Visible spectrophotometer	(FAITHFUL) model /721 (China)
Vortex mixer	945307 /THE.U.S.A
Water bath	England /Gallenkamp

4.3.2 Chemicals

The chemicals used in this study are summarized in Table (4-2)

Table (4-2): The chemicals used in this study

Material	Company
Calcium chloride	BDH Chemical
Sodium oxalate	BDH Chemical
Tris-HCl buffer	Himedia, India
Anhydrous sodium carbonate	Merck, Germany
Sodium chloride	Hi-Media
α -amylase	Macklin /china
Phosphate buffer	Grainland Chemical Company
3,5-dinitrosalicylic acid	Analar trade mark
Acarbose	Germany / Company
α -glucosidase	Macklin /china
<i>P</i> -nitrophenyl-D-glucopyranoside	Macklin /china
Starch	Himedia, India
Cystone	Indian/ Company
Normal saline	RASAN Sulaymaniyah / Iraq
Triton X-100	BDH Chemical

4.4 Methods

4.4.1 Urolithiasis Assay

4.4.1.1 Nucleation Assay

- **Procedure**

The nucleation test was carried out using the method given in refs. [177,178]. Calcium chloride (4 mM) and sodium oxalate (7.5 mM) solution were prepared in a Tris-HCl buffer (Tris-HCl 0.05 M and NaCl 0.15 M) at pH 6.5. A 95 μ L of calcium chloride solution was added to 10 μ L of each different concentration (50, 100, 150, 200, 250 μ g/mL) of the synthesis compounds (**G2_(a)**, **G3_(b)**, **G2_(b)**, **G3_(b)**, **4a**, **4b**, **4e**, **4f**, **5a**, **5b**, **5f**, and **5g**) and the cystone drug was used as a positive control in a 96-well plate. To start the crystallization process, a 95 μ L of sodium oxalate was added to the mixture.

The negative control was prepared in the same way but without the sample. The mixture was incubated at 37°C for 0, 30, 60, 180, and 360 minutes respectively. The optical density was measured at 620 nm.

- **Calculation**

The percentage inhibition of nucleation was calculated using eq.1.

$$\% \text{ Inhibition} = (\text{OD control} - \text{OD test} / \text{OD control}) \times 100 \dots \dots \dots \text{eq.1}$$

where OD test is the optical density of the sample or cystone, and OD control is the optical density of the negative control.

4.4.1.2 Aggregation Assay

- **Procedure**

The aggregation test for calcium oxalate crystals was performed as described in refs.[179,180]. The preparation of calcium oxalate crystals was initiated by mixing (10mL) the solutions of CaCl₂ (50 mM) and Na₂C₂O₄ (50 mM). Both solutions were heated at 60°C in a water bath for 1 hour to form the crystals, then cooled down to 37°C to give a final concentration of 0.8 mg/mL, which was dissolved in a Tris-HCl buffer (Tris-HCl 0.05 M and NaCl 0.15 M) at pH 6.5. A 100 µL of prepared compounds (**G2_(a)**, **G3_(b)**, **G2_(b)**, **G3_(b)**, **4a**, **4b**, **4e**, **4f**, **5a**, **5b**, **5f** and **5g**) were separately added to the calcium oxalate crystal solution and incubated at 37°C for 0, 30, 60, 180, and 360 minutes respectively. The optical density was measured at 620 nm. The absorbance was measured in triplicate.

- **Calculation**

The percentage inhibition was calculated as indicated in eq. 1.

- **Statistical analysis**

The statistical package for social science (SPSS) version 28 (IBM,SPSS, Chicago,USA) was used for data analysis. One-way analysis of variance (ANOVA) followed by the Tukey's post Hoc test was used for all pairwise differences. *P*- values ≤ 0.05 are considered to be statistically significant.

4.4.2 Antidiabetic Assay

4.4.2.1 Inhibition Activity of α -Amylase

- **Procedure**

The inhibitory activity of the α -amylase enzyme was measured using the standard reference approach [181]. An α -amylase enzyme (500 μ L) 1 U/mL was incubated in a tube with 1000 μ L of phosphate buffer (pH 6.8, 50 mM) and 250 μ L of starch solution (2%w/v) for 10 minutes at 37°C. To the previously incubated enzyme solution. A 1000 μ L of different concentrations (50,100,150,200 and 250 μ g/mL) of prepared compounds (**G2_(a)**, **G3_(b)**, **G2_(b)**, **G3_(b)**, **4a**, **4b**, **4e**, **4f**, **4g**, **5a**, **5b**, **5f** and **5g**) were separately added. Thereafter, 1000 μ L of 3,5-dinitro salicylic acid (DNS) was added. Then the samples were placed in a water bath for 15 minutes. The contents of the tubes were cooled to room temperature and the final volume of each was diluted with 9 mL of deionized water, and the absorbance was determined at 540 nm using a UV-Vis spectrophotometer. The negative control was prepared without any test material. Acarbose was utilized as a positive control.

- **Calculation**

The percentage of enzyme inhibition was calculated as in equation 2.

$$(\%) \text{ Inhibition of enzyme} = \left[\frac{\text{Abs}_{540} (\text{control}) - \text{Abs}_{540} (\text{sample})}{\text{Abs}_{540} (\text{control})} \right] \times 100 \dots\dots\dots \text{eq.2}$$

4.4.2.2 Inhibition Activity of α -Glucosidase

- **Procedure**

The study of α -glucosidase inhibition was determined according to [182]. The 10 μ L of various concentrations (50,100,150,200 and 250 μ g/mL) of the prepared derivatives (**G2_(a)**, **G3_(b)**, **G2_(b)**, **G3_(b)**, **4a**, **4b**, **4e**, **4f**, **4g**, **5a**, **5b**, **5f** and **5g**) were placed in a 96-well plate. Acarbose (10 μ L) was utilized as a reference drug. A 135 μ L of phosphate buffer (pH 6.8) was added and the substrate *p*-nitrophenyl-D-glucopyranoside (PNPG) (25 μ L, 4 mM) was added to the mixture and incubated at 37°C for 5 minutes. A 50 μ L of α -glucosidase solution (0.15 U/mL) was prepared in phosphate buffer (pH 6.8) added to every well and incubated at 37°C for 15 minutes. A 100 μ L of sodium carbonate (200 mM) was added to the mixture to spotted the reaction. Finally, the absorbance at 405 nm was measured using an ELISA microplate reader. The control was prepared without any test material. All tests were carried out in triplicate.

- **Calculation**

The percentage inhibition was determined according to the equation 3.

$$(\%) \text{ Inhibition of enzyme} = \left[\frac{\text{Abs}_{405} (\text{control}) - \text{Abs}_{405} (\text{sample})}{\text{Abs}_{405} (\text{control})} \right] \times 100 \dots\dots\dots \text{eq.3}$$

Where Abs= Absorbance

4.4.3 Anti-bacterial Assay

4.4.3.1 Minimum Inhibitory Concentrations (MICs) Method

Antibacterial activity was tested by determining the minimum inhibitory concentration (MIC) using the microdilution plate method with resazurin. Briefly, Double serial dilutions (100, 200, 300, and 400 μ g/mL) of samples (**G2_(a)**, **G3_(a)**, **G2_(b)**, **G3_(b)**, **4a**, **4b**, **4e**, **4f**, **5g**, **5a**, **5b**, **5c**, **5f** and **5g**) and drugs (Amoxicillin-clavulanic acid and Azithromycin) which were prepared from a stock (500 μ g/mL) and added to the 96-well microtiter plate using Mueller-Hinton broth as a diluent

which prepared by dissolving 21mg of Mueller Hinton broth powder in 100 mL of distilled water and thoroughly mixing until dissolved. This media was sterilized by autoclaving at (121°C) for 15 minutes and 15 (Psi) pressure. All wells were inoculated with 20µl of bacteria suspension (isolate from UTI infections) comparable to McFarland standard No.0.5 (1.5×10^8 CFU/ mL) except for the negative control wells as a reference for the Antibiotic Susceptibility Study (AST), McFarland standard No.0.5 is performed by mixing 9.95 mL of 1% H₂SO₄ solution with 0.05 mL of 1% barium chloride (BaCl₂). Microtiter plates were incubated at 37°C for 18-20 hrs. Finally, 10 µL of resazurin solution prepared by dissolving 15 mg of resazurin in 100 mL of sterile distilled water using a vortex mixer until completely dissolved was added. Resazurin is an oxidation-reduction indicator used for the evaluation of microbial growth. It is a blue non-fluorescent dye that becomes pink and fluorescent when reduced to resorufin by oxidoreductases within viable cells. The inoculated plates were incubated at 37°C for 2h. MIC was defined as the lowest concentration of the tested samples that prevented resazurin color change from blue to pink. Antibiotic Amoxicillin-clavulanic acid and Azithromycin were used as positive control. The sub-MIC concentrations were determined visually in broth micro dilutions as the lowest concentrations at which color changed from blue to pink in the resazurin broth assay [183].

4.4.3.2 Agar Well Diffusion Method

Agar well diffusion is a common method for determining antimicrobial activity. It is the method of inhibiting microorganism growth and reducing their shelf life, as well as preventing the generation of microbial groups. This process may be carried out by microorganisms in a variety of ways. Like disc diffusion method, agar well diffusion, agar plug diffusion method, etc., using the agar well diffusion method, the antibacterial activity of some synthesized dendrimers (**G2_(a)**, **G3_(a)**, **G2_(b)** and **G3_(b)**) and imidazole derivatives (**4a,4b,4e,4f** and **4g**) and (**5a,5b,5c**, **5e** and **5f**) was evaluated against Gram-positive bacteria (*Staphylococcus aureus* and *Streptococcus*

agalactiae) and Gram-negative bacteria (*Proteus mirabilis*, and *Escherichia coli*). A volume of the inoculum of bacteria is dispersed throughout the entire surface of the agar to inoculate the agar plate surface. After that, a hole with a diameter of 6 to 8 mm is made carefully with a sterilized corn borer or the tip, and a volume of test sample solution (100 μ L) at various concentrations (200,300,400 and 500 μ g/mL) is introduced into the well. The diameter of the inhibitory zone was determined in millimeters (mm) for each sample. Amoxicillin-clavulanic acid and Azithromycin were utilized as standard drugs [184].

4.4.4 Hemolytic Assay

- **Procedure**

This study included ten healthy non-smoking donors ranging in age from 18 to 30 years. Blood was collected via venipuncture into test tubes containing heparinized human blood [185].

Different concentrations (500, 400, 300, 250, 200, and 100 μ g/mL respectively) of prepared compounds (**G2_(a)**, **G3_(a)**, **G2_(b)**, **G3_(b)**, **4a**, **4b**, **4e**, **4f**, **5a**, **5b**, **5f**, and **5g**) (30 μ L) was added to 0.2 mL of the blood specimen. The mixture was then thoroughly stirred for 10 seconds. To avoid severe hemolysis, 10 mL of normal saline (0.9%) was added. For 10 minutes, the resulting mixture was centrifuged at 4000xg. The mixture's absorbance was measured at 540 nm. Blood has been diluted 100-fold in distilled water to achieve complete hemolysis (100%) of the sample. Normal saline was utilized as the negative control and Triton X-100 as the positive control.

- **Calculation**

After the determination of absorbance, the percentage of hemolysis was calculated using the equation 4.

$$\% \text{ of Hemolysis} = [(AT - AS) / (A_{100\%} - AS)] * 100 \% \dots \dots \dots \text{eq.4}$$

Where:

AT=Absorption of the test sample.

AS= Absorption of control (normal saline solution.)

A100% =Absorption of 100 percent hemolysis

4.5 Results

4.5.1 Urolethiasis Assay for Dendrimer (**G2_(a)**, **G3_(a)**, **G2_(b)**, and **G3_(b)**)

The effect of compounds (**G2_(a)**, **G3_(a)**, **G2_(b)** and **G3_(b)**.) on calcium oxalate nucleation and aggregation was investigated using the UV/visible spectroscopic method via measuring optical density (OD) at 620 nm in the presence of inhibitor (tested sample and cystone) and in the absence of inhibitor. The percentage of inhibition was determined. Figures 4-4 and 4-5 (a, b, c, d, and e) illustrate the % inhibition of calcium oxalate formation by each tested sample and the cystone. Based on the findings, all of the tested samples inhibited the calcium oxalate formation in a dose-dependent manner.

In the nucleation assay, compound **G2_(a)** showed 55% and 58% significant inhibition ($p < 0.001$) in the rate of crystal formation at the concentrations 50 μ g/mL and 100 μ g/mL respectively, after 360 minutes of incubation compared with cystone. The compounds **G2_(a)** and **G3_(a)** had shown 65% and 64% inhibition ($p < 0.05$ and $p < 0.001$) in the rate of crystal formation at the concentration of 150 mg/mL after 360 min of incubation compared with the drug whereas compound **G2_(b)** showed 60%, 66%, and 67% crystal growth inhibition ($p < 0.001$) at the concentration 150 mg/mL after 60, 180 and 360 minutes of incubation compared with the cystone. The results of compounds **G2_(b)** and **G3_(b)** showed excellent *in vitro* inhibition of CaOx crystal formation, that is, (67 %-84%), (85%- 91%), (63%-76%), and (80%-90%) respectively, at the concentration in 200 μ g/mL and 250 μ g/mL after 30, 60, 180, 360 minutes of incubation compared with cystone and other tested. As shown in Figure 4-4 (a, b, c, d, and e).

In the Aggregation assay, the inhibition percentage on calcium oxalate crystal of tested samples and standard drug cystone was shown in Figure 4-5 (a, b, c, d, and e), based on the results, compound **G2_(a)** exhibited the highest inhibition percentage ($p < 0.001$) with (52%,58%) and (67%,69%) respectively, in 200 μ g/mL and 250 μ g/mL concentration after 180, and 360 minutes of incubation as compared to other tested sample and positive control. The inhibition of aggregation activities of all tested samples did not exceed 50%, at concentrations 50 μ g/mL, 100 μ g/mL, and 150 μ g/mL after 0,30,60,180,360 minutes of incubation which is considerably high when compared to the standard control.

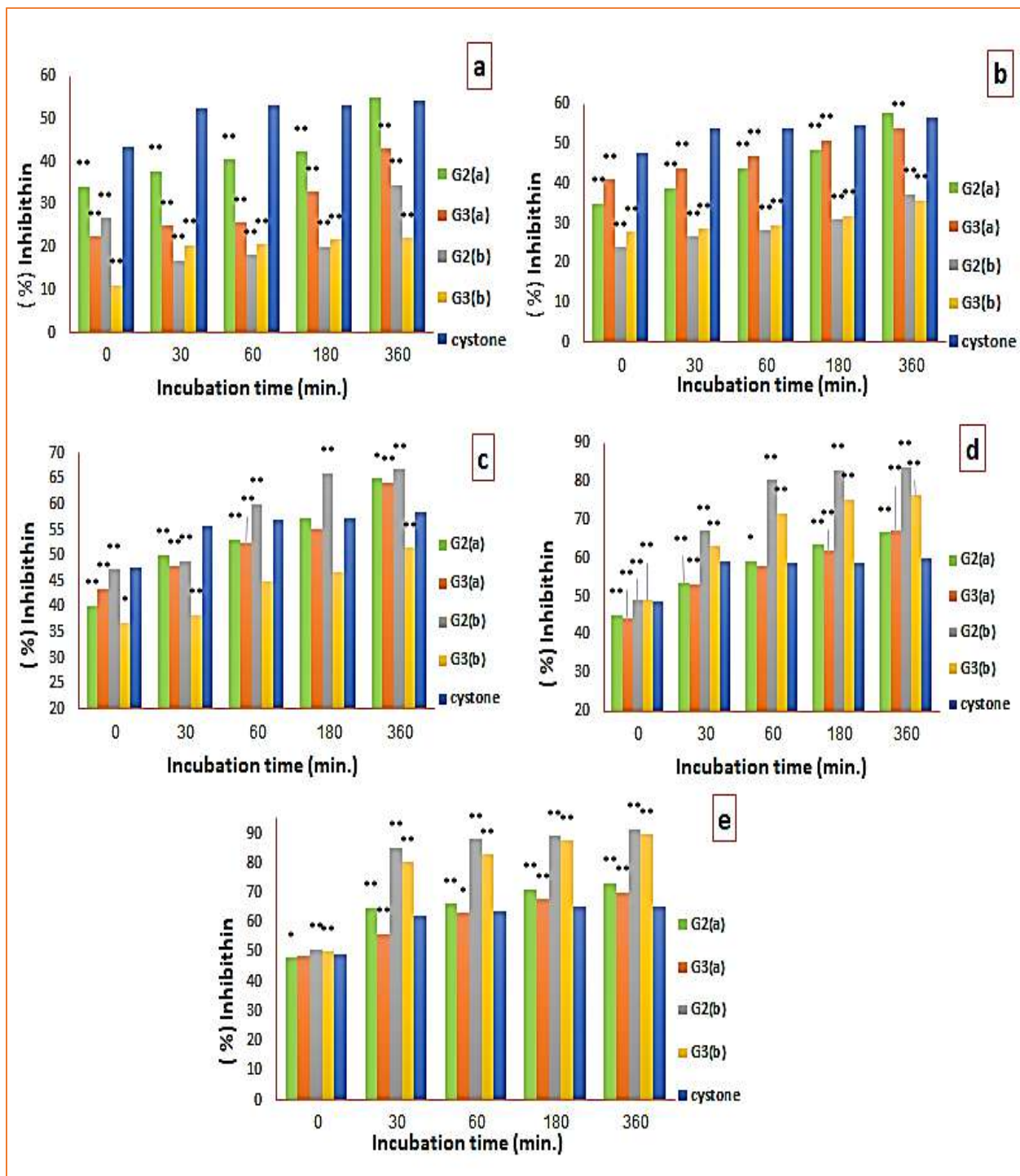


Figure 4-4: Effect of the G2(a), G3(a), G2(b), and G3(b) compounds and cysteine (a) at 50 µg/mL (b) at 100 µg/mL (c) at 150 µg/mL (d) at 200 µg/mL (e) at 250 µg/mL on nucleation of calcium oxalate crystallization **p*-value ≤ 0.05 vs. cysteine, ***p*-value ≤ 0.001 vs. cysteine

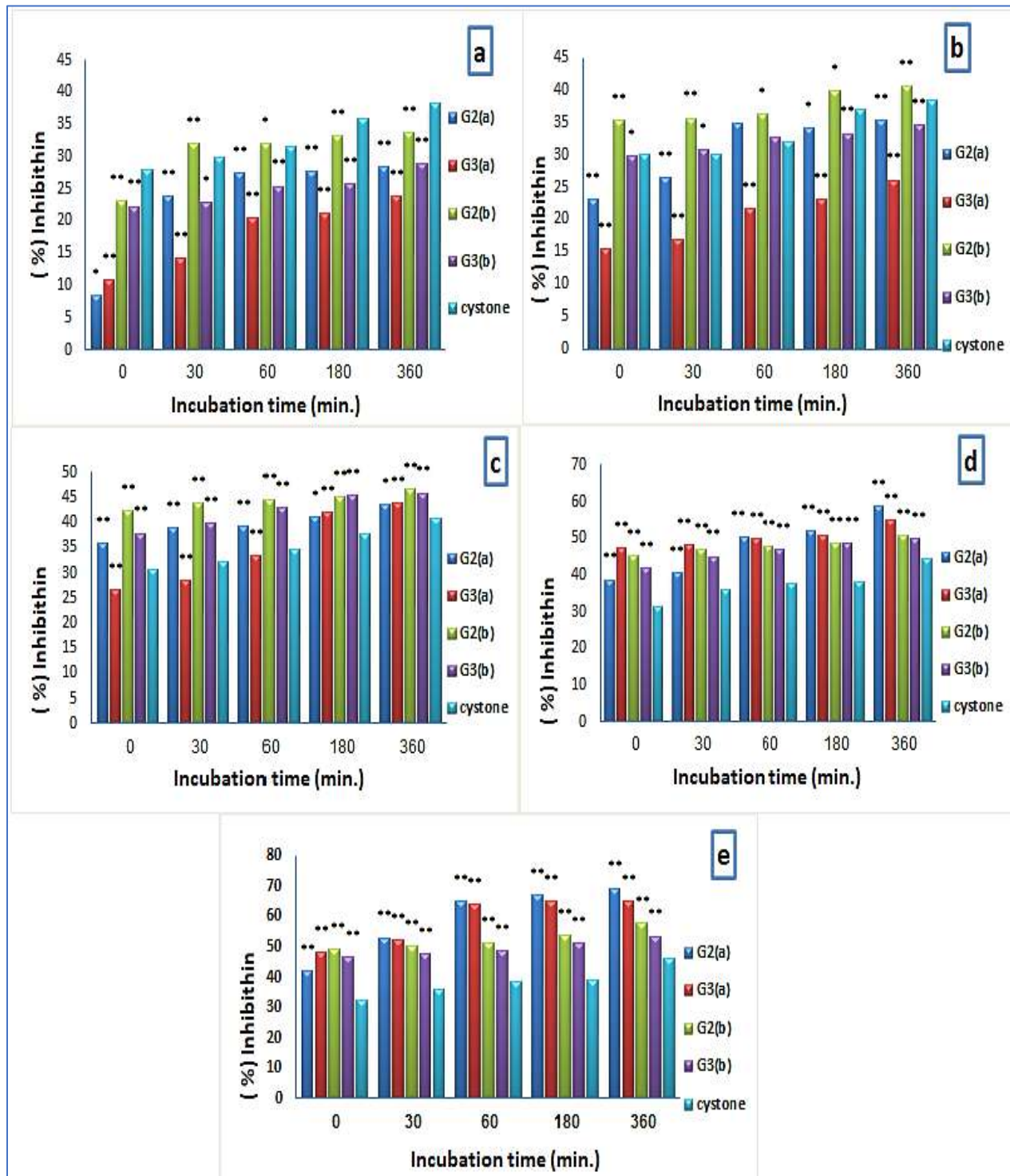


Figure 4-5: Effect of the G2(a), G3(a), G2(b), and G3(b) compounds and cystone (a) at 50 µg/mL (b) at 100 µg/mL (c) at 150 µg/mL (d) at 200 µg/mL (e) at 250 µg/mL on aggregation of calcium oxalate crystallization * p -value ≤ 0.05 vs. cystone, ** p -value ≤ 0.001 vs. cystone

4.5.2 Urolethiasis Assay for Tri-imidazole Derivatives (4a,4b,4e, and 4f)

The inhibitory effects of tested compounds (**4a**, **4b**, **4e**, and **4f**), and cystone on nucleation and aggregation of calcium oxalate crystals were determined based on the spectrophotometric assay at 620 nm in different concentrations (50,100,150, 200 and 250µg/mL) and incubation at different times (0, 30, 60, 180, and 360 minutes) at a temperature of 37 °C. The rate of nucleation was determined by comparing the induction time of crystals in the presence of the tested sample and those of the controls without the tested sample (negative control) and cystone (positive control). The effects of **4b** on nucleation are more potent than cystone and other tested samples with % inhibition in the range 64%-73%, 66%-73%, and 68%-74% ($p < 0.001$) at concentrations 150 µg/mL, 200 µg/mL, and 250 µg/ml after 60,180,360 minutes of incubation. Also, compound **4f** exhibited higher % inhibition ($p < 0.001$) of nucleation compared with cystone, besides, compounds **4a** and **4e** in the range of inhibition 64%-68%, 69% -72%, and 70% -73% at concentrations 150 µg/mL, 200µg/mL, and 250µg/ml respectively, after 180 and 360 minutes of incubation as explained in Figure 4-6 (a, b, c, d, and e).

The results of the aggregation assays which are shown in Figure 4-7 (a, b, c, d, and e) showed that all tested compounds have % inhibition higher than cystone at all concentrations after 0, 30,60,180,360 minutes of incubation. Compound **4b** had more potent calcium oxalate anti-crystallization activity than the activity of other tested compounds at concentrations of 50µg /mL (42%-52%), 100 µg /mL (43%-55%),150µg /mL (43%-57%),200µg/mL (43%-65%) and 250µg /mL (47%-68%) respectively, after 0, 30,60,180,360 minutes of incubation. The order of potency for the tested compounds was **4b** > **4f** > **4a** > **4e**. Compound **4b** was found to be most active in inhibiting of CaOx crystallization in both nucleation and aggregation assays.

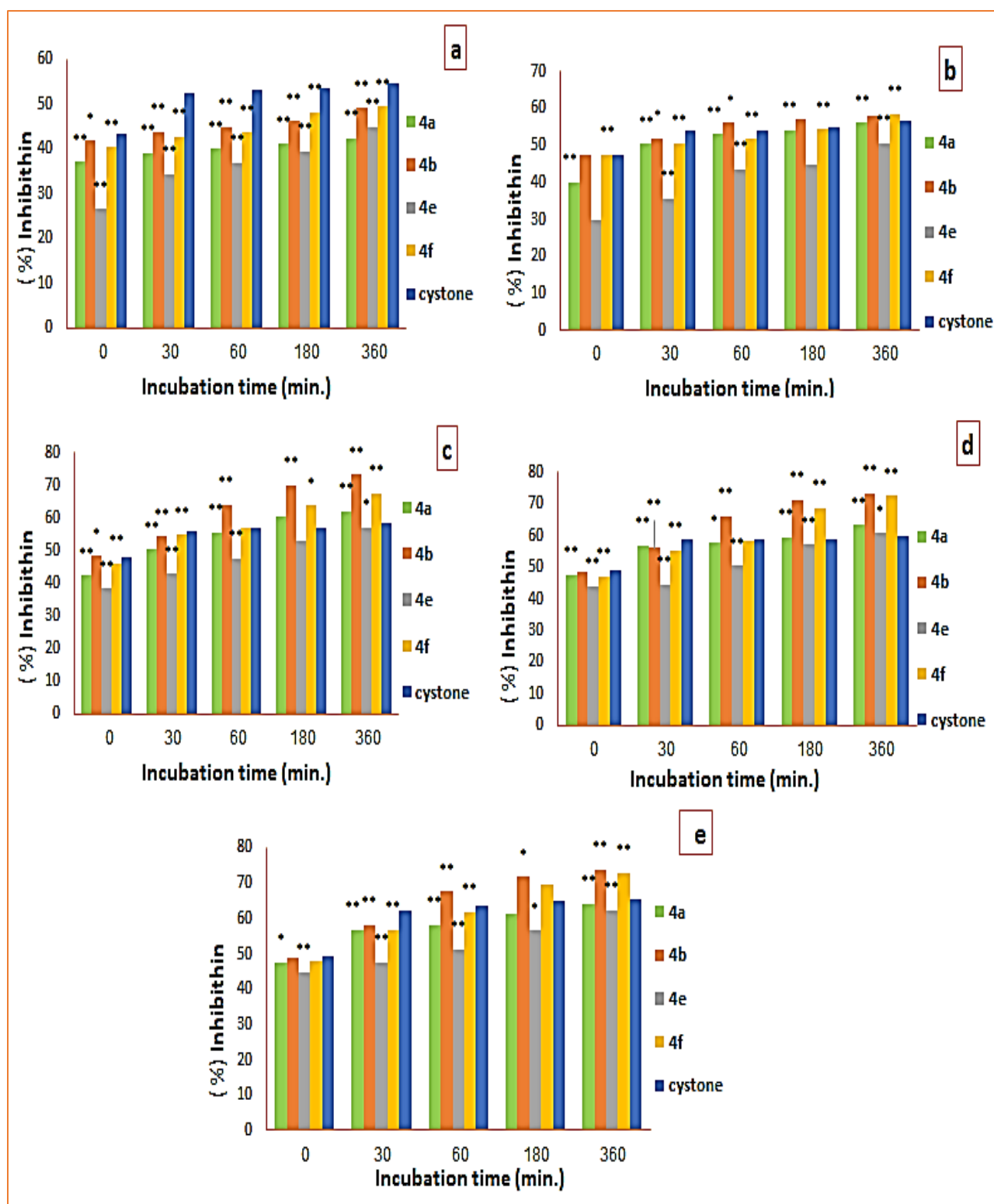


Figure 4-6: Effect of the 4a, 4b, 4e, and 4f compounds and cystone (a) at 50 µg/ml (b) at 100 µg/mL (c) at 150 µg/mL (d) at 200 µg/mL (e) at 250 µg/mL on nucleation of calcium oxalate crystallization **p*-value ≤ 0.05 vs. cystone, ***p*-value ≤ 0.001 vs. cystone

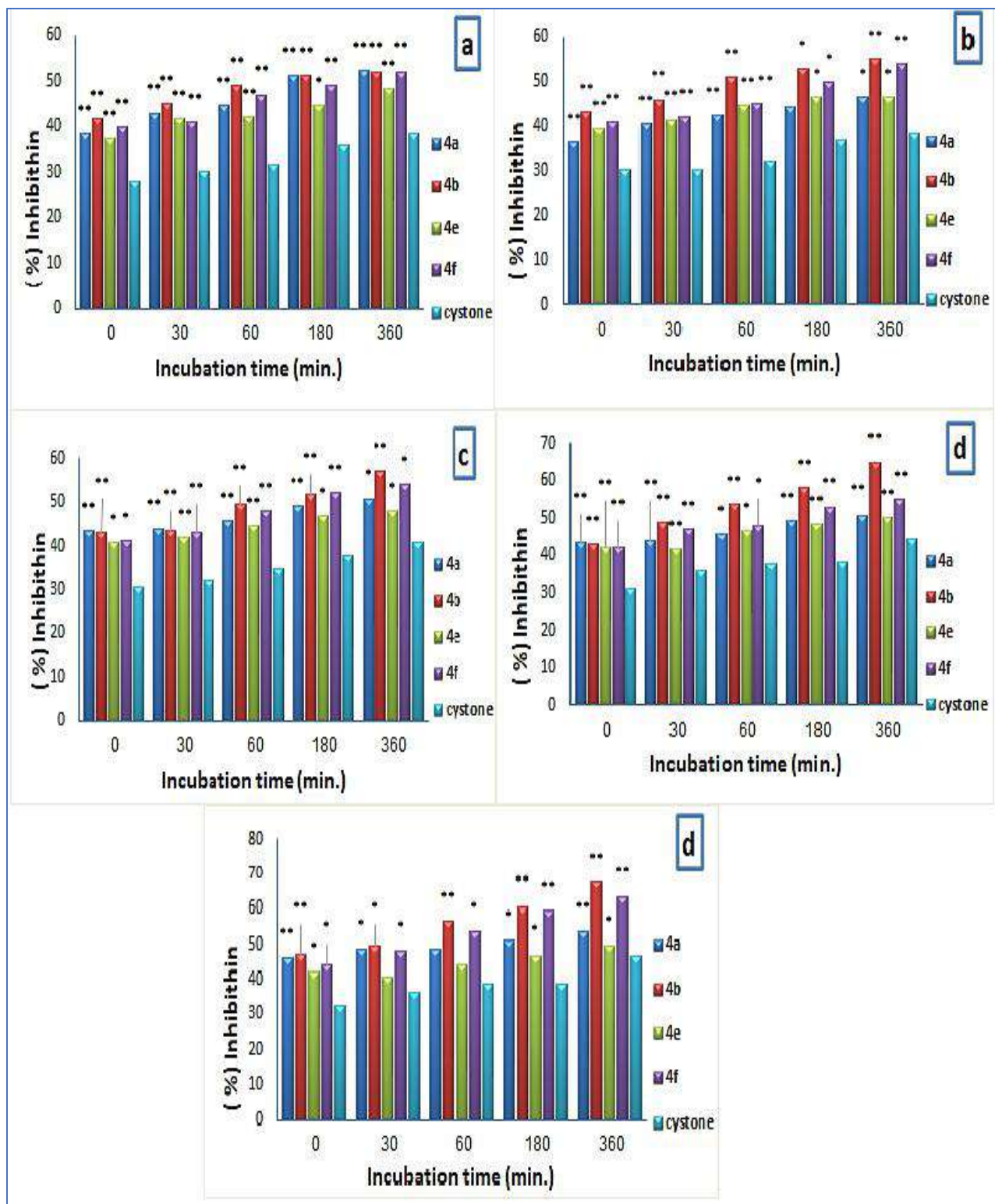


Figure 4-7: Effect of the 4a, 4b, 4e, and 4f compounds and cystone (a) at 50 µg/mL (b) at 100 µg/mL (c) at 150 µg/mL (d) at 200 µg/mL (e) at 250 µg/mL on aggregation of calcium oxalate crystallization **p*-value ≤ 0.05 vs. cystone, ***p*-value ≤ 0.001 vs. cystone

4.5.3 Urolethiasis Assay for Tetra-imidazole Derivatives (**5a**, **5b**, **5f**, and **5g**).

The percentage nucleation inhibition for various concentrations of the tested compounds (**5a**, **5b**, **5f** and **5g**) is shown in Figure 4-8 (a, b, c, d, and e). All the tested compounds at concentrations of 50 µg/mL, 100 µg/mL, and 150 µg/mL, after 0, 30, 60, 180, and 360 minutes, showed a lower percentage inhibition in the ranges 35%-52%, 30%-54%, and 44%-56%, respectively ($p < 0.001$) compared with the reference standard cysteine (43%-54%, 48%-57%, and 48%-59%, respectively). The highest inhibition of nucleation activity was obtained for the **5a** compound at 200 µg/mL and 250 µg/mL, after 0, 30, 60, 180, and 360 minutes in the ranges 47%-67% and 49%-71%, respectively, ($p < 0.001$) as compared to the cysteine, (49%-60% and 49%-65%). The second-highest inhibition of nucleation activity was the **5g** compound at 200 µg/mL and 250 µg/mL, after 0, 30, 60, 180, and 360 minutes in the ranges 45% -61% and 47%-67%, respectively, ($p < 0.05$) as compared to the control cysteine.

Figure 4-9 (a, b, c, d, and e) illustrates the activity of the various tested compounds in the aggregation inhibiting. All compounds **5a**, **5b**, **5f**, and **5g** at concentrations of 50 µg/mL, 100 µg/mL, 150 µg/mL, and 200 µg/mL, after 0, 30, 60, 180, and 360 minutes, showed the lowest percentage of inhibition ($p < 0.001$) in the ranges 8%-31%, 10%-34%, 14%-36%, and 14%-47% respectively, compared with the reference at 28-38%, 30-38%, 31-41%, and 31-44%, while the most significant inhibition against aggregation was obtained from compound **5a** at 250 µg/mL after 0, 30, 60, 180, and 360 minutes, which increased from 29% to 57% ($p < 0.001$) higher than cysteine (31%-46%) respectively.

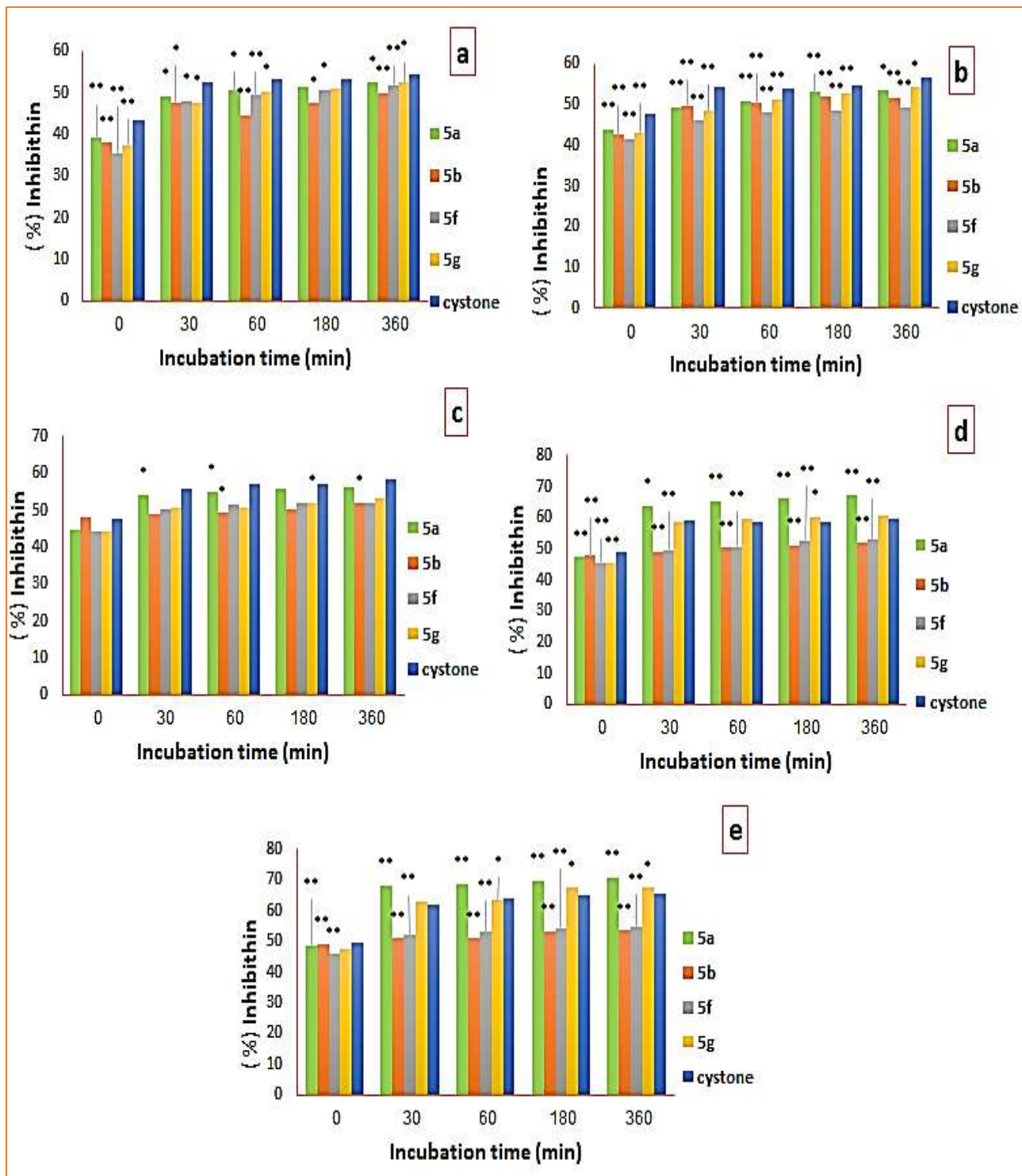


Figure 4-8: Effect of the 5a, 5b, 5f, and 5g compounds and cysteine (a) at 50 µg/mL (b) at 100 µg/mL (c) at 150 µg/mL (d) at 200 µg/mL, (e) at 250 µg/mL on nucleation of calcium oxalate crystallization *P-value ≤ 0.05 vs. cysteine, **P-value ≤ 0.001 vs. cysteine

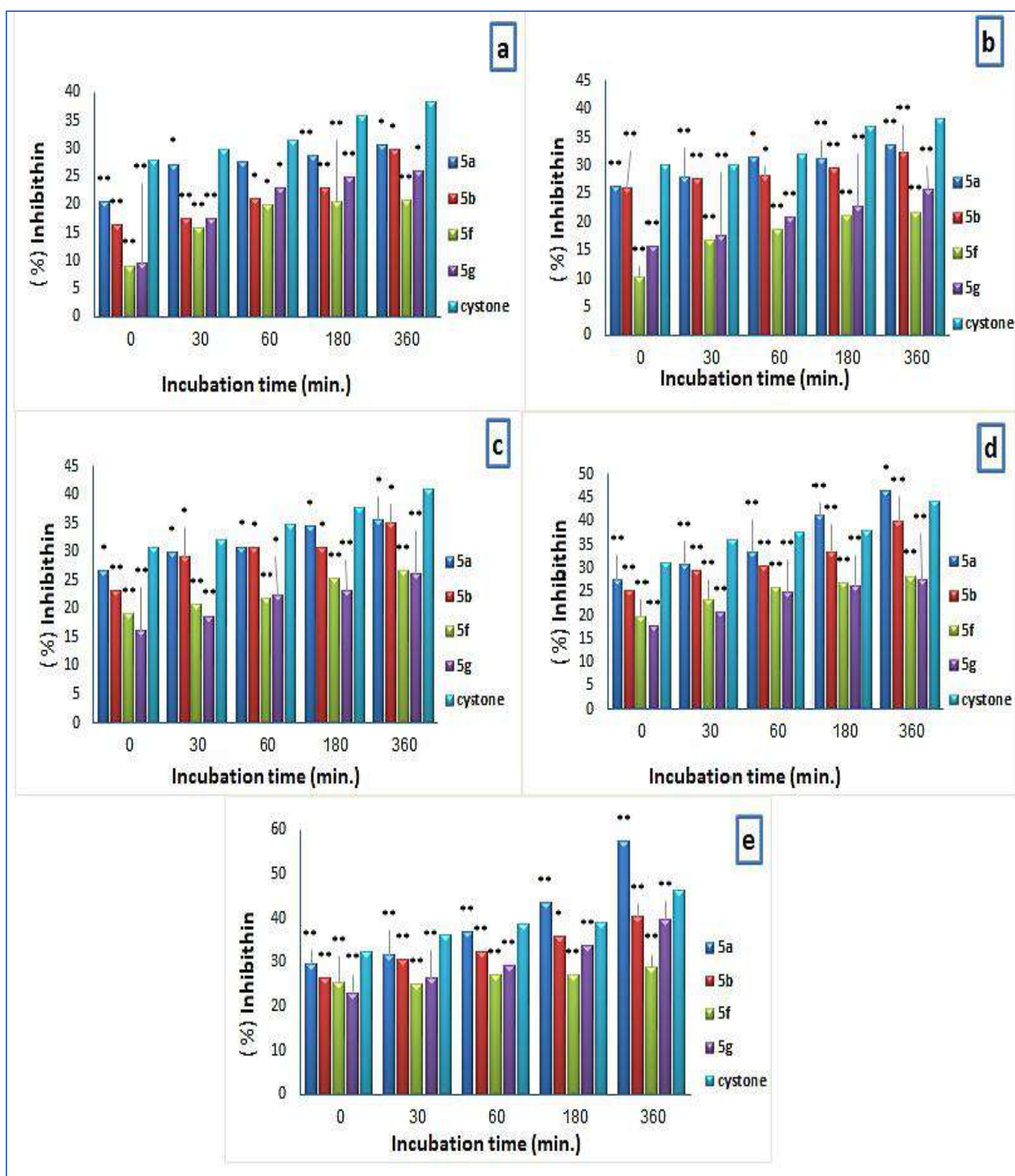


Figure 4-9: Effect of the 5a, 5b, 5f, and 5g compounds and cystone (a) at 50 µg/mL (b) at 100 µg/mL (c) at 150 µg/mL (d) at 200 µg/mL (e) at 250 µg/mL on the aggregation of calcium oxalate crystallization **p*-value ≤ 0.05 vs. cystone, ***p*-value ≤ 0.001 vs. cystone

4.5.4 Microscopy Study on the Changes of CaOx Crystals in Nucleation and Aggregation Assays

The images were obtained with a light microscope at a magnification of 40X. On the glass slide, a drop of the crystallizable or inhibitory solution mixture is poured and promptly placed under the microscope's lenses. The nucleation and aggregation activities were validated by examining the changes in the CaOx crystals. Figures 4-10 (a, b, and c) demonstrate the proportion of nucleation inhibition by the **G2_(b)** compound compared to the negative control and the positive control (cystone). The inhibition of CaOx crystal in nucleation assay was caused by the **G2_(b)** compounds and cystone, as the CaOx crystals were fewer in number when compared to the negative control indicating that the **G2_(b)** compound might prevent the chemical reaction of calcium chloride and sodium oxalate to producing CaOx crystals, demonstrating its activity as anti-urolithiasis.

The microscopic images of the aggregation inhibition by the **G2_(a)**, negative control, and positive control are shown in Figure 4-11 (a, b, and c). The number and shape of the CaOx crystals revealed that the **G2_(a)** had a stronger potential for crystal aggregation inhibition at higher concentrations (250 μ g/mL). The reduction of the size of crystals shows that the **G2_(a)** could reduce stone sizes.

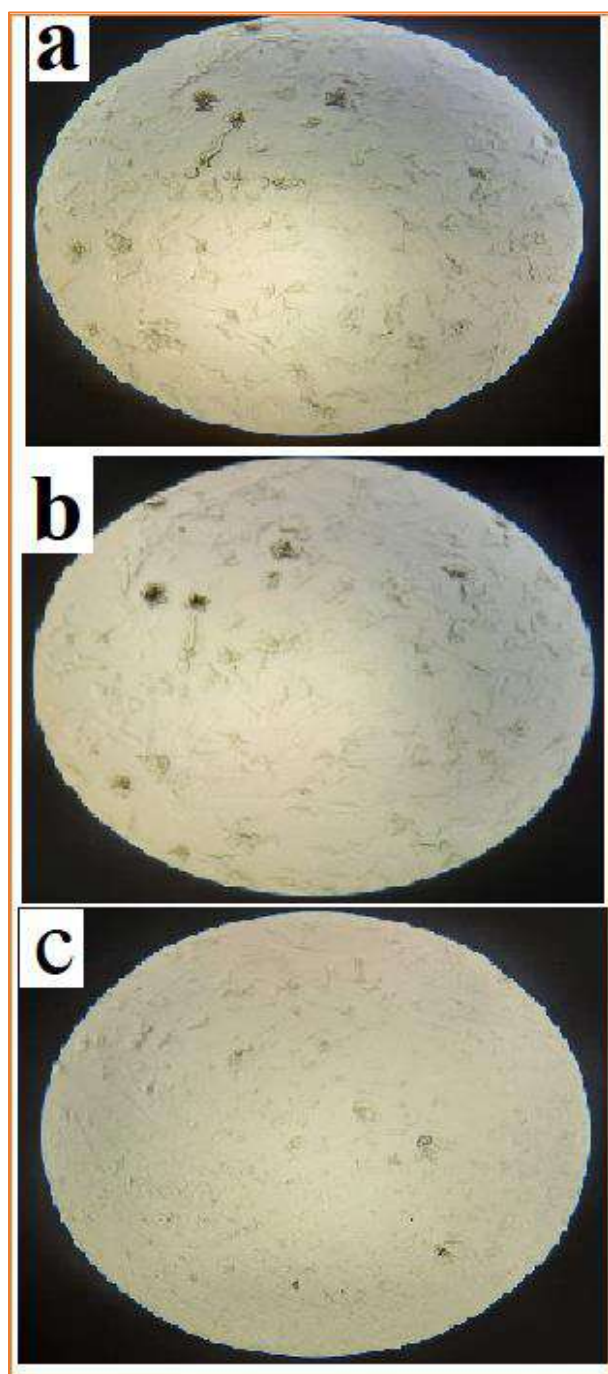


Figure 4-10: Light microscopic image of nucleation inhibition activity (40X) magnification (a) negative control (no treatment) (b) positive control (cystone) (250 mg/mL) (c) compound G2_(b) (250 µg/mL)

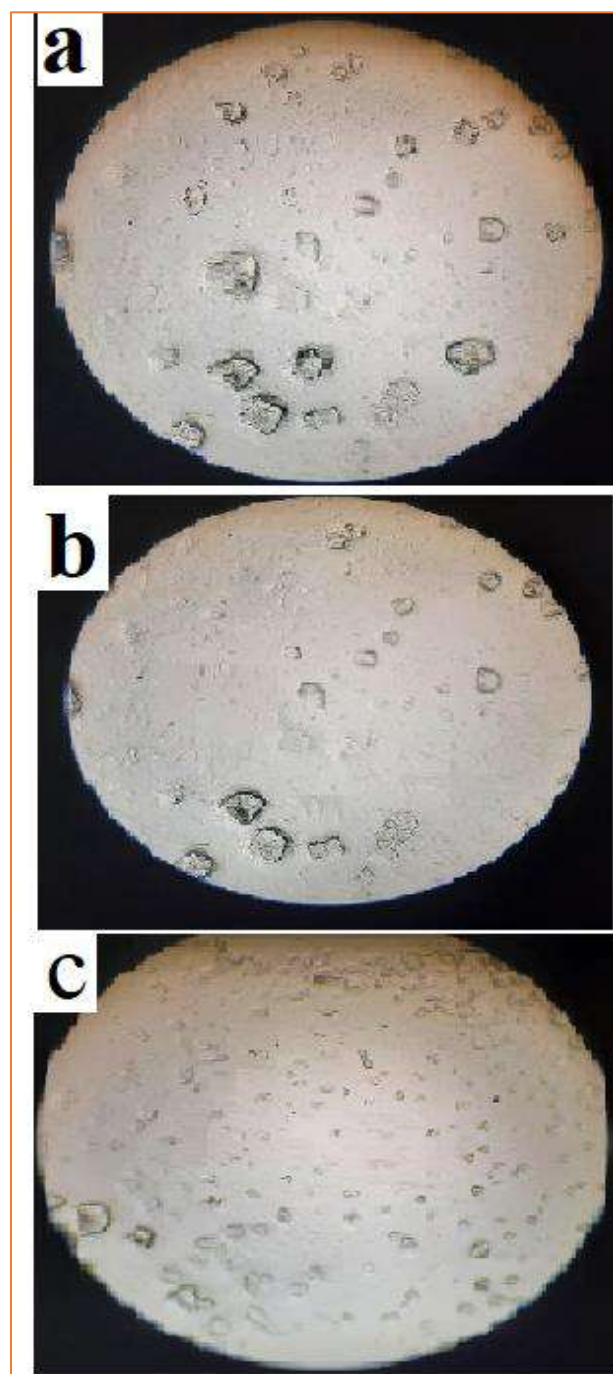


Figure 4-11: Light microscopic image of aggregation inhibition activity (40X) magnification (a) negative control (no treatment) (b) positive control (cystone) (250 mg/mL) (c) compound G2_(a) (250 µg/mL)

4.5.5 Antidiabetic Effect of Dendrimers (G2_(a), G3_(b), G2_(a) and G3_(b))

The activities of α -amylase and α -glucosidase for the tested compounds were measured spectrophotometrically at 540 nm for α -amylase and 410 nm for α -glucosidase and the percentage inhibition values for these enzymes at concentrations of 50,100,150,200 and 250 μ g/mL were calculated Table (4-3). All of the examined compounds inhibited α -amylase and α -glucosidase in a concentration-dependent comparable to acarbose, the standard anti-diabetic drug, Figure (4-12) displays a graph of percentage inhibition vs concentration (μ g/mL) of tested compounds and cystone. In α -amylase assays, the preliminary results revealed that compounds G2_(a) and G2_(b) exhibited the maximum percentage inhibition of 67% and 65% compared to the reference drug acarbose 63%, and other remaining compounds (G3_(a) and G3_(b) at 250 μ g/mL).

Table 4-3: The percentage inhibition of the enzymes α -amylase and α -glucosidase by compounds G2_(a), G3_(a), G2_(b), and G3_(b) at different concentrations

Conc. (μ g /mL)	(%) inhibition α -amylase					(%) inhibition α -glucosidase				
	G2 _(a)	G3 _(a)	G2 _(b)	G3 _(b)	acarbose	G2 _(a)	G3 _(a)	G2 _(b)	G3 _(b)	acarbose
50	37	17	25	10	32	45	46	41	42	43
100	41	22	34	16	42	47	51	46	48	47
150	47	29	46	25	55	50	53	49	51	54
200	59	34	55	39	59	53	55	51	55	61
250	67	48	65	49	63	56	58	54	57	66

EC₅₀ for G2_(a) and G2_(b) = 200 (μ g /mL) for α -amylase

EC₅₀ for G2_(a) and G3_(b) = 150 (μ g /mL) for α -glucosidase

EC₅₀ for G3_(a) = 100 (μ g /mL) for α -glucosidase

EC₅₀ for G2_(b) = 200 (μ g /mL) for α -glucosidase

In α -glucosidase assays, acarbose exhibits the highest inhibition (66%) followed by G3_(a) (58%), G3_(b) (57%), G2_(a) 56%, and G2_(b) 54% respectively, at their highest concentration 250 μ g /mL.

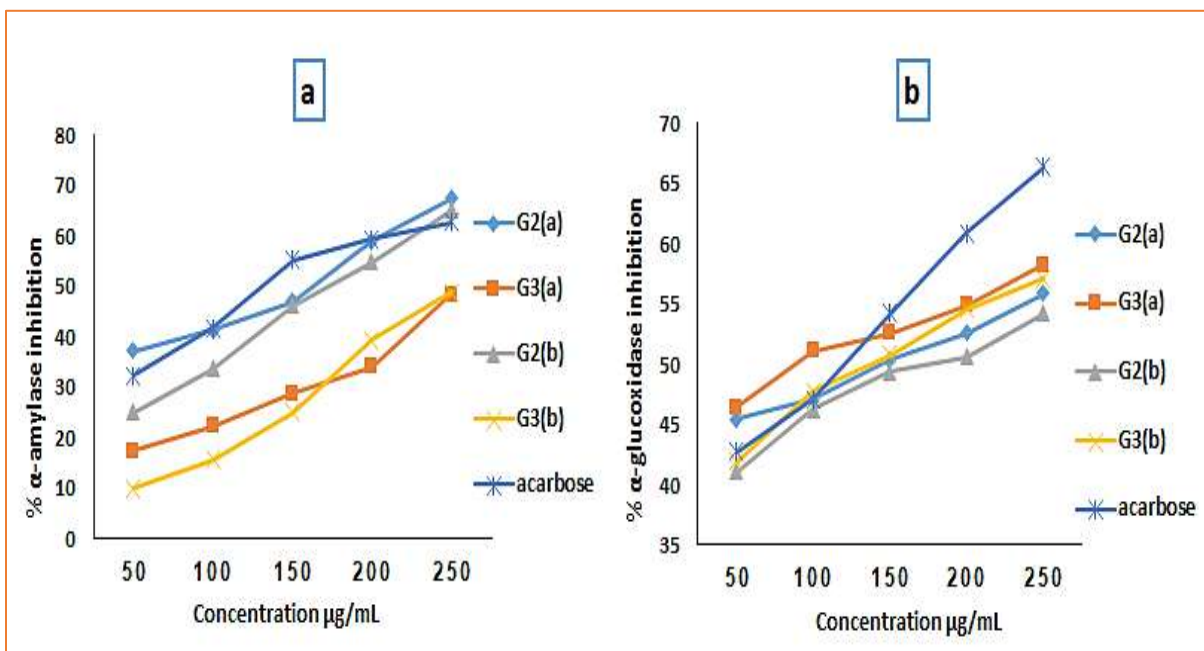


Figure 4-12: Antidiabetic activity (a) α -amylase inhibition (b) α -glucosidase inhibition by dendrimers G2(a), G3(a), G2(b) and G3(b)

4.5.6 Antidiabetic Effect of Tri-imidazole derivatives (4a, 4b, 4e, 4f and 4g)

The *in vitro* inhibitory activity of compounds (4a, 4b, 4e, 4f and 4g) was evaluated spectrophotometrically at 540 nm for α -amylase and 410 nm for α -glucosidase. In this study, the inhibitory activity of tested compounds for α -amylase and α -glucosidase was examined and the results are shown in Table (4-4). The findings that resulted from the antidiabetic assay towards α -amylase activity of compounds 4a, 4b, 4e, 4f, and 4g revealed that all five compounds were effective against enzyme activity, Figure 4.13 shows a plot of percentage inhibition vs. concentration. According to the inhibitory results of α -amylase activity at a concentration of 250 $\mu\text{g/mL}$ during inhibition measurements, it was found that all compounds had a stronger inhibitory effect on α -amylase than acarbose, which serves as a positive control; among all the examined compounds, 4f showed the highest inhibition at 90%, whereas compounds 4a, 4b, 4e and 4g exhibited good to

moderate inhibition of 64%, 75%, 78%, and 70%, respectively, in comparison to acarbose (63%) for the **4a**, **4b**, **4e**, **4f** and **4g**.

Table 4-4: The percentage inhibition of the enzymes α -amylase and α -glucosidase by compounds 4a, 4b, 4e, 4f, and 4g at different concentrations

Conc. ($\mu\text{g}/\text{mL}$)	(%) inhibition α -amylase						(%) inhibition α -glucosidase					
	enzyme						enzyme					
	4a	4b	4e	4f	4g	acarbose	4a	4b	4e	4f	4g	acarbose
50	53	55	53	54	51	32	24	26	26	27	22	43
100	55	66	58	59	55	42	26	31	31	33	24	47
150	59	67	68	80	60	55	32	36	39	41	28	54
200	61	69	71	87	62	59	43	47	47	52	34	61
250	64	75	78	90	70	63	56	58	51	61	38	66

EC_{50} for 4a,4b,4e,4f, and 4g = 50 ($\mu\text{g}/\text{mL}$) for α -amylase.

EC_{50} for 4f = 200($\mu\text{g}/\text{mL}$) for α -glucosidase.

EC_{50} for 4a,4b and 4e = 250($\mu\text{g}/\text{mL}$) for α -glucosidase

In the α -glucosidase assay, the investigated compounds demonstrated reasonable inhibitory activity at a concentration of 250 $\mu\text{g}/\text{mL}$ when compared to the reference inhibitor (Fig. 4-13). Among all the tested compounds, 4e showed the least activity at 38%, when compared to the standard, whereas compounds **4a**, **4b** and **4f** exhibited better activity at 56%, 58%, and 61%, respectively, which were found to be closer to the activity of the reference inhibitor (66%). All tested compounds exhibited concentration-dependent activity and it was observed that the inhibitory activity increased as the compounds' concentration increased.

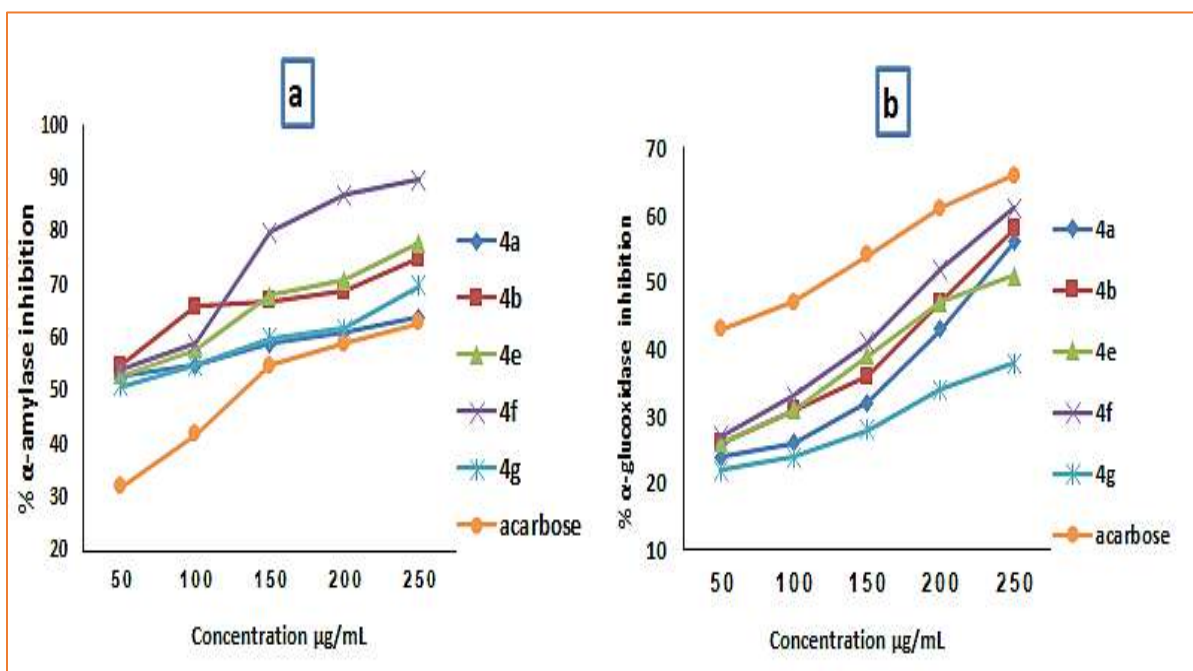


Figure 4-13: Antidiabetic activity (a) α -amylase inhibition (b) α -glucosidase inhibition by triimidazole 4a,4b,4e,4f, and 4g

4.5.7 Antidaibetic Effect of Tetra-imidazole derivatives (5a, 5b, 5f and 5g)

The inhibition of α -amylase and α -glucosidase activity by the tested compounds (5a, 5b, 5f and 4g) were measured at concentrations of 50,100,150, 250, and 250 $\mu\text{g/mL}$ and the percentage inhibition values of these compounds against α -amylase are presented in Table (4-5). In α -amylase assays, the results showed that all target compounds had a stronger inhibitory effect at a high concentration than acarbose (63%), whereas 5b was the most active inhibitor (77%) followed by 5a (73%), 5f (70%), and 5g (64%).

In α -glucosidase assays, the inhibitory activities of the tested compounds and acarbose (standard drug) are displayed in Table 4.5. In general, the results showed that all tested compounds (5a, 5b, 5f, and 4g) exhibited the lowest percentage inhibitory activity toward α -glucosidase activity at different concentrations in the range of 27% - 46%, 33% -51%, 31% -51%, and 22% -47% respectively in comparison to acarbose with an % inhibition value in the range of 43%-66%. The comparative percentage inhibition values of α -amylase and α -glucosidase of the

tested compounds with acarbose are shown in Figure 4-14 (a and b). It is clear from the graph (a), that the inhibition potential of tested compounds is better than that of the reference drug.

Table 4-5: The percentage inhibition of the enzymes α -amylase and α -glucosidase by compounds 5a, 5b, 5f, and 5g at different concentrations

Conc. ($\mu\text{g}/\text{ml}$)	(%) inhibition α -amylase enzyme					(%) inhibition α -glucosidase enzyme				
	5a	5b	5f	5g	acarbose	5a	5b	5f	5g	acarbose
50	38	41	37	32	32	27	33	31	22	43
100	55	52	50	41	42	33	38	38	28	47
150	61	64	61	49	55	37	41	42	37	54
200	64	69	68	58	59	43	47	45	42	61
250	70	77	73	64	63	46	51	51	47	66

EC_{50} for 5a , 5b and 5f = 100 ($\mu\text{g}/\text{mL}$) for α -amylase

EC_{50} for 5g = 200 ($\mu\text{g}/\text{mL}$) for α -amylase

EC_{50} for 5b and 5f = 250($\mu\text{g}/\text{mL}$) for α -glucosidase

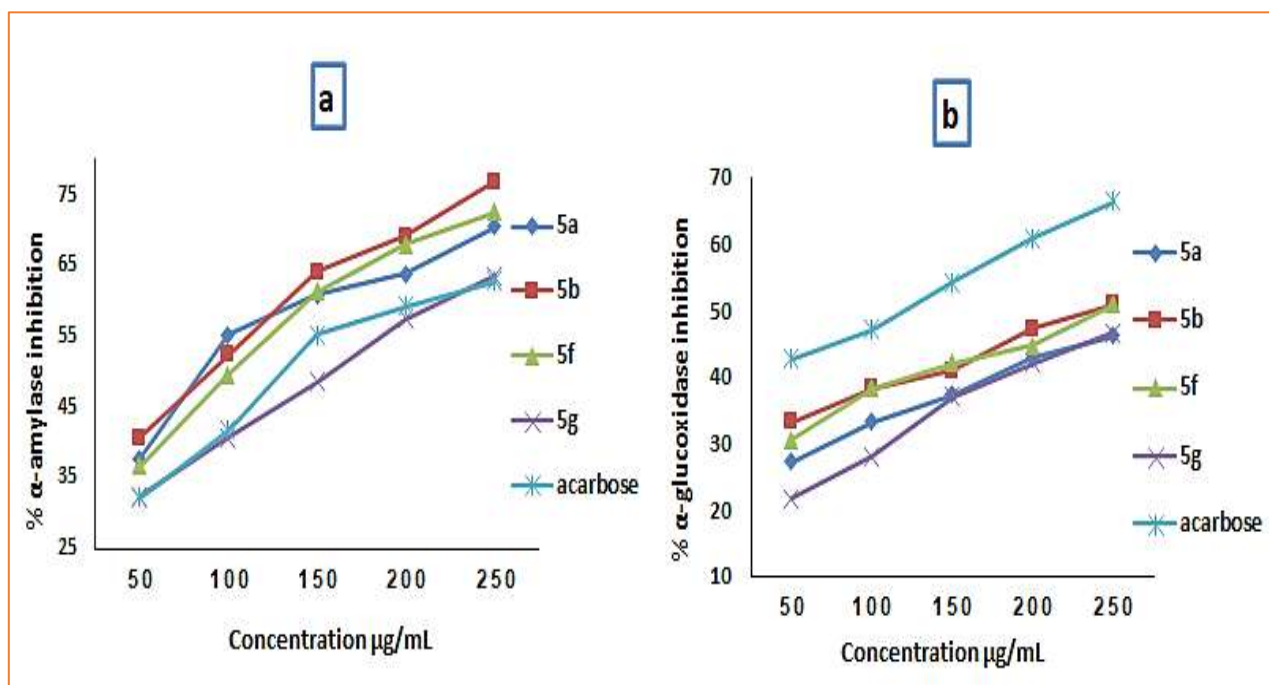


Figure 4-14: Aantidiabetic activity (a) α -amylase inhibition (b) α -glucosidase inhibition by tetraimidazole 5a, 5b, 5f, and 5g

4.5.8 Anti-bacterial Activity of Dendrimer (Minimum Inhibitory Concentrations (MICs))

The antibacterial study was evaluated using a microtiter plate assay with resazurin dye to determine the minimum inhibitory concentration (MICs) at various concentrations ranging from (100 $\mu\text{g/mL}$ to 500 $\mu\text{g/mL}$). Some of the newly synthesized dendrimers (**G2_(a)**, **G3_(a)**, **G2_(b)** and **G3_(b)**) have been investigated for their antibacterial activity. For this, *Staphylococcus aureus*, *Streptococcus agalactiae*, *Proteus mirabilis*, and *E. coli*, bacteria isolated from UTI infections were utilized. All examined compounds exhibited lower inhibitory activities when compared to standard antibiotics Azithromycin and Amoxicillin-clavulanic acid, which exhibited MICs of 200 $\mu\text{g/mL}$ and 300 $\mu\text{g/mL}$, respectively. As mentioned in Table (4-6) and (Fig. 4-15).

Table 4-6: MICs test results of Dendrimer (G2_(a), G3_(a), G2_(b), and G3_(b)) against selected Gram-positive and Gram-negative bacteria using resazurin dilution in broth assays at concentrations (100-500 $\mu\text{g/mL}$).

Compound	MIC: Minimum Inhibition Concentration ($\mu\text{g/mL}$)							
	Gram-positive bacteria				Gram-negative bacteria			
	<i>Staphylococcus aureus</i>		<i>Streptococcus agalactiae</i>		<i>Proteus mirabilis</i>		<i>Escherichia coli</i>	
	MIC	SUB	MIC	SUB	MIC	SUB	MIC	SUB
G2_(a)	300	200	400	300	400	300	500	400
G3_(a)	400	300	500	400	400	300	500	400
G2_(b)	300	200	400	300	400	300	500	400
G3_(b)	400	300	500	400	400	300	400	300
Azithromycin	200	200	300	300	200	200	200	300
Amoxicillin-clavulanic acid	200	100	300	200	200	100	300	200

SUB means no inhibition

4.5.9 Anti-bacterial Activity of Tri-imidazole derivatives (Minimum Inhibitory Concentrations (MICs))

The minimum inhibitory concentrations (MICs) of the tri-imidazole samples (**4a**, **4b**, **4e**, **4f**, and **4g**) were also determined using a microtiter plate assay with resazurin dye against four isolates of *Staphylococcus aureus*, *Streptococcus agalactiae*, *Proteus mirabilis*, and *E. coli*. The isolates, such as *Staphylococcus aureus*, were affected by the concentration 200 µg/ mL for **4a** and **4e**, and at 300 µg/ mL for **4b**, **4f**, and at 400 µg/ mL for **4g**, while other isolates, like *Streptococcus agalactiae*, was inhibited by 300 µg/ mL for **4e**, 400 µg/ mL for **4a**, **4b**, and **4f** and 500 µg/ mL for **4g**. The MICs of the isolate *Proteus mirabilis* were 300 µg/ mL for **4a** and **4g** and 400 µg/ mL for **4b**, **4e**, and **4f**, and finally, *E. coli* was also inhibited by 400 µg/mL for **4a** and **4g** and 500 µg/ mL for **4b**, **4e** and **4f**. Also, the results showed that the concentration of 200µg/mL and 300µg/ mL to four isolates was the MICs of Azithromycin and Amoxicillin-clavulanic acid which can inhibit growth, Table (4-7) and (Fig. 4-15).

Table 4-7: MICs test results of tri-imidazoles (4a,4b,4e,4f, and 4g)

Compound	MIC: Minimum Inhibition Concentration (µg/mL)							
	Gram-positive bacteria				Gram-negative bacteria			
	<i>Staphylococcus aureus</i>		<i>Streptococcus agalactiae</i>		<i>Proteus mirabilis</i>		<i>Escherichia coli</i>	
	MIC	SUB	MIC	SUB	MIC	SUB	MIC	SUB
4a	200	100	400	300	300	200	400	300
4b	300	200	400	300	300	300	500	400
4e	200	100	300	200	400	300	500	400
4f	300	200	400	300	400	400	500	400
4g	400	300	500	400	300	200	400	300
Azithromycin	200	200	300	300	200	200	200	300
Amoxicillin-clavulanic acid	200	100	300	200	200	100	300	200

SUB means no inhibition

4.5.10 Anti-bacterial Activity of Tetra-imidazole Derivatives (Minimum Inhibitory Concentrations (MICs))

The anti-bacterial activity of **5a**, **5b**, **5c**, **5e**, and **5f** was as previously mentioned. Antibacterial investigation revealed that most of the synthesized compounds have shown good to moderate activity against tested microorganisms. In particular, compounds **5b** and **5c** exhibited activity equal to that of standard drugs Azithromycin and Amoxicillin-clavulanic acid against *Staphylococcus aureus* with a MICs value of 200 µg/mL, Table (4-8) and (Fig. 4-15).

Table 4-8: MICs test results of teraimidazoles (**5a**,**5b**,**5c**,**5e** and **5f**)

Compound	MIC: Minimum Inhibition Concentration (µg/mL)							
	Gram-positive bacteria				Gram-negative bacteria			
	<i>Staphylococcus aureus</i>		<i>Streptococcus agalactiae</i>		<i>Proteus mirabilis</i>		<i>Escherichia coli</i>	
	MIC	SUB	MIC	SUB	MIC	SUB	MIC	SUB
5a	300	200	500	400	400	300	500	400
5b	200	100	300	200	400	300	400	300
5c	200	100	400	300	400	300	500	400
5e	500	400	400	300	500	400	400	300
5f	300	200	400	300	300	200	500	400
Azithromycin	200	200	300	300	200	200	200	300
Amoxicillin-clavulanic acid	200	100	300	200	200	100	300	200

SUB means no inhibition

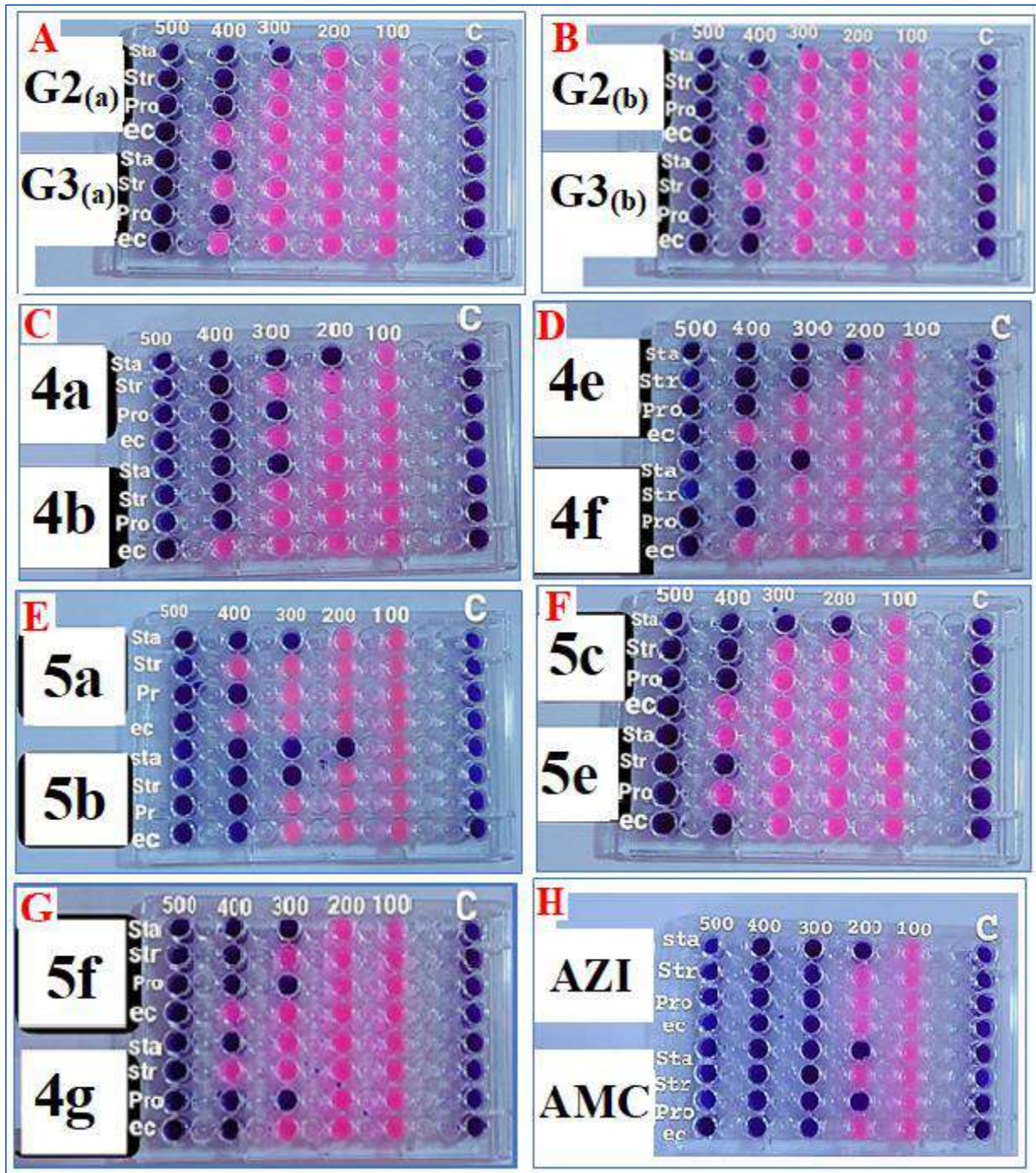


Figure 4-15: A schematic representation the (MICs) of the 96-well resazurin broth microdilution model (A) for G2 (a) and G3(a) (B) for G2(b) and G3(b) (C) for 4a and 4b (D) for 4e and 4f (E) for 5a and 5b (F) for 5c and 5e (G) for 5f and 4g and (H) for AZI and AMC against *Staphylococcus aureus*, *Streptococcus agalactiae*, *Proteus mirabilis*, and *E. coli*, **observation:** The pink color shows that organisms are active, whereas the blue color shows that growth has been inhibited

Compound **5b** has shown similar activity as that of standard drugs Azithromycin and Amoxicillin-clavulanic acid with a MICs value of 300 µg/mL against *Streptococcus agalactiae*. The remaining compounds exhibited lower inhibitory activities when compared to standard antibiotics Azithromycin and Amoxicillin-clavulanic acid against all four tested microorganisms as explained in Table (4-8) and (Fig. 4.15).

4.5.11 Agar Well Method for Dendrimer (**G2**_(a), **G3**_(a), **G2**_(b), and **G3**_(b))

Some of the newly synthesized compounds (**G2**_(a), **G3**_(a), **G2**_(b), and **G3**_(b)) were examined for their antibacterial activity (*in vitro*) against *Staphylococcus aureus*, *Streptococcus agalactiae*, *Proteus mirabilis* and *E. coli*, and their activity was compared to that of a well-known commercialized antibiotic, Amoxicillin-clavulanic acid and Azithromycin. The zone of inhibition of antibacterial activity was measured using the "Agar well Diffusion" method. The tested compounds exhibited variable antibacterial activity against the above-tested bacterial strains. The results indicated that among the tested compounds, **G2**_(a) and **G2**_(b) showed very excellent antibacterial activity towards all bacterial strains when compared with standard drugs Azithromycin and Amoxicillin-clavulanic acid. The rest of the compounds showed equipotent activity towards *Proteus mirabilis* and *E. coli* compared with reference drugs. These compounds are also found to be slightly active against *Staphylococcus aureus* and *Streptococcus agalactiae* compared to reference drugs. The findings of antibacterial studies are depicted in Table (4-9) and Figure (4-16).

4.5.12 Agar Well Method for Tri-imidazole Derivatives (**4a**, **4b**, **4e**, **4f**, and **4g**)

The new compounds (**4a**, **4b**, **4e**, **4f**, and **4g**) were tested for their antibacterial activity (*in vitro*) against *Staphylococcus aureus*, *Streptococcus agalactiae*, *Proteus mirabilis*, and *E. coli* and their activity was compared to antibiotic, Azithromycin and Amoxicillin-clavulanic acid. The zone of inhibition of antibacterial activity was

measured using the "Agar well Diffusion" method. Antibacterial results revealed that most of the tested compounds showed moderate to good bacterial inhibition (Table 4.9 and Fig. 4.17). Compound **4b**, exhibited excellent antibacterial activity against *Staphylococcus aureus* compared to the standard drug Azithromycin and exhibited equipotent activity as that of standard Azithromycin against *Proteus mirabilis* and *E. coli*, **4f** also inhibited the growth of *Staphylococcus aureus* similarly as that of standard Azithromycin whereas exhibited equipotent activity as that of standard Azithromycin against *Proteus mirabilis* and *E. coli*, **4a**, **4e**, and **4g** showed equipotent activity as that of standard Azithromycin against *Staphylococcus aureus*, *Proteus mirabilis*, and *E. coli*, all tested compounds showed moderate activity against *Streptococcus agalactiae* compared to reference drug Azithromycin also all examined compounds exhibited less inhibition against *Staphylococcus aureus* and *Streptococcus agalactiae* compared to reference drug Amoxicillin-Clavulanic whereas showed equipotent activity against *Proteus mirabilis* and *E. coli* as that of standard Amoxicillin-Clavulanic acid.

4.5.13 Agar Well Method for Tetra-imidazole Derivatives (**5a**, **5b**, **5c**, **5e**, and **5f**)

The diameter of the inhibition zone (mm) was measured in Mueller-Hinton Agar utilizing the "Agar well Diffusion" method to evaluate the *in vitro* antibacterial activity of newly prepared compounds against the above-mentioned bacteria and their activity was compared to the antibiotic, Azithromycin, and Amoxicillin-clavulanic acid. The evaluation of antibacterial screening results of compounds (**5a**, **5b**, **5c**, **5e**, and **5f**) demonstrated that most of the investigated compounds inhibit bacteria moderately to well against different tested bacterial strains, Table (4.9) and (Fig. 4-17). Among all of the examined compounds, **5a** showed excellent activity against *Staphylococcus aureus* when compared with standard Azithromycin. Compounds **5c** and **5e** showed inhibition activity close to the standard against *Staphylococcus aureus*. All compounds showed comparable activity to standard

Azithromycin and Amoxicillin-Clavulanic acid against *Proteus mirabilis* and *Escherichia coli*, these compounds are also found to be slightly active against *Streptococcus agalactiae* compared to the standard drugs.

Table 4-9: Antibacterial activities of all tested compounds

Compound	Zone of inhibition (mm)			
	Gram (+) bacteria		Gram (-) bacteria	
	<i>Staphylococcus aureus</i>	<i>Streptococcus agalactiae</i>	<i>Proteus mirabilis</i>	<i>Escherichia coli</i>
G2(a)	45	40	40	38
G3(a)	13	15	13	15
G2(b)	45	40	40	35
G3(b)	18	22	17	16
4a	14	14	15	12
4b	22	19	16	15
4e	18	14	14	13
4f	21	17	16	14
4g	16	15	15	12
5a	20	18	16	14
5b	15	15	15	13
5c	17	17	16	14
5e	19	19	15	14
5f	14	14	15	14
AZI	21	30	18	15
AMC	35	30	20	18
H ₂ O	-	-	-	-
ETOH+H ₂ O	-	-	-	-

AZI =Azithromycin

AMC =Amoxicillin-Clavulanic acid

ETOH= ethanol.

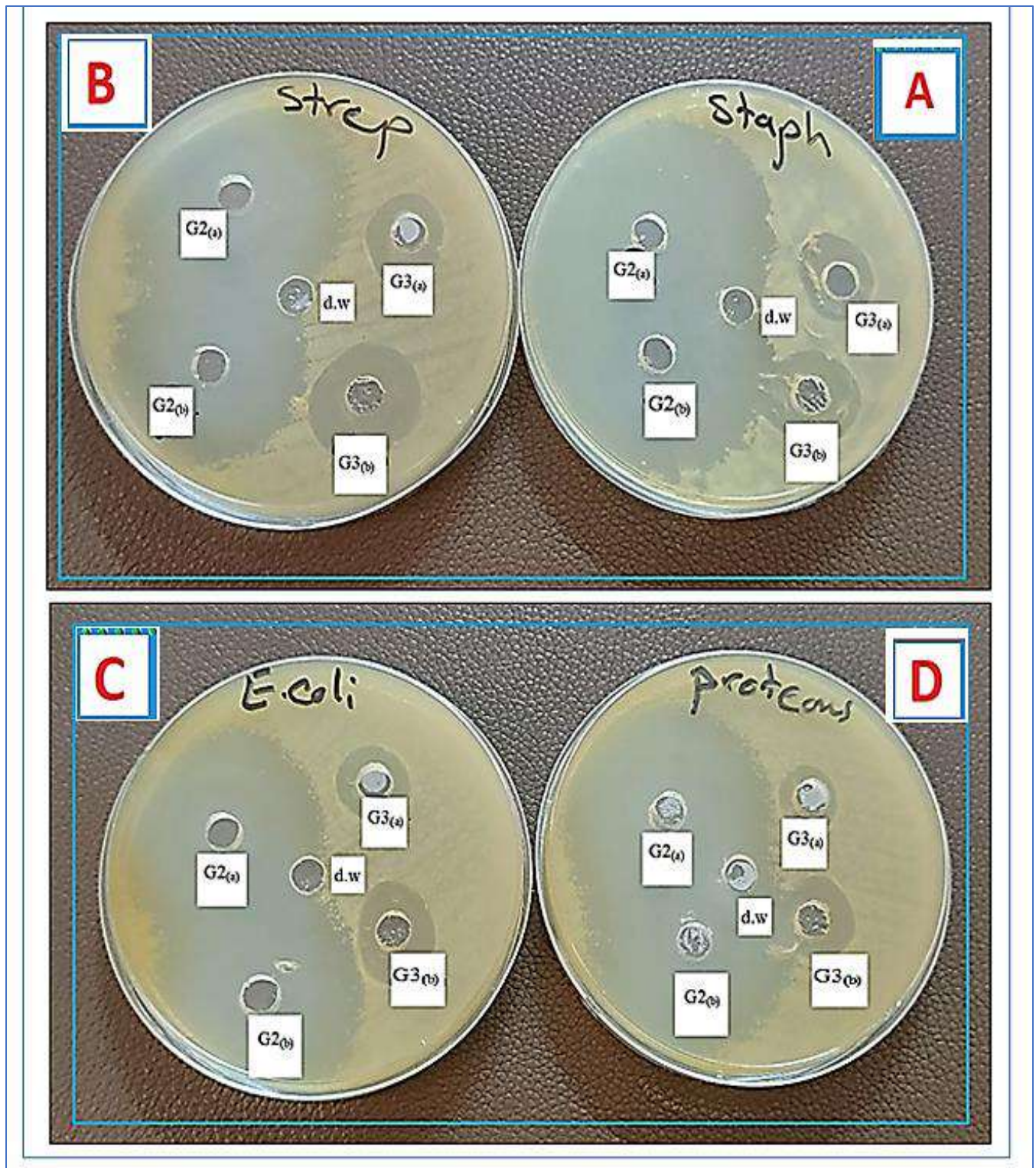


Figure 4-16: The antibacterial activity of G2(a), G3(a), G2(b) and G3(b) (A) and (B) against Gram-positive bacteria (*Staphylococcus aureus* and *Streptococcus agalactiae*) (C) and (D) against Gram-negative bacteria (*Proteus mirabilis* and *E. coli*), Negative control represents solvent, (Azithromycin and Amoxicillin-Clavulanic acid) represents positive control

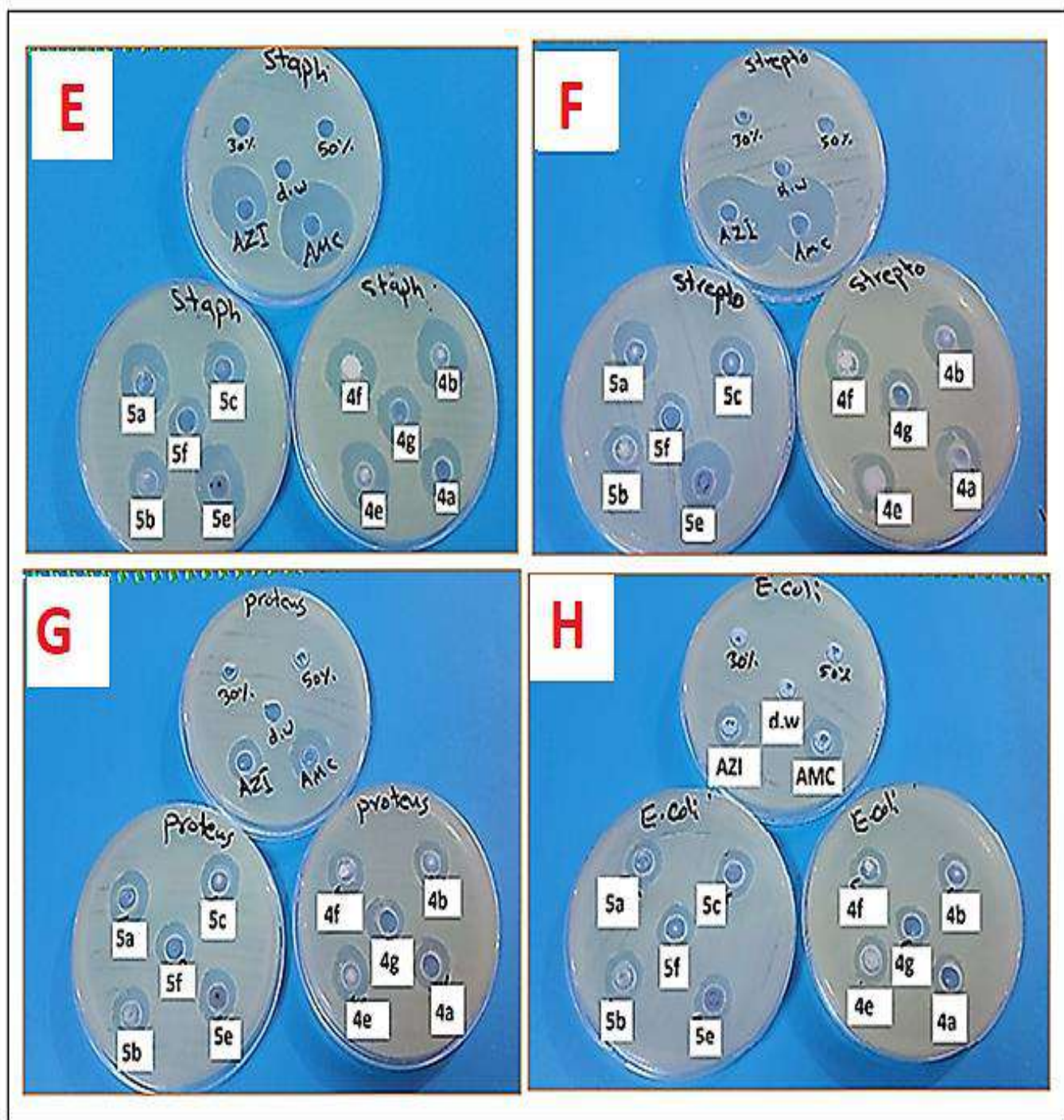


Figure 4-17: The antibacterial activity of 4a,4b,4e,4f,4g 5a,5b,5c,5e and 5f (E) and (F) against Gram-positive bacteria (*Staphylococcus aureus* and *Streptococcus agalactiae*) (G) and (H) against Gram-bacteria (*Proteus mirabilis* and *E. coli*), Negative control represents solvent, (Azithromycin and Amoxicillin-Clavulanic acid) represents positive control

4.5.14 Hemolytic Activity of Dendrimer (**G2_(a)**, **G3_(a)**, **G2_(b)** and **G3_(b)**)

At concentrations of 100, 200, 250, 300, 400, and 500 $\mu\text{g/mL}$, the *in vitro* hemolysis assay of the four active compounds **G2_(a)**, **G3_(a)**, **G2_(b)** and **G3_(b)** revealed that they were nontoxic and had low hemolytic activity. The hemolytic activity of the examined samples is represented as a percentage. The permitted limit of hemolysis for biomedical products has been extensively demonstrated to be less than 5% in all conditions [186]. All the tested compounds do not exceed the 5% percentage of hemolysis at all concentrations. Hemolysis rates were found to be dose-dependent and appeared to increase with increasing concentration (Fig. 4-18) and Table (4-10). The **G2_(b)** compound was the least cytotoxic owing to its lower hemolytic activity (0.71–1.61%) compared to the standard Triton X-100 (a positive control), which exhibited 97.3%. The hemolytic activity of compound **G3_(a)** was (0.796 %-1.63%), and the compound **G2_(b)** showed hemolysis of (1.00%-1.73%), whereas compound **G3_(b)** exhibited of (1.64%-2.68)..

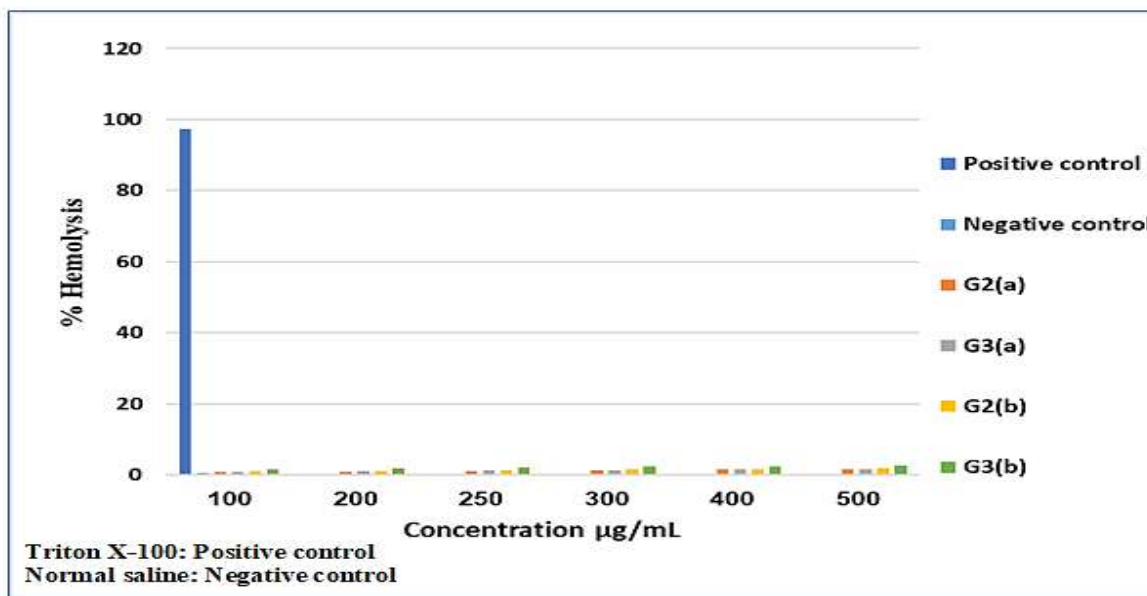


Figure 4-18: Hemolytic activities of **G2_(a)**, **G3_(a)**, **G2_(b)** and **G3_(b)** at the concentrations of 100, 200, 250, 300, 400, and 500 $\mu\text{g/mL}$

4.5.15 Hemolytic Activity of Tri-imidazole Derivatives (4a, 4b, 4e and 4f)

Compounds **4a**, **4b**, **4e**, and **4f** were evaluated for hemolytic activity versus normal human erythrocytes. The hemolytic activity of tested samples is presented as a percentage. Hemolysis rates were measured at six different concentrations: 100, 200, 250, 300, 400, and 500 $\mu\text{g/mL}$. The results showed that hemolysis rates were dosage-dependent. The rates increased relatively with concentrations of **4a**: 2.58% - 7.93%, **4b**: 0.97%-3.50%, **4e**: 4.09% -8.97%, and **4f**: 1.02%-3.14%, respectively (Fig. 4-19) and Table (4-10). The findings of the hemolytic activity of the tested compounds reveal that compounds **4b** and **4f** have lower hemolytic activity than compounds **4a** and **4e**.

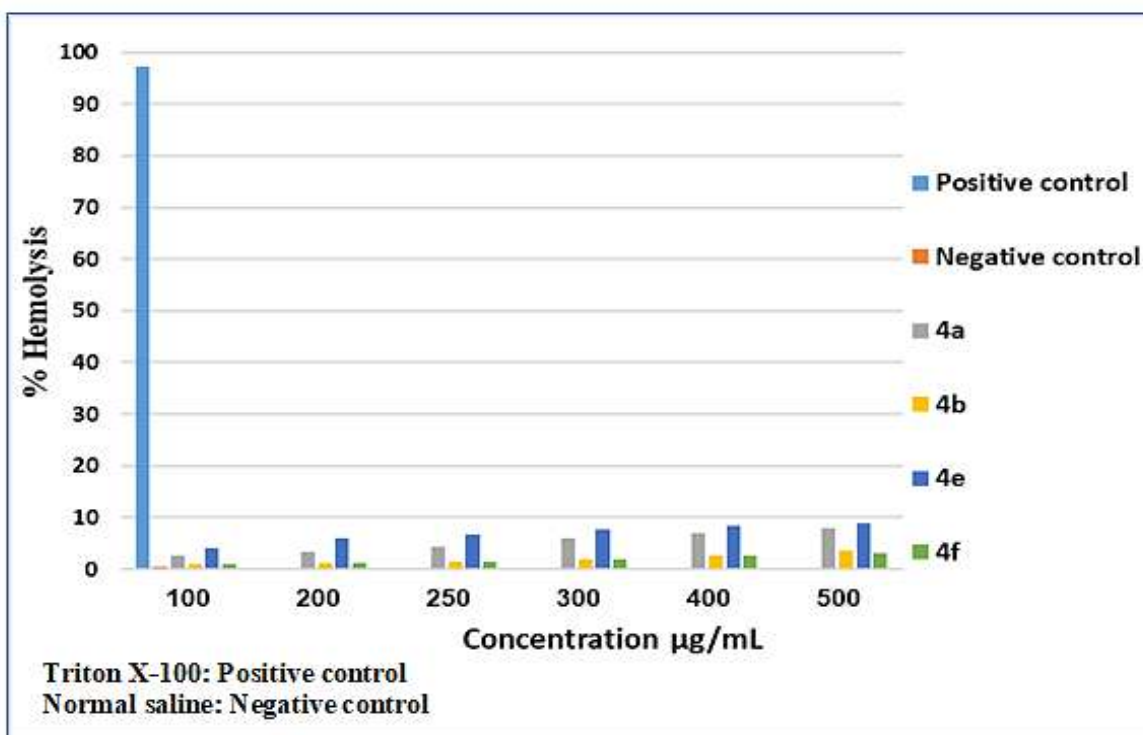


Figure 4-19: Hemolytic activities of 4a,4b,4e, and 4f at the concentrations of 100, 200, 250, 300, 400 and 500 $\mu\text{g/mL}$

4.5.16 Hemolytic Activity of Tetra-imidazole Derivatives (5a, 5b, 5f, and 5g)

In vitro, the hemolysis assay was utilized to demonstrate the effectiveness of **5a**, **5b**, **5f**, and **5g** samples as a bioactive compound free from adverse effects of toxicity. To test the preliminary toxicity, the compounds were treated with human erythrocytes (red blood cells). The percent of hemolysis increased when increasing the concentration of compounds. The obtained results demonstrate that most of the compounds have lower hemolytic activity against erythrocytes compared with positive control. Among the four tested compounds, compound **5g** has the lowest % hemolysis in the ranges of 0.95%-2.45% at concentrations (100, 200, 250, 300, 400, and 500 $\mu\text{g}/\text{mL}$) whereas, the percentage of hemolytic activity of the other synthesized compounds **5a**, **5b**, and **5f** were in the ranges of 1.126%- 3.205%, 1.708%- 2.988%, 1.358%- 3.879% at concentrations (100, 200, 250, 300, 400, and 500 $\mu\text{g}/\text{mL}$) respectively, (Fig. 4-20) and Table (4-10).

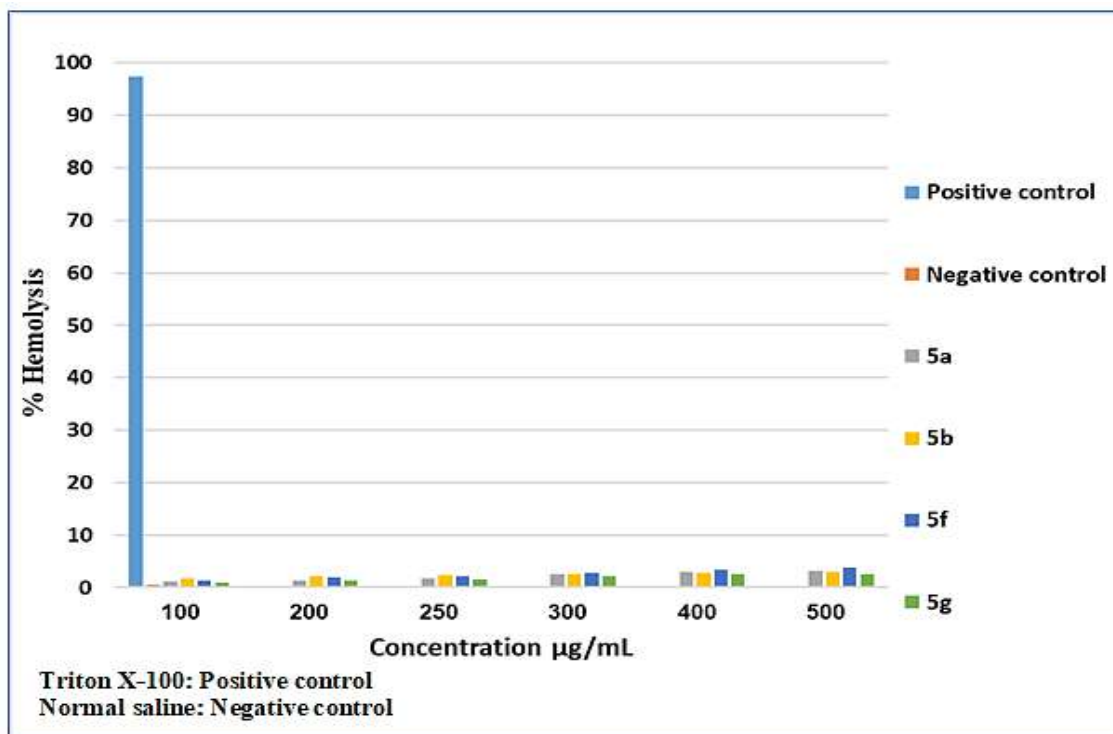


Figure 4-20: Hemolytic activities of 5a, 5b, 5f, and 5g at the concentrations of 100, 200, 250, 300, 400 and 500 $\mu\text{g}/\text{mL}$

Table 4-10: Hemolytic activity of all tested compounds

Test sample	% Hemolysis of RBCs					
	100µg/mL	200µg/mL	250µg/mL	300µg/mL	400µg/mL	500µg/mL
G2(a)	0.718	0.882	0.970	1.219	1.465	1.619
G3(a)	0.796	0.921	1.170	1.299	1.495	1.637
G2(b)	1.003	1.154	1.292	1.439	1.588	1.739
G3(b)	1.645	1.880	2.048	2.221	2.452	2.688
4a	2.581	3.471	4.461	6.131	7.111	7.931
4b	0.971	1.153	1.423	1.835	2.664	3.523
4e	4.091	6.067	6.766	7.653	8.387	8.971
4f	1.028	1.328	1.558	1.888	2.628	3.142
5a	1.126	1.357	1.648	2.642	2.935	3.205
5b	1.708	2.154	2.432	2.571	2.810	2.988
5f	1.358	1.870	2.145	2.692	3.393	3.879
4g	0.953	1.229	1.565	2.168	2.542	2.654

4.6 Discussion

Urolithiasis is a global disease that is becoming increasingly prevalent. Since ancient times, people have suffered from urolithiasis, a very painful condition [187]. Medical researchers have become interested in the mechanism of calcium oxalate renal calculi formation due to the condition's frequent clinical occurrence and challenging therapeutic options. Dietary and lifestyle habits play a role in the complexity of this condition. Hyperoxaluria is one of the main risk factors for human idiopathic calcium oxalate disease[188] . The results investigated that the inhibitory effect of the tested compounds on nucleation and aggregation were compared using cysteine as a positive control. The nucleation process is a crucial first step at the beginning of crystals, which eventually grow and form aggregates[189] . As a result, an *in vitro* anti-urolithiasis test was used to investigate the potential of (**G2_(a)**, **G3_(b)**, **G2_(b)** and **G3_(b)**), (**4a**, **4b**, **4e** and **4f**) and (**5a**, **5b**, **5f** and **5g**) to inhibit the formation of calcium oxalate. The findings of the nucleation and aggregation assays demonstrated that some of these compounds are nucleation and aggregation-preventing compounds.

By comparing the tested synthesized compounds in nucleation assay, it is found that compounds **G2_(b)** and **G3_(b)** show higher inhibition activity than compounds **G2_(a)** and **G3_(a)**. This may be attributed to the presence of amino-terminated and methoxy-terminated groups. Also, it is found that compounds **4b**, **5a** and **5g** show higher inhibition activity than compounds **4a**, **4e**, **4f**, **5b** and **5f**. This could be attributed to the higher electron-withdrawing inductive effect moiety.

Aggregation is arguably the second major factor in the formation of kidney stones; it is the mechanism that increases the particle size, chemical composition, and crystalline structure of the urinary stones. The crystals that adhered to one another are difficult to separate and remain in position. This procedure serves a crucial role in lithiasis [190].

The **G2_(a)** and **G3_(a)** contain amino-terminated and methoxy-terminated groups that may inhibit calcium oxalate crystal retention, as large crystals are less likely to pass spontaneously in the urinary tract. Thereby calcium oxalate crystals can be easily eliminated from the urinary tract which helps to prevent kidney stone formation due to properties of **G2_(b)** and **G3_(b)**, also it may cause the particles to be dispersed and reduce the crystal growth thereby reducing the urinary tract. Also, in the aggregation assay, the results found that the withdrawing group -Cl which is found in compounds **4b** and **5a** gave a percentage inhibition higher than the other donating group such as -OH, -OCH₃, which is found in compounds **4a,4e** and **5b** the reason could be the chloride is a good leaving group.

Diabetes therapy aims to decrease postprandial hyperglycemia by inhibiting the digestive enzymes responsible for carbohydrate hydrolysis (α -amylase and α -glucosidase), and glucose absorption is reduced. Inhibitors of these enzymes slow and prolong the digestion of carbohydrates, which in turn reduces the rate of glucose absorption and, as a result, reduces the increase in plasma glucose levels that occurs after a meal[191]. α -amylase and α -glucosidase inhibitors are extremely significant because the unclear inhibition of other glycosidases, particularly pancreatic α -Amylase, may be the cause of an increase in non-processed sugars in the gut, resulting in stomach pain and looseness of the bowels [192].

The activity of examined compounds (**4a,4b,4e,4f** and **4g**) against these enzymes may be because of the presence of free amino hydrogen inside the imidazole ring [193] and also, maybe due to different substituents found in various positions of imidazole derivatives are responsible for the inhibition of enzyme activity [194].

By comparing the findings of **5b** and **5f** with **5a** and **5g** the compounds **5b** and **5f** demonstrated a better inhibition potential than those of **5a** and **5g**. It has been postulated that the presence of both hydroxyl and methoxy groups may be involved in the formation of hydrogen bonding with the active region of the enzyme, thereby enhancing the inhibitory potential. The EC₅₀ (the concentration at which 50% of α -

amylase and α -glucosidase activity is inhibited) was calculated for all tested compounds.

The structure-activity relation of synthesized compounds demonstrates that the very excellent antibacterial activity of **G2_(a)** and **G2_(b)** is due to the presence of an amino-terminated PAMAM moiety which has the strongest antibacterial activity. It is generally believed that protonated amino groups on PAMAM enhance the rupturing of anionic bacterial cell membranes via electrostatic interactions and that they are required for the release of lipids[195].

The excellent antibacterial activity exhibited by the compound **4b** may be attributed to the presence of a 4-chlorophenyl substituent on the imidazole ring. Further, the presence of p-carboxyl phenyl substituent in the second position on the imidazole ring in compound **4f** can be attributed to its good activity. In addition, the presence of electrons donating groups such as 4-methoxy substituent, 4-hydroxy substituent, and dimethylsulfane (-SCH₃) substituent in compounds **4a,4e** and **4f** respectively, exhibited moderate activity against all of the bacterial strains that were tested.

Regarding the relationships between the design of the heterocyclic scaffold and the detected antibacterial properties, it is clear that the enhanced activity of **5a** and **5c** can be attributed to the presence of a 4-chlorophenyl group attached to the first position of the imidazole ring and the presence of a benzo[d] thiazole substituent at the same position. In addition, it was found that substituents such as the 6-methoxybenzo[d] thiazole moiety of compound **5e**, which is attached to the first position of the imidazole ring, exhibited good antibacterial activity against the microorganisms under study. In the case of **5b** and **5f**, however, a decrease in activity may be observed due to the presence of hydroxy and methoxy phenyl attached to the imidazole. In general, compounds containing halogen substituents exhibited greater antibacterial activity than those with other substituents.

The hemolysis is related to the compound's concentration and potency. In addition, each compound's hemolytic activity relates to the chemical composition. The lowest hemolytic activity of the tested dendrimer compounds (**G2_(a)**, **G3_(a)**, **G2_(b)** and **G3_(b)**) can be related to the varied functional groups' positions, which could impact the hemolytic activity. It has been assumed that the attached groups' electron-withdrawing and electron-donating properties might affect the hemolytic activity of various compounds [196]. The lowest hemolytic activity of the active derivatives (**4a**, **4b**, **4e** and **4f**) and (**5a**, **5b**, **5f**, and **5g**) can be related to the different functional groups' positions, which could impact the hemolytic action. It has been proposed that the attached groups' electron-withdrawing groups like -NO₂, -Cl and electron-donating groups like OH, and CH₃ might affect the hemolytic activity of various compounds. Most of the tested compounds were nontoxic even at high concentrations, and they were found to be safe.

CONCLUSIONS AND

FUTURE WORKS

Conclusions

Dendrimers are distinctive synthetic macromolecules that have attracted significant attention as biomedical systems. As well as the imidazole ring plays a vital role in a variety of aspects of biological functioning and structure.

The following reactions have been carried out during the present research work:

1. Various generations (G1 to G3) of PAMAM dendrimers have been successfully synthesized through divergent approaches by utilizing two iterative steps, namely Michael addition and amidation. For dendrimers that undergo the Michael addition reaction, (ester-terminated PAMAM dendrimers) were produced. In the amidation reaction, (amine-terminated PAMAM dendrimers) were formed.
2. A series of new 2,4,5 Triimidazoles and 1,2,4,5 Tetraimidazoles were synthesized using conventional methods in one-step, three- and four-component coupling reactions with cost-effective and readily available catalysts such as AcOH and H₂SO₄.
3. Ultrasonic and microwave irradiation techniques efficiently, rapidly, and conveniently synthesize substituted imidazoles. These methods have many advantages, such as a faster reaction time, better yields, and easier experimental and work-up processes.
4. The products are purified using simple techniques like recrystallization, and no costly column chromatographic techniques were employed.
5. The anti-urolithiasis assay of the screened compounds **G2_(a)** and **G3_(b)** showed the highest inhibition against CaOx crystal formation so maybe they can be used in the pharmaceutical or medical field to treat stones or inhibit their formation after conducting more studies in this field.
6. The antidiabetic results of the selected compounds also indicated that the compounds **G3_(a)**, **4b**, **4e**, **4f**, and **5b** exhibited the highest inhibition activity against

Conclusions and future works

α -amylase and α - α -glucosidase enzymes, these findings imply that these compounds have the potential to reduce blood sugar levels and may be valuable for future research.

7. The antibacterial studies indicated that among all the tested compounds, **G2_(a)** and **G2_(b)** exhibit the highest activity against all types of bacteria (Gram-positive and Gram-negative). Hence it can be concluded that these compounds can be used as antibiotics after conducting further studies in this field.
8. The hemolysis results also indicated that among tested compounds, **G2_(a)**, **G3_(a)**, and **G2_(b)** showed the highest activity and the experimental studies revealed that these compounds were quite safe even at higher concentrations and may be safe for therapeutic use.

Future Works

1. Synthesis of new dendrimer by selecting an alternative core.
2. Synthesis of a dendrimer with a larger generation and more terminal groups
3. Synthesis of different Tri-substituted imidazole or Tetra -substituted imidazole derivatives via the condensation reaction with other aromatic aldehydes or aromatic amines In addition, the synthesized compounds can be used as ligands in the formation of different organometallic complexes which have a wide range of applications in the fields of medical treatment, catalytic reactions, and material science.
4. The newly prepared compounds that displayed excellent *in vitro* biochemical and biological activity can be further evaluated for *in vivo* biological activities.
5. More biological evaluations of synthesized compounds for antioxidant, antiviral, anti-inflammatory, and antifungal properties
6. Investigating the molecular docking of the prepared compounds.

REFERENCES

References

- [1] Y. Kim and S. C. Zimmerman, “Applications of dendrimers in bio-organic chemistry,” *Curr. Opin. Chem. Biol.*, vol. 2, no. 6, pp. 733–742, 1998.
- [2] G. M. Dykes, “Dendrimers: A review of their appeal and applications,” *J. Chem. Technol. Biotechnol.*, vol. 76, no. 9, pp. 903–918, 2001.
- [3] A. K. Sharma, A. Gothwal, P. Kesharwani, H. Alsaab, A. K. Iyer, and U. Gupta, “Dendrimer nanoarchitectures for cancer diagnosis and anticancer drug delivery,” *Drug Discov. Today*, vol. 22, no. 2, pp. 314–326, 2017
- [4] A. Santos, F. Veiga, and A. Figueiras, “Dendrimers as pharmaceutical excipients: Synthesis, properties, toxicity and biomedical applications,” *Materials*, vol. 13, no. 1, pp. 1–31, 2020.
- [5] P. Kesharwani, K. Jain, and N. K. Jain, “Dendrimer as nanocarrier for drug delivery,” *Prog. Polym. Sci.*, vol. 39, no. 2, pp. 268–307, 2014.
- [6] F. Paquin, J. Rivnay, A. Salleo, N. Stingelin, and C. Silva, “Multi-phase semicrystalline microstructures drive exciton dissociation in neat plastic semiconductors,” *J. Mater. Chem. C*, vol. 3, pp. 10715–10722, 2015.
- [7] D. A. Tomalia and J. M. J. Fréchet, “Discovery of dendrimers and dendritic polymers: A brief historical perspective,” *J. Polym. Sci. Part A Polym. Chem.*, vol. 40, no. 16, pp. 2719–2728, 2002.
- [8] M. Wojcik, “Herstellung und Charakterisierung schallaktiver Polymerpartikel im nanoskaligen Bereich,” 2017.
- [9] J. Khandare and M. Calderón, “Dendritic polymers for smart drug delivery applications,” *Nanoscale*, vol. 7, no. 9, pp. 3806–3807, 2015.
- [10] S. S. Gillani, M. A. Munawar, K. M. Khan, and J. A. Chaudhary, “Synthesis, characterization and applications of poly-aliphatic amine dendrimers and dendrons,” *J. Iran. Chem. Soc.*, vol. 17, no. 11, pp. 2717–2736, 2020.
- [11] S. Chemical, “Dendritic Macromolecules:’ Synthesis of Starburst Dendrimers,” *Macromolecules*, pp. 2466–2468, 1986.
- [12] P. Kesharwani, K. Jain, and N. K. Jain, “Dendrimer as nanocarrier for drug delivery,” *Prog. Polym. Sci.*, vol. 39, no. 2, pp. 268–307, 2014.
- [13] N. N. Hoover, B. J. Auten, and B. D. Chandler, “Tuning supported catalyst reactivity with dendrimer-templated Pt-Cu nanoparticles,” *J. Phys. Chem. B*, vol. 110, no. 17, pp. 8606–8612, 2006.
- [14] S. Choudhary, L. Gupta, S. Rani, K. Dave, and U. Gupta, “Impact of

References

- dendrimers on solubility of hydrophobic drug molecules,” *Front. Pharmacol.*, vol. 8, no. MAY, pp. 1–23, 2017.
- [15] E. Beeram, “International Pharmaceutical Research of Modern,” *Int. J. Mod. Pharm. Res.*, vol. 3, no. 1, pp. 16–23, 2022.
- [16] R. Esfand and D. A. Tomalia, “Poly(amidoamine) (PAMAM) dendrimers: From biomimicry to drug delivery and biomedical applications,” *Drug Discov. Today*, vol. 6, no. 8, pp. 427–436, 2001.
- [17] S. Svenson and D. A. Tomalia, “Dendrimers in biomedical applications- reflections on the field,” *Adv. Drug Deliv. Rev.*, vol. 64, pp. 102–115, 2012 .
- [18] E. Potter, “Dendrimeric micelles for controlled drug release and targeted delivery,” *Mol Pharm*, vol. 2, no. 4, pp. 264–272, 2005,
- [19] R. Y. Patle and J. S. Meshram, “The advanced synthetic modifications and applications of multifunctional PAMAM dendritic composites,” *React. Chem. Eng.*, vol. 7, no. 1, pp. 9–40, 2022.
- [20] B. Klajnert and M. Bryszewska, “Dendrimers : properties and applications,” *Acta Biochim. Pol.*, vol. 48, no. 1, pp. 199–208, 2001.
- [21] U. Singh, M. M. Dar, and A. A. Hashmi, “Dendrimers: Synthetic strategies, properties and applications,” *Orient. J. Chem.*, vol. 30, no. 3, pp. 911–922, 2014.
- [22] H. baker, J. Dewald, M. hall, G. kallos, S. martin, J. rocker, J. ryder, and P. smith, “A New Class of Polymers : Starburst-Dendritic,” *Polym. J.*, vol. 17, no. 1, pp. 117–132, 1985.
- [23] V. Gawande, H. Choudhury, and P. Kesharwani, “Chapter 6 - Dendrimer nomenclature and synthesis methods,” in *Dendrimer-Based Nanotherapeutics*, P. Kesharwani, Ed. Academic Press, 2021, pp. 75–94.
- [24] P. Patel, V. Patel, and P. M. Patel, “Synthetic strategy of dendrimers: A review,” *J. Indian Chem. Soc.*, vol. 99, no. 7, p. 100514, 2022.
- [25] H. C. Kolb, M. G. Finn, and K. B. Sharpless, “Click Chemistry: Diverse Chemical Function from a Few Good Reactions,” *Angew. Chemie - Int. Ed.*, vol. 40, no. 11, pp. 2004–2021, 2001 .
- [26] Z. H. Aliand and N. R. Jber, “A Review on Synthesis, Properties, of Liquid Crystal Dendrimers,” *Al-Nahrain J. Sci.*, vol. 24, no. 4, pp. 15–25, 2021.
- [27] J. Haensler and F. C. Szoka, “Polyamidoamine Cascade Polymers Mediate Efficient Transfection of Cells in Culture,” *Bioconjug. Chem.*, vol. 4, no. 5, pp. 372–379, 1993.

References

- [28] P. Mehta, S. Kadam, A. Pawar, and C. Bothiraja, "Dendrimers for pulmonary delivery: Current perspectives and future challenges," *New J. Chem.*, vol. 43, no. 22, pp. 8396–8409, 2019.
- [29] J. Satija, V. V. R. Sai, and S. Mukherji, "Dendrimers in biosensors: Concept and applications," *J. Mater. Chem.*, vol. 21, no. 38, pp. 14367–14386, 2011.
- [30] P. Singh, T. Onodera, Y. Mizuta, K. Matsumoto, N. Miura, and K. Toko, "Dendrimer modified biochip for detection of 2,4,6 trinitrotoluene on SPR immunosensor: Fabrication and advantages," *Sensors Actuators, B Chem.*, vol. 137, no. 2, pp. 403–409, 2009.
- [31] J. Yan and J. Pei, "Chromophore-functionalized dendrimers for sensing applications," *Front. Chem. China*, vol. 5, no. 2, pp. 134–149, 2010.
- [32] A. Myc, I. J. Majoros, T. P. Thomas, and J. R. Baker, "Dendrimer-based targeted delivery of an apoptotic sensor in cancer cells," *Biomacromolecules*, vol. 8, no. 1, pp. 13–18, 2007.
- [33] A. Nantalaksakul, R. R. Dasari, T. S. Ahn, R. Al-Kaysi, C. J. Bardeen, and S. Thayumanavan, "Dendrimer analogues of linear molecules to evaluate energy and charge-transfer properties," *Org. Lett.*, vol. 8, no. 14, pp. 2981–2984, 2006.
- [34] T. Fernandes, A. L. Daniel-da-Silva, and T. Trindade, "Metal-dendrimer hybrid nanomaterials for sensing applications," *Coord. Chem. Rev.*, vol. 460, p. 214483, 2022.
- [35] M. Karadag, C. Geyik, D. O. Demirkol, F. N. Ertas, and S. Timur, "Modified gold surfaces by 6-(ferrocenyl)hexanethiol/dendrimer/gold nanoparticles as a platform for the mediated biosensing applications," *Mater. Sci. Eng. C*, vol. 33, no. 2, pp. 634–640, 2013.
- [36] G. Eric Oosterom, J. N. H. Reek, P. C. J. Kamer, and P. W. N. M. Van Leeuwen, "Transition metal catalysis using functionalized dendrimers," *Angew. Chemie - Int. Ed.*, vol. 40, no. 10, pp. 1828–1849, 2001.
- [37] A. S. H. King and L. J. Twyman, "Heterogeneous and solid supported dendrimer catalysts," *J. Chem. Soc. Perkin 1*, vol. 2, no. 20, pp. 2209–2218, 2002.
- [38] M. Zhao and R. M. Crooks, "Homogeneous Hydrogenation Catalysis with," *Angew. Chemie Int. Ed.*, vol. 38, no. 3, pp. 364–366, 1999.
- [39] Y. C. Lu, R. Anedda, and L. L. Lai, "Shape-Persistent Dendrimers," *Molecules*, vol. 28, no. 14, pp. 17–22, 2023.
- [40] D. Lenoir, R. B. C. Ber, and R. Schmidt, "Rapid Construction of Large-size Phenylacetylene Dendrimers up to 12.5 Nanometers in Molecular Diameter,"

References

- Angrw. Chem. Ini. Ed. Engl*, vol. 32, no. 9, pp. 70–73, 1993.
- [41] A. Chauhan, C. Patil, P. Jain, and H. Kulhari, “Dendrimer-based marketed formulations and miscellaneous applications in cosmetics, veterinary, and agriculture,” *Pharm. Appl. Dendrimers*, pp. 325–334, 2020.
- [42] D. A. Tomalia, *Dendrimers and Other Dendritic Polymers*, vol. 1. 2001.
- [43] R. Singh, M. Singh, N. Kumari, Janak, S. Maharana, and P. Maharana, “A comprehensive review of polymeric wastewater purification membranes,” *J. Compos. Sci.*, vol. 5, no. 6, 2021.
- [44] O. Bernardo, S. González-Pelayo, and L. A. López, “Synthesis and Applications of Ferrocene-Fused Nitrogen Heterocycles,” *Eur. J. Inorg. Chem.*, vol. 2022, no. 8, 2022.
- [45] Y. Sun, Y. Gu, and J. Yang, “Adsorption of N-heterocyclic compounds from aqueous solutions by sulfonic acid-functionalized hypercrosslinked resins in batch experiments,” *Chem. Eng. J.*, vol. 428, p. 131163, 2021.
- [46] A. Siwach and P. K. Verma, “Synthesis and therapeutic potential of imidazole containing compounds,” *BMC Chem.*, vol. 15, no. 1, pp. 1–69, 2021.
- [47] S. Y. Atanasova-Stamova, S. F. Georgieva, and M. B. Georgieva, “Reaction strategies for synthesis of imidazole derivatives: a review,” *Scr. Sci. Pharm.*, vol. 5, no. 2, p. 7, 2018.
- [48] P. K. Rahul Godge, Amol Dighe, “An Overview of Imidazole, Derivatives Ofimidazole and its Pharmacological Applications,” *Asian J. Research Chem.*, vol. 16, no. 1, pp. 1–6, 2023.
- [49] H. V. Tolomeu and C. A. M. Fraga, “Imidazole: Synthesis, Functionalization and Physicochemical Properties of a Privileged Structure in Medicinal Chemistry,” *Molecules*, vol. 28, no. 2, pp. 1–27, 2023.
- [50] H. S. Jabbar, A. K. Al-Edan, A. A. H. Kadhum, W. N. Roslam, and M. Sobri, “Synthesis and characterization of imidazole derivatives and catalysis using chemical pharmaceutical compounds,” *J. Adv. Res. Dyn. Control Syst.*, vol. 11, no. 3, pp. 1928–1939, 2019.
- [51] X. Zheng, Z. Ma, and D. Zhang, “Synthesis of imidazole-based medicinal molecules utilizing the van Leusen imidazole synthesis,” *Pharmaceuticals*, vol. 13, no. 3, pp. 1–19, 2020.
- [52] D. Chaudhury, J. Banerjee, N. Sharma, and N. Shrestha, “Routes of synthesis and biological significances of Imidazole derivatives : Review,” *World J. Pharm. Sci.*, vol. 3, pp. 1668–1681, 2015.

References

- [53] P. Manocha, D. S. Wakode, A. Kaur, K. Anand, and H. Kumar, "A review: Imidazole synthesis and its biological activities," *Int J Pharm Sci Res*, vol. 1, no. 7, pp. 12–16, 2016.
- [54] S. Saxer, C. Marestin, R. Mercier, and J. Dupuy, "The multicomponent Debus-Radziszewski reaction in macromolecular chemistry," *Polym. Chem.*, vol. 9, no. 15, pp. 1927–1933, 2018.
- [55] L. and M. H. and C. D. G. Rajiv Bhalla, "Synthesis and structure of a 2 CuII 2 CuI constellation ligated by the new biimidazole, bis(1-methyl-4,5-diphenylimidaz-2-oyl)carbin," *Chem. Commun*, vol. 13, pp. 921–922, 1996.
- [56] N. A. Boland, M. Casey, S. J. Hynes, J. W. Matthews, M. P. Smyth, and M.P. Smyth, "A Novel General Route for the Preparation of Enantiopure Imidazolines" *J. Org. Chem.*, vol. 67, no. 16, pp. 3919–3922, 2002.
- [57] A. Puratchikody and M. Doble, "Antinociceptive and antiinflammatory activities and QSAR studies on 2-substituted-4,5-diphenyl-1*H*-imidazoles," *Bioorganic Med. Chem.*, vol. 15, no. 2, pp. 1083–1090, 2007.
- [58] H. Zang, Q. Su, Y. Mo, B. W. Cheng, and S. Jun, "Ionic liquid [EMIM]OAc under ultrasonic irradiation towards the first synthesis of trisubstituted imidazoles," *Ultrason. Sonochem.*, vol. 17, no. 5, pp. 749–751, 2010.
- [59] A. Mirjafari, "Direct synthesis of 2,4,5-trisubstituted imidazoles from alcohols and α -hydroxyketones by microwave," *Environ. Chem. Lett.*, vol. 12, no. 1, pp. 177–183, 2014.
- [60] F. Nemati, M. M. Hosseini, and H. Kiani, "Glycerol as a green solvent for efficient, one-pot and catalyst free synthesis of 2,4,5-triaryl and 1,2,4,5-tetraaryl imidazole derivatives," *J. Saudi Chem. Soc.*, vol. 20, pp. 503–508, 2016.
- [61] A. Hariharan, S. Kumar, M. Alagar, K. Dinakaran, and K. Subramanian, "Synthesis, photophysical and electrochemical properties of polyimides of tetraaryl imidazole," *Polym. Bull.*, vol. 75, no. 1, pp. 93–107, 2018.
- [62] W. Sun, M. Zhang, P. Li, and Y. Li, "One-Pot Synthesis of Polysubstituted Imidazoles Based on Pd(OAc)₂/Ce(SO₄)₂/Bi(NO₃)₃ Trimetallic Cascade of Decarboxylation/Wacker-Type Oxidation/Debus-Radziszewski Reaction," *Synth.*, vol. 51, no. 17, pp. 3221–3230, 2019.
- [63] G. Patel, A. R. Patel, and S. Banerjee, "Visible light-emitting diode light-driven one-pot four component synthesis of poly-functionalized imidazoles under catalyst- And solvent-free conditions," *New J. Chem.*, vol. 44, no. 31, pp. 13295–13300, 2020.

References

- [64] D. Sinha, S. Biswas, M. Das, and A. Ghatak, "An eco-friendly, one pot synthesis of tri-substituted imidazoles in aqueous medium catalyzed by RGO supported Au nano-catalyst and computational studies," *J. Mol. Struct.*, vol. 1242, pp. 1–8, 2021.
- [65] L. Maintz and N. Novak, "Histamine and histamine intolerance," *Am. J. Clin. Nutr.*, vol. 85, no. 5, pp. 1185–1196, 2007
- [66] R. V. Shingalapur, K. M. Hosamani, and R. S. Keri, "Synthesis and evaluation of in vitro anti-microbial and anti-tubercular activity of 2-styryl benzimidazoles," *Eur. J. Med. Chem.*, vol. 44, no. 10, pp. 4244–4248, 2009,
- [67] S. Zhao, L. Zhao, X. q. Zhang, P. Wei, M. Wu, X. Su, B. Sun, D. Zhao and M. Cheng, "Design, synthesis and evaluation of biphenyl imidazole analogues as potent antifungal agents," *Bioorganic Med. Chem. Lett.*, vol. 29, no. 17, pp. 1–13, 2019.
- [68] A. H. Abdelazeem, M. T. El-Saadi, A. G. Safi El-Din, H. A. Omar, and S. M. El-Moghazy, "Design, synthesis and analgesic/anti-inflammatory evaluation of novel diarylthiazole and diarylimidazole derivatives towards selective COX-1 inhibitors with better gastric profile," *Bioorganic Med. Chem.*, vol. 25, no. 2, pp. 665–676, 2017.
- [69] A. K. Jain, V. Ravichandran, M. Sisodiya, and R. K. Agrawal, "Synthesis and antibacterial evaluation of 2-substituted-4,5-diphenyl-N-alkyl imidazole derivatives," *Asian Pac. J. Trop. Med.*, vol. 3, no. 6, pp. 471–474, 2010.
- [70] F. Chaudhry *et al.*, "Imidazole-pyrazole hybrids: Synthesis, characterization and in-vitro bioevaluation against α -glucosidase enzyme with molecular docking studies," *Bioorg. Chem.*, vol. 82, pp. 267–273, 2019.
- [71] M. Gaba, D. Singh, S. Singh, V. Sharma, and P. Gaba, "Synthesis and pharmacological evaluation of novel 5-substituted-1-(phenylsulfonyl)-2-methylbenzimidazole derivatives as anti-inflammatory and analgesic agents," *Eur. J. Med. Chem.*, vol. 45, no. 6, pp. 2245–2249, 2010.
- [72] A. Goyal, J. Singh, and D. P. Pathak, "Synthesis and Pharmacological Evaluation of Some Novel Imidazole Derivatives for Their Potential Anti-Hypertensive Activity," *J. Pharm. Technol. Res. Manag.*, vol. 1, no. 1, pp. 69–79, 2013.
- [73] B. K. Verma, S. Kapoor, U. Kumar, S. Pandey, and P. Arya, "Synthesis of new Imidazole Derivatives as effective Antimicrobial Agents," *Indian J. Pharm. Biol. Res.*, vol. 5, no. 01, pp. 01–09, 2017.
- [74] A. A. Adeniji, K. E. Knoll, and D. T. Loots, "Potential anti-TB investigational compounds and drugs with repurposing potential in TB therapy: a conspectus,"

References

- Appl. Microbiol. Biotechnol.*, vol. 104, no. 13, pp. 5633–5662, 2020.
- [75] X. Zhang, H. Zhang, Y. Ma, W. Che, and M. R. Hamblin, “Management of Hypertension Using Olmesartan Alone or in Combination,” *Cardiol. Ther.*, vol. 6, no. 1, pp. 13–32, 2017.
- [76] S. S. Ebada, N. A. Al-Jawabri, F. S. Youssef and A. Alboh, “In vivo antiulcer activity, phytochemical exploration, and molecular modelling of the polyphenolic-rich fraction of *Crepis sancta* extract,” *Inflammopharmacology*, vol. 28, no. 1, pp. 321–331, 2020.
- [77] C. Zhang, B. Zhong, S. Yang, L. Pan, S. Yu and Z. Li, “Synthesis and biological evaluation of thiabendazole derivatives as anti-angiogenesis and vascular disrupting agents,” *Bioorganic Med. Chem.*, vol. 23, no. 13, pp. 3774–3780, 2015.
- [78] A. S. Salman, A. Abdel-aziem, and M. J. Alkubbat, “Design, Synthesis of Some New Thio-Substituted Imidazole and Their Biological Activity,” *Am. J. Org. Chem.*, vol. 5, no. 2, pp. 57–72, 2015.
- [79] N. Srestha, J. Banerjee, and S. Srivastava, “A review on chemistry and biological significance of benzimidazole nucleus,” *IOSR J. Pharm.*, vol. 04, no. 12, pp. 28–41, 2014.
- [80] H. Y. Gondal, S. Tariq, S. Akhter, A. R. Raza, M. F. ur Rehman, and S. L. Rubab, “Synthesis, characterization, and in vitro anti-cholinesterase screening of novel indole amines,” *RSC Adv.*, vol. 13, no. 2, pp. 1203–1215, 2023.
- [81] B. K. Pawan Kumar and M. G. Reena Gupta, “Imidazole: Chemistry and biological activities,” *Think India J.*, vol. 22, no. 37, pp. 359–380, 2019.
- [82] S. S. Dipake, M. K. Lande, A. S. Rajbhoj, and S. T. Gaikwad, “Zeolite ZSM-11 as a reusable and efficient catalyst promoted improved protocol for synthesis of 2,4,5-triarylimidazole derivatives under solvent-free condition,” *Res. Chem. Intermed.*, vol. 47, no. 6, pp. 2245–2261, 2021.
- [83] J. Jayram and V. Jeena, “An iodine/DMSO-catalyzed sequential one-pot approach to 2,4,5-trisubstituted-1H-imidazoles from α -methylene ketones,” *RSC Adv.*, vol. 8, no. 66, pp. 37557–37563, 2018.
- [84] G. Gupta, N. Rani, and V. Kumar, “Microwave Assisted Synthesis of Imidazoles - A Review,” *Mini. Rev. Org. Chem.*, vol. 9, no. 3, pp. 270–284, 2012.
- [85] V. Santagada, E. Perissutti, and G. Caliendo, “The Application of Microwave Irradiation as New Convenient Synthetic Procedure in Drug Discovery,” *Curr. Med. Chem.*, vol. 9, no. 13, pp. 1251–1283, 2002.

References

- [86] L. B. Richard Gedye, F. Smith, K. Westaway, H. Ali and L. L. and J. Rousell, "The use of Microwave ovens for rapid organic synthesis," *Tetrahedron Lett.*, vol. 27, no. 3, pp. 279–282, 1986.
- [87] M. S. Tople, N. B. Patel, and P. P. Patel, "Microwave irradiation for the synthesis of quinoline scaffolds: a review," *J. Iran. Chem. Soc.*, vol. 20, no. 1, pp. 1–28, 2023.
- [88] M. Nüchter and B. Ondruschka, "Tools for microwave-assisted parallel syntheses and combinatorial chemistry," *Mol. Divers.*, vol. 7, no. 2, pp. 253–264, 2003.
- [89] S. Gulati, S. E. John, and N. Shankaraiah, "Microwave-assisted multicomponent reactions in heterocyclic chemistry and mechanistic aspects," *Beilstein J. Org. Chem.*, vol. 17, pp. 819–865, 2021.
- [90] A. Nurdiana, L. Astuti, R. P. Dewi, R. Ragadhita, A. B. D. Nandiyanto, and T. Kurniawan, "Techno-economic Analysis on the Production of Zinc Sulfide Nanoparticles by Microwave Irradiation Method," *ASEAN J. Sci. Eng.*, vol. 2, no. 2, pp. 143–156, 2022.
- [91] R. S. Varma, "Clay and clay-supported reagents in organic synthesis," *Tetrahedron*, vol. 58, no. 7, pp. 1235–1255, 2002.
- [92] N. Elander, J. R. Jones, S.-Y. Lu, and S. Stone-Elander, "Microwave-enhanced radiochemistry," *Chem. Soc. Rev.*, vol. 29, no. 4, pp. 239–249, 2000.
- [93] A. de la Hoz, Á. Díaz-Ortiz, A. Moreno, A. Sánchez-Migallón and P. Prieto, "Microwave-Assisted Reactions in Heterocyclic Compounds with Applications in Medicinal and Supramolecular Chemistry," *Comb. Chem. High Throughput Screen.*, vol. 10, no. 10, pp. 877–902, 2007.
- [94] X. Luo, H. Gong, Z. He, P. Zhang, and L. He, "Recent advances in applications of power ultrasound for petroleum industry," *Ultrason. Sonochem.*, vol. 70, p. 105337, 2021.
- [95] R. Javahershenas and S. Nikzat, "Recent advances in the multicomponent synthesis of heterocycles using tetronic acid," *RSC Adv.*, vol. 13, no. 24, pp. 16619–16629, 2023.
- [96] M. A. Schiel, A. B. Chopa, G. F. Silbestri, M. B. Alvarez, A. G. Lista, and C. E. Domini, *Use of Ultrasound in the Synthesis of Heterocycles of Medicinal Interest*. Elsevier Inc., 2015.
- [97] C. Domini, L. Vidal, G. Cravotto, and A. Canals, "A simultaneous, direct microwave/ultrasound-assisted digestion procedure for the determination of total Kjeldahl nitrogen," *Ultrason. Sonochem.*, vol. 16, no. 4, pp. 564–569,

References

- 2009.
- [98] J. L. Luche, "A few questions on the sonochemistry of solutions," *Ultrason. Sonochem.*, vol. 4, no. 2, pp. 211–215, 1997.
- [99] S. Chaudhuri, A. Ghosh, and S. K. Chattopadhyay, "Chapter 14 - Green synthetic approaches for medium ring-sized heterocycles of biological and pharmaceutical interest," in *Green Synthetic Approaches for Biologically Relevant Heterocycles (Second Edition)*, Second Edi., G. Brahmachari, Ed. Elsevier, 2021, pp. 617–653.
- [100] L. H. Thompson and L. K. Doraiswamy, "Sonochemistry: Science and Engineering," *Ind. Eng. Chem. Res.*, vol. 38, pp. 1215–1249, 1999.
- [101] M. J. Lo Fiego, M. A. Badajoz, C. Domini, A. B. Chopa, and M. T. Lockhart, "Indium-mediated regioselective synthesis of ketones from arylstannanes under solvent-free ultrasound irradiation," *Ultrason. Sonochem.*, vol. 20, no. 3, pp. 826–832, 2013.
- [102] L. S. Gadekar, B. R. Arbad, and M. K. Lande, "Eco-friendly synthesis of benzimidazole derivatives using solid acid scolecite catalyst," *Chinese Chem. Lett.*, vol. 21, no. 9, pp. 1053–1056, 2010.
- [103] K. Bahrami, M. M. Khodaei, and F. Naali, "Mild and Highly Efficient Method for the Synthesis of 2-Arylbenzimidazoles and 2-Arylbenzothiazoles" *J. Org. Chem.*, vol. 73, no. 19, pp. 6835–6837, 2008.
- [104] K. Jadidi, R. Gharemanzadeh, M. Mehrdad, H. R. Darabi, H. R. Khavasi, and D. Asgari, "A facile synthesis of novel pyrrolizidines under classical and ultrasonic conditions," *Ultrason. Sonochem.*, vol. 15, no. 2, pp. 124–128, 2008.
- [105] P. Magdolen, M. Mečiarová, and Š. Toma, "Ultrasound effect on the synthesis of 4-alkyl-(aryl)aminobenzaldehydes," *Tetrahedron*, vol. 57, no. 22, pp. 4781–4785, 2001, doi: 10.1016/S0040-4020(01)00403-3.
- [106] G. Cravotto, S. Tagliapietra, M. Caporaso, D. Garella, E. Borretto, and A. Di Stilo, "Recent advances in the cyclization of N-heterocycles: The role of enabling techniques (review)," *Chem. Heterocycl. Compd.*, vol. 49, no. 6, pp. 811–826, 2013.
- [107] R. Cella and H. A. Stefani, "Ultrasound in heterocycles chemistry," *Tetrahedron*, vol. 65, no. 13, pp. 2619–2641, 2009.
- [108] W. T. Richards and A. L. Loomis, "The chemical effects of high frequency sound waves I. A preliminary survey," *J. Am. Chem. Soc.*, vol. 49, no. 12, pp. 3086–3100, 1927.
- [109] R.W.Bailey, "Isolation of Alkaloids using Ultrasonic Energy," *Nature*, vol.

References

- 199, pp. 1292–1293, 1963.
- [110] J. Am and T. Ni, “The Sonochemistry of Zn Powder,” *J. Am. Chem. SOC*, vol. 2, no. 1, pp. 2342–2344, 1989.
- [111] M. Mamaghani, A. Loghmanifar, and M. R. Taati, “An efficient one-pot synthesis of new 2-imino-1,3-thiazolidin-4-ones under ultrasonic conditions,” *Ultrason. Sonochem.*, vol. 18, no. 1, pp. 45–48, 2011.
- [112] Z. Lyu, L. Ding, A. Y. T. Huang, C. L. Kao, and L. Peng, “Poly(amidoamine)dendrimers: covalent and supramolecular synthesis,” *Mater. Today Chem.*, vol. 13, pp. 34–48, 2019.
- [113] P. Tarach and A. Janaszewska, “Recent advances in preclinical research using pamam dendrimers for cancer gene therapy,” *Int. J. Mol. Sci.*, vol. 22, no. 6, pp. 1–31, 2021.
- [114] R. V. de Araújo, S. da Silva Santos, E. I. Ferreira, and J. Giarolla, “New advances in general biomedical applications of PAMAM dendrimers,” *Molecules*, vol. 23, no. 11, pp. 1–27, 2018, doi: 10.3390/molecules23112849.
- [115] R. Esfand and D. A. Tomalia, “Laboratory Synthesis of Poly(amidoamine)(PAMAM) Dendrimers,” *Dendrimers Other Dendritic Polym.*, vol. 1, pp. 587–604, 2002.
- [116] G. Lucotte, “Skin Debris on the Face of the Turin Shroud: A SEM-EDX Analysis,” *Archaeol. Discov.*, vol. 4, no. 2, pp. 103–117, 2016.
- [117] A. Hasaninejad, A. Zare, M. Shekouhy, and J. Ameri Rad, “Catalyst-free one-pot four component synthesis of polysubstituted imidazoles in neutral ionic liquid 1-butyl-3-methylimidazolium bromide,” *J. Comb. Chem.*, vol. 12, no. 6, pp. 844–849, 2010.
- [118] D. Strübing, H. Neumann, S. Klaus, S. Hübner, and M. Beller, “A facile and efficient synthesis of enyne-reaction precursors by multicomponent reactions,” *Tetrahedron*, vol. 61, no. 48, pp. 11333–11344, 2005.
- [119] M. A. Zolfigol *et al.*, “Design of ionic liquid 1,3-disulfonic acid imidazolium hydrogen sulfate as a dual-catalyst for the one-pot multi-component synthesis of 1,2,4,5-tetrasubstituted imidazoles,” *J. Ind. Eng. Chem.*, vol. 19, no. 3, pp. 721–726, 2013.
- [120] H. D. Hanoon, E. Kowsari, M. Abdouss, M. H. Ghasemi, and H. Zandi, “Highly efficient and simple protocol for synthesis of 2,4,5-triarylimidazole derivatives from benzil using fluorinated graphene oxide as effective and reusable catalyst,” *Res. Chem. Intermed.*, vol. 43, no. 7, pp. 4023–4041, 2017.
- [121] R. S. Ghogare, “Mandelic acid: an efficient and green organo-catalyst for

References

- synthesis of 2,4,5-trisubstituted Imidazoles under solvent-free conditions,” *Org. Commun.*, vol. 15, no. 1, pp. 44–58, 2022.
- [122] D.L. Pavia, M. Lampman, G. S. Kriz and J. R. Vyvyan, Introduction to spectroscopy, Department of Chemistry Western Washington University Bellingham, Washington, 2015, pp.262-264.
- [123] M. Kaurav, S. Ruhi, H. A. Al-Goshae, A. K. Jeppu, D. Ramachandran, R. K. Sahu, A.K. Sarkar, J.Khan and A.M. Ashif Ikbal, “Dendrimer: An update on recent developments and future opportunities for the brain tumors diagnosis and treatment,” *Front. Pharmacol.*, vol. 14, pp. 1–20, 2023.
- [124] N. Mody, R. K. Tekade, N. K. Mehra, P. Chopdey, and N. K. Jain, “Dendrimer, liposomes, carbon nanotubes and PLGA nanoparticles: One platform assessment of drug delivery potential,” *AAPS PharmSciTech*, vol. 15, no. 2, pp. 388–399, 2014.
- [125] A. I. Lopez, R. Y. Reins, A. M. McDermott, B. W. Trautner, and C. Cai, “Antibacterial activity and cytotoxicity of PEGylated poly(amidoamine) dendrimers,” *Mol. Biosyst.*, vol. 5, no. 10, pp. 1148–1156, 2009.
- [126] M. Ficker, J. F. Petersen, J. S. Hansen, and J. B. Christensen, “Guest-host chemistry with dendrimers-binding of carboxylates in aqueous solution,” *PLoS One*, vol. 10, no. 10, pp. 1–12, 2015.
- [127] J. Rojo and R. Delgado, “Glycodendritic structures: Promising new antiviral drugs,” *J. Antimicrob. Chemother.*, vol. 54, no. 3, pp. 579–581, 2004.
- [128] C. C. Michelle, K. Calabretta, A. Kumar and A. M. McDermott, “Antibacterial Activities of Poly(amidoamine) Dendrimers Terminated with Amino and Poly(ethylene glycol) Groups,” *Biomacromolecules*, vol. 8, no. 6, pp. 1807–1811, 2007.
- [129] K. Winnicka, M. Wroblewska, P. Wieczorek, P. T. Sacha, and E. A. Tryniszewska, “The effect of PAMAM dendrimers on the antibacterial activity of antibiotics with different water solubility,” *Molecules*, vol. 18, no. 7, pp. 8607–8617, 2013.
- [130] M. M. Heravi, M. Daraie, and V. Zadsirjan, “Current advances in the synthesis and biological potencies of tri- and tetra-substituted 1H-imidazoles,” *Mol. Divers.*, vol. 19, no. 3, pp. 577–623, 2015.
- [131] S. S. Alghamdi, R. S. Suliman, K. Almutairi, K. Kahtani, and D. Aljatli, “Imidazole as a promising medicinal scaffold: Current status and future direction,” *Drug Des. Devel. Ther.*, vol. 15, pp. 3289–3312, 2021.
- [132] R. A. Devkar, S. Chaudhary, S. Adepu, S. K. Xavier, K. S. Chandrashekar, and

References

- M. M. Setty, "Evaluation of antiurolithiatic and antioxidant potential of *Lepidagathis prostrata*: A Pashanbhed plant," *Pharm. Biol.*, vol. 54, no. 7, pp. 1237–1245, 2016.
- [133] V. Chandel, A. Choubey, and S. Asati, "Evaluation of in Vitro Antiurolithiatic Activity of *Thunbergia Erecta*," *Plant Arch.*, vol. 20, no. 2, pp. 4295–4299, 2020.
- [134] V. Butterweck and S. R. Khan, "Herbal medicines in the management of urolithiasis: Alternative or complementary?," *Planta Med.*, vol. 75, no. 10, pp. 1095–1103, 2009.
- [135] N. V. L. Suvarchala Reddy, M. Ganga Raju, and M. Mamatha, "Antilithiatic activity of leaf extract of *Citrus medica* on sodium oxalate urolithiasis-in-vitro and in-vivo evaluation," *Int. J. Pharm. Sci. Res.*, vol. 12, no. 7, pp. 3709–3715, 2021.
- [136] K. Spandana, M. Shivani, J. Himabindhu, and K. Ramanjaneyulu, "Evaluation of in vitro Antiurolithiatic Activity of *Gossypium Herbaceum*," *Res. J. Pharm. Technol.*, vol. 11, no. 12, pp. 5455–5457, 2018.
- [137] A. Nagal and R. K Singla, "Herbal Resources with Antiurolithiatic Effects: A Review," *Indo Glob. J. Pharm. Sci.*, vol. 03, no. 01, pp. 06–14, 2013.
- [138] K. M. Chinnala, S. Shanigarm and M.M.Elsani, "Antiurolithiatic activity of the plant extracts of *Solanum virginianum* on ethylene glycol induced urolithiasis in rats," *Int J Pharm Bio Sci*, vol. 3, no. 4, pp. 328–334, 2013.
- [139] N. Vyas and A. Argal, "Antiuroolithiatic Activity of Extract and Oleanolic Acid Isolated from the Roots of *Lantana camara* on Zinc Disc Implantation Induced Urolithiasis," *ISRN Pharmacol.*, vol. 2013, pp. 1–5, 2013.
- [140] S. B. Erickson, T. J. Vrtiska, and J. C. Lieske, "Effect of Cystone® on urinary composition and stone formation over a one year period," *Phytomedicine*, vol. 18, no. 10, pp. 863–867, 2011.
- [141] M. Tsujihata, "Mechanism of calcium oxalate renal stone formation and renal tubular cell injury," *Int. J. Urol.*, vol. 15, no. 2, pp. 115–120, 2008.
- [142] H.-J. Chung, H. M. Abrahams, M. V. Meng, and M. L. Stoller, "Theories of Stone Formation," *Urinary Stone Disease*, no. 1, 2007, pp. 55–68.
- [143] C. Senthil Kumari, "Efficacy and Safety of Herbal Medicine for Urolithiasis- A Systemic Review," *Int. J. Innov. Sci. Res. Technol.*, vol. 6, no. 2, pp. 491–498, 2021.
- [144] D. J. Kok and S. R. Khan, "Calcium oxalate nephrolithiasis, a free or fixed particle disease," *Kidney Int.*, vol. 46, no. 3, pp. 847–854, 1994.

References

- [145] S. P. Hewagama and R. P. Hewawasam, "Antiuro lithiatic Potential of Three Sri Lankan Medicinal Plants by the Inhibition of Nucleation, Growth, and Aggregation of Calcium Oxalate Crystals In Vitro," *Sci. World J.*, vol. 2022.
- [146] T.H.-Truc Phan¹, K. Hengphasatporn, Y. Shigeta W. Xie. P. Maitarad, T. Rungrotmongkol and W.Chavasiril "Designing Potent α -Glucosidase Inhibitors: A Synthesis and QSAR Modeling Approach for Biscoumarin Derivatives," *ACS Omega*, vol. 8, no. 29, pp. 26340–26350, 2023.
- [147] R. A. Defronzo, "Pathogenesis of type 2 diabetes mellitus," *Med. Clin. North Am.*, vol. 88, no. 4, pp. 787–835, 2004.
- [148] S. Padhi, A. K. Nayak, and A. Behera, "Type II diabetes mellitus: a review on recent drug based therapeutics," *Biomed. Pharmacother.*, vol. 131, p. 110708, 2020.
- [149] A. Fagot-Campagna A.A. Engelgau and David J. Pettitt,, "Type 2 diabetes among North American children and adolescents: An epidemiologic review and a public health perspective," *J. Pediatr.*, vol. 136, no. 5, pp. 664–672, 2000.
- [150] A. N. Nagappa, P. A. Thakurdesai, N. V. Rao, and J. Singh, "Antidiabetic activity of Terminalia catappa Linn fruits," *J. Ethnopharmacol.*, vol. 88, no. 1, pp. 45–50, 2003.
- [151] J. Jonusas, K. Aleknavicius, and S. Valinskas, "Klinio mobile app for diabetes self-care: A pilot study of HbA1c improvement in type 2 diabetes patients," *Smart Heal.*, vol. 29, p. 100404, 2023.
- [152] H.Yuan, X. Li, G.Wan, L. Sun, X. Zhu, F.Che and Z. Yang, "Type 2 diabetes epidemic in East Asia: A 35-year systematic trend analysis," *Oncotarget*, vol. 9, no. 6, pp. 6718–6727, 2018.
- [153] M. N. Piero, "Diabetes mellitus – a devastating metabolic disorder," *Asian J. Biomed. Pharm. Sci.*, vol. 4, no. 40, pp. 1–7, 2015.
- [154] K. Dabie, F. Adulley, B. A. Ababio, E. P. Yamoah, and E. Owusuaa, "Alpha (α)-amylase Inhibitory Property of Anthocleista nobilis Leaf Extract," *European J. Med. Plants*, vol. 33, no. 5, pp. 31–39, 2022.
- [155] E. J. Mayer-Davis, "Incidence Trends of Type 1 and Type 2 Diabetes among Youths, 2002–2012," *N. Engl. J. Med.*, vol. 376, no. 15, pp. 1419–1429, 2017.
- [156] M. B. Adinortey, "Biochemicophysiological Mechanisms Underlying Signs and Symptoms Associated with Diabetes mellitus," *Adv. Biol. Res. 11*, vol. 11, no. 6, pp. 382–390, 2017.
- [157] E. K. Hoogeveen, "The Epidemiology of Diabetic Kidney Disease," *Kidney Dial.*, vol. 2, pp. 433–442, 2022.

References

- [158] S. D. Bhinge, M. A. Bhutkar, D. S. Randive, G. H. Wadkar, and T. S. Hasabe, "In vitro hypoglycemic effects of unripe and ripe fruits of *Musa sapientum*," *Braz. J. Pharm. Sci.*, vol. 53, no. 4, pp. 1–6, 2017.
- [159] J. Blahova, M. Martiniakova, M. Babikova, V. Kovacova, V. Mondockova, and R. Omelka, *Pharmaceutical drugs and natural therapeutic products for the treatment of type 2 diabetes mellitus*, vol. 14, no. 8. 2021.
- [160] U. F. Magaji, O. Sacan, and R. Yanardag, "Alpha amylase, alpha glucosidase and glycation inhibitory activity of *Moringa oleifera* extracts," *South African J. Bot.*, vol. 128, pp. 225–230, 2020.
- [161] N. M. Alikunhi, K. Kandasamy, C. Manoharan, and M. Subramanian, "Insulin-like antigen of mangrove leaves and its anti-diabetic activity in alloxan-induced diabetic rats," *Nat. Prod. Res.*, vol. 26, no. 12, pp. 1161–1166, 2012.
- [162] K. S. Wagh, M. R. Khan, and S. Khan, "Investigation of Antioxidants , Antidiabetic and Antihyperlipidemic Activity of *Ficus Racemosa* leaves," *Eur. Chem. Bull.*, vol. 12, no. 4, pp. 5742–5750, 2023.
- [163] S. Alam *et al.*, "Antidiabetic Phytochemicals From Medicinal Plants: Prospective Candidates for New Drug Discovery and Development," *Front. Endocrinol. (Lausanne)*, vol. 13, no. February, pp. 1–35, 2022.
- [164] Y. A. Helmy, "Antimicrobial Resistance and Recent Alternatives to Antibiotics for the Control of Bacterial Pathogens with an Emphasis on Foodborne Pathogens," *Antibiotics*, vol. 12, no. 2, pp. 6–52, 2023.
- [165] H. Ullah. and S. Ali "Classification of Anti-Bacterial Agents and Their Functions," *Intech*, 2017, pp. 2–17
- [166] A. T. Sheldon, "Antibiotic resistance: a survival strategy.," *Clin. Lab. Sci.*, vol. 18, no. 3, pp. 170–180, 2005.
- [167] D. I. Edwards, "Nitroimidazole drugs - action and resistance mechanisms I. Mechanisms of action," *J. Antimicrob. Chemother.*, vol. 31, pp. 9–20, 1993.
- [168] R. A. Helmick, "Imidazole antibiotics inhibit the nitric oxide dioxygenase function of microbial flavohemoglobin," *Antimicrob. Agents Chemother.*, vol. 49, no. 5, pp. 1837–1843, 2005.
- [169] W. H. Miller ,M.A.seefled andK.A.Newlander "Discovery of aminopyridine-based inhibitors of bacterial enoyl-ACP reductase (FabI)," *J. Med. Chem.*, vol. 45, no. 15, pp. 3246–3256, 2002.
- [170] R. C. Chisté, M. Freitas, A. Z. Mercadante, and E. Fernandes, "Carotenoids are Effective Inhibitors of in vitro Hemolysis of Human Erythrocytes, as Determined by a Practical and Optimized Cellular Antioxidant Assay," *J. Food*

References

- Sci.*, vol. 79, no. 9, pp. H1841–H1847, 2014.
- [171] M. Gondwal and G. Joshi Nee Pant, “Synthesis and Catalytic and Biological Activities of Silver and Copper Nanoparticles Using *Cassia occidentalis*,” *Int. J. Biomater.*, vol. 8, pp. 4–11, 2018.
- [172] M. G. Davanc, A. Caroline, L. A. dos Santos, E.C. Padilha, M. L. Campos and C. R. de Andrade, “Evaluation of antimalarial activity and toxicity of a new primaquine prodrug,” *PLoS One*, vol. 9, no. 8, pp. 1–10, 2014.
- [173] J. Choi, V. Reipa, V. M. Hitchins, P. L. Goering, and R. A. Malinauskas, “Physicochemical Characterization and in vitro hemolysis evaluation of silver nanoparticles,” *Toxicol. Sci.*, vol. 123, no. 1, pp. 133–143, 2011.
- [174] S. G. Nayak, B. Poojary, and V. Kamat, “Novel pyrazole-clubbed thiophene derivatives via Gewald synthesis as antibacterial and anti-inflammatory agents,” *Arch. Pharm. (Weinheim)*, vol. 353, no. 12, pp. 1–13, 2020.
- [175] H. Huang, W. Lai, M. Cui, L. Liang, Y. Lin and Q. Fang, “An Evaluation of Blood Compatibility of Silver Nanoparticles,” *Sci. Rep.*, vol. 6, no. January, pp. 1–15, 2016.
- [176] M. Podsiedlik, M. Markowicz-Piasecka, and J. Sikora, “Erythrocytes as model cells for biocompatibility assessment, cytotoxicity screening of xenobiotics and drug delivery,” *Chem. Biol. Interact.*, vol. 332, pp. 1–77, 2020.
- [177] M. Abu Zarin, J. S. Tan, P. Murugan, and R. Ahmad, “Investigation of potential anti-urolithiatic activity from different types of *Musa pseudo-stem* extracts in inhibition of calcium oxalate crystallization,” *BMC Complement. Med. Ther.*, vol. 20, no. 1, pp. 1–12, 2020.
- [178] S. Vishnupriya, “A study on phytochemical screening and antilithiatic activity on *Aerva lanta* (L.) Juss. ex Schult. leaves extract,” *Asian J. Innov. Res.*, vol. 6, no. 1, pp. 10–13, 2022.
- [179] P. Rajeshwari, G. Rajeswari, S. Jabbarulla, and I. Vishnu Vardhan, “Evaluation of invitro anti-urolithiasis activity of *Convolvulus arvensis*,” *Int. J. Pharm. Pharm. Sci.*, vol. 5, no. 3, pp. 599–601, 2013.
- [180] R. K. Chilivery, S. Alagar, and T. P. Darsini, “In Vitro Anti-Urolithiasis Potentials of *Argemone mexicana* L. Leaves,” *Curr. Clin. Pharmacol.*, vol. 11, no. 4, p. 286–290, 2016.
- [181] M. I. Kazeem, R. Balogun, and A. L. Ogundajo, “Comparative Study on the α -Amylase and α -Glucosidase Inhibitory Potential of Different Extracts of *Bhlgia Sapida* Koenig,” *Am. J. Res. Commun.*, vol. 1, no. 7, pp. 178–192, 2013.

References

- [182] M. Govindappa, B. Hemashekhar, M. Arthikala, V. R. Rai, and Y. L. Ramachandra, "Characterization, antibacterial, antioxidant, antidiabetic, anti-inflammatory and antityrosinase activity of green synthesized silver nanoparticles using *Calophyllum tomentosum* leaves extract," *Results Phys.*, vol. 9, pp. 400–408, 2018.
- [183] F. U. Ohikhena, O. A. Wintola, and A. J. Afolayan, "Evaluation of the Antibacterial and Antifungal Properties of *Phragmanthera capitata* (Sprengel) Balle (Loranthaceae), a Mistletoe Growing on Rubber Tree, Using the Dilution Techniques," *Sci. World J.*, vol. 3, pp. 1–10, 2017.
- [184] K. G. Bhat and T. M. Nalawade, "Antimicrobial Activity of Endodontic Medicaments and Vehicles using Agar Well Diffusion Method on Facultative and Obligate Anaerobes," *Int. J. Clin. Pediatr. Dent.*, vol. 9, no. 4, pp. 335–341, 2016.
- [185] S. A. Mohammed, H. M. Mousa, and A. H. Alwan, "Determination of hemolytic cytotoxicity and antibacterial activity of *Conocarpus lancifolius* aqueous leaves extract," *IOP Conference Series: Materials Science and Engineering*, 2019, vol. 571, no. 1, pp. 2–10.
- [186] K. Babijczuk, B. Warzajtis, J. Starzyk, L. Mrówczyńska, and B. Jasiewicz, "Synthesis, Structure and Biological Activity of Indole–Imidazole Complexes with $ZnCl_2$: Can Coordination Enhance the Functionality of Bioactive Ligands?," *Molecules*, vol. 28, no. 10, pp. 1–19, 2023.
- [187] M. A. Zarin, J. S. Tan, R. Ahmad, N. Z. Jin, and N. F. H. A. Aziz, "Determination of nucleation assay for anti-urolithiasis activity from bagasse *Musa acuminata* x *balbisiana* Colla cv. Pisang Awak Legor methanolic extracts using uv-spectrometer and size measurement," *IOP Conf. Ser. Mater. Sci. Eng.*, vol. 716, no. 1, pp. 1–9, 2020.
- [188] R. Siener, D. Ebert, C. Nicolay, and A. Hesse, "Dietary risk factors for hyperoxaluria in calcium oxalate stone formers," *Kidney Int.*, vol. 63, no. 3, pp. 1037–1043, 2003.
- [189] S. Suman and S. V. S. Kumar, "Anti-urolithiatic activity of ethanolic extract of *Piper cubeba* dried fruits: An in-vitro and in-vivo study," *Pharmacogn. J.*, vol. 12, no. 6, pp. 1289–1296, 2020.
- [190] V. B., "Kidney Stone Disease: A Brief Review," *Acta Sci. Pharmacol.*, vol. 2, no. 2, pp. 17–21, 2021.
- [191] F. O. Balogun and A. O. T. Ashafa, "Aqueous root extracts of *Dicoma anomala* (Sond.) extenuates postprandial hyperglycaemia in vitro and its modulation on the activities of carbohydrate-metabolizing enzymes in streptozotocin-induced

References

- diabetic Wistar rats,” *South African J. Bot.*, vol. 112, pp. 102–111, 2017.
- [192] A. S. Alqahtani, S. Hidayathulla, and Md Tabish Rehman, “Alpha-amylase and alpha-glucosidase enzyme inhibition and antioxidant potential of 3-oxolupenal and katononic acid isolated from *Nuxia oppositifolia*,” *Biomolecules*, vol. 10, no. 1, pp. 1–19, 2020.
- [193] N. Lohitha and V. Vijayakumar, “Imidazole Appended Novel Phenoxyquinolines as New Inhibitors of α -Amylase and α -Glucosidase Evidenced with Molecular Docking Studies,” *Polycycl. Aromat. Compd.*, vol. 42, no. 8, pp. 5521–5533, 2022.
- [194] D. G. Aguila-Muñoz, “Synthesis and Molecular Docking Studies of Alkoxy- and Imidazole-Substituted Xanthenes as α -Amylase and α -Glucosidase Inhibitors,” *Molecules*, vol. 28, no. 10, 2023.
- [195] M. Gholami, R. Mohammadi, and M. A. D. Arzanlou, “In vitro antibacterial activity of poly (amidoamine)-G7 dendrimer,” *BMC Infect. Dis.*, vol. 17, no. 1, pp. 1–11, 2017.
- [196] H. Ali Mohamed, Y. A. Ammar, G. A. m. Elhagali, H. A. Eyada, D. S. Aboul-Magd, and A. Ragab, “In Vitro Antimicrobial Evaluation, Single-Point Resistance Study, and Radiosterilization of Novel Pyrazole Incorporating Thiazol-4-one/Thiophene Derivatives as Dual DNA Gyrase and DHFR Inhibitors against MDR Pathogens,” *ACS Omega*, vol. 7, no. 6, pp. 4970–4990, 2022.

APPENDIX



Appendix A

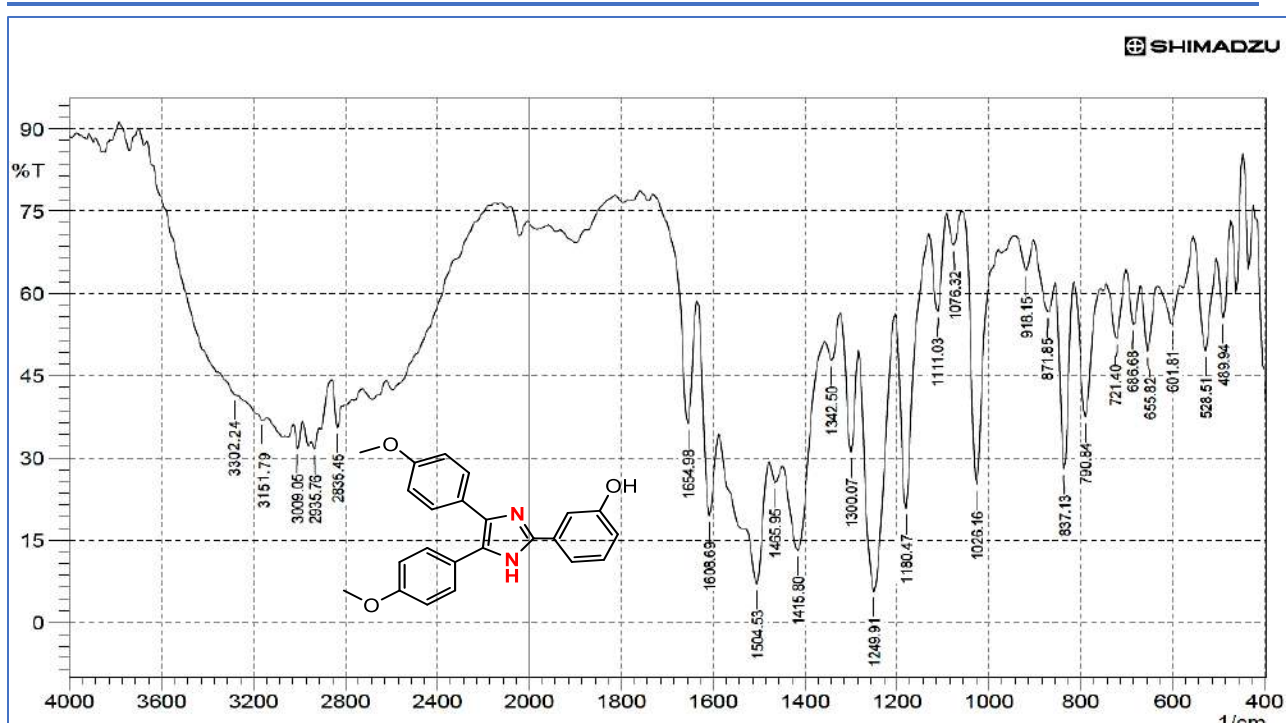


Figure 1: FTIR spectrum of 4a

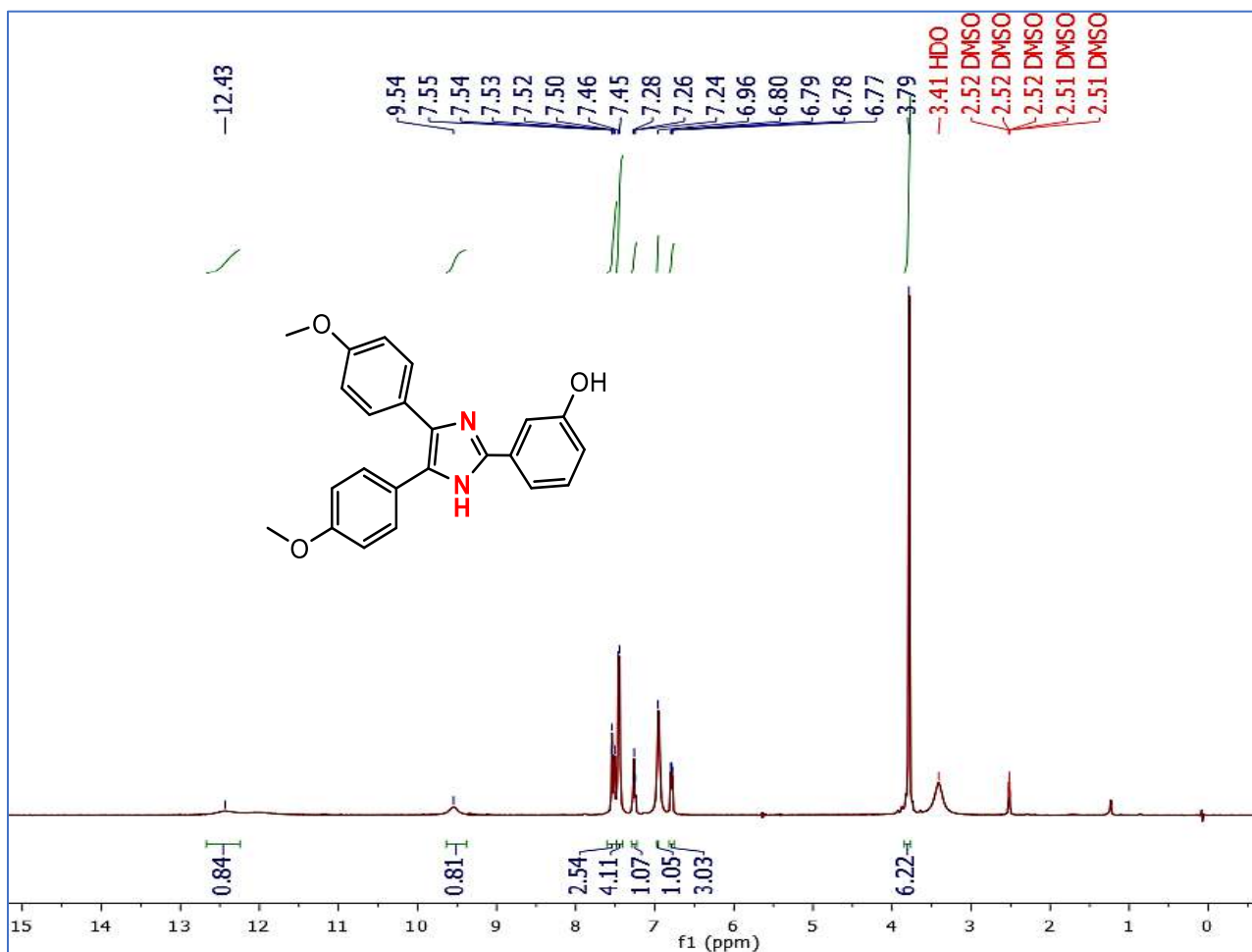


Figure 2: ¹H NMR spectrum of 4a

Appendix A

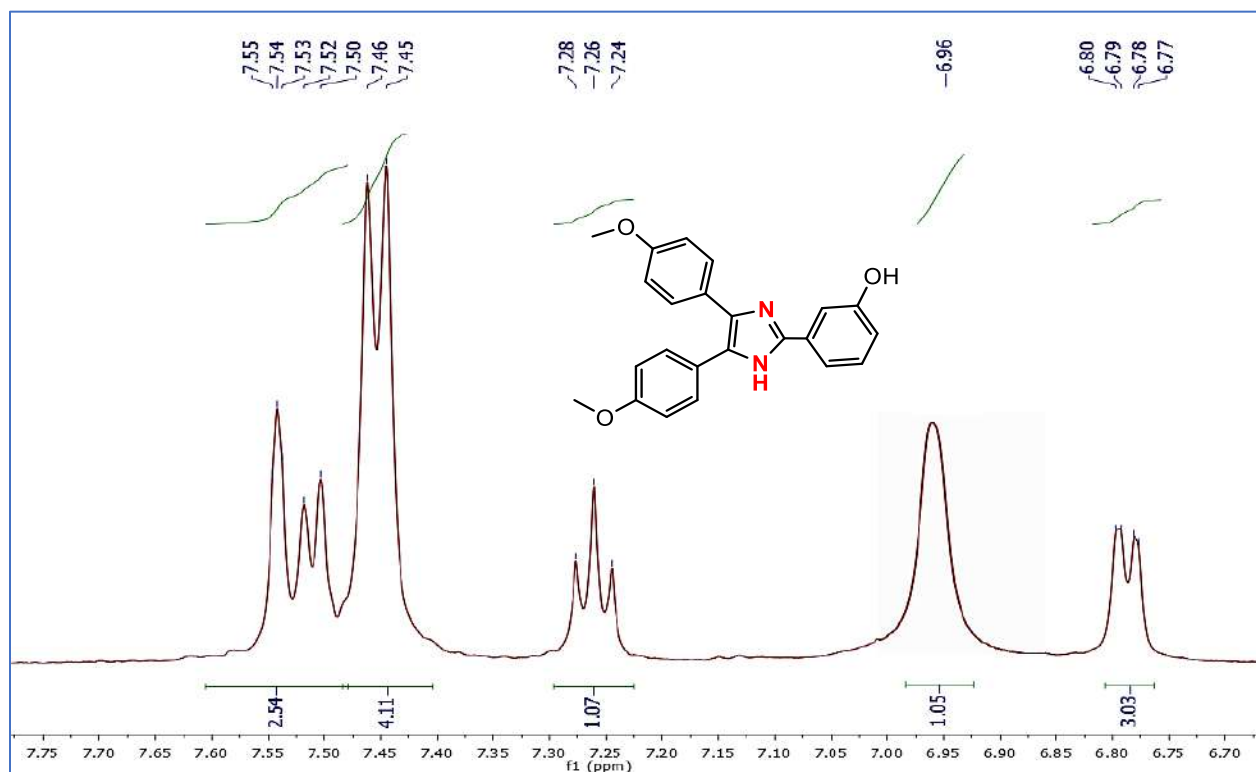


Figure 3: Expanded ^1H NMR spectrum of 4a

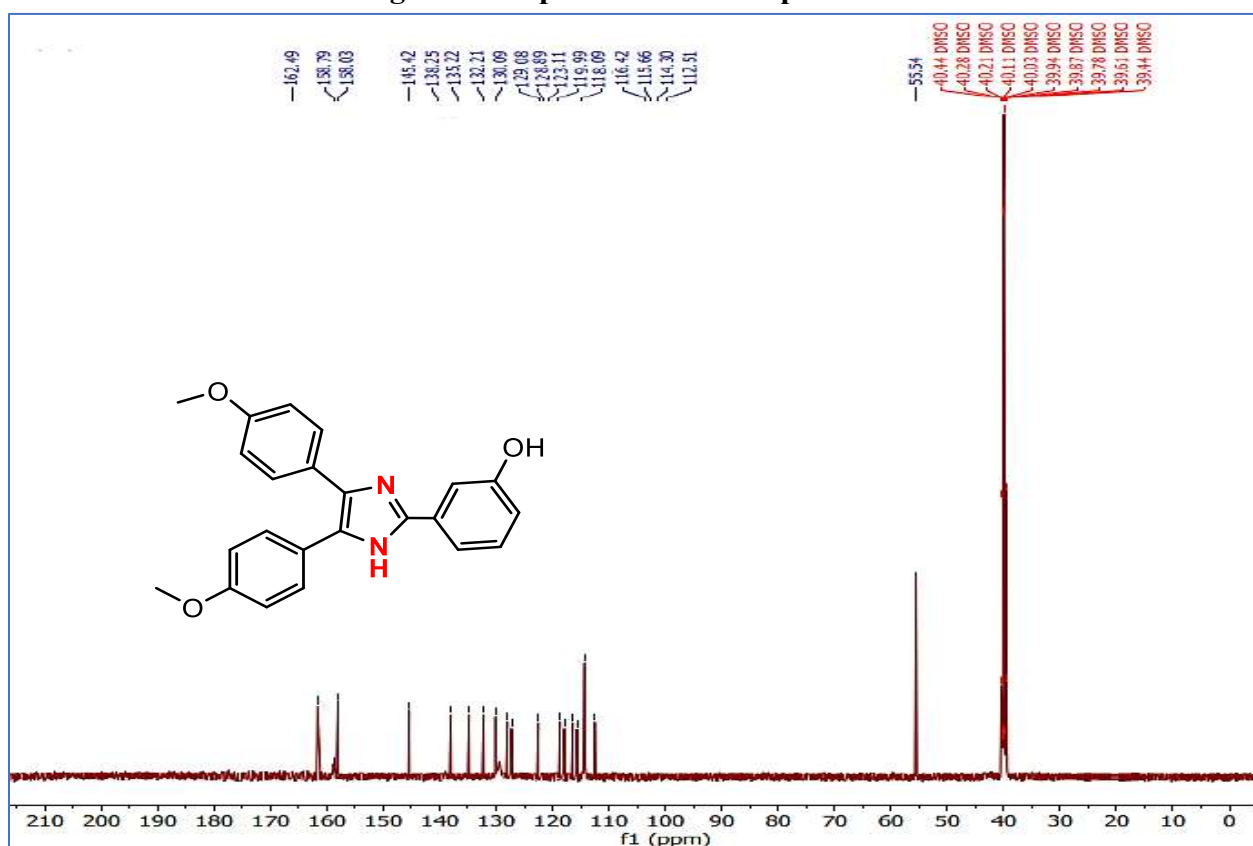


Figure 4: ^{13}C NMR spectrum of 4a

Appendix A

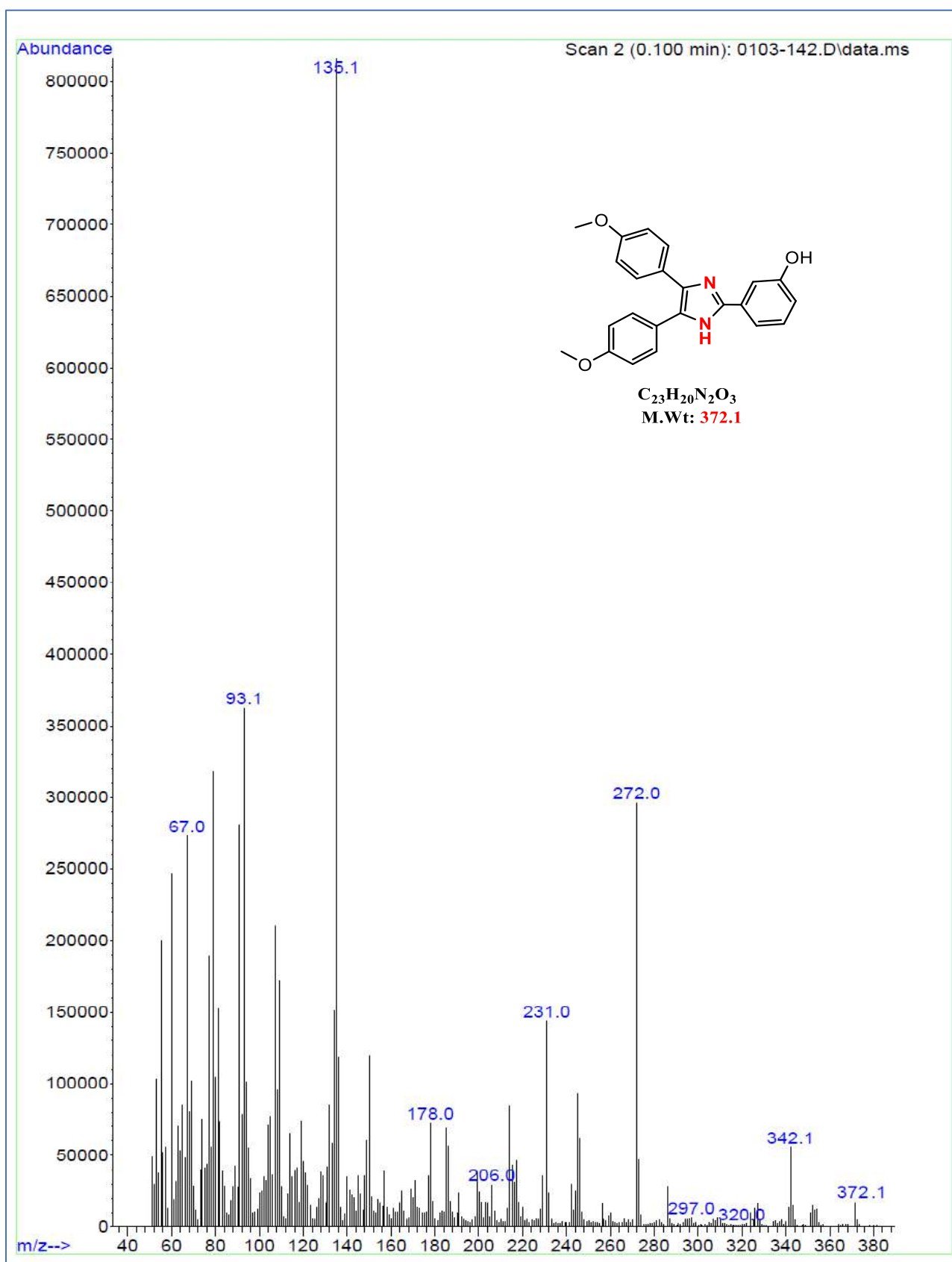


Figure 5: Mass spectrum of 4a

Appendix A

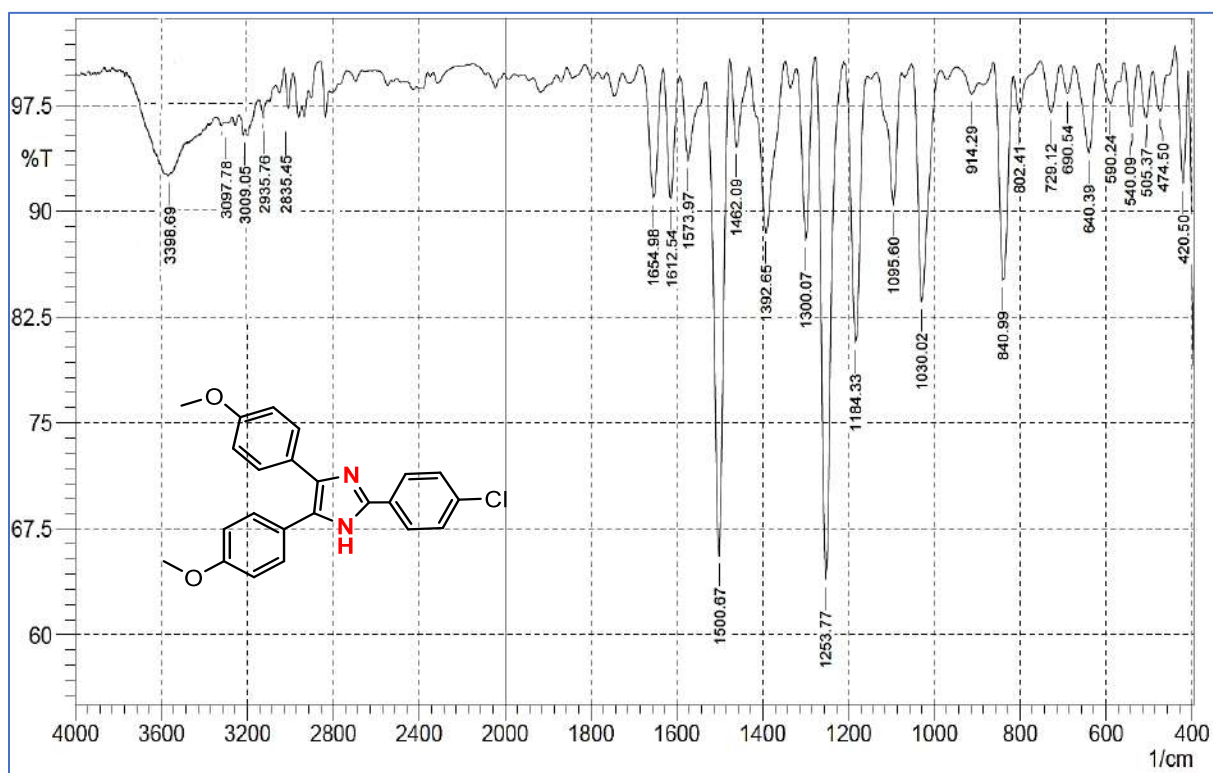


Figure 6: FTIR spectrum of 4b

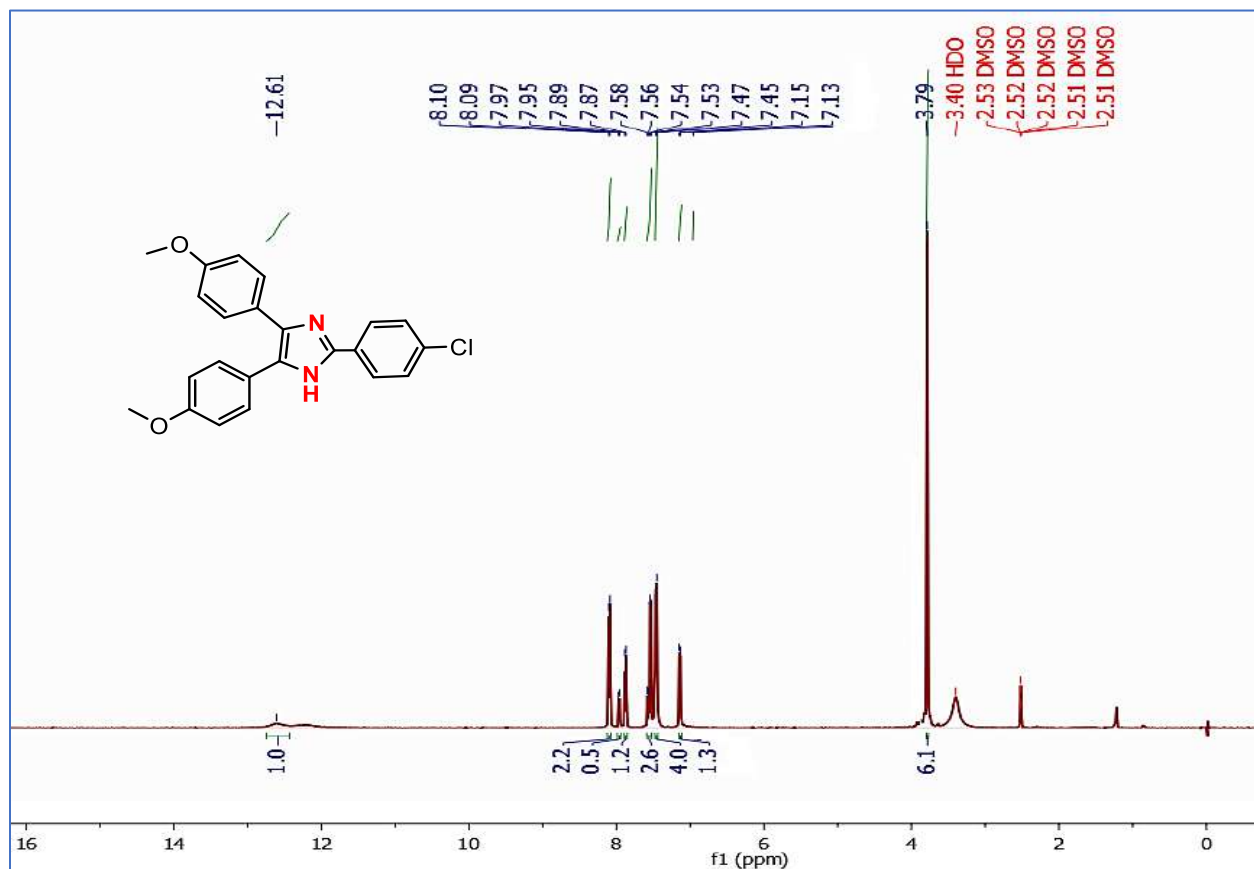


Figure 7: ^1H NMR spectrum of 4b

Appendix A

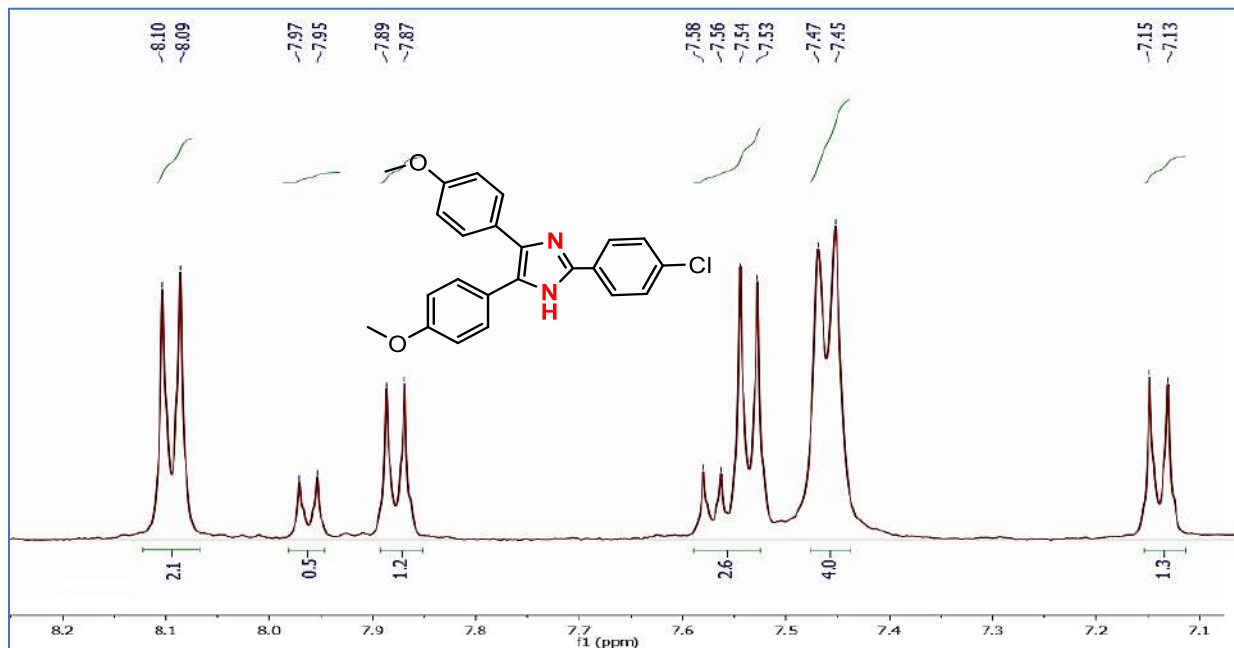


Figure 8: Expanded ^1H NMR spectrum of 4b

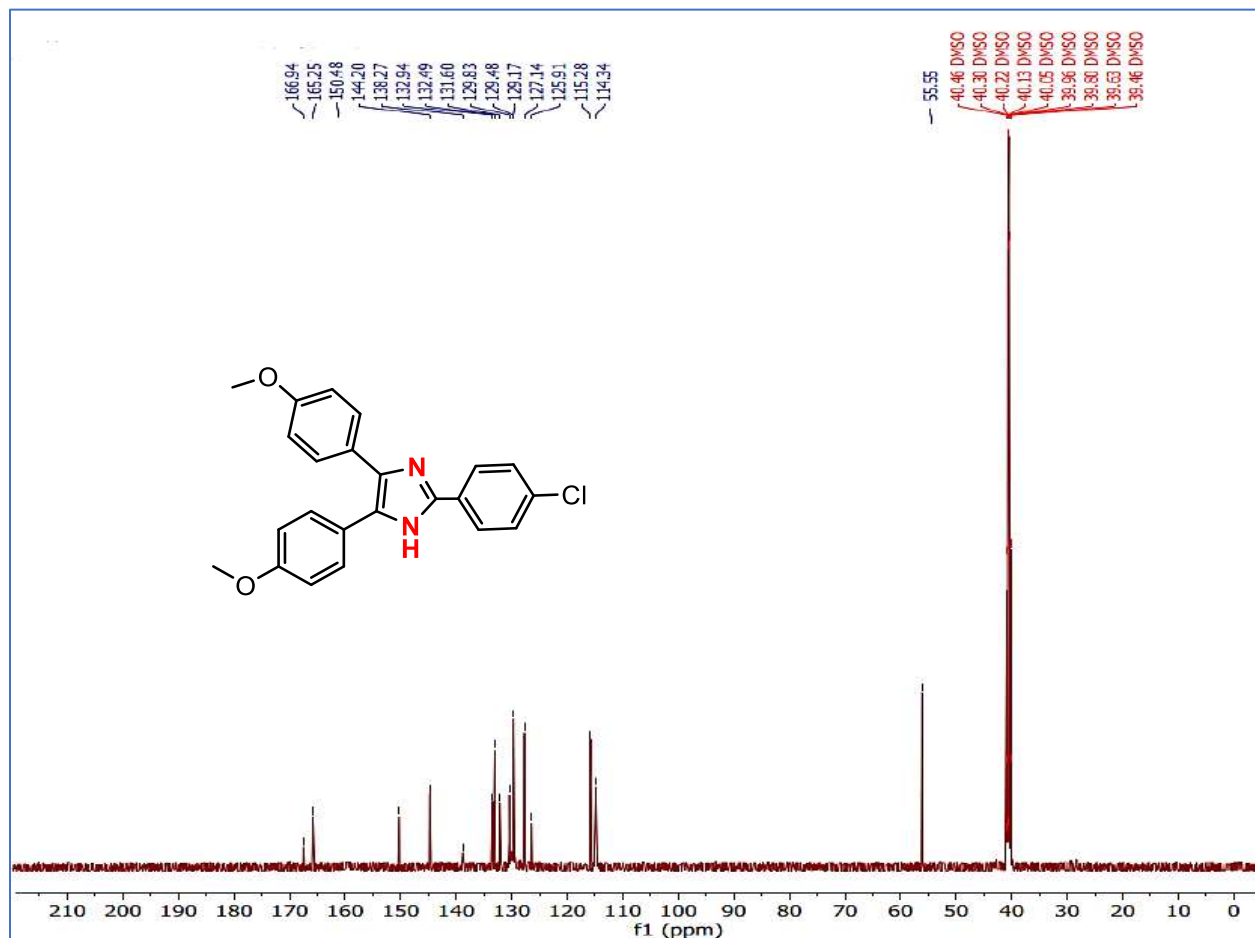


Figure 9: ^{13}C NMR spectrum of 4b

Appendix A

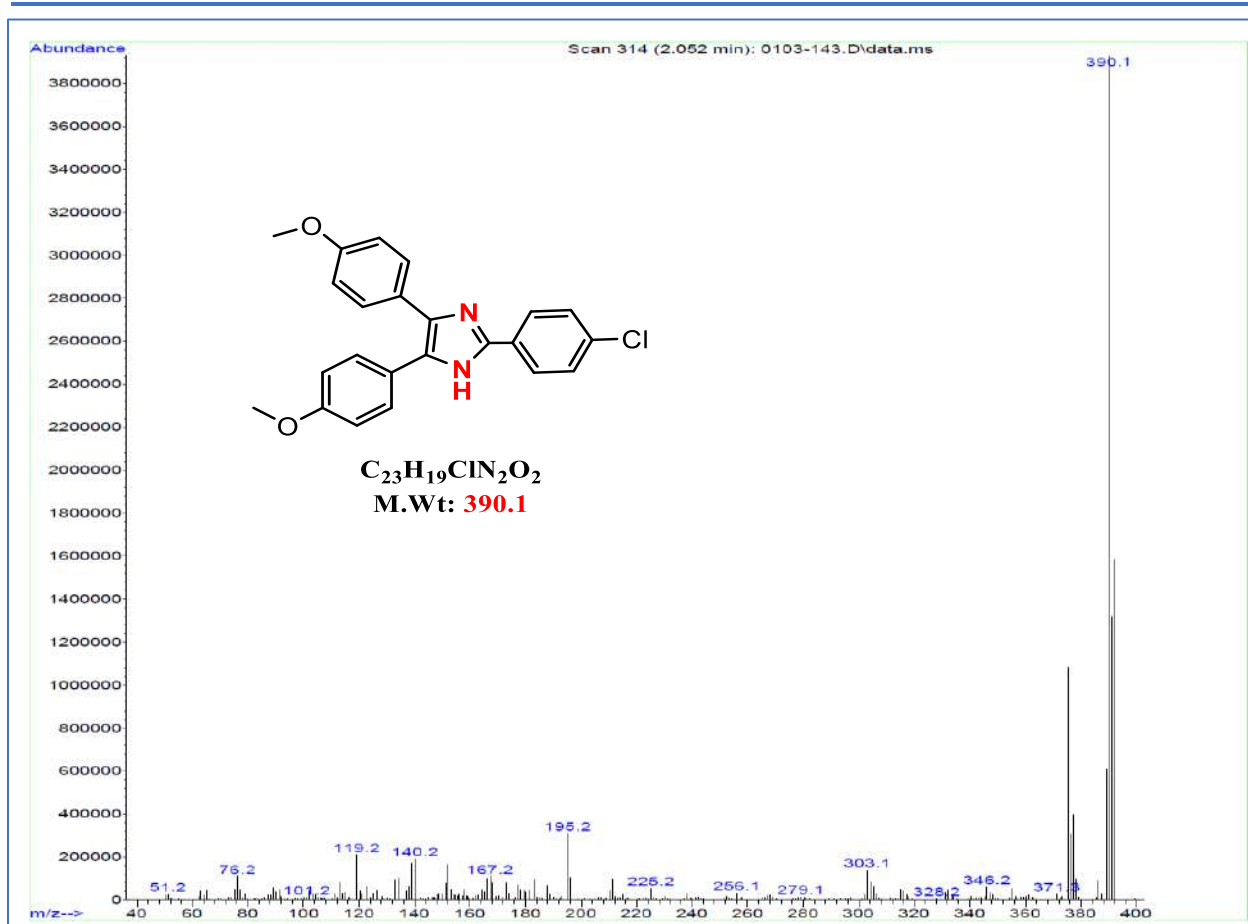


Figure 10: Mass spectrum of 4b

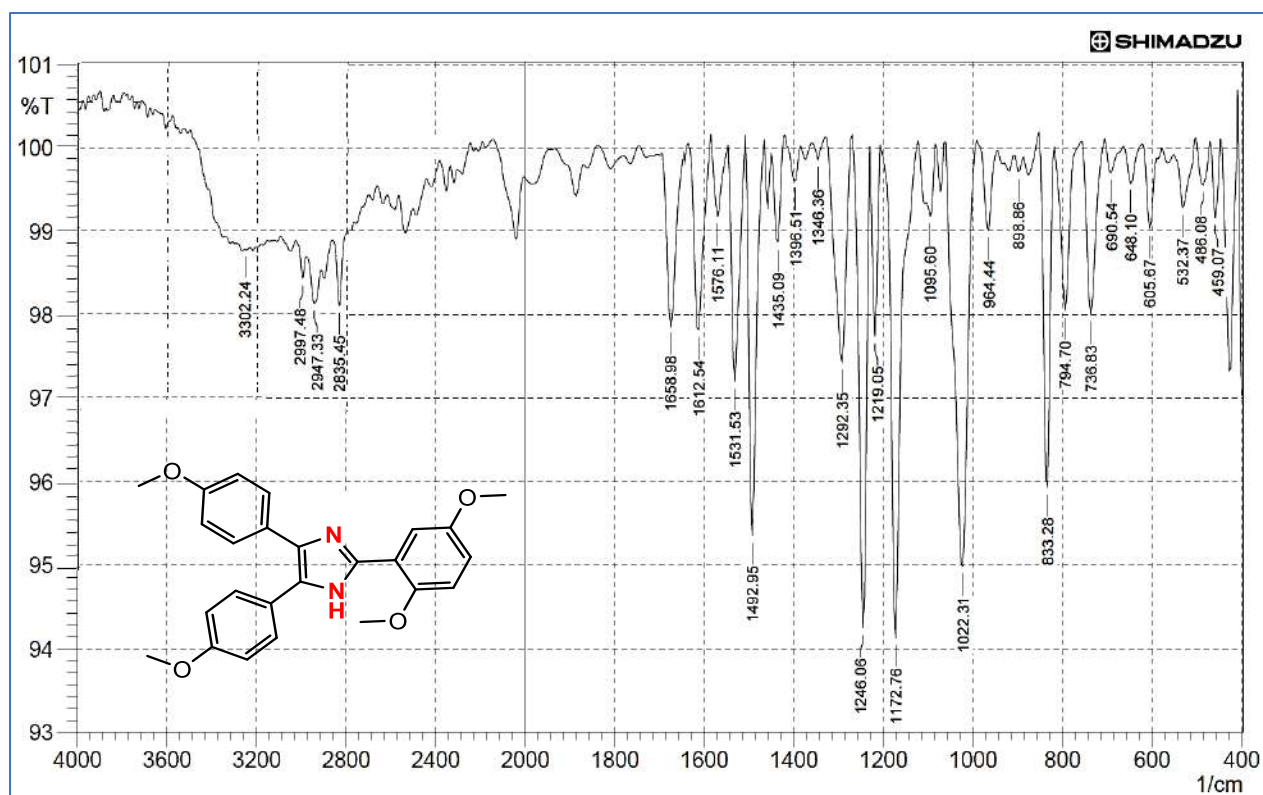


Figure 11: FTIR spectrum of 4c

Appendix A

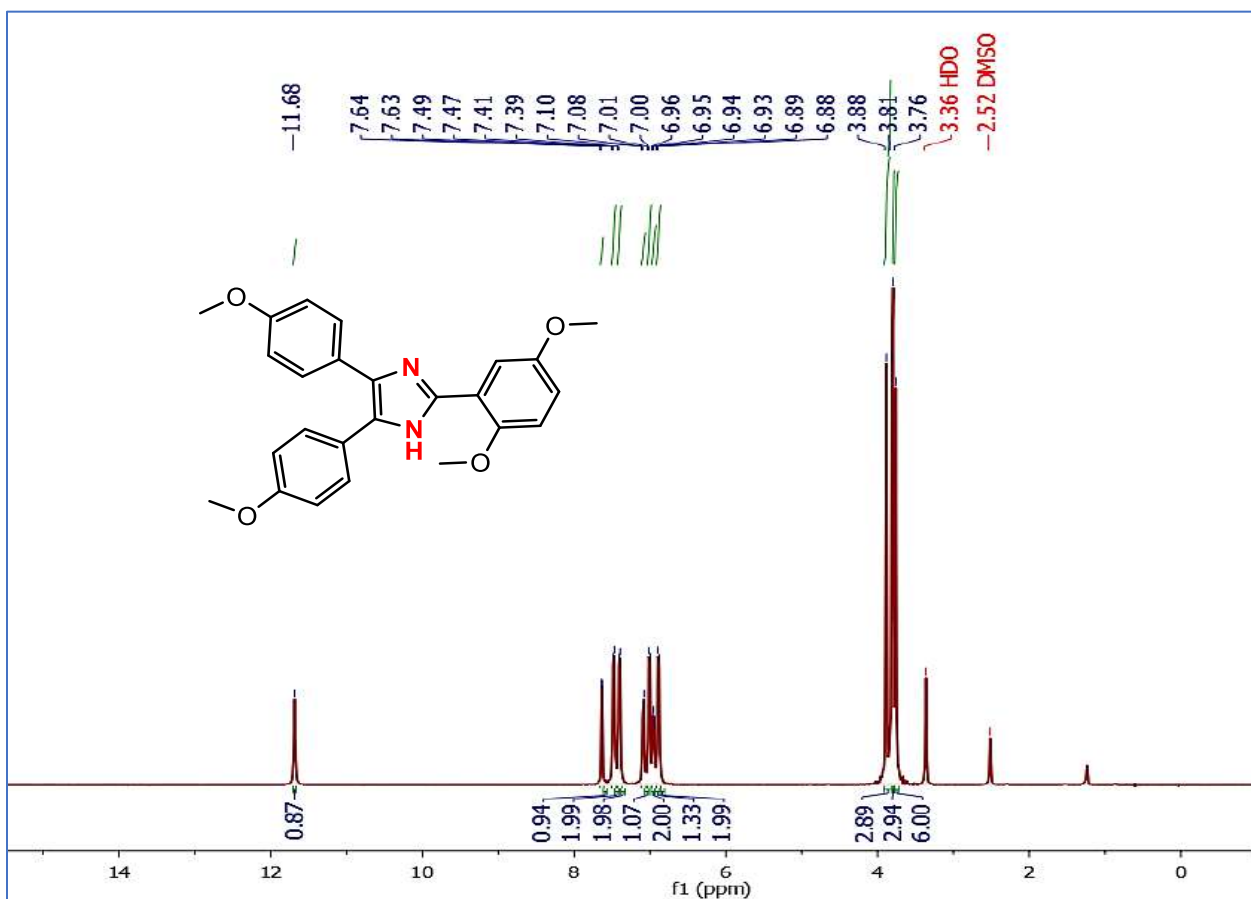


Figure 12: ^1H NMR spectrum of 4c

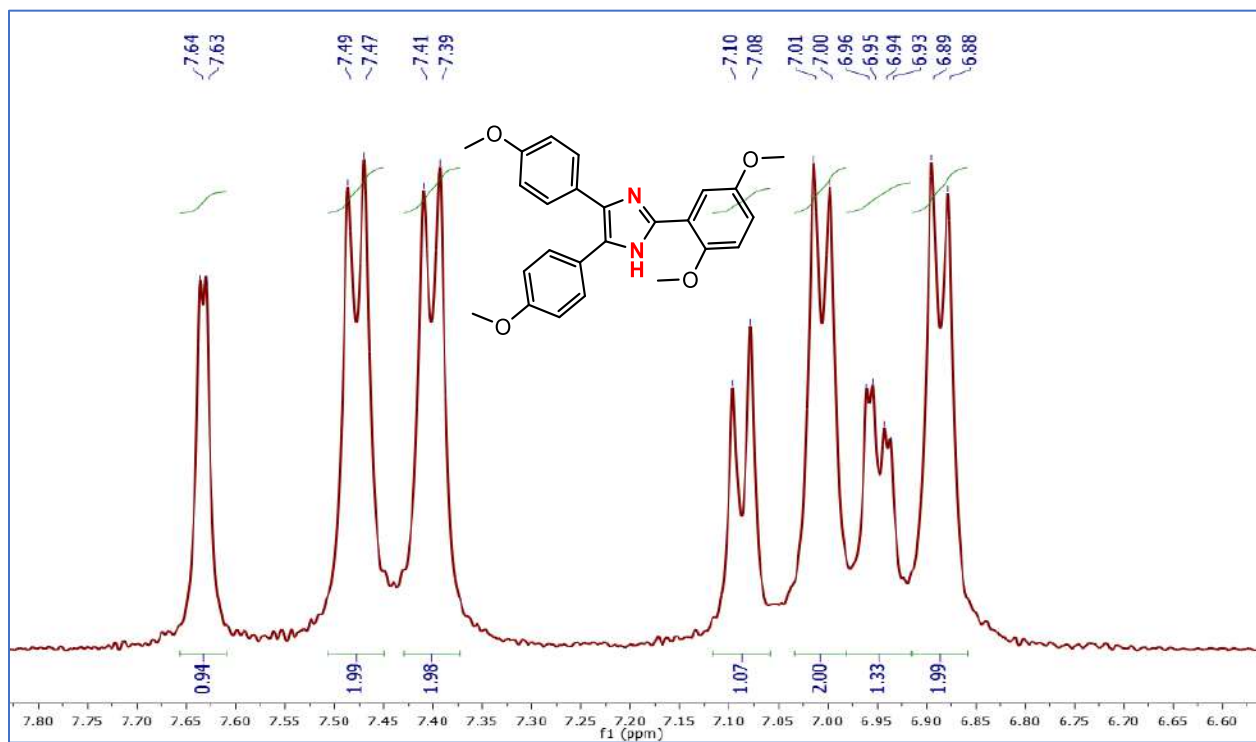


Figure 13: Expanded ^1H NMR spectrum of 4c

Appendix A

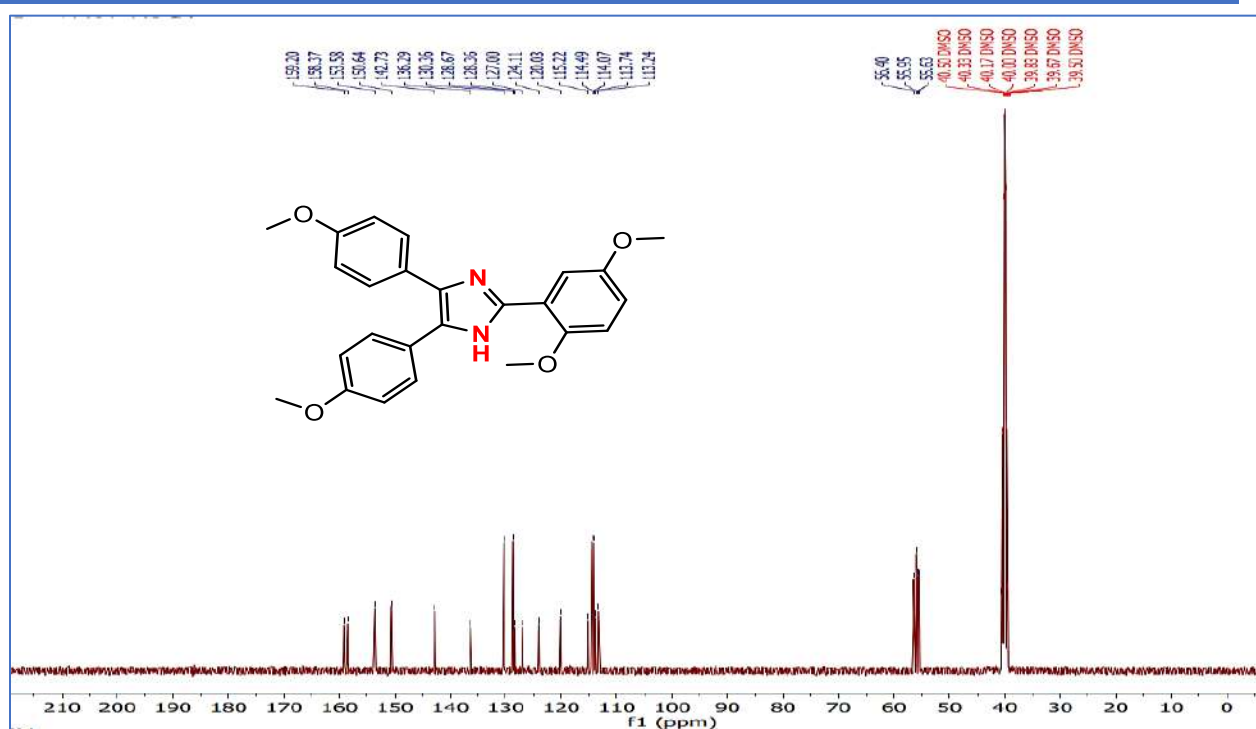


Figure 14: ¹³C NMR spectrum of 4c

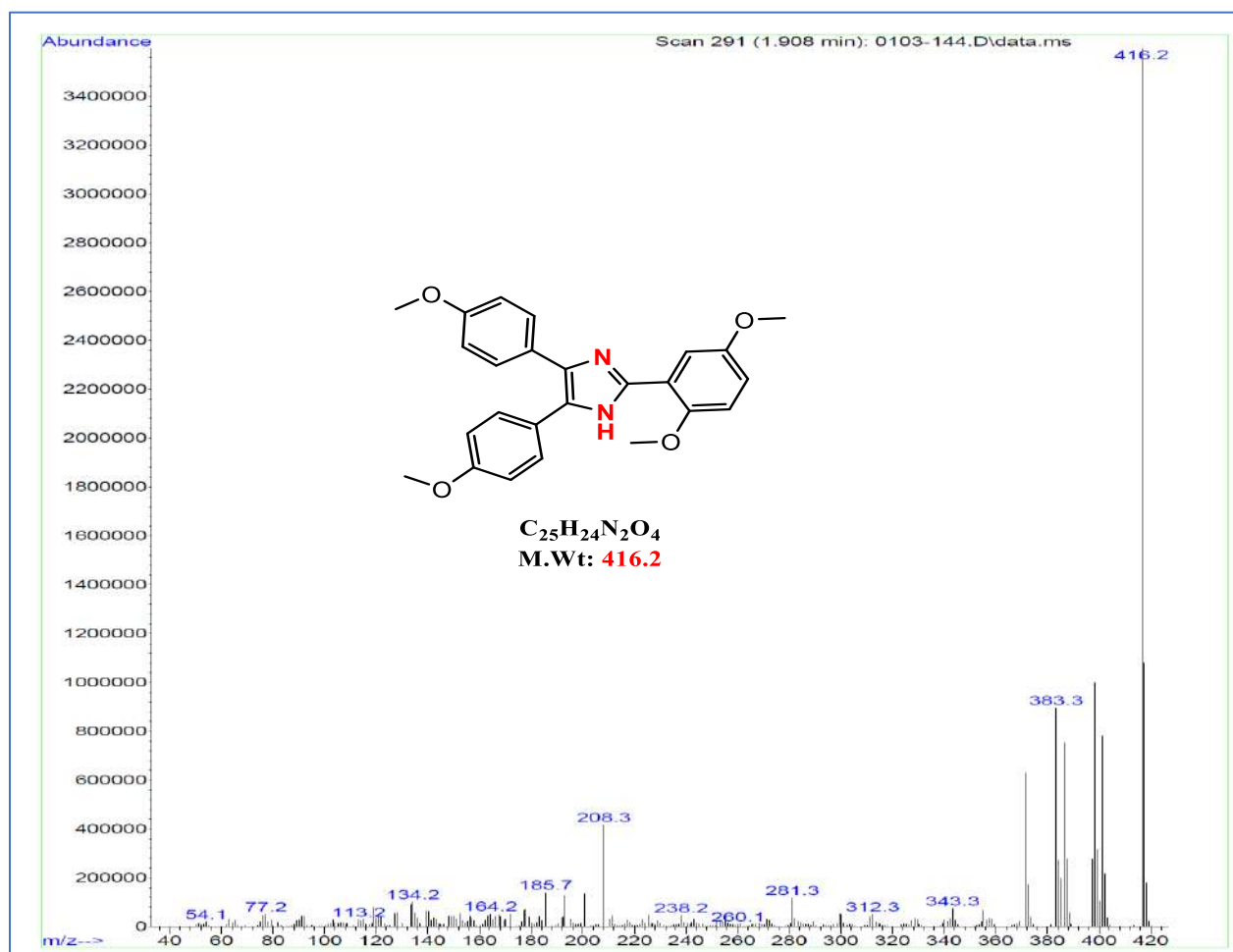


Figure 15: Mass spectrum of 4c

Appendix A

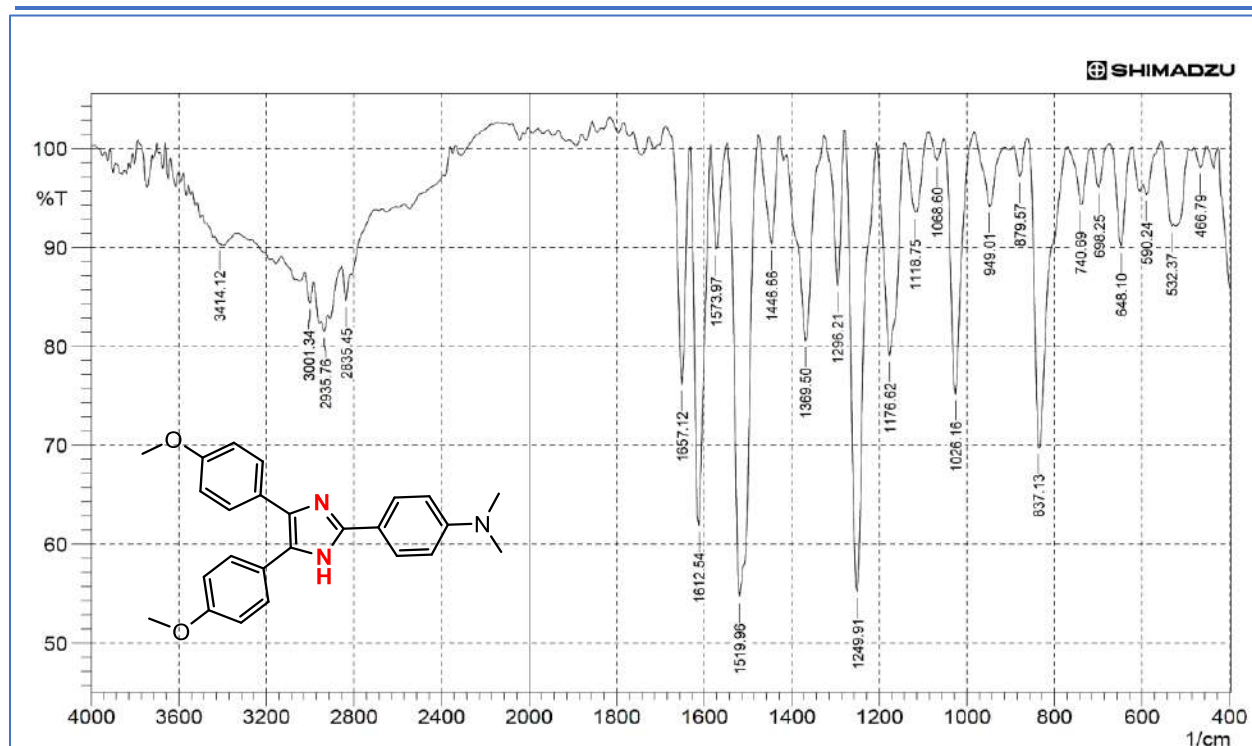


Figure 16: FTIR spectrum of 4d

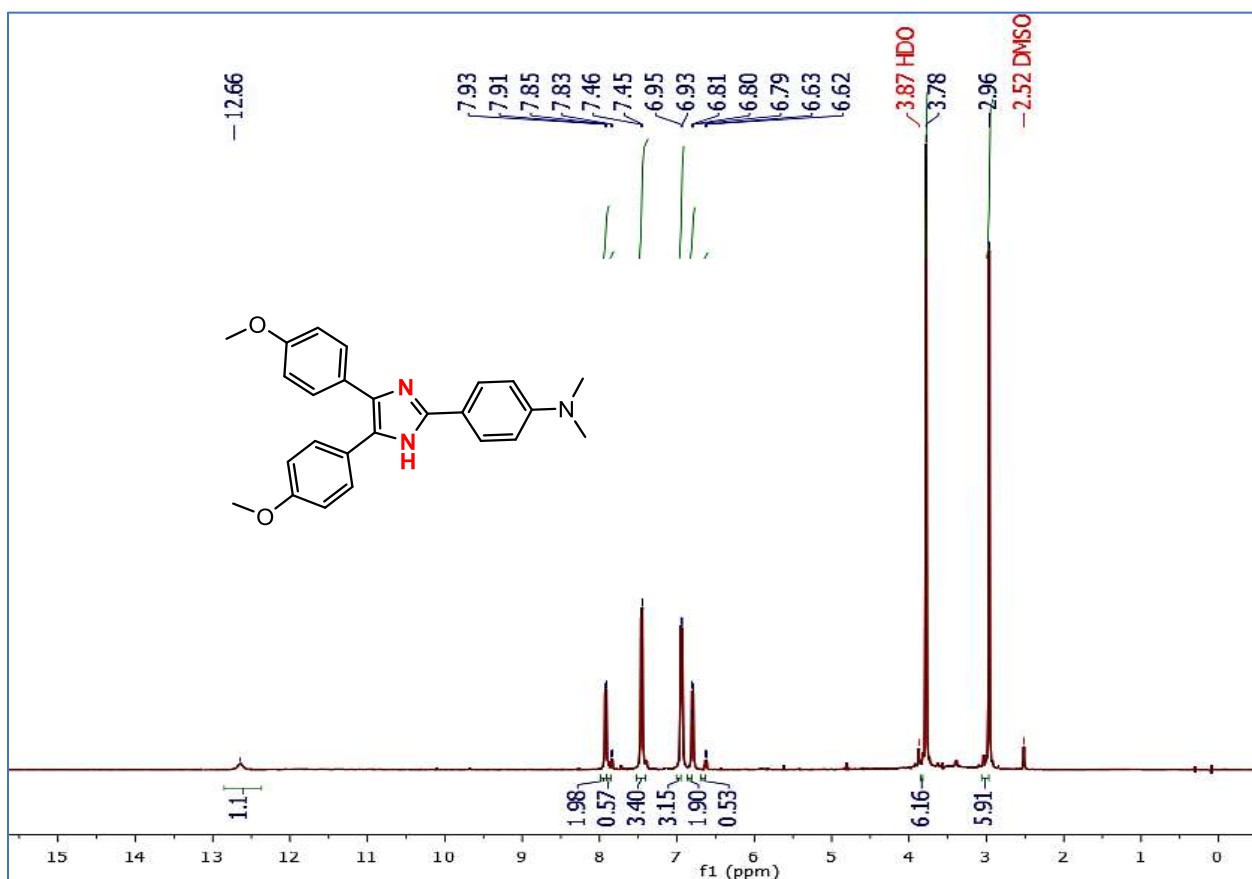


Figure 17: ^1H NMR spectrum of 4d

Appendix A

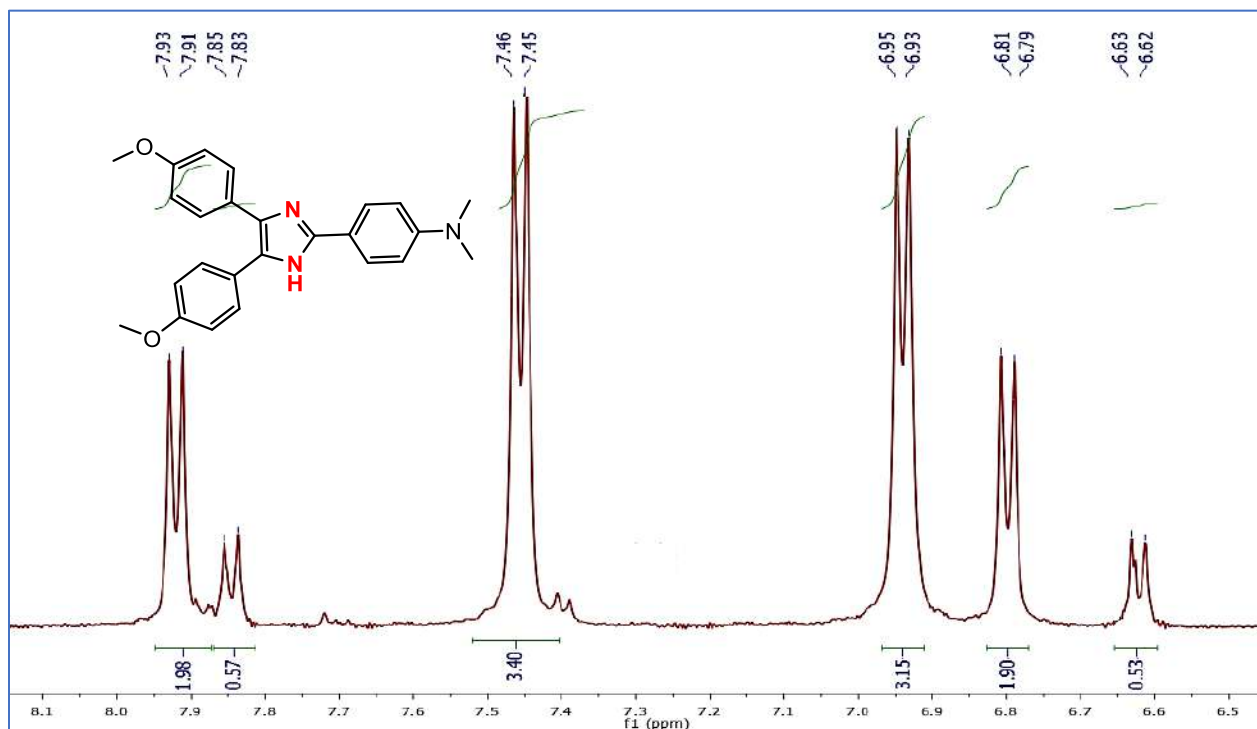


Figure 18: Expanded ^1H NMR spectrum of 4d

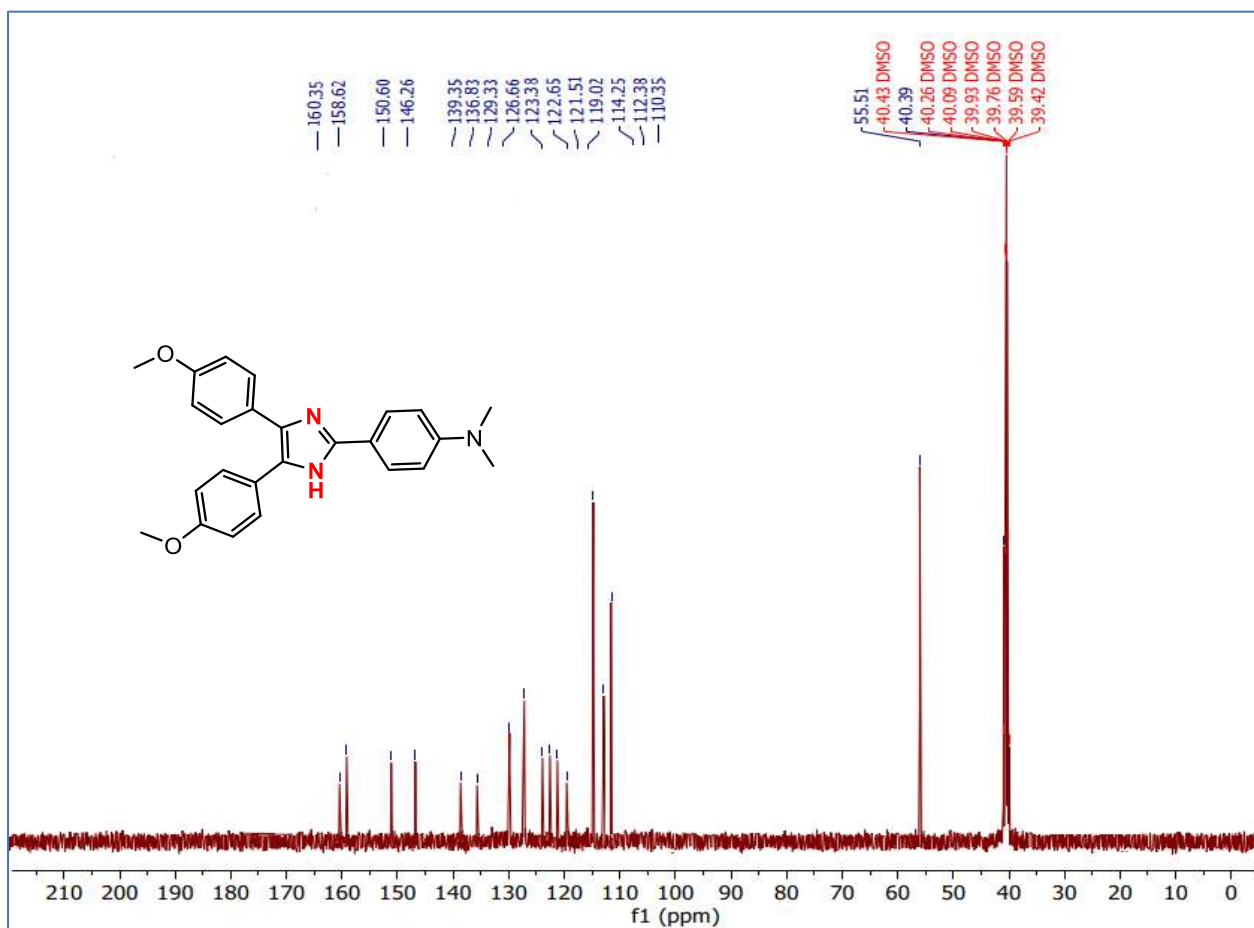


Figure 19: ^{13}C NMR spectrum of 4d

Appendix A

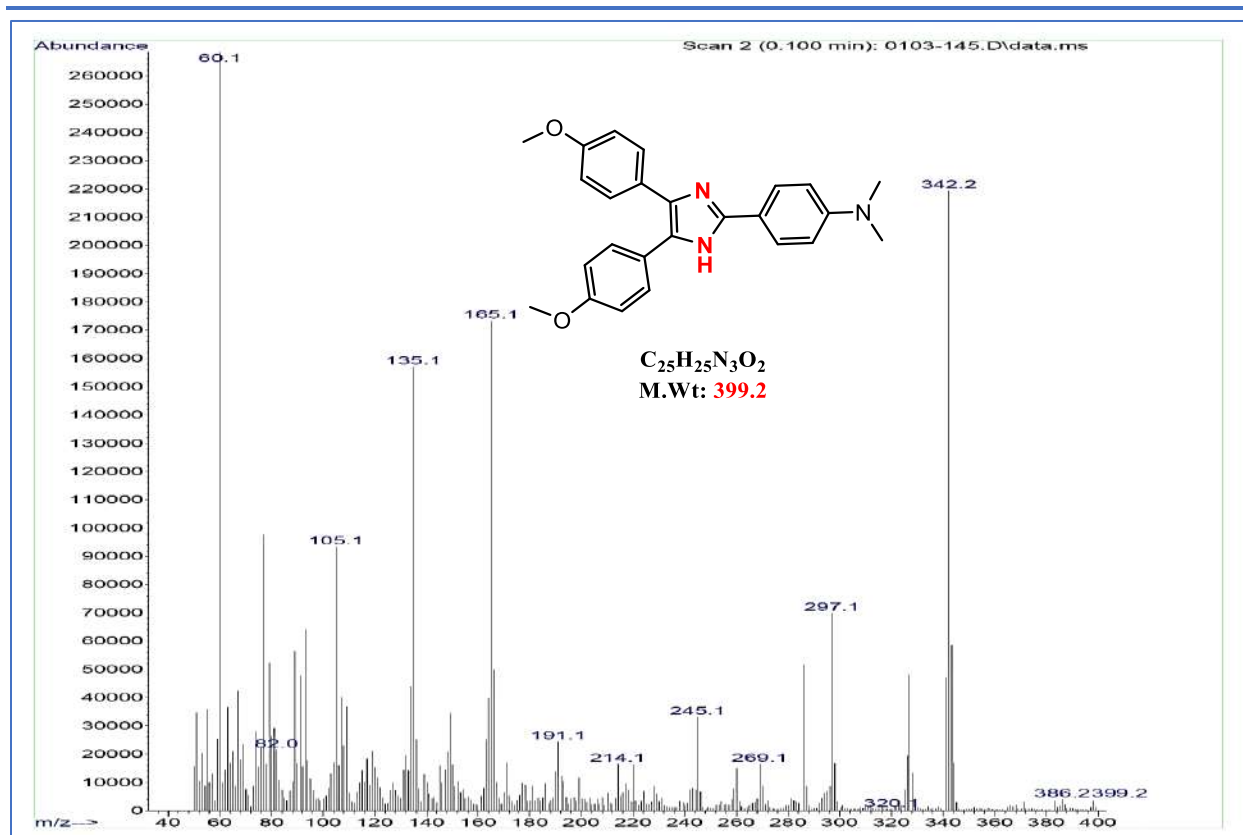


Figure 20: Mass spectrum of 4d

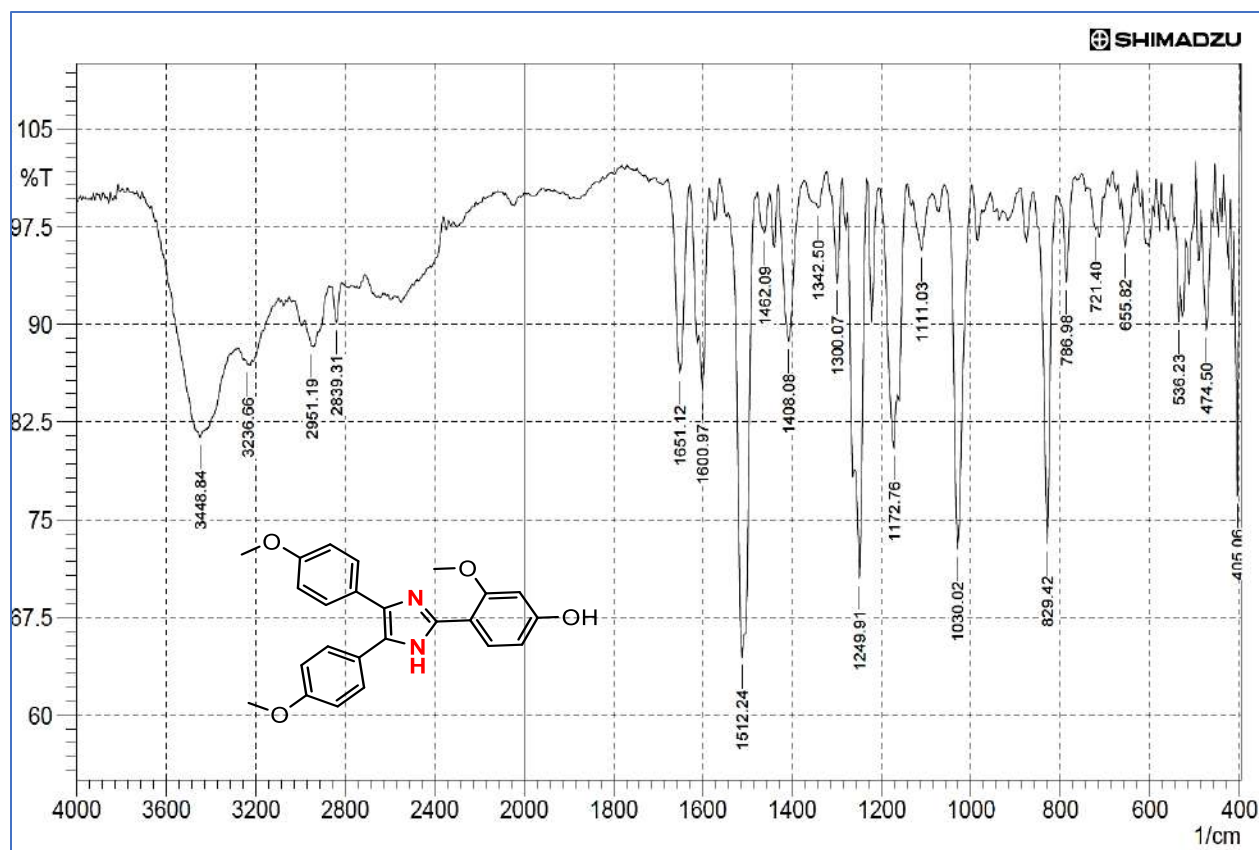


Figure 21: FTIR spectrum of 4e

Appendix A

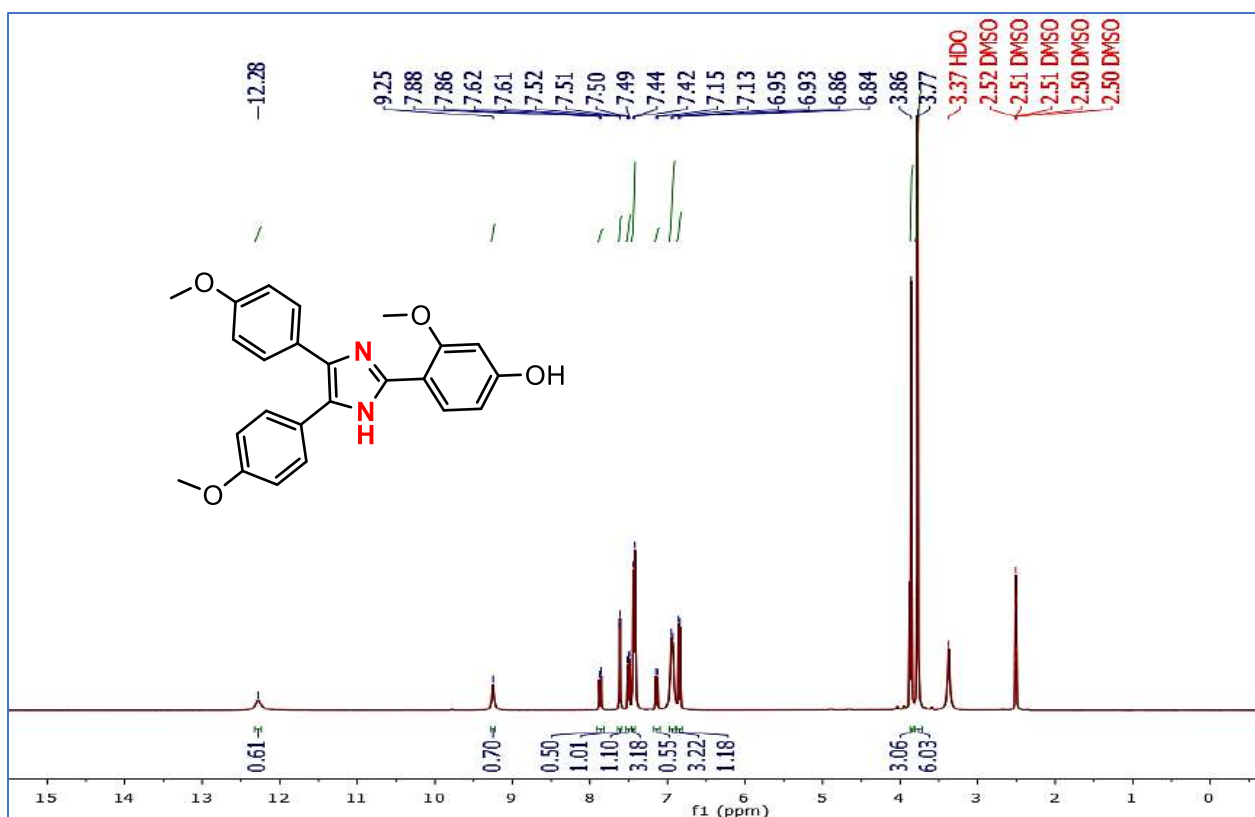


Figure 22: $^1\text{H NMR}$ spectrum of 4d

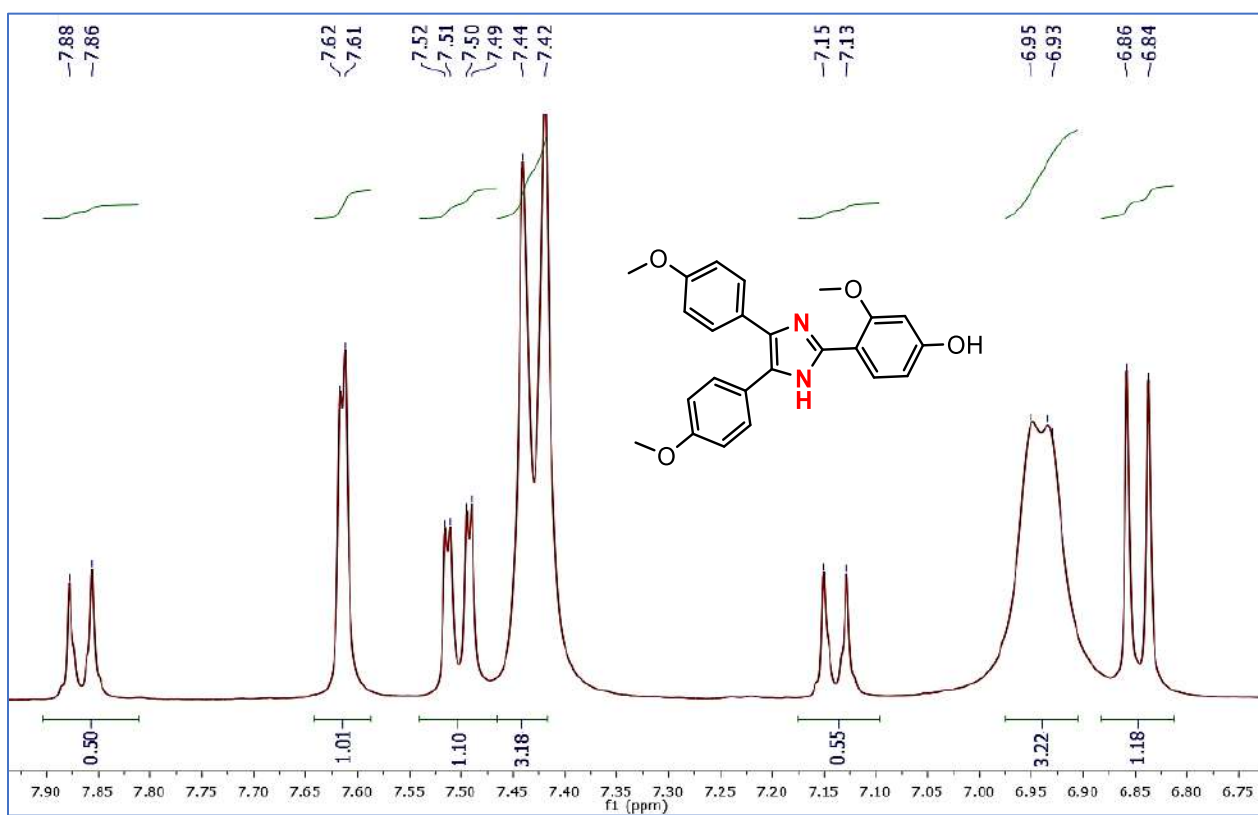


Figure 23: Expanded $^1\text{H NMR}$ spectrum of 4e

Appendix A

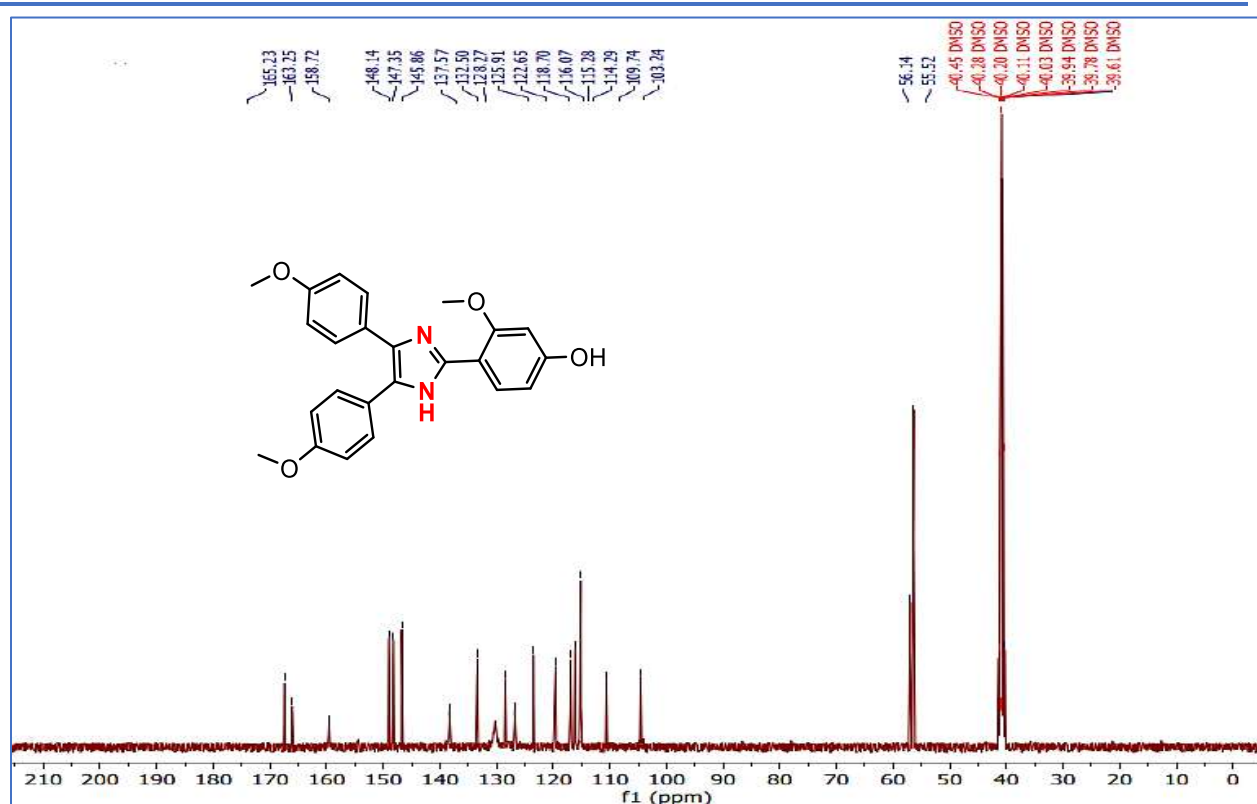


Figure 24: ¹³C NMR spectrum of 4e

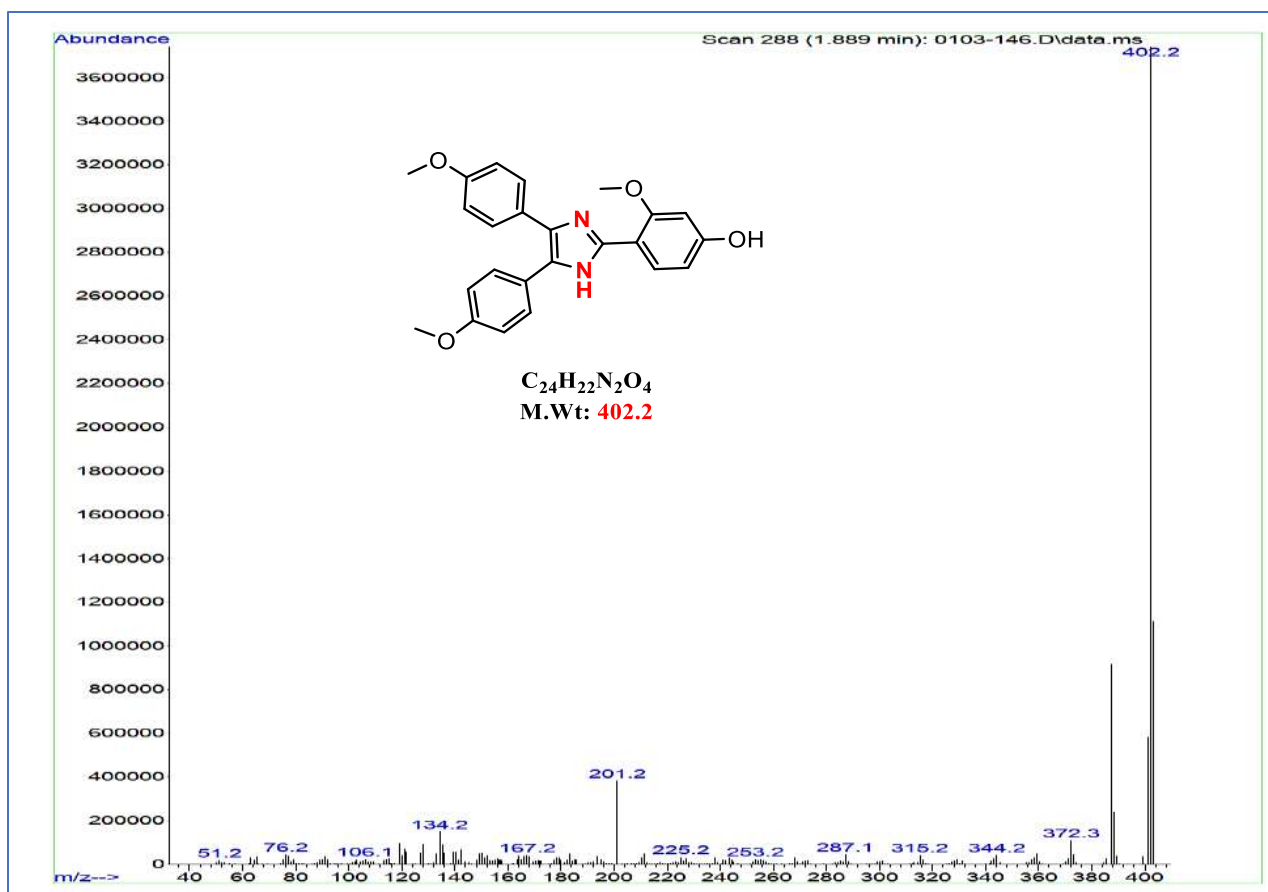


Figure 25: Mass spectrum of 4e

Appendix A

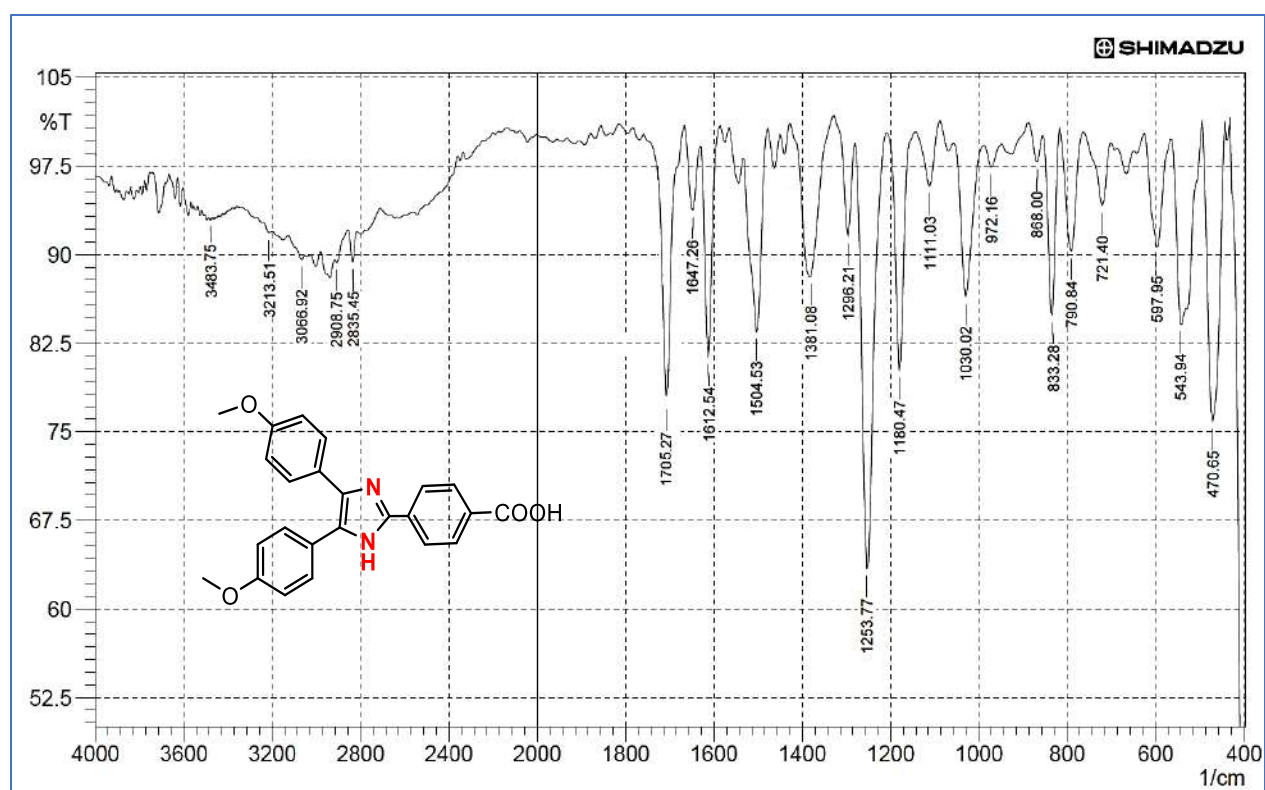


Figure 26: FTIR spectrum of 4f

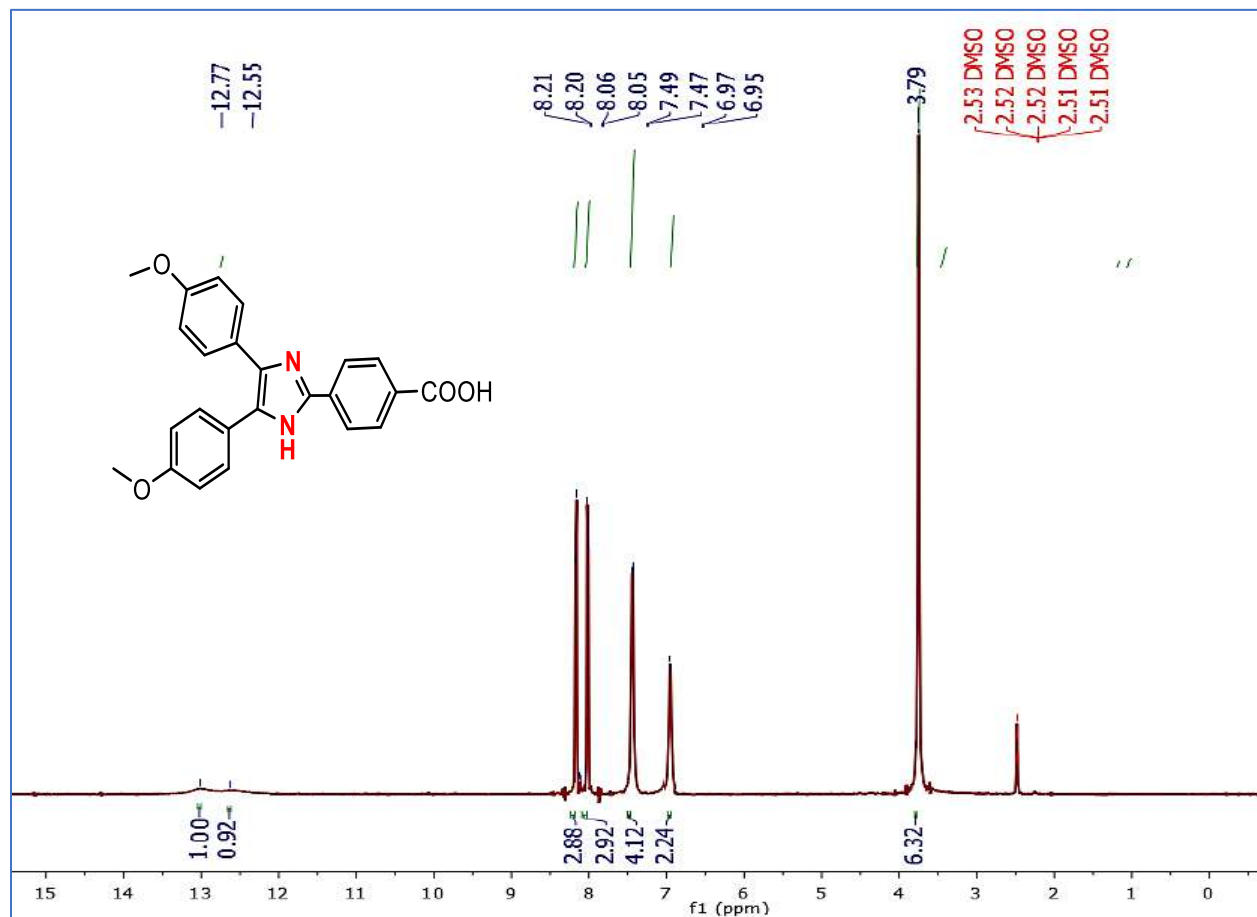


Figure 27: ¹H NMR spectrum of 4f

Appendix A

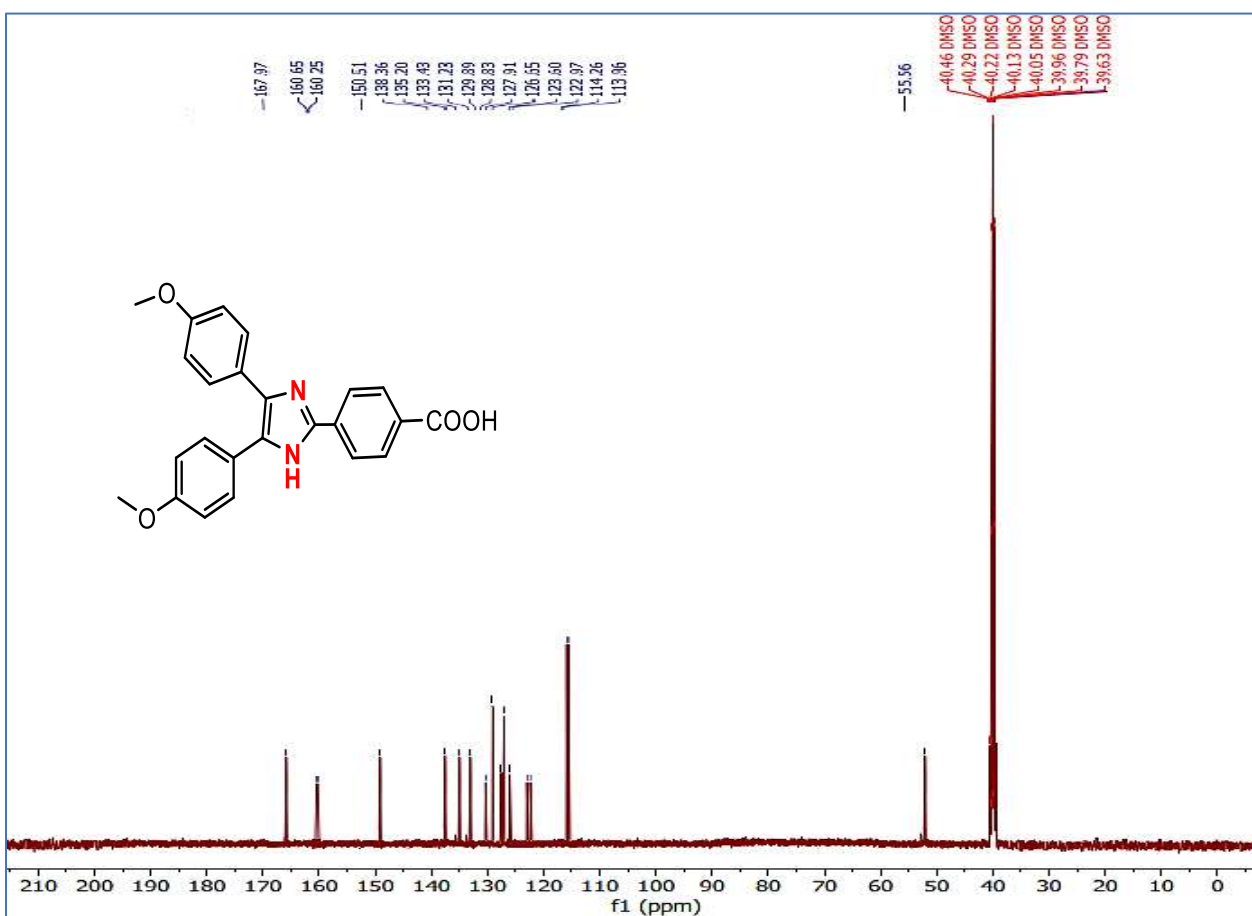
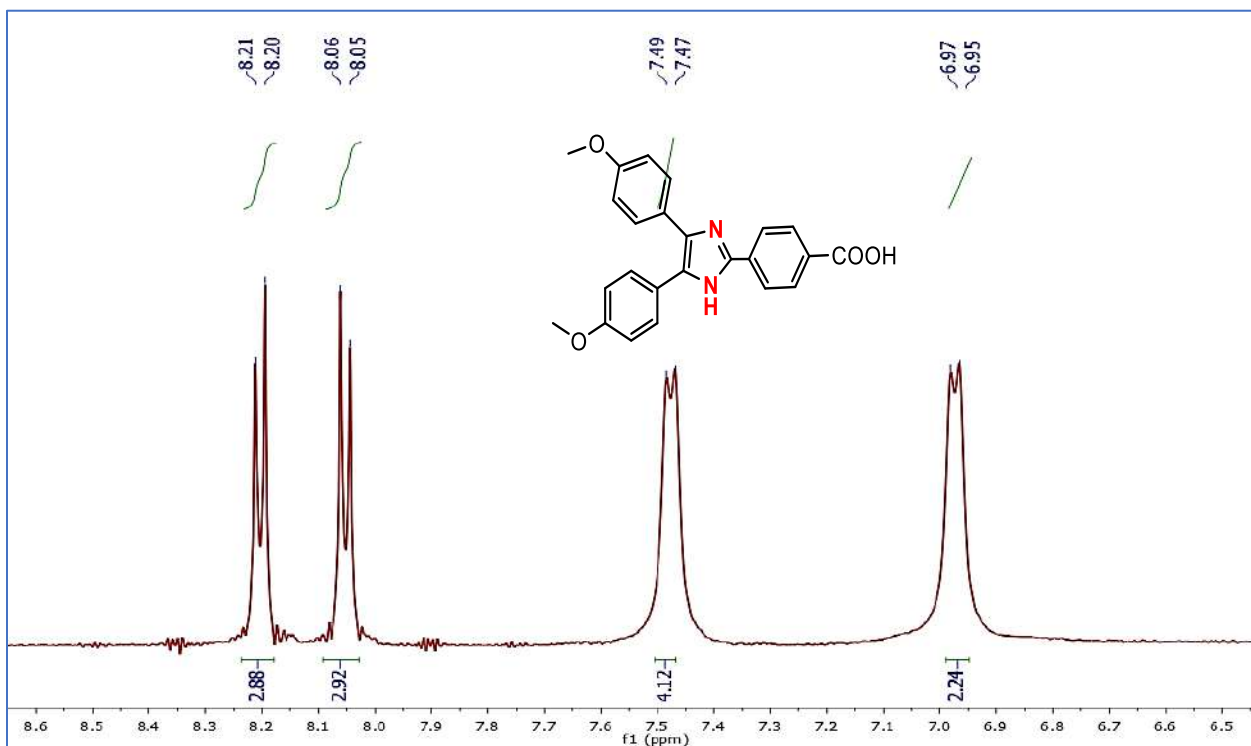


Figure 29: ^{13}C NMR spectrum of 4f

Appendix A

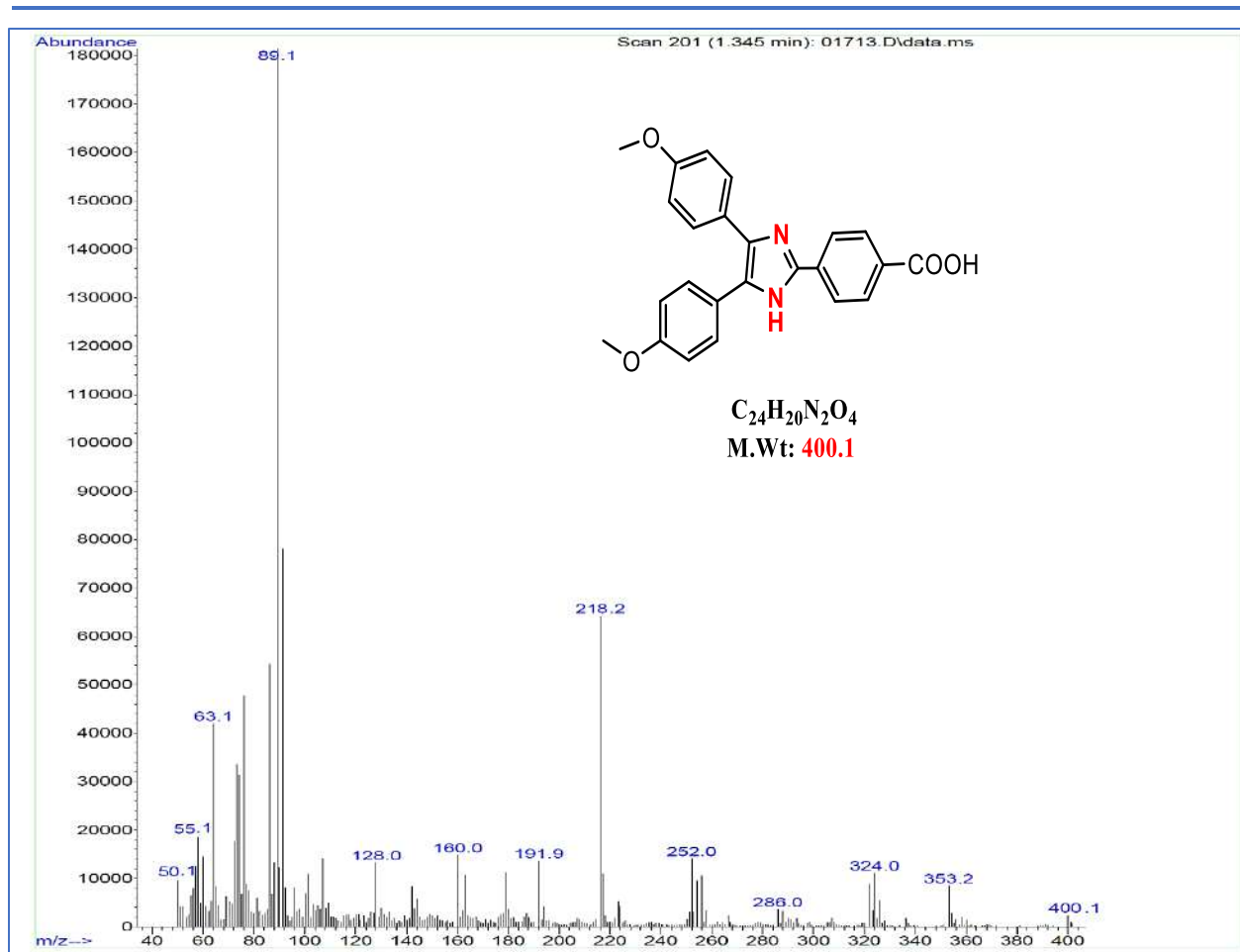


Figure 30: Mass spectrum of 4f

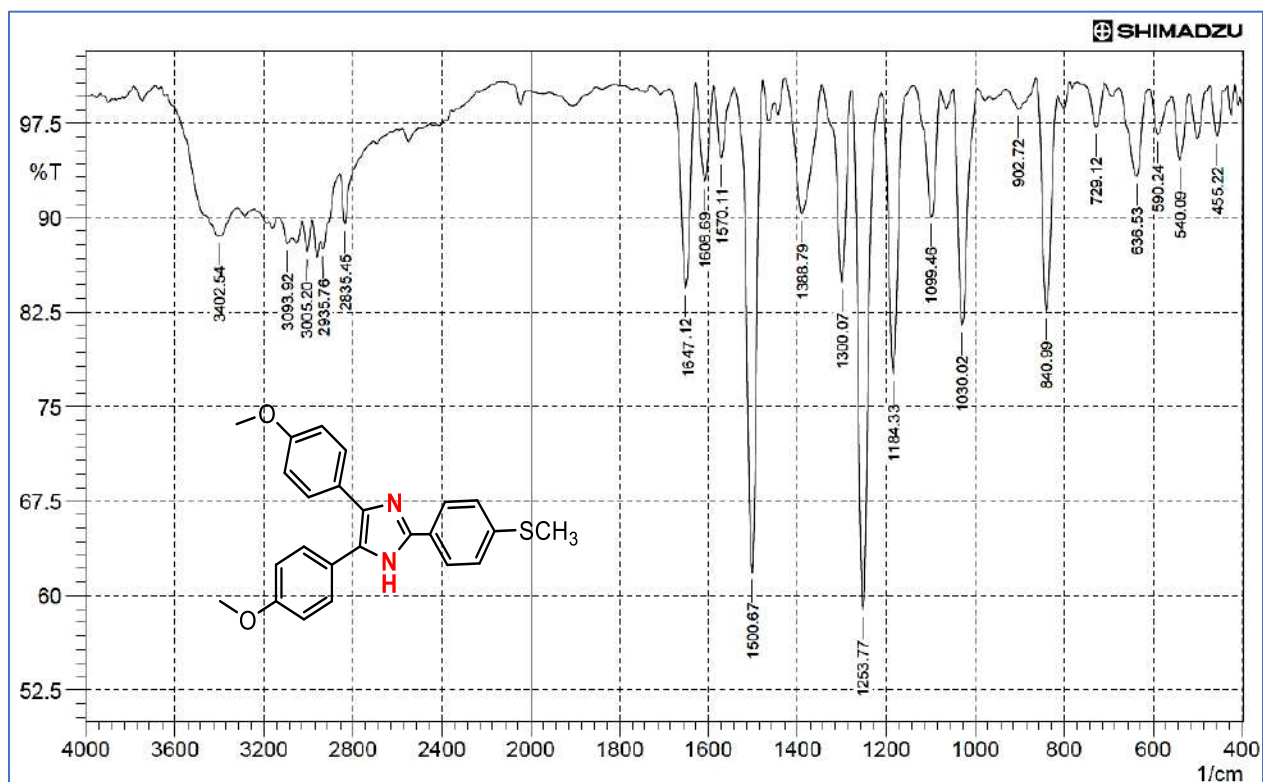


Figure 31: FTIR spectrum of 4g

Appendix A

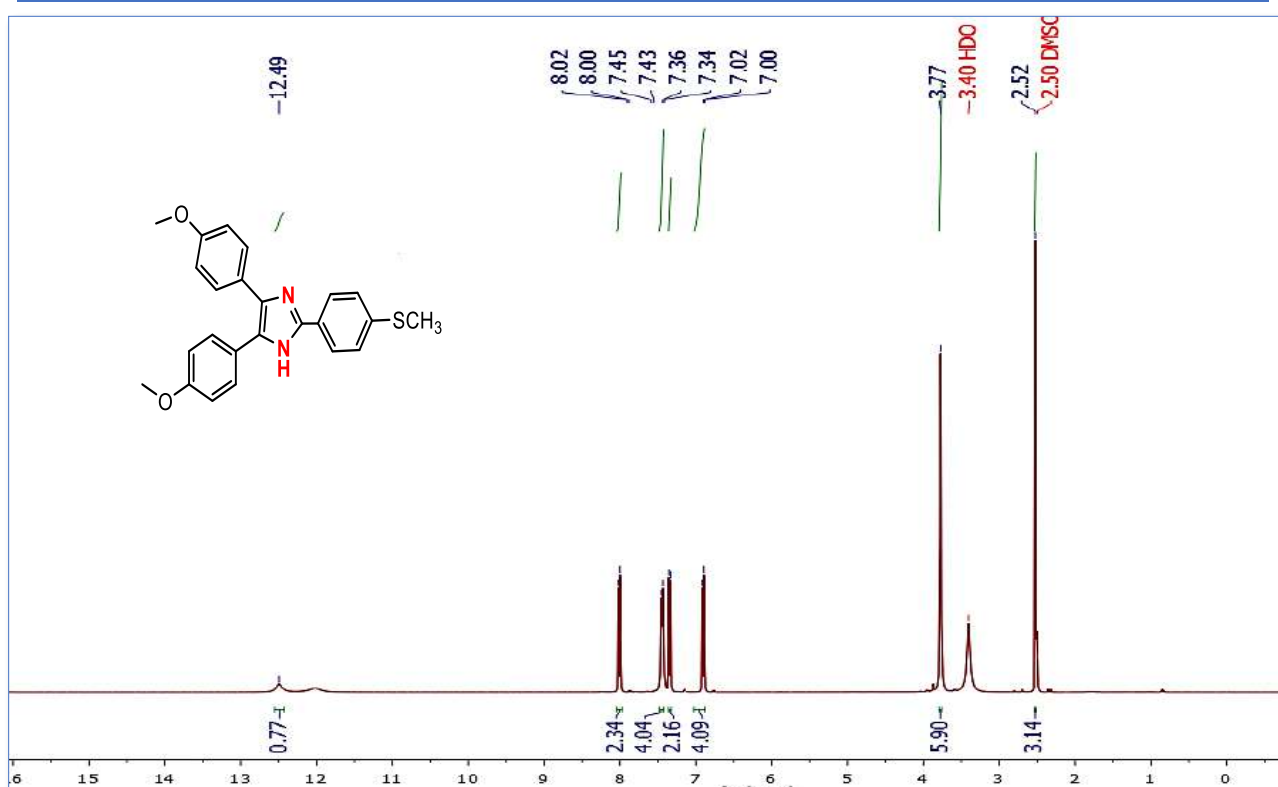


Figure 32: ^1H NMR spectrum of 4g

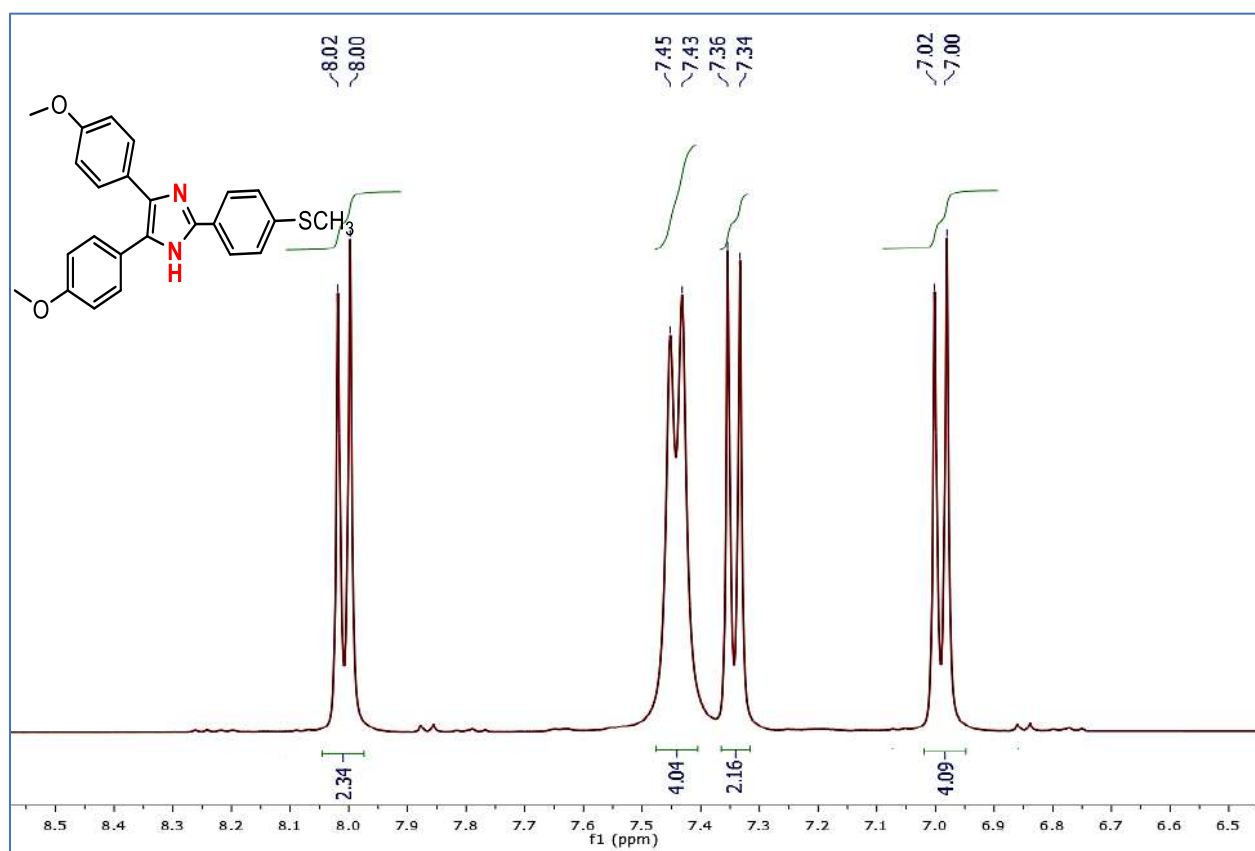


Figure 33: Expanded ^1H NMR spectrum of 4g

Appendix A

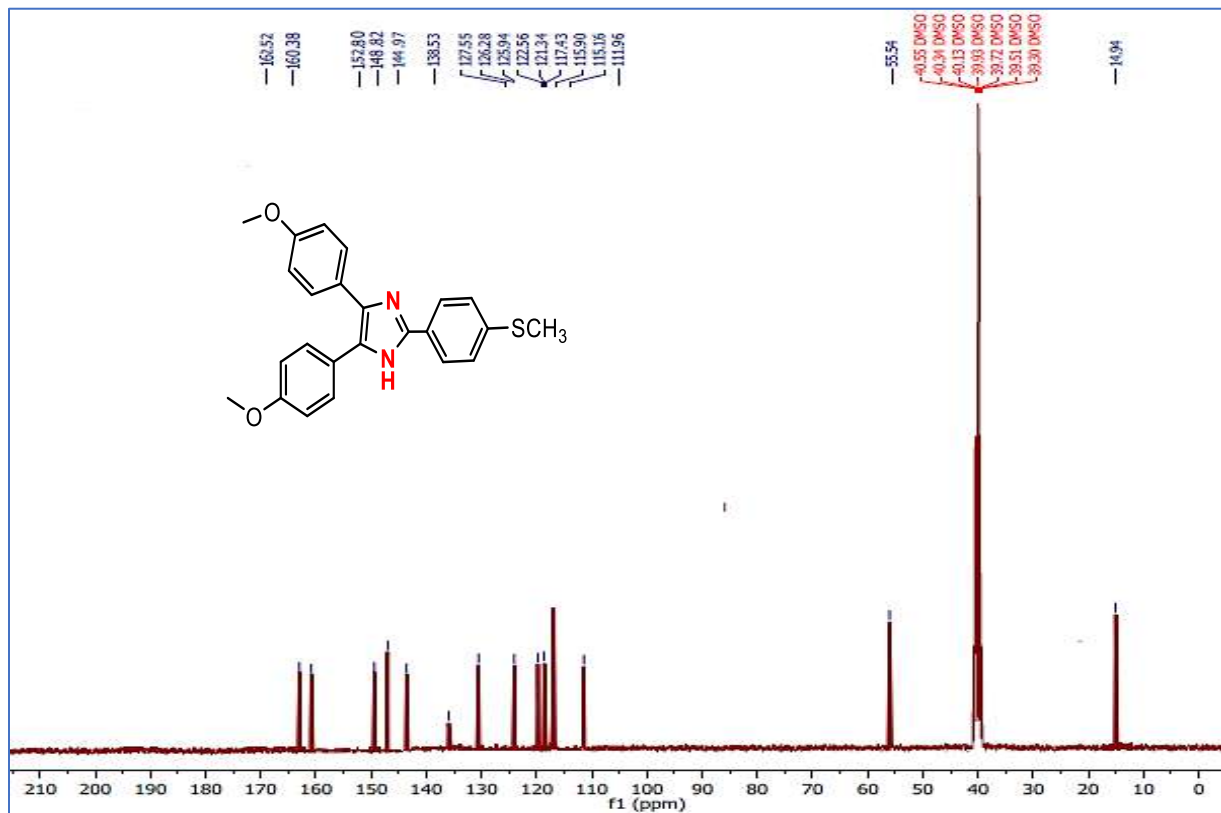


Figure 34: ¹³C NMR spectrum of 4g

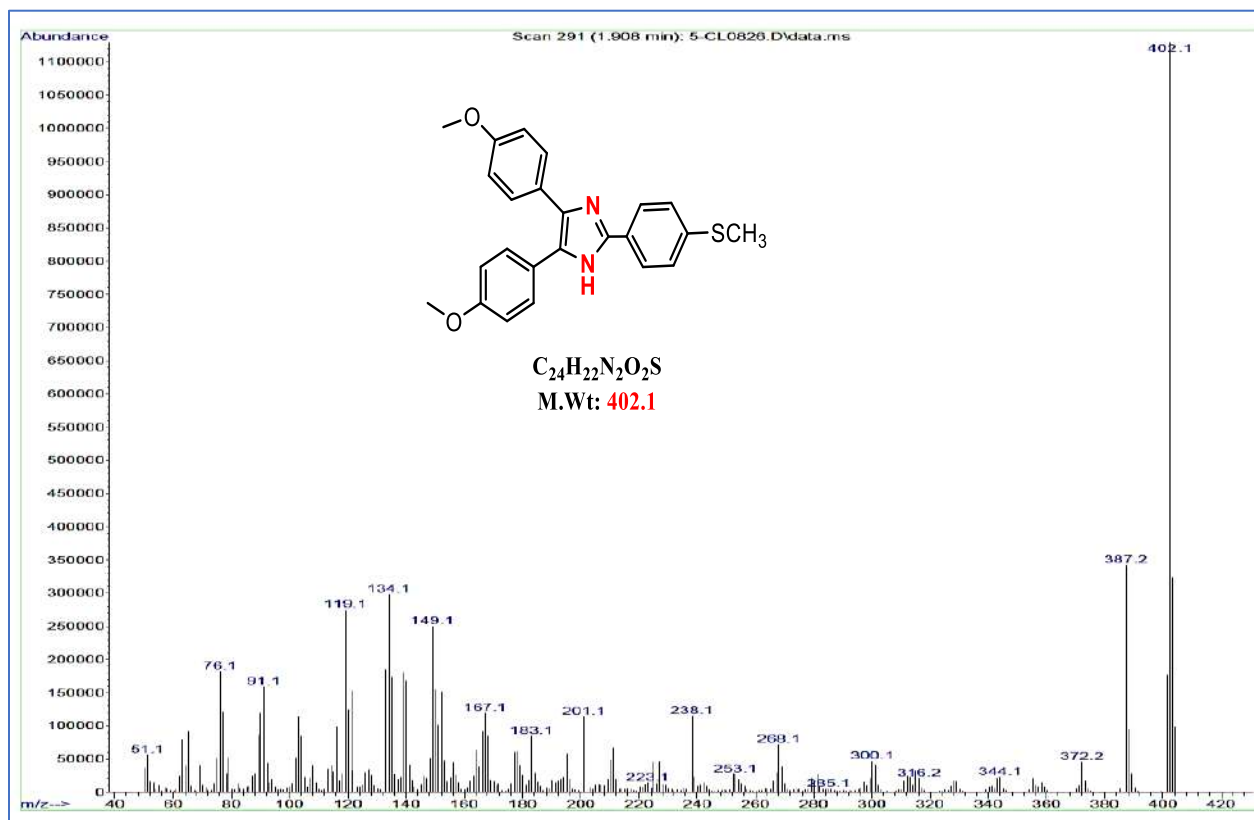


Figure 35: Mass spectrum of 4g

Appendix A

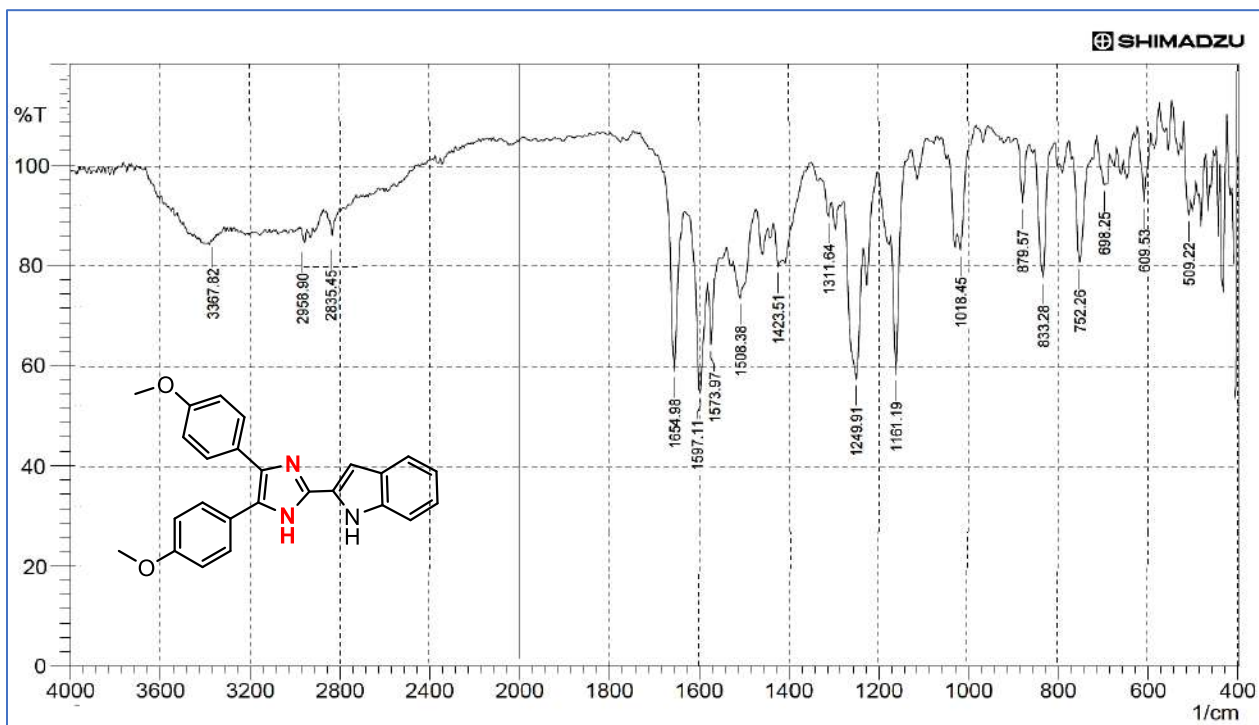


Figure 36: FTIR spectrum of 4h

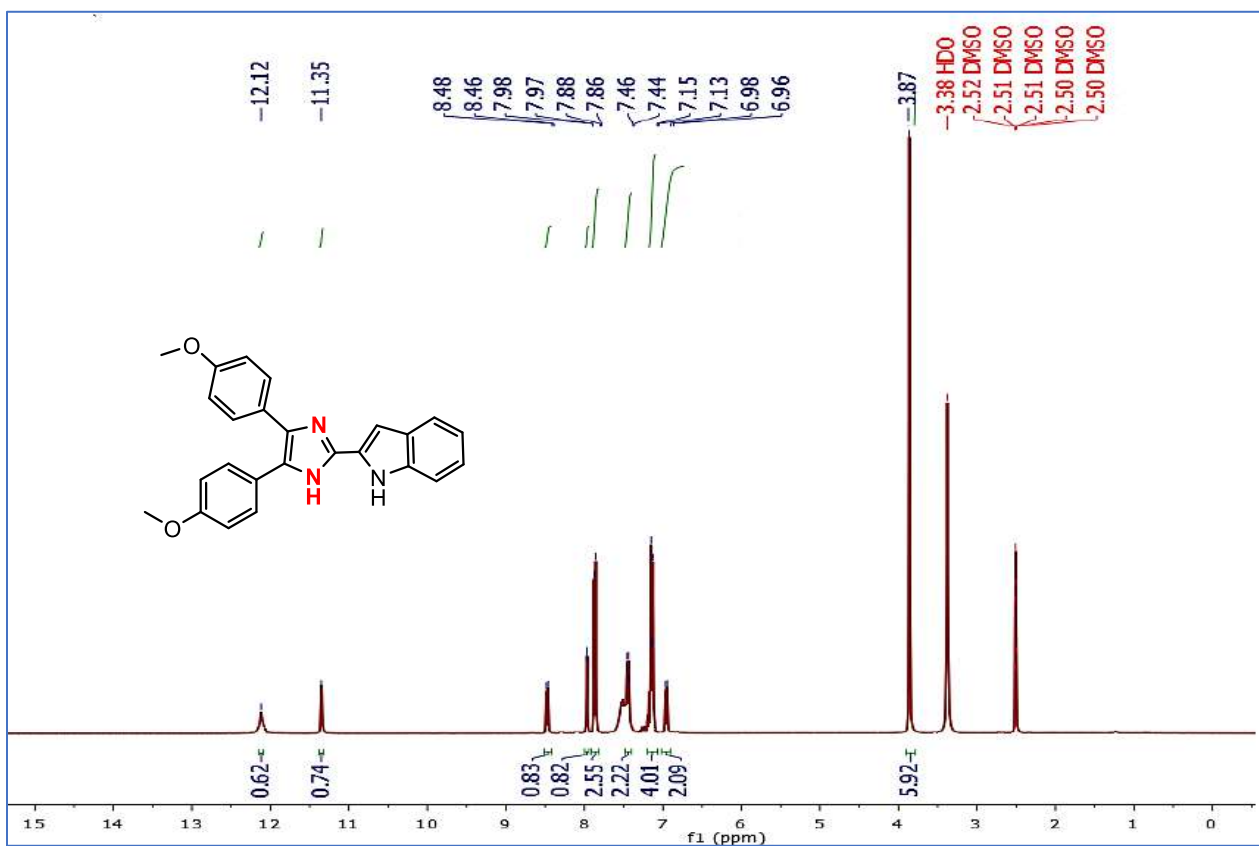


Figure 37: ^1H NMR spectrum of 4h

Appendix A

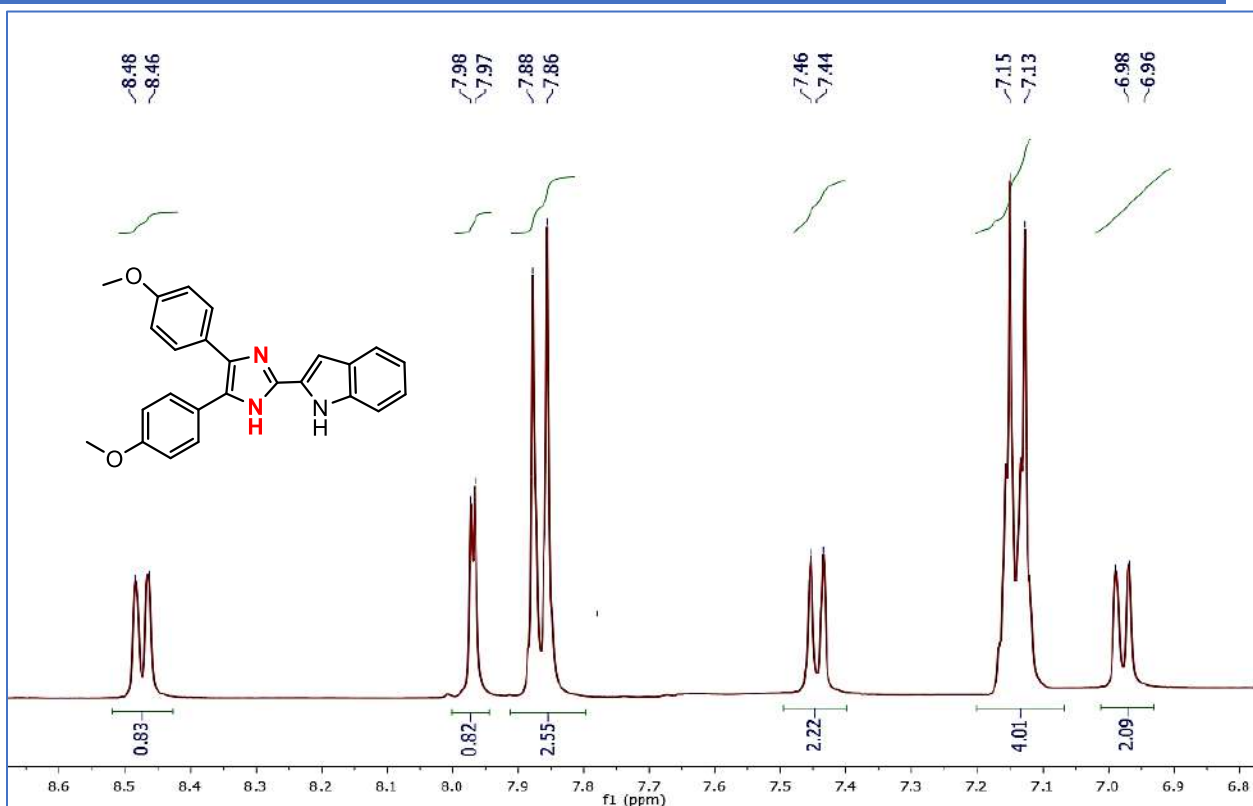


Figure 38: Expanded ^1H NMR spectrum of 4h

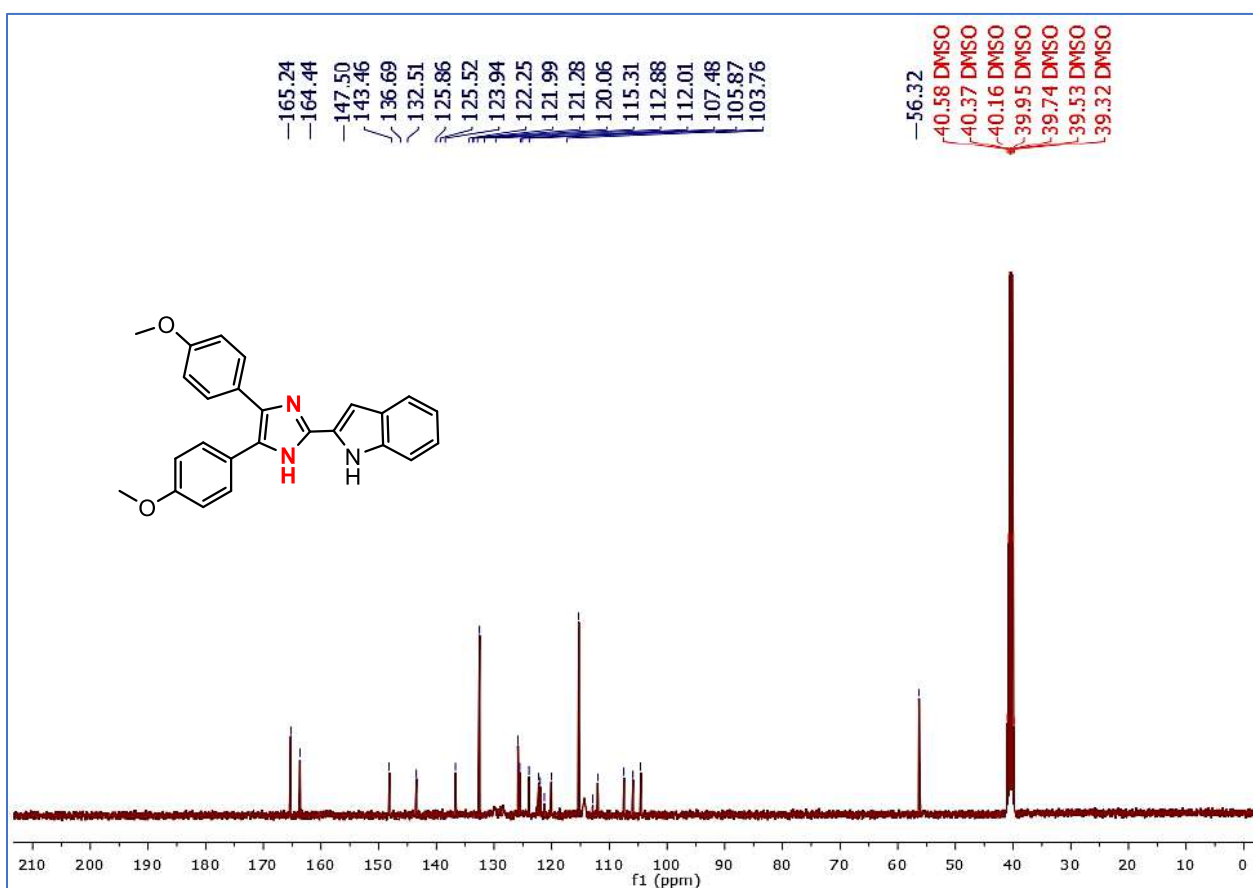


Figure 39: ^{13}C NMR spectrum of 4h

Appendix A

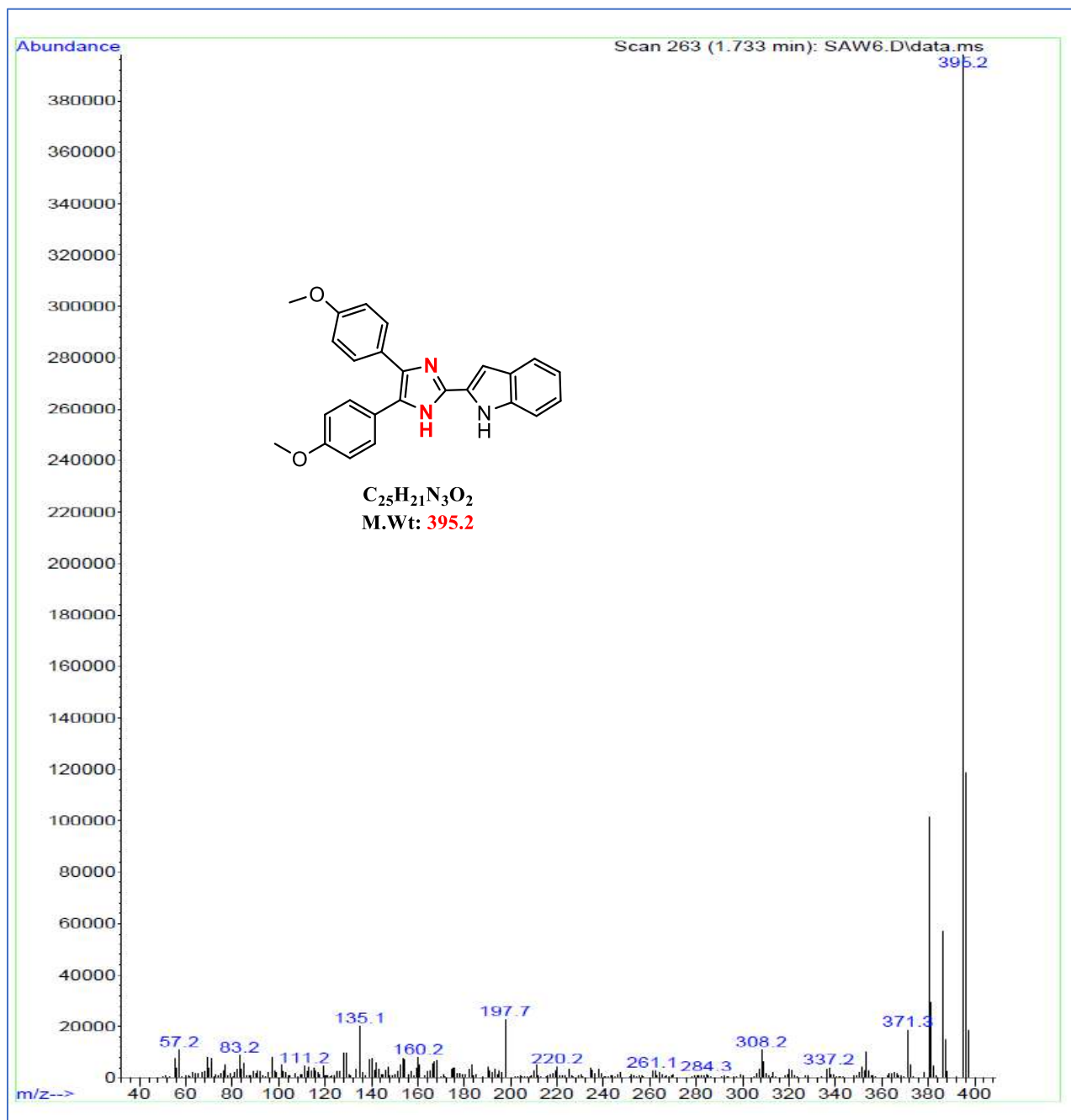
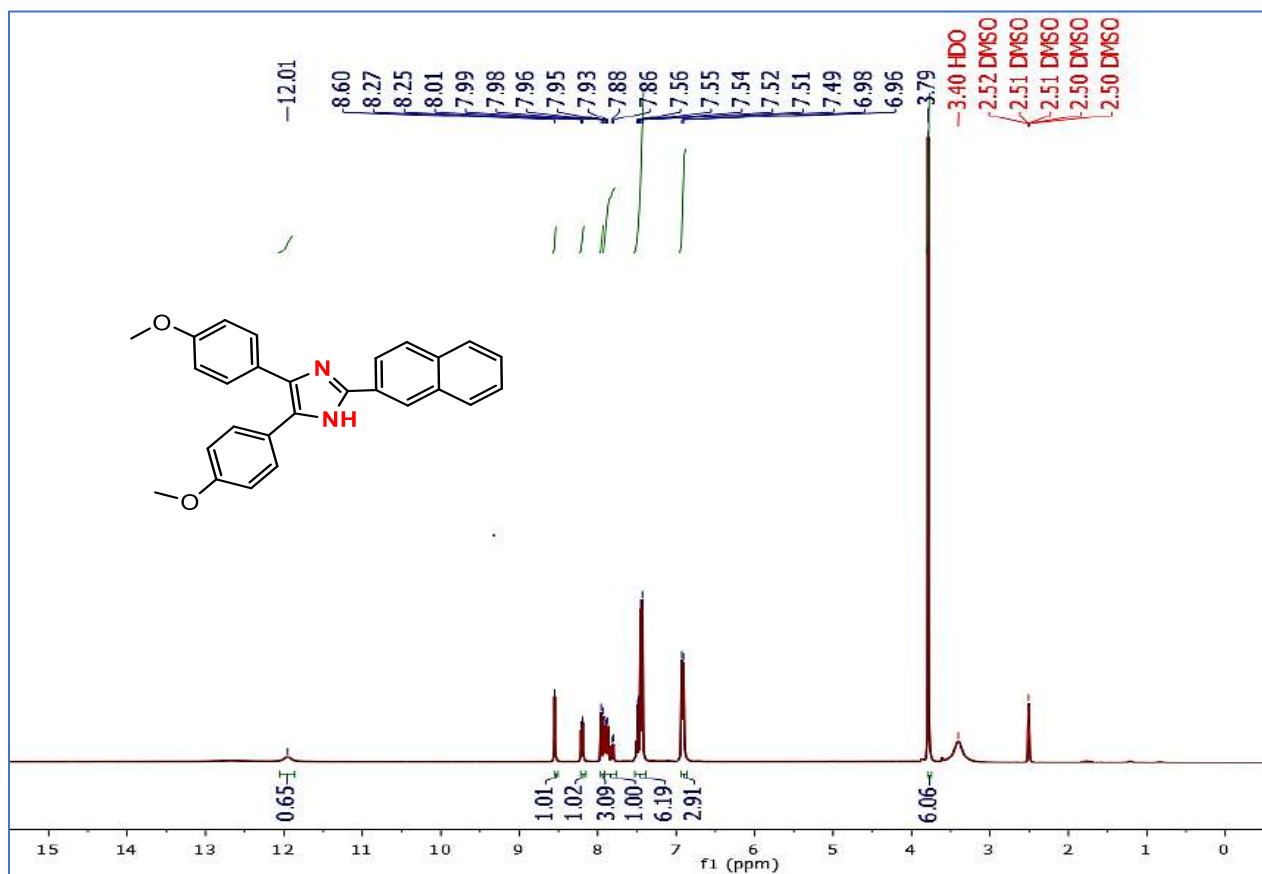
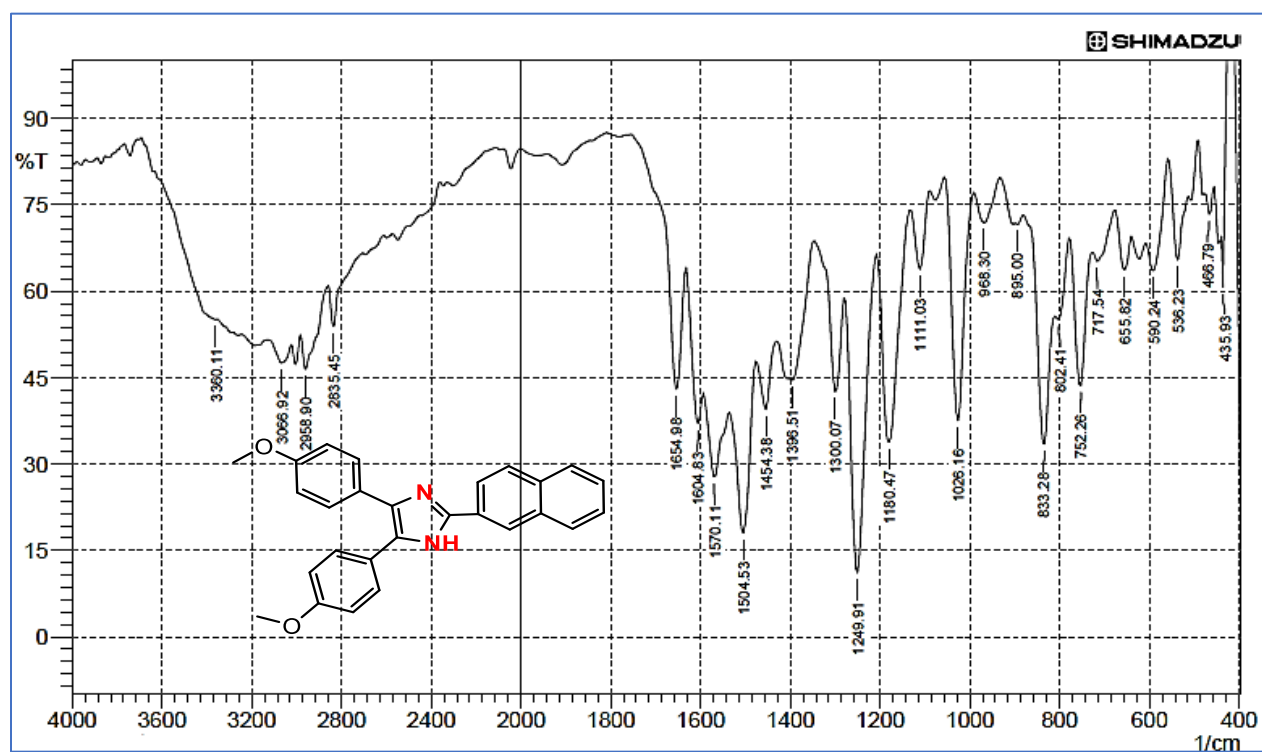
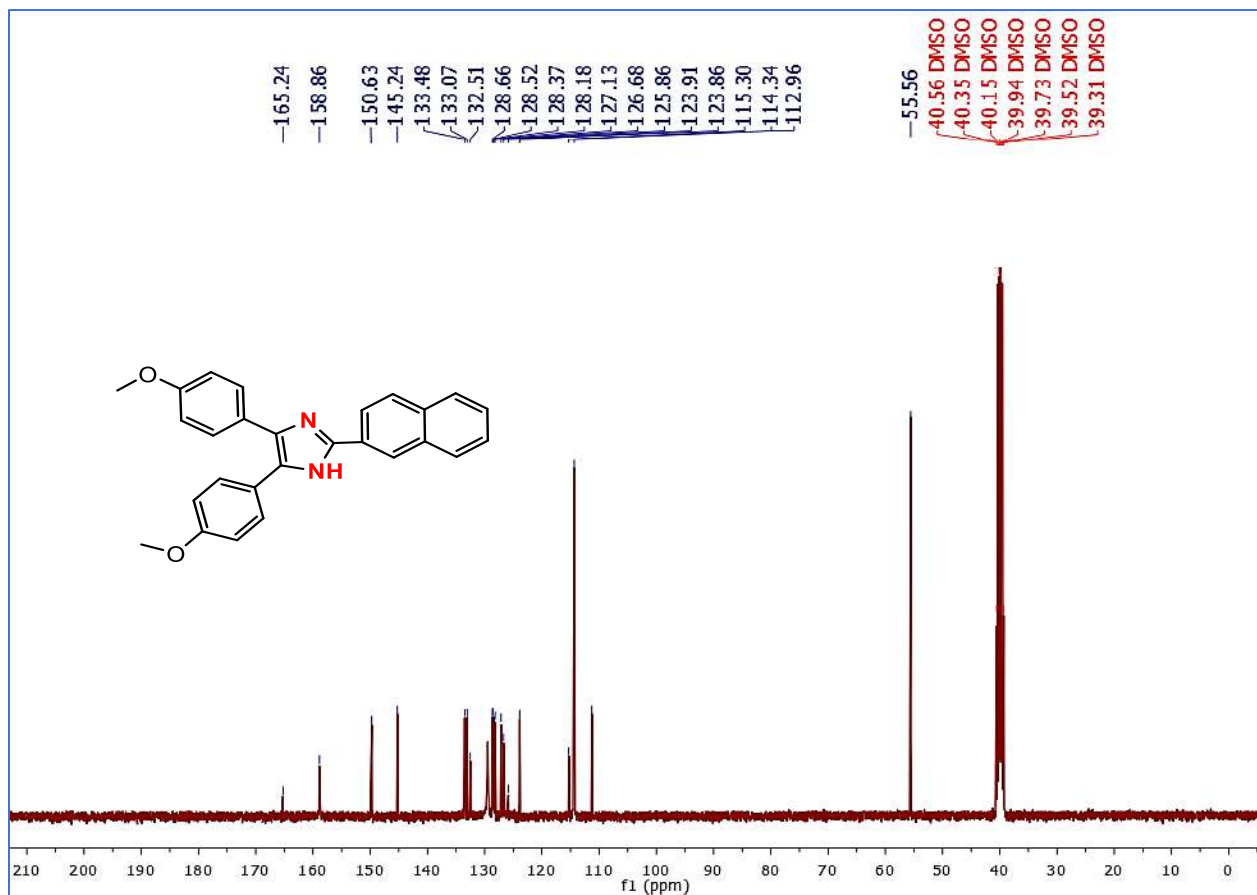
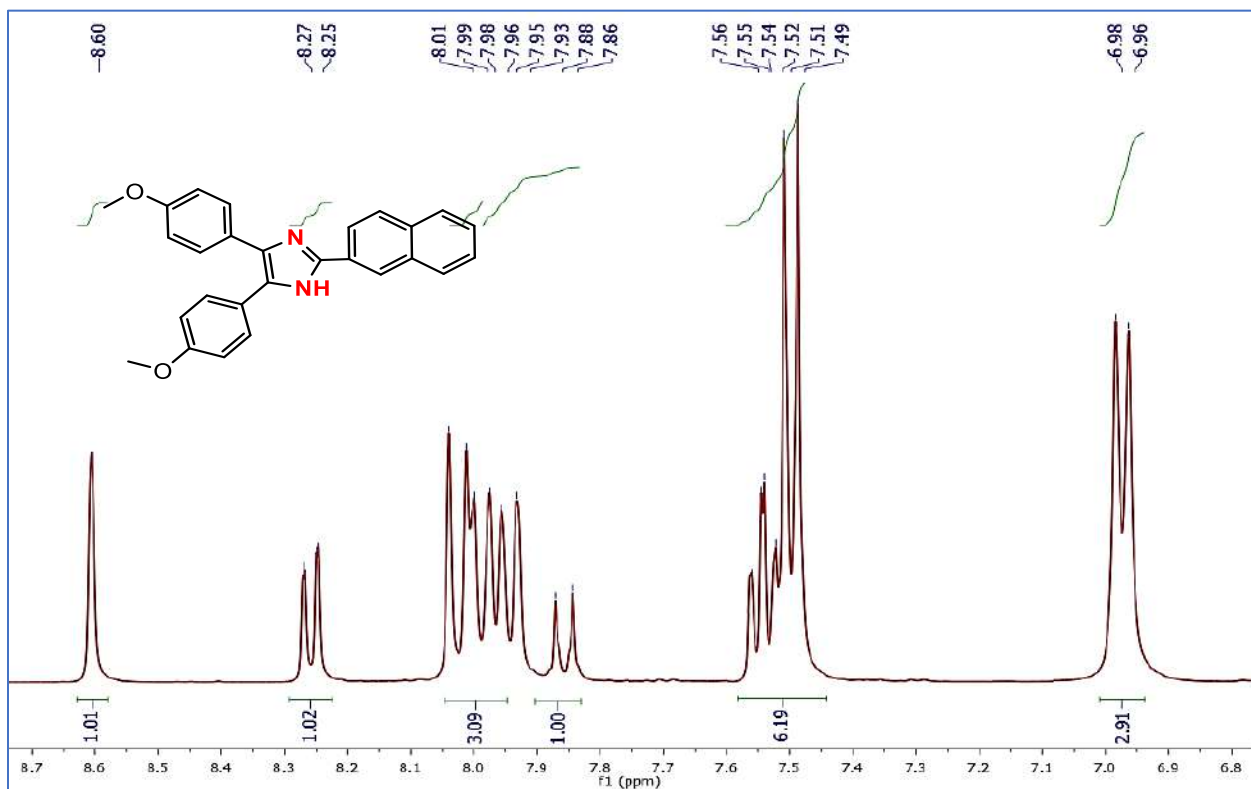


Figure 40: Mass spectrum of 4h

Appendix A



Appendix A



Appendix A

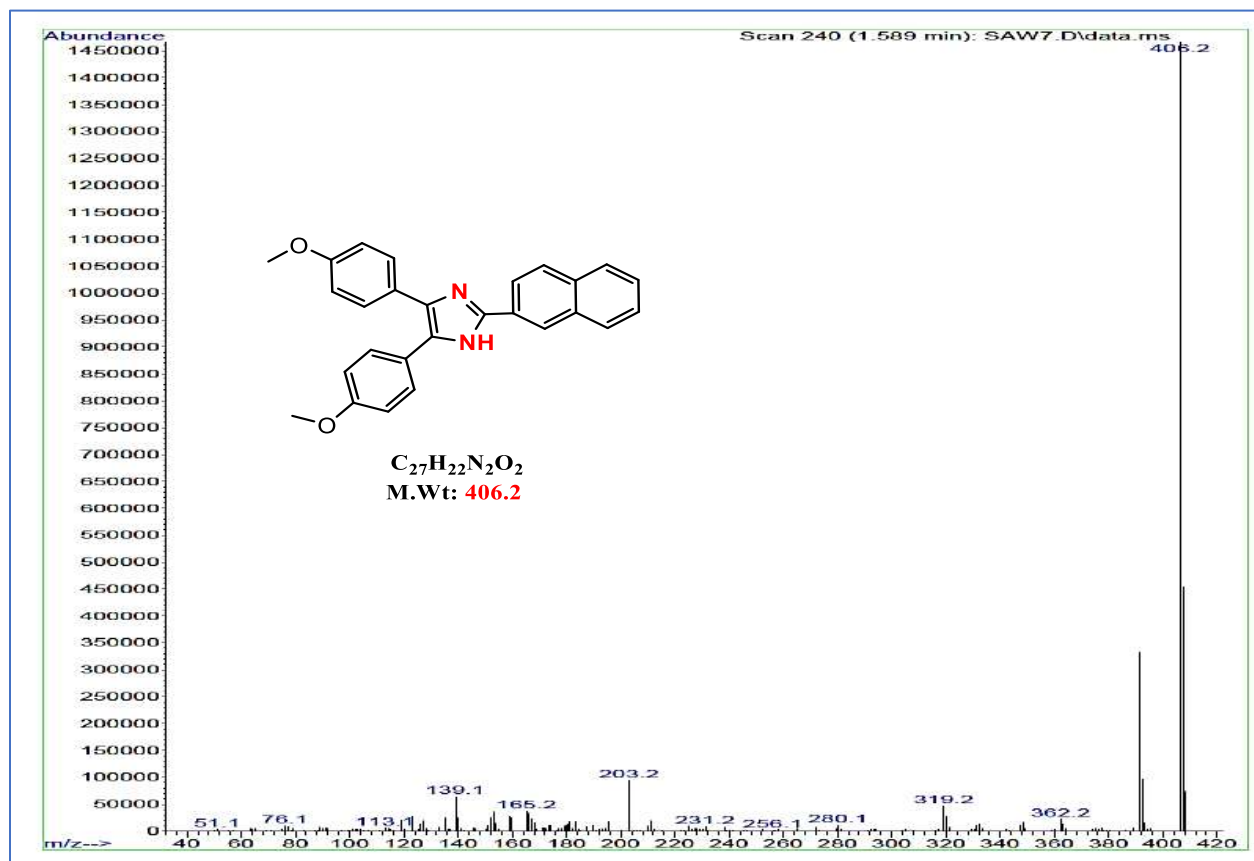


Figure 45: Mass spectrum of 4i

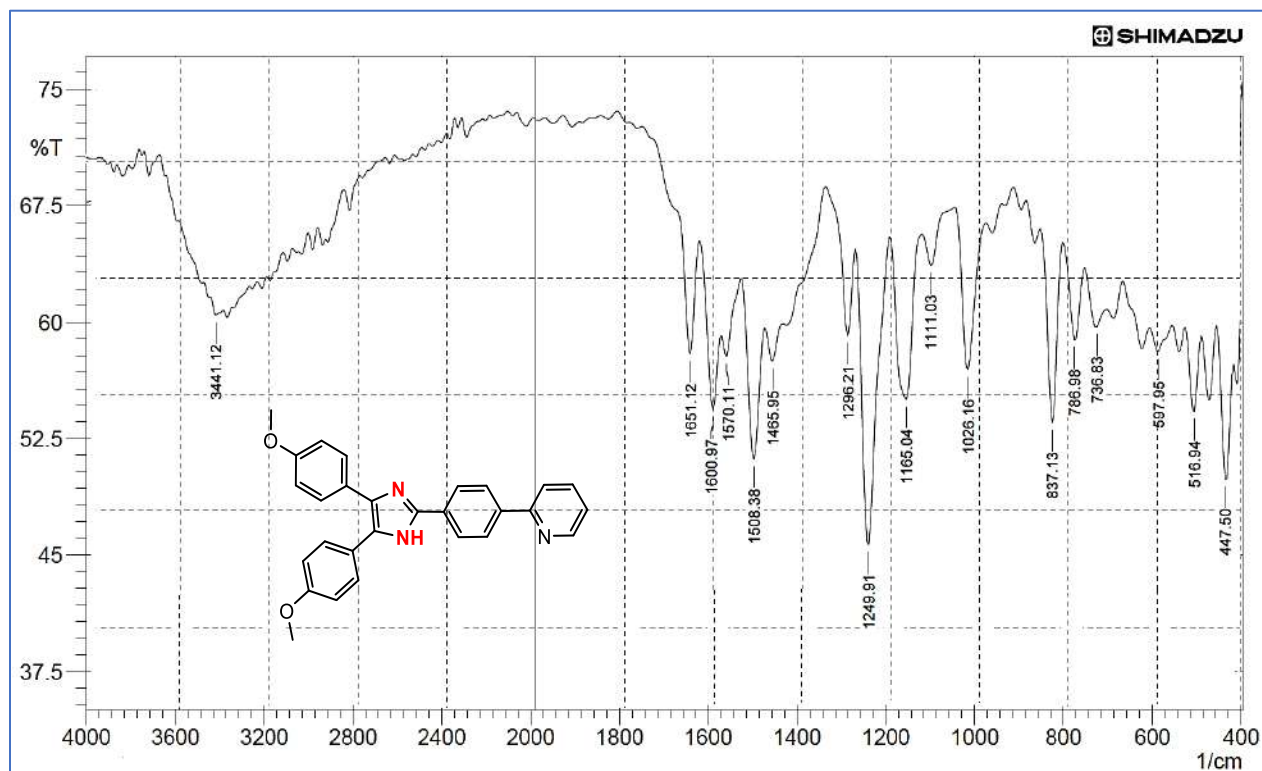


Figure 46: FTIR spectrum of 4j

Appendix A

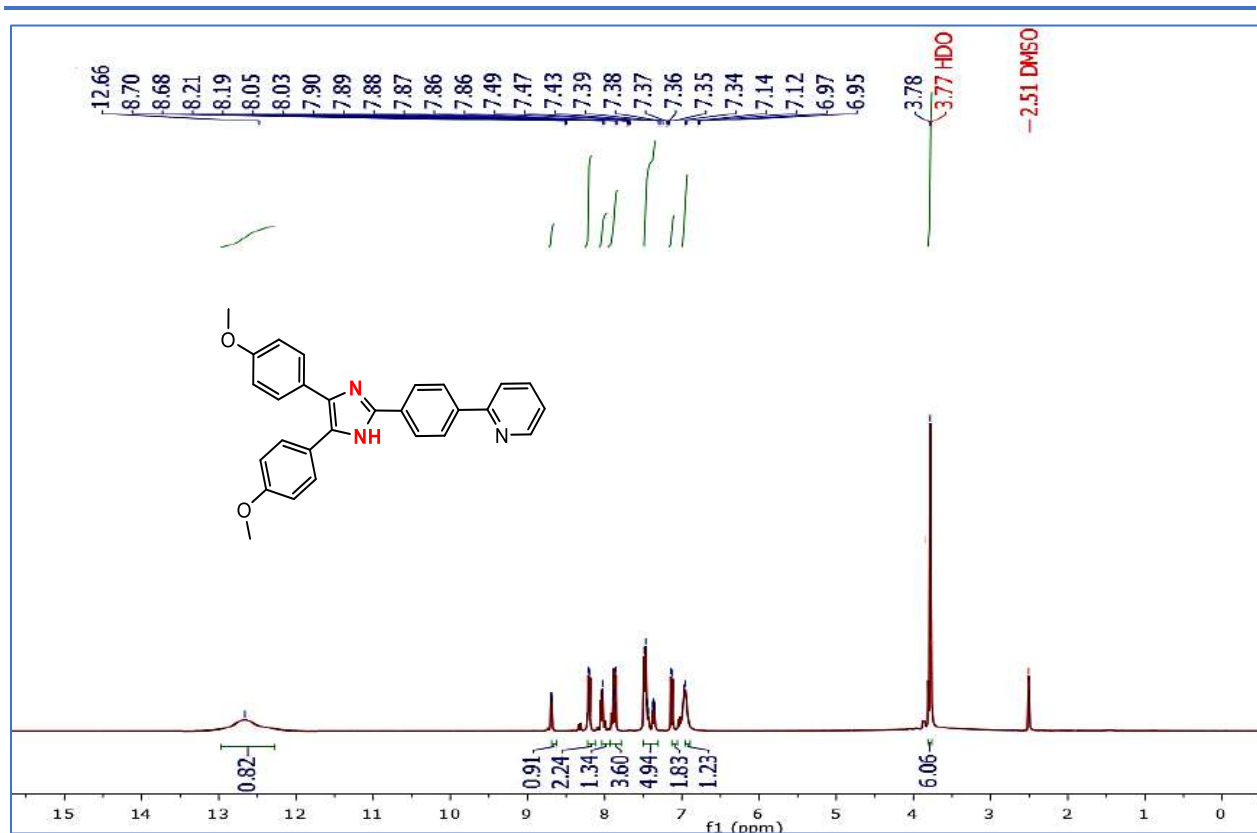


Figure 47: ^1H NMR spectrum of **4j**

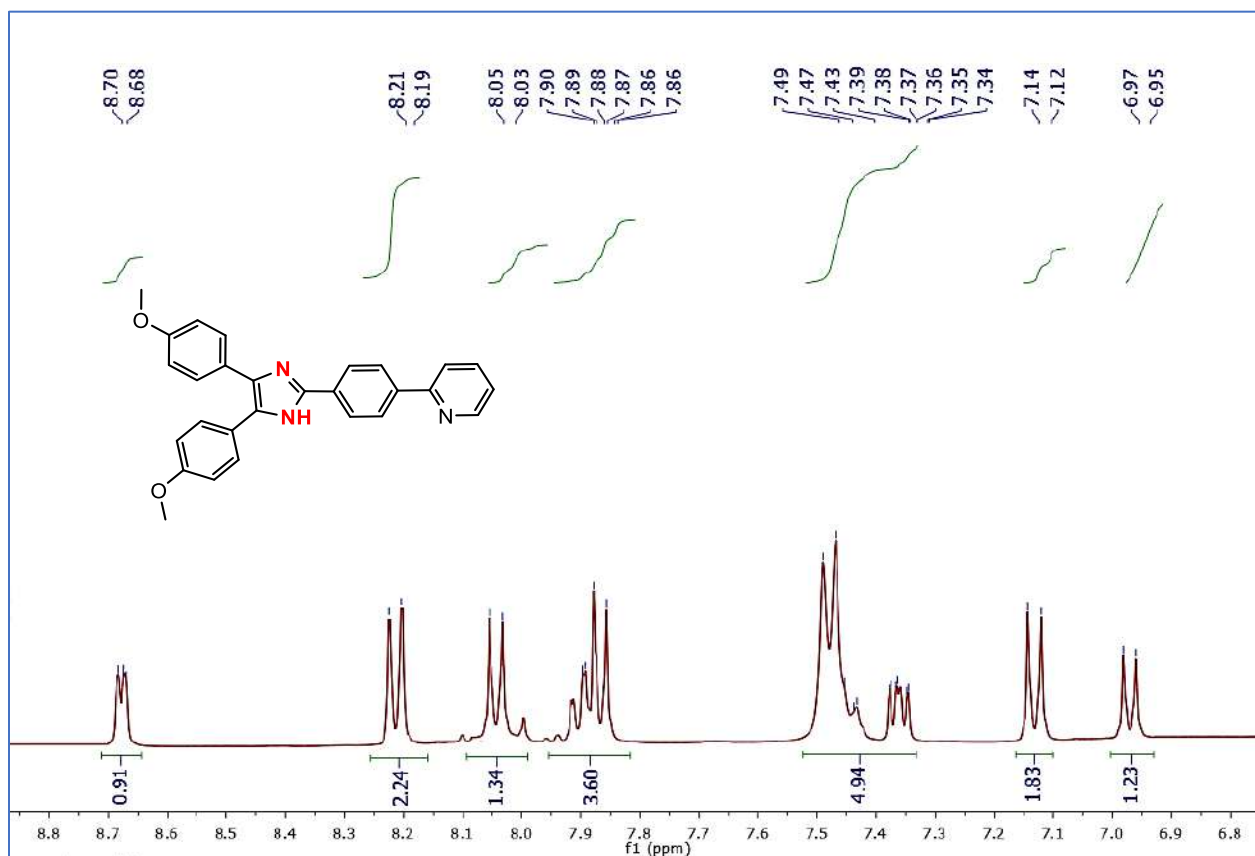


Figure 48: Expanded ^1H NMR spectrum of **4h**

Appendix A

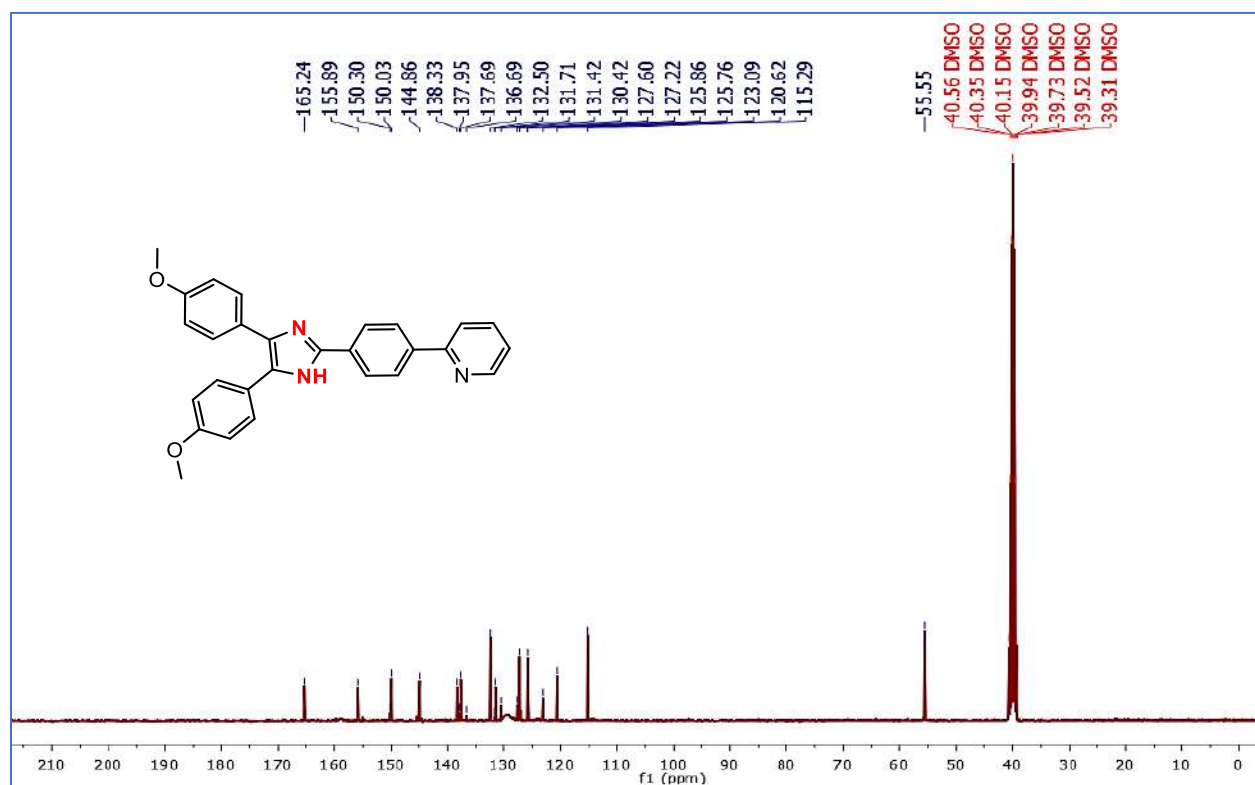


Figure 49: ¹³C NMR spectrum of 4j

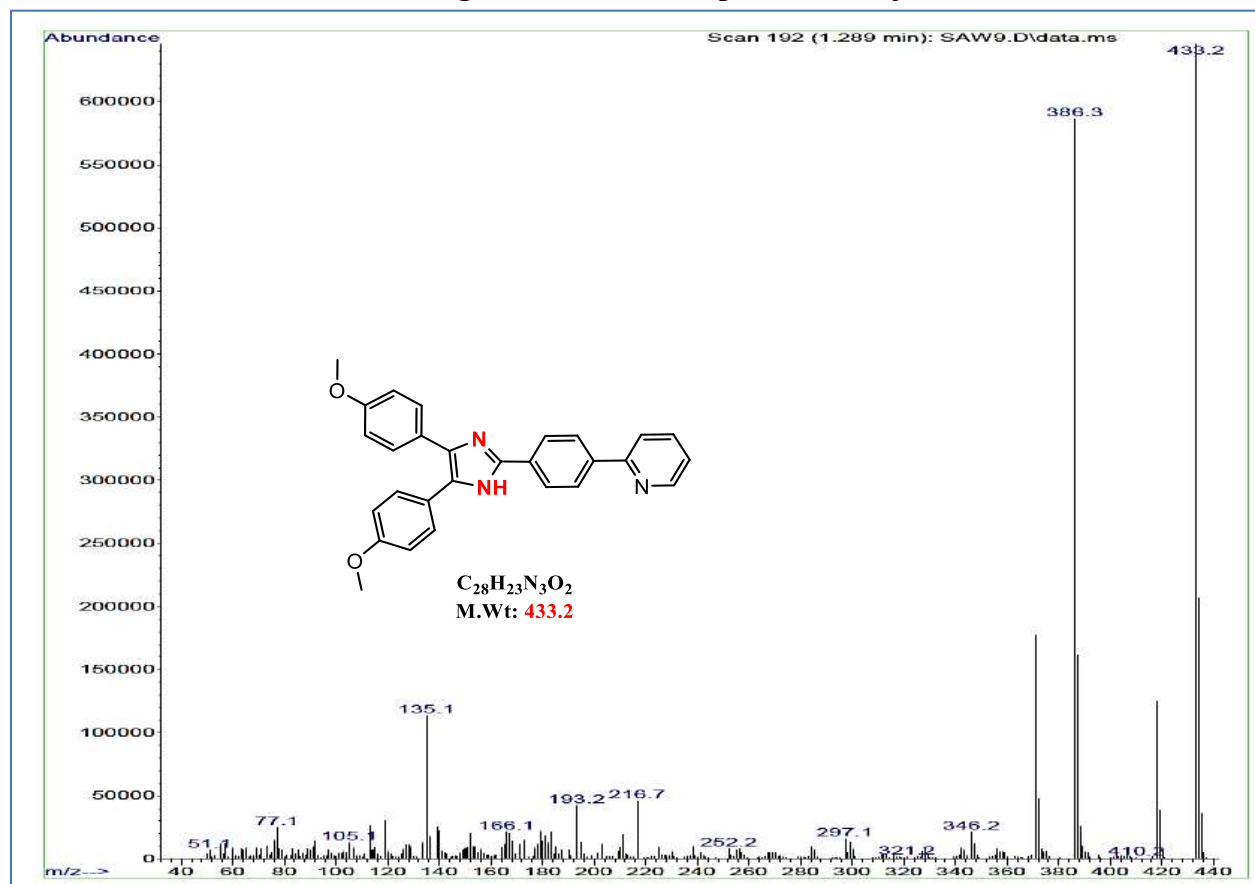


Figure 50: Mass spectrum of 4j

Appendix A

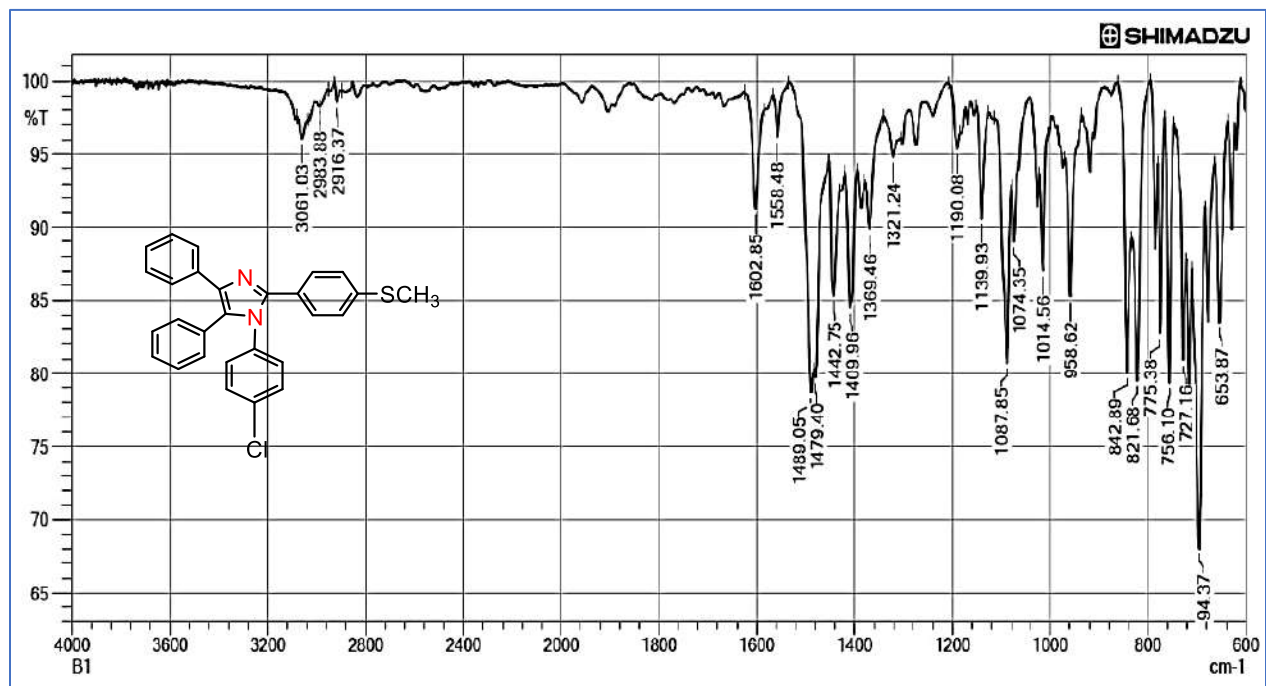


Figure 51: FTIR spectrum of 5a

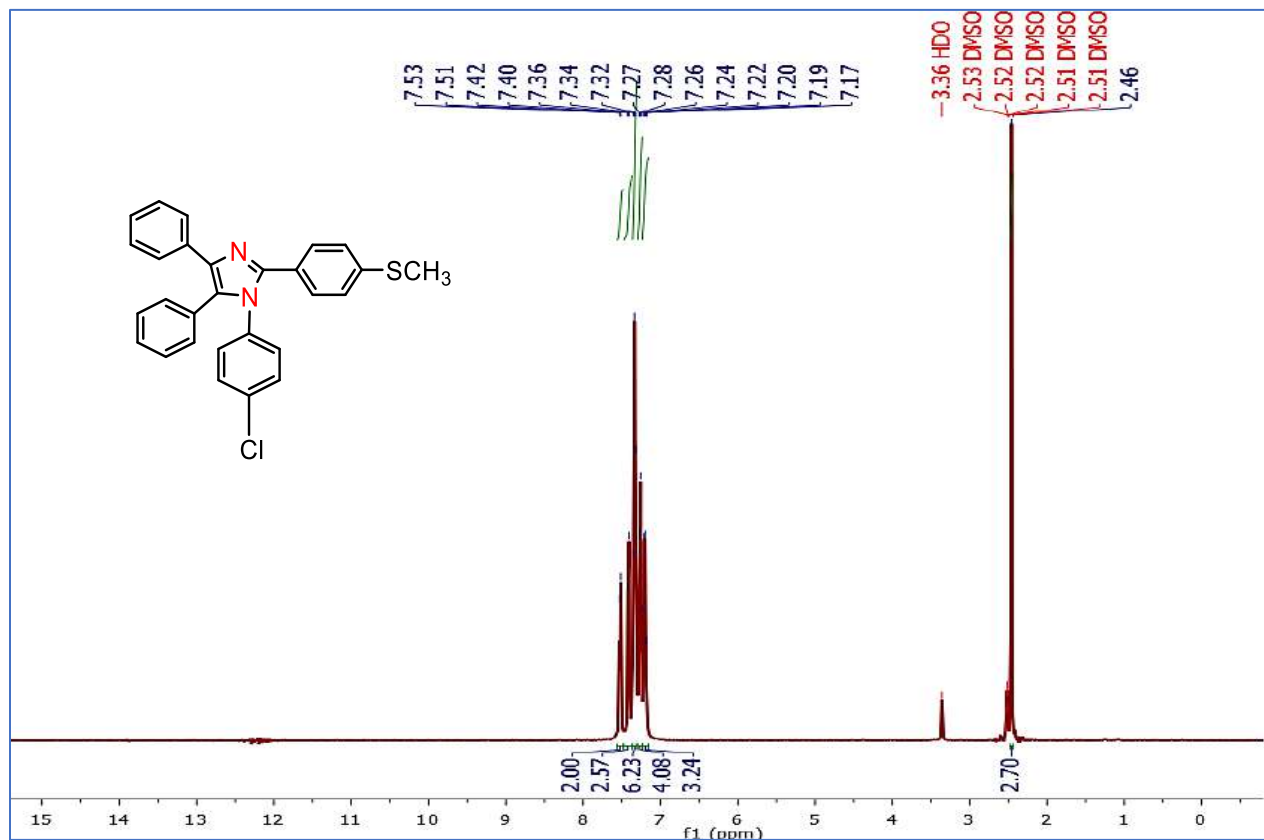


Figure 52: ¹H NMR spectrum of 5a

Appendix A

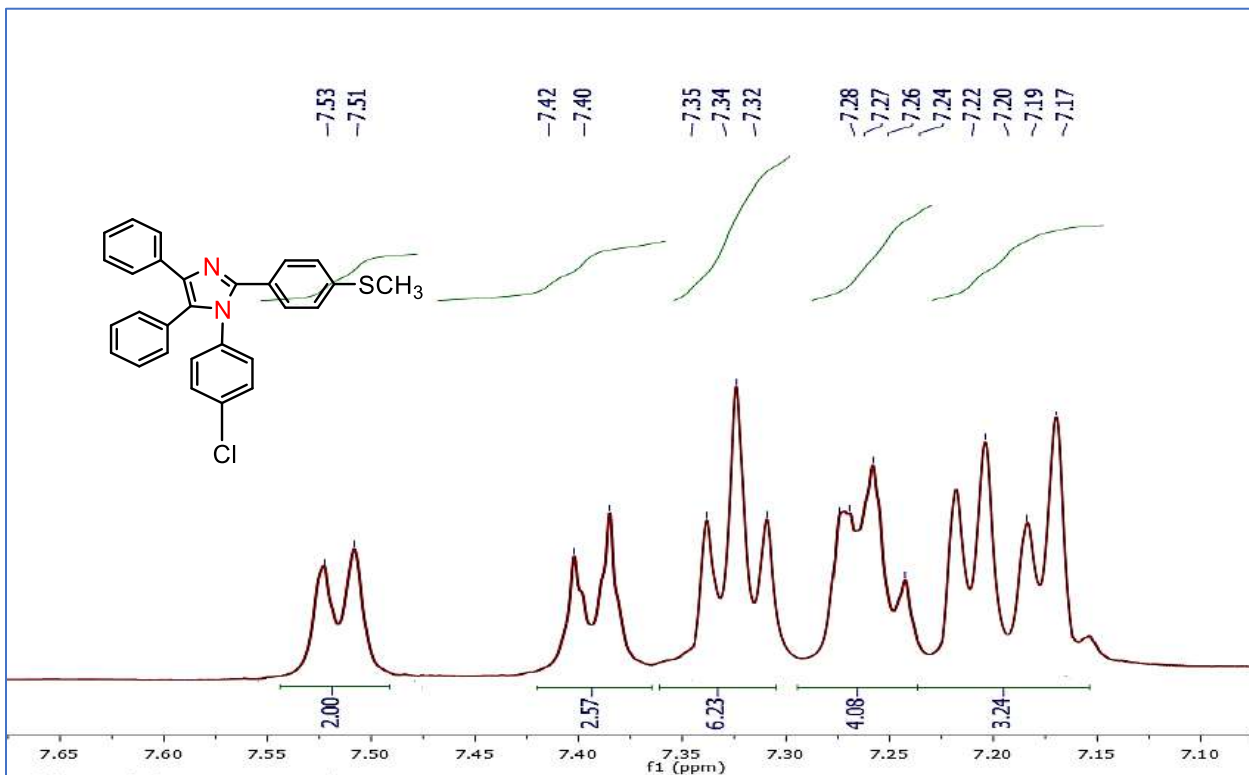


Figure 53: Expanded ¹H NMR spectrum of 5a

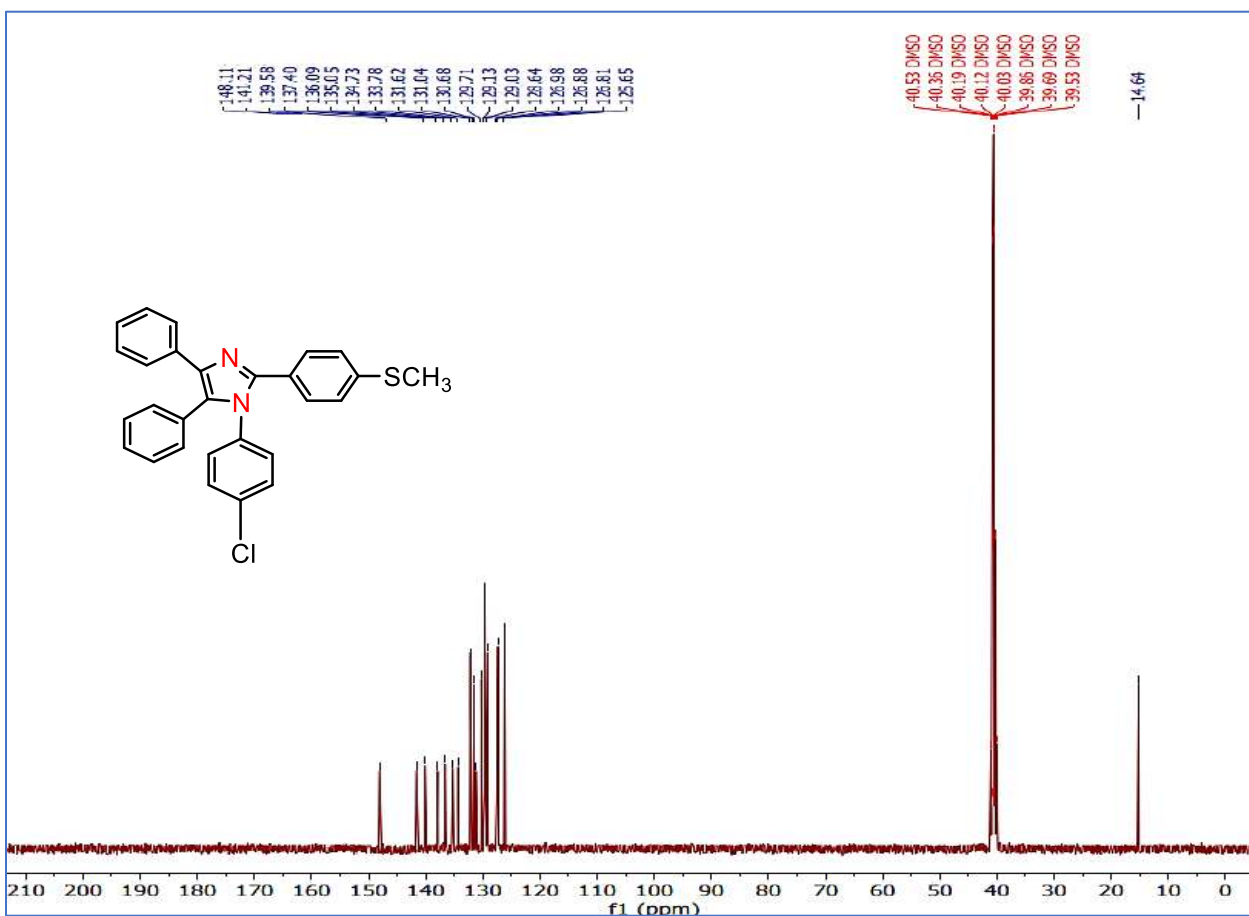


Figure 54: ¹³C NMR spectrum of 5a

Appendix A

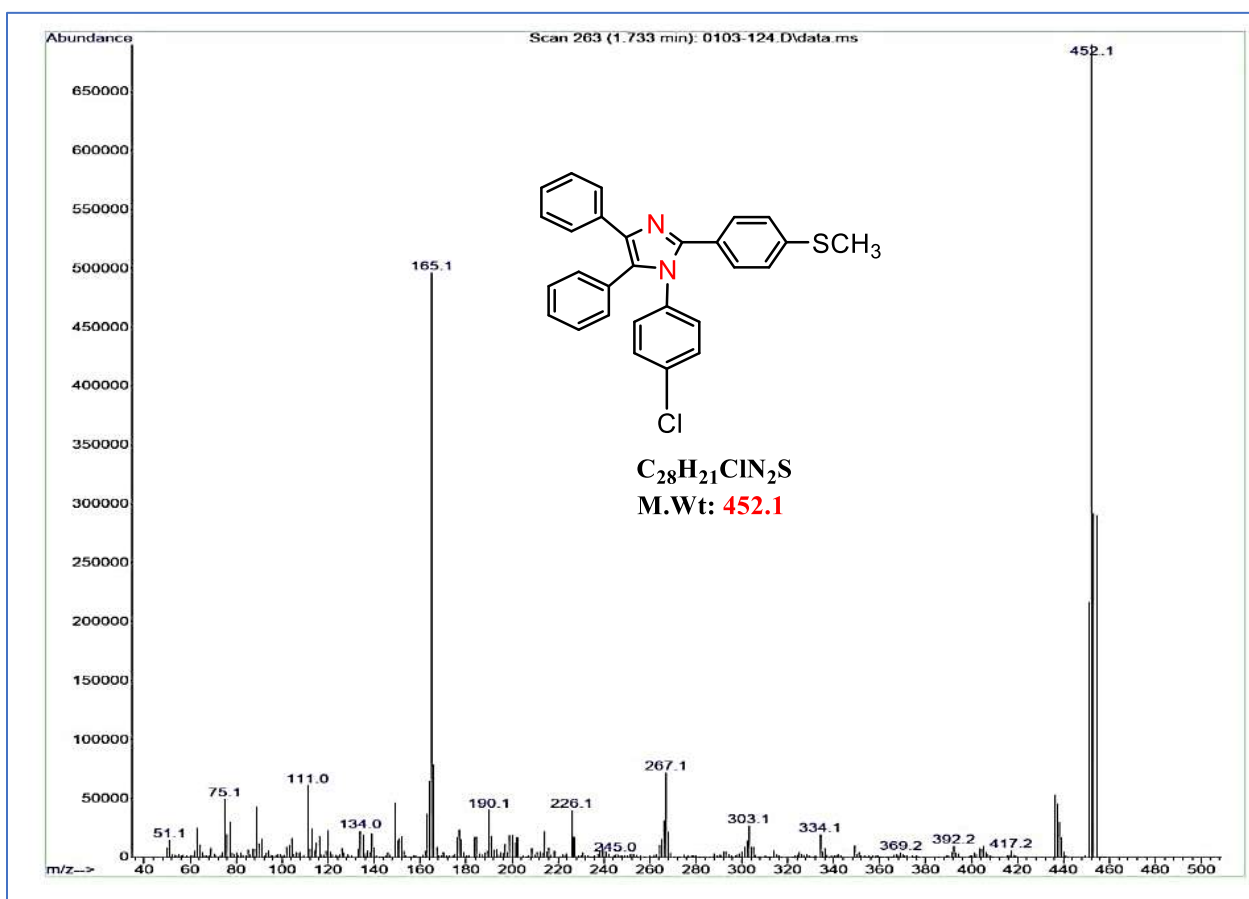


Figure 55: Mass spectrum of 5a

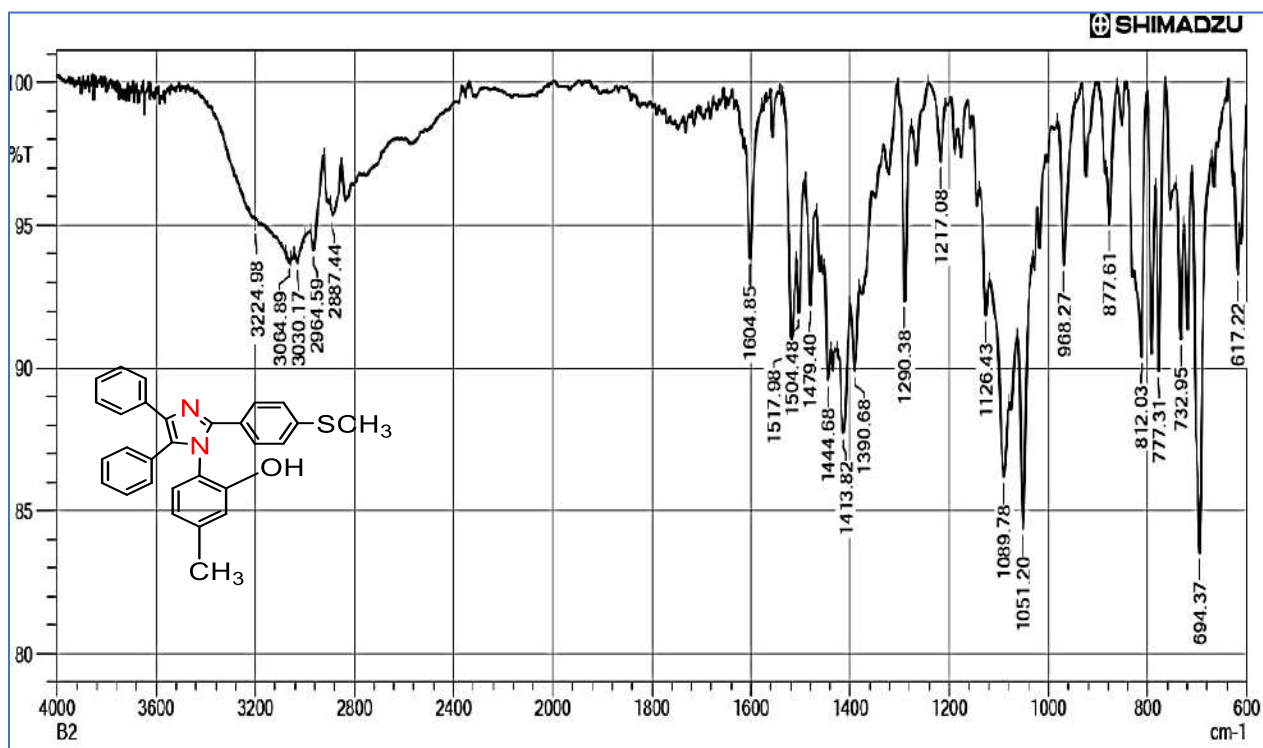


Figure 56: FTIR spectrum of 5b

Appendix A

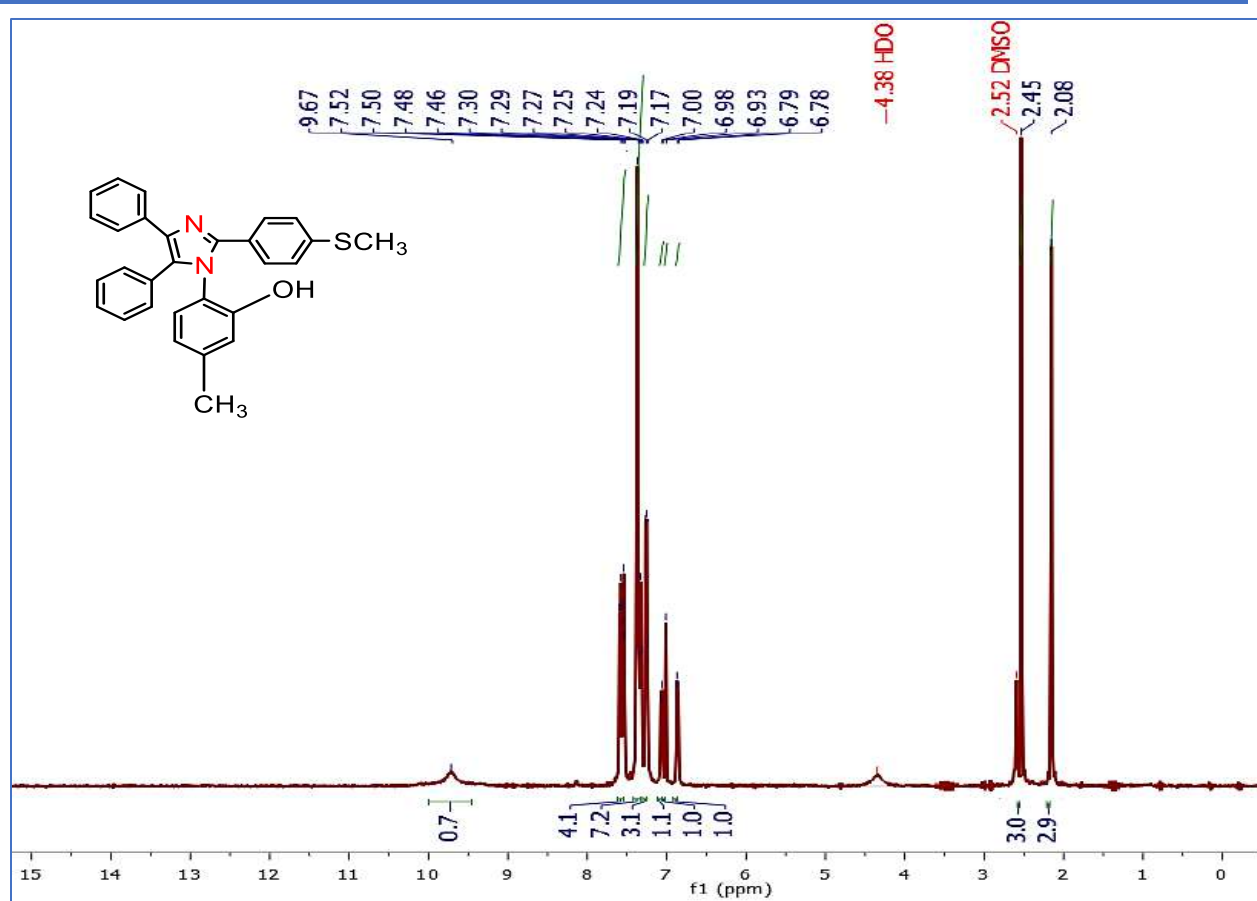


Figure 57: $^1\text{H NMR}$ spectrum of **5b**

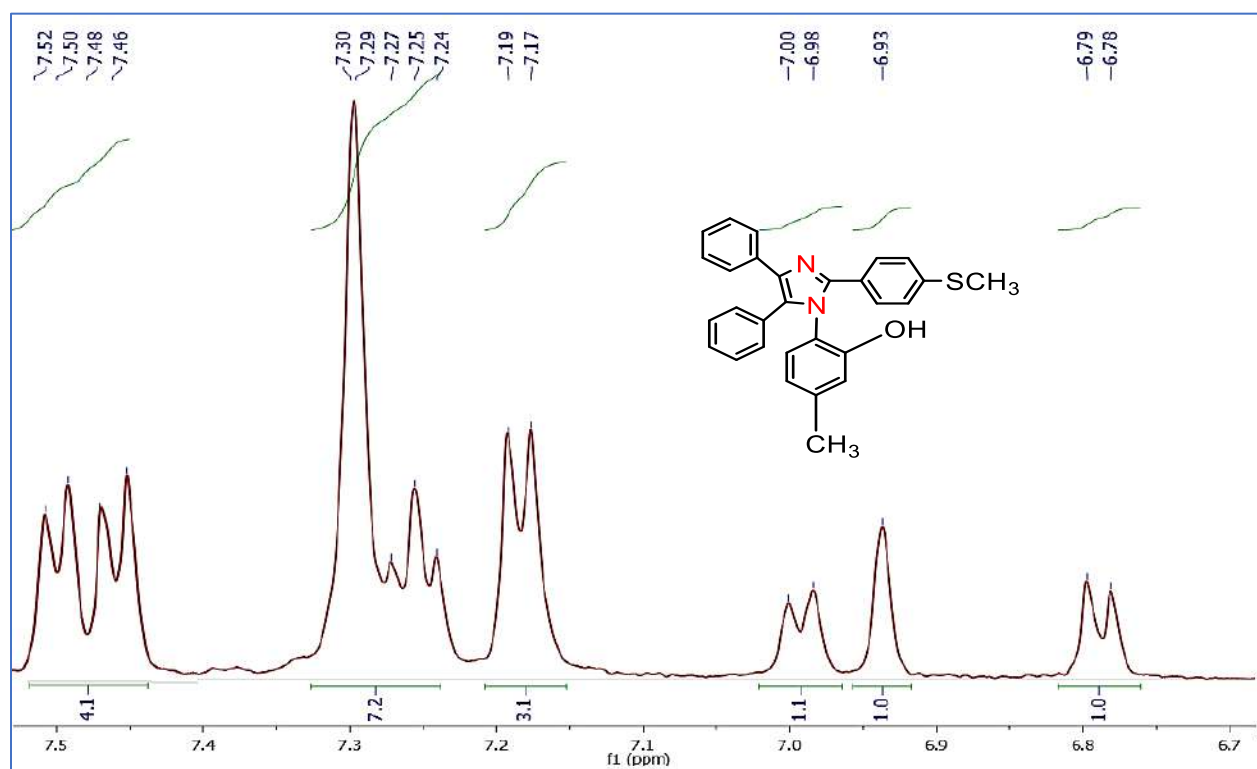


Figure 58: Expanded $^1\text{H NMR}$ spectrum of **5b**

Appendix A

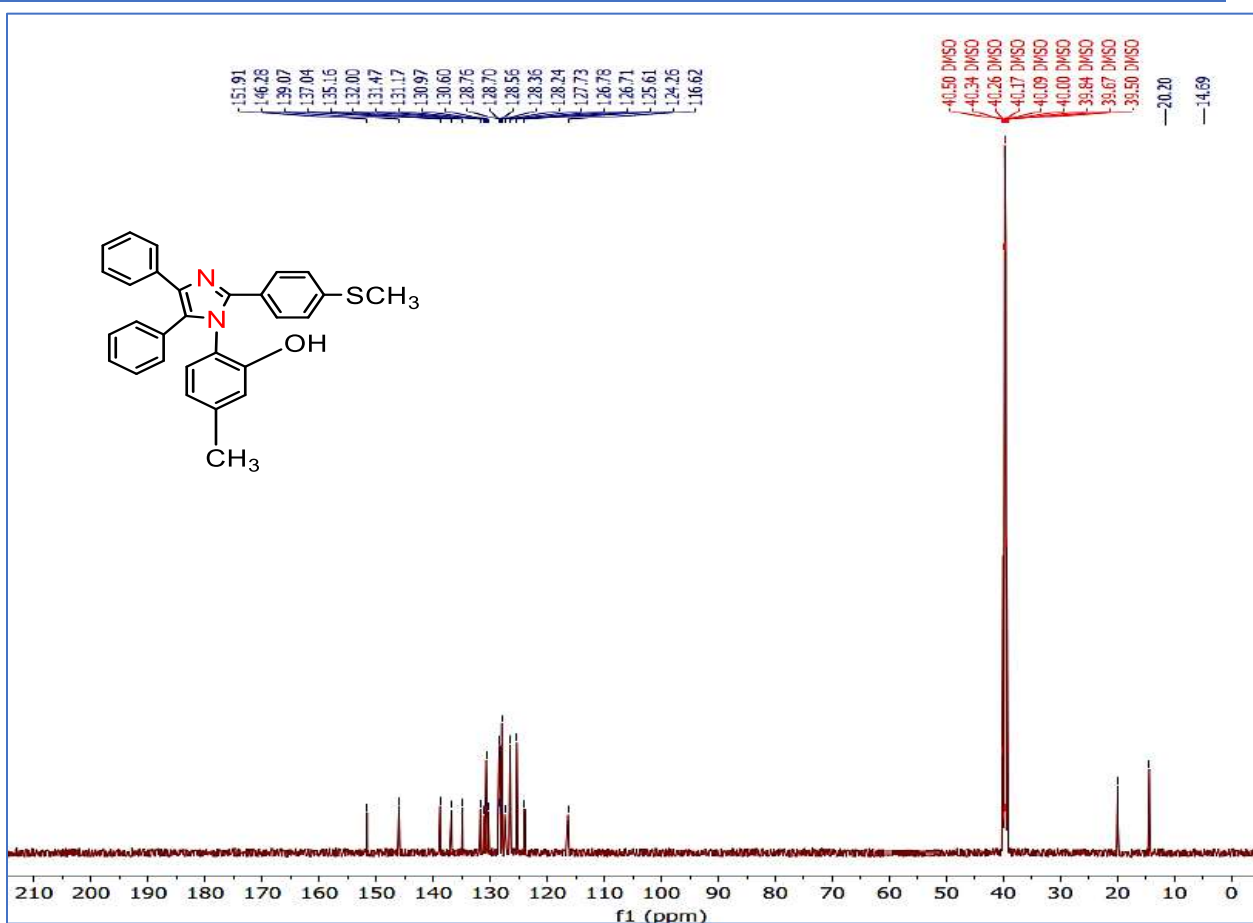


Figure 59: ¹³C NMR spectrum of 5b

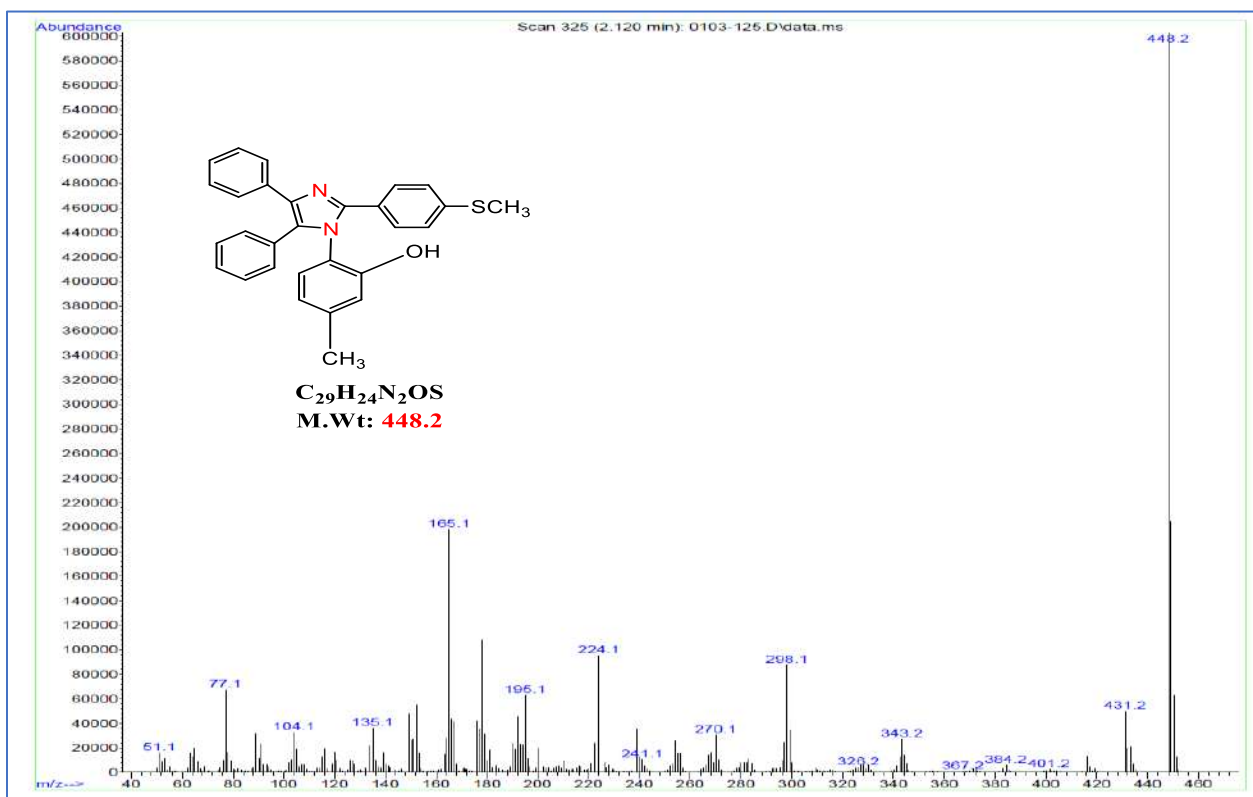


Figure 60: Mass spectrum of 5b

Appendix A

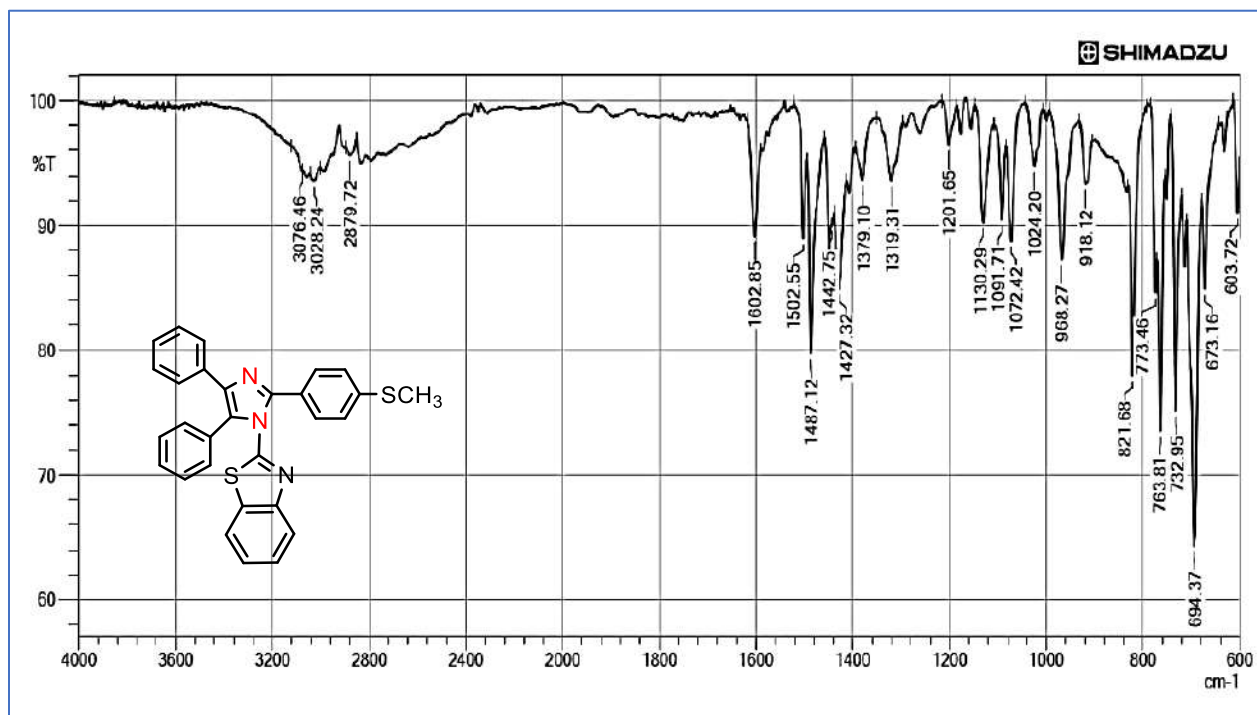


Figure 61: FTIR spectrum of 5c

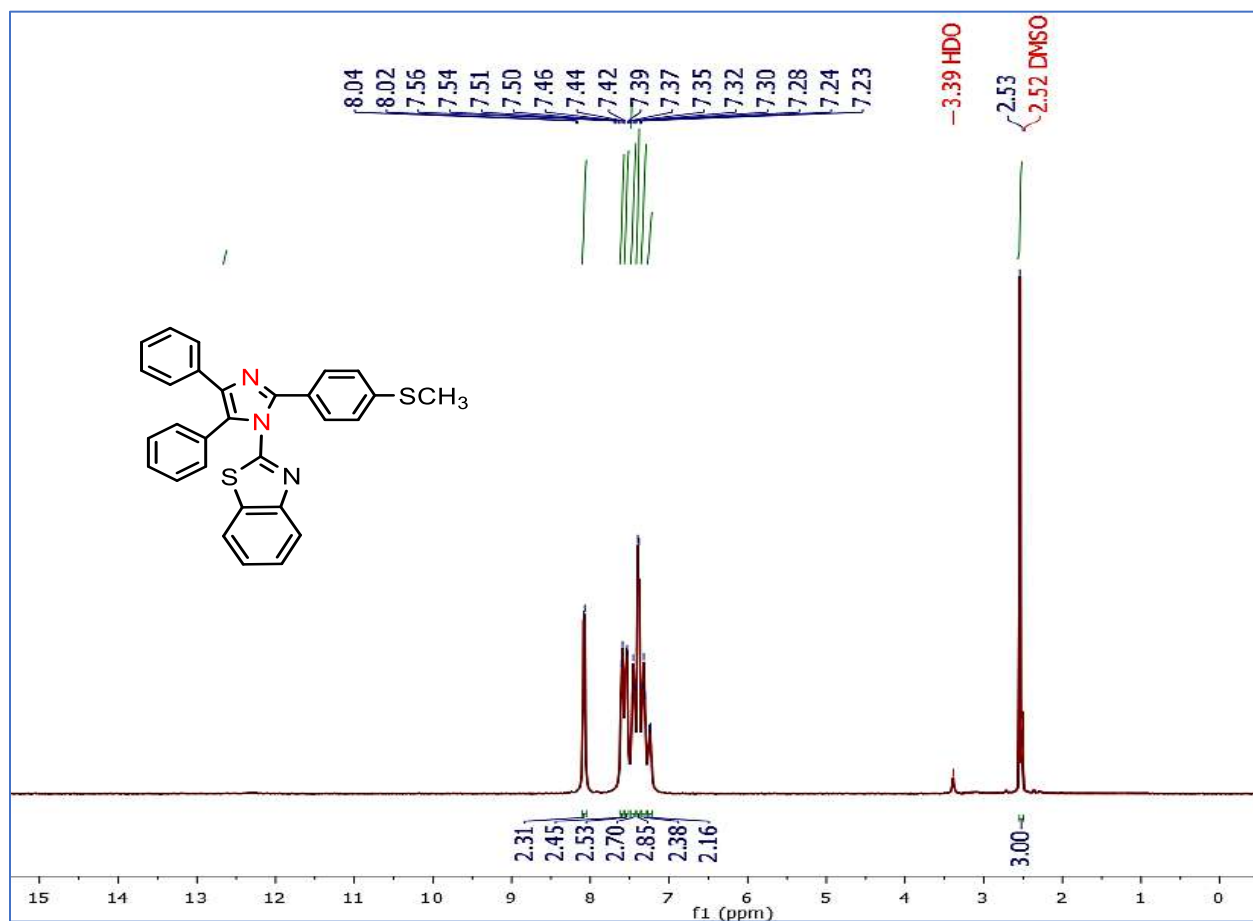


Figure 62: ¹H NMR spectrum of 5c

Appendix A

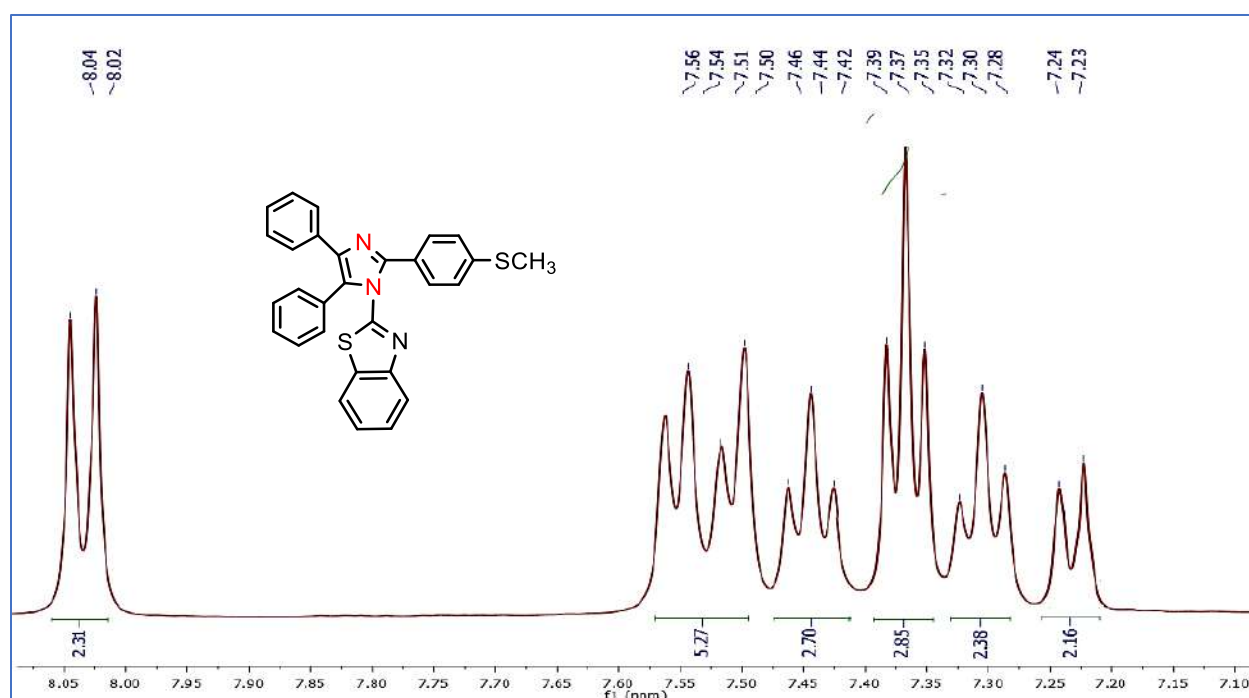


Figure 63: Expanded ^1H NMR spectrum of 5c

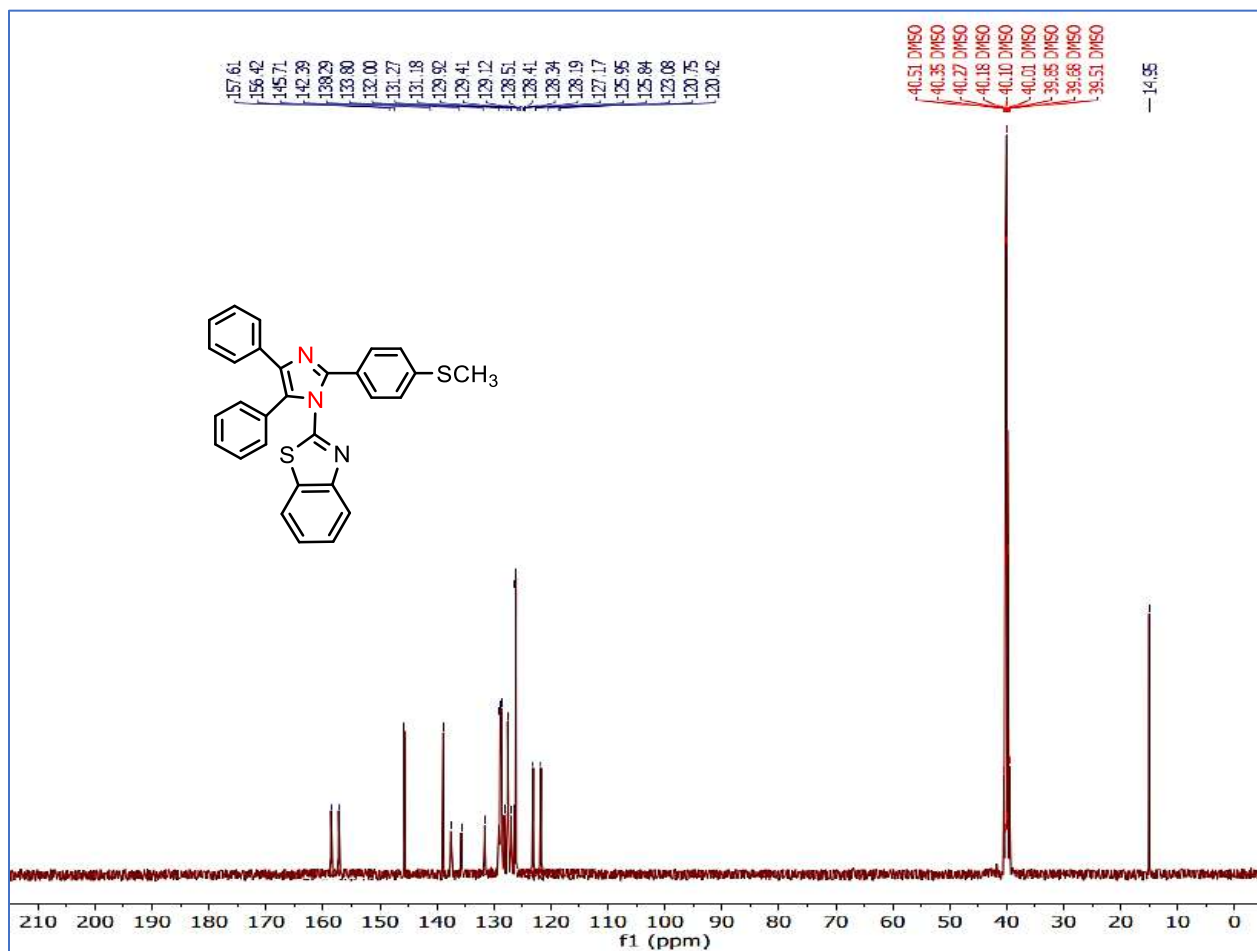


Figure 64: ^{13}C NMR spectrum of 5c

Appendix A

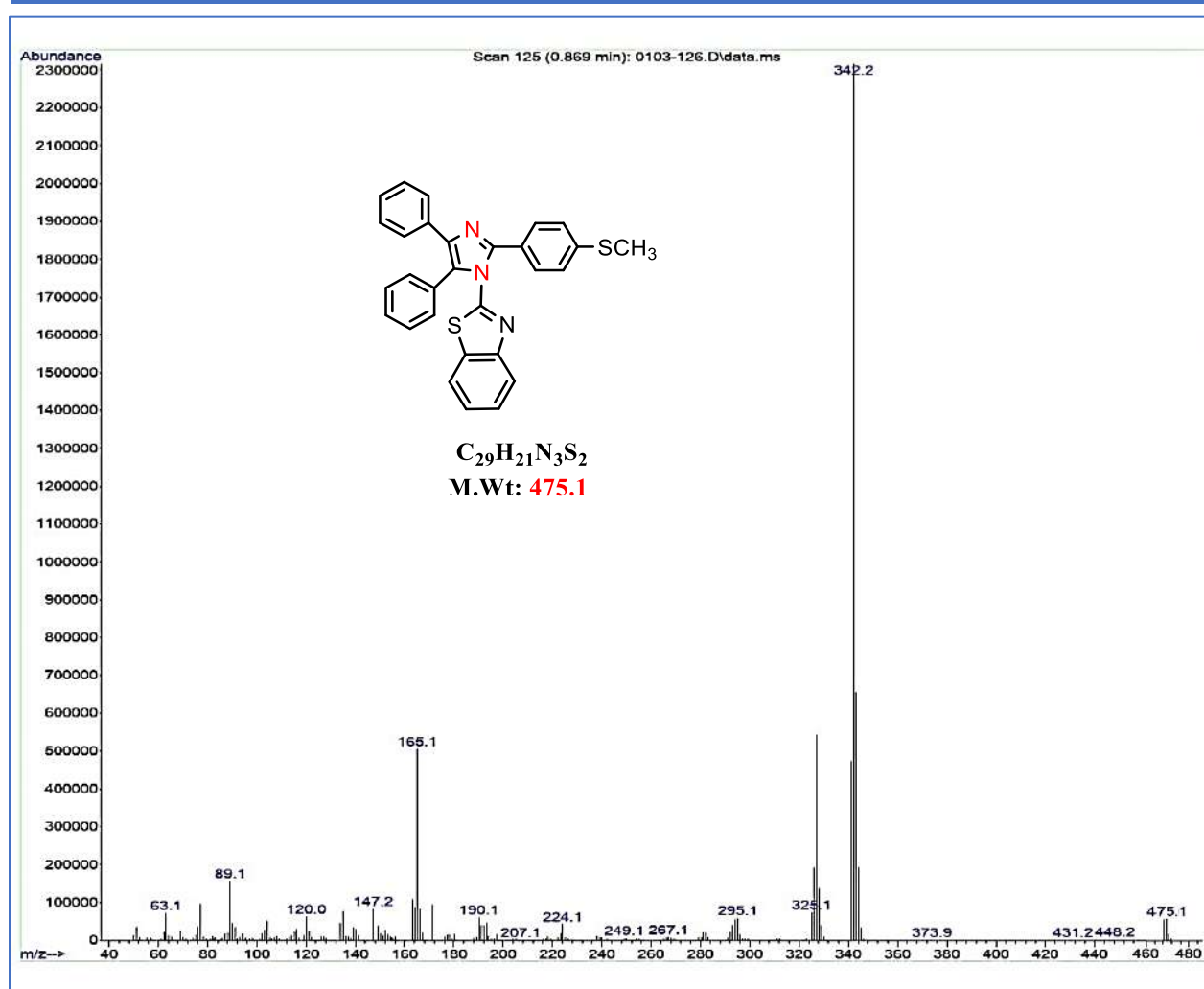


Figure 65: Mass spectrum of 5c

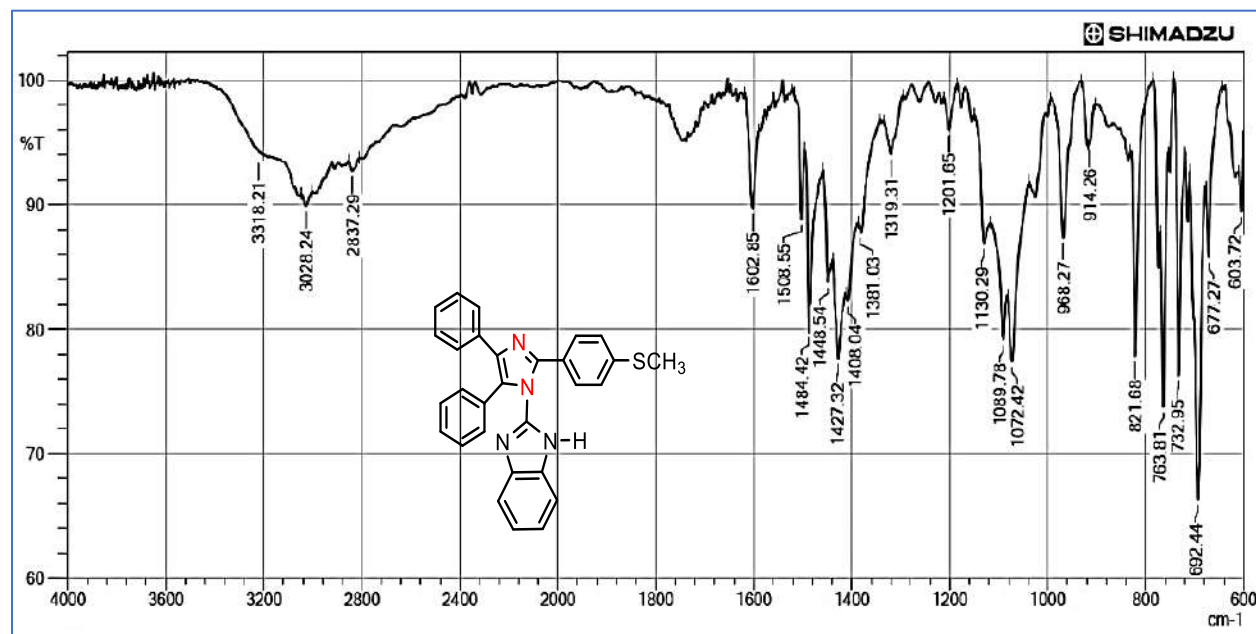


Figure 66: FTIR spectrum of 5d

Appendix A

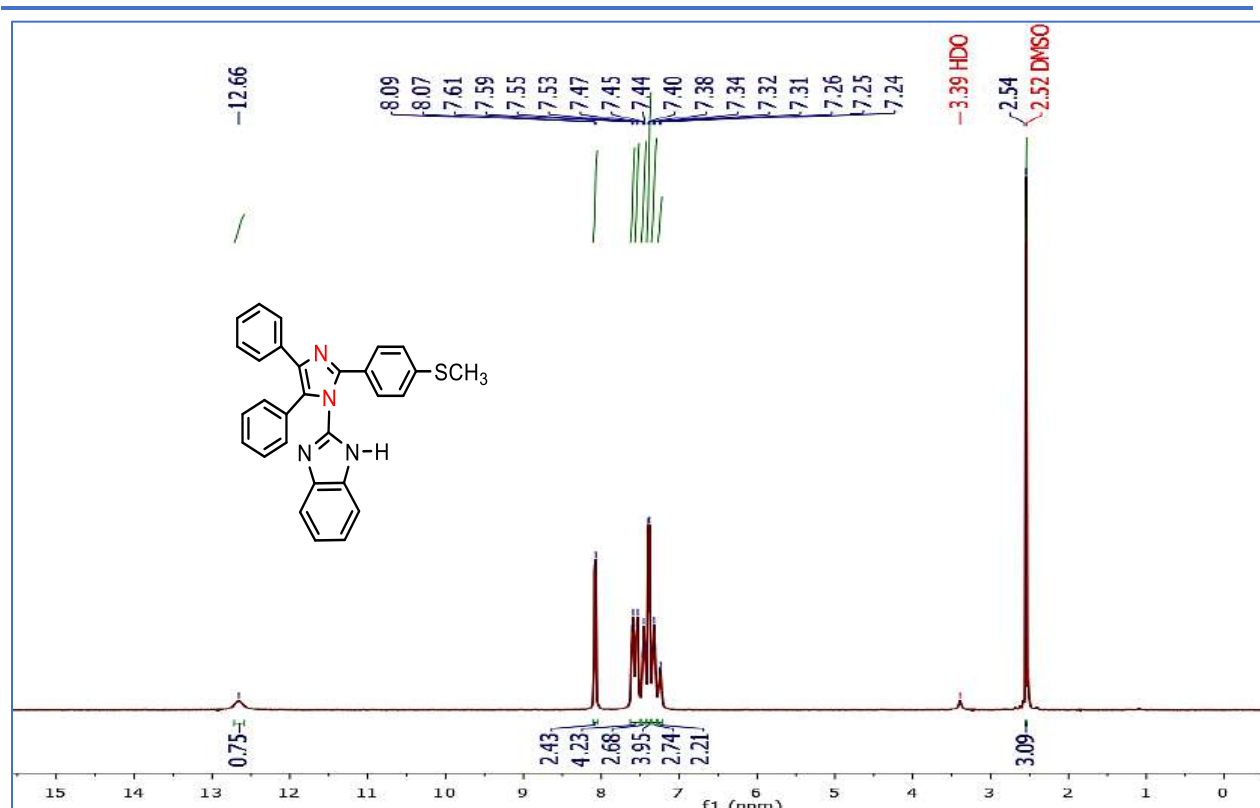


Figure 67: $^1\text{H NMR}$ spectrum of **5d**

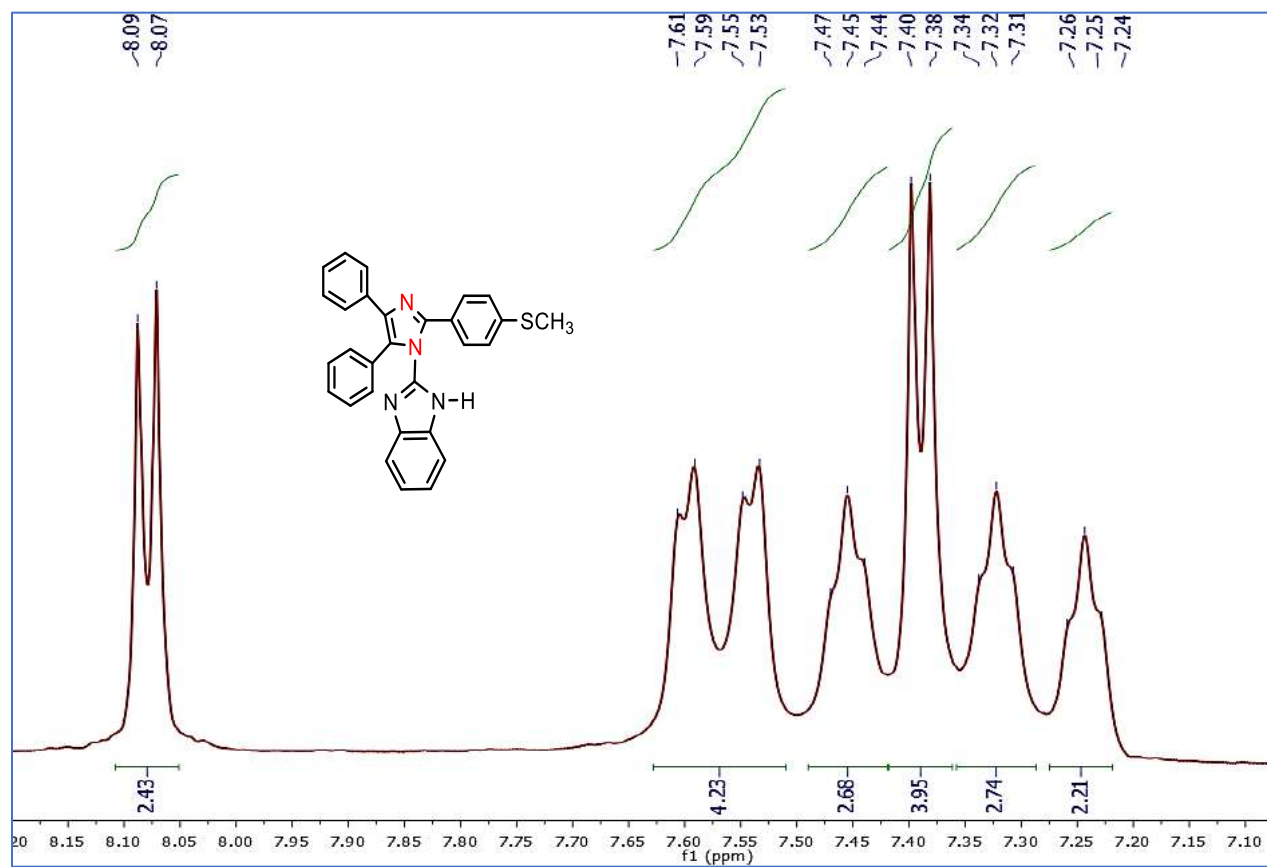


Figure 68: Expanded $^1\text{H NMR}$ spectrum of **5d**

Appendix A

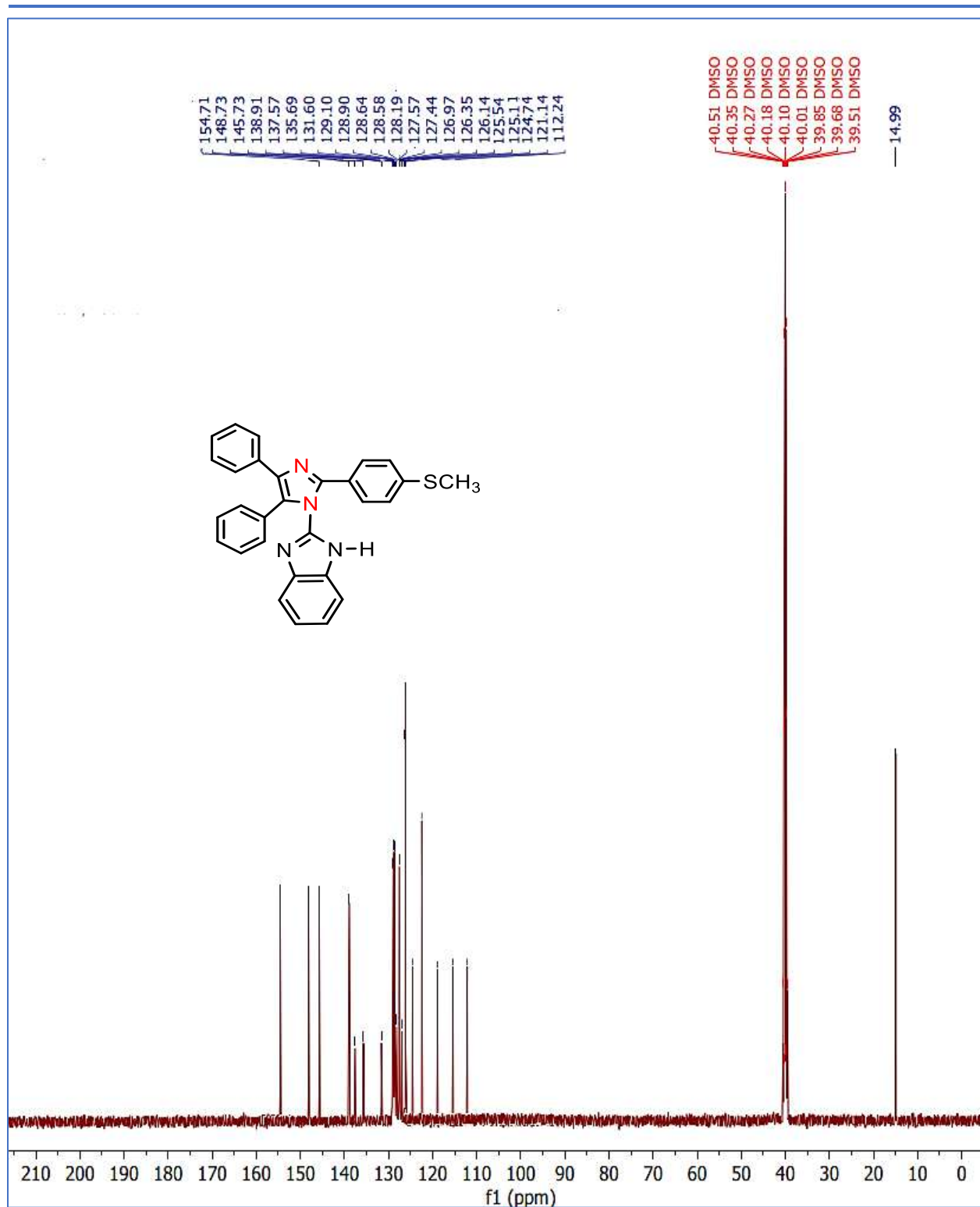


Figure 69: ¹³C NMR spectrum of 5d

Appendix A

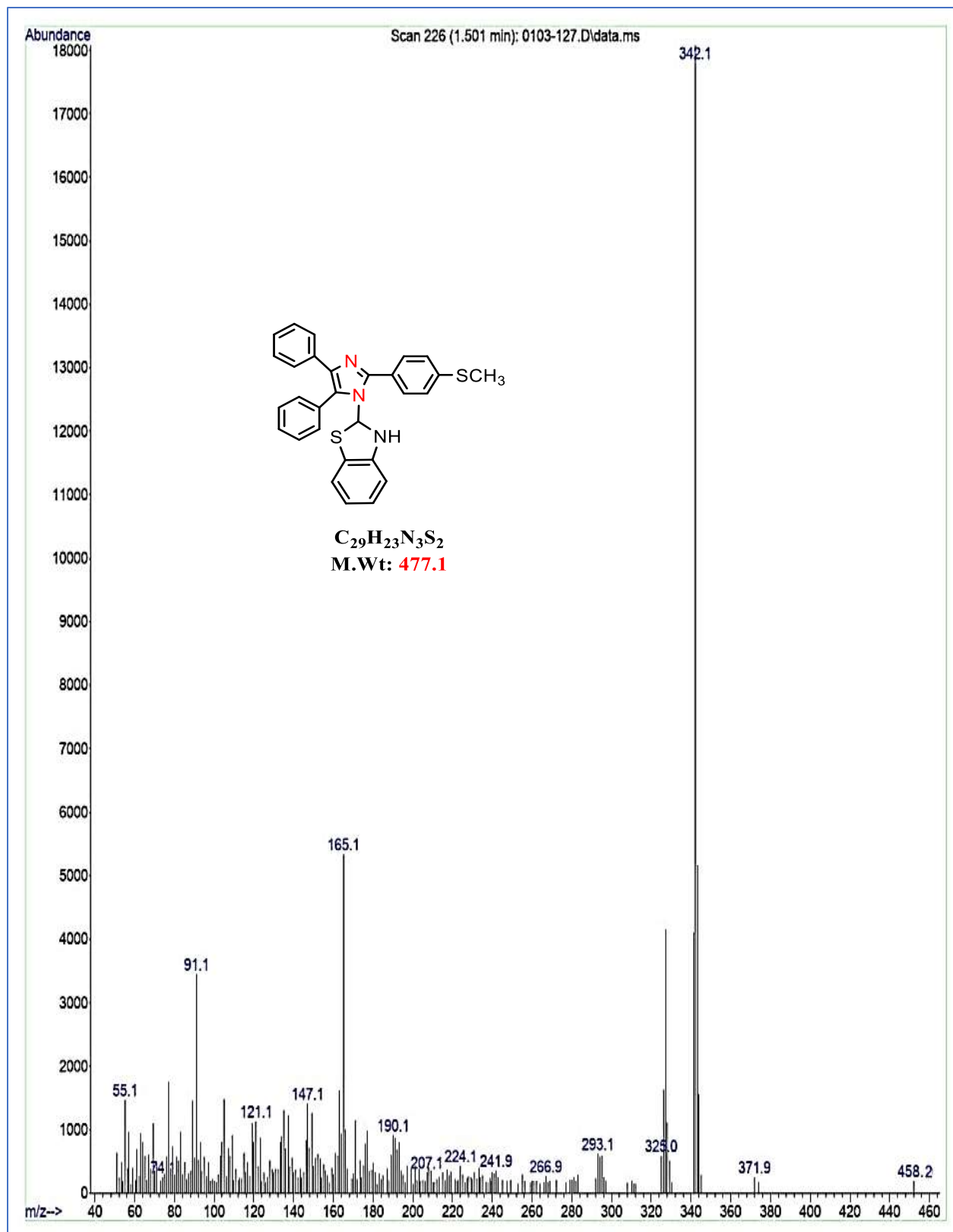


Figure 70: Mass spectrum of 5d

Appendix A

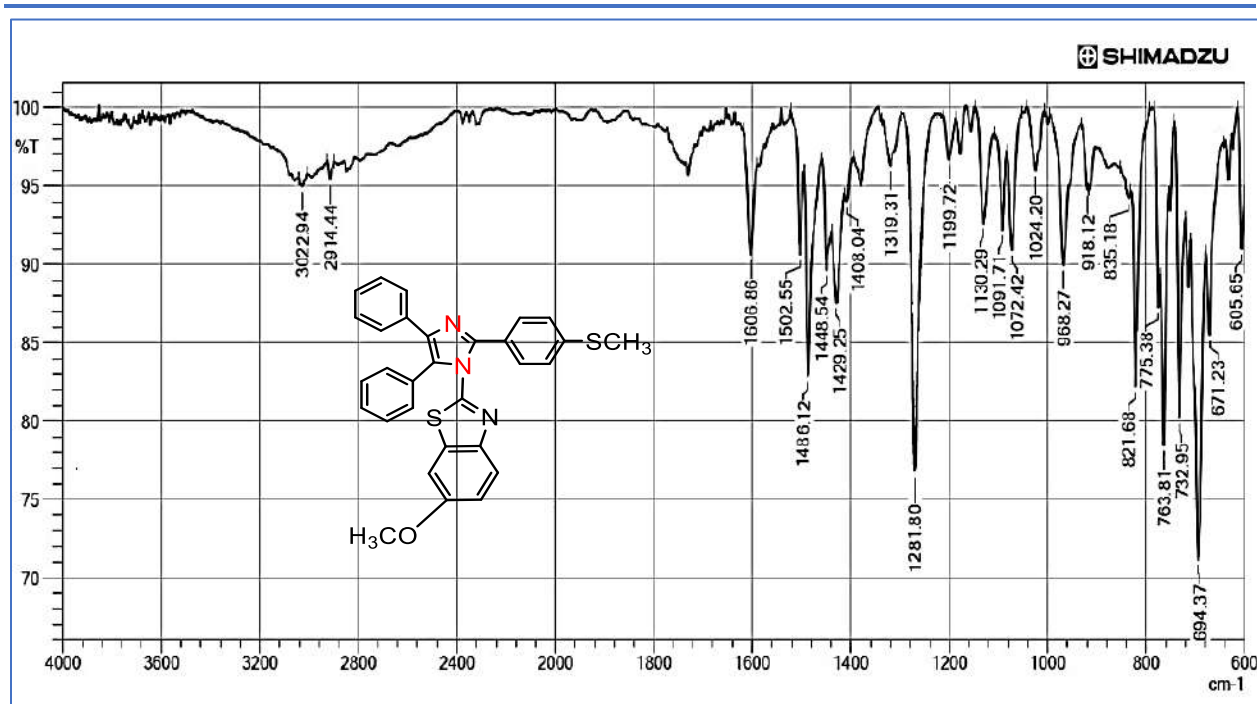


Figure 71: FTIR spectrum of 5e

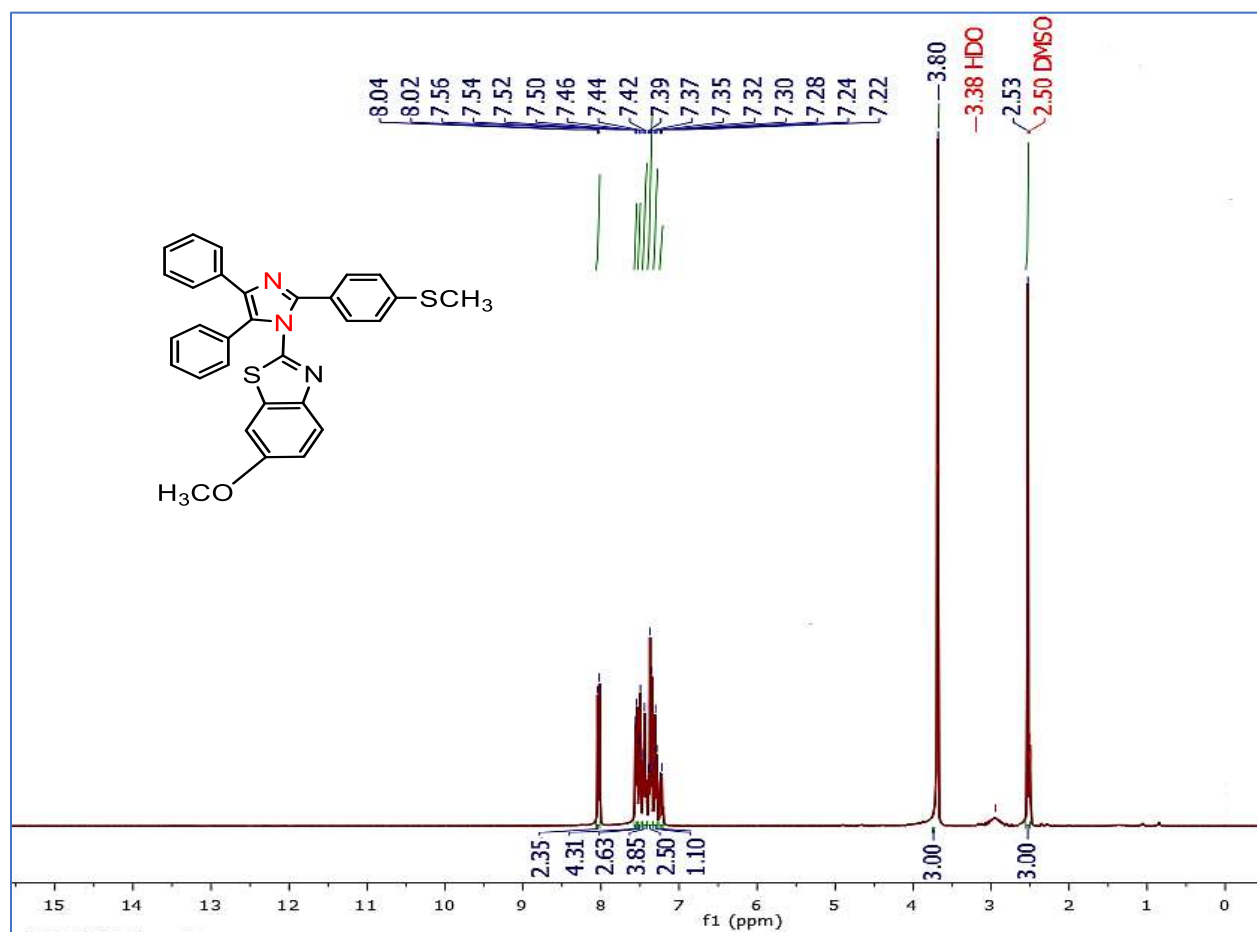


Figure 72: ¹H NMR spectrum of 5e

Appendix A

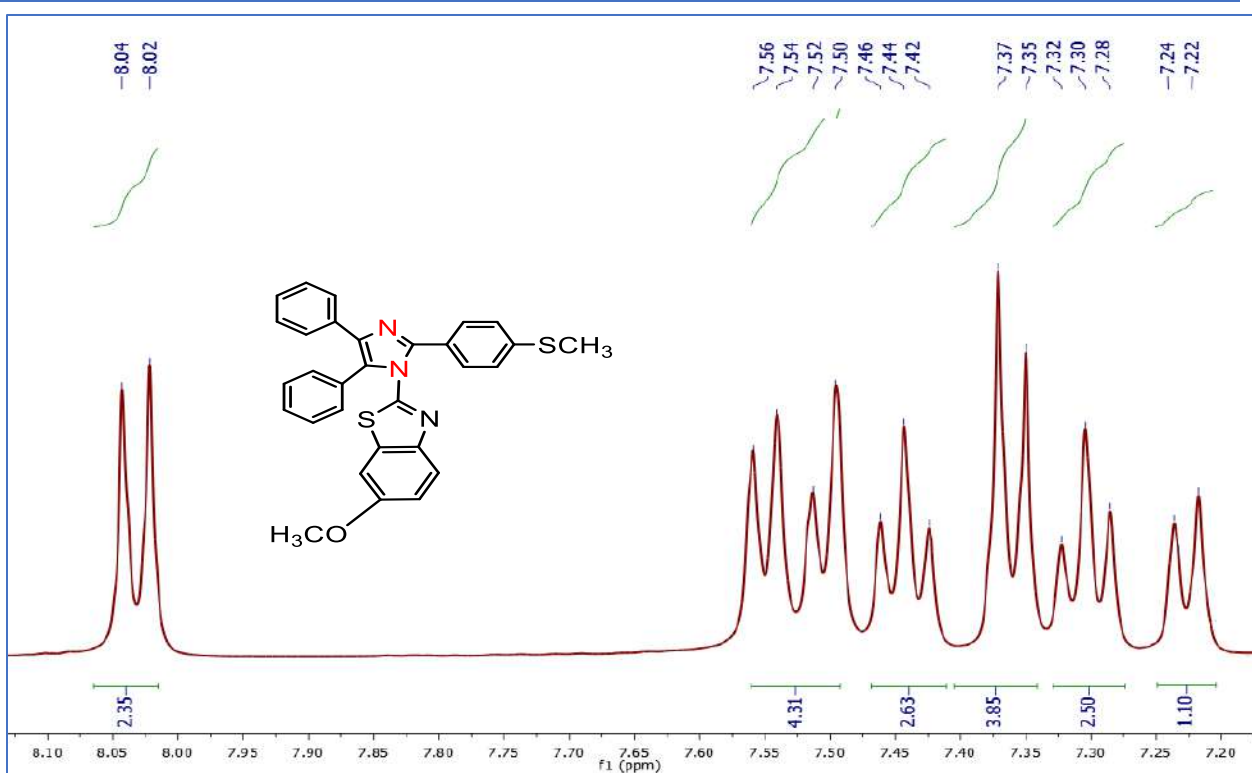


Figure 73: Expanded ¹H NMR spectrum of 5e

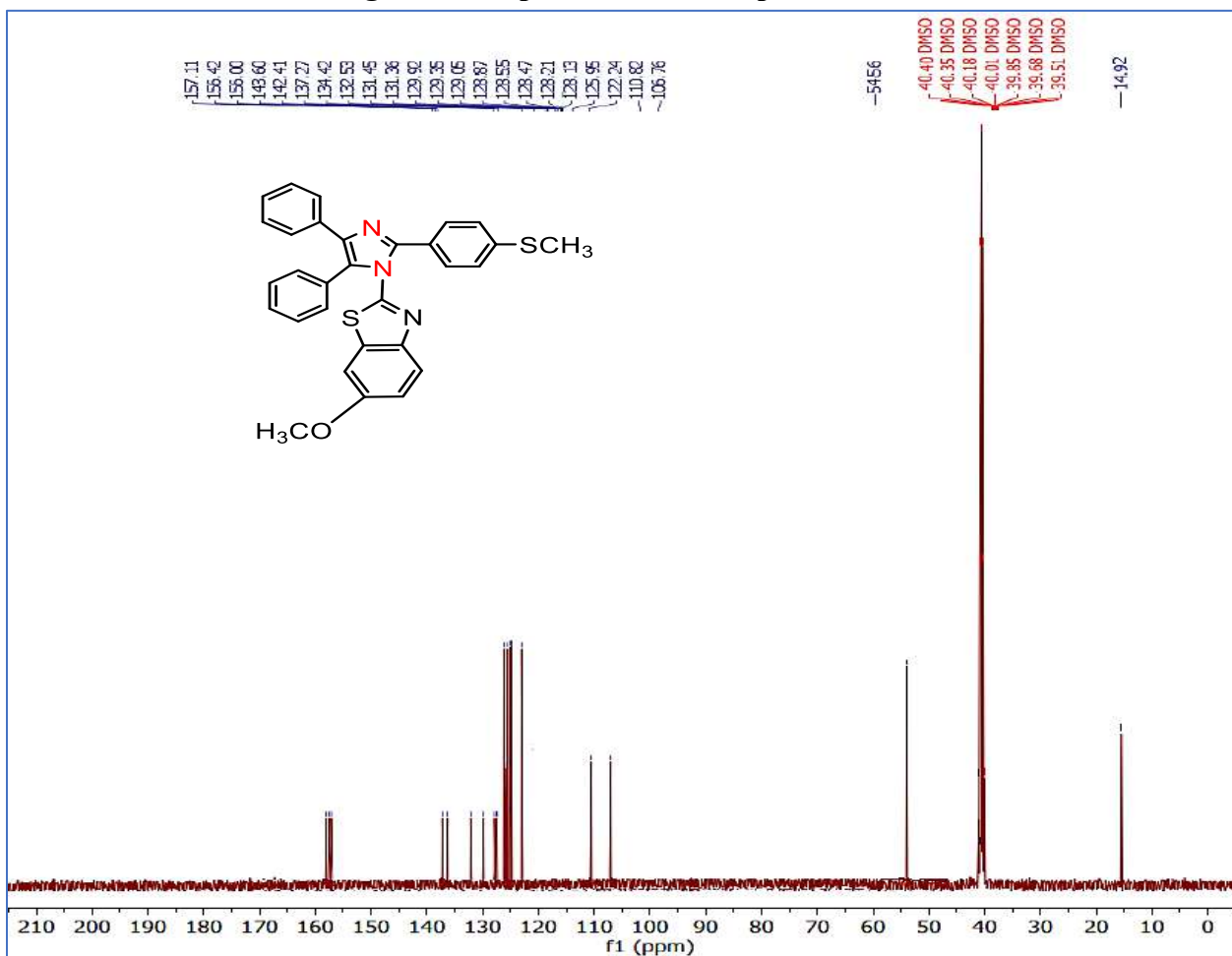


Figure 74: ¹³C NMR spectrum of 5e

Appendix A

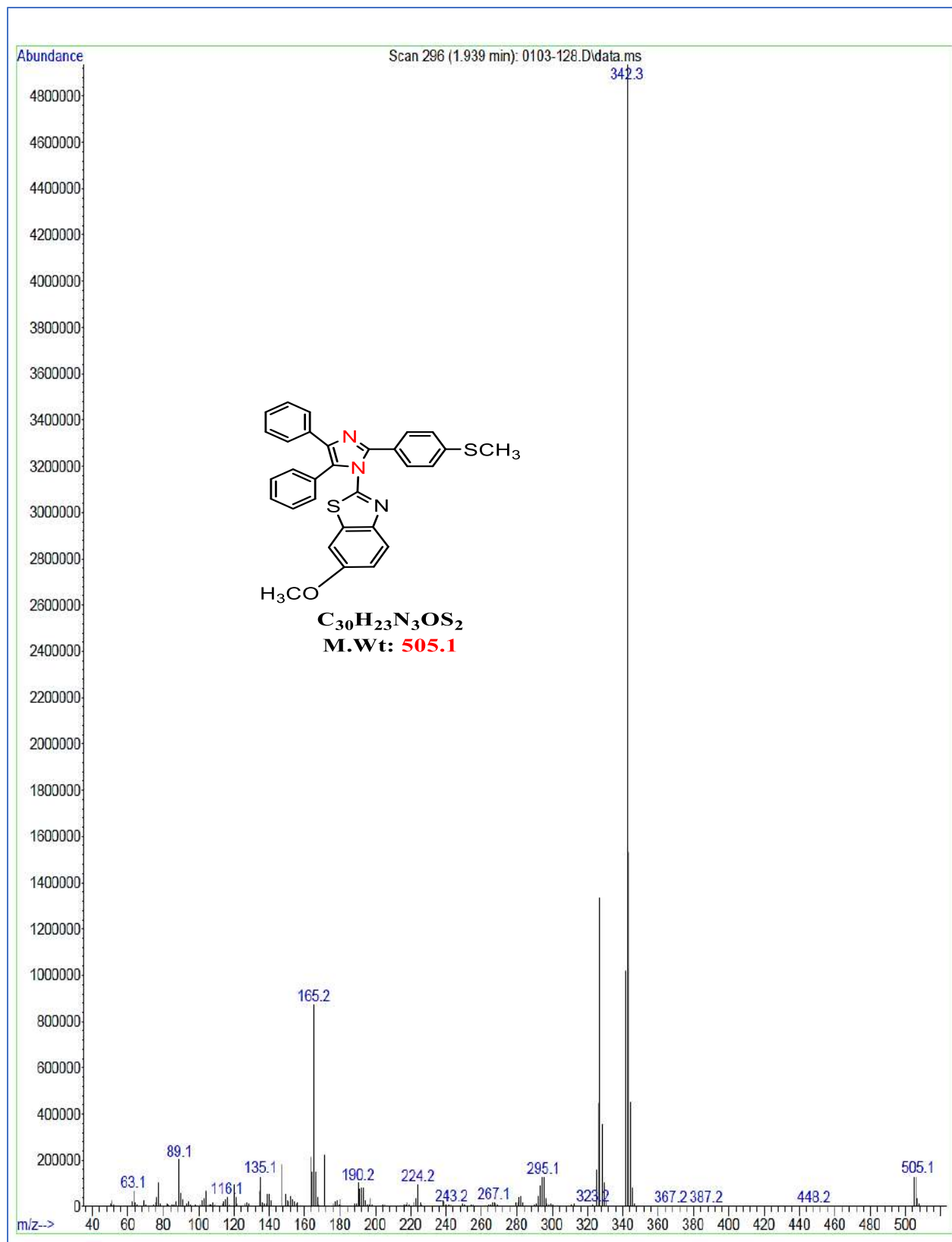


Figure 75: Mass spectrum of 5e

Appendix A

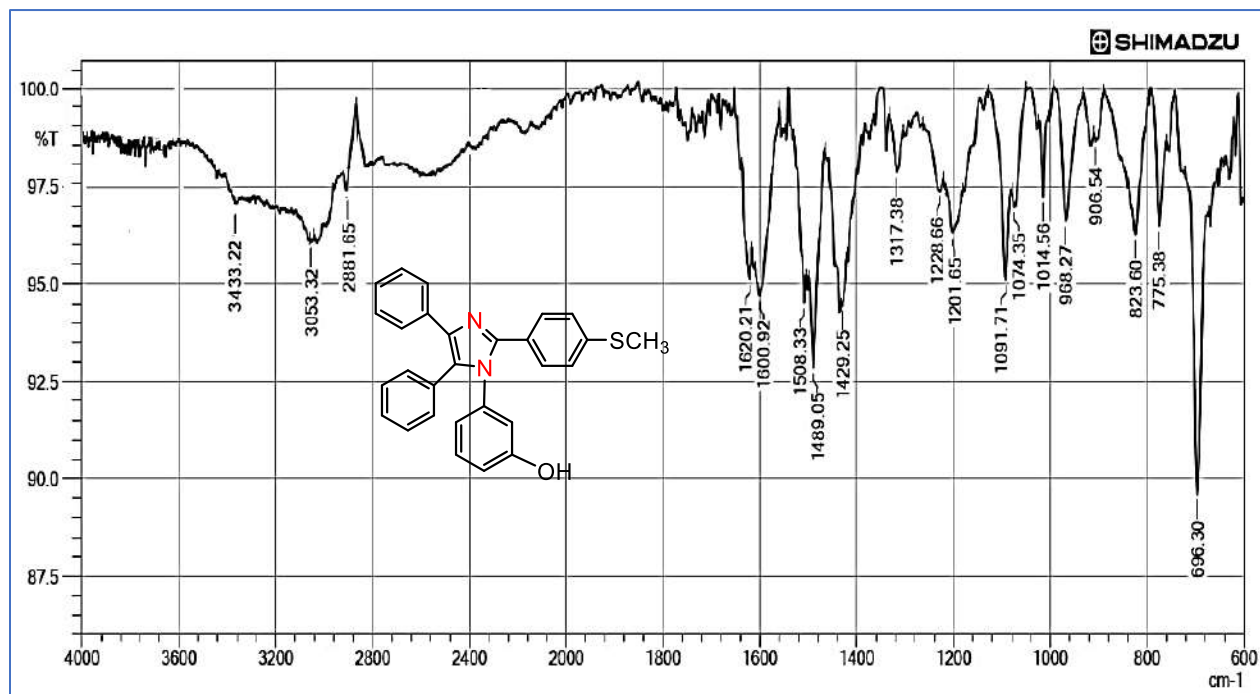


Figure 76: FTIR spectrum of 5f

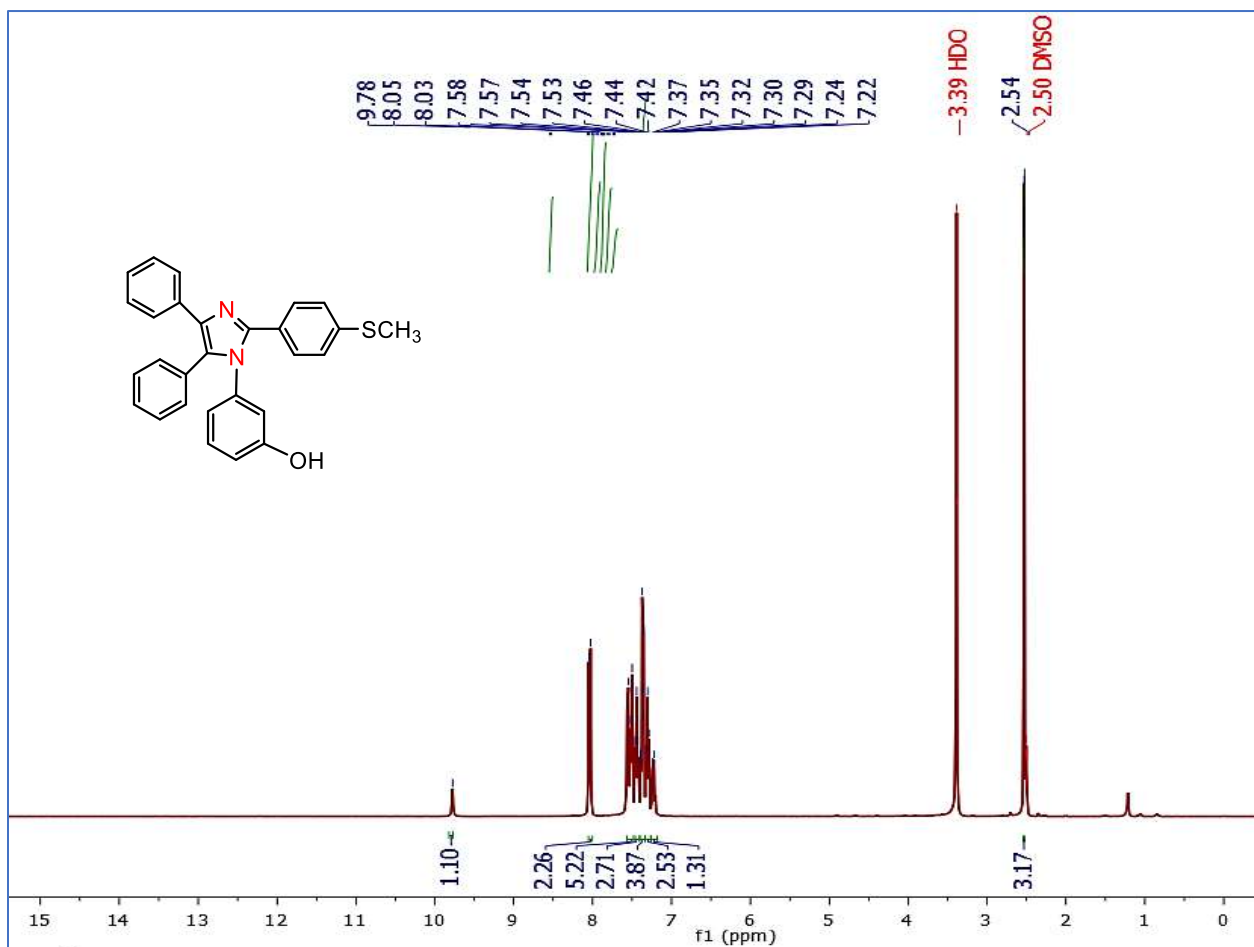


Figure 77: ¹H NMR spectrum of 5f

Appendix A

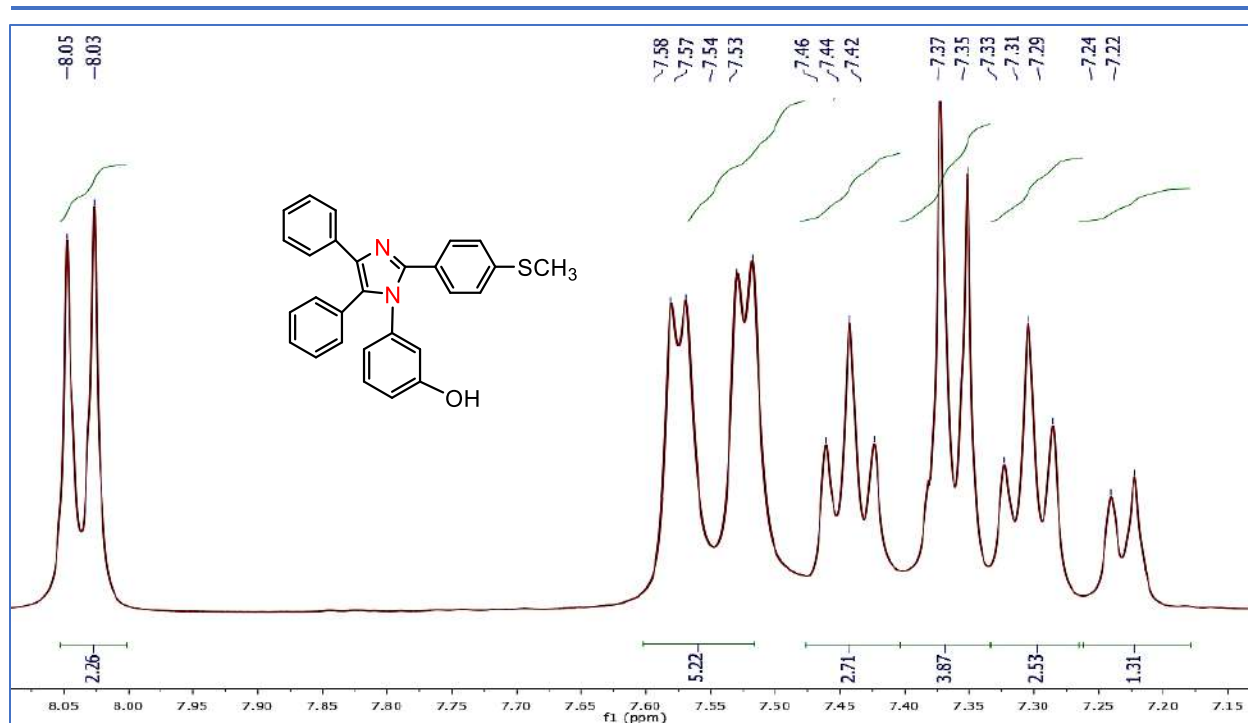


Figure 78: Expanded ^1H NMR spectrum of 5f

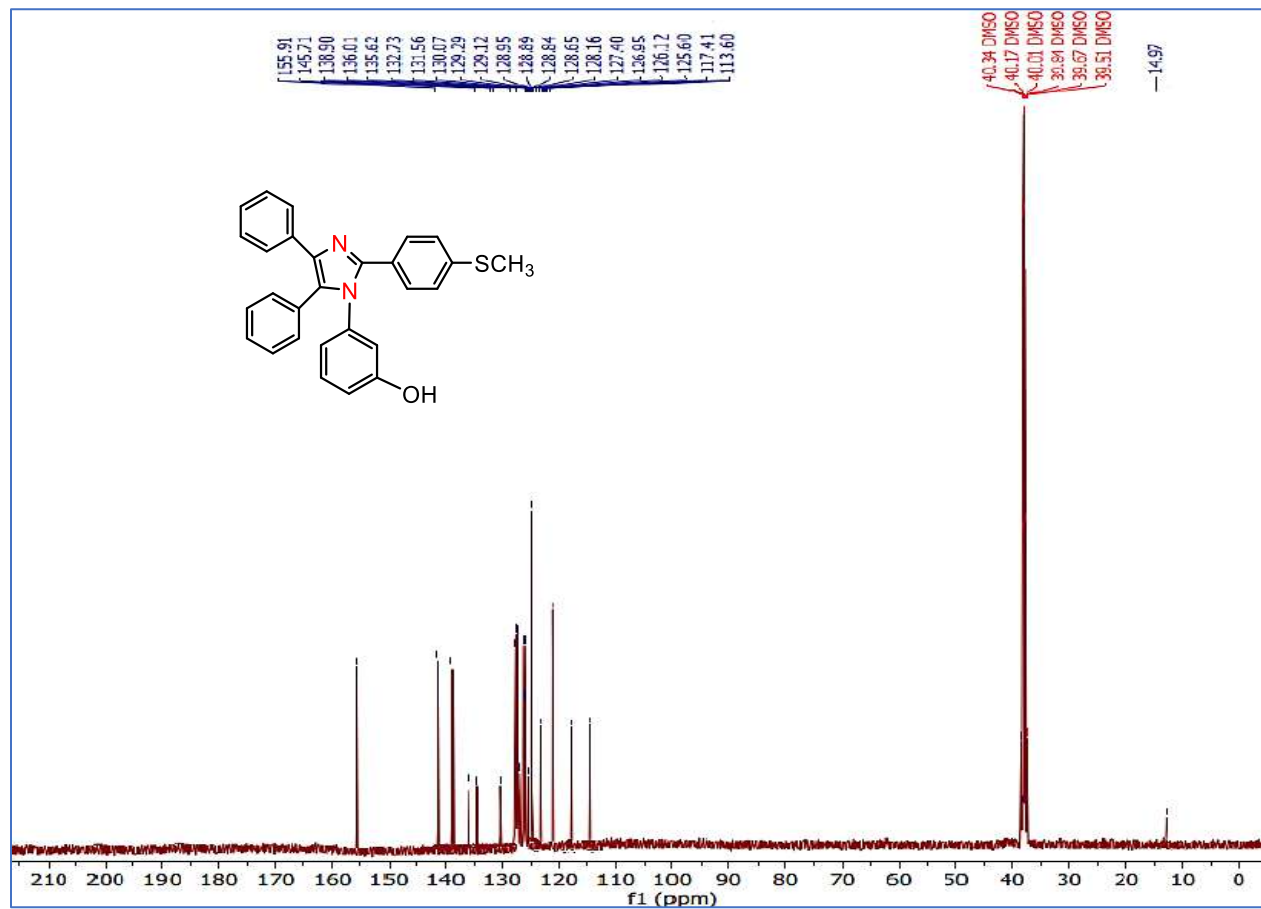


Figure 79: ^{13}C NMR spectrum of 5f

Appendix A

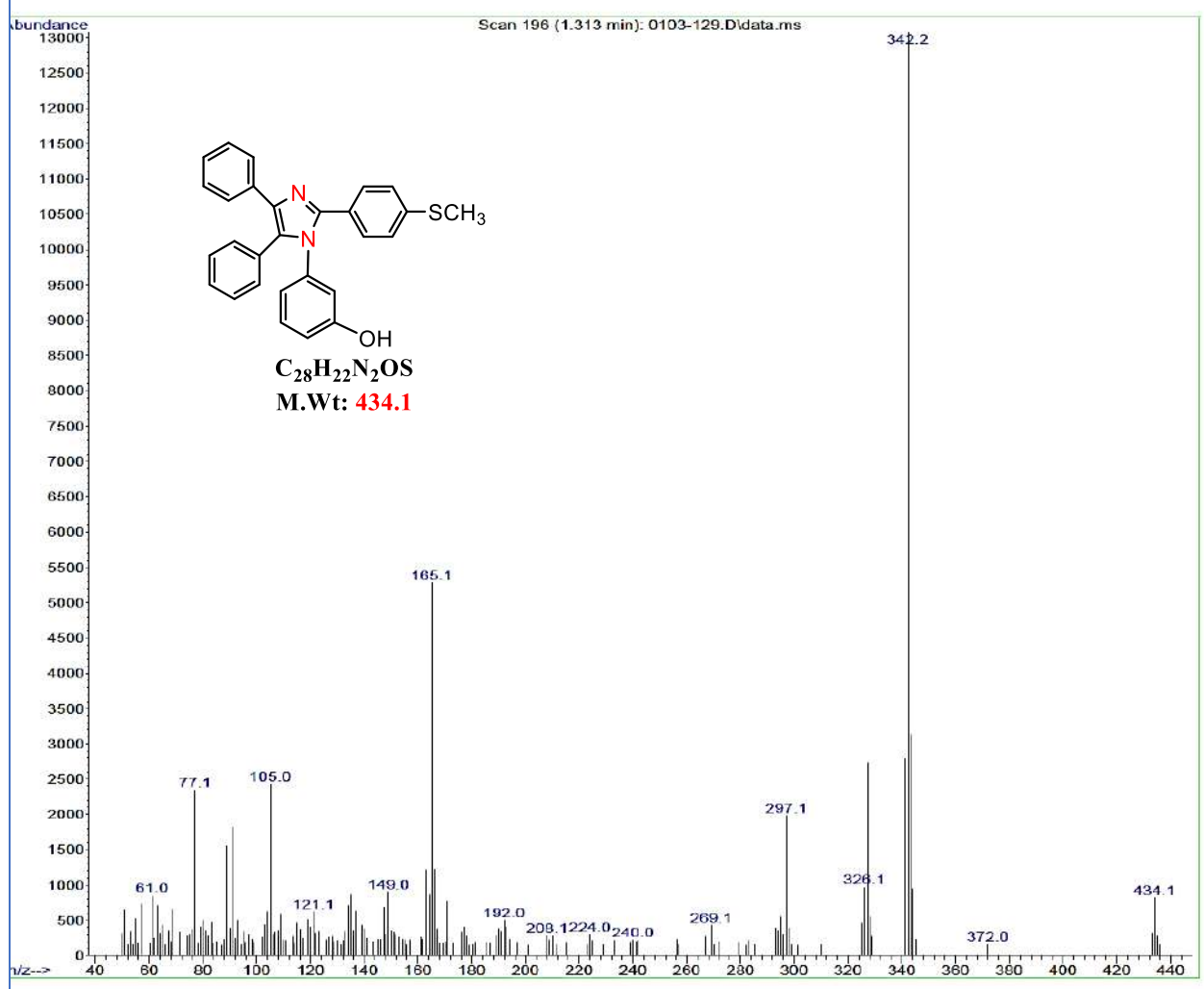


Figure 80: Mass spectrum of 5f

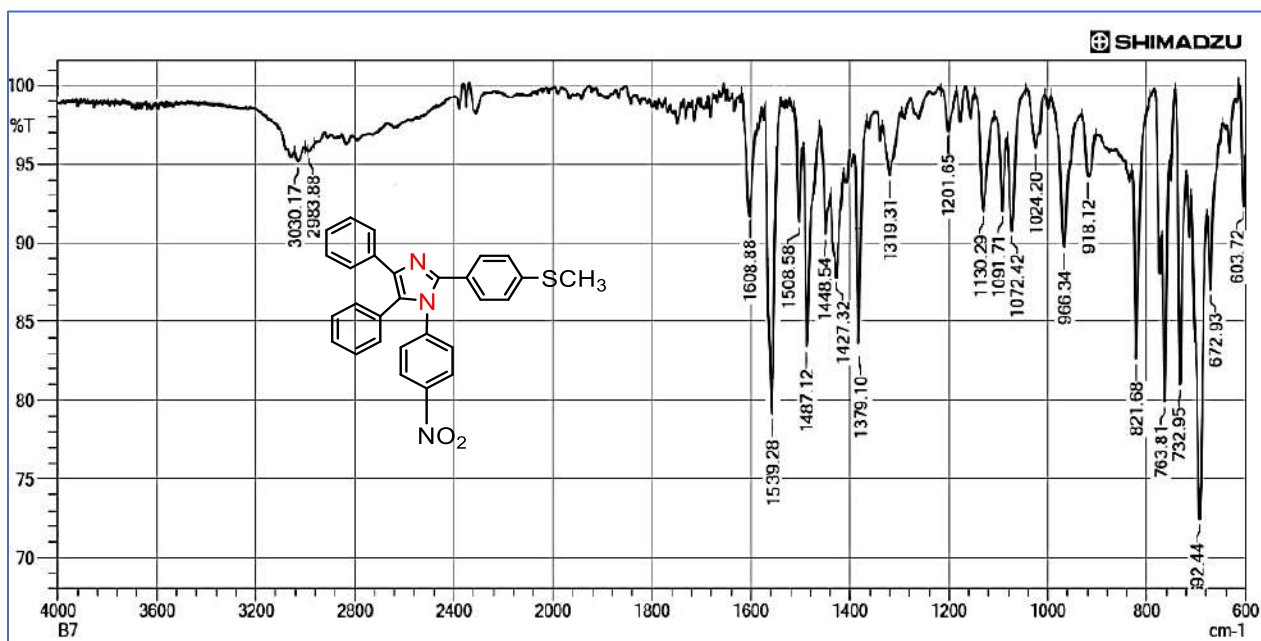


Figure 81: FTIR spectrum of 5g

Appendix A

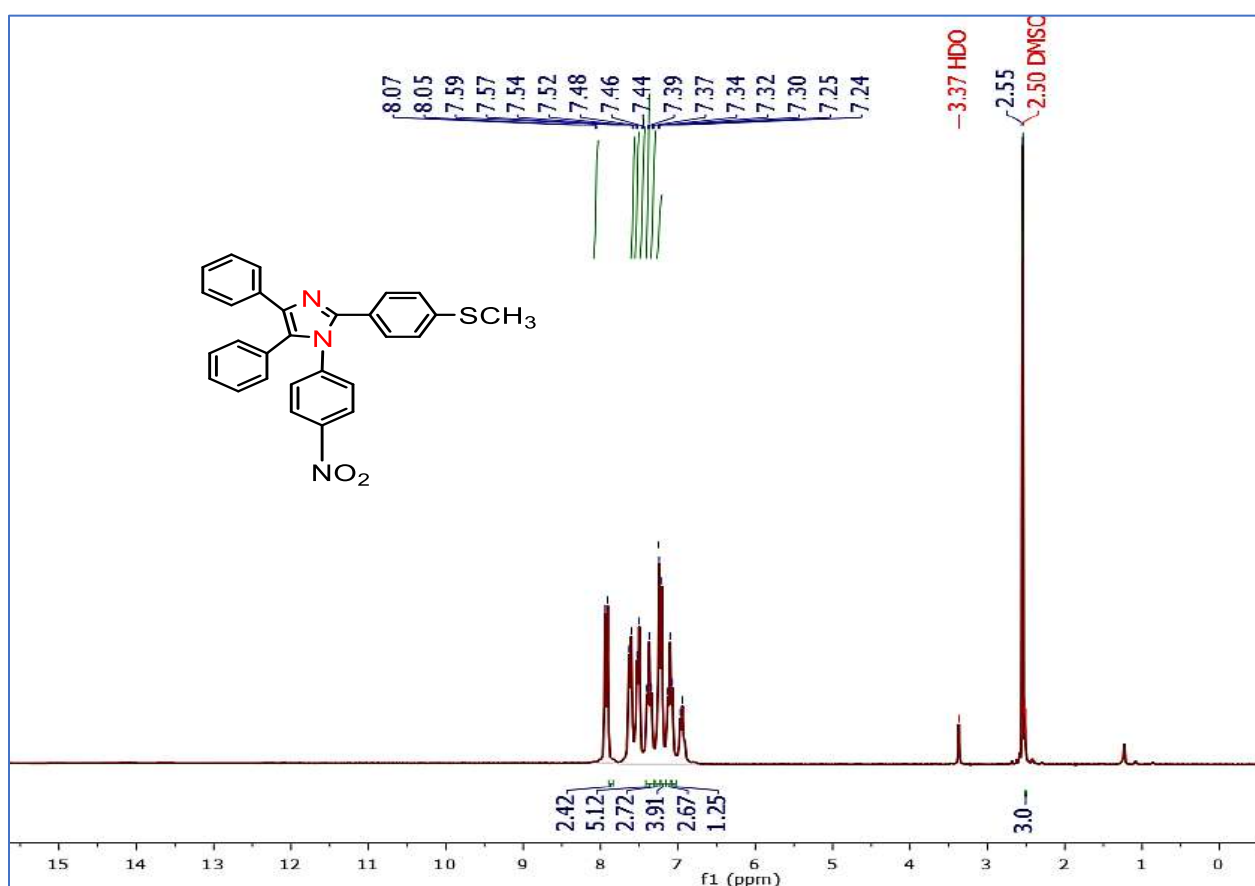


Figure 82: $^1\text{H NMR}$ spectrum of 5g

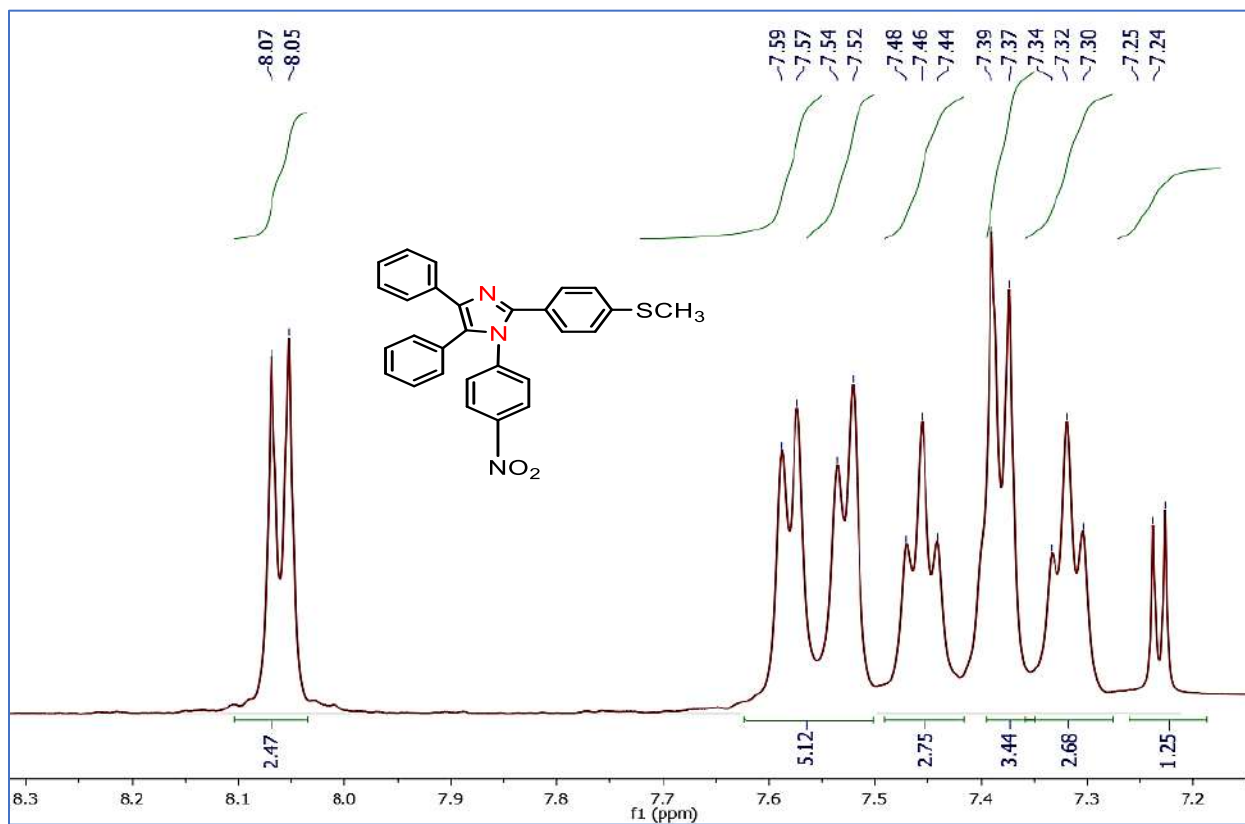


Figure 83: Expanded $^1\text{H NMR}$ spectrum of 5g

Appendix A

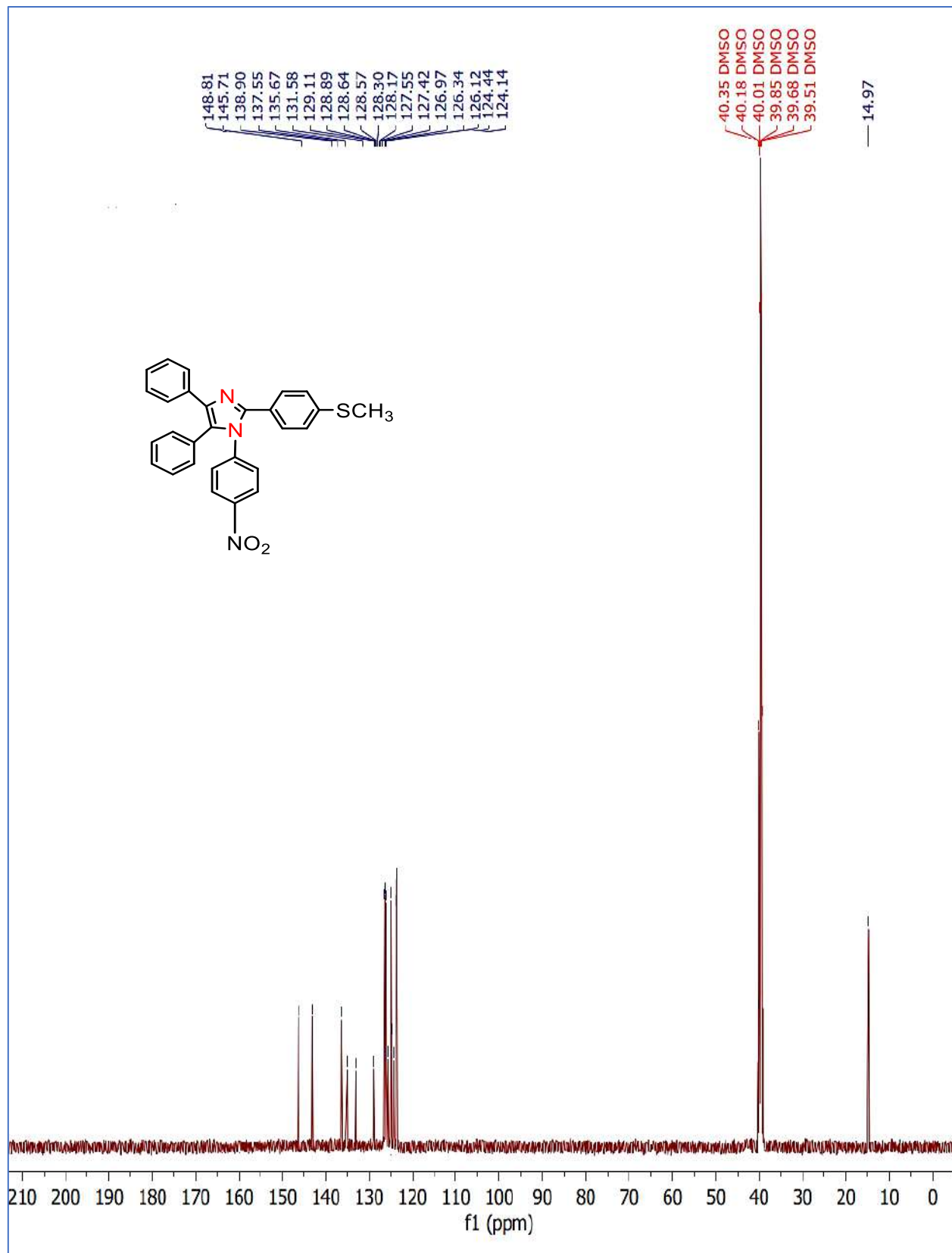


Figure 84: ¹³C NMR spectrum of 5g

Appendix A

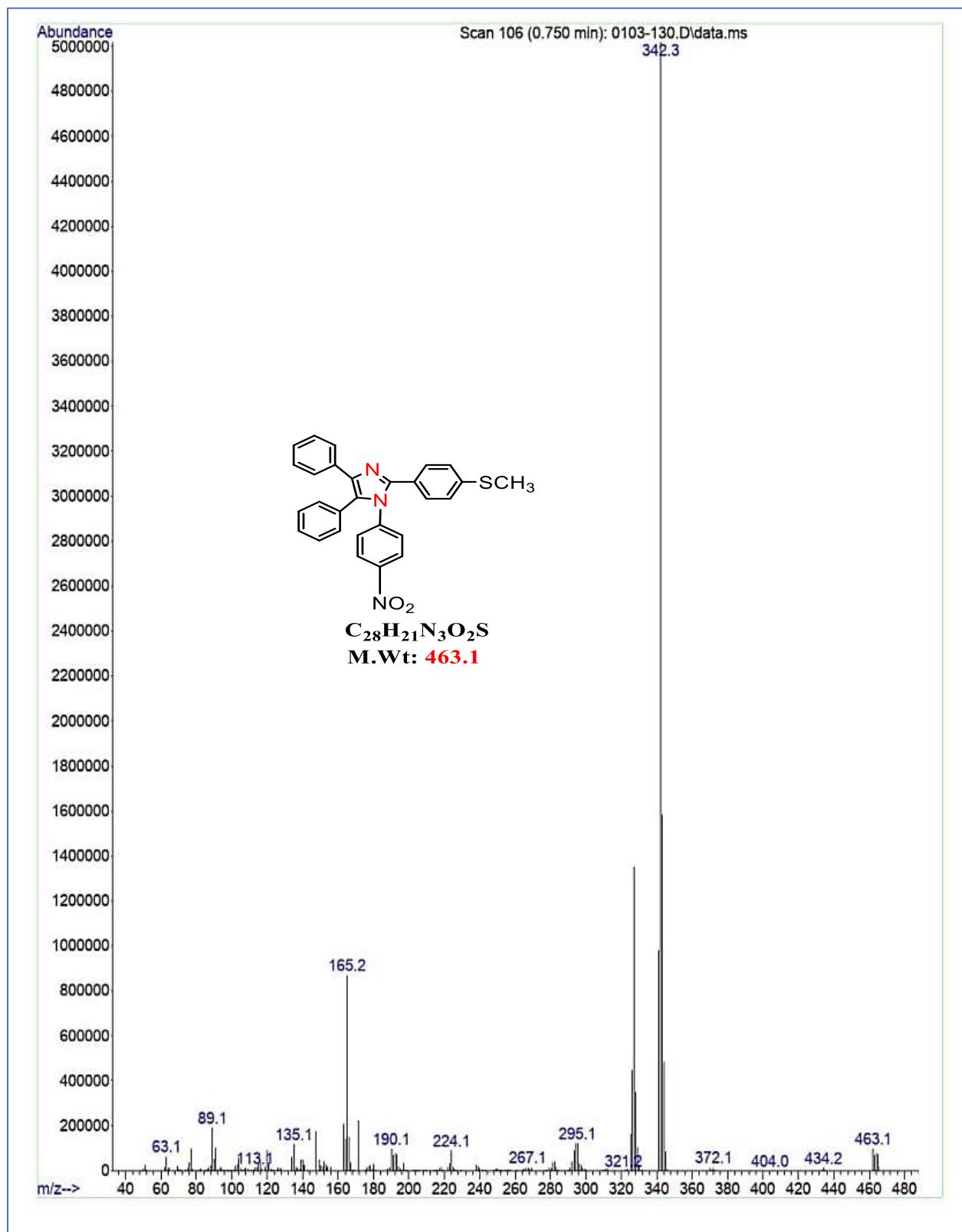


Figure 85: Mass spectrum of 5g

Appendix A

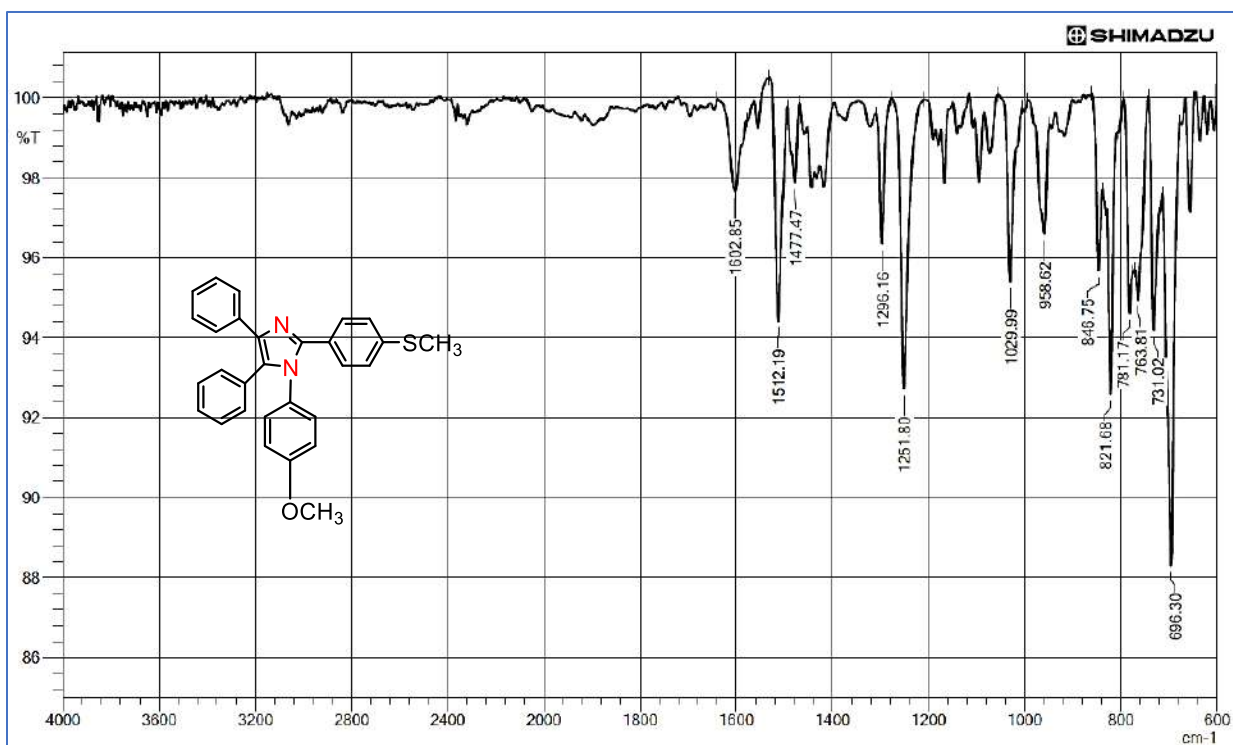


Figure 86: FTIR spectrum of 5h

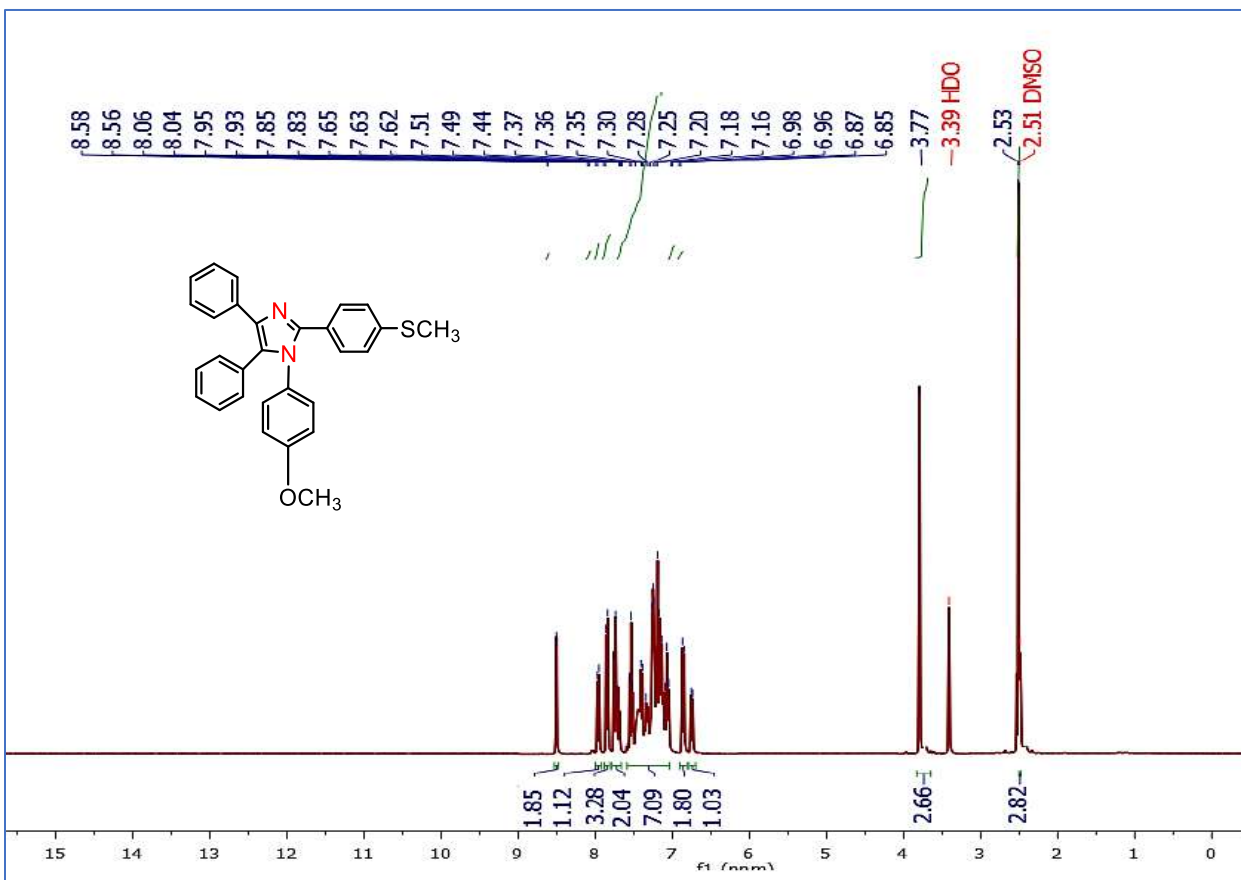


Figure 87: ¹H NMR spectrum of 5h

Appendix A

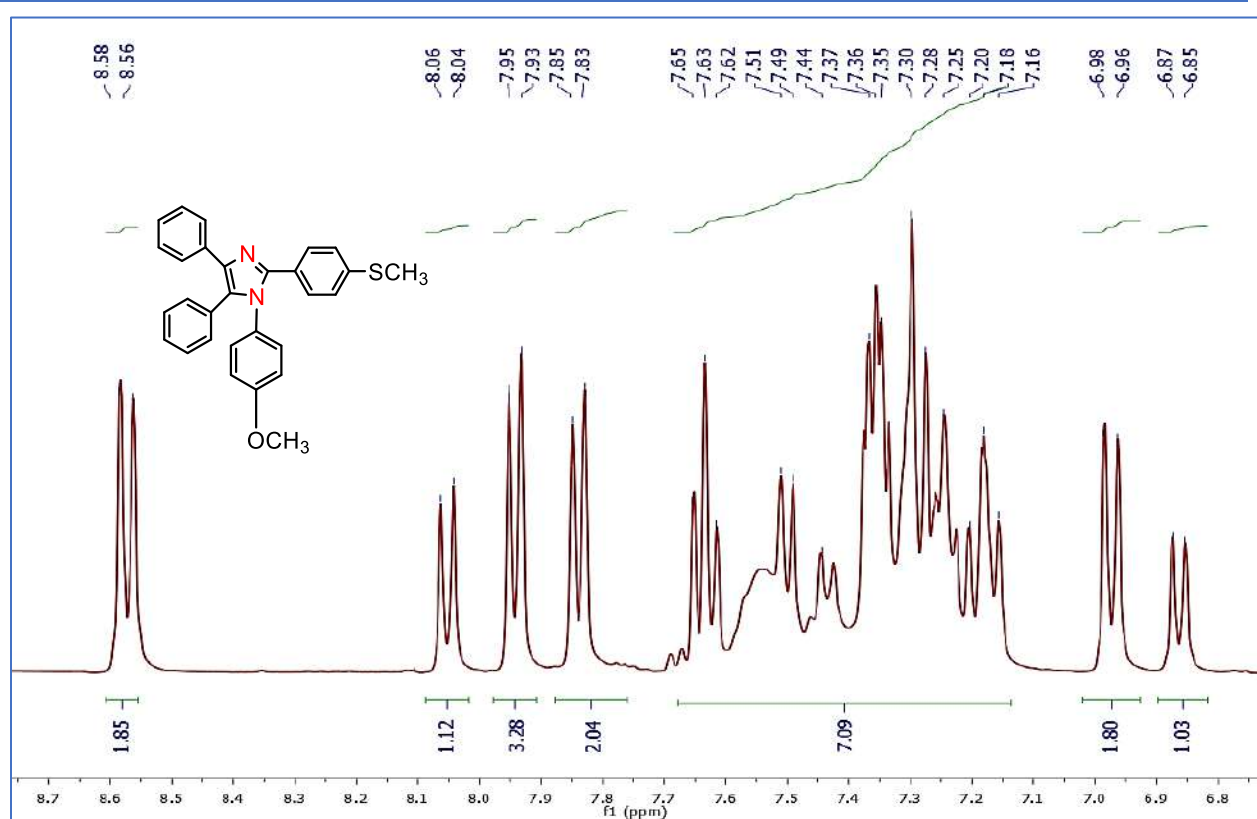


Figure 88: Expanded ^1H NMR spectrum of 5h

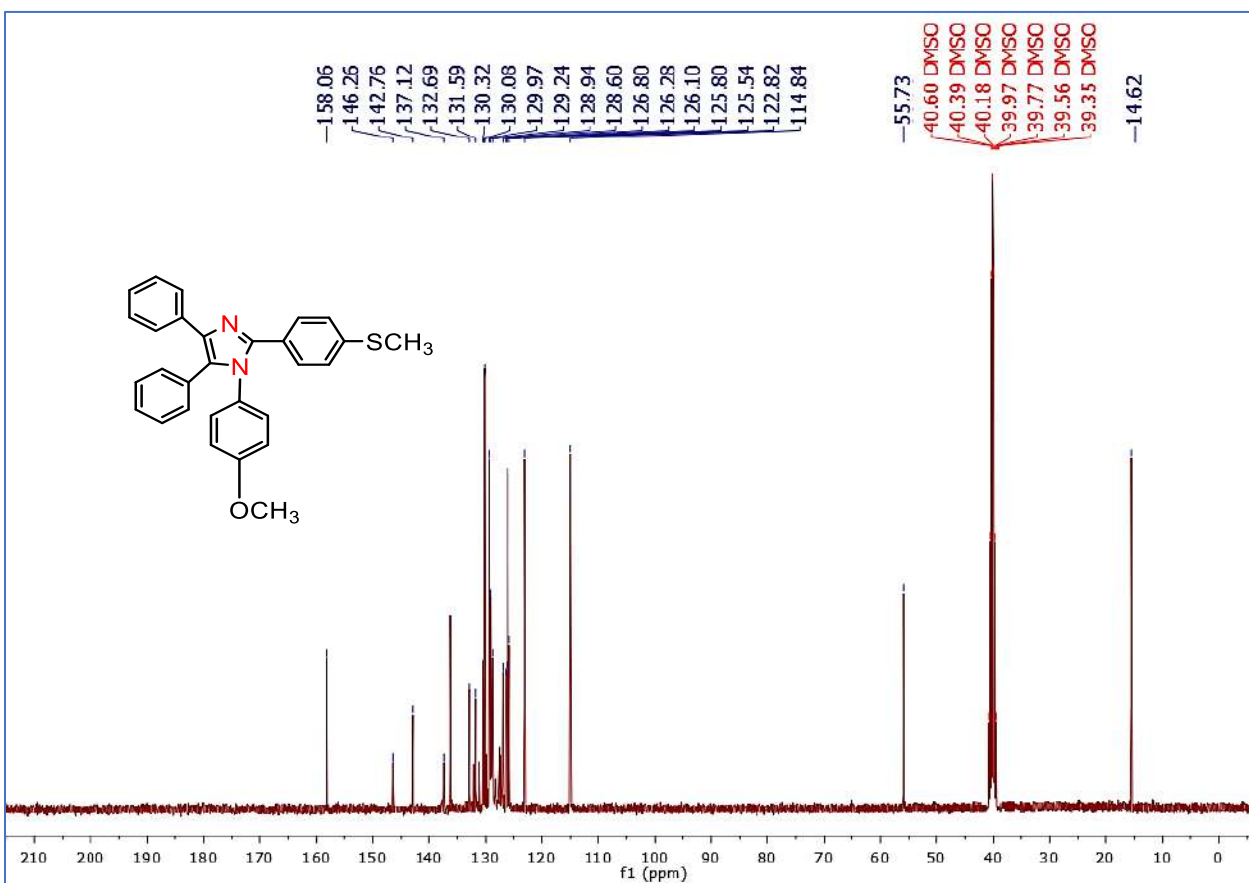


Figure 89: ^{13}C NMR spectrum of 5h

Appendix A

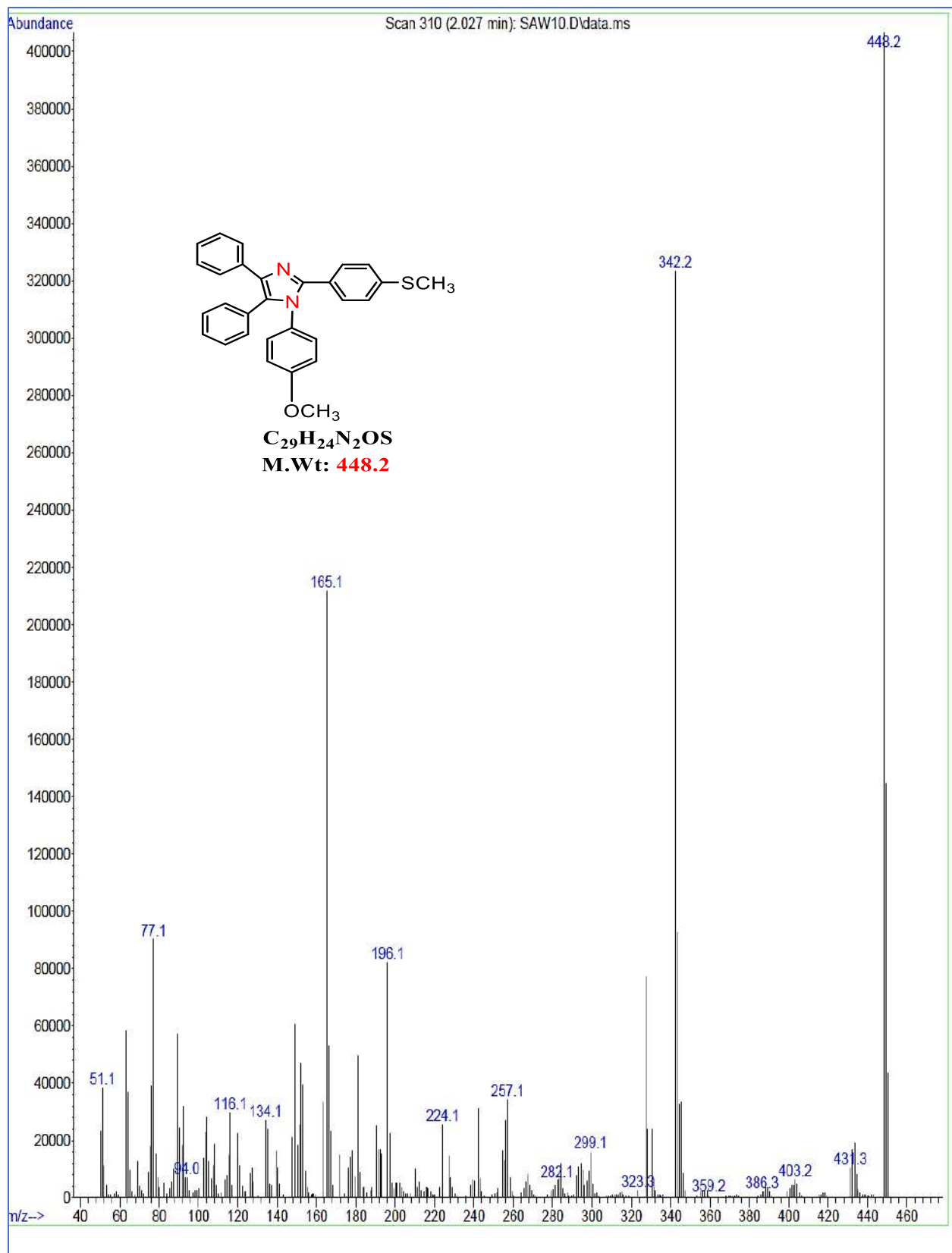


Figure 90: Mass spectrum of 5h

Appendix A

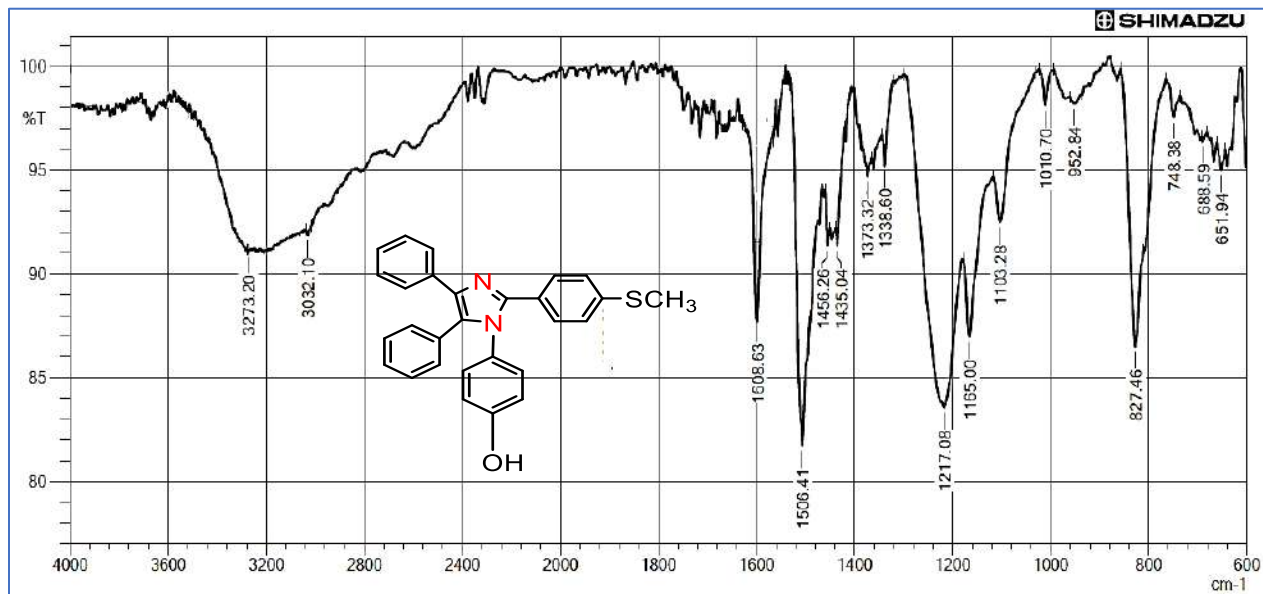


Figure 91: FTIR spectrum of 5i

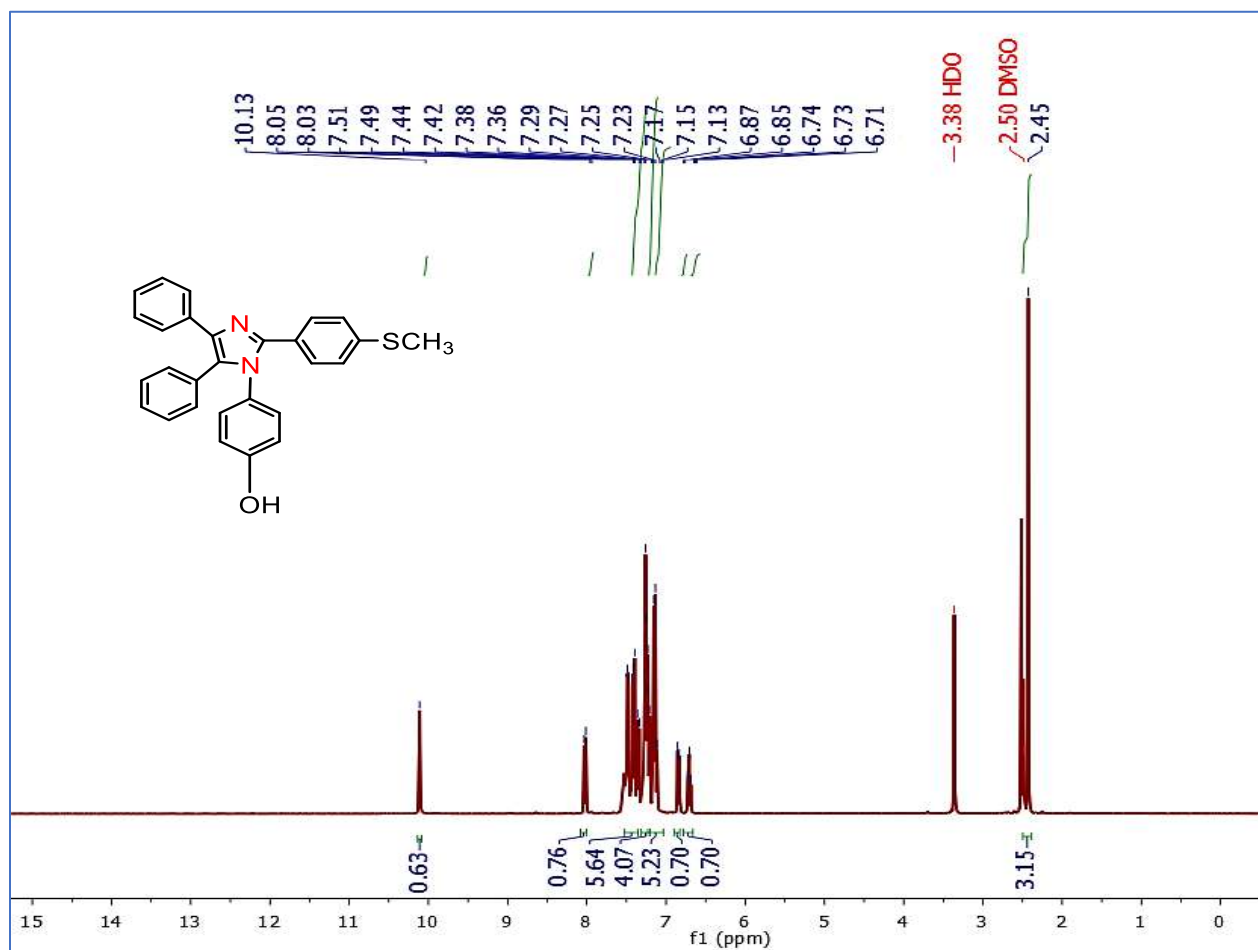


Figure 92: ¹H NMR spectrum of 5i

Appendix A

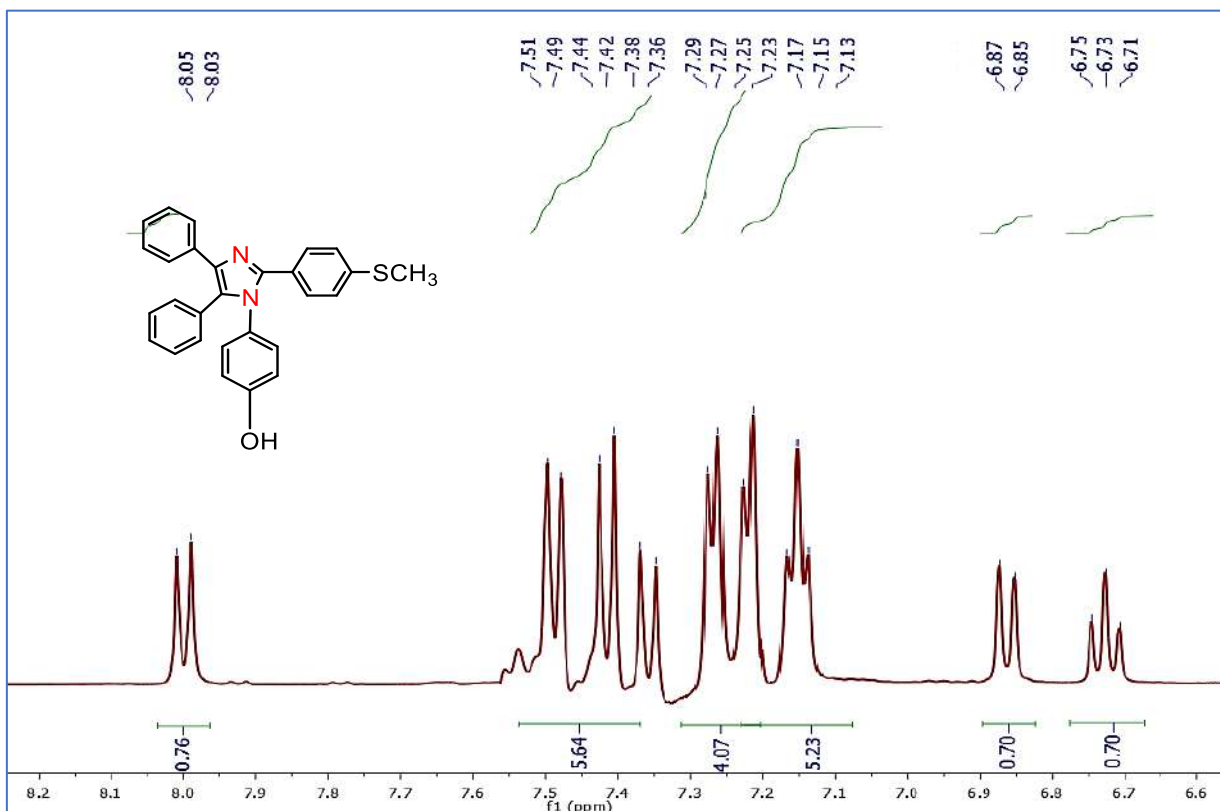


Figure 93: Expanded ¹H NMR spectrum of 5i

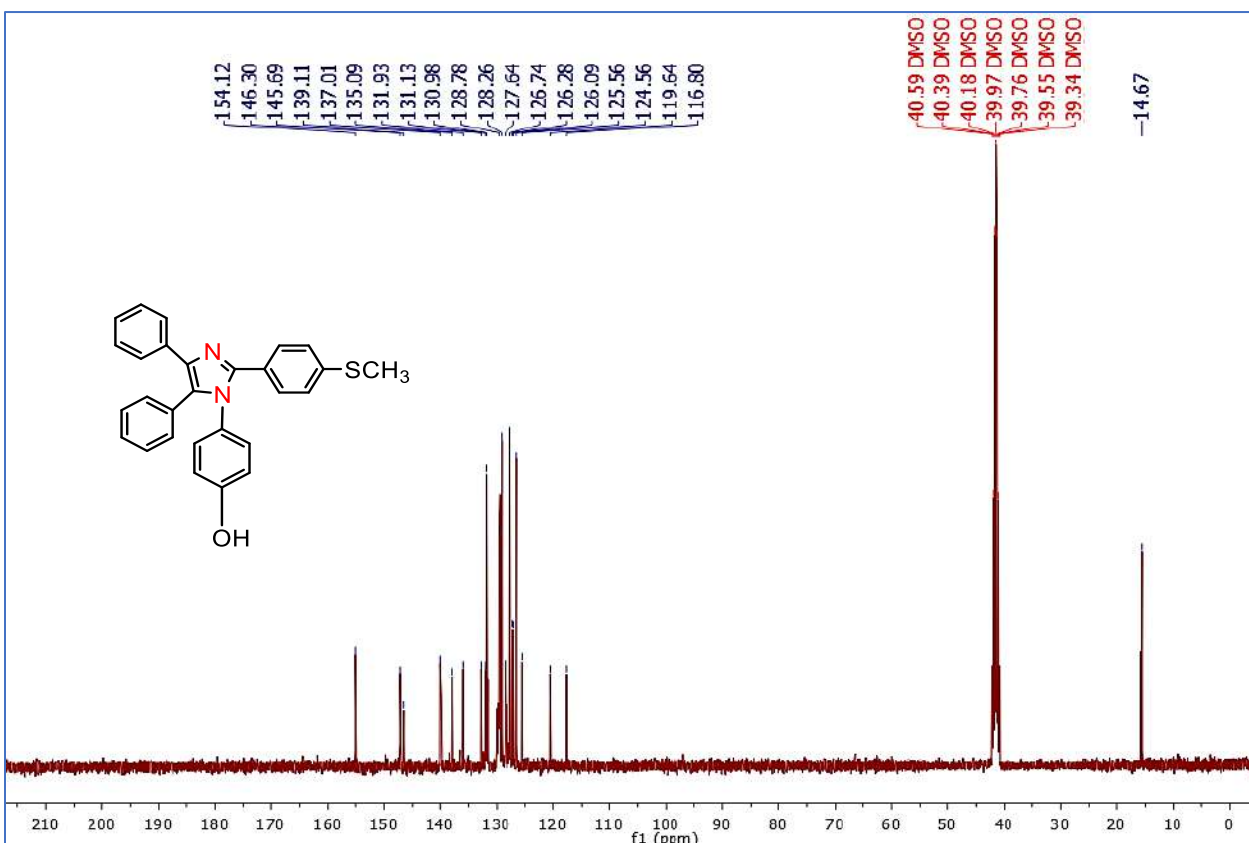


Figure 94: ¹³C NMR spectrum of 5i

Appendix A

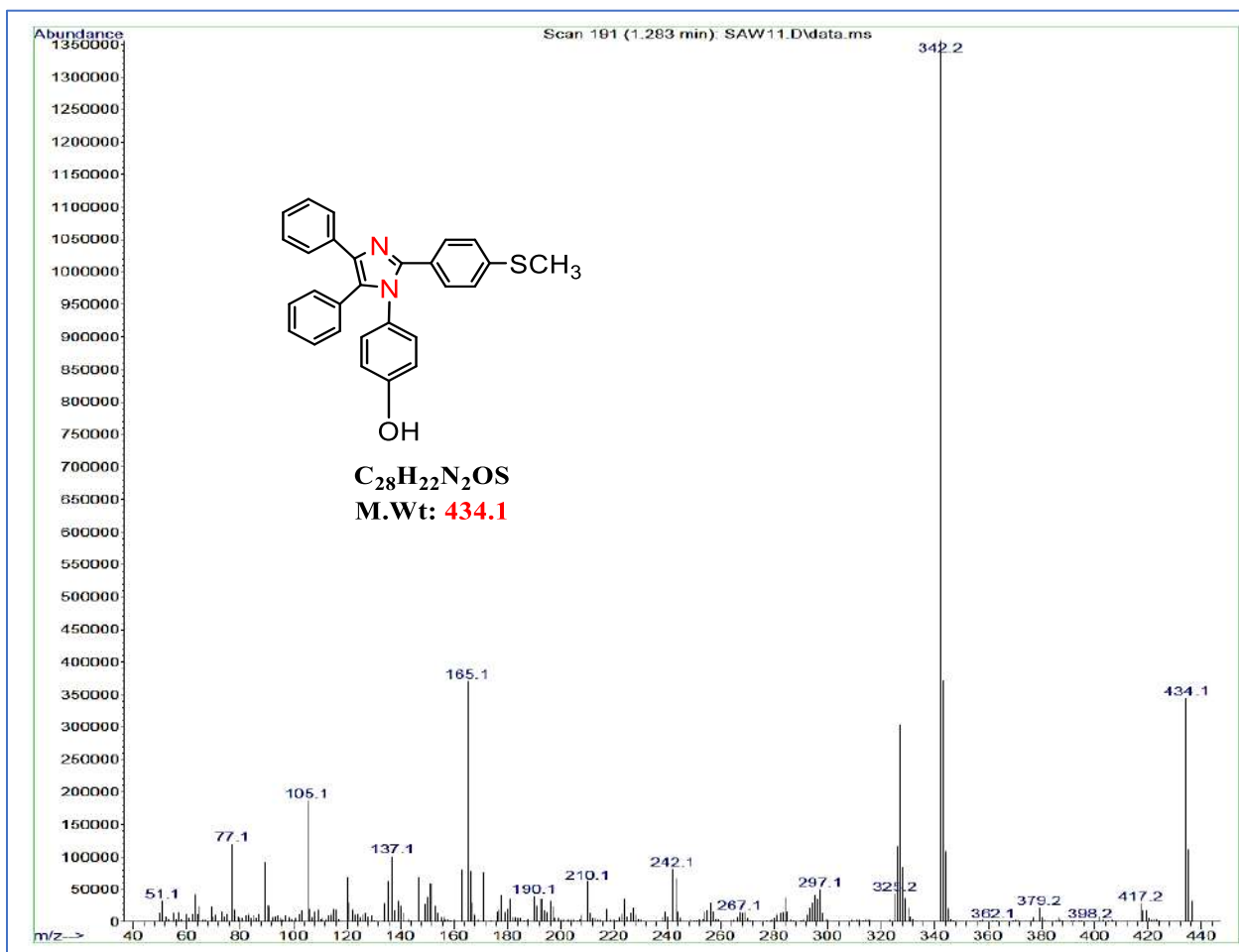


Figure 95: Mass spectrum of 5i

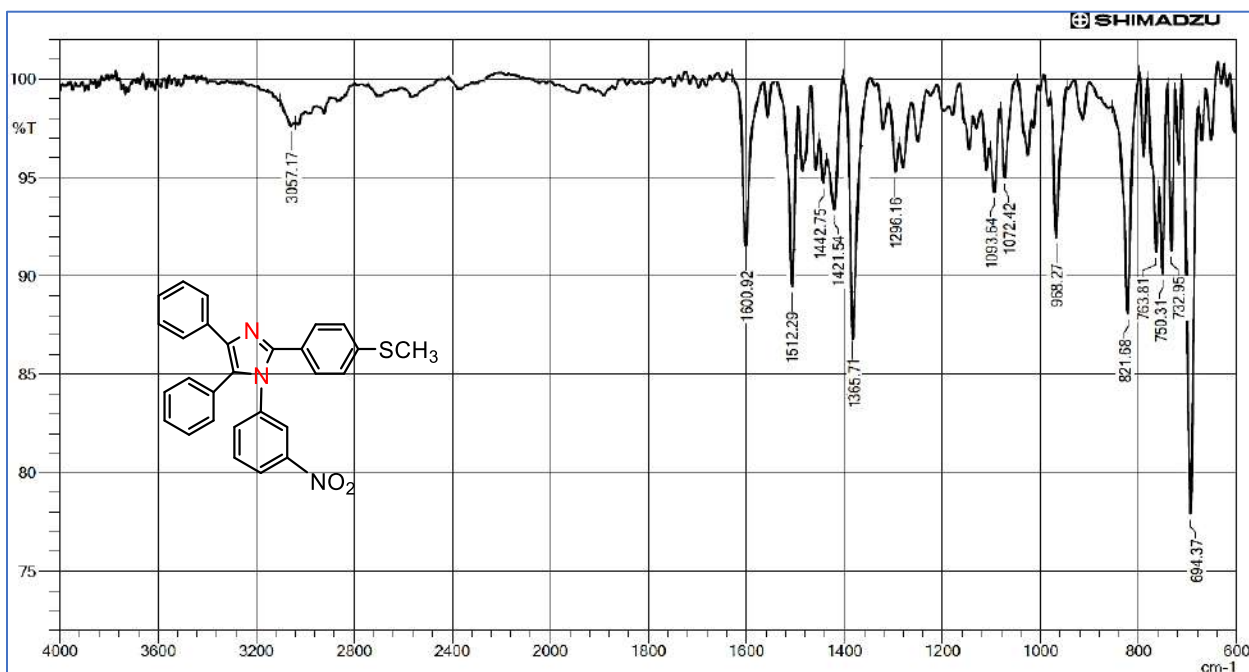


Figure 96: FTIR spectrum of 5j

Appendix A

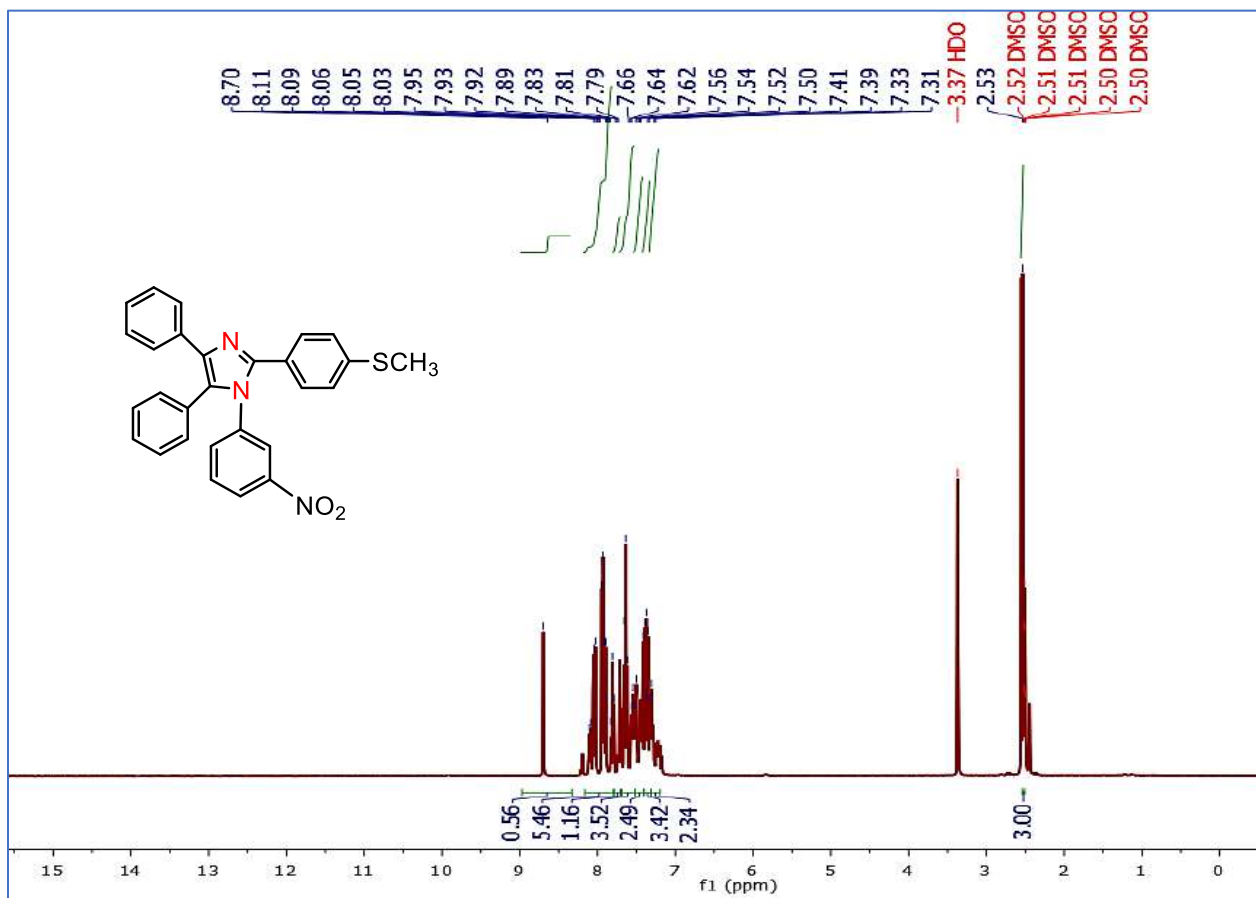


Figure 97: ^1H NMR spectrum of 5j

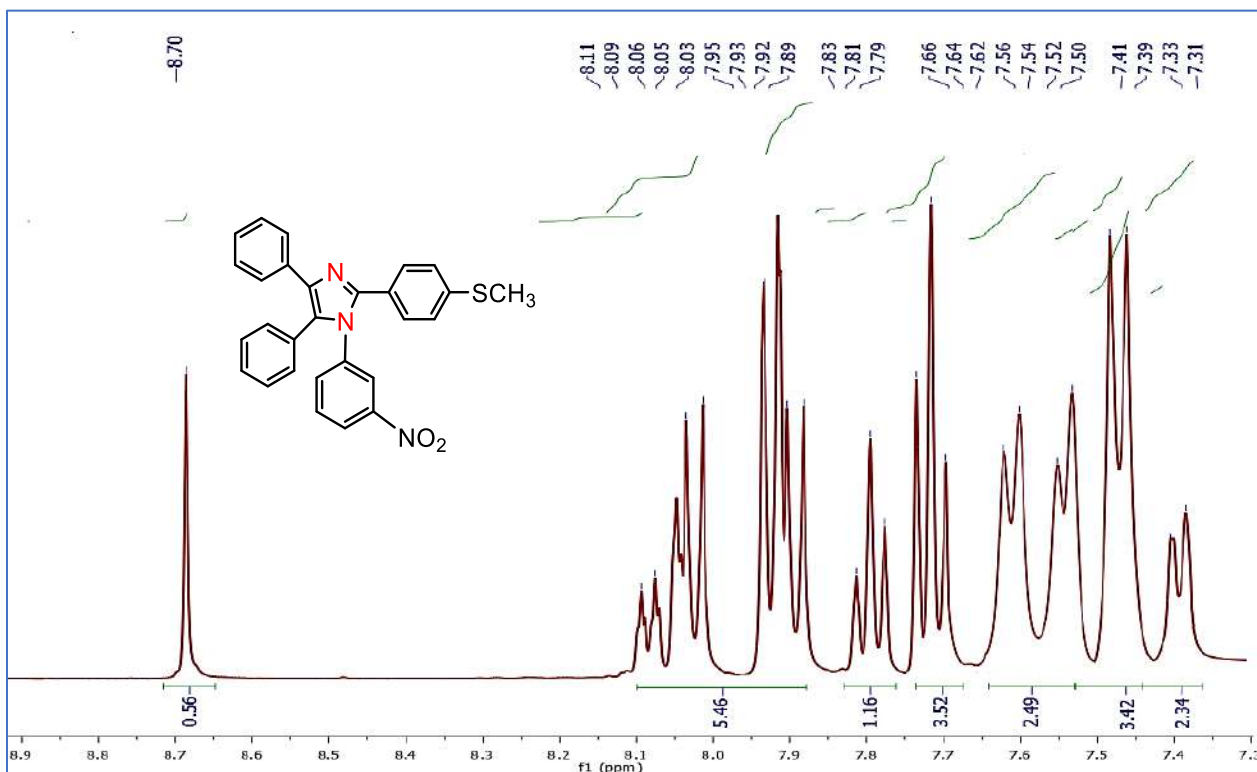


Figure 98: Expanded ^1H NMR spectrum of 5j

Appendix A

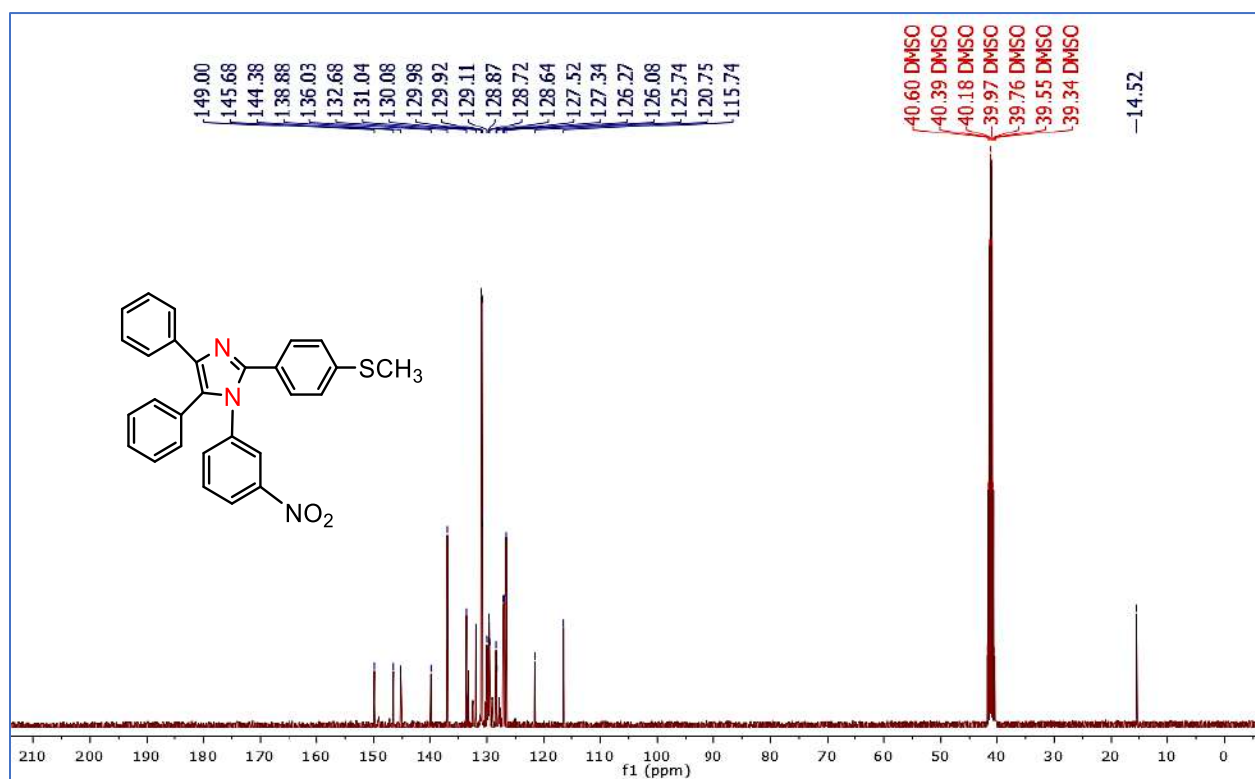


Figure 99: ¹³C NMR spectrum of 5j

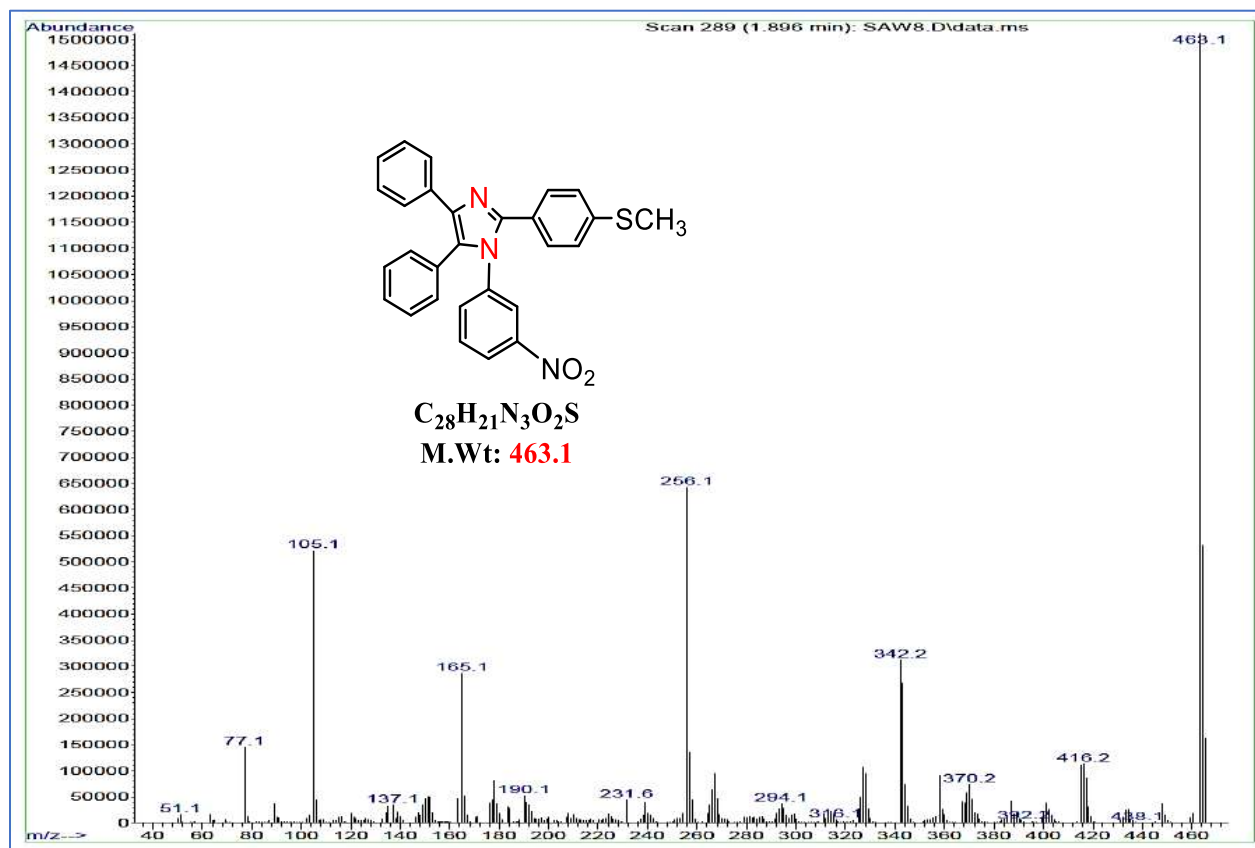


Figure 100: Mass spectrum of 5j

APPENDIX

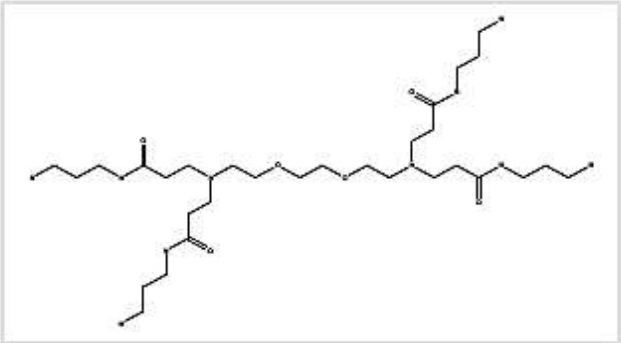
B

SciFinder® Page 1

CAS SciFinder® Task History

Initiating Search July 19, 2023, 10:03AM

References:
Filtered By:

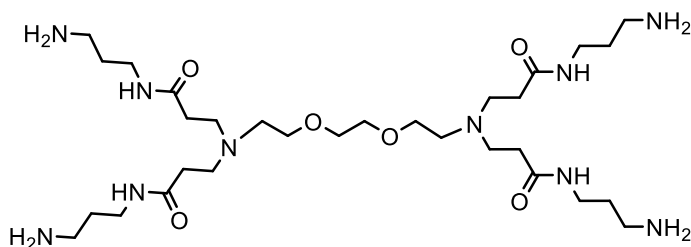


Structure Match: As Drawn

Search Tasks

Task	Search Type	View
Exported: Returned Reference Results + Filters (0)	References	View Results

Copyright © 2023 American Chemical Society (ACS). All Rights Reserved.
Internal use only. Redistribution is subject to the terms of your SciFinder® License Agreement and CAS Information Use Policies.



[G2(b)]

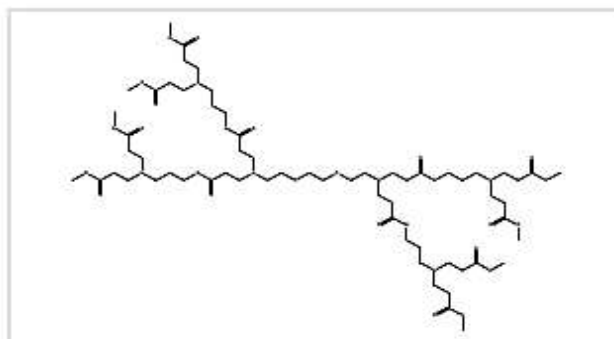
N1,N16-bis(3-aminopropyl)-4,13-bis(3-((3-aminopropyl)amino)-3-oxopropyl)-7,10-dioxa-4,13-diazahexadecanediamide

Initiating Search

July 19, 2023, 10:06AM

References:

Filtered By:



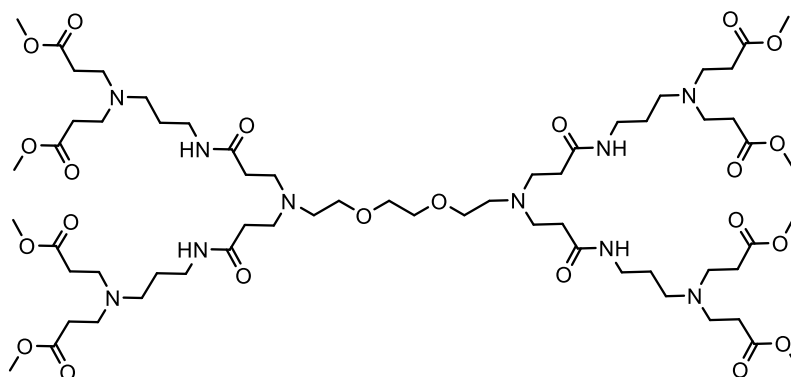
Structure Match: As Drawn

Search Tasks

Task	Search Type	View
Exported: Returned Reference Results + Filters (0)	<input checked="" type="checkbox"/> References	View Results

Copyright © 2023 American Chemical Society (ACS). All Rights Reserved.

Internal use only. Redistribution is subject to the terms of your SciFinder® License Agreement and CAS information Use Policies.

**[G3(b)]**

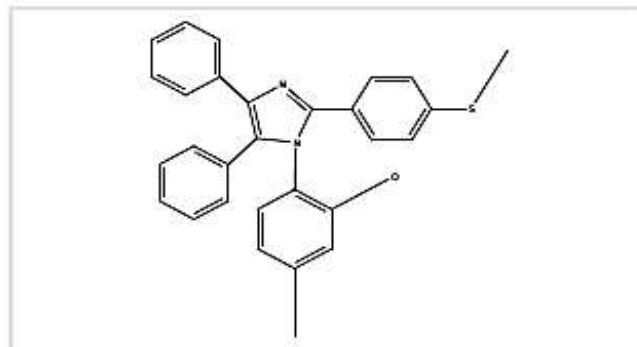
dimethyl 12,21-bis(3-((3-(bis(3-methoxy-3-oxopropyl)amino)propyl)amino)-3-oxopropyl)-4,29-bis(3-methoxy-3-oxopropyl)-9,24-dioxo-15,18-dioxa-4,8,12,21,25,29-hexaazadotriacontanedioate

Initiating Search

July 19, 2023, 10:11AM

References:

Filtered By:



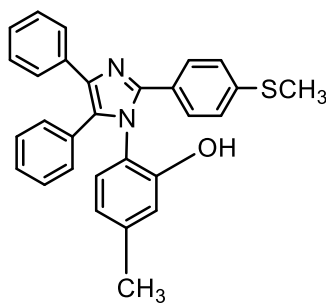
Structure Match: As Drawn

Search Tasks

Task	Search Type	View
Exported: Returned Reference Results + Filters (0)	References	View Results

Copyright © 2023 American Chemical Society (ACS). All Rights Reserved.

Internal use only. Redistribution is subject to the terms of your SciFinder® License Agreement and CAS information Use Policies.

**[5b]**

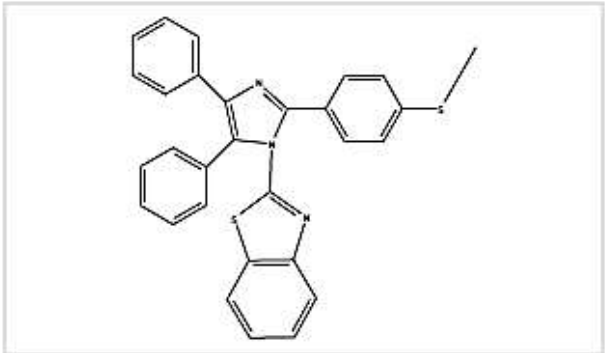
5-methyl-2-(2-(4-(methylthio)phenyl)-4,5-diphenyl-1H-imidazol-1-yl)phenol

SciFinder®Page 1

CAS SciFinder® Task History

Initiating Search July 19, 2023, 10:13AM

References:
Filtered By:

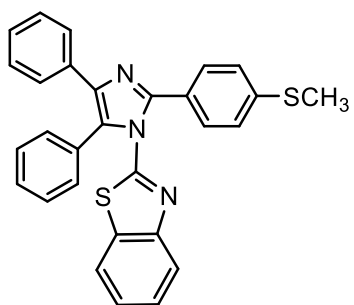


Structure Match: **As Drawn**

Search Tasks

Task	Search Type	View
Exported: Returned Reference Results + Filters (0)	<input checked="" type="checkbox"/> References	View Results

Copyright © 2023 American Chemical Society (ACS). All Rights Reserved.
Internal use only. Redistribution is subject to the terms of your SciFinder® License Agreement and CAS Information Use Policies.



[5c]

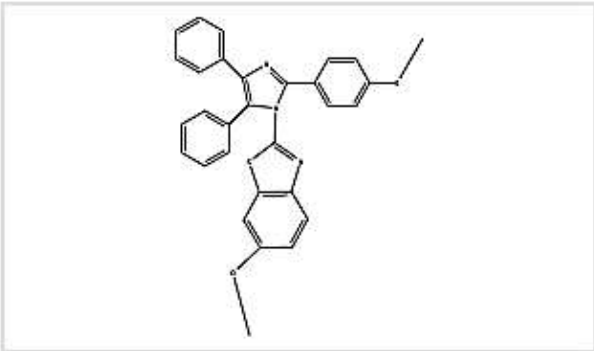
2-(2-(4-(methylthio)phenyl)-4,5-diphenyl-1Himidazol-1-yl)benzo[d]thiazole

SciFinder® Page 1

CAS SciFinder® Task History

Initiating Search July 19, 2023, 10:14AM

References:
Filtered By:

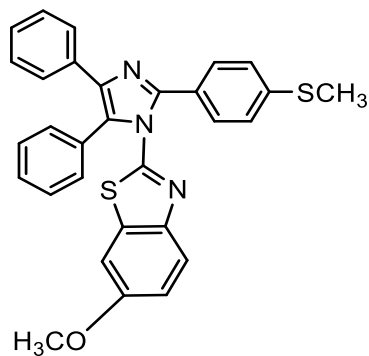


Structure Match: **As Drawn**

Search Tasks

Task	Search Type	View
Exported: Returned Reference Results + Filters (0)	<input checked="" type="checkbox"/> References	View Results

Copyright © 2023 American Chemical Society (ACS). All Rights Reserved.
Internal use only. Redistribution is subject to the terms of your SciFinder® License Agreement and CAS information Use Policies.



[5e]

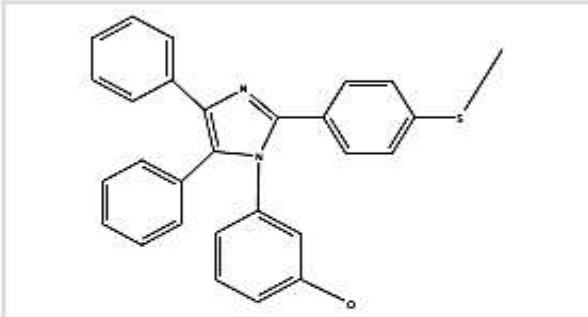
6-methoxy-2-(2-(4-(methylthio)phenyl)-4,5-diphenyl-1H-imidazol-1-yl)benzo[d]thiazole

SciFinder® Page 1

CAS SciFinder® Task History

Initiating Search July 19, 2023, 10:16AM

References:
Filtered By:

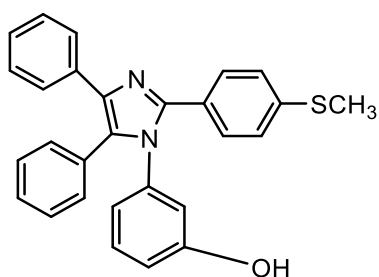


Structure Match: **As Drawn**

Search Tasks

Task	Search Type	View
Exported: Returned Reference Results + Filters (0)	<input checked="" type="checkbox"/> References	View Results

Copyright © 2023 American Chemical Society (ACS). All Rights Reserved.
Internal use only. Redistribution is subject to the terms of your SciFinder® License Agreement and CAS Information Use Policies.



[5f]

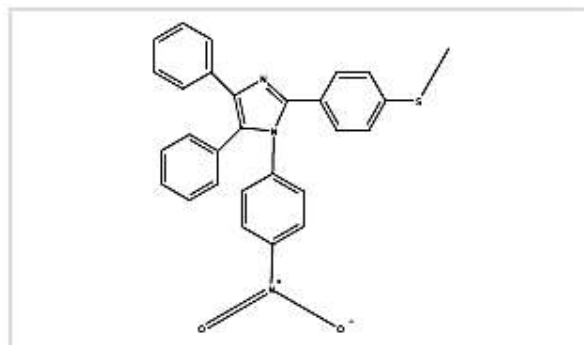
3-(2-(4-(methylthio)phenyl)-4,5-diphenyl-1H-imidazol-1-yl)phenol

Initiating Search

July 19, 2023, 10:15AM

References:

Filtered By:



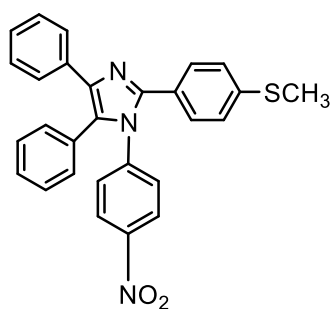
Structure Match: As Drawn

Search Tasks

Task	Search Type	View
Exported: Returned Reference Results + Filters (0)	 References	View Results

Copyright © 2023 American Chemical Society (ACS). All Rights Reserved.

Internal use only. Redistribution is subject to the terms of your SciFinder® License Agreement and CAS Information Use Policies.

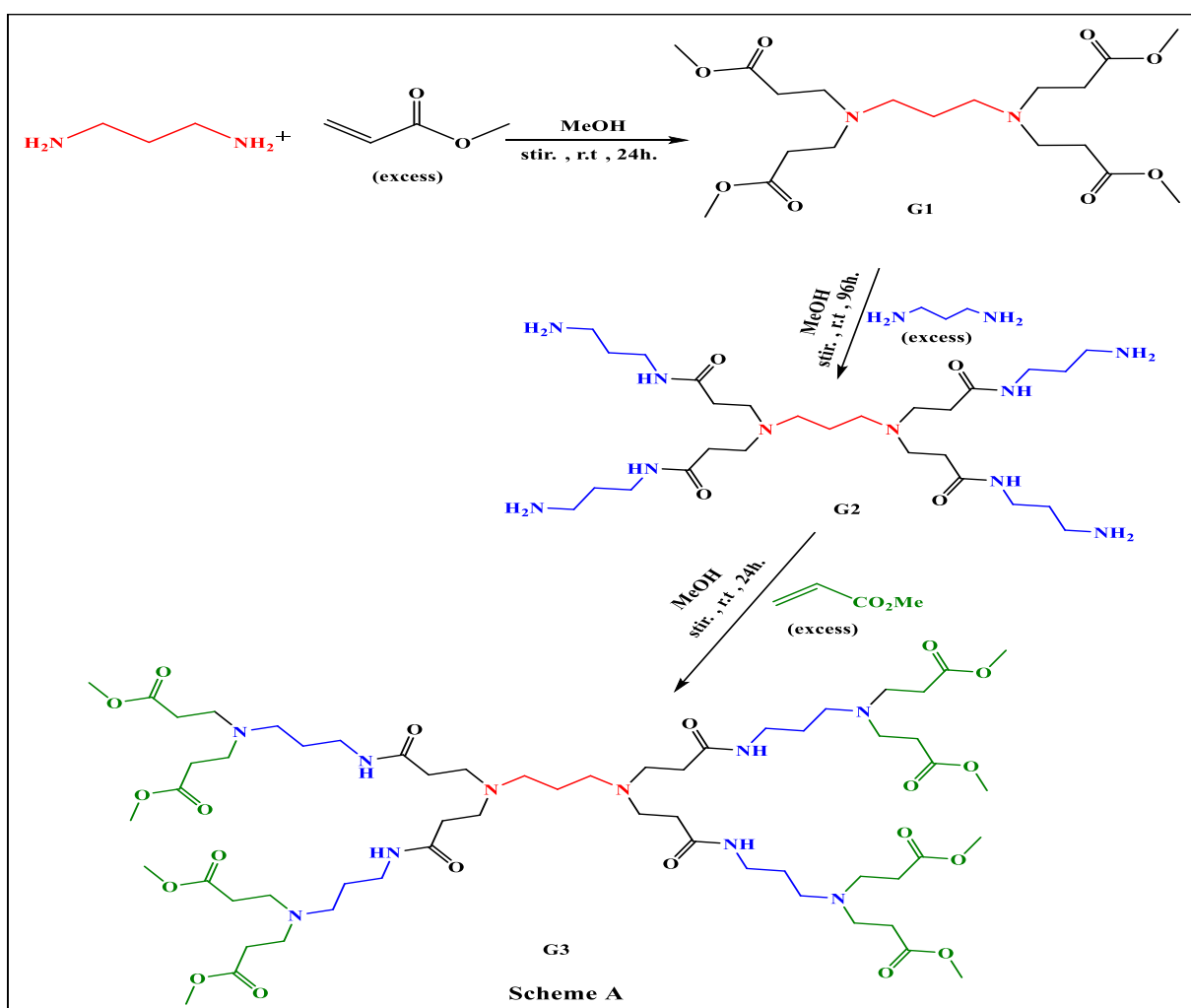
**[5g]**

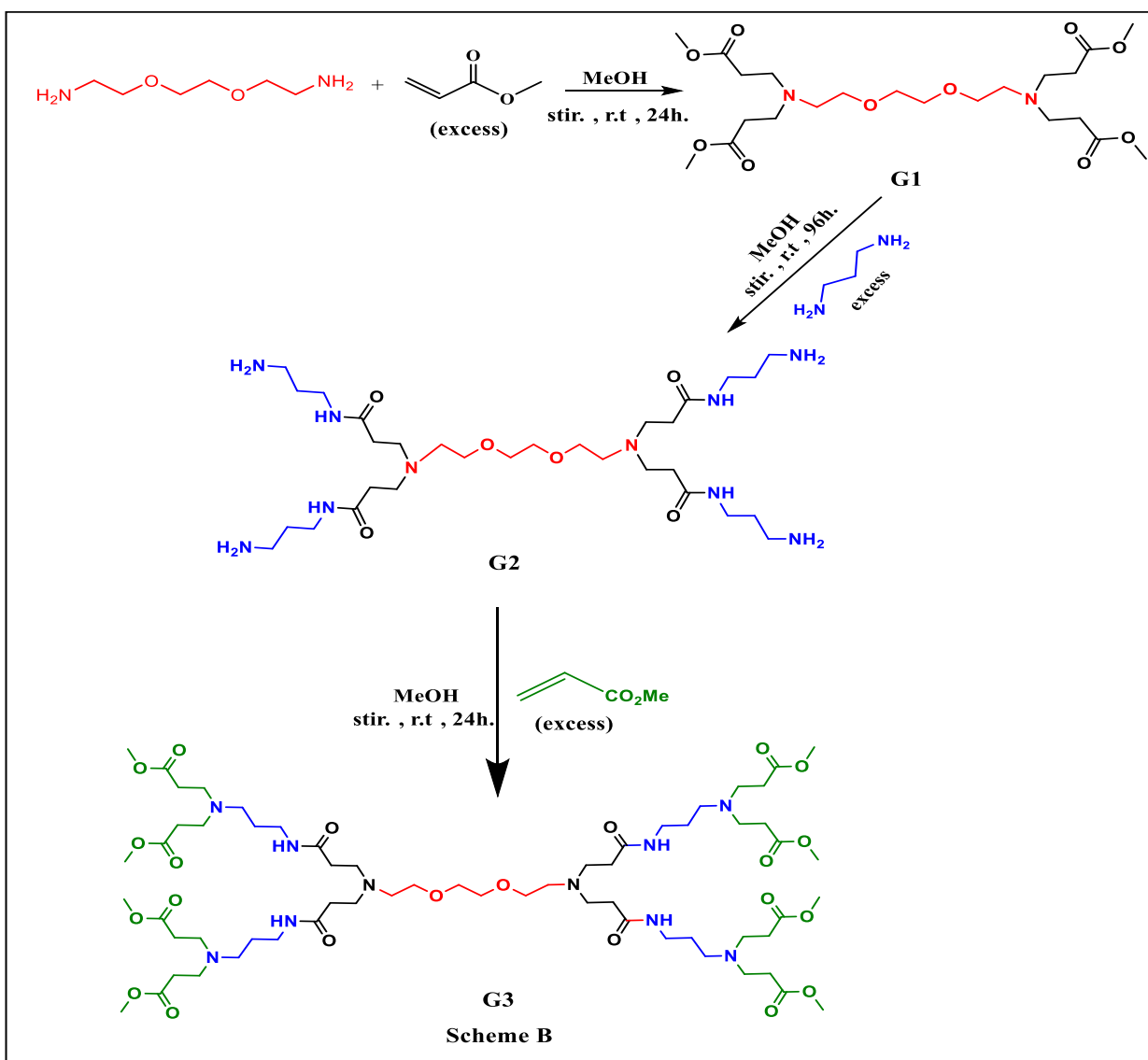
2-(4-(methylthio)phenyl)-1-(4-nitrophenyl)-4,5-diphenyl-1H-imidazole

الخلاصة

تعد متشعبات ال PAMAM ومشتقات الإيميدازول من المركبات العضوية المهمة حيث تلعب دورًا مهمًا في الكيمياء الطبية. نتيجة لذلك، تركّز هذه الدراسة على تحضير وتشخيص المتشعبات عاليه التفرع (PAMAM dendrimers) ومشتقات الايميدازول (ثلاثي إيميدازول ورباعي ايميدازول) بالإضافة إلى دراسته خصائصها في التطبيق البيوكيميائي والبيولوجي. تضمن البحث الحالي ثلاثة أجزاء.

يتضمن الجزء الأول من الأطروحة تحضير متشعبات PAMAM من G1 إلى G3 من خلال تفاعل كيميائي يتضمن خطوتين؛ إضافة مايكل ينتج عنها تحضير داندرامر (متشعب منتهي بالإستر) وخطوة وسطية لتحضير متشعب منتهي بالأمين. تم اختيار البروبان-1,3-ديامين و 1,2-ثنائي (2-أمينوايثوكسي) إيثنان كإنويه مختلفة لتحضير المتشعبات لإنتاج الأمينات الأولية والثانوية داخل هيكل الجزيئة (المخططان A و B).

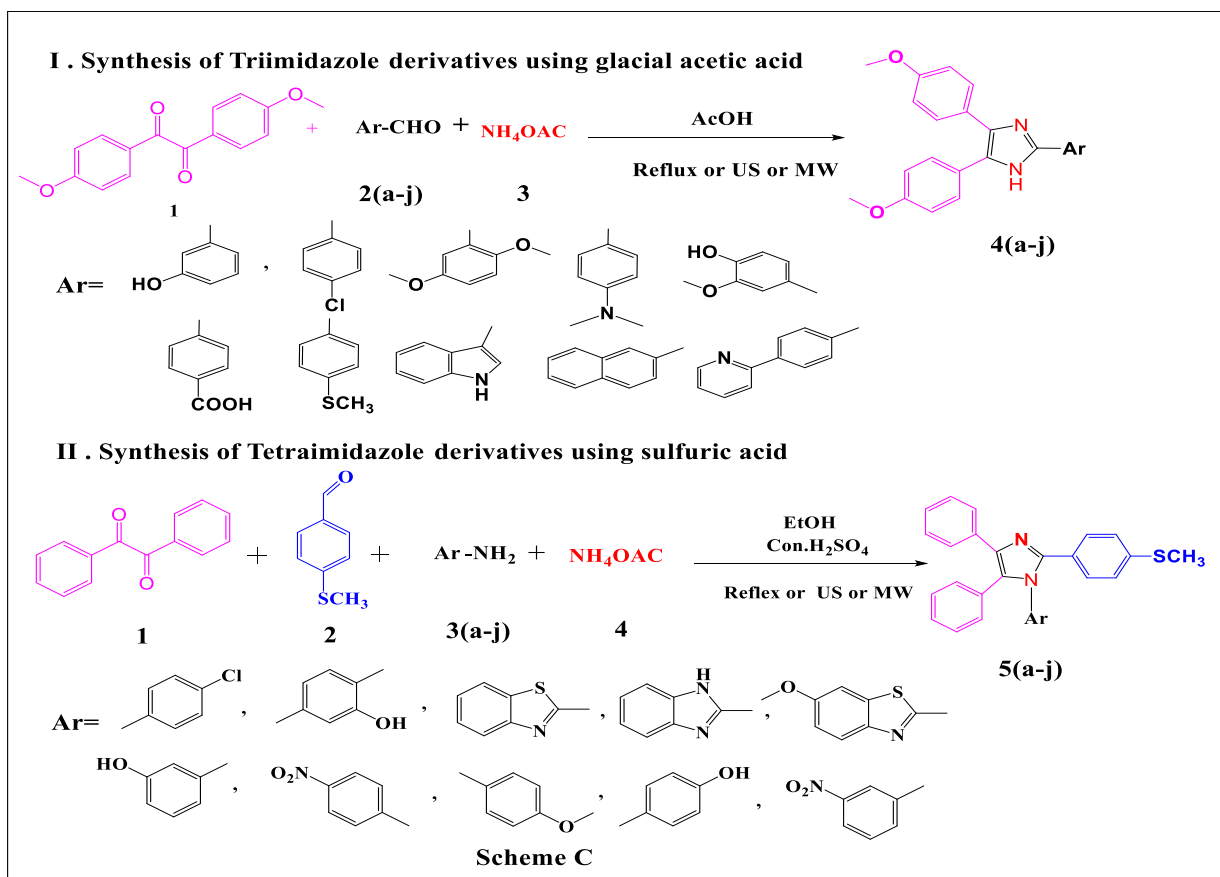




للتأكد من ان المتشعبات قد تم تحضيرها بنجاح، تم استخدام تقنيات طيفية مختلفة مثل مطيافيه الأشعة تحت الحمراء (FT-IR) , ومطيافيه الرنين النووي المغناطيسي (^{13}C , $^1\text{H-NMR}$) , وقياس طيف الكتلة (ESI) بالإضافة إلى المجهر الإلكتروني لمسح الانبعاث الميداني (FE-SEM) والتحليل الطيفي للأشعة السينية المشتتة للطاقة (EDX) .

يصف الجزء الثاني من الدراسة تفاعل تكثيف أحادي الوعاء والذي يسمى Debus-Radziszewski لتحضير مشتقات إلاميدازول ثلاثيه التعويض **4a** إلى **4j** باستخدام البنزاييل وبعض الألدهيدات الاروماتيه المتنوعه وخلات الأمونيوم في وجود حامض الخليك الثلجي كعامل مساعد . أيضاً تم تحضير مشتقات الأميدازول رباعيه التعويض **5a** إلى **5j** باستخدام البنزاييل والألدهيد الاروماتي ومجموعة متنوعة من الأمينات

الاروماتيه وخلات الامونيوم في وجود حامض الكبريتيك كعامل مساعد باستخدام عمليه التصعيد (ظروف تسخين). كما تم استخدام التشعيع بالموجات فوق الصوتية والتشعيع بالأشعة المايكرويه لتحضير هذه المركبات، تمت مقارنة التفاعلات في ظروف التسخين التقليديه مع التشعيع بالموجات فوق الصوتية وتفاعلات إشعاع المايكرويف حيث يتم استخدام هذه التقنيات كأحد طرق الكيمياء الخضراء. بالمقارنة مع الطرق التقليديه ، فإن الموجات فوق الصوتية وموجات المايكرويف لها نسبه ناتج أفضل ووقت تفاعل أسرع وانتقائية أعلى وآثار جانبية أقل (المخطط C). تم تشخيص المركبات المحضره باستخدام درجه الانصهار (Melting point)، مطيافيه الاشعه تحت الحمراء (FTIR) ، والتحليل الطيفي النووي المغناطيسي (^{13}C ، ^1H -NMR) وتحليل طيف الكتله (ESI-MS).



يتضمن الجزء الثالث من العمل التطبيقات البيوكيميائية والبيولوجية لبعض المركبات التي تم تحضيرها ، حيث تم اخضاع بعض المركبات المحضره للنشاط المضاد لتحصي المسالك البولية ، كما تم فحص نشاطها المضاد لمرض السكري والنشاط المضاد للبكتيريا بالإضافة إلى فحوصات تحلل الدم من أجل فهم أفضل للدراسه السمية لهذه المركبات, لفحص امكانيه بعض المركبات المحضره المضادة لتحصي المسالك البولية ، تم اختبار الأنشطة المثبته لمضادات التبول في المختبر باستخدام الأكاربوز كدواء مرجعي. أظهرت النتائج أن المركب (b) **G2**

كان له أعلى نسبة تثبيط في اختبار التنوي ، والتي كانت 91% بتركيز 250 ميكروغرام / مل بعد 360 دقيقة من فترة الحضانه في درجه حراره 37م° ، مقارنة بالعقار المرجعي cystone ، والذي كان له نسبة مئوية بحدود 65%. من ناحية أخرى، أظهر المركب G2(a) أعلى نسبة تثبيط في اختبار التجمع عند 360 دقيقة من الحضانه عند تركيز 250 ميكروغرام / مل ، والتي كانت 69% ؛ 24% أعلى من cystone 46%.

أظهر الفحص المضاد لمرض السكري نتائج تثبيط متوسطه إلى جيدة ، بقيم تثبيط تتراوح من 48% إلى 90% ضد α -amylase و 38% إلى 61% ضد α -glucosidase. كانت هذه النتائج مشجعة للغاية. تمت مقارنة النتائج التي تم الحصول عليها مع عقار ألكاربوز كمرجع قياسي، والذي كانت قيمته 65% لـ α -amylase و 66% لـ α -glucosidase وعلى وجه الخصوص، كانت المركبات 4f و 4e و 5b و 4b هي الأكثر نشاطاً، حيث بلغت قيم تثبيط النسبة المئوية 90% و 78% و 77% و 75% على التوالي ضد α -amylase والمركبات 4f و 4b، مع قيم تثبيط بنسبة 61% و 58% ضد α -glucosidase.

كما تم فحص المركبات فيما يتعلق بنشاطها المضاد للبكتيريا في المختبر ضد أربعة بكتيريا معزولة موجبة الجرام (*Streptococcus agalactiae* ، *Staphylococcus aureus*) وسالبة الجرام (*Proteus mirabilis* و *E. coli*). أظهرت نتائج الحد الأدنى من التراكيز المثبطة (MICs) قيمة مماثلة للمضادات الحيوية المعيارية Azithromycin و Amoxicillin-clavulanic acid وأبرزها 4a و 4e و 5b و 5c ضد *Staphylococcus aureus* و 4e و 5b ضد *Streptococcus agalactiae*.

أظهرت نتائج اختبار انحلال الدم أن معظم المركبات التي تم فحصها لها تأثير منخفض على خلايا الدم الحمراء البشرية (أقل من 5%). وعلى وجه التحديد، تم إثبات أن المركبات G2(a) و G3(a) و G2(b) و G3(b) و 5g نشطة بشكل ملحوظ مع نسبة انحلال الدم والتي تتراوح من 0.718% إلى 2.654% مقارنة بمعيار Triton X-100 ، والذي أظهر نتيجة إيجابية بنسبة 97.3% . اشارت نتائج الدراسات الأولية لهذه الفحوصات ان بعض المركبات اظهرت نشاطا قويا اعلى من الدواء المرجعي لكل فحص تم اجراءه، مما قد يجعلها دواءً واعدًا للعلاج.



جامعة كربلاء
كلية العلوم
قسم الكيمياء

تحضير منشعبات، أيميدازولات ودراسة تطبيقاتها البيوكيميائية والبايولوجية

اطروحة مقدمة
الى مجلس كلية العلوم- جامعة كربلاء
كجزء من متطلبات نيل درجة الدكتوراه فلسفة في
العلوم/علوم الكيمياء

من قبل

سوسن خضير عباس

بكالوريوس علوم كيمياء / جامعة بابل 2002
ماجستير علوم كيمياء / جامعة كربلاء 2014

بأشراف

أ.د نرجس هادي منصور السعدي
دكتوراه في الكيمياء الحياتية

أ.د هيثم دلول حنون الشبلي
دكتوراه في الكيمياء العضوية